A COMBINED MODELLING APPROACH FOR SIMULATING CHANNEL–WETLAND EXCHANGES IN LARGE AFRICAN RIVER BASINS

A thesis submitted in fulfilment of the requirements for the degree of

DOCTOR OF PHILOSOPHY

of

RHODES UNIVERSITY

By

EUNICE J MAKUNGU

APRIL 2019

DEDICATION

This thesis is dedicated to my daughter, Elmarie.

ABSTRACT

In Africa, many large and extensive wetlands are hydrologically connected to rivers, and their environmental integrity, as well as their influence on downstream flow regimes, depends on the prevailing channel–wetland exchange processes. These processes are inherently complex and vary spatially and temporally. Understanding channel–wetland exchanges is therefore, indispensable for the effective management of wetlands and the associated river basins. However, this information is limited in most of the river basins containing large wetlands in Africa. Furthermore, it is important to understand the links between upstream and downstream flow regimes and the wetland dynamics themselves, specifically where there are water resource developments that may affect these links (upstream developments), or be affected by them (downstream developments).

Hydrological modelling of the entire basin using basin-scale models that include wetland components in their structures can be used to provide the information required to manage water resources in such basins. However, the level of detail of wetland processes included in many basin-scale models is typically very low and the lack of understanding of the wetland dynamics makes it difficult to quantify the relevant parameters. Detailed hydraulic models represent the channel-wetland exchanges in a much more explicit manner, but require relatively more data and time resources to establish than coarser scale hydrological models. The main objective of this study was, therefore, to investigate the use of a detailed hydraulic wetland model to provide a better understanding of channel–wetland exchanges and wetland dynamics, and to use the results to improve the parameterisation of a basin-scale model.

The study focused on improving the water resource assessments modelling of three data-scarce African river basins that contain large wetlands: the floodplains of the Luangwa and Upper Zambezi River basins and the Usangu wetland in the Upper Great Ruaha River basin. The overall objective was achieved through a combined modelling approach that uses a detailed high-resolution LISFLOOD-FP hydraulic model to inform the structure and parameters of the GW Pitman monthly hydrological model. The results from the LISFLOOD-FP were used to improve the understanding of the channel–wetland exchange dynamics and to establish the wetland parameters required in the GW Pitman model. While some wetland parameters were directly quantified from the LISFLOOD-FP model results, others, which are highly empirical, were estimated by manually calibrating the GW Pitman wetland sub-model

implemented in excel spreadsheets containing the LISFLOOD-FP model results. Finally, the GW Pitman model with the inclusion of the estimated wetland parameters was applied for each basin and the results compared to the available downstream observed flow data. The two models have been successfully applied in southern Africa, with the GW Pitman model being one of the most widely applied hydrological models in this region. To address the issue of data scarcity, during setup of these models, the study mainly relied on the global datasets which clearly adds to the overall uncertainty of the modelling approach. However, this is a typical situation for most of the data scarce regions of the continent.

A number of challenges were, however, faced during the setup of the LISFLOOD-FP, mainly due to the limitations of the data inputs. Some of the LISFLOOD-FP data inputs include boundary conditions (upstream and downstream), channel cross-sections and wetland topography. In the absence of observed daily flows to quantify the wetland upstream boundary conditions, monthly flow volumes simulated using the GW Pitman monthly model (without including the wetland sub-model) were disaggregated into daily flows using a disaggregation sub-model. The simulated wetland inflows were evaluated using the observed flow data for downstream gauging stations that include the wetland effects. The results highlighted that it is important to understand the possible impacts of each wetland on the downstream flow regime during the evaluations of the model simulation results. Although the disaggregation approach cannot be validated due to a lack of observed data, it at least enables the simulated monthly flows to be used in the daily time step hydraulic model. One of the recommendations is that improvements are required in gauging station networks to provide more observed information for the main river and the larger tributary inflows into these large and important wetland systems. Even a limited amount of newly observed data would be helpful to reduce some of the uncertainties in the combined modelling approach. The SRTM 90 m DEM (used to represent wetland topography) was filtered to reduce local variations and noise effects (mainly vegetation bias), but there were some pixels that falsely affect the inundation results, and the recently released vegetation-corrected DEMs are suggested to improve the simulation results. Channel cross-section values derived from global datasets should be examined because some widths estimated from the Andreadis *et al.* (2013) dataset were found to be over-generalised and did not reflect widths measured using high-resolution Google Earth in many places. There is an indication that channel cross-sections digitised from Google Earth images can be successfully used in the model setup except in densely vegetated swamps where the values are difficult to estimate, and in such situations, field measured cross-section data are required. Small channels such as those found in the Usangu wetland could play major role in the exchange dynamics, but digitising them all was not straightforward and only key ones were included in the model setup. Clearly, this inevitably introduced uncertainties in the simulated results, and future studies should consider applying methods that simplify extractions of most of these channels from high-resolution images to improve the simulated results.

The study demonstrated that the wetland and channel physical characteristics, as well as the seasonal flow magnitude, largely influence the channel–wetland exchanges and wetland dynamics. The inundation results indicated that the area–storage and storage–inflow relationships form hysteretic curves, but the shape of these curves vary with flood magnitude and wetland type. Anticlockwise hysteresis curves were observed in both relationships for the floodplains (Luangwa and Barotse), whereas there appears to be no dominant curve type for the Usangu wetlands. The lack of well-defined hysteretic relationships in the Usangu could be related to some of the difficulties (and resulting uncertainties) that were experienced in setting up the model for this wetland. The storage–inflow relationships in all wetlands have quite complex rising limbs due to multiple flow peaks during the main wet season. The largest inundation area and storage volume for the Barotse and Usangu wetlands occurred after the peak discharge of the wet season, a result that is clearly related to the degree of connectivity between the main channel and those areas of the wetlands that are furthest away from the channel. Hysteresis effects were found to increase with an increase in flood magnitudes and temporal variations in the wetland inflows. Overall, hysteresis behaviour is common in large wetlands and it is recommended that hysteresis curves should be reflected in basin-scale modelling of large river basins with substantial wetland areas. At a daily time scale, inflow–outflow relationships showed a significant peak reduction and a delayed time to peak of several weeks in the Barotse and Usangu wetlands, whereas the attenuation effects of the Luangwa floodplain are minimal.

To a large extent, the LISFLOOD-FP results provided useful information to establish wetland parameters and assess the structure of Pitman wetland sub-model. The simple spreadsheet used to estimate wetland parameters did not account for the wetland water transfers from the upstream to the next section downstream (the condition that is included in the LISFLOOD-FP model) for the case when the wetlands were distributed across more than one sub-basin. It is recommended that a method that allows for the upstream wetland inflows and the channel inflows should be included in the spreadsheet. The same is true to the Pitman model structure, and a downstream transfer of water can be modelled through return flows to the channel. The structure of the wetland sub-model was modified to allow an option for the return flows to occur at any time during the simulation period to provide for types of wetlands (e.g. the Luangwa) where spills from the channel and drainage back to the channel occur simultaneously. The setup of the GW Pitman model with the inclusion of wetland parameters improved the simulation results. However, the results for the Usangu wetlands were not very satisfactory and the collection of additional field data related to exchange dynamics is recommended to achieve improvements. The impacts of the Luangwa floodplain on the flow regime of the Luangwa River are very small at the monthly time scale, whereas the Barotse floodplain system and the Usangu wetlands extensively regulate flows of the Zambezi River and the Great Ruaha River, respectively. The results highlighted the possibilities of regionalising some wetland parameters using an understanding of wetland physical characteristics and their water exchange dynamics. However, some parameters remain difficult to quantify in the absence of site-specific information about the water exchange dynamics. The overall conclusion is that the approach implemented in this study presents an important step towards the improvements of water resource assessments modelling for research and practical purposes in data-scarce river basins. This approach is not restricted to the two used models, as it can be applied using different model combinations to achieve similar study purpose.

TABLE OF CONTENTS

DEDICATION i

ABSTRACT ii

TABLE OF CONTENTS vi

ACRONYMS xii

LIST OF FIGURES xiii

LIST OF TABLES xxiii

ACKNOWLEDGEMENT xxvi

CHAPTER ONE: INTRODUCTION 1

1.1 General introduction 1

1.2 Research problem 5

1.3 Research aim 5

1.4 Significance of the study 7

1.5 Thesis structure 7

CHAPTER TWO: LITERATURE REVIEW 8

2.1 Wetland definition, distribution and the processes responsible for wetland formation in Africa 8

2.2 Large inland wetlands in Africa 11

2.3 Channel–wetland exchanges 16

2.3.1 General overview 16

2.3.2 Hysteretic behaviour in channel–wetland processes 18

2.4 Quantification of wetland form and dynamics in data-scarce river basins 19

2.5 Hydrological models 24

2.5.1 ACRU hydrological model 25

2.5.2 SWAT hydrological model 28

2.5.3 Pitman hydrological model 29

2.6 Parameterization and calibration of hydrological models 33
2.7 Hydraulic modelling in wetlands 35
2.7.1 MIKE 21 hydraulic model 36
2.7.2 LISFLOOD-FP hydraulic model 36
2.8 Uncertainties in hydrological and hydraulic modelling 39
2.8.1 Model input data uncertainty 39
2.8.2 Model structure uncertainty 42
2.8.2 Model parameter uncertainty 43
2.9 Dealing with uncertainty in hydrological modelling 44
2.10 Uncertainty analysis framework for ungauged basins in the southern African region . 46
2.11 Conclusions 48
CHAPTER THREE: BASIN CHARACTERISTICS, DATA SOURCES AND QUALITY . 49
3.1 Summary of the datasets used in this study 50
3.2 Luangwa River Basin 52
3.2.1 Topography and slope 53
3.2.2 Geology and soil characteristics 54
3.2.3 Land cover and land use 56
3.2.4 Climate 57
3.2.4.1 Rainfall 57
3.2.4.2 Temperature and potential evapotranspiration (PET) 62
3.2.4.3 Streamflow 65
3.2.5 Water use 67
3.2.6 Luangwa floodplain 69
3.3 Upper Zambezi River basin 72
3.3.1 Topography and slope 73
3.3.2 Geology and soil characteristics 74
3.3.3 Land cover and land use 75

3.3.4 Climate 76
3.3.4.1 Rainfall 76
3.3.4.2 Temperature and potential evapotranspiration (PET) 79
3.3.4.3 Streamflow 81
3.3.5 Water use 84
3.3.6 Barotse floodplain and associated flats 84
3.4 The Upper Great Ruaha River Basin 88
3.4.1 Topography and slope characteristics 89
3.4.2 Geology and soil characteristics 90
3.4.3 Land cover and land use 91
3.4.4 Climate 92
3.4.4.1 Rainfall 93
3.4.4.2 Temperature and potential evapotranspiration (PET) 96
3.4.4.3 Streamflow 98
3.4.5 Water use 103
3.4.6 Usangu Wetlands 105
3.5 Conclusions 108
CHAPTER FOUR: METHODOLOGICAL FRAMEWORK 109
4.1 Data preparation for modelling 110
4.1.1 Sub-basin delineation 110
4.1.2 Extracting physical and hydrological characteristics for each sub-basin 113
4.1.3 Sub-basin similarity analysis 116
4.2 Spatial and Time Series Information Modelling (SPATSIM) 117
4.3 The GW Pitman model 119
4.3.1 The structure and parameters of the GW Pitman model 119
4.3.2 Versions of the Pitman model 126
4.3.2.1 The structured uncertainty version of the GW Pitman model. 126

4.3.2.2 The single-run version 127

4.3.2.3 The 2-stage model 128

4.3.3 Model performance measures 128

4.3.4 GW Pitman model setup for this study 130

4.4 Pitman Disaggregation sub-model 131

4.5 LISFLOOD-FP hydraulic model 133

4.5.1 The structure and parameters of the LISFLOOD-FP hydraulic model 133

4.5.2 LISFLOOD-FP hydraulic model setup for this study 135

4.5.3 Validation of the LISFLOOD-FP model results 139

4.6 Re-run and evaluation of the GW Pitman model for the entire basin 140

4.6.1 Establishment of Pitman wetland sub-model parameters from the LISFLOOD-FP model results 140

4.6.2 Re-run the Pitman model with the inclusion of wetland sub-model parameters. 140

4.7 Regionalisation or direct estimation of wetland parameters of the basin-scale model 141

4.8 Conclusions 141

CHAPTER FIVE: A COMBINED MODELLING APPROACH: RESULTS AND DISCUSSION 142

5.1 The Luangwa River basin 143

5.1.1 Sub-basin delineated 143

5.1.2 Sub-basin groups formed. 145

5.1.3 Parameter sampling using the structured uncertainty version of the GW Pitman model 148

5.1.4 Simulation of wetland inflows using a single-run version of the GW Pitman model 152

5.1.5 Disaggregation of simulated monthly flows into daily flows using the Pitman disaggregation sub-model 155

5.1.6 Simulation of wetland inundation characteristics using LISFLOOD-FP model. 159

5.1.7 Quantification of Pitman wetland parameters 182

5.1.8 Re-run the Pitman model for the entire basin with the wetland sub-model included 187

5.2 The Upper Zambezi River basin 191

5.2.1 Sub-basin delineated...191

5.2.2 Sub-basin groups formed...191

5.2.3 Parameter sampling using structured uncertainty version of the GW Pitman model. 194

5.2.4 Simulation of wetland inflows using GW Pitman monthly model......................198

5.2.5 Disaggregation of simulated monthly flows into daily flows using the Pitman disaggregation sub-model 203

5.2.6 Simulation of wetland inundation characteristics using LISFLOOD-FP model.204

5.2.7 Quantification of Pitman wetland parameters 217

5.2.8 Re-run the Pitman model for the entire basin with the wetland sub-model included 218

5.3 The Upper Great Ruaha River basin (UGRRB) 222

5.3.1 Disaggregation of simulated monthly flows into daily flows.............................222

5.3.2 Simulation of wetland inundation characteristics using LISFLOOD-FP model.224

5.3.3 Quantification of Pitman wetland parameters 239

5.3.4 Re-run the Pitman model for the entire basin with the wetland sub-model included 242

5.4 Regionalisation or direct estimation of wetland parameters of the basin-scale model..... 244

5.5 General discussions and conclusions 248

CHAPTER SIX: CONCLUSIONS AND RECOMMENDATIONS 254

6.1 Conclusions...254

6.1.1 Establishment of wetland inflows 254

6.1.2 Understanding the wetland–channel exchange processes and quantification of the wetland parameters of the basin-scale model 255

6.1.3 Re-calibration of the basin-scale model with a channel–wetland exchange function included 257

6.1.4 Regionalisation of the estimated wetland parameters 258

6.2 Recommendations 258

6.2.1 Simulation of wetland inflows 258

6.2.2 Simulation of wetland inundation characteristics 259

6.2.3 Pitman wetland parameter estimations and revision of the GW Pitman model 260

6.2.4 Recommendations for further studies 260

REFERENCES 262

ACRONYMS

ACRU	Agricultural Catchments Research Unit
ASTER	Advanced Spaceborne Thermal Emission and Reflection Radiometer
BARE	Bayesian Recursive parameter Estimation
BATEA	Bayesian Total Error Analysis
DEM	Digital Elevation Model
EO	Earth Observation
FAI	Flood Area Index
GIS	Geographic Information System
GLWD	Global Lakes and Wetland Database
GTOP30	Global Arc-Second Elevation
HWSD	Harmonised World Soil database
IQQM	Integrated Quality and Quantity Modelling
ITCZ	Inter-Tropical Convergent Zone
LiDAR	Light Detection and Ranging
MODIS	Moderate-resolution Imaging Spectroradiometer
MPSO	Multi-objective Particle Swarm Optimisation
MSSE-PSO	Master-slave Swarms Shuffling based on self-adaptive PSO
PSO	Particle Swarm Optimisation
PCA	Principal Component Analysis
SAR	Synthetic Aperture Radar
SCE-UA	Shuffled Complex Evolution
SPOT	Satellite Pour l'Observation de la Terre
SRTM	Shuttle Radar Topographic Mission
SUFI-2	Sequential Uncertainty Fitting, version 2
SWAT	Soil and Water Assessment Tool
UGRRC	Upper Great Ruaha River Catchment

LIST OF FIGURES

Figure 1.1: A combining modelling appriioach at a basin scale. 6

Figure 2.1 The distribution of wetlands in the GLWD dataset (Lehner and Döll, 2004) across southern Africa region (top) and selected three wetlands in this study (bottom). 10

Figure 2.2: Changes in channel morphology for two different sections of the Luangwa floodplain between 1957 and 1983 (Source: Gilvear *et al*., 2000). 12

Figure 2.3: Google Earth images of two sections of the Luangwa floodplain indicating different floodplain features. 14

Figure 2.4: Google Earth image showing the Lukanga depression wetland 16

Figure 2.5: One of the classifications of hydrological models (Source: Xu, 2002) 25

Figure 2.6: General structure of the Agricultural Catchments Research Unit (ACRU) model (Source: Schulze, 1995) 27

Figure 2.7: Wetland processes in the Agricultural Catchments Research Unit (ACRU) model (Source: Schulze and Pike, 2004). 27

Figure 2.8: Schematic representation of water movement in the Soil and Water Assessment Tool (SWAT) model (Source: SWAT2005 user manual) 29

Figure 2.9: Structure of the GW Pitman model (Source: Hughes *et al*., 2014) 32

Figure 2.10: Conceptual diagram of the LISFLOOD-FP base model (a), sub-grid solver (b), and sub-grid section (c) (Source: Neal *et al*., 2012). 38

Figure 2.11: A two-stage approach to uncertainty analysis used within the GW Pitman model (Source: Hughes, 2015a). 47

Figure 3.1: Locations of the three selected basins in southern Africa. 50

Figure 3.2: Location of the Luangwa River basin in the Zambezi River system. 53

Figure 3.3: Slope characteristics of the Luangwa River basin. 54

Figure 3.4: Soil distribution in the Luangwa River basin (Source: Hengl *et al*., 2014). 55

Figure 3.5: Land cover distribution in the Luangwa River basin (source: Broxton *et al*., 2014). 56

Figure 3.6: Location of the CRU TS 3.22 grids and the local rainfall stations in Luangwa River basin. 59

Figure 3.7: Comparison of the annual rainfall values between the CRU grids and some of the available local rainfall gauging stations in the Luangwa River basin. 60

Figure 3.8: Rainfall seasonality and the spatial variation of the mean annual rainfall for some of the sub-basins in the Luangwa River basin. 61

Figure 3.9: Variation of the mean annual temperature in the Luangwa River basin. 63

Figure 3.10: Variation of the mean annual potential evapotranspiration (PET) in the Luangwa River basin. 65

Figure 3.11: Mean monthly hydrograph for the Great East Road station (L28) in the Luangwa River basin. 67

Figure 3.12: Mita-Hills or Lusemfwa Dam (Source: https://www.snpower.com/history/entering-3-new-markets-article757-271.html). 68

Figure 3.13: Google Earth image showing some irrigation farms in the Luangwa River basin. 69

Figure 3.14: Google Earth image showing lodges and camping sites on the Luangwa floodplain. 70

Figure 3.15: The Luangwa River in the dry season (Source: http://www.patrickbentley.com/). 71

Figure 3.16: The Luangwa River in the wet season (Source: http://www.patrickbentley.com/) 71

Figure 3.17: Location of the Upper Zambezi River basin in the Zambezi River system. 73

Figure 3.18: Slope characteristics of the Upper Zambezi River basin. 74

Figure 3.19: Distribution of different soils in the Upper Zambezi River basin (Source: Hengl *et al*., 2014). 75

Figure 3.20: Land cover in Upper Zambezi River basin (Source: Broxton *et al*., 2014). 76

Figure 3.21: Rainfall seasonality in the Upper Zambezi River basin. 78

Figure 3.22: Variation of the mean annual temperature in the Upper Zambezi River basin. ..79

Figure 3.23: Variation of the mean annual potential evapotranspiration (PET) in the Upper Zambezi River basin. 80

Figure 3.24: Location of the streamflow gauging stations in the Upper Zambezi River basin. 82

Figure 3.25: Mean monthly hydrograph for three gauges in the Upper Zambezi basin. 83

Figure 3.26: A 3D Google Earth image showing detail of the geomorphology of the main channel and other floodplain features in the Barotse floodplain (Source: https://earth.google.com/web/@-14.8480635,22.98257525,1029.26325177a,6877.27730748d,35y,0.91172863h,67.15028773t,0r). 85

Figure 3.27: Natoga village in the Barotse floodplain (Source: https://farm6.staticflickr.com/5507/14158410929_22e59f4527_z.jpg). 86

Figure 3.28: Some temporary rural houses on the Barotse floodplain (Source: http://mw2.google.com/mw-panoramio/photos/medium/22959134.jpg). 86

Figure 3.29: Barotse floodplain and its associated flats and plains (source: LandsatLook image; 30th April 2016): 1) swamps and floodplain of the Lungue-Bungo, 2) Liuwa plains National Park, 3) Luena flats, 4) Luanguinga floodplain, 5) Barotse floodplain, 6) Lui floodplain and 7) a broad floodplain which carries the overspill from the high floods of the Cuado River. 87

Figure 3.30: The Upper Great Ruaha River Basin and the Usangu wetlands.........................89

Figure 3.31: Slope characteristics of the Upper Great Ruaha River basin. 90

Figure 3.32: Distribution of the soils types in the Upper Great Ruaha River basin (Source: Hengl *et al.*, 2014). 91

Figure 3.33: Land cover in the Upper Great Ruaha River basin (Source: Broxton *et al.*, 2014). 92

Figure 3.34: Rainfall seasonality for some of the sub-basins in the Upper Great Ruaha River Basin. 94

Figure 3.35: Spatial variations of the mean annual rainfall and the inter-annual rainfall variations for some of the sub-basins in the Upper Great Ruaha River basin for the period 1960 – 2009..95

Figure 3.36: Variation of the mean annual potential evapotranspiration in the Upper Great Ruaha basin. 98

Figure 3.37: Location of the streamflow gauging stations in the Upper Great Ruaha River basin. 100

Figure 3.38: Streamflow seasonality for some gauged sub-basins in the Upper Great Ruaha River basin. 102

Figure 3.39: Location of the large-scale irrigation farms in the Upper Great Ruaha River basin (Source: SMUWC, 2001). 104

Figure 3.40: Google Earth images showing different paddy rice farms in the Usangu plains. 105

Figure 3.41: The Usangu wetlands (modified from Mwakalila, 2011). 107

Figure 3.42: Google Earth image showing the distribution of different channels in the eastern wetland. 107

Figure 4.1: Flow chart diagram illustrating the combined modelling approach used in this study 110

Figure 4.2: Original sub-basins and the created sub-basin nodal points in the Luangwa River basin. Note: Sub-basin name starts with ‘L’ and sub-basin node with ‘N’. 112

Figure 4.3: A screenshot of the CRU time series data extract program of SPATISM. 115

Figure 4.4: A screenshot of the ARC2 satellite time series data extract program. 116

Figure 4.5: Structure of the GW Pitman model (Source: Hughes *et al*., 2014). 120

Figure 4.6: Frequency distribution of basin absorption rate, Z (A) and cumulative frequency curve of generated surface runoff, r is the rate of rainfall input (B). 122

Figure 4.7: Soil moisture storage and subsurface runoff generation parameter relationship (Source: Kapangaziwiri, 2008). 123

Figure 4.8: The geometry of the groundwater component in the GW Pitman model (Source: Hughes, 2013). 124

Figure 4.9: Conceptual diagram of the LISFLOOD-FP base model (a), sub-grid solver (b), and sub-grid section (c) (Source: Neal *et al*., 2012). 134

Figure 4.10: Comparison between two river networks generated from two different DEMs. 137

Figure 5.1: Sub-basins and sub-basin nodes formed in the Luangwa River basin. 144

Figure 5.2: PCA biplot for the 9 variables of the Luangwa River basin. 146

Figure 5.3: The sub-basin groups generated by the PCA and the location of sub-basin nodes used in the final model runs of the Luangwa River basin...147

Figure 5.4: The FDCs of the observed and simulated bounds for the N21 sub-basin node of the Luangwa River basin. 150

Figure 5.5: Scatterplots of the variation in CE and CE (ln) against ST and ZMAX parameter values for the N21 sub-basin node of the Luangwa River basin. 151

Figure 5.6: Scatterplots of the variation in CE and CE (ln) against FT/POW + GW/GPOW index for the N21 sub-basin node of the Luangwa River basin..152

Figure 5.7 Observed and simulated monthly flow duration curves for N21 sub-basin node for the period 1930 – 1991. 154

Figure 5.8: Time series of observed and simulated monthly flows for the N21 sub-basin node for the period October 1930 – September 1960 (top) and October 1960 – September 1991 (bottom)..155

Figure 5.9: Screenshot of the published information on early 2007 floods in the Luangwa (Source: http://robinpopesafaris.net/blog/2000/01/its-monday-5th-feb-2007-and-the-flood/) 157

Figure 5.10: Disaggregated mean daily flows for some sub-basin nodes of the Luangwa River (October 2005 to September 2013)..158

Figure 5.11: The location of the Luangwa floodplain in the Luangwa River basin 161

Figure 5.12: The elevation and channel width values for the upper section of the Luangwa floodplain. 162

Figure 5.13: The elevation and channel width values for the middle section of the Luangwa floodplain. 163

Figure 5.14: The elevation and channel width values for the lower section of the Luangwa floodplain. 164

Figure 5.15: Channel depth values for upper and middle sections of the Luangwa floodplain. 165

Figure 5.16: Channel depth values for the lower section of the Luangwa floodplain. 166

Figure 5.17: Comparison between observed and simulated flooding extents 26th March 2010 in the Luangwa floodplain (simulation for entire floodplain as a single unit).......................169

Figure 5.18: Comparison between observed and simulated flooding extents 26th March 2010 in the Luangwa River floodplain (simulation for entire floodplain as a single unit).............170

Figure 5.19: Comparison between observed and simulated flooding extents 26th March 2010 in the middle section of the Luangwa floodplain..171

Figure 5.20: Comparison between observed and simulated flooding extents 26th March 2010 in the lower section of the Luangwa floodplain...172

Figure 5.21: Comparison between the observed and simulated flooding extents on 21st May in the middle section of the Luangwa floodplain. 173

Figure 5.22: Storage–inflow and area–storage 7-day anticlockwise hysteresis for the wet (2006/07: Left) and normal (20012/13: Right) years in the entire Luangwa floodplain. 175

Figure 5.23: Standardised storage–inflow and area–storage 7-day anticlockwise hysteresis for the wet (2006/07: Left) and normal (20012/13: Right) years in the entire Luangwa floodplain. 175

Figure 5.24: Storage–inflow and area–storage 7-Day hysteresis for wet (2006/07: Left) and normal (20012/13: Right) years in the upper section of the Luangwa floodplain. 176

Figure 5.25: Standardized storage–inflow and area–storage 7-day hysteresis for wet (2006/07: Left) and normal (20012/13: Right) years in the upper section of the Luangwa floodplain. 177

Figure 5.26: Storage–inflow and area–storage 7-day anticlockwise hysteresis for the wet (2006/07) and normal (20012/13) years in the middle section of the Luangwa floodplain. .178

Figure 5.27: Standardised storage–inflow and area–storage 7-day anticlockwise hysteresis for the wet (2006/07) and normal (20012/13) years in the middle section of the Luangwa floodplain. 178

Figure 5.28: Storage–inflow and area–storage 7-day hysteresis for the wet (2006/07) and normal (20012/13) years in the lower section of the Luangwa floodplain. 179

Figure 5.29: Standardised storage–inflow and area–storage 7-day hysteresis for the wet (2006/07) and normal (20012/13) years in the lower section of the Luangwa floodplain. ...180

Figure 5.30: Mean daily inflows and outflows for the wet (2006/07) and normal (20012/13) years in the entire Luangwa floodplain. 181

Figure 5.31: Mean daily inflows and outflows in the upper section of the Luangwa floodplain. 181

Figure 5.32 Mean daily inflows and outflows in the middle section of the Luangwa floodplain. 182

Figure 5.33: Mean daily inflows and outflows in the lower section of the Luangwa floodplain. 182

Figure 5.34: Comparison between the volume and flows simulated by the LISFLOOD-FP and Pitman wetland sub-model in the Luangwa floodplain (simulated as a single unit) for the period October 2011 to September 2013. 184

Figure 5.35: Comparison between the volume and flows simulated by the LISFLOOD-FP and Pitman wetland sub-model in the upper section (NF1) of the Luangwa floodplain for the period October 2011 to September 2013. 185

Figure 5.36: Comparison between the volume and flows simulated by the LISFLOOD-FP and Pitman wetland sub-model in the middle section (NF2) of the Luangwa floodplain for the period October 2005 to September 2007. 186

Figure 5.37: Comparison between the volume and flows simulated by the LISFLOOD-FP and Pitman wetland sub-model in the lower section (NF3) of the Luangwa floodplain for the period October 2005 to September 2007. 187

Figure 5.38: Observed and simulated flows (before and after wetland parameters) for sub-basin node N21 in the Luangwa River basin. 189

Figure 5.39 Observed and simulated FDCs (before and after wetland sub-model) for sub-basin node N21 in the Luangwa River basin. 190

Figure 5.40: Sub-basins and sub-basin nodes in the Upper Zambezi River basin. 191

Figure 5.41: PCA biplot for the 9 variables of the Upper Zambezi River basin. 193

Figure 5.42: FDC of Observed and Simulated bounds for BP7 and BP9 sub-basin nodes. ..196

Figure 5.43: Scatterplots of the variation in CE and CE (ln) against ST and ZMAX parameter values for the BP7 sub-basin node of the Upper Zambezi River basin. 197

Figure 5.44: Scatterplots of the variation in CE and CE (ln) against FT/POW + GW/GPOW index for the BP7 sub-basin node of the Upper Zambezi River basin..................................198

Figure 5.45: Observed and simulated monthly flows volumes for the period October 1958 – September 1978 (Top) and October 1978 – September 1992 for BP7sub-basin node. 200

Figure 5.46: The FDCs of the observed and simulated monthly flows volumes for BP7sub-basin node for the period October 1958 – September 1992..201

Figure 5.47 Observed and simulated monthly flows volumes for the period October 1948 – September 1963 (Top) and October 1963 – September 1979 for BP9 sub-basin node. 202

Figure 5.48: The FDCs of the observed and simulated monthly flows volumes for BP9sub-basin node for the period October 1948 – September 1979..203

Figure 5.49: Mean daily flows for two sub-basins in Upper Zambezi River basin (Oct 2003 to Sept 2013). 204

Figure 5.50: The location of the Barotse floodplain system in the Upper Zambezi River basin. 206

Figure 5.51: Elevation and channel width values in the Barotse floodplain system 207

Figure 5.52: Elevation and channel depths in the Barotse floodplain system 208

Figure 5.53: Comparison between observed and simulated flooding extents on 12 March 2004 in the upper section of the Barotse floodplain system. 210

Figure 5.54: Comparison between observed and simulated flooding extents on 12 March 2004 in the middle and lower sections of the Barotse floodplain system. 211

Figure 5.55: Comparison between observed and simulated flooding extents on 22 April 2007 in the upper section of the Barotse floodplain system. 212

Figure 5.56: Comparison between observed and simulated flooding extents on 22 April 2007 in the middle and lower sections of the Barotse floodplain system......................................213

Figure 5.57: Storage–inflow and area–storage anti-clockwise hysteresis for the wet (left) and normal (right) years in the Barotse floodplain system. 215

Figure 5.58: Standardised storage–inflow and area–storage anti-clockwise hysteresis for the wet (left) and normal (right) years in the Barotse floodplain system. 215

Figure 5.59: Daily inflows and outflows in the Barotse floodplain system for the period January 2003 to September 2007. 216

Figure 5.60: Comparison between observed and simulated daily flows (a gap on the observed flows indicates missing values) for the period January 2003 to September 2007. 216

Figure 5.61: Monthly volume and flow simulated by LISFLOOD-FP and Pitman wetland sub-model in the Barotse Floodplain. 218

Figure 5.62: Observed and simulated flows (before and after wetland sub-model) for sub-basin BP9 in the Upper Zambezi River basin. 220

Figure 5.63: Observed and simulated FDCs before and after wetland sub-model for BP9 sub-basin in the Upper Zambezi River basin. 221

Figure 5.64: Comparison between observed and simulated monthly flows at BP9 (a gap on the observed flows indicates missing values) for the period January 2003 to September 2007. 221

Figure 5.65: FDC of the observed (daily and monthly) and simulated daily flows after the establishment of the final scaling parameters. 222

Figure 5.66: Disaggregated mean daily flows for 1KA33, UG21 and UG6 sub-basins of the Upper great Ruaha River basin (October 2000 to September 2009). 223

Figure 5.67: The location of the Usangu wetlands in the Upper Great Ruaha River basin. ..227

Figure 5.68: Channel depth values in the Usangu wetlands. 228

Figure 5.69: Elevation and channel widths in the western (Top) and eastern (Bottom) wetlands 229

Figure 5.70: Simulated daily flows from the wetland outlet and wetland storage before and after increasing evaporation values by 4 mm in the Upper Great Ruaha River basin. 230

Figure 5.71 Storage–inflow and area–storage mean monthly hysteresis for 2001/02 (left) and 2002/03 (right) years in the Usangu wetlands (simulated as a single unit). 232

Figure 5.72: Standardised storage–inflow and area–storage mean monthly hysteresis for 2001/02 (left) and 2002/03 (right) years in the Usangu wetlands (simulated as a single unit). 233

Figure 5.73: Storage–inflow and area–storage mean monthly hysteresis for 2001/02 and 2002/03 years in the western Usangu wetland (1ka71). 234

Figure 5.74: Standardised Storage–inflow and area–storage mean monthly hysteresis for wet (left) and normal (right) years in the western Usangu wetland (1ka71). 235

Figure 5.75: Storage–inflow and area–storage 7-day hysteresis for wet (left) and normal (right) years in the eastern Usangu wetland (1ka27). 236

Figure 5.76: Standardised Storage–inflow and area–storage mean monthly hysteresis for wet (left) and normal (right) years in the eastern Usangu wetland (1ka27). 237

Figure 5.77: Daily inflows and outflows in the Usangu wetlands (simulated as a single unit). 238

Figure 5.78: Daily inflows and outflows in the western Usangu wetland (1ka71)....................238

Figure 5.79: Daily inflows and outflows in the eastern Usangu wetland (1ka27)....................239

Figure 5.80: Observed (1ka59) and simulated daily outflows in the Usangu wetlands. 239

Figure 5.81: Monthly volume and flow simulated by LISFLOOD-FP and Pitman wetland sub-model in the Usangu wetlands (simulated as a single unit). 241

Figure 5.82: Monthly volume and flow simulated by LISFLOOD-FP and Pitman wetland sub-model in the western Usangu wetland (1ka71 sub-basin)....................241

Figure 5.83: Monthly volume and flow simulated by LISFLOOD-FP and Pitman wetland sub-model in the eastern Usangu wetland (1ka27 sub-basin)....................242

Figure 5.84: Observed and simulated uncertainty bounds after inclusion of wetland parameters in the Pitman model....................243

Figure 5.85: Interactions between the Luangwa River and the floodplain features (left), the Zambezi River and Barotse floodplain features (right). 246

Figure 5.86: Return flows against standardised plot of the stored volume relative to the residual volume. 247

LIST OF TABLES

Table 3.1: FAO slope classication 54

Table 3.2: Sub-basin mean monthly potential evapotranspiration (PET) in the Luangwa River basin 64

Table 3.3: Catchment areas for sub-basins in the Luangwa River basin 66

Table 3.4: Sub-basin monthly and annual potential evapotranspiration in the Upper Zambezi River basin. 80

Table 3.5: Catchment areas for sub-basin nodes in the Upper Zambezi River basin. 82

Table 3.6: Streamflow gauging stations in the Upper Zambezi River basin. 83

Table 3.7: Sub-basin average monthly potential evapotranspiration in the upper Great Ruaha River basin. 97

Table 3.8: Catchment areas for the sub-basins in the Upper Great Ruaha River basin 99

Table 3.9: Streamflow gauging stations in the Upper Great Ruaha River basin 100

Table 3.10: Mean annual runoff for some gauged sub-basins in the Upper Great Ruaha River basin. 101

Table 4.1: Catchment areas of the original sub-basins and the new sub-basins nodes. 113

Table 4.2: The GW Pitman model attributes in the Spatial and Time Series Information Modelling (SPATSIM) platform..119

Table 4.3: The GW Pitman model parameters..121

Table 4.4: Parameters used within the Pitman wetland sub-model 126

Table 5.1: Characteristics and indices for each sub-basin that were entered into the PCA...143

Table 5.2: Areal characteristics upstream of each sub-basin node in the Luangwa River basin. 145

Table 5.3: Total variance explained by 9 variables in the PCA..146

Table 5.4: Sub-basin node groups formed in the Luangwa River basin 148

Table 5.5: The parameter ranges used to set the uncertainty model 149

Table 5.6: The initial set of calibration parameters for the GW Pitman model. 153

Table 5.7: Final set of calibration parameters for the GW Pitman model 153

Table 5.8: Parameter ranges used to setup the LISFLOOD-FP model 167

Table 5.9: Magnitude of the hysteresis curve in the Luangwa floodplain 181

Table 5.10: Estimated parameter set for the Pitman wetland sub-model 183

Table 5.11: Final parameter values established after inclusion of wetland sub-model in the model setup. 188

Table 5.12: Summarised model performance measures for sub-basin node N21 188

Table 5.13: Characteristics and indices for each sub-basin node that were entered in the PCA 192

Table 5.14: Total variance explained for the 9 variables in the PCA 193

Table 5.15: Sub-basin groups generated by the PCA for the Upper Zambezi River basin ... 193

Table 5.16: Final parameter ranges used to set the uncertainty model 194

Table 5.17: Final set of calibration parameters for the GW Pitman model 199

Table 5.18: Parameter ranges used to set up the LISFLOOD-FP model 208

Table 5.19: Magnitude of the hysteresis curve in the Barotse floodplain 216

Table 5.20: Estimated parameters for the Pitman wetland sub-model 217

Table 5.21: Final parameter values established after inclusion of wetland sub-model in the model setup. 219

Table 5.22: Summarised model performance measures for BP9 and BP7 sub-basin nodes. 219

Table 5.23: Summarised model performance measures for the LISFLOOD-FP and the Pitman model 220

Table 5.24: Parameter ranges used to setup the LISFLOOD-FP model 230

Table 5.25: Magnitude of the hysteresis in the Usangu wetlands 238

Table 5.26 Estimated parameter set for the Pitman wetland sub-model in the Usangu wetlands 240

Table 5.27: Summarised model performance measures for 1ka59 sub-basin 243

Table 5.28: Summary of the estimated wetland sub-model parameters 246

ACKNOWLEDGEMENT

I express my greatest thanks to my supervisor Prof. Hughes; his supports, guidance and constructive comments have made this work to be accomplished. I also acknowledge the supports and advice from my co-supervisor, Dr. Mantel. Thanks for the LISFLOOD-FP team (Prof. Bates, Dr. Trigg, and Dr. Neal) for all the supports you gave me especially on how to set and run the LISFLOOD-FP model.

Special thanks to the Carnegie Corporation of New York through the Regional Initiative in Science and Education (RISE) Programme and the Sub-Saharan African Water Resources Network (SSAWRN) for full funding my PhD research and different International conferences which I attended during the course of my study.

My gratitude is extended to Dr. Valimba for sharing this PhD opportunity with me, and for his constructive advice. Thanks to Dr. Ndomba, Dr. Tirivarombo, and Dr. Madaka, for sharing me with some data which actually made this study possible.

To my husband, special thanks to you honey. It wasn’t easy leaving you home, a 1 month after our wedding. Thanks for the patience and understanding, thanks for all the supports you gave me though the entire period of my study.

I convey my gratitude to my parents, thanks for your endless love, supports, and prayers. I wouldn’t be where I am without you. God bless you. Thanks to my siblings (Leah and Enos), my cousin Barak, and friends for their moral supports.

Special thanks to my colleagues at the Institute for Water Research (Dionis, Onna, Zwido, Coli, Emanuel Dr. Slaughter, Dr. Jane, Sibo and others) for the supports through the entire period of my study.

CHAPTER ONE: INTRODUCTION

1.1 General introduction

Wetlands are formed at the interface between terrestrial and aquatic areas (Curie *et al*., 2007; Tooth and McCarthy, 2007; Ellery *et al*., 2009). Their formation is mainly determined by a combination of geological, hydrological and geomorphic factors (Ellery *et al*., 2009; Grenfell *et al*., 2010) or tectonic activities (Sivan *et al*., 2011). As a result, wetlands formed by different processes have different characteristics, and they are expected to function differently (Tooth and McCarthy, 2007; McCartney *et al*., 2010; Acreman and Holden, 2013).

Globally, wetlands are regarded as valuable freshwater ecosystems because of the functions and services they deliver (Hooijer, 2003; Berkowitz and White, 2013; Heimhuber *et al.*, 2016; Tomscha *et al*., 2017). Wetlands provide many useful benefits, including the effective attenuation of floods, maintaining base flow, recharging groundwater, providing habitats for aquatic species, supporting biodiversity, recycling nutrients and purifying water. Moreover, the presence of fertile soils in wetlands encourages agriculture, ranging from small to large scale (Kakuru *et al*., 2013). Some human populations, particularly in developing regions in Africa, derive more than 50% of their income from wetlands (Schuijt, 2002; Schuyt, 2005). For example, approximately 100% of the water used for domestic activities by the community living near the Yala swamp in Kenya is abstracted from this wetland, and 86% of their building materials, such as soils, woods and papyrus, are similarly obtained from this wetland (Schuyt, 2005). In general, wetland functions can be divided into three broad categories: 1) hydrological; 2) biological, and; 3) geochemical (Wang *et al*., 2008). The hydrological functions, in particular, are regarded as the driving force of other wetland functions (Acreman and Miller, 2007; Todd *et al*., 2010; Mitsch and Gosselink, 2015; Zhiqiang *et al*., 2016). For example, the ecological health, biodiversity and water quality of wetlands are highly influenced by the wetland hydrology (i.e. the amount and movement of water in the wetland). Moreover, the hydrological functions of wetlands account for the importance of these ecosystems in the hydrological cycle (Bullock and Acreman, 2003; Négrel *et al*., 2005; Fossey *et al.*, 2015). Therefore, wetland hydrological variables (e.g. duration, timing, frequency and the extent of inundation) have been widely assessed in many wetland studies.

Although the importance of wetlands is widely recognised, anthropogenic activities, either upstream or within wetlands, modify the natural characteristics, functions and processes of wetlands (Grundling *et al.*, 2013; Mcclain, 2013; Matthew and Day, 2014). Channel slopes, roughness and velocity may be significantly altered by anthropogenic activities to an extent that the duration, timing, frequency, magnitude and the extent of inundation are affected (Hattermann *et al*., 2008). As a result, apart from other factors, such as climate change and natural variability, anthropogenic activities have contributed substantially to changes in wetland dynamics (Kashaigili *et al*., 2006a; Tockner *et al*., 2008; Harrison, 2013).

In Africa, many large and extensive wetlands are hydrologically connected to large rivers (Tooth *et al.*, 2002; Hughes *et al.*, 2014). Examples of these wetlands include the wetlands in the upper reaches of the Congo River, the Barotse floodplain of the Zambezi River, the Niger River Delta and many other large rivers across the continent. The total integrity of the two systems (i.e. river channels and wetland) depends on how they interlink (Thoms *et al*., 2005; Frazier and Page, 2006; Heimhuber *et al*., 2016). The channel–wetland exchange processes are inherently complex, particularly in large wetlands (Phillips, 2013; Hughes *et al*., 2014; Karim *et al.*, 2015; Vanderhoof *et al*., 2015; Larocque *et al*., 2016), and they vary spatially and temporally. Variation in the exchange processes has impacts on both the wetland water balance and river flow regimes (Wang *et al*., 2010; Hughes *et al*., 2014; Fossey *et al*., 2015). An improved understanding of the spatial and temporal variation of the exchange processes between river channels and wetlands is indispensable for the effective management of wetlands and river basins (Frazier and Page, 2009; Kupfer and Meitzen, 2012; Hughes *et al*., 2014; Karim *et al*., 2015). However, this information remains limited for many river basins containing large wetlands in Africa. This is because collecting ground-based data particularly in large and remote river basins is a challenging task, and high-quality Earth Observation (EO) data are not always available for these basins. Modelling can be an alternative approach for understanding different processes in wetlands, including channel–wetland exchange dynamics.

Hydraulic models are widely used to understand the channel–wetland exchange dynamics, including the occurrence and magnitude of flood inundation in terms of spatial extents and depths (Patro *et al*., 2009; Karim *et al*., 2012; Neal *et al*., 2012). However, a comprehensive understanding of the influence of these dynamics on flow regimes at the basin scale should also consider the impacts of upstream changes on wetland hydrological inputs. As a result, this requires basin-scale modelling (Zhang *et al*., 2013), and many studies have applied basin-scale models to understand different processes in wetlands and their impacts on the downstream hydrological regime of river basins (Ndomba *et al*., 2010; Gray *et al*., 2012; Zhang *et al.*, 2013; Hughes *et al*., 2014; Rahman *et al.*, 2016). Basin-scale models vary from simple to complex, based on the required amount of input data and parameters, basin processes captured in the model structure and the spatial and temporal resolution used (Hughes, 2015a). Existing models either directly incorporate or indirectly model wetland processes (Rahman *et al*., 2016), although many models ignore or oversimplify the natural wetland processes e.g. the channel–wetland exchange processes (Hattermann *et al*., 2008; Martinez-Martinez *et al*., 2014). For example, the earliest version of the Pitman model (Pitman, 1973) represented a wetland as a simple reservoir. A model structure that is not sufficiently detailed in terms of wetland processes will inevitably produce simulation results of low reliability (Hughes *et al*., 2006).

In an effort to improve model simulations, various researchers have modified the wetland components of some basin-scale models to include relevant wetland processes (Hattermann *et al*., 2008; Wang *et al*., 2008; Liu *et al*., 2010; Gray *et al*., 2012; Zhang *et al*., 2013; Hughes *et al*., 2014; Mekonnen *et al*., 2016). For example, a study by Gray *et al*. (2012) modified the wetland component of the Agricultural Catchments Research Unit (ACRU) model, and applied it to assess the influence of a wetland on hydrological responses in the Thukela Basin in South Africa, whereas Zhang *et al*. (2013) modified the wetland component in the Soil and Water Assessment Tool (SWAT) model to simulate the hydrological processes of the Zhalong Wetland in northeast China. Liu *et al*. (2010) developed an extension of SWAT's wetland module that can be used to assess the wetland–river interactions in large catchments, whereas Rahman *et al*. (2016) further developed SWAT's wetland module to simulate hydraulic interactions between rivers, riparian depression wetlands and aquifers in the Barak-Kushiyara River Basin in India. Hughes *et al*. (2014) introduced a wetland component for the modified version of the Pitman model (GW Pitman model, Hughes et *al*., 2004) that includes a channel–wetland exchange function, mainly including wetland processes that are important for the generation of downstream flows.

Despite the improvements of the wetland components of many basin-scale models, the application of these models to data-scarce basins of Africa remains a challenge (Hughes, 2015a), as the inclusion of more processes within a model structure requires a greater amount of observed data for model calibration. Climatic data required to establish and validate models as well as the physical data required to estimate model parameters are generally insufficient and generally not accurate (Hughes, 2006; 2015a). Some researchers have attempted to integrate Earth Observation (EO) data and Geographic Information System (GIS) into models to understand various wetland characteristics and channel–wetland exchanges in many river basins in Africa (Griensven *et al*., 2008; Jung *et al.*, 2010; Leauthaud *et al.*, 2013; Lee *et al.*, 2015). Hughes *et al*. (2014) acknowledged the importance of EO data to understand complex processes associated with channel–wetland exchanges, such as wetland return flow. However, although EO data have proved to be valuable in many studies, particularly in the developed world, remote sensing images of high quality (e.g. Satellite Pour l'Observation de la Terre (SPOT), Synthetic Aperture Radar (SAR) and light detection and ranging (LiDAR)) are expensive to acquire, and in some cases, are not available (Frazier and Page, 2009). Freely available satellite images are affordable for use in river basins studies in Africa (Yan *et al*., 2015) but they are subject to a series of uncertainties. For that reason, the application of EO data as alternative data to force and validate models for data-scarce basins in Africa remains largely problematic.

A further challenge in applying basin-scale models in river basins containing large wetlands is that the level of detail included in these models, especially for large wetlands, is very low. Thus, setting up models in these wetlands is always difficult. If detailed hydraulic models (e.g. LISFLOOD-FP, MIKE 21 and SOBEK) that include different conceptual processes can be used to understand the hydraulic characteristics and inundation dynamics associated with these wetlands, it is likely that this information can help to set up basin-scale model. Recently, the LISFLOOD-FP model has been successfully applied to many river basins containing large wetlands in Africa (Jung *et al*., 2010; Neal *et al*., 2012; Schumann *et al*., 2013; Fernández *et al*., 2016). In most of these studies, the LISFLOOD-FP model was established using limited ground-based climatic data, free EO data such as the Shuttle Radar Topography Mission (SRTM) data to represent the topographical characteristics, and the freely available satellite imagery, such as Landsat images, to calibrate and/or validate model simulations. This suggests that, despite the challenge presented by data scarcity, detailed hydraulic models, which can be set up in data-scarce basins and provide satisfactory results, are available.

1.2 Research problem

Surface freshwater resources continue to be the main source of water for many African countries; therefore, socio-economic development of these countries is dependent on the availability of surface water (Mwanza, 2003; Mcclain, 2013). Yet, most water resources are dynamic, resulting in the unpredictability of water availability (Valimba, 2004; Mazvimavi and Wolski, 2006; Oguntunde *et al.*, 2006; Conway, 2009). Unless there is an understanding of the processes influencing the dynamics of these water resources, it is unlikely that sustainable management of water resources can be implemented. Most large rivers are hydrologically connected with large wetlands. Although wetlands owe their sustainability to the balance between inflows and outflows from their source river, the flow regime of a river is also highly influenced by wetland dynamics. As the integrity of both systems depends on their connectivity, the channel–wetland exchange dynamics have impacts on the flow regimes of both the wetland and the river. Channel–wetland exchange dynamics require quantification to facilitate the understanding of water resource dynamics.

To enable an improved understanding of the impacts of different upstream water resource developments on large wetlands, and in turn, the influence of channel–wetland exchange on water resources dynamics (i.e. river flow regimes), a basin-scale model which includes a wetland component is required (Wen *et al*., 2013; Zhang *et al*., 2013). However, the flow routing components in most of these models are simplified and do not realistically represent the flow dynamics of large wetlands (Goteti *et al*., 2008; Trigg *et al*. 2009; Valentová *et al*., 2010). Despite several recent studies on the inundation dynamics of large wetlands using available ground and/or satellite observations, this approach is always constrained by the availability and quality of both ground and satellite observation data. Ground-based observations of water surface elevation and discharge often do not exist, particularly for the upper catchments that contribute to wetland inflows. It is difficult to establish plausible model parameter values when modelling basins that include large wetlands. Therefore, a new approach is required for modelling African river basins that contain large wetlands.

1.3 Research aim

The overall purpose of the study is to improve water resource assessment modelling of data-scarce large African river basins that include large wetlands. This will be achieved through a combined modelling approach that allows the use of a detailed hydraulic model to inform the structure and parameters of the basin-scale model, as summarised in Figure 1.1. The approach involves the following steps:

- ❖ To apply an initially calibrated, monthly time step and coarse spatial scale hydrological model, coupled with a monthly to daily disaggregation approach, to establish the upstream boundary conditions required for setting up the hydraulic model.

- ❖ To calibrate the hydraulic model using a limited number of seasonal flood sequences to understand and quantify the wetland–channel exchange processes and to assist with the quantification of the parameters of the much simpler basin-scale model.

- ❖ To re-calibrate the basin-scale model that includes a wetland–channel exchange function and to validate the model using any available data.

- ❖ To assess the possibility of regionalising or directly estimating the wetland parameters of the basin-scale model on the basis of the wetland characteristics.

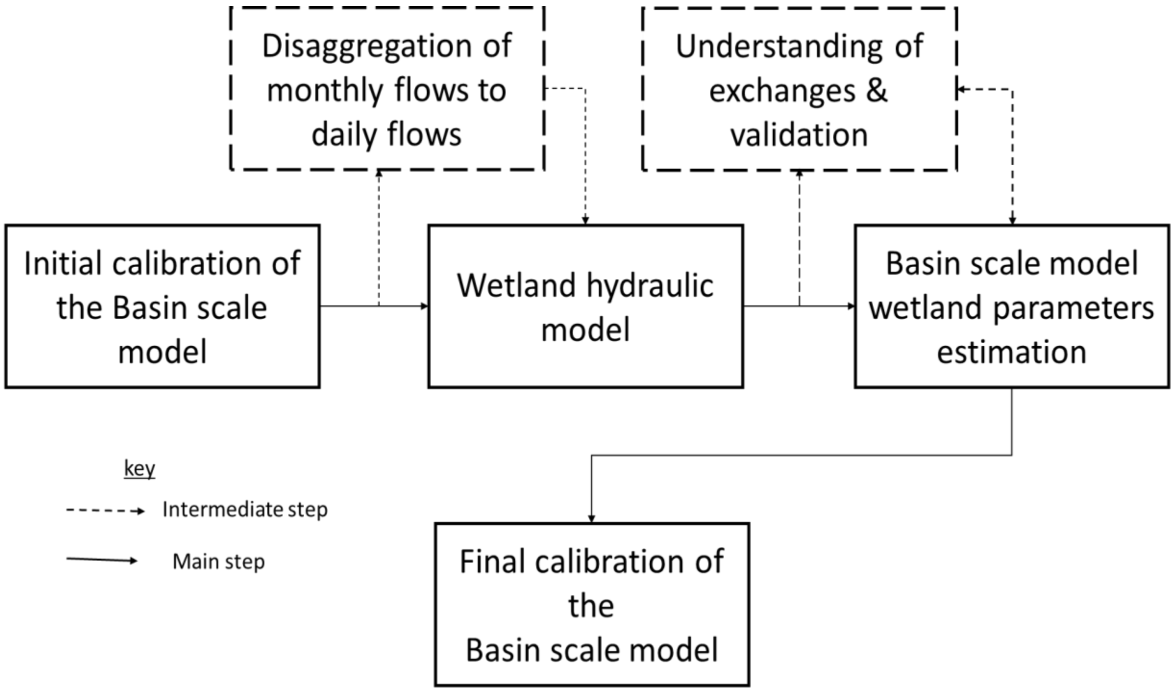

Figure 1.1: A combined modelling approach at a basin scale.

1.4 Significance of the study

Generally speaking, the hydrology of wetlands as well as the interactions between wetlands and rivers can potentially be assessed through ground-based monitoring; however, this is only possible in relatively small wetlands where interactions among hydrological processes can be monitored over small spatial scales (Clilverd *et al*., 2013; Rahman *et al*., 2016). It is not practical to implement gauging and monitoring of a large basin possibly containing one large or numerous wetlands (Alsdorf *et al*., 2007). A combined modelling approach applied in this study is expected to improve the understanding and accomplish efficient modelling for practical purposes at the basin scale.

1.5 Thesis structure

Chapter 2 covers a review on channel–wetland exchanges including hydrological and hydraulic modelling (and a combined modelling approach) of river basins containing large wetlands. Study areas and their physical characteristics are presented in **Chapter 3**. This chapter also introduces sources and quality of the data that were used in the study. **Chapter 4** covers different methods used to attain the overall aim of the study. Results and general discussions are presented in **Chapter 5**, while the conclusions and recommendations of the study are in **Chapter 6**.

CHAPTER TWO: LITERATURE REVIEW

This chapter presents a review of the different aspects related to channel–wetland exchanges in large river basins. Various methods related to modelling large basins containing substantial wetland areas are reviewed, such as the use of EO data, GIS and models, or a combination of these methods (e.g. Kashaigili *et al*., 2006a; Rayburg and Thoms, 2009; Schumann *et al*., 2013; Trigg *et al*., 2013; Heimhuber *et al*., 2016). A review of a combined modelling approach that integrates both hydraulic and hydrological models to improve model simulation results in different wetland studies is also included. Since the study focuses on southern African river basins containing large wetlands, sections 2.1 and 2.2 briefly introduce the distributions and common types of large wetlands in Africa.

2.1 Wetland definition, distribution and the processes responsible for wetland formation in Africa

There is no single agreed definition of wetlands; however, the definition provided by the Ramsar Convention on Wetlands (1971) has been widely accepted with some minor modifications. The Convention's definition of wetlands is: '*areas of marsh, fen, peatland or water, whether natural or artificial, permanent or temporary, with water that is static or flowing, fresh, brackish or salty, including areas of marine water the depth of which at low tide does not exceed six metres*'. Some organisations, such as the South African National Biodiversity Institute (SANBI, 2009), have modified the stipulation within the Ramsar definition of six metres of marine water to ten metres for low tides and replaced the term 'fen' with 'peatland'. Thus, SANBI defines a wetland as: *'an area of marsh, peatland or water, whether natural or artificial, permanent or temporary, with water that is static or flowing, fresh, brackish or salty, including areas of marine water the depth of which at low tide does not exceed ten metres'*. This definition has been adopted in most areas within southern Africa.

Wetlands in Africa vary from saline coastal lagoons in West Africa to fresh and brackish water lakes in East Africa (Hughes and Hughes, 1992). A large number of wetlands are found between 15° N and 20° S, such as wetlands of the four major rivers in Africa (i.e. Congo, Zambezi, Niger and Nile), the Okavango Delta in Botswana, the Sudd in southern Sudan and

Ethiopia and others found along the coastlines (Hails, 1996; Schuijt, 2002). Some wetlands are also found outside 15° N and 20° S. These include inland oases, wadis and chotts in north-west Africa, the Qualidia and Sidi Moussa lagoons in Morocco, the Limpopo River floodplain in Mozambique and other parts of South Africa, the Banc d'Arguin of Mauritania, and the St. Lucia wetland in South Africa (Hails, 1996). Large wetlands cover about 2×10^6 km^2 of the land mass in the sub-Saharan region (Mitchell, 2012), with more than 20 listed as Ramsar sites, and they are located in both coastal and inland areas (Tooth and McCarthy, 2007).

The three wetlands used in this study are part of the list of large wetlands in Africa (with area greater than 1000 km^2) and are included in the Ramser sites. Lehner and Döll (2004) dataset (GLWD-3) represents the spatial distribution of wetlands, reservoirs, lakes, and rivers in the world and the selected wetlands are part of the dataset. Wetlands in the Zambezi River basin covers about 19% of the total wetland coverage in the southern Africa region. The Barotse floodplain for instance is the second largest wetland in the Zambezi basin approximately 240 km long and 40 km wide whereas the Luangwa floodplain coverage is about 2 500 km^2 (Euroconsult, 2008). The Usangu depression wetland found in the Upper Great Ruaha River basin (Tanzania) is approximately 2 000 km^2. Figure 2.1 represents the spatial distribution of wetlands in the GLWD dataset (Lehner and Döll, 2004) within southern Africa region and the zoomed image in the bottom indicates spatial location of the selected wetlands in this study.

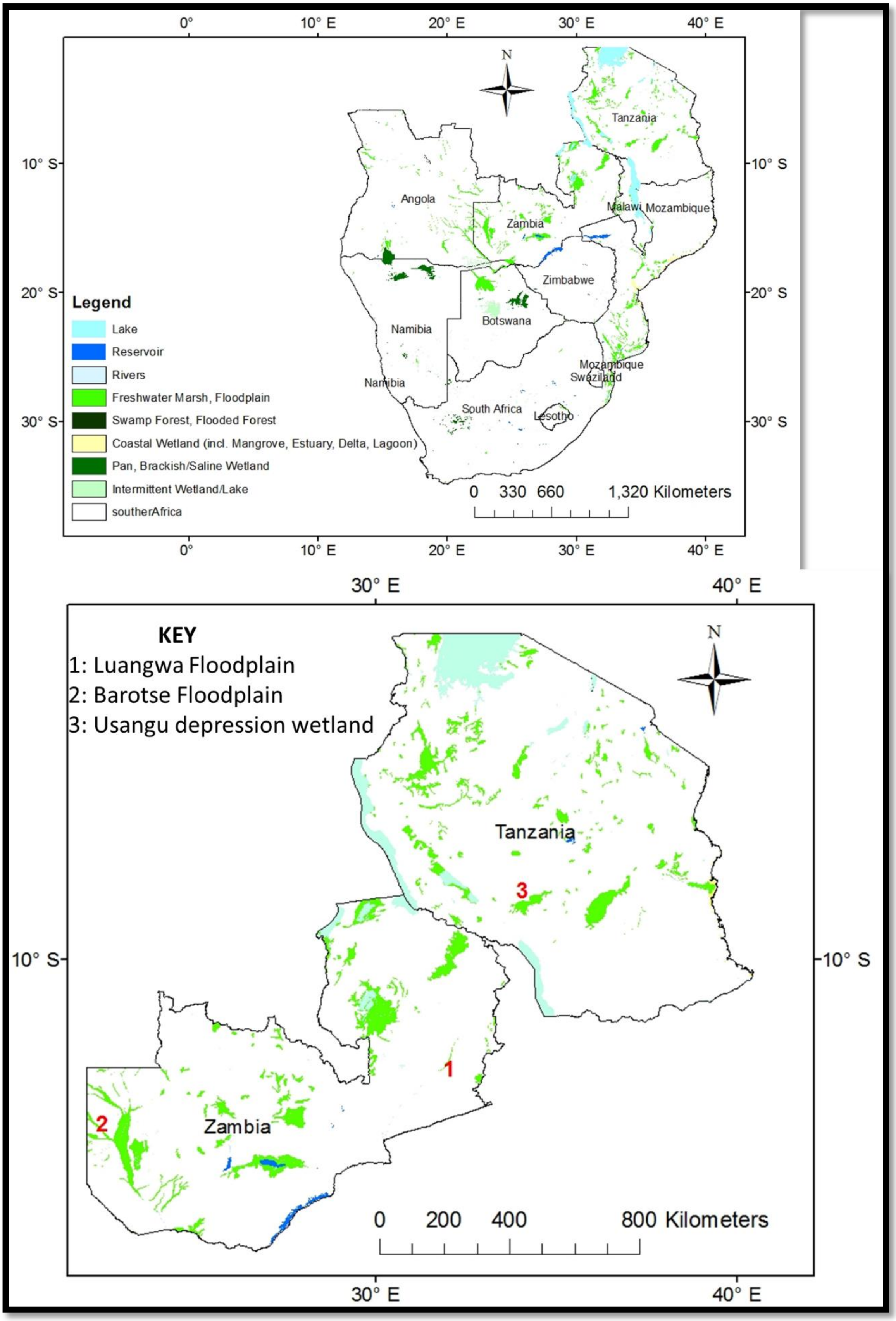

Figure 2.1 The distribution of wetlands in the GLWD dataset (Lehner and Döll, 2004) across southern Africa region (top) and selected three wetlands in this study (bottom).

2.2 Large inland wetlands in Africa

There are different types of large inland wetlands in Africa, of which floodplains dominate. Floodplains are low-relief features dominated by fluvial deposition and can develop at different locations along the river corridor (Lewin, 1978; Tockner *et al*., 2008; 2010). According to Tooth *et al*. (2012), inland floodplains are mostly formed in low-gradient river corridors characterised by low energy and strong interactions between flow, sediments and biota. Moreover, fluvial features (e.g. levees, backwater depressions, old infilled channels, meanders cut-offs, backwater depressions, ridges and swales) formed as a result of erosion and deposition processes in the river corridor are also common in floodplains (Amoros and Bornette, 2002; Tooth *et al*., 2002; Tooth and McCarthy, 2007). They are evenly distributed along the river corridor or cluster into distinct physical landforms (Scown *et al*., 2015). Their interactions with the main channel, and/or among each other, occur over scales of decades or centuries, thereby modifying their sizes and shapes and resulting in complex floodplain geomorphology (Gilvear *et al.*, 2000; Amoros and Bornette, 2002; Tooth *et al.*, 2002; Thoms *et al*., 2005; McCarthy *et al*., 2010; Tooth *et al*., 2012). The study by Gilvear *et al.* (2000) on the Luangwa floodplain revealed that high rates of channel migration and cut-offs of meandering sections significantly shifted the Luangwa river, which resulted in the formation of abandoned channels, meander cut-offs, and anabranches within the period between 1957 and 1983 (Figure 2.2). The interactions between floodplain features and/or the main river modify the local geomorphological settings of the floodplain, and this transformed landscape determines how water and sediment move from the main river onto the floodplain and back to the main river. Therefore, a floodplain forms a complex mosaic of landforms which have great influence on the river–floodplain interactions, including inundation patterns (Tockner *et al*., 2008; Scown *et al*., 2015). An attempt to modify the geomorphological setup of a river–floodplain system affects not only its connectivity but also the key functions of the floodplain (e.g. hydrological and ecological functions) (Edwards *et al*., 2016).

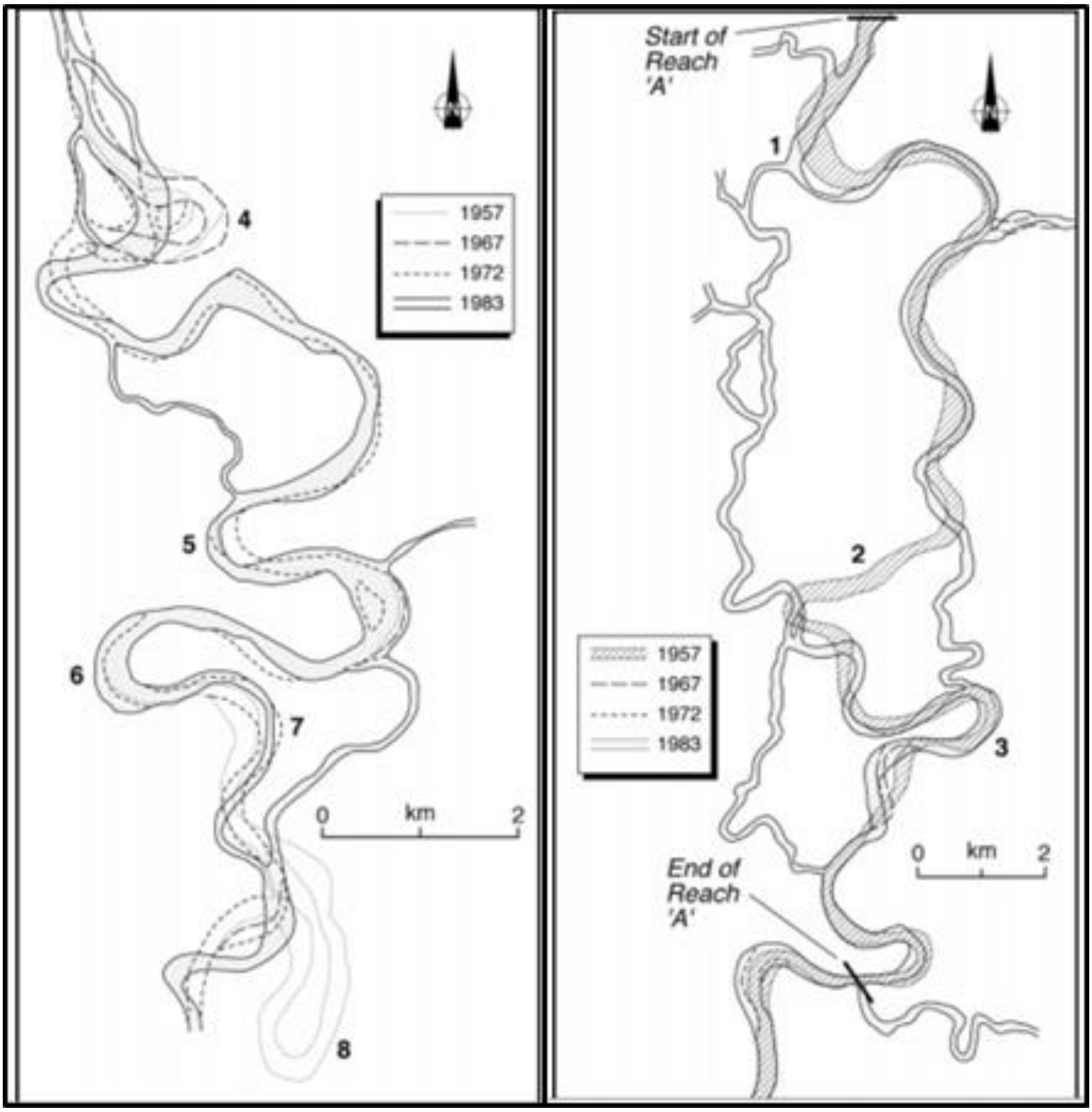

Figure 2.2: Changes in channel morphology for two different sections of the Luangwa floodplain between 1957 and 1983 (Source: Gilvear *et al*., 2000).

Apart from floodplain features that define the geomorphological complexity of many floodplains, evidence of more than one type of wetland in many river basins exists, and these types display different characteristics and interact differently with the main river. The study by Gilvear *et al*. (2000) on the middle section of the Luangwa floodplain revealed the existence of both meandering and anastomosing floodplain types. Anastomosing occurs when the river flows over a low gradient, results in the formation of multiple channels that tend to separate and rejoin (anabranches); they are connected to the main river during high flows and completely disconnect during flow recession. As a result, anabranches transfer sediment loads and disperse water into different parts of the floodplain. In the meandering floodplain section, the main river has sufficient energy to erode and deposit, and the overbank spill is common. Moreover, floodplain features such as old infilled channels and oxbows are found in these sections. The study by Gilvear *et al*. (2000) determined the existence of different floodplain types in the Luangwa floodplain, suggesting that morphological and micro-topographical settings of this floodplain are complex because they vary across different sections within the floodplain. Apart from the Luangwa floodplain, complex morphological settings have been observed in other floodplains, such as the wetland associated with Congo River (Jung *et al.*, 2010; O'Loughlin *et al*., 2013), the Kafue floodplain (Hughes *et al*., 2014), Blood River floodplain (McCarthy *et al*., 2010), Faguibine floodplain in Mali (Hamerlynck *et al*., 2016) and several floodplains outside Africa, such as the Amazon floodplain (Mertes, 1997; Trigg *et al*., 2012), a wetland linked to the Fly River in New Guinea (Day *et al*., 2008) and floodplains in the Murray-Darling basin in Australia (Scown *et al.*, 2016). Figure 2.3 presents the two different sections of the Luangwa floodplain indicating the anastomosing (top) and meandering (bottom) with different geomorphological features. The features in Figure 2.3 justify the argument by Lewin and Ashworth (2014) that large floodplains are plural (reflecting the activities of several channels and sub-systems, with a partial disconnect with main channel activity), complex (with zonal differences in processing and rates of activity) and diachronous (contain different forms that have developed over a range of timescales).

Figure 2.3: Google Earth images of two sections of the Luangwa floodplain indicating different floodplain features.

There are other wetlands situated in topographic depressions with closed or nearly-closed elevation contours (i.e. basin-like wetlands), and their formation is related to tectonic activities such as rifting and volcanic events (Tooth and McCarthy, 2007; Ellery *et a*l., 2009; Ollis *et al.*, 2015). These wetlands are mostly known as depression wetlands. Depression wetlands may have a single or combination of inlets, and generally, they get inundated from rivers, direct precipitation, overland flows from adjacent uplands and/or groundwater discharge (USDA, 2008; Ollis *et al.,* 2015). They are characterised by gentle slopes, as a result, many rivers entering depression wetlands reduce their energy, deposit sediments and over time, most rivers tend to split into small channels and/or disappear within the wetland (e.g. the Lukanga depression in Zambia, the Bahi and Usangu depression wetlands in Tanzania). Furthermore, many depression wetlands have no outlet, and where available, is confined in such a way that the surface outflow is limited (Ellery *et a*l., 2009).

Figure 2.4 illustrates that apart from direct rainfall (not shown here), the Lukanga depression wetland (Lukanga swamp) receives water from the Lukanga River and other seasonal streams as well as spill from the Kafue River especially when the river is at high flows. The dominant features include the small ponds scatted in the entire depression, permanent swamp, termitaria grasslands, dambos and channels (Mccartney, 2007). These features in totality form a major lacustrine (i.e. open water), and palustrine (i.e. marsh) system with the palustrine dominating (Mccartney *et al.*, 2011). Other depression wetlands that form more than one type is the Usangu depression in Tanzania (see section 3.4.6). The total depression contains two types of wetlands (eastern and western wetlands) which are separated by elevated land at the centre (SMUWC, 2001). The eastern wetland is very flat, and covers a permanent swamp and small ponds, whereas the western part is slightly steeper, and is generally seasonally inundated (Kashaigili *et al.*, 2006a; McCartney *et al.*, 2008). Therefore, like floodplains, a single large depression wetland may contain different wetland types.

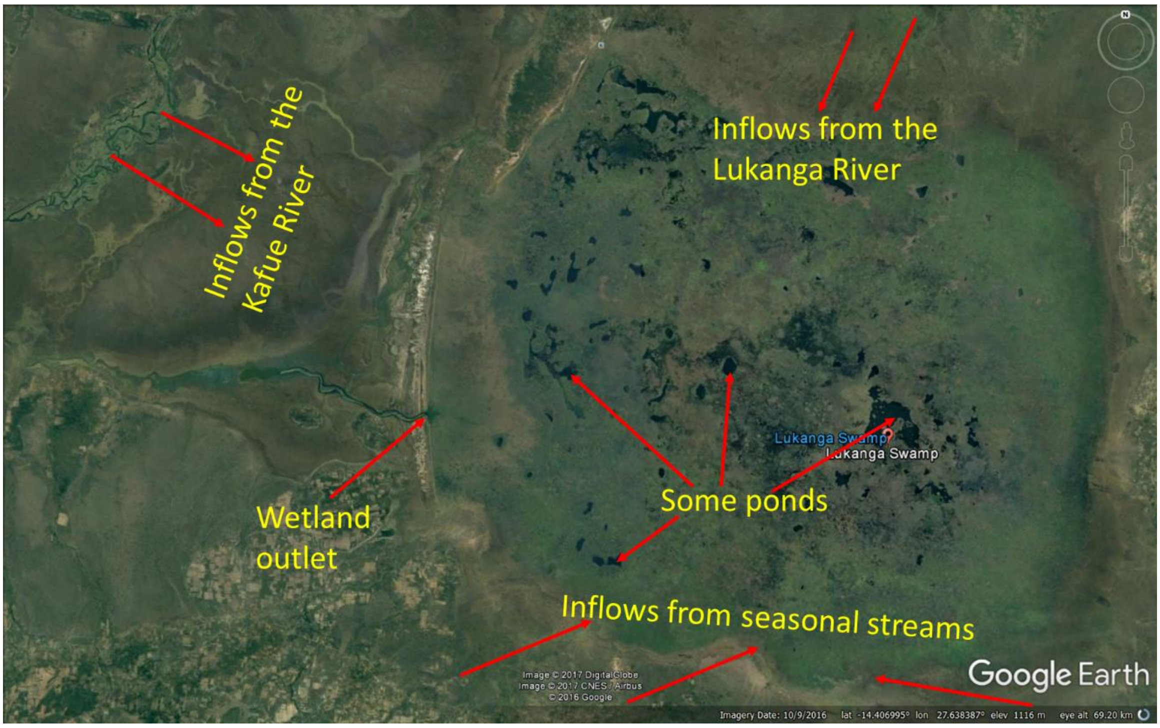

Figure 2.4: Google Earth image showing the Lukanga depression wetland

2.3 Channel–wetland exchanges

2.3.1 General overview

Globally, there have been many attempts to better understand the relationships between wetlands and channels (Popov and Gavrin, 1970; Hughes, 1980; Lewin and Hughes, 1980; Junk *et al.*, 1989; Mertes, 1997), and a considerable amount of research on this aspect has been conducted during the last two decades (Hudson *et al*., 2013). In large river basins, the interactions between the channels and wetlands are complex, and some of these complexities have been described by earlier studies (e.g. Hughes, 1980; Lewin and Hughes, 1980; Mertes, 1997). The channel–wetland exchange process is primarily controlled by flood pulses (Junk *et al.*, 1989; Tockner *et al.*, 2000) and have been reported in many studies worldwide (Gallardo *et al*., 2009; Opperman *et al*., 2010; Karim *et al*., 2012; Schumann *et al*., 2013; Trigg *et al*., 2013). The number, duration and frequency of flood pulses control the exchanges in different ways (Junk *et al*., 1989; Tockner *et al*., 2000), and the whole process is important for ecological, geomorphological and hydrological processes in river basins (Hudson *et al.*, 2013; Kupfer *et al*., 2015; Karim *et al*., 2016). The exchange of water occurs through overbank diffuse flows or channelized flows (Junk *et al*., 1989; Mertes, 1997; Trigg *et al*., 2012; 2013) and through sub-surface flow (Tockner *et al*., 2000). Apart from water volumes, different materials (e.g. soil and nutrients) and aquatic species are exchanged between the two systems (Clilverd *et al*., 2013). Most of the wetland functions are related to how the two systems are connected (Frazier and Page, 2006; Tockner *et al*., 2010; Karim *et al*., 2012; Chen *et al*., 2015). For example, the ecological and hydrological importance of a wetland connected with a river channel is highly dependent on how the two systems are connected (Mcginness *et al*., 2002; Tockner *et al*., 2008; Karim *et al*., 2013; Allen, 2015). Water resources development upstream of the floodplain may change the size and shape of the flood hydrograph (i.e. magnitude of flood and time to peak). Some of these upstream development structures include large and small dams, irrigation schemes, and Hydropower systems. This can have significant impacts on channel–wetland exchange behaviour (Thoms *et al.*, 2005; Kupfer and Meitzen, 2012; Morris *et al*., 2013). For example, upstream changes tend to modify the spatial and temporal inundation patterns (Wiens, 2002), and when wetting and drying processes in the floodplain are altered, the downstream flow regime is also affected.

Although a flood pulse is regarded as the main driving force of the exchanges, geomorphological variations among wetland features and the main channel determine the movement of water from, and back to, the main channel. Floodplain processes related to sediment deposition (e.g. the formation of natural levees) can modify the local morphology of the floodplain (Day *et al*., 2008; Lewin and Ashworth, 2014). For instance, natural levees elevate the river banks and create a barrier for surface water connectivity between the river and adjacent low-lying backwater areas (Newman and Keim, 2013). Unless the flow depth exceeds this height, water movement from the main river to the wetland through the river banks may not occur. Apart from natural levees, the relative elevation between different floodplain features influences how water diffuses within the floodplain. For example, if a backwater depression is located adjacent to the main channel and receives water immediately after the channel overtops its bank, the distribution of water from this depression into other parts of the floodplain will depend on elevation differences. In most cases, multiple channels found within the floodplain play an important role in dispersing water from the main channel to different parts of the floodplain (Trigg *et al.*, 2012). Anabranches, which are common in an anastomosing floodplain, are examples of floodplain channels that carry sediment-laden river water into the floodplain.

2.3.2 Hysteretic behaviour in channel–wetland processes

Hysteretic behaviour occurs when the output response is dependent on both the immediate input and the history of the input (Zhang and Werner, 2015). This phenomenon is common in different hydrological processes, such as discharge–groundwater relationships, water retention–soil moisture tension relationships and stage–discharge relationships (O'Kane, 2005; Beven, 2006; Norbiato and Borga, 2008). The relationship between the channel discharge and inundation characteristics in wetlands also forms a hysteresis curve (Chen *et al*., 2015; Zhang and Werner, 2015), and the shape of this curve varies with flood hydrology, wetland surface roughness, wetland topographical setting and internal flow connectivity between wetland features (Hughes, 1980; Lewin and Hughes, 1980). For example, large hysteresis effects are expected for wetlands characterised by a large area below bank height (Hughes *et al*., 2014).

Although earlier studies (Hughes, 1980; Lewin and Hughes, 1980) demonstrated the use of hysteresis curves to understand the interactions between channels and wetlands of different types under different flood magnitudes, studies that maximised the use of hysteresis behaviour to understand inundation characteristics, particularly in large wetlands, were reported more recently (Chen *et al*., 2015). In recent years, quite a number of studies have incorporated the use of hysteresis curves to understand inundation characteristics in both floodplain and depression wetlands (e.g. Shook and Pomeroy, 2011; Shook *et al*., 2013; Hughes *et al*., 2014; Rudorff *et al*., 2014; Chen *et al*., 2015; Zhang and Werner, 2015; Mengistu and Spence, 2016; Huang *et al*., 2017). For example, Zhang and Werner (2015) explored the hysteresis behaviour in the flooding dynamics of a large lake–floodplain system of Poyang Lake in China, whereas Chen *et al*. (2015) observed a hysteresis relationship of inundation area/volume–discharge in a channel–floodplain system of the Truckee River in Nevada. The authors of the latter study argued that the observed hysteresis can be useful for water resource management, and can be used in similar basins with substantial floodplain areas. Hughes *et al.* (2014) pointed out that prior knowledge of hysteretic effects of floodplain inundation can be used to establish a plausible model parameter set when using a relatively simple water balance model to simulate wetland processes. A recent study by Huang *et al*. (2017) explored different characteristics and factors that have influence on the hysteresis of water area–stage curves in for Poyang Lake in China.

2.4 Quantification of wetland form and dynamics in data-scarce river basins

In the absence of ground-based observation data, wetland form and dynamics can be determined from satellite observation data and/or modelling approaches. The use of EO data coupled with a GIS has made substantial contributions to wetland studies (Jones *et al*., 2009; MacKay *et al*., 2009; Rebelo *et al*., 2009; Mwita *et al*., 2013; Heimhuber *et al*., 2016). Remote sensing products with different spatial resolutions and temporal coverage such as Landsat, SPOT (Satellite Pour l'Observation de la Terre), NOAA-AVHRR (Advanced Very High Resolution Radiometer), SAR (Synthetic Aperture Radar), LiDAR (Light Detection and Ranging), Radar systems, and TerraSAR-X are suitable for different wetland studies (Mwita *et al*., 2013). For example, satellite images provide useful information for remote wetlands where the collection of ground-based data is expensive and time-consuming (Overton, 2005). EO data can also be used in conjunction with models to understand different wetland characteristics, including wetland dynamics in data-scarce areas. Winsemius (2009) incorporated available ground-based and EO data from the GRACE satellite to build a robust model for the Luangwa River basin, which is an example of a data-scarce river basin in southern Africa. Milzow *et al*. (2009) and Bauer *et al*. (2002) used remote sensing data to establish some model inputs (e.g. topographical variability, evapotranspiration, channel positions and precipitation) for the Okavango Delta. Different studies (e.g. Frazier and Page, 2006; Schumann *et al*., 2013; Trigg *et al*., 2013; Heimhuber *et al*., 2016) have applied EO data to calibrate and/or validate models used to understand channel–wetland exchange processes. Neal *et al*. (2012) used satellite images to establish river cross-sections as well as to validate the calibrated model results in the Niger Inland Delta. Notwithstanding the usefulness of EO data in wetland studies, most of the high-resolution satellite data are not freely available in many areas in Africa and most studies rely on no-fee available satellite data (Patro *et al*., 2009; Yan *et al*., 2015). Since the present study focuses on large wetlands in Africa, it is important to discuss some of the no-fee available satellite-based data that are mostly used to understand wetland form and dynamics in data-scarce areas and to make their limitations transparent.

A Digital Elevation Model (DEM) is a computerised model that represents the Earth's surface elevation, including the heights of different features found on the Earth's surface (Sulebak, 2000; Kiamehr and Sjöberg, 2005). These topographical data can be integrated with GIS to delineate the catchments and derive wetland slopes, stream flow directions and channel cross-sections (Wang, 2000; Paz *et al*., 2006; Patro *et al*., 2009; Kreiselmeier, 2015). Moreover, a DEM is a very important input into hydrodynamic models which are used to define the topographical variations and flow directions (Sanders, 2007; Patro *et al*., 2009). Currently, different types of freely (no-fee) available DEM exist, such as Shuttle Radar Topographic Mission (SRTM), Advanced Spaceborne Thermal Emission and Reflection Radiometer (ASTER) and Global Arc-Second Elevation (GTOP30). However, their accuracy is not uniform because they normally use different data sources in their constructions (Kiamehr and Sjöberg, 2005; Li and Wong, 2010).

The SRTM is an example of a freely available DEM that has been applied in many wetland inundation studies in data-scarce basins (Neal *et al*., 2012; Schumann *et al*., 2013; Mukolwe *et al*., 2015; Yan *et al*., 2015; Domeneghetti, 2016). One of the challenges experienced when applying the SRTM relates to its vertical accuracy, as its vertical accuracy is affected by the presence of vegetation signals contained within the SRTM. As a result, the DEM values are over-elevated (i.e. they do not represent ground surface elevations) (Sanders, 2007; Baugh *et al.*, 2013; Bates *et al*., 2014). Despite some initiatives to reduce vegetation bias in this DEM, as yet, there is a limited number of globally established methods for correcting the vegetation effects (e.g. O'Loughlin *et al*., 2016; Yamazaki *et al*., 2017; Allen and Pavelsky, 2018; Zhao *et al.*, 2018). Some studies have used an already available vegetation height map and subtracted a uniform percentage of each height value from the SRTM (Wilson *et al*., 2007), or subtracted a uniform vegetation artefact height value from the entire DEM (Coe *et al.*, 2008; Paiva *et al*., 2011). Baugh *et al*. (2013) applied the use of an available global vegetation height dataset (Simard *et al.*, 2011) to determine the percentage of vegetation height to be subtracted from the SRTM and then filtered the DEM to remove the random error noise. A percentage of the vegetation height was removed because the radar technology used by SRTM could not fully penetrate the vegetation before reflecting (Sanders, 2007; O'Loughlin *et al.*, 2016). Even though the last method appears to be an attractive option, the percentage of vegetation height that should be subtracted from the SRTM remains unclear. Moreover, the resolutions of most of the available vegetation datasets are low relative to the resolution of the DEM itself, e.g. 1 km for Simard *et al.* (2011) and 500 m for Lefsky (2010). An additional issue affecting the quality of the SRTM is the presence of random noise (Falorni *et al*., 2005; Sanders, 2007; Bates *et al*., 2014; Mukolwe *et al.*, 2015). In most cases, this error is resolved by average filtering of the SRTM (Wilson *et al.* 2007; Neal *et al*., 2012;

Baugh *et al.*, 2013). However, in some cases, the filtering processes may result in a misrepresentation of some channels which are important in connecting the floodplain areas with the main river (Trigg *et al.*, 2012; Baugh *et al.*, 2013).

Grid size or DEM resolution (e.g. 30 m and 90 m) is another challenge hindering the application of the SRTM in hydraulic modelling. Some of the channels, especially small channels, are hardly represented in the SRTM. For example, small channels (e.g. width < 30 m) cannot be captured in the 30 m resolution SRTM. In addition, other wetland micro-topography variations are not clearly presented in this DEM (Bates *et al*., 2014). Therefore, an attempt to use this DEM in such conditions would not effectively simulate wetland dynamics because in some wetlands these small channels contribute to wetland inundation dynamics. To account for small channels that influence hydraulic characteristics of wetlands, Neal *et al.*, (2012) included a sub-grid solver in the LISFLOOD-FP hydraulic model, which allows any size of the river channel below the grid resolution of the DEM to be included in the model setup. However, these sub-grid channels should be quantified from high-resolution images or DEM, and included in the model setup.

Optical remote sensors such as Landsat (30 m resolution) are also important sources of data to understand wetland dynamics as well as the channel–wetland exchanges (Kashaigili *et al.*, 2006a; Frazier and Page, 2009; Rowberry *et al*., 2011; Niu *et al.*, 2012; Ward *et al*., 2013; Tulbure *et al*., 2016). Landsat is one of the most accurate satellite images for understanding wetland dynamics due to its high-resolution (Chang *et al.*, 2012). Moreover, these images are used to establish river width values especially when river bathymetry data are missing (Andreadis *et al.*, 2013; O'Loughlin *et al*., 2013). They can also be used to distinguish different floodplain features such as levees, ox-bows, meander bends, ridges and swales (Syvitski *et al*., 2012). Despite their applications, Landsat images are sometimes obscured by cloud cover, and their temporal coverage (i.e. revisit cycle of 16 days) does not correlate with the inundation period in many wetlands (Feng *et al.*, 2012; Bates *et al*., 2014; Long *et al*., 2014). Recently, images from the Moderate-resolution Imaging Spectroradiometer (MODIS) have been applied in wetland inundation dynamics studies because these images are available daily or at 8-day time scale (Sakamoto *et al*., 2007; Chang *et al.*, 2012). However, the MODIS images can also be obscured by cloud cover, and their spatial resolution (250–1 000 m) is too coarse. It is likely that under this resolution, MODIS data cannot represent shallow inundation and/or inundation that cover small extents. Moreover, small channels below the MODIS resolution and those flowing in denser vegetation cannot be clearly represented (Chen *et al*., 2013; Ticehurst et al., 2014; Tulbure *et al.*, 2016). According to Chen *et al*. (2013), the accuracy of the MODIS data to detect inundation in wetlands can also be limited by the spectral confusion of background materials and depth of water. For instance, dark alluvial soils can be detected as inundated areas.

An additional challenge in applying both Landsat and MODIS images is related to the method used to extract water pixels. The approaches used to detect and extract inundated areas from satellite images can be grouped into single-band and multi-band methods (Xu, 2006). In the former method, a single band is selected from a multispectral image using a specified threshold. However, the possibility of a mixing of pixels representing water with those of other land cover types exists, and this is regarded as a weakness of this method (Rokni *et al*., 2014). In the multi-band method, different reflective bands are combined, following which a threshold is used to extract the water pixels (Xu, 2006; Rokni *et al*., 2014). The multi-band method provides a variety of spectral identifications that make it easy to identify different land cover features, including water pixels. However, the threshold value used to identify water pixels is not fixed and there is the possibility of under- or over-estimating the derived water pixels.

Google Earth images are also recognised as being useful in wetland studies (Mahay, 2008; Karim *et al*., 2011; Zahera, 2011; Teng *et al*., 2015; Nguyen *et al*., 2016). Visual inspections using Google Earth images make it possible to delineate inundation areas, river width, topographical differences between the main channel and the wetland, and to formulate assumptions about vegetation cover and soil characteristics. Mccorquodale *et al*. (2010) and Zahera (2011) used Google Earth images to determine channel cross-sections, whereas Karim *et al*. (2011) used these images to estimate the Manning's roughness coefficient when setting up a hydraulic model.

The available satellite-based global datasets that provide river width estimates are also widely used in data-scarce areas (Andreadis *et al.*, 2013; Yamazaki *et al.*, 2015). However, they have some limitations that are worth discussing. For example, the dataset used by Andreadis *et al.* (2013) estimated widths and depths as a function of drainage area and bankfull discharge, it is likely that the uncertainty in estimating the bankfull discharge (a 2-year return period discharge was assumed to represent bankfull discharge) was propagated to the final estimated values of widths and depths. Furthermore, the estimated values were evaluated using the Landsat-derived river width values; therefore, they might not have represented the bankfull conditions for some rivers (Andreadis *et al*., 2013). An additional issue with this dataset is that the location of the river network was adopted from the HydroSHEDS dataset by Lehner et al. (2006), which contains a number of errors. The HydroSHEDS river network was generated from a low-resolution DEM (15 arc-seconds) and there is a high possibility that most of the river channels with a width of less than 15 arc-seconds will not be captured (Lehner *et al*., 2008), which in turn affects the quality of the estimated width values in the simple global river bankfull width and depth dataset by Andreadis *et al*. (2013).

In the absence of direct observations of inundation patterns, hydraulic models are widely used to understand wetland dynamics (Patro *et al*., 2009; Jung *et al.*, 2010; Karim *et al*., 2012; Schumann *et al*., 2013). However, it is always important to understand the links between upstream and downstream flow regimes and the wetland dynamics themselves. This can be possible by setting up a basin-scale model for the entire basin (Zhang *et al*., 2013) and such models that include a wetland component include the Pitman (Pitman, 1973; Hughes, 2013), SWAT (Arnold *et al.*, 1993), ACRU (Schulze *et al*., 1987), MIKE SHE (DHI, 2004) and WATFLOOD (Kouwen, 1988) models. These models tend to either directly incorporate or indirectly model wetland processes (Rahman *et al.*, 2016). However, it is clear that the level of detail included in these models, especially in relation to their application to a large wetland, is very low. For instance, most semi-distributed models use empirical power equations that define the relationships between volume, area and depth, and incorporate these relationships in the model structure to define different wetland processes (Rahman *et al.*, 2016). In a river basin where river channels are integrated with multiple storage systems in a large wetland, the application of these models may lead to unacceptable or, at the very least, highly uncertain model results (Rayburg and Thoms, 2009). This is because most of the processes occurring in a large wetland remain poorly understood. As a result, the parameterization of these models remains a challenge. Understanding hydraulic characteristics related to wetland dynamics, such as spatial and temporal inundation characteristics, will assist in establishing different model parameters required to setup the wetland component of a basin-scale model. This information can be obtained from detailed hydraulic models (e.g. LISFLOOD-FP, MIKE 21 and SOBEK). This suggests the usefulness of an approach that can maximise the benefits of using a combination of hydraulic and hydrological models in large river basins containing wetlands.

A number of studies that used both hydraulic and hydrological models are represented in the literature, where one model generates the data inputs for the other model (Biancamaria *et al*., 2009; Rayburg and Thoms, 2009; Bravo *et al*., 2012; Schumann *et al*., 2013; Wen *et al.*, 2013b; Amarnath *et al*., 2015). Schumann *et al*. (2013) combined hydrological and hydraulic models to simulate inundation extents in the lower Zambezi floodplain, whereas Rayburg and Thoms (2009) incorporated these models to predict the inundation characteristics in the Narran River floodplain in Australia. The former study applied a hydrological model to simulate floodplain inflows and used a hydraulic model to simulate the inundation extents. In the latter study, the authors used a hydraulic model for understanding the water dynamics and the hydrological model to predict the water levels. The following sections provide a more detailed review of different basin-scale models as well as hydraulic models that can be applied to these river basins.

2.5 Hydrological models

Hydrological models are mathematical representations of the hydrological cycle. The motivations for their developments differ, including predicting and understanding of the hydrological processes in a basin, the generation of hydrological state variable data and the exploration of different scenarios used in water resources management (Xu, 2002; Silberstein, 2006). Hydrological models have been classified in many ways (Singh and Woolhiser, 2002; Xu, 2002; Viessman and Lewis, 2003; Hughes, 2004a). According to Xu (2002), mathematical models are sub-divided into categories of theoretical, empirical and conceptual, depending on the way they represent the basin processes (Figure 2.5). Theoretical models represent real basin processes, whereas empirical models do not consider physical processes in the basin. Conceptual models can be considered to fall between these two model extremes, as they consider physical processes in a simplified manner. The most often used classification of hydrological models is based on their spatial and temporal resolution: lumped and distributed models. Lumped models do not take into account the spatial variability of processes, inputs, boundary conditions and system geometric characteristics, whereas distributed models do (Singh, 1995). Within distributed models, the modelled basin is divided into smaller units, and each of these units is modelled independently. The structures of distributed models are generally complex, and therefore require a lot of input data (Xu, 2002). For this reason, semi-distributed models, which represent a compromise between lumped and distributed models, have been used in many studies worldwide.

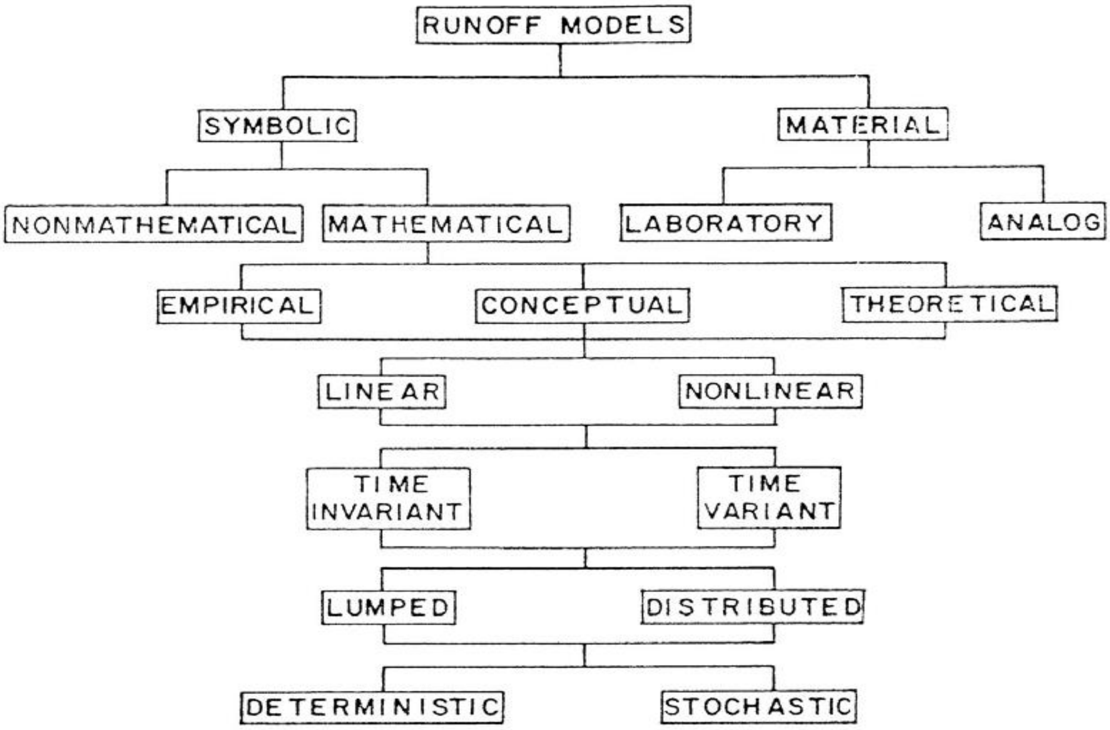

Figure 2.5: One of the classifications of hydrological models (Source: Xu, 2002)

Many different hydrological models have been developed to date, including models that can be applied to large river basins which include large wetlands. The choices of appropriate model are constrained by 1) the purpose of the study; 2) the availability of data to run the model; 3) the hydrological processes captured in the model structure; 4) the previously demonstrated applicability of the model to the specific study region and; 5) the time required to understand and become proficient at using a model. Based on these criteria, three hydrological models were reviewed in the present study.

2.5.1 ACRU hydrological model

The Agricultural Catchments Research Unit (ACRU) hydrological model is a physically-based distributed daily time step model developed by the School of Bio-resources Engineering and Environmental Hydrology at the University of KwaZulu-Natal (Schulze, 1984). The original purpose of the model was to quantify impacts of land-use change on runoff in both gauged and poorly gauged basins. This model has undergone several modifications to improve its structure (Schulze *et al.*, 1989; Schulze, 1995). Currently, it is regarded as a versatile model that can be applied to a variety of modelling applications, such as stream flow simulation, crop yield assessment, reservoir yield modelling, ecological requirements, irrigation demand and supply, planning optimal water resources utilisation and climate change impact studies (Schulze *et al*., 2003). The model inputs include catchment area, altitude, daily rainfall, potential evaporation (A-pan), land cover and soils, irrigation scheme as well as reservoir dimensions. ACRU is not a model that utilises parameter fitting or optimisation; rather, parameters are estimated from physical catchment characteristics. The model has been used for small and large-scale projects within southern Africa (e.g. South Africa, Zimbabwe, Lesotho, Swaziland and Namibia). Figure 2.6 shows the dominant catchment processes represented in the ACRU model structure.

The wetland component in ACRU was initially introduced by Schulze *et al*. (1987) and was tested in a study which assessed the hydrological impacts of a proposed reservoir upstream of a wetland situated in East Griqualand (Schulze *et al*., 1987). An initial modification to improve its structure was conducted by Schulze (2001), and Figure 2.7 depicts the idealised wetland processes after this modification. Schulze and Smithers (2002) provide a list of studies that applied the modified wetland component of the ACRU model. The most recent modification by Gray *et al*. (2012) involves an extension that allows excess river flow to flood riparian areas or wetland response units. This version of the model provided satisfactory results in some wetland studies in South Africa where it was tested (Gray *et al.*, 2012; Rebelo *et al*., 2015). Gray *et al*. (2012) applied the model to simulate the impacts of wetlands on catchment hydrological processes in the Thukela River catchment in South Africa.

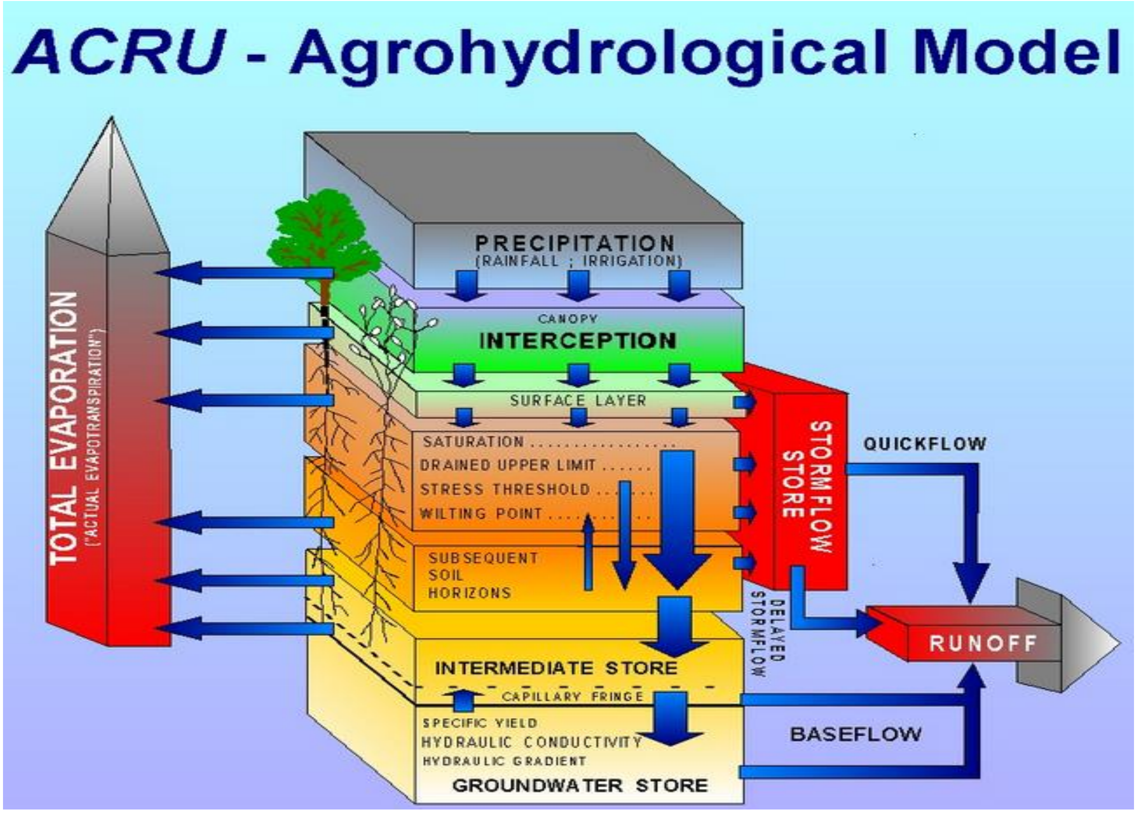

Figure 2.6: General structure of the Agricultural Catchments Research Unit (ACRU) model (Source: Schulze, 1995)

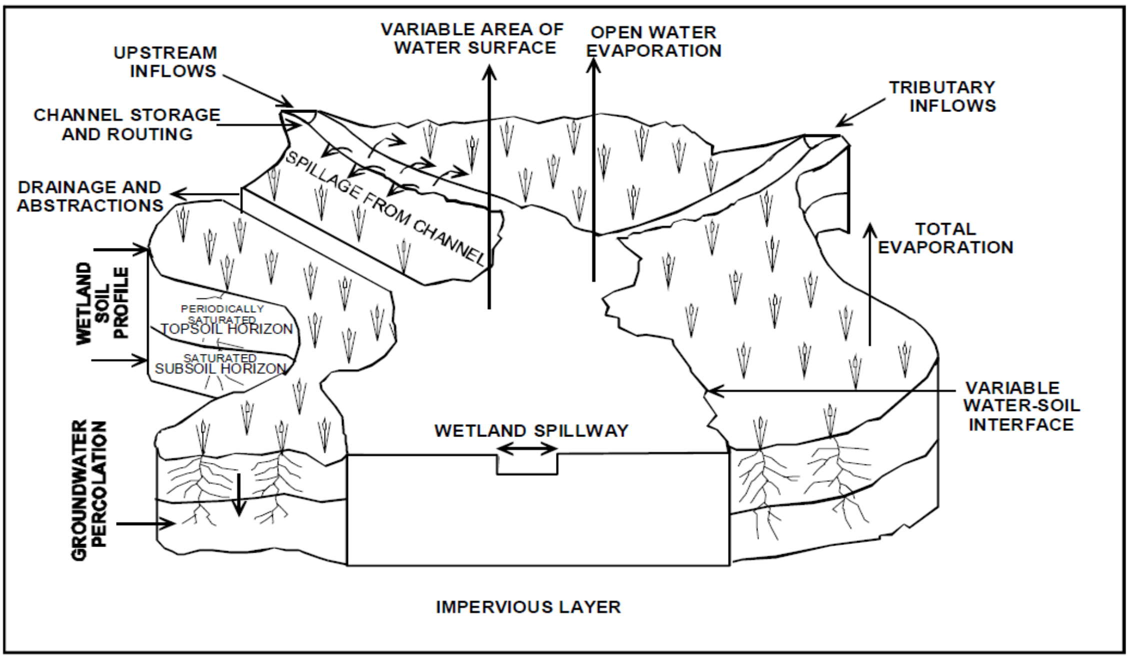

Figure 2.7: Wetland processes in the Agricultural Catchments Research Unit (ACRU) model (Source: Schulze and Pike, 2004).

2.5.2 SWAT hydrological model

The Soil and Water Assessment Tool (SWAT) model is a semi-distributed physically-based model that operates on a daily time step (Arnold *et al*., 1998). The SWAT model was developed by the Agricultural Research Service within the Department of Agriculture (USDA) in the United States. The main purpose of the model was to predict the impacts of land management practices on water, sediments and agricultural chemical yields in large complex watersheds with varying soils, land use and management conditions over a long period of time (Neitsch *et al*., 2005; Griensven *et al*., 2008). Figure 2.8 shows the dominant watershed processes represented in the SWAT model structure. The SWAT model has undergone several modifications, including the incorporation of spatial units based on Hydrological Response Units (HRUs). The most recent version of this model enables parameter calibration as well as uncertainty and sensitivity analysis (Pagliero *et al*., 2014). Depending on the processes included in the SWAT model, a large number of parameters are required for setting up the model, resulting in the parameterization and calibration of the model being a particularly challenging task (Arnold *et al*., 2012). Different techniques have been developed to improve the parameterization of the SWAT model, including both manual and automated approaches using SUFI 2 (Guillermo *et al*., 2015; Arnold *et al*., 2012). The SWAT model has been applied in many studies worldwide, as presented by Gassman *et al*. (2007) and Rahman *et al*. (2016).

Wetlands are represented in two ways in SWAT: 1) as a reservoir on the main channel and; 2) located off-channel and receiving loadings only from the portion of the sub-basin where it is located (Martinez-Martinez *et al*., 2014). The model has been applied in different wetland studies outside Africa (Vining, 2002; Du *et al*., 2005; Wang *et al*., 2008; Zhang *et al*., 2013, Martinez-Martinez *et al*., 2014 and Mekonnen *et al*., 2016) and in Africa (Griensven *et al.*, 2008; Ndomba *et al*., 2010; Liersch and Hattermann, 2011; Liechti *et al*., 2014). Griensven *et al*. (2008) incorporated remote sensing in the SWAT model to understand the processes of a riverine wetland in the Kagera River basin in Tanzania. Ndomba *et al*. (2010) applied the model to understand the hydrological characteristics of the Rugezi Wetland in Rwanda. Despite the fact that the SWAT model is a semi-distributed physical model, some wetland processes are not well captured in the model (Schuol and Abbaspour, 2006; Wang *et al*., 2008; Zhang *et al*., 2013; Rahman *et al*., 2016). As a result, a number of researchers (e.g. Hattermann *et al.*, 2008; Wang *et al*., 2008; Liu *et al*., 2010; Zhang *et al*., 2013; Mekonnen *et al*., 2016; Rahman *et al*., 2016) have modified the SWAT wetland module to improve its structure in their studies. For example, Zhang *et al*. (2013) modified the SWAT wetland component to simulate hydrological processes within the Zhalong Wetland in northeast China, whereas Wang *et al*. (2008) represented wetlands using a hydrologic equivalent wetland (HEW) to simulate the stream flows in different wetland types of the Otta River watershed, northwest of Minnesota. The most recent wetland module of SWAT is SWATrw (Rahman *et al*., 2016), in which the unidirectional hydrological interactions between wetlands and the river or aquifer have been modified, with a bidirectional approach to represent the interactions between riparian wetlands and the river.

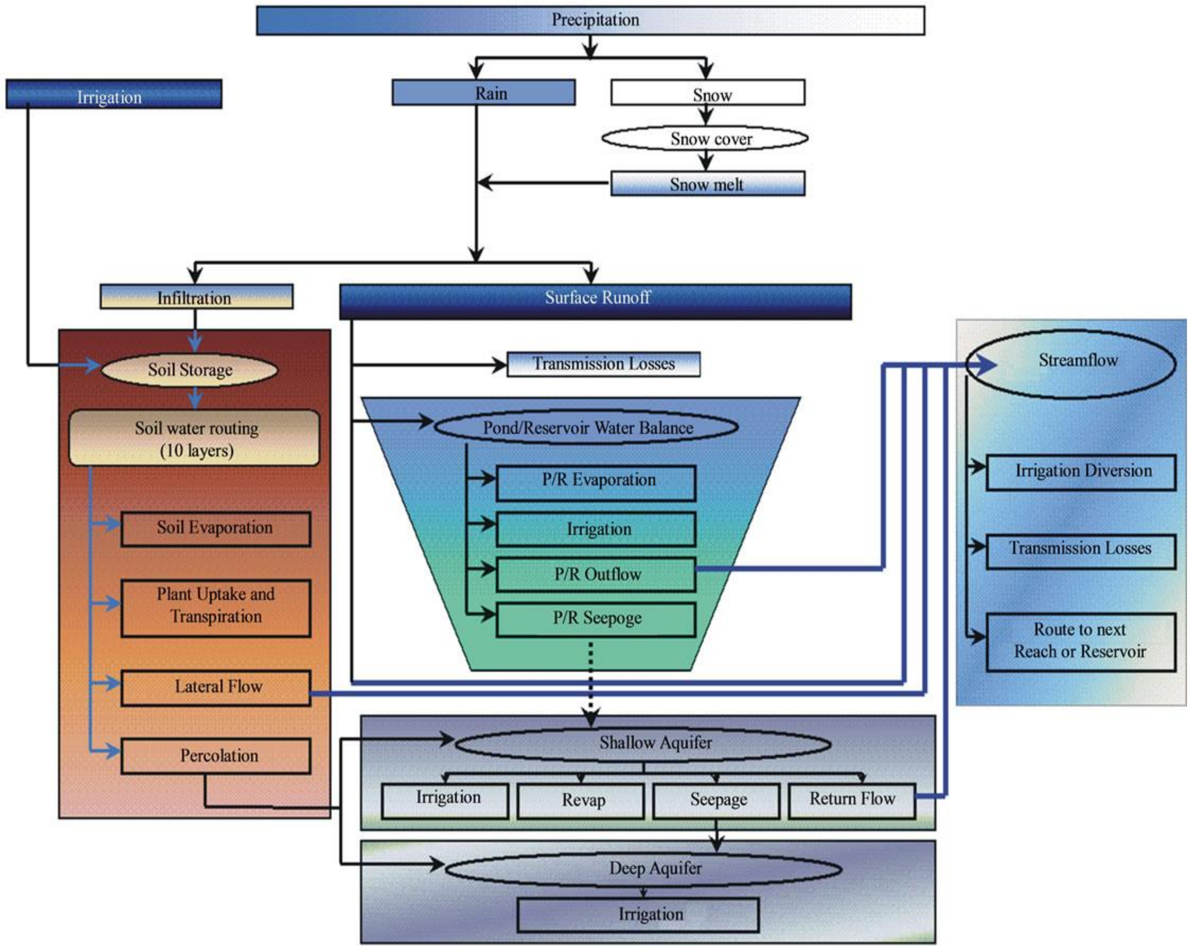

Figure 2.8: Schematic representation of water movement in the Soil and Water Assessment Tool (SWAT) model (Source: SWAT2005 user manual)

2.5.3 Pitman hydrological model

Pitman (1973) developed the original version of the Pitman model for simulating runoff in both gauged and ungauged catchments in South Africa. The model primarily operates on a monthly time scale and its main inputs are rainfall and potential evapotranspiration. The model has undergone several modifications since its inception to improve its structure. The most recent modifications include the addition of surface–groundwater interactions (GW Pitman: Hughes, 2004b), the inclusion of the model into a comprehensive uncertainty framework (Hughes *et al*., 2010; Kapangaziwiri *et al*., 2012), a wetland component (Hughes *et al*., 2014) and a sub-model to disaggregate monthly flow values to daily discharge using daily rainfall data (Slaughter *et al*., 2015). The semi-distributed concept has been applied to the recent versions of the model in which a basin is divided into discrete areas (sub-basins), and these units are modelled independently. The Pitman model is one of the most frequently used hydrological models for research and practical water resource assessments in southern Africa. Apart from the applications of the earlier version of the model (Pitman, 1973), the recent versions of the model have been widely applied in the sub-Saharan region (e.g. Andersson *et al*., 2006; Mazvimavi *et al*., 2006; Wolski *et al*., 2006; Hughes *et al*., 2010; Tshimanga *et al*., 2011; Kapangaziwiri *et al*., 2012; Hughes *et al*., 2014; Tumbo and Hughes, 2015). Moreover, the model has been used for climate change studies (Tshimanga and Hughes, 2012; Tirivarombo, 2013; Hughes, 2015b; Mohobane, 2015).

The original version of the model (Pitman, 1973) treated the wetland as a reservoir. However, following the recognition of the importance of wetland processes in the basin–water balance dynamics, there was a need to include wetland processes in the model structure. The Pitman wetland sub-model was therefore included in the GW Pitman model by Hughes *et al.* (2014). Among the processes represented in the wetland sub-model is the channel–wetland exchange function, which is important for representing the interaction between the wetland and river channels and the impacts of the wetland on the hydrological regime of the basin (Hughes *et al*., 2014). This sub-model can simulate seasonally inundated wetlands as well as natural lake conditions. Wetland–groundwater interactions are not included in the Pitman wetland sub-model as most of the groundwater–wetland processes are reported to have minor effects on the monthly water balance in large river–wetland systems in southern Africa (Wamulume *et al*., 2011; Hughes *et al*., 2014). In the wetland sub-model, wetland inflows occur as the proportion of channel flows above a given threshold, whereas wetland return flow is the proportion of the excess volume above the wetland residual volume (the volume below which there are no returns to the river). The relationship between area and storage of inundation is assumed to be a power function defined by scale and power parameters. There are currently 13 parameters required for setting up the Pitman wetland sub-model, of which some can be more-or-less directly estimated, whereas others are highly empirical and their estimation requires a good understanding of channel–wetland exchange processes and/or hysteresis effects. For instance, the maximum and residual wetland volumes and the maximum inundated area are some of the parameters required to set up the Pitman wetland sub-model. These parameters can either be estimated from area–volume curves or from available satellite images. The available area–volume curves can also be used to establish the two parameters that define the area and volume of inundation in the model. Other parameters, such as the proportions that control wetland inundation volume and wetland return flow, cannot be easily estimated without prior knowledge of exchange processes. The Pitman wetland sub-model has been applied in river basins that include large wetlands within the southern African region. These include the Congo River basin (Tshimanga *et al*., 2011), the Zambezi River basin (Tirivarombo, 2013), the Kafue and Okavango river basins (Hughes *et al*., 2014) as well as the Great Ruaha River basin (Tumbo and Hughes, 2015). The structure of the GW Pitman model, including the wetland sub-model, is presented in Figure 2.9.

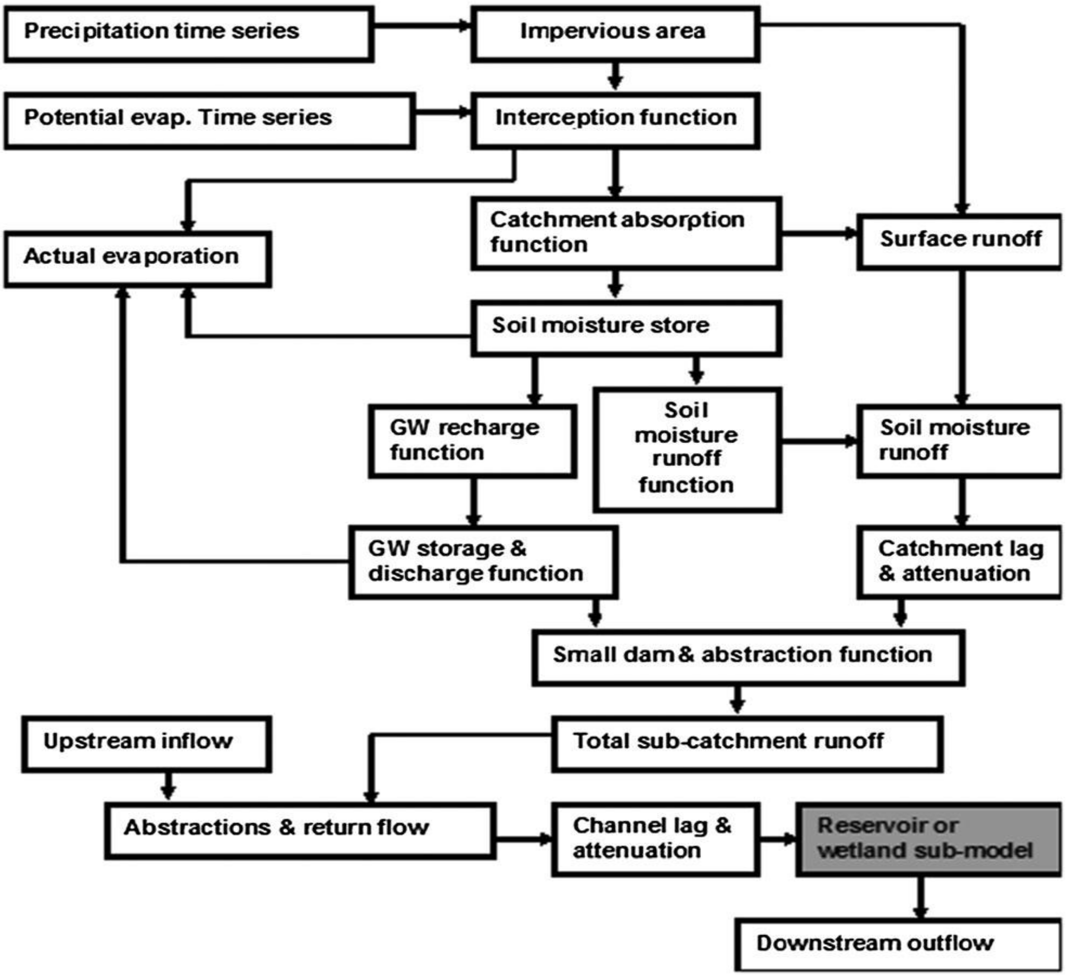

Figure 2.9: Structure of the GW Pitman model (Source: Hughes *et al*., 2014)

2.6 Parameterization and calibration of hydrological models

Model parameters represent hydrological processes occurring in a specific catchment or basin under study. Usually, a more detailed hydrological model requires more parameters (Hughes, 2004b; Schuol and Abbaspour 2006; Arnold *et al*., 2012). For example, a larger number of parameters are required in distributed models compared to lumped models and different approaches are required to parameterize the two types of models (Beven, 1989; Refsgaard, 1997; Beven, 2006). Generally, the parameterization processes is never a straightforward task (Dams *et al*., 2009; Chen *et al.*, 2015; Malone *et al.*, 2016) and there are relatively few guidelines on how to parameterise hydrological models (Malone *et al*., 2016). One of the reasons for this could be the spatial–temporal heterogeneity of physical characteristics within the basin, which make it difficult to pre-define model parameters for every single hydrological model (Chen *et al*., 2015). Efficient model parameterization is expected to improve the model calibration process and in turn the final model results (Refsgaard, 1997).

Calibration processes are conducted with the aim of identifying the optimal parameter set that simulates characteristics of the catchment or basin (Sahoo *et al.*, 2006). Manual and automatic calibration approaches have been proposed for establishing appropriate model parameters, however, they all have limitations in their applicability. Manual calibration, for instance, is argued to be infeasible (Schuol and Abbaspour, 2006), very tedious and time-consuming (Jiang *et al.*, 2013; Seong *et al.*, 2015), especially for models with large numbers of parameters. Moreover, the successful application of manual calibration is dependent on the modeller’s experience, skills, and understanding of basin processes captured in the model (Boyle *et al*., 2000; Confesor and Whittaker, 2007). In general, a broad understanding of the model and real basin processes is important for effectively modelling using manual calibration (Boyle *et al*., 2000). Refsgaard (1997), Andersen *et al.* (2001) and Blasone *et al*. (2008a) acknowledged the use of rigorous parameterization and reduction of parameter space to facilitate manual calibration processes. This might be possible through sensitivity analysis to identify parameters that greatly influence model results and/or adopting values estimated from previous model simulations (Blasone *et al*., 2008a).

During automatic calibration, parameters are adjusted automatically using a specific search scheme and numerical measures of goodness of fit (i.e. objective functions are used to assess the simulated and observed values), and the process is repeated until a specified termination criterion is satisfied (Boyle *et al*., 2000; Madsen, 2001). In most cases, the modeller has to specify the initial range for each parameter, and this parameter space is assumed to contain behavioural parameter values. Different algorithms are used in the automatic calibration processes, such as Shuffled Complex Evolution (SCE-UA) (Duan *et al*., 1992), Particle Swarm Optimisation (PSO) (Eberhart and Kennedy, 1995), Shuffled Complex Evolution Metropolis algorithm (SCEM-UA) (Vrugt, 2003), Multi-objective Particle Swarm Optimisation (MPSO) (Gill *et al*., 2006), Master-slave Swarms Shuffling based on self-adaptive PSO (MSSE-PSO) (Jiang *et al*., 2010) and Bayesian Recursive parameter Estimation (BARE) (Thiemann *et al*., 2001). The first two algorithms use single objective functions, whereas the remaining algorithms apply multi-objectives. It has been argued that a single objective function cannot clearly measure all important characteristics of the observed data and provide the most appropriate parameter set (Wagener *et al.*, 2001; Vrugt, 2003; Gill *et al*., 2006). As a result, multi-objective algorithms have recently been used to automatically calibrate many hydrological models (e.g. Confesor and Whittaker, 2007; Zhang *et al.*, 2013; Wang and Brubaker, 2015; Jung *et al*., 2017).

Although automatic calibration is recognised as quicker and less labour intensive, Boyle *et al*. (2000) noted that some automatic calibration methods might fail to produce acceptable parameter values and simulated hydrographs. Moreover, they require extensive mathematical formulations and computations which hamper their application in many hydrological models. Automated calibration is always difficult in ungauged basins where there are no observed data to quantify measures of goodness-of-fit (Hughes, 2006; Hughes, 2015a). These problems have been overcome by some authors through the use of regionalised constraints on basin response (Bloschl, 2005; Merz *et al*., 2006; Yadav *et al*., 2007; Zhang *et al*., 2008; Tumbo and Hughes, 2015). In most of these approaches, the hydrological response behaviour of the basins are estimated and then regionalised in an uncertainty framework (Yadav *et al.*, 2007; Tumbo and Hughes, 2015). Tumbo and Hughes (2015) used an approach that is implemented in an uncertainty framework within the GW Pitman hydrological model, and involves the use of hydrogical signatures such as mean monthly streamflow (MMQ), mean monthly groundwater recharge, Q10, Q50 and Q90 on the flow duration curve as well as the percent time of zero flows to constrain generated ensembles from which behavioural parameter sets are identified. A detailed explanation of this approach is presented in section 2.11. It can be concluded that automatic and manual calibration approaches in hydrological models have both merits and drawbacks. An approach that considers the strengths of both approaches (manual and automatic), similar to that developed by Boyle *et al.* (2000), could improve calibration of hydrological models.

2.7 Hydraulic modelling in wetlands

The importance of two-dimensional (2D) hydraulic modelling in understanding hydraulic characteristics of wetlands has been recognised by many authors (e.g. Nicholas and Mitchell, 2003; Thompson, 2004; Trigg *et al*., 2009; Karim e*t al*., 2011; Schumann *et al*., 2013; Chen *et al*., 2015). Unlike remote sensing data which have spatial and temporal limitations, 2D models can provide useful information to understand wetland dynamics, including spatial and temporal inundation extents and water depths (Shen *et al*., 2015; Teng *et al*., 2015). Some of the well-known 2D hydraulic models include LISFLOOD-FP (Bates and De Roo, 2000; Bates *et al*., 2010), MIKE 21 (DHI, 2007), SOBEK (Stelling *et al*., 1998), ISIS-2D (Liang *et al*., 2006) and TUFLOW (Syme, 1991). These models vary according to their algorithms and spatial applicability (Gall *et al*., 2007; Pender and Néelz, 2007). A full solution of the Saint-Venant shallow water equations or simplified representations (i.e. a version in which the inertia terms are ignored in the Saint-Venant shallow water equations) can be used in these models (Hunter *et al*., 2007). However, in most cases, the application of the full Saint-Venant shallow water equations in very complex topographies using finite difference, finite element or finite volume approaches may result in model instability due to the highly nonlinear and hyperbolic nature of the governing equations (Hunter *et al*., 2007). Thus, the simplified Saint-Venant shallow water equations have been used in many 2D hydraulic models (Teng *et al*., 2017). In shallow water equations, the vertical component of flow is assumed to be considerably smaller compared to the horizontal component of flow (Dawson and Mirabito, 2008). Among the various hydraulic models, MIKE21 and the LISFLOOD-FP have recently been applied to a number of studies in Africa e.g. Beck and Basson (2008), Schoen *et al.* (2014), Pamba *et al*. (2016), Schumann *et al*. (2013), Zahera (2011); Neal *et al.* (2012); Coulthard *et al*. (2013), Fernández *et al*. (2016). The LISFLOOD-FP model is a non-commercial model, whereas MIKE 21 model is commercial. The two models are described in the following sections.

2.7.1 MIKE 21 hydraulic model

The MIKE 21 hydraulic model is a professional engineering software package developed by the Danish Hydrological Institute (DHI) with the main purpose of simulating surface flows, water quality, sediment transport, and waves in coastal and estuarine environments. However, the model can also be applied to floodplains, lakes and reservoirs (DHI, 2007). The model applies depth-averaged Saint-Venant equations and uses an implicit finite difference scheme to solve for continuity and momentum on each grid mesh covering the whole model domain (Petersen and Fohrer, 2010; Karim *et al.*, 2012; Teng *et al*., 2015). The main model inputs include topography (DEM), boundary conditions (inflows and outflows), initial conditions, rainfall, evaporation, infiltration, bed roughness and other parameters such as eddy viscosity (DHI, 2003; 2007; Karim *et al*., 2015). The main outputs of the model consist of time series of water depths and flow for each grid mesh defined in the model domain (Karim *et al*., 2015). The original version of the model has undergone several modifications, including the improvements to the flooding and drying routines, the incorporation of routines for describing hydraulic structures (broad-crested weir flows, hydraulic jumps, dam-break flows), and modelling supercritical flows (McCowan, 2001). Some of the applications of MIKE21 in Africa include Beck and Basson (2008), Schoen *et al.* (2014) and Pamba *et al*. (2016), whereas applications outside Africa include Karim *et al.* (2012), Wen *et al.* (2013a), Karim *et al*. (2014), Teng *et al*. (2015), Zhang and Werner (2015) and Czgani *et al.* (2016). However, it can be noted that there are relatively few reported applications of this model in Africa.

2.7.2 LISFLOOD-FP hydraulic model

The LISFLOOD-FP model was developed at Bristol University in the United Kingdom for the purpose of simulating river flooding and floodplain inundation in data-scarce areas (Bates and De Roo, 2000; Bates *et al*., 2010). The model includes two equations that solve continuity of mass for each cell and continuity of momentum between cells (Neal *et al*., 2012). The model uses an explicit finite difference technique to solve the Saint Venant shallow water equation with the advection component ignored and the acceleration, water slope and friction slope components retained (Schumann *et al*., 2013; Fernández *et al*., 2016). The motivation for the above approach is that the advection component is considered to be negligible in most floodplains (Hunter *et al*., 2007; Bates *et al.*, 2010). The most recent versions of this model include the introduction of a local inertial term to the diffusive wave equation with the aim of reducing the computation cost (Bates *et al.*, 2010) and the inclusion of a sub-grid approach (Neal *et al*., 2012). The sub-grid approach is incorporated in the base model (Bates *et al*., 2010), and provides for hydraulic characteristics of channels that are smaller in size compared to the grid size. Additionally, the LISFLOOD-FP has speed advantages for large domains as well as application in data scarce areas. A full description of the development of the sub-grid approach can be found in Neal *et al*. (2012), while Figure 2.10b presents a summary of the structure of the sub-grid approach.

The model inputs include upstream and downstream boundary conditions (discharge and water level), topography (DEM), river bathymetry (width and depth, bed elevation) and channel and floodplain roughness. In data-scarce areas where most of the river bathymetry data are not available (e.g. bankfull depths, bed elevation), the model estimates these variables using the hydraulic geometry equation of Leopold and Maddock (1953) that defines the relationship between width and depth. The simulated results consist of time series of channel and floodplain inundation extent, storage and water depths in the wetland. The model is capable of simulating inundation for both small and large wetlands (1 000 to 100 000 km^2) at a high spatial-temporal resolution. Some of the LISFLOOD-FP model applications in Africa include to the Lower Zambezi Delta (Schumann *et al*., 2013), the Inner Niger Delta (Zahera, 2011; Neal *et al.*, 2012; Coulthard *et al*., 2013), the Blue Nile (Yan *et al.*, 2014), the Logone floodplain in Cameroon (Fernández *et al*., 2016) and a significant number of studies outside of Africa (e.g. Hunter *et al*., 2005a; Alsdorf *et al.*, 2007; Wilson *et al.*, 2007; Biancamaria *et al.,* 2009; Trigg *et al.,* 2009; de Almeida and Bates, 2013; Trigg *et al.*, 2013; Wood *et al.*, 2016).

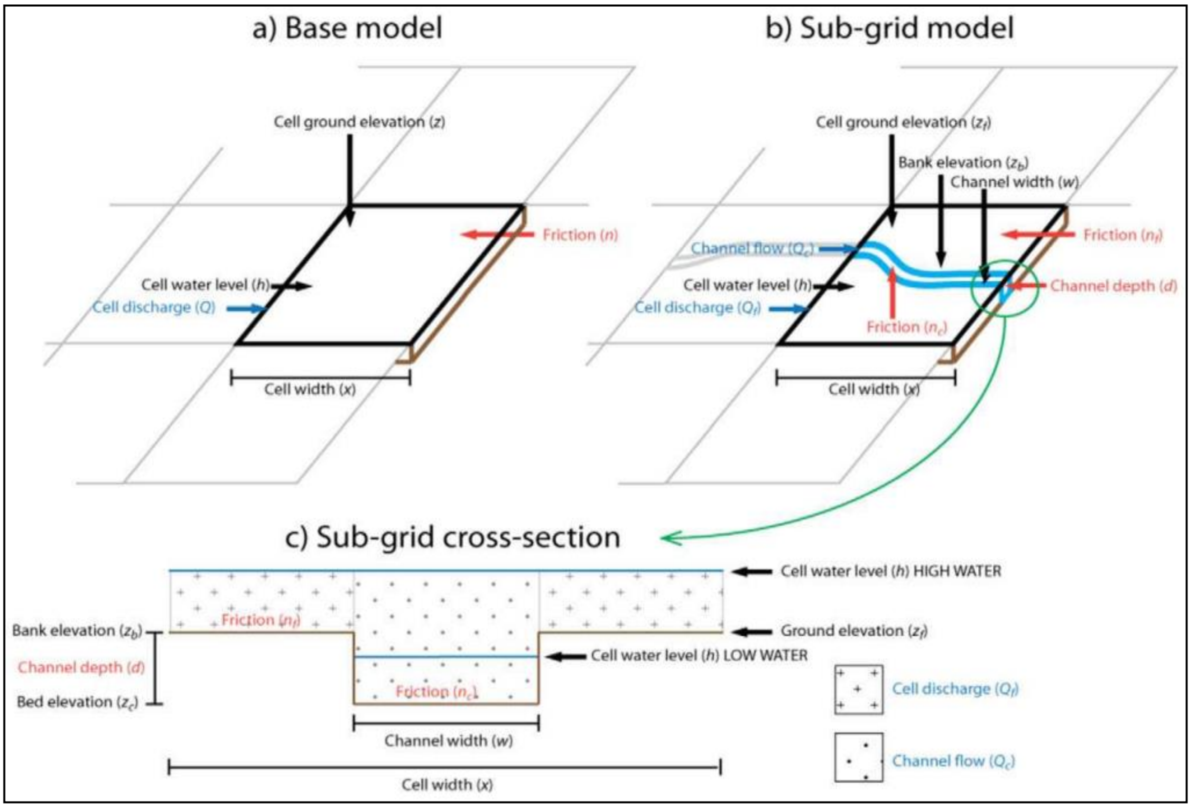

Figure 2.10: Conceptual diagram of the LISFLOOD-FP base model (a), sub-grid solver (b), and sub-grid section (c) (Source: Neal *et al*., 2012).

2.8 Uncertainties in hydrological and hydraulic modelling

In recent years, the need to explicitly quantify uncertainty in modelling results has been widely advocated (Sivapalan *et al*., 2003; Wagener *et al*., 2003; Pappenberger and Beven, 2006; Yadav *et al*., 2007; Hughes *et al*., 2010; Sawicz *et al*., 2011; Kapangaziwiri *et al*., 2012). Uncertainty analysis provides a fundamental guide to quantify the reliability of model simulations for both research and practical uses (Wagener and Gupta, 2005; Pappenberger *et al*., 2006). Liu and Gupta (2007) argued that to address uncertainty issues, uncertainty should be well understood, quantified and reduced to an acceptable degree. Therefore, understanding of uncertainty is vital for its quantification and reduction in modelling. The three major sources of uncertainty in modelling include those associated with the model structure, model input data and model parameters (Refsgaard *et al*., 2005; Di Baldassarre and Montanari, 2009). These sources of uncertainty are not necessarily independent, as they can interact in complex ways (Beven, 2005; Renard *et al*., 2010; Beven, 2016; Jensen and Wu, 2016). For example, a perfect model structure will not produce acceptable results if both model inputs and parameters are not correct (Beven, 2005). Moreover, model structural uncertainty can hinder identification of a parameter to represent a certain process, and the uncertainty in the calibrated parameters may affect model results (Wagener and Wheater, 2006). Thus, uncertainty analysis should consider all sources of uncertainty together as they interlink.

2.8.1 Model input data uncertainty

Input data uncertainties may arise from different sources related to sampling, measurements and interpolation methods (Renard *et al*., 2010). Uncertainties due to model input data are generally high in data-scarce regions (Hughes *et al*., 2010; Hughes and Mantel, 2010; Mcmillan *et al*., 2012; Hrachowitz, *et al*., 2013; Hughes, 2013). Discharge data are needed to validate both hydrological and hydraulic model simulations or as inputs to hydraulic models. Unfortunately, many rivers in Africa are not gauged, and where rivers are gauged, data are generally of poor quality (i.e. short periods and contain outliers), and in some cases, are affected by upstream water resource developments (Hughes *et al*., 2010; Hughes and Mantel, 2010). Although some wetlands are linked to narrow river channels upstream and downstream, where inflows and outflows can be quantified, flow patterns in these channels are frequently unknown (Fekete *et al*., 2012). The majority of wetlands remain totally ungauged (Griensven *et al*., 2008; Wen *et al*., 2013; Bates *et al*., 2014). Many gauging stations are based on rated natural river sections rather than flow gauging structures (Di Baldassarre and Montanari, 2009; Guerrero *et al*., 2012). The stage-discharge relationships need to be based on gauging observations across a representative range of discharges (Coxon *et al*., 2015). It is not only difficult to achieve this with limited resources and remote locations, but there is also the possibility that channel hydraulic characteristics might change over time due to scouring or sedimentation (Di Baldassarre and Claps 2010; Westerberg *et al*., 2011). This, therefore, necessitates frequent updating of the stage–discharge relationships. However, most of the stage–discharge relationships are not updated frequently, and this inevitably introduces uncertainty in discharge data and in turn the validation of model simulation results (Guerrero *et al*., 2012; Sikorska *et al*., 2013; Coxon *et al*., 2015).

Rainfall, as one of the major inputs to hydrological models, varies in time, space and altitude because of multi-climatic mechanisms. The measurement of rainfall requires weather stations appropriately distributed across the basin; however, this is not the case in many basins in Africa (Hughes, 2006; Nicholson, 2013; Awange *et al*., 2016). Apart from the spatial distribution of gauges, uncertainty in ground-based rainfall data is also associated with gauge type and height, windshield, exposure, and interpolation methods (WMO, 1983). Although gridded and satellite rainfall datasets are used as alternative sources of rainfall data, they are associated with a number of uncertainties related to estimation, and sampling techniques, retrieval algorithms and topography (Villarini *et al*., 2008; Aghakouchak *et al*., 2010; Awange *et al*., 2016; Dahri *et al.*, 2016). The other sources of uncertainties in satellite-based rainfall are related to estimation techniques based on cloud top reflectance and thermal radiance, as well as infrequent satellite overpasses (AghaKouchak *et al*., 2009; Bytheway and Kummerow, 2013). For instance, the use of high-resolution infrared spectral band has resulted in the unrealistic estimation of rainfall values because the rainfall is estimated from cloud-top temperature, which is highly affected by the height of the clouds, and as a result, orographic rainfall events in mountainous areas are frequently not captured (Gebregiorgis and Hossain, 2013; Awange *et al*., 2016). Generally, the influence of altitude on rainfall variation is ignored in many satellite-based rainfall datasets (Hughes, 2006; Dahri *et al.*, 2016). The CRU (Climate Research Unit) gridded long-term monthly rainfall (1901 to date) was estimated using available local ground-based rainfall (i.e. fewer stations were used in some areas which affect the interpolation process) (Harris *et al*., 2014). Moreover, some of the earlier records are clearly unreliable, and it is evident that they were infilled using long-term mean monthly values.

Potential evapotranspiration (PET) is an additional important hydrological model input which is normally estimated from climate variables (i.e. solar radiation, wind, temperature, atmospheric pressure and water vapour deficit), using different empirical formulas such as that by Penman (Penman, 1948; Allen *et al*., 1998), Hargreaves (Hargreaves and Allen, 2003) and others as presented by Lu *et al*. (2005) and Esmaeilabadi (2014). The PET data estimated using these methods vary with data inputs and assumptions made during computations (Grismer *et al.*, 2002). The climatic variables used to estimate the PET data are mostly estimated from meteorological stations which are point-based stations. As a result, the computed PET values are not representative of the basin PET (Hughes, 2007; Long *et al.*, 2014). The introduced errors in the estimated basin PET can inevitably affect the simulated model results. Global satellite-based PET datasets have recently been used as another source of PET data (Allen *et al.*, 2011). One of the major challenges in applying some of the global satellite-based PET datasets is related to their resolution and they tend to be too coarse for application at small scales (Allen *et al.*, 2011; Westerhoff, 2015). The MODIS 16 PET product has a pixel resolution of 1 km × 1 km and is derived from remote sensing data and global meteorological data (Mu *et al*., 2011). The use of global meteorological data, which are mostly not representative of climatic variations, for the computation of the MODIS16 PET, is regarded as one of the weaknesses of this product (Trambauer *et al*., 2014; Westerhoff, 2015). As a result, application of the MODIS16 PET in modelling has resulted in under- or over-estimation of model simulations (Mu *et al*., 2011; Jovanovic *et al*., 2015; Westerhoff, 2015; Rafiei *et al*., 2017). Moreover, in some global datasets, the PET values are derived using simplified assumptions as applied in the Penman method or interpolated from a limited number of available ground-based values.

Topography is one of the key model inputs in hydraulic models. In data-scarce regions of Africa, ground-based topographical data are frequently not available, and freely-available DEMs are therefore used to represent topographical characteristics in the model setup (e.g. SRTM, ASTER and GTOP30). These DEMs vary depending on the method of acquisition (Rodriguez *et al*., 2006; Bates *et al.*, 2014; Yan *et al*., 2015). For example, Radar-based technology applied in the SRTM could neither penetrate the water surface nor the full vegetation height (Sanders, 2007; O'Loughlin *et al.*, 2016). As a result, the SRTM elevation data are elevated in some places (i.e. they do not represent ground elevations). Thus, unless the vegetation effects are corrected, the application of this DEM, particularly in densely vegetated areas, would result in unrealistic model results (Baugh *et al*., 2013; Teng *et al*., 2017).

Channel bathymetry data are also required in setting up hydraulic models. Generally, this information is rarely available for many rivers. In some cases, the river bathymetry data are estimated through surveying river reaches (Trigg *et al*., 2009; Di Baldassarre *et al*., 2010; Rudorff *et al*., 2014) for a few representative sections. Clearly, this technique is always expensive, and sometimes the few selected sections might not be representative of the entire river network. In some studies, river bathymetry data have been extracted from high-resolution satellite data (Biancamaria *et al*., 2009; Neal *et al*., 2012; Kreiselmeier, 2015; Yan, 2015; Edwards *et al*., 2016). Even though this approach appears to be an attractive option, high-resolution satellite images are often not available for many regions in southern Africa. It is also possible to obtain the river bathymetry data from the available global datasets, such as Andreadis *et al*. (2013) and Yamazaki *et al*. (2014). In most datasets, the river cross-section values were derived from low-resolution DEMs (e.g. the 15-arcsecond SRTM DEM), which do not correctly represent the river morphology and the estimated values are unrealistic. Within other datasets, empirical equations (e.g. Leopold and Maddock, 1953; Dingman and Sharma, 1997) were applied to derive river cross-section values, but it is clear most of the local channel variations are not captured by the empirical equations (Yamazaki *et al.*, 2014).

2.8.2 Model structure uncertainty

A model is an abstract and simplified representation of the real-world basin processes (Refsgaard *et al*., 2005). Basin processes interact in a complicated manner, and oversimplification of these processes in a model structure may affect the quality of model results (Renard *et al.,* 2010; Hughes *et al.*, 2011; Gupta *et al.*, 2012). Moreover, the spatial and temporal scale of analysis contributes to structural uncertainty in modelling (Wagener and Gupta, 2005; Refsgaard *et al*., 2007; Beven *et al*., 2008; Hrachowitz, *et al*., 2013; Hughes *et al*., 2013). Despite the recognised sources of structural uncertainty, only a few studies have focused on assessing model structure uncertainty (e.g. Butts *et al*., 2004; Refsgaard *et al*., 2006; Zhang *et al*., 2011), because it is often difficult to separate these uncertainties from those derived from other sources, and structural uncertainty depends heavily on other sources of uncertainty (Beven, 2005; Warmink *et al*., 2010; Zhang *et al*., 2011). For example, a more detailed model structure requires a large number of parameters, and quantification of these parameters is often difficult. As a result, the model predictability becomes low. Therefore, an attempt to change the model structure will inevitably affect both model inputs and model parameters. Refsgaard *et al*. (2006) provide a review of different strategies developed to assess structure uncertainties. These strategies include an increase of the parameter space to account for structural uncertainty, as applied by Van Griensven and Meixner (2004), estimation of the structural uncertainty term, as applied by Radwan *et al*. (2004), the use of multiple conceptual models, as applied by Butts *et al*. (2004) and Visser *et al*. (2000) and the use of expert elicitation, as applied by Meyer *et al*. (2004).

2.8.2 Model parameter uncertainty

Parameter uncertainty arises from different sources, which affects model accuracy and reliability (Ao *et al*., 2006). According to Ao *et al*. (2006), parameter uncertainty can be due to 1) quality and quantity of model input data; 2) model structure; 3) initial parameter ranges; 4) choice of objective functions to evaluate the model; 5) optimisation algorithms and; 6) equifinality. The lack of accurate basin physical characteristics (e.g. soils, geological, topographical and land cover) which are used to estimate model parameters affects the parameterization processes. In most cases, these data are typically not available locally, and global datasets offer an alternative source for these types of data (e.g. Lehner *et al.*, 2006; Rodriguez *et al*., 2006; Andreadis *et al*., 2013; Hengl *et al*., 2014). However, in most cases, they are inconsistent, erroneous and not available at the required resolution or in the correct form (Andersson *et al*., 2015). For example, soil depths and/or water capacity are required to derive parameters related to soil infiltration and subsurface storage; however, these datasets mostly provide information only on soil types. Moreover, other datasets provide information on geological formations, with no details of fracture density, storativity and transmissivity values, which are required for model calibration. This suggests that inappropriate basin physical data may lead to incorrect estimates of parameter values. Thus, it is always vital to examine and identify the datasets that suit the intended purpose (Winsemius, 2009; Yan *et al*., 2015). Discharge data used in calibration have been found to contain a number of types of errors, including measurement errors, leading to incorrectly estimated parameter values (Ao *et al.*, 2006). Uncertainties in the objective functions used during calibration have impacts on the final parameter values. Different objective functions may lead to different parameter sets after calibration. Several frameworks are available to understand and reduce parameter uncertainties, including *a priori* parameter estimation, which is appropriate for data-scarce areas (Duan *et al*., 2006; Zhang *et al*., 2008; Kapangaziwiri and Hughes, 2008; Hughes *et al*., 2010).

2.9 Dealing with uncertainty in hydrological and hydraulic modelling

Different uncertainty frameworks are available to quantify the sources of uncertainty and facilitate parameter estimation and data assimilation (Beven and Binley, 1992; Beven and Freer, 2001; Vrugt *et al*., 2003; Wagener *et al*., 2003; Abbaspour, 2004; Moradkhani *et al*., 2005; Rubarenzya *et al*., 2007; Wagener and Kollat, 2007; Yadav *et al*., 2007; Wagener and Montanari, 2011; Kapangaziwiri *et al*., 2012). Some of these frameworks include GLUE (Beven and Binley, 1992), DYNIA (Wagener *et al*., 2003), SCEM-UA (Vrugt *et al*., 2003), BATEA (Kavetski *et al*., 2006) and SUFI-2 (Abbaspour, 2004).

The *Generalised Likelihood Uncertainty Estimation (GLUE; Beven and Binley, 1992):* The main purpose of the development of GLUE was to account for different sources of uncertainty, such as that associated with the model structure, model parameter values and model inputs in hydrological modelling. A Monte Carlo sampling technique is used to generate parameter sets from *a priori* distributions of parameter values, and likelihood measures are used to separate non-behavioural and behavioural sets. This technique is one of the most widely-applied uncertainty approaches, and an example application of this framework in data-poor basins of Africa is a study by Winsemius *et al*. (2009) in the Luangwa River basin. GLUE framework has also been applied together with the LISFOOD-FP in different studies to estimate uncertainties in the simulated inundation characteristics (e.g. Bates *et al*., 2004; Hunter *et al*., 2005b; Pappenberger *et al*., 2006; Pappenberger *et al*., 2007; Di Baldassarre *et al*., 2009). For example, Pappenberger *et al*. (2007) developed a fuzzy methodology that applied this uncertainty framework together with the LISFLOOD-FP to estimate uncertainties in the model results whereas, Hunter et *al*., (2005b) applied the framework to estimate uncertainties in the model inputs. Despite its application, other studies such as Christensen (2004), Montanari (2005), Montovan and Todini (2006) and Stedinger *et al*. (2008) have reported some drawbacks to this framework. Montovan *et al*. (2007) argued that the prediction limits derived from the GLUE tend to be different from those estimated from other classical and widely-accepted statistical methods. Moreover, there is as yet no method developed to establish the threshold values used to distinguish behavioural and non-behavioural model runs (Montanari, 2005; Blasone *et al*., 2008b; Winsemius *et al*., 2009).

The *Dynamic Identifiability Analysis (DYNIA: Wagener et al. (2003):* The main purpose of DYNIA was to reduce the effects of parameter non-identifiability through identifying the model structure and estimation of parameters that are most appropriate. The method locates periods of high identifiability for each parameter and detects the failure of the model structure (Ouyang *et al.,* 2014). Based on the uniform prior distribution of the feasible parameter space, a Monte Carlo sampling technique is used to examine the behavioural parameter space. The objective function associated with each parameter set is transformed, and the gradient of the cumulative probability distribution of the transformed values can be used to estimate the degree of identifiability of each parameter within a parameter space (Wagener *et al*., 2003). One of the strengths of this method is its ability to measure the changing levels of parameter identifiability over time, and the flexibility of choosing model performance criteria (Wagener *et al*., 2003). Moreover, this approach can be applied in any model to evaluate its structure.

Bayesian Total Error Analysis (BATEA) by Kavetski et al. (2002; 2006): The main purpose of this approach was to understand data and model uncertainties in hydrological modelling. The method identifies sources of uncertainties that affect calibration and prediction of hydrological models (Thyer *et al.,* 2009; Renard *et al.*, 2010). The method is among few frameworks that consider most of the sources of uncertainty in modelling (Ajami *et al.*, 2007). Its major strength is the ability to use the independent prior information to obtain a well-posed and useful inference, even when the data alone may not be sufficient (Kavetski *et al*., 2006a; Thyer *et al*., 2009). Conversely, the BATEA approach is computationally intensive as it includes different numerical methods. For example, Monte Carlo sampling is combined with fast Newton-type optimisation methods and Hessian-based covariance (Kavetski *et al*., 2006b).

The Shuffled Complex Evolution Metropolis (SCEM-UA) by Vrugt et al. (2003): This framework uses a Markov Chain Monte Carlo (MCMC) sampling algorithm to infer the posterior distribution of hydrological parameters. According to Efstratiadis and Koutsoyiannis (2010), SCEM-UA combines both uncertainty assessment and parameter optimisation procedures using a modified version of the Shuffled Complex Evolution (SCE-UA) method for global optimisation developed by (Duan *et al.,* 1992). The method generates explicit estimates of parameter uncertainty as well as the prediction of uncertainty bounds (Vrugt *et al*., 2003; Ajami *et al*., 2007). Moreover, SCE-UA is one of the most-used methods for the automatic calibration of hydrological models (Ndiritu, 2009).

Sequential Uncertainty Fitting, version 2 (SUFI-2) by Abbaspour et al. (2004): SUFI-2 is mainly used for uncertainty analysis and calibration in the SWAT model (Abbaspour *et al.*, 2004; 2015). It is a multi-site and semi-automated global search procedure that is used to combine parameter calibration and uncertainty predictions in the SWAT model (Schuol and Abbaspour, 2006). Generally, parameter uncertainty assessment is used to represent uncertainties from all other sources in the model, and Latin hypercube sampling is used to identify independent parameter sets (Abbaspour *et al.*, 2007; Yang *et al.*, 2008). Objective functions and parameter ranges are defined from physical understanding of the basin, and parameters are adjusted manually in an iterative mode between auto-calibration runs (Schuol and Abbaspour, 2006). The results from uncertainty and sensitivity analyses can be used to estimate optimal parameter sets depending on an understanding of the basin processes (Arnold *et al*., 2012). Among the drawbacks of the method is that a modeller is required to check the suggested posterior parameter sets; thus, there is a need to have a prior understanding of the parameters and their impacts on model outputs (Yang *et al*., 2008).

2.10 Uncertainty analysis framework for ungauged basins in the southern African region

Although it would be challenging to apply the majority of uncertainty frameworks in data-scarce areas (Hughes, 2015a), a few approaches suitable for application to these regions are available (e.g. Ao *et al*., 2006; Duan *et al*., 2006; Yadav *et al*., 2007; Kuzmin *et al*., 2008; Zhang *et al*., 2008; Yao *et al*., 2012). In recent years, uncertainty approaches for hydrological predictions in southern Africa with the GW Pitman model have been proposed (Kapangaziwiri and Hughes, 2008; Hughes *et al*., 2010; Tumbo and Hughes, 2015). The Kapangaziwiri and Hughes (2008) approach is based on the use of the basin physical and climatological characteristics (e.g. land cover, topography, geology, soils, rainfall and evapotranspiration) to establish *a priori* parameter sets using different empirical formulas and a regionalisation of the stream flow signatures used to constrain behavioural ensembles. This approach was applied in different studies within southern African basins (e.g. Kapangaziwiri *et al*., 2012; Tshimanga 2012). One of the recent approaches focused on using hydrological signatures as constraints (Hughes, 2015a; Tumbo and Hughes, 2015). The hydrological constraints used in this approach include mean monthly streamflow (MMQ), mean monthly groundwater recharge, Q10, Q50 and Q90 on the flow duration curve as well as the percent time of zero flows. The method involves two steps, as indicated in Figure 2.11. The initial step uses *a priori* parameter distributions under Monte Carlo sampling to generate ensembles for the incremental natural flows of each sub-basin, and hydrological signatures are used to constrain all possible outputs to those considered behavioural. An ensemble can be considered behavioural when its bounds fall within all established constraints. In step 2 the behavioural parameter sets are re-sampled and the entire model is run for all sub-basins linked together to generate the cumulative streamflow volumes at the outlets of all sub-basins. The final simulated flows can be further constrained using available observed data. This approach is simple and flexible and is, therefore, suitable for ungauged basins as it does not rely on the time series of observed data to establish the constraints. The approach has been successfully applied to the Great Ruaha River basin (Tumbo and Hughes, 2015), Caledon River basin (Hughes, 2015b) and five river basins in Swaziland (Ndzabandzaba and Hughes, 2017).

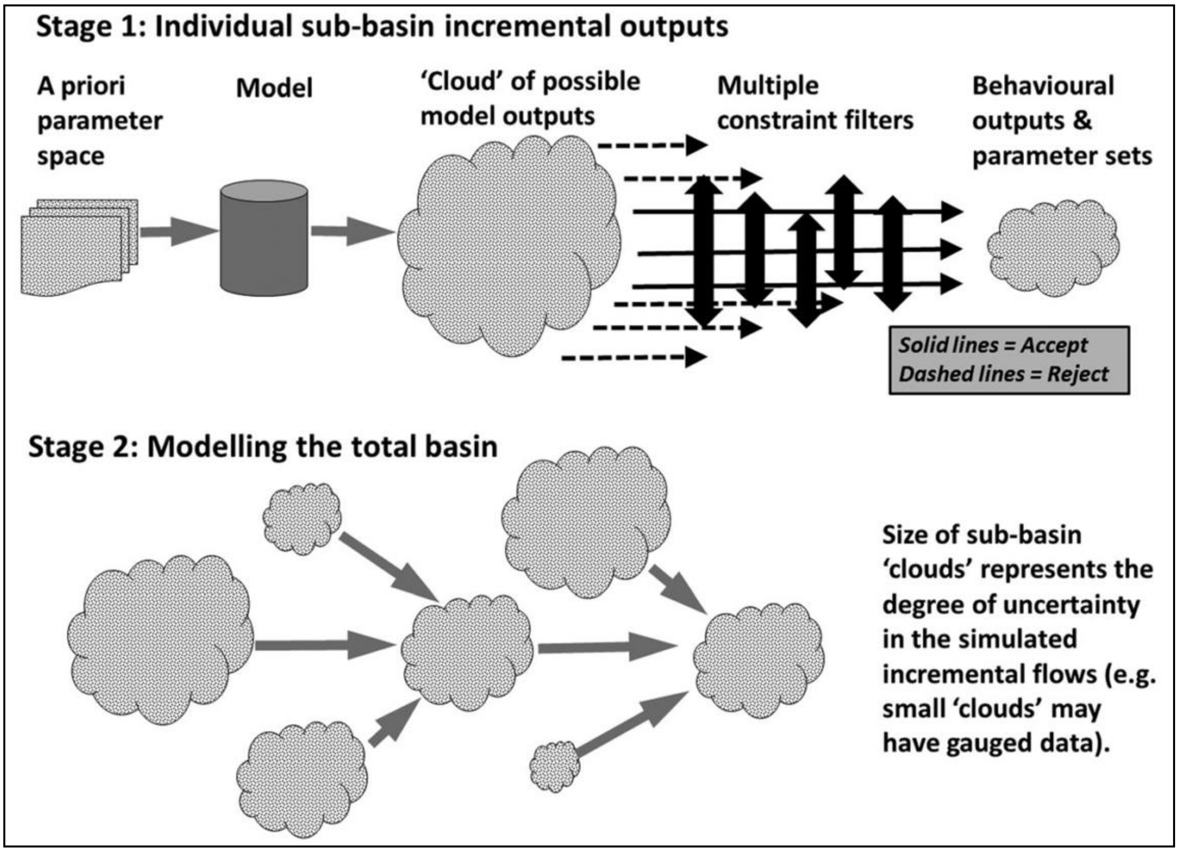

Figure 2.11: A two-stage approach to uncertainty analysis used within the GW Pitman model (Source: Hughes, 2015a).

2.11 Conclusions

In Africa, many river basins contain substantial wetland areas, and these wetlands are hydrologically connected to river channels. The total integrity of the two systems depends on how they interact. There is evidence to illustrate how upstream water resource development changes affect wetland hydrological inputs, and these impacts inevitably modify channel–wetlands exchanges as well as downstream river flow regimes. Understanding of both the impacts upstream changes have on wetlands and the channel–wetland exchanges is important to achieve sustainable management of many river basins in Africa. This chapter discusses different issues related to large wetlands and their exchanges with river channels, and different methods to quantify channel–wetland exchanges in data-scarce river basins. The literature reviewed in this chapter suggests that freely-available EO data can provide useful information for understanding wetland dynamics; however, their application is limited due to their spatial resolution and temporal coverage. Modelling approaches remain useful for understanding wetland dynamics and their influence on flow regimes at the basin scale.

Different types of basin-scale models are available for modelling different basin processes; however, in large wetlands, the details captured in these models cannot effectively represent the interactions of these wetlands with river channels. As a result, calibration of these models in large wetlands is very difficult and does not provide satisfactory model simulations. The available detailed hydraulic models can provide information related to wetland dynamics, and this information can be used to establish parameters required in basin-scale models. For example, Wen *et al.* (2013b) applied a MIKE FLOOD hydrodynamic model to understand wetland dynamics and used the simulated results (i.e. water level, inundation area and relationship between stream and wetlands and among wetlands) to estimate data and parameters required in the Integrated Quality and Quantity Modelling (IQQM) hydrological model in the Macquarie floodplain in Australia. Therefore, the approach that uses both hydraulic and basin-scale models to model the influences of large wetlands on river flow regime is suitable for river basins that include large wetlands.

CHAPTER THREE: BASIN CHARACTERISTICS, DATA SOURCES AND QUALITY

The physical and climatic settings (e.g. rainfall, evapotranspiration, topography, slope, geology, and land cover) influence basin processes including the generation of runoff. Physical characteristics determine the understanding of hydrological processes that is used to derive different model parameters, whereas rainfall and evapotranspiration are the main inputs for most hydrological models. Although these characteristics are generally important for the modelling process, in the southern African region they are frequently not available. Global datasets provide alternative data sources to understand the different characteristics and processes in basins and have been applied in different studies in this region (e.g. Kashaigili, *et al*., 2006; Winsemius *et al*., 2009; Tshimanga *et al*., 2011; Neal *et al*., 2012; Hughes and Slaughter, 2015; Tumbo and Hughes, 2015; Masafu, 2016; Kossi, 2017). Some of the global datasets include the SRTM (Farr and Kobrick, 2000); the SoilGrids 1 km (Hengl *et al*., 2014); the USGS land cover (USGS LCI: Broxton *et al*., 2014); the ARC2 satellite rainfall (Novella and Thiaw, 2013); and the CRU TS v. 3.22 monthly rainfall (Harris *et al*., 2014) which provide topography, soil, land cover and rainfall data, respectively. Satellite images have also been used to detect different land cover types such as vegetation and open water bodies in many places in the southern African region and the results have been used to calibrate and/or validate models (Milzow *et al.*, 2009; Meier *et al*., 2011).

The current study focused on three basins containing large wetlands within southern Africa: 1) the Upper Zambezi River basin, 2) the Luangwa River basin, and 3) the Upper Great Ruaha River basin as indicated in Figure 3.1. The first two are part of the Zambezi River system, and the latter is part of the Great Ruaha River system in Tanzania. The southern African region is characterised by variable climatic conditions from tropical dry to humid tropical (Valimba, 2004). As a result, the three basins experience different climatic conditions depending on their spatial proximity. Apart from the climatic conditions, physical characteristics such as topography, soils, and geology vary extensively within the region. Therefore, this chapter discusses in detail the physical and climatic settings of the three selected basins and their associated wetlands using information that was obtained from local and global datasets.

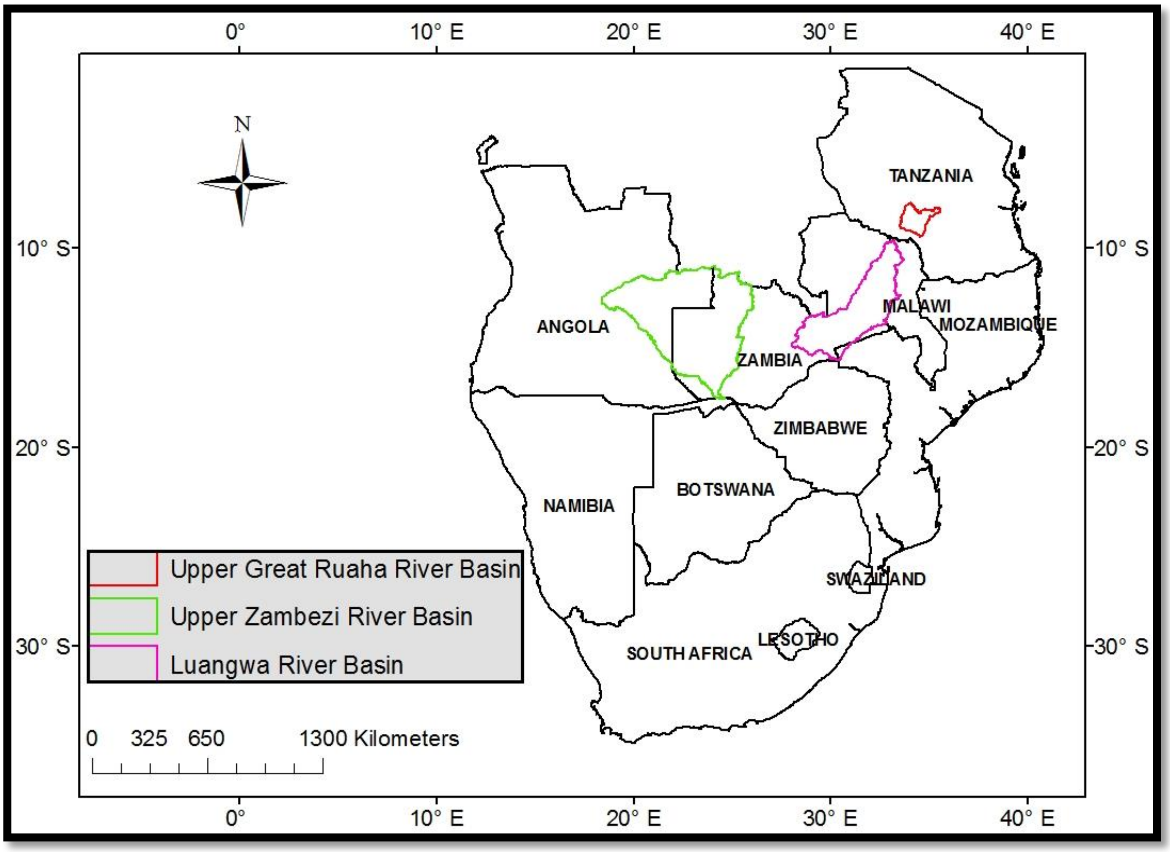

Figure 3.1: Locations of the three selected basins in southern Africa.

3.1 Summary of the datasets used in this study

Most of the data used in this study were obtained from global datasets. The topography and slope distributions were derived from the SRTM 90 m resolution dataset (Farr and Kobrick, 2000). This DEM has an absolute vertical error of 5.6 m and a relative error of 9.8 m in Africa (Rodriguez *et al*., 2006) and has been widely applied in both hydrological (e.g. Tirivarombo, 2013; Tumbo and Hughes 2015; Mohobane, 2015), and hydraulic studies (e.g. Neal *et al*., 2012; Coulthard *et al*., 2013; Schumann *et al*., 2013; Fernández *et al*., 2016) in southern Africa. The Harmonised World Soil database (HWSD) version 1.2 (Nachtergaele *et al*., 2008) and the SoilGrids 1 km (Hengl *et al*., 2014) are the most recent available global soil datasets. Despite their low spatial resolution, they provide useful information that can be used to understand soil types and soil distribution in the basins where local data are not available. Hengl *et al*. (2014) provided some limitations associated with the SoilGrids 1 km dataset such as their coarse resolution and the use of low sampling density which is not representative of the spatial variation of soils. However, in comparison to the HWSD which has not been recently updated, the SoilGrids 1 km dataset (http://soilgrids.org) is the most recent soil dataset which is automated and flexible to use (Hengl *et al*., 2014; Nachtergaele, 2014). Thus, this dataset was used to evaluate the distribution of the soil types found in the three selected basins.

Global land cover datasets that are freely available include the Global Land Cover map (GLOBCOVER: Bontemps *et al*., 2011), Global Land Cover Facility (GLCF: Channan *et al*., 2014), the Global Land Cover Characterisation (GLCC: Loveland *et al*., 2000) and the USGS Land Cover dataset (USGS LCI: Broxton *et al*., 2014). Recently, the USGS LCI has released a 0.5 km MODIS-based Global Land Cover Climatology for Africa. The dataset was prepared based on the collection of 5.1 MCD12Q1 land cover type data for 10 years starting from 2001 to 2010 (Broxton *et al*., 2014). Compared to other global datasets, such as the Global Land Cover Characterisation (GLCC) data, which were developed using one year of Advanced Very High Resolution Radiometer (AVHRR) land cover data (1992 to 1993), the USGS LCI included the variations of land cover for a period of 10 years and validated the results using high quality data (Broxton *et al.*, 2014). Therefore, USGS LCI dataset is more accurate compared to the GLCC dataset and was therefore selected to inform the understanding of the land cover in all the study basins.

Climatic data were obtained from both local and global datasets. Generally, there are a limited number of rainfall stations in these basins and, where available, they predominantly contain records with either missing values or poor quality data. Under these conditions, global rainfall datasets are the only data sources that provide continuous time series over the full spatial extent of the basins. The long-term monthly and daily rainfall data required for this study were obtained from the Climate Research Unit (CRU) at East Anglia University, UK (http://www.cru.uea.ac.uk/cru/data/hrg/cru ts 3.22/) (CRU TS v. 3.22: Harris *et al*., 2014) and the Climate Prediction Centre (CPC) within NOAA (National Oceanic and Atmospheric Administration) (ftp://ftp.cpc.ncep.noaa.gov/fews/fewsdata/africa/arc2/bin) (ARC2: Novella and Thiaw, 2013), respectively. The ARC2 dataset contains satellite-derived daily rainfall data gridded at 0.1° resolution and its records extend from 1983 to the present day (Novella and Thiaw, 2013). The CRU TS v. 3.22 (Harris *et al*., 2014) are long-term series of monthly rainfall data available at a coarse resolution (0.5° × 0.5° grids) and contain no missing values for the entire data period from 1901 to date. They were established by interpolation of available local rainfall data. However, due to the limitation of local rainfall stations in southern Africa, it is likely that the number of stations that contributed to the CRU rainfall estimation is very low in this region, thereby affecting the quality of the estimated rainfall values. The average monthly potential evapotranspiration (PET) and the mean monthly temperature data were obtained from the Climatic Data Portal within the International Water Management Institute (IWMI) (http://wcatlas.iwmi.org/) (New *et al*., 2002). These PET values were computed from the FAO Penman-Monteith equation (Allen *et al*., 1998) using 30 years of observations of temperature, humidity, sunshine and wind speed from different weather stations around the world (Droogers and Allen, 2002). The computed values are presented in a grid format at a resolution of approximately 18 km × 18 km (New *et al*., 2002). The number of stations used to compute PET varies spatially according to the climatic variables used, hence errors in the calculated PET and temperature values are expected in areas where there are a limited number of meteorological stations.

3.2 Luangwa River Basin

The Luangwa River basin (approximately $15 \times 10^4\,km^2$) is located in the eastern part of Zambia and it forms part of the Zambezi River system (Figure 3.2). This basin includes the Luangwa Rift Valley which is an extension of the Great East Africa Rift Valley (Beilfuss and Santos, 2001; Meier *et al*., 2011) and is bounded by the Nyika and the Viphya plateaus in the north and the Muchinga escarpment in the west (Ashton *et al*., 2001). The Luangwa River emerges from the north-east part of Zambia close to the Malawi border at 9°53'S and 33°20'E, and it meanders along the Luangwa Rift Valley southwards until its confluence with the Zambezi River just upstream of the Cahora Bassa Dam in Mozambique (Figure 3.2). In the middle section of the Luangwa Rift Valley, the river flows across a large floodplain characterised by different floodplain features including old infilled channels, anabranches, small depressions and ox-bows (Gilvear *et al*., 2000). These features may influence the flow dynamics of the Luangwa River. While a number of hydrological studies have been conducted in the Luangwa River basin (e.g. Winsemius *et al*., 2008; 2009; Meier *et al*., 2011), to the best knowledge of the author, there is no detailed study that has attempted to understand the influence of the Luangwa floodplain on the flow regime of the Luangwa River. The information on the factors that affect the flow regime of the Luangwa River is important not only for the operation of the Cahora Bassa Dam (Winsemius *et al*., 2008; Beilfuss, 2012; Kling *et al*., 2014), but also for the reduction of flood impacts downstream (Hrachowitz *et al*., 2013).

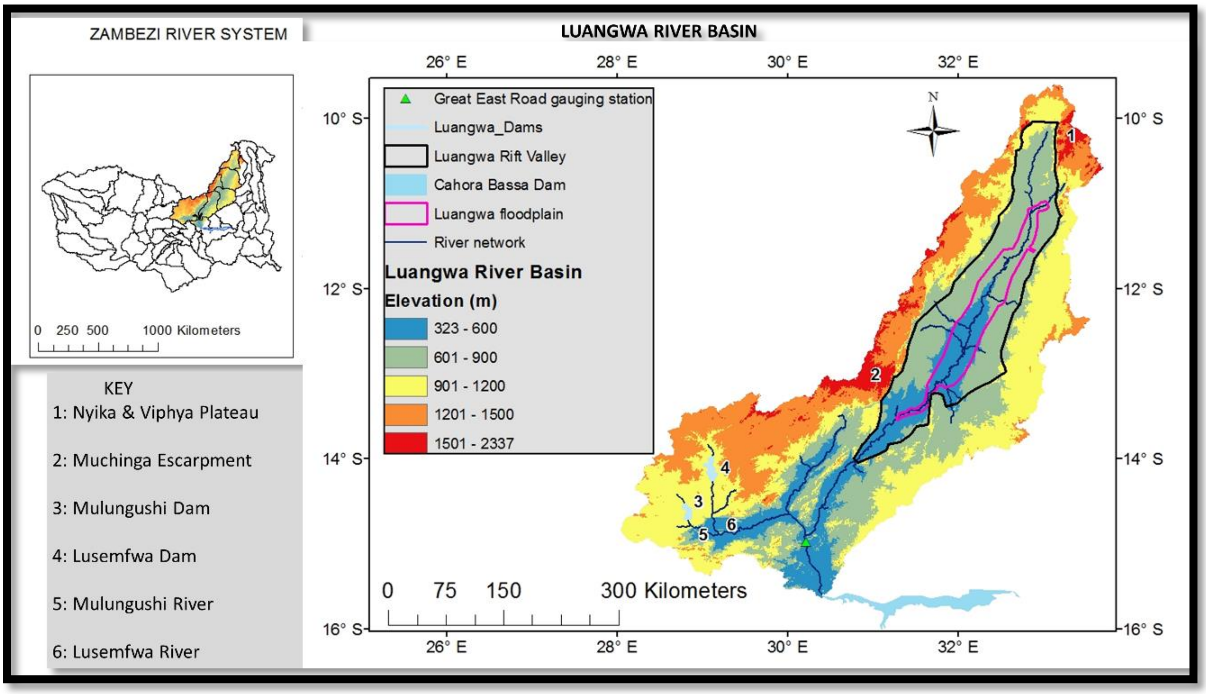

Figure 3.2: Location of the Luangwa River basin in the Zambezi River system.

3.2.1 Topography and slope

Topography is regarded as the first-order control of the hydrological response in basins (Sørensen *et al*., 2006; Milzow *et al.*, 2009). In most cases, topography influences channel origins and the spatial distribution of the climatic variables such as rainfall, temperature and evaporation, whereas slope guides both the surface and the subsurface movement of water in a basin (Jarvis *et al*., 2004; Dennis and Dennis, 2012). Topography can also influence the movement and spatial variation/distribution of water in the wetlands. Sichingabula (1998) classified the topography of the Luangwa River basin into six zones: 1) escarpment, 2) hills, 3) ridges and undulating surfaces, 4) plains and pans, 5) old alluvial zone, and 6) floodplain. Figure 3.2 and 3.3 present the topography and the slope distributions of the Luangwa River basin, respectively. Following the FAO slope classes (Table 3.1) (Jahn *et al*., 2006), high elevated areas such as the Muchinga escarpment and the Nyika plateau are classified as sloping to moderately sloping areas (i.e. slope values between 10% and 30%), whereas the Luangwa Rift Valley has low elevation values (mostly 254 m to 900 m) and slope values between 0% and 2%. The transitional areas between the highlands and the valley are characterised by the highest slope values (>31%).

Table 3.1: FAO slope classification

Class	Description	%
1	Flat	0-0.2
2	Level	0.2-0.5
3	Nearly level	0.5-1
4	Very gently sloping	1-2
5	Gently sloping	2-5
6	Sloping	5-10
7	Strongly sloping	10-15
8	Moderately steep	15-30
9	Steep	30-60
10	Very steep	>60

Modified from Jahn *et al*. (2006)

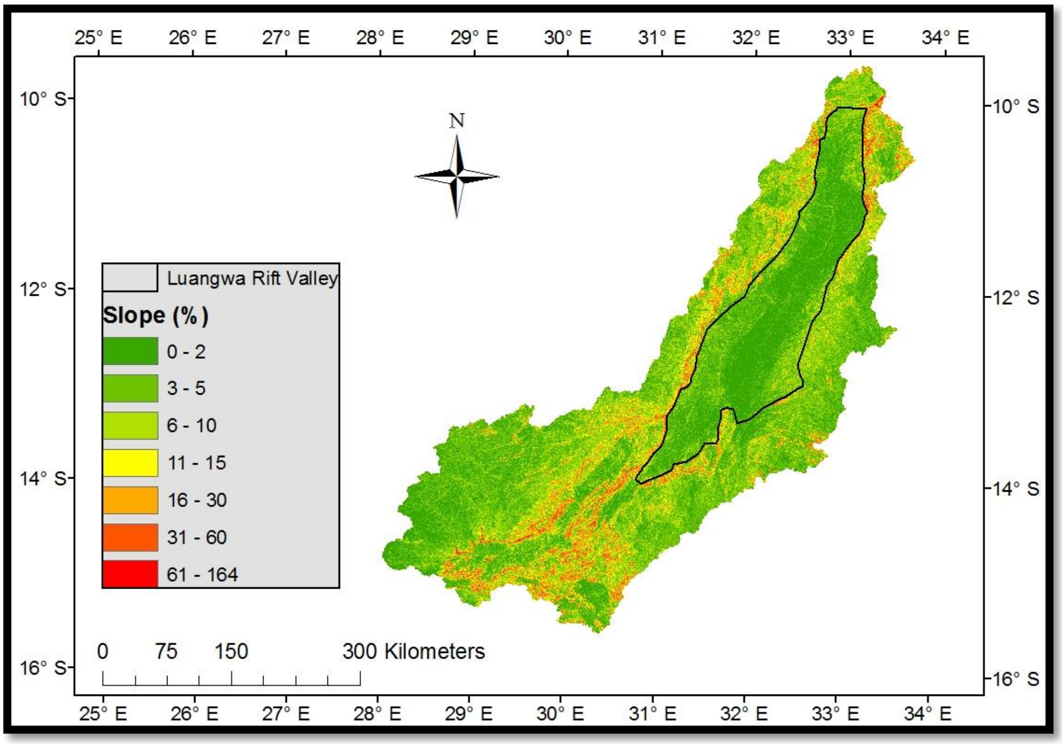

Figure 3.3: Slope characteristics of the Luangwa River basin.

3.2.2 Geology and soil characteristics

Geological and soil characteristics influence surface and subsurface flow patterns and the distribution of the basin vegetation. The geology of the Luangwa River basin is characterised by Permian-Carboniferous, Jurassic-Carboniferous, Paleozoic-Precambrian (Persits *et al*., 2002) and Karoo age sediments including sandstone, siltstone, mudstone and grit along the Luangwa Rift Valley (Astle *et al*., 1969; Gilvear *et al*., 2000; Van Straaten, 2002; Nyirenda, 2012). The fault scarp is characterised by hard crystalline, igneous and metamorphic rocks of

Pre-Cambrian age (Astle *et al*., 1969), whereas the plateaus are dominated by quartzite, sandstones, granites and gneisses underlain by sedimentary rocks (Ashton *et al*., 2001).

Ashton *et al*. (2001) grouped the soils of this basin into three groups: 1) moderately deep, well-leached feralitic soils dominating the northern, western and southeastern parts; 2) moderately deep sandy soils derived from quartzite, sandstones and alluvial material dominating the floor of the Luangwa Rift Valley; and 3) moderately deep, sandy loams particularly in areas underlain by limestone deposits. Figure 3.4 illustrates the distribution of the soil types found in the Luangwa River basin derived from the SoilGrids 1 km dataset. Ferralsols, Cambisols and Rigosols cover about 79% of the basin. Most of the highlands are covered by Ferralsols which are physically stable, deep and strongly weathered soils. The Regosols dominate large areas of the Luangwa Rift Valley, whereas the Arenosols dominate the upper sections of this valley. The Cambisols are weak and moderately developed soils whereas the Regosols are soils with very limited development that are of alluvial origin (Meek *et al*., 2016; Chesworth *et al*., 2016).

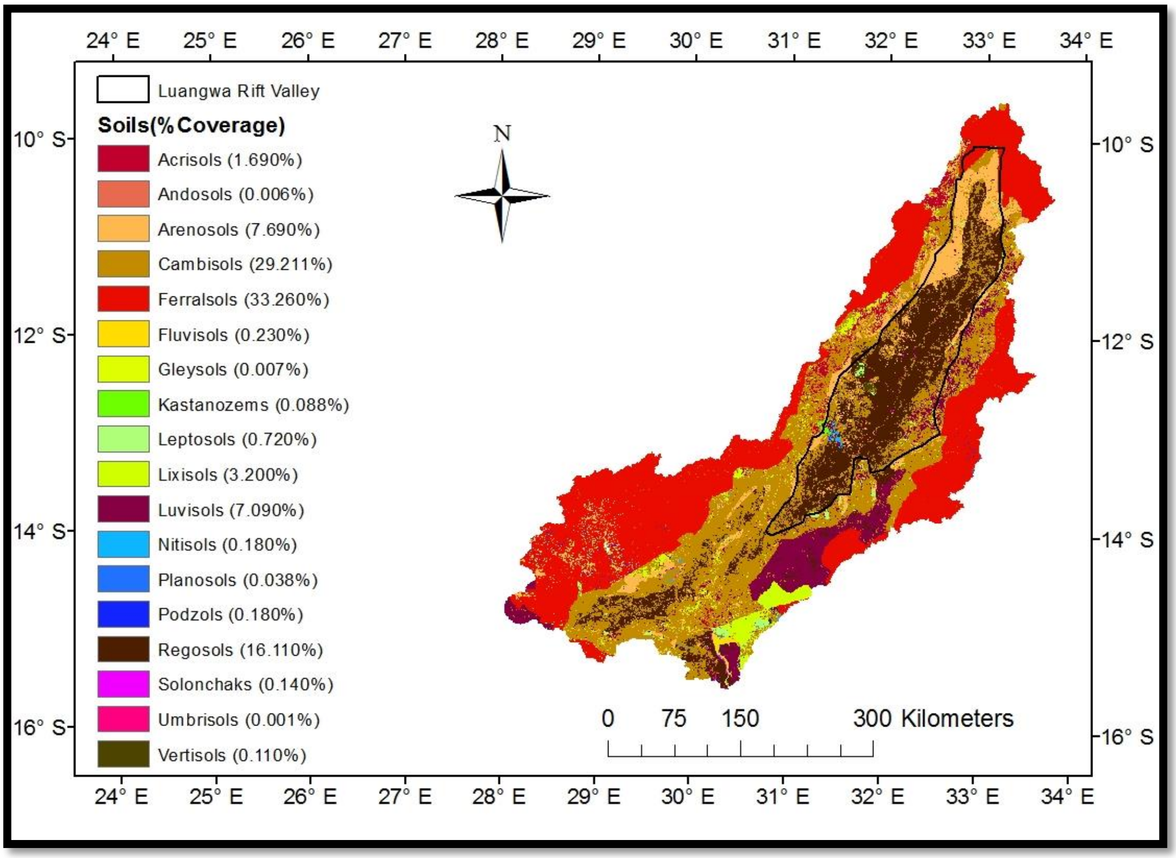

Figure 3.4: Soil distribution in the Luangwa River basin (Source: Hengl *et al.*, 2014).

3.2.3 Land cover and land use

Land cover and land use control basin processes such as infiltration and evapotranspiration, thereby influencing the basin water balance. A detailed classification of land cover in the Luangwa River basin was documented by Astle *et al*. (1969). However, due to land cover changes, including self-modification of the river morphology as reported by Gilvear *et al*. (2000), it is important to understand the recent distribution of land cover in this basin. The land cover types displayed in Figure 3.5 show that wood-savannas dominate the highly elevated areas particularly in the north-west and western parts of the basin, while the Luangwa Rift Valley is characterised by a mixture of savanna types (e.g. Miombo-Mopane, Acacia-Combretum, Faidherbia-Combretum, and riparian woodland; Timberlake, 2000; Nyirenda, 2012). Permanent wetlands occupy 0.04% of the total basin area and are mostly located in the Luangwa Rift Valley. The main land use activities in this basin include tourism especially in the South and North Luangwa National Parks (located within the Luangwa Rift Valley), subsistence agriculture in rural areas, commercial farming such as maize and tobacco, as well as livestock rearing (Ashton *et al*., 2001).

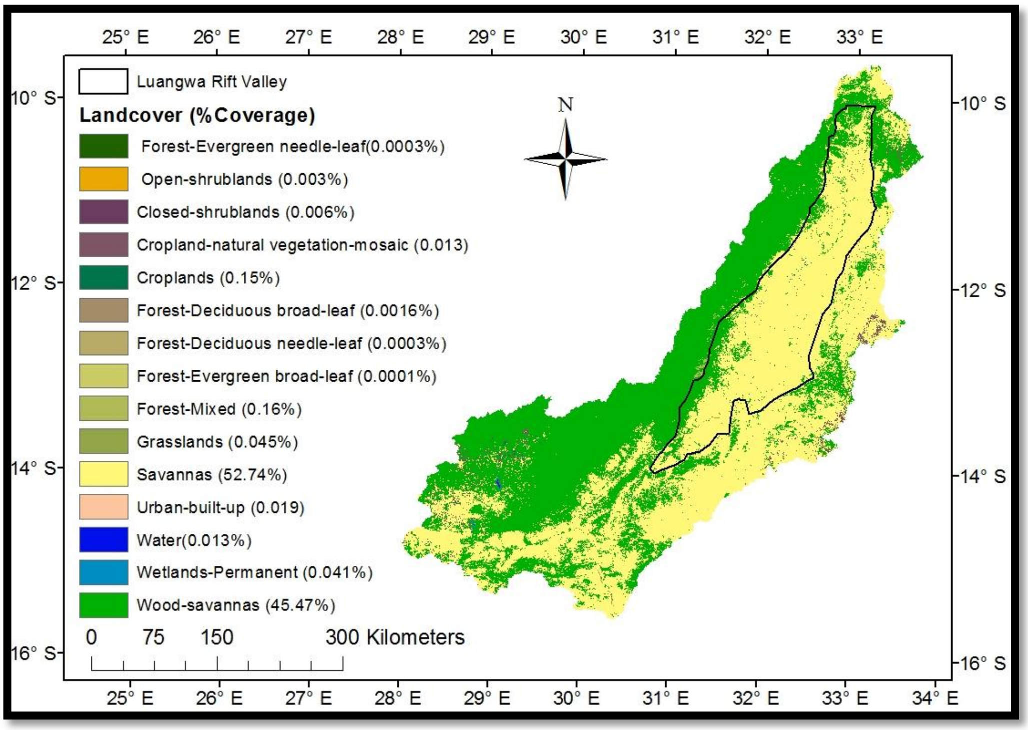

Figure 3.5: Land cover distribution in the Luangwa River basin (source: Broxton *et al*., 2014).

3.2.4 Climate

A large part of the Luangwa River basin is located in Zambia whose climatic variables (e.g. temperature and rainfall) are highly influenced by altitude (Musambachime, 2016). Within the Luangwa River basin, the Luangwa Rift Valley experiences higher mean daily temperature (>38°C) than the surrounding plateau areas (e.g. Nyika) which are the coldest areas. October is the hottest month and July is the coldest month. Rainfall is highly controlled by the movement of the Inter-Tropical Convergent Zone (ITCZ), which occurs when the moist Congo air mass encounters the humid air from the South East Trade winds (Beilfuss and dos Santos, 2001; Musambachime, 2016). There are three dominant climatic seasons: cool dry (April to August), hot dry (September to October), and warm wet season (November to April) (Winsemius *et al*., 2008; Nyirenda *et al*., 2013). The southward movement of the ITCZ marks the beginning of the rainy season in the Luangwa basin especially starting from November. The dry season starts when the ITCZ reverses its movement towards the north around April (Musambachime, 2016). Considerable spatial and temporal variation in rainfall has been reported (Nyirenda *et al*., 2013; Tirivarombo, 2013). Tirivarombo (2013) noted that there is evidence of inter-annual rainfall variation in the Luangwa River basin which is related not only to change in the position of the ITCZ but also to the El Niño Southern Oscillation and La Niña (cold phase). For example, the El Niño in 1997/98 caused severe droughts in the surrounding region which resulted in significant reduction in stream flow in the Luangwa River (Beilfuss and Santos, 2001).

3.2.4.1 Rainfall

The monthly and daily rainfall data from the CRU TS V. 3.22 (Harris *et al*., 2014) and the ARC2 (Novella and Thiaw, 2013) were used in this study but in order to assess the reliability of these datasets, the rainfall estimates were compared with rainfall records from the local stations. A comparison was made between the annual rainfall values from local gauging stations and the CRU data for a similar period. Daily data are used in disaggregation of monthly to daily flows; where only the rainfall frequencies are used (see section 4.4 and Slaughter *et al.*, 2015). Thus, there was no need to evaluate the daily rainfall magnitudes. Figure 3.6 illustrates the location of the local rainfall gauging stations and the respective CRU grids, and a comparison of annual rainfall from the local and the nearest CRU grid is shown in Figure 3.7. The relationship was fitted by a linear curve, and the results indicated high values of coefficient of determination (R^2) ($R^2 > 0.7$). Despite some differences, this analysis indicated that the rainfall data from CRU TS can be used for this study.

The long-term mean monthly rainfall data from area-averaged CRU monthly data for selected sub-basins were used to understand the rainfall seasonality in the Luangwa River basin. The seasonal analysis indicated that the Luangwa River basin receives a unimodal type of rainfall (Figure 3.8). Monthly peak values greater than 200 mm month^{-1} are experienced in the high elevated areas such as the Muchinga escarpment in the west. Moreover, the spatial variations of the annual rainfall indicate a considerable decrease in rainfall from mountainous areas (north and north-east) toward the centre of the Luangwa Rift Valley. These variations have been reported by other researchers such as Beilfuss and Santos (2001), Nyirenda (2012) and Nyirenda *et al*. (2013).

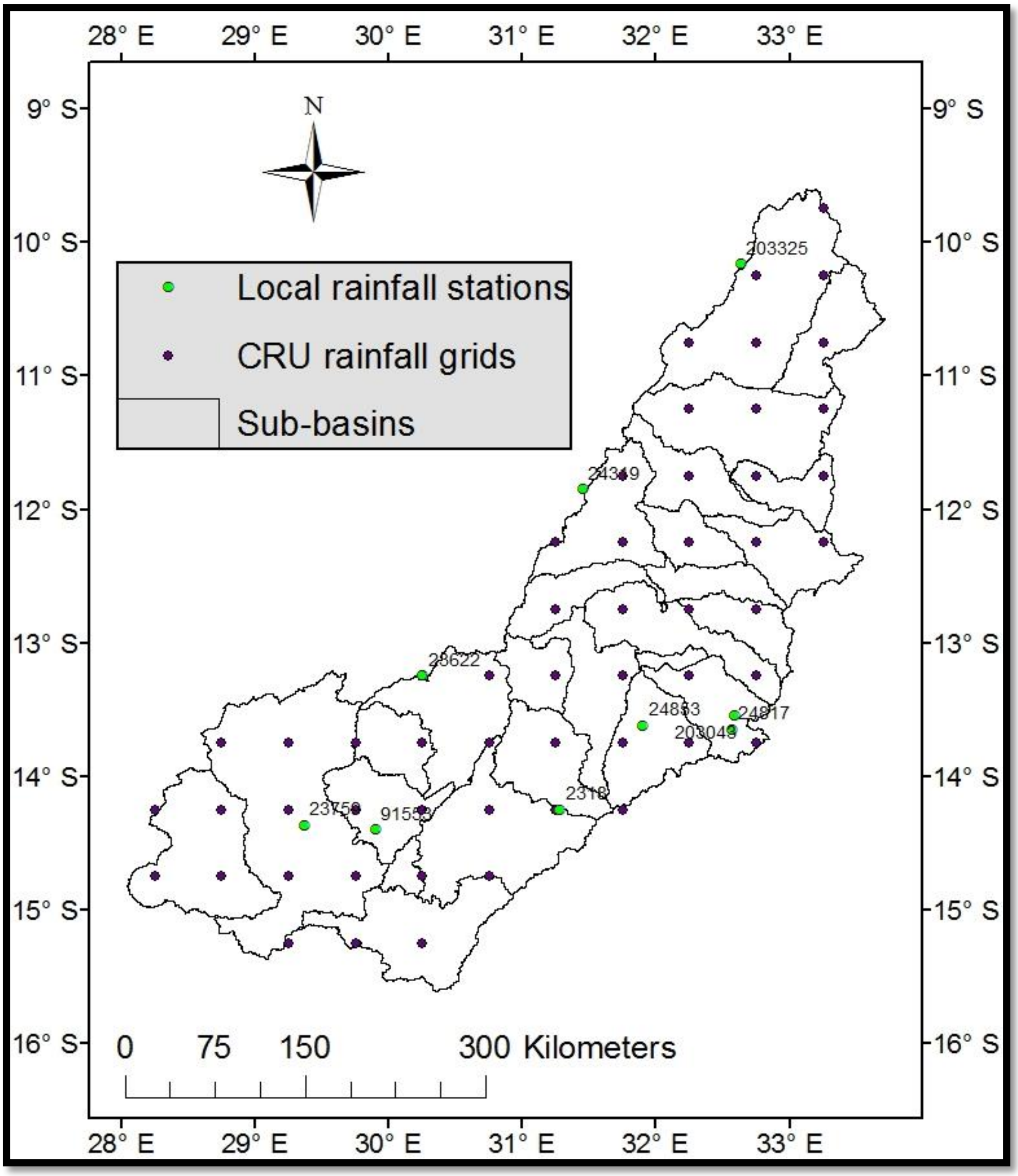

Figure 3.6: Location of the CRU TS 3.22 grids and the local rainfall stations in Luangwa River basin.

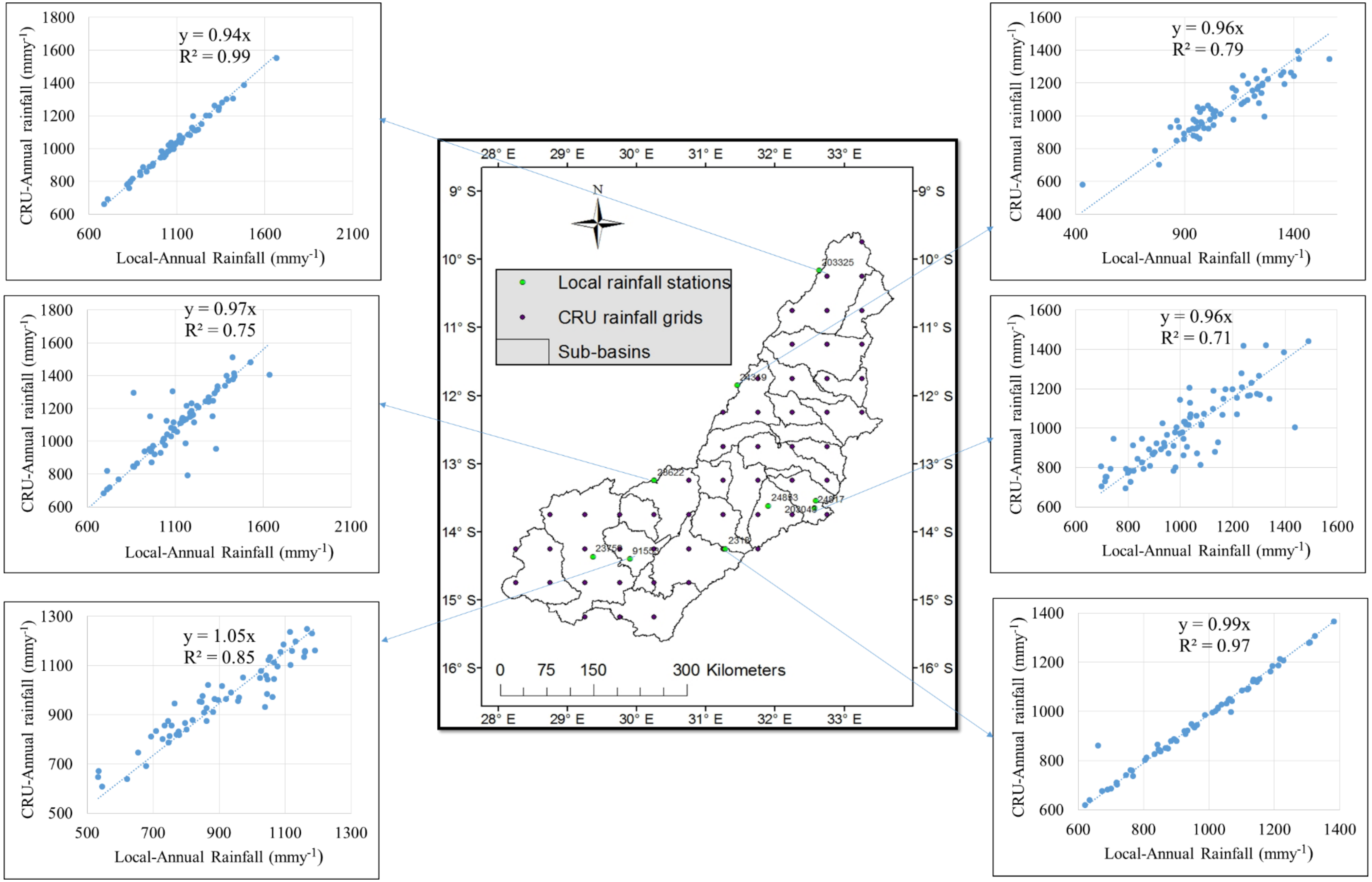

Figure 3.7: Comparison of the annual rainfall values between the CRU grids and some of the available local rainfall gauging stations in the Luangwa River basin.

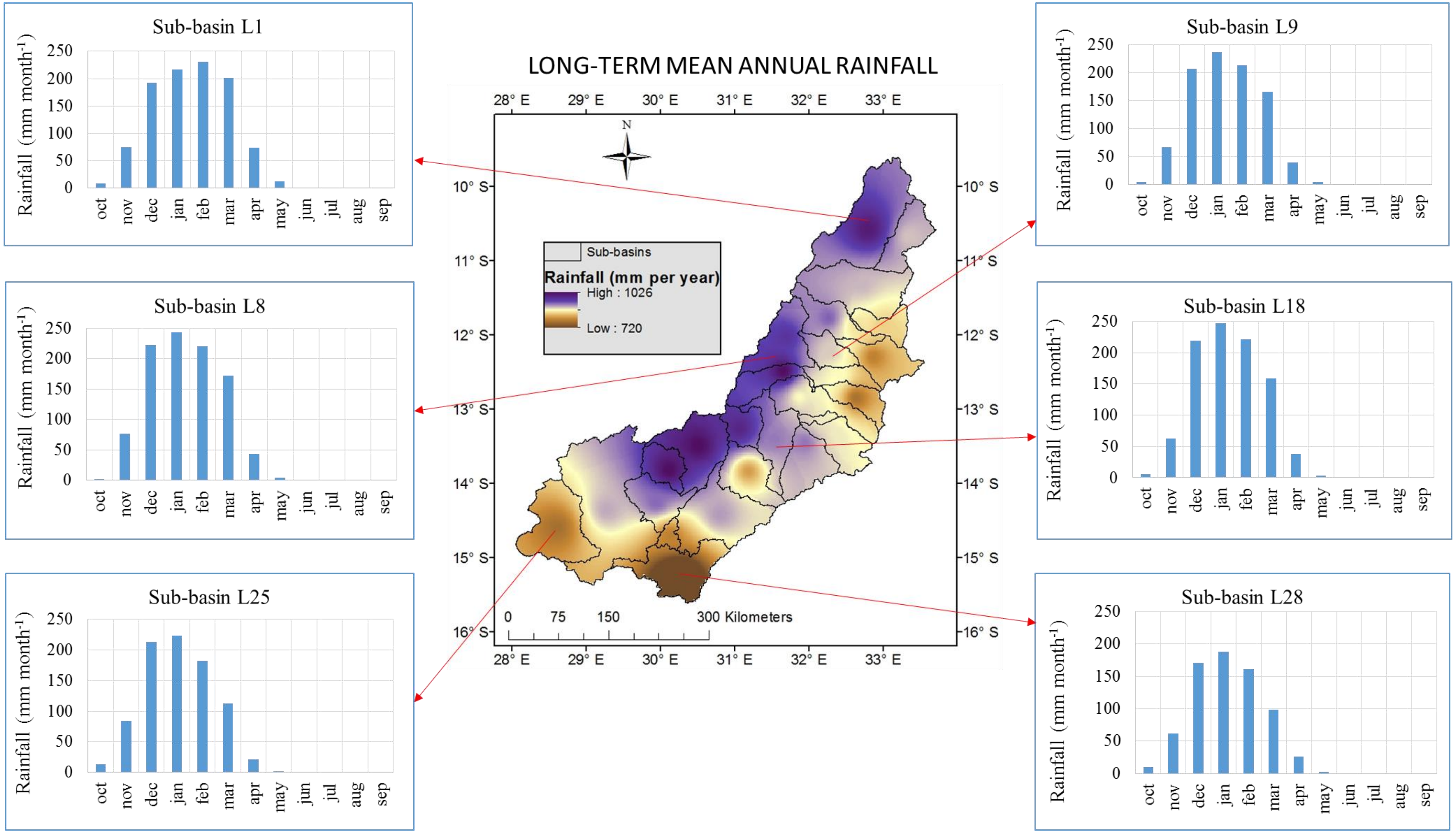

Figure 3.8: Rainfall seasonality and the spatial variation of the mean annual rainfall for some of the sub-basins in the Luangwa River basin.

3.2.4.2 Temperature and potential evapotranspiration (PET)

The minimum and maximum mean temperatures in the area are 15^{o}C (June to July) and 36^{o}C (October), respectively (Nyirenda *et al*., 2012). In October, the Luangwa Rift Valley experiences higher temperatures of up to 38^{o}C whereas high elevated areas have temperatures between 25^{o}C and 30^{o}C (Nyirenda *et al*., 2013). Figure 3.9 indicates the spatial variation of the mean annual temperatures from the IWMI Climatic Data Portal (New *et al*., 2002). There is not a significant variation in the mean annual temperature in this basin, although somewhat higher temperature values have been recorded along the Luangwa Rift Valley (central part) and further downstream, suggesting the reason for the higher evapotranspiration rates in these areas (Ashton *et al*., 2001). The mean monthly potential evapotranspiration data were obtained from the IWMI Climatic Data Portal (New *et al*., 2002). September, October and November contribute more to annual evapotranspiration (≥ 9.4%) than other months (Table 3.2). However, the October contribution to the annual value is the highest in all sub-basins (≥ 12%) and this can be related to the higher temperatures and low rainfall experienced during this month. Generally, the mean annual potential evapotranspiration for the Luangwa River sub-basins ranges between 1 476 mm y^{-1} and 1 756 mm y^{-1} (Table 3.2). Figure 3.10 shows the spatial variation of the mean annual potential evapotranspiration and indicates that the central and lower parts of the basin are characterised by higher potential evapotranspiration compared to the other parts of the basin.

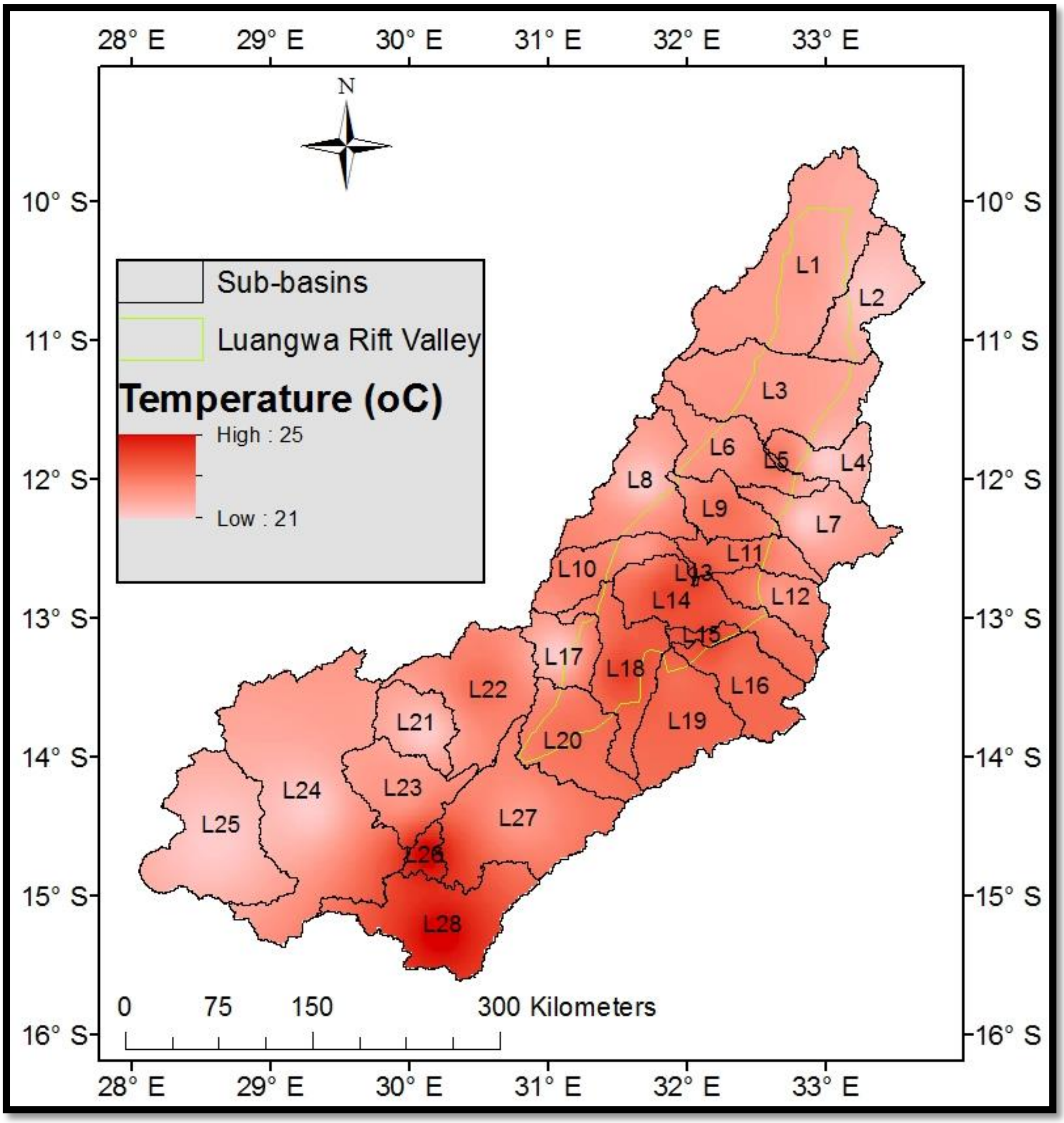

Figure 3.9: Variation of the mean annual temperature in the Luangwa River basin.

Table 3.2: Sub-basin mean monthly potential evapotranspiration (PET) in the Luangwa River basin

Sub-basin	Potential evapotranspiration (mm month^{-1})												Annual (mm)
	Oct	Nov	Dec	Jan	Feb	Mar	Apr	May	Jun	Jul	Aug	Sept	
L1	195	153	118	109	101	117	115	117	112	126	152	182	1598
L2	200	166	123	110	102	117	114	114	109	122	147	178	1600
L3	195	152	114	104	97	112	111	111	103	118	144	175	1536
L4	204	171	125	114	105	119	116	116	105	116	142	177	1608
L5	180	150	109	99	90	100	99	100	90	97	127	153	1497
L6	203	152	114	104	97	112	111	111	103	118	144	175	1536
L7	201	172	127	115	109	125	120	120	110	122	150	189	1669
L8	198	159	115	108	102	118	115	115	104	116	145	182	1593
L9	201	172	127	115	109	125	120	120	110	122	150	189	1669
L10	200	147	107	103	97	110	107	109	98	111	140	171	1486
L11	201	172	127	115	109	125	120	120	110	122	150	189	1669
L12	201	172	127	115	109	125	120	120	110	122	150	189	1669
L13	201	172	127	115	109	125	120	120	110	122	150	189	1669
L14	201	172	127	115	109	125	120	120	110	122	150	189	1669
L15	200	186	139	125	114	134	127	123	111	125	158	197	1756
L16	200	186	139	125	114	134	127	123	111	125	158	197	1756
L17	201	148	111	105	98	111	107	105	95	108	138	172	1479
L18	201	148	108	105	98	111	106	105	95	108	137	171	1477
L19	201	148	111	105	98	111	107	105	95	108	138	172	1479
L20	201	148	108	105	98	111	106	105	95	108	137	171	1477
L21	197	147	114	109	100	115	111	108	96	108	138	169	1497
L22	197	147	114	109	100	115	111	108	96	108	138	169	1497
L23	198	153	121	118	105	119	115	107	96	109	140	175	1550
L24	190	150	118	113	102	116	110	102	92	104	137	169	1551
L25	192	152	120	117	105	119	111	103	94	103	138	170	1563
L26	198	171	131	126	113	130	121	115	101	115	150	186	1663
L27	213	189	146	138	122	139	131	121	105	121	156	201	1699
L28	205	181	139	131	116	133	123	113	97	111	148	188	1679

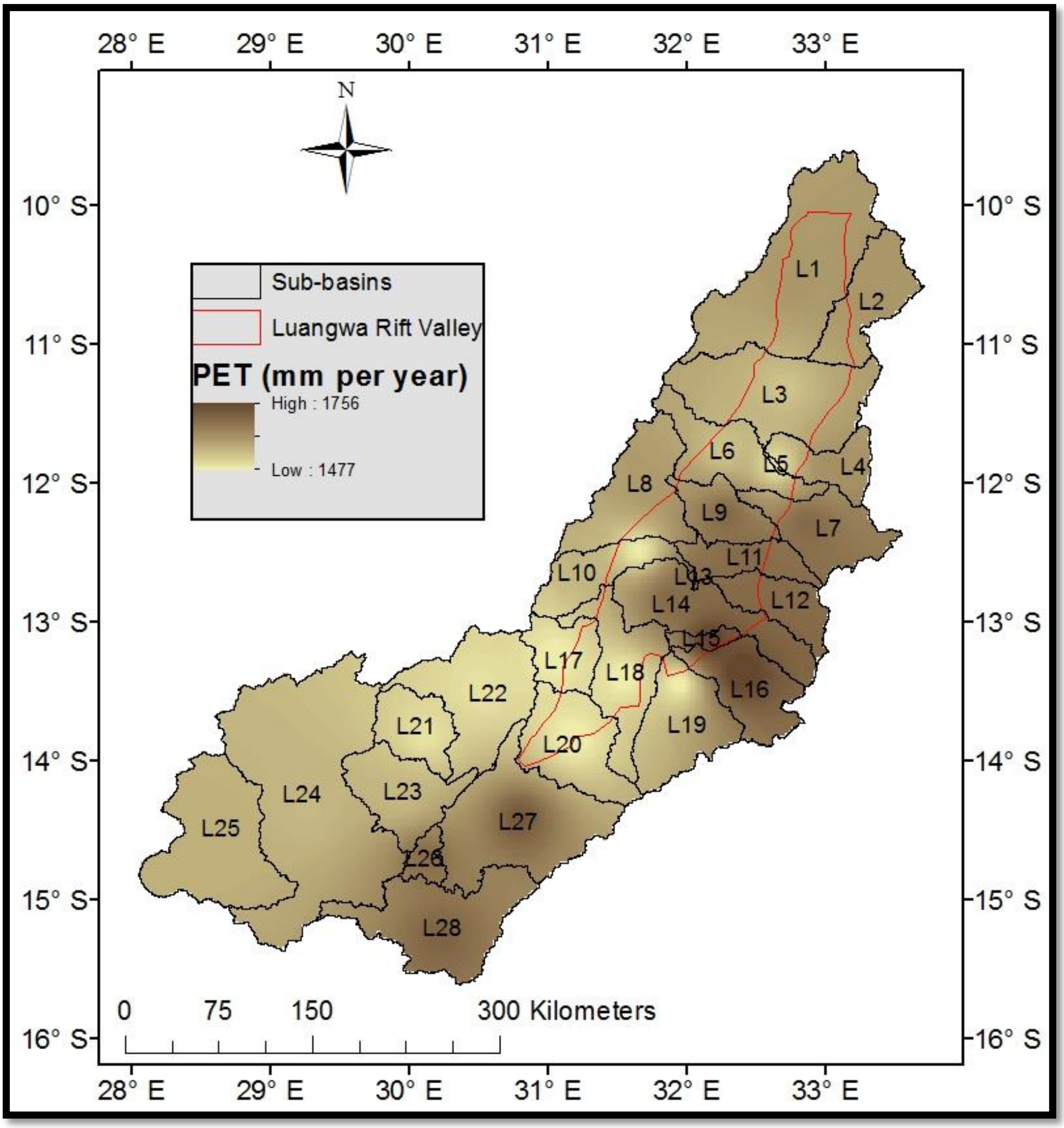

Figure 3.10: Variation of the mean annual potential evapotranspiration (PET) in the Luangwa River basin.

3.2.4.3 Streamflow

The Luangwa River, which meanders along the Luangwa Rift Valley, is mainly characterised by a sand-bed (Gilvear *et al*., 2000). It receives water from perennial and non-perennial tributaries draining from highly elevated areas including the escarpment (Winsemius *et al.*, 2009; Meier *et al*., 2011). The Lusemfwa River is the major tributary of the Luangwa River which drains an area of about 44×10^3 km^2 (see Figure 3.2). The Lusemfwa River joins the

Luangwa River a few kilometres before the confluence with the Zambezi River (Beilfuss and Santos, 2001). The Luangwa River basin is divided into 28 sub-basins and their areas are presented in Table 3.3.

There is a single gauging station on the Luangwa River (Great East Road station or L28 in this study) located at 14.9°S and 30.2°E close to its confluence with the Zambezi River (Figure 3.2). This gauging station measures the river discharge generated from an area of about 95% of the whole Luangwa River basin. The accessed data record is from 1930 to 1991, which has no missing data. Based on the monthly flow data from this station, the streamflow displays a unimodal pattern with the rising limb starting in mid-November and peaking in February (1 860 $m^3 s^{-1}$). The rising limb of the hydrograph responds quickly to the peak rainfall amounts, and the recession limb starts rapidly from March until May and then decreases slowly up to September (Figure 3.11). The calculated mean annual runoff for the record period (1930 – 1991) is 18×10^9 m^3 with an annual coefficient of variation (CV) of 0.46 which indicates a year-to-year variation of the annual runoff.

Table 3.3: Catchment areas for sub-basins in the Luangwa River basin

Sub-basin ID	Area (km^2)	Sub-basin ID	Area (km^2)
L1	12742	L15	668
L2	4465	L16	4478
L3	9168	L17	2841
L4	2744	L18	5339
L5	86	L19	5482
L6	4647	L20	5426
L7	4710	L21	3164
L8	6150	L22	7231
L9	2837	L23	4571
L10	3490	L24	19235
L11	2645	L25	8762
L12	3063	L26	997
L13	29	L27	9633
L14	5950	L28	7617

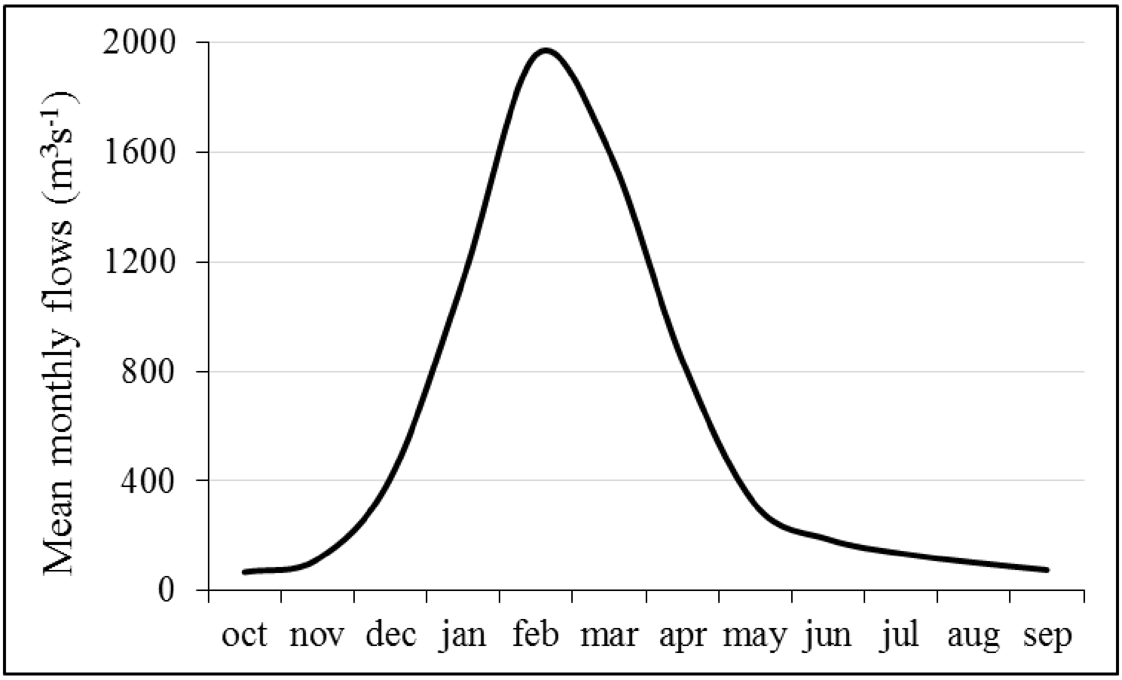

Figure 3.11: Mean monthly hydrograph for the Great East Road station (L28) in the Luangwa River basin.

3.2.5 Water use

Generally, water is abstracted for domestic, industrial and agricultural use as well as the generation of Hydro Electric Power (HEP). A large part of the Luangwa River basin is dominated by rural populations, hence abstraction for domestic uses is minimal (Ashton *et al*., 2001). There are two main HEP dams linked to the Lusemfwa and the Mulungushi tributaries (Figure 3.2). The two tributaries join the Luangwa River a few kilometres upstream of its confluences with the Zambezi River, hence they have no direct impact on the Luangwa floodplain which is located on the middle section of the Luangwa River basin. The Mulungushi Dam has a surface area of 31 km^2 and a storage capacity of 49.6×10^6 m^3 whereas the values for Lunsemfwa Dam are 45 km^2 and 72×10^6 m^3 (Figure 3.12) (Imasiku and Feilberg, 2012).

Figure 3.12: Mita-Hills or Lusemfwa Dam (Source: https://www.snpower.com/history/entering-3-new-markets-article757-271.html).

The irrigation area in the Luangwa River basin is approximately 101 km^2 with 91 km^2 along the Lusemfwa tributary and the rest in the eastern part of the basin (World Bank, 2010). Beilfuss (2012) and Spalding-Fecher *et al*. (2014) reported that about 120×10^6 m^3yr^{-1} of water (i.e. less than 1% of the mean annual runoff) is abstracted for irrigation purposes in the entire basin. Water abstractions from small dams and weirs have been reported (World Bank, 2010), however, there is no reliable information on how they are operated. Figure 3.13 illustrates some patches of the irrigation land in the Luangwa River basin. Although there are HEP and irrigation farms, their impacts on the total annual runoff of the Luangwa River basin are considered to be minimal (Beilfuss, 2012).

Figure 3.13: Google Earth image showing some irrigation farms in the Luangwa River basin.

3.2.6 Luangwa floodplain

The floodplain is located along the Luangwa Rift Valley and it has been included in the list of wetlands of international importance (Ramsar site) since 2007. The Luangwa floodplain also includes the South and North Luangwa National Park, as well as various game reserves (Ramsar, 2007). The Luangwa floodplain is approximately 340 km in length and covers an area of about 2 500 km^2 (Euroconsult, 2008; Meier *et al*., 2011) and its width varies between 5 and 12 km. The inundation characteristics (i.e. extent and depths) are influenced by the topographical and morphological settings of the area between the river channels and the floodplain. For example, the middle section is wide with minor topographical variation, whereas the top and bottom sections tend to be narrow and somewhat steep. Most of the Luangwa River tributaries that originate from steep areas are responsible for the inundation of the floodplain. Thus, the Luangwa floodplain responds quickly to flooding water at the beginning of the wet season and depending on the local topography setup, water diffuses throughout the floodplain, and returns back to the main channel through different channels found in the floodplain.

Generally, a large part of the floodplain is seasonally inundated with the exception of a few meander cut-offs and other depressions (Hughes and Hughes, 1992; Ashton *et al*., 2001). For example, there are various lodges and camping sites along the floodplain, and some of them are adjacent to the main river (Figure 3.14). Figure 3.15 and 3.16 show a meander section of the Luangwa River during the wet and the dry seasons. During the wet season, water in the main channel is at bank height and the floodplain is inundated. In the dry season, the main channel in this section has low flow, and most of the floodplain areas are dry except for some areas with shallow water depths. The floodplain vegetation is sparse and includes a variety of species such as grasses, herbs, riparian and Miombo woodland, *Berchemia discolor*, *Breonadia salicina*, *Diospyros mespiliformis*, *Trichilia emetic*, Mopane African ebony, and *Acacia albida* (Hughes and Hughes, 1992; Gilvear *et al*., 2000; Ramsar, 2007).

Figure 3.14: Google Earth image showing lodges and camping sites on the Luangwa floodplain.

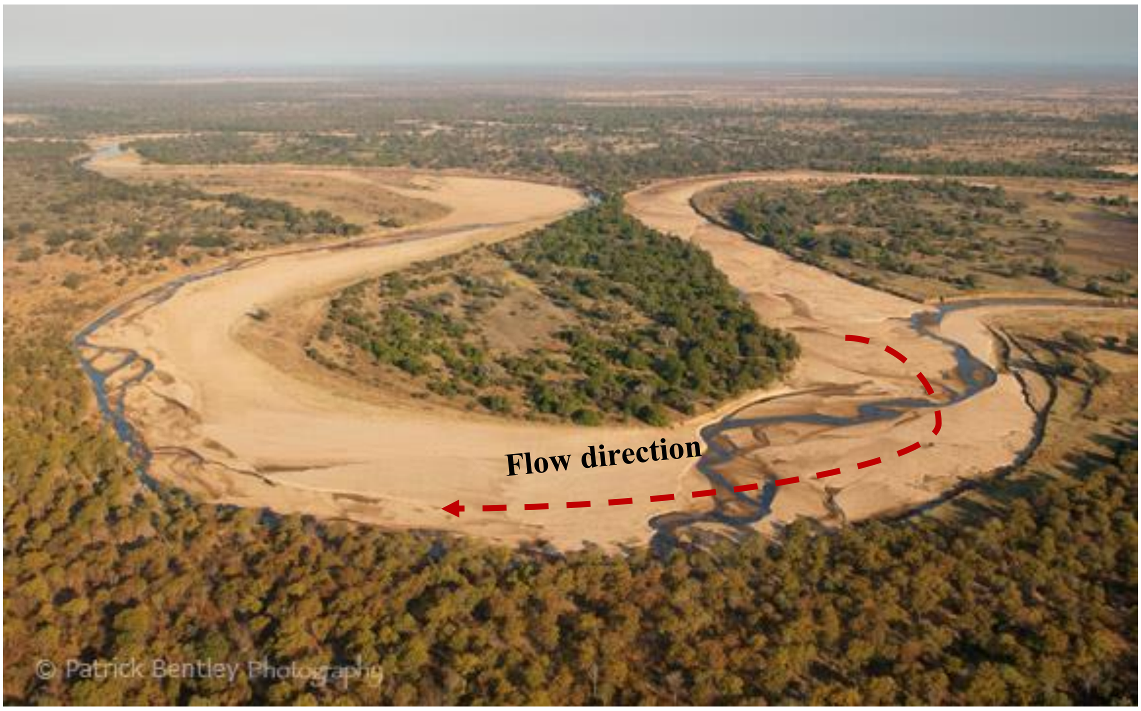

Figure 3.15: The Luangwa River in the dry season (Source: http://www.patrickbentley.com/).

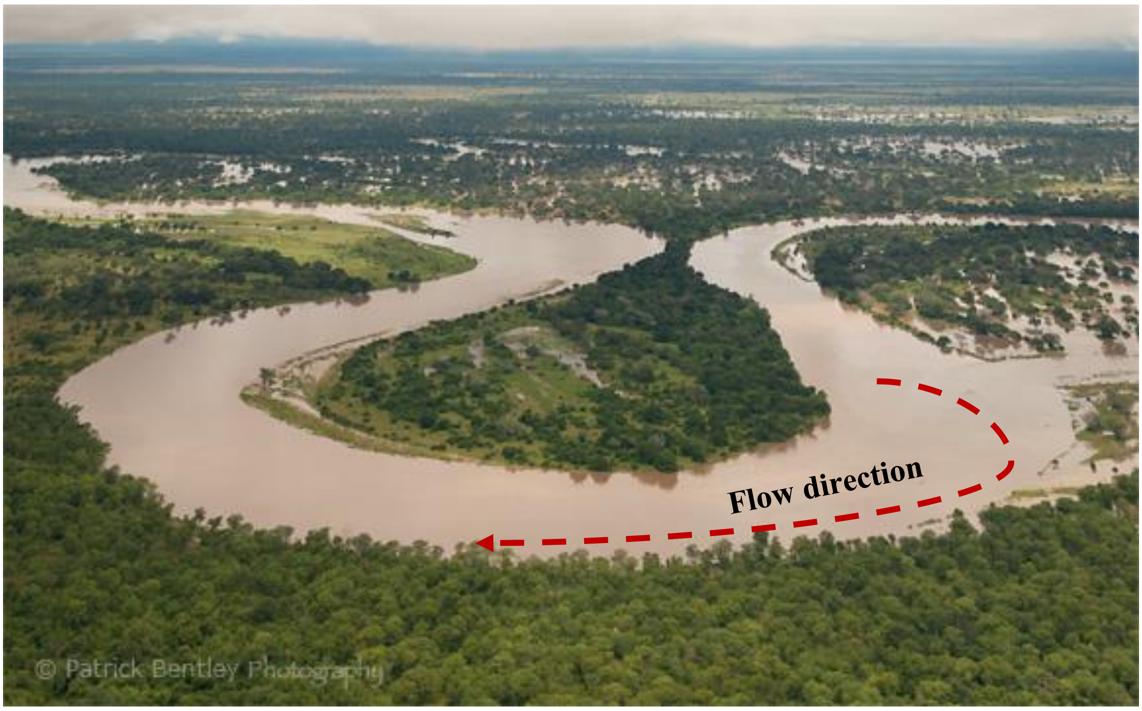

Figure 3.16: The Luangwa River in the wet season (Source: http://www.patrickbentley.com/)

3.3 Upper Zambezi River basin

The Upper Zambezi River basin extends down to the Victoria Falls (e.g. Beilfuss and Santos, 2001; World Bank, 2010; Kling *et al*., 2014). However, the current study only considers the delineated area as shown in Figure 3.17 because the main focus of this study was to capture the Barotse floodplain and its entire drainage area. Therefore, the delineated areas include the Luena, Luanguinga, Lungue-Bungo and the Kabompo River sub-basins as well as the Barotse floodplain at the centre (Figure 3.17). Apart from the Barotse floodplain, some of these sub-basins are characterised by small plains and flatlands such as the Lungue-Bungo River floodplain and the Lui River floodplain (Timberlake, 2000). The Barotse floodplain, as the second largest floodplain in the Zambezi River system, extensively regulates the flows of the Zambezi River (Moore *et al*., 2008; Beilfuss, 2012). Beilfuss (2012) reported that about 17×10^9 m^3 of water was stored in the floodplain during the large flood of 1958. Despite its importance, the spatial and temporal variation of the water exchange processes between the Barotse floodplain and the river channels are not well known. As the Upper Zambezi River basin is regarded as the 'water tower' for the Zambezi River basin (Beilfuss, 2012), understanding the floodplain-channel exchange processes is useful not only for sustainability of the floodplain but also for other water resource developments downstream.

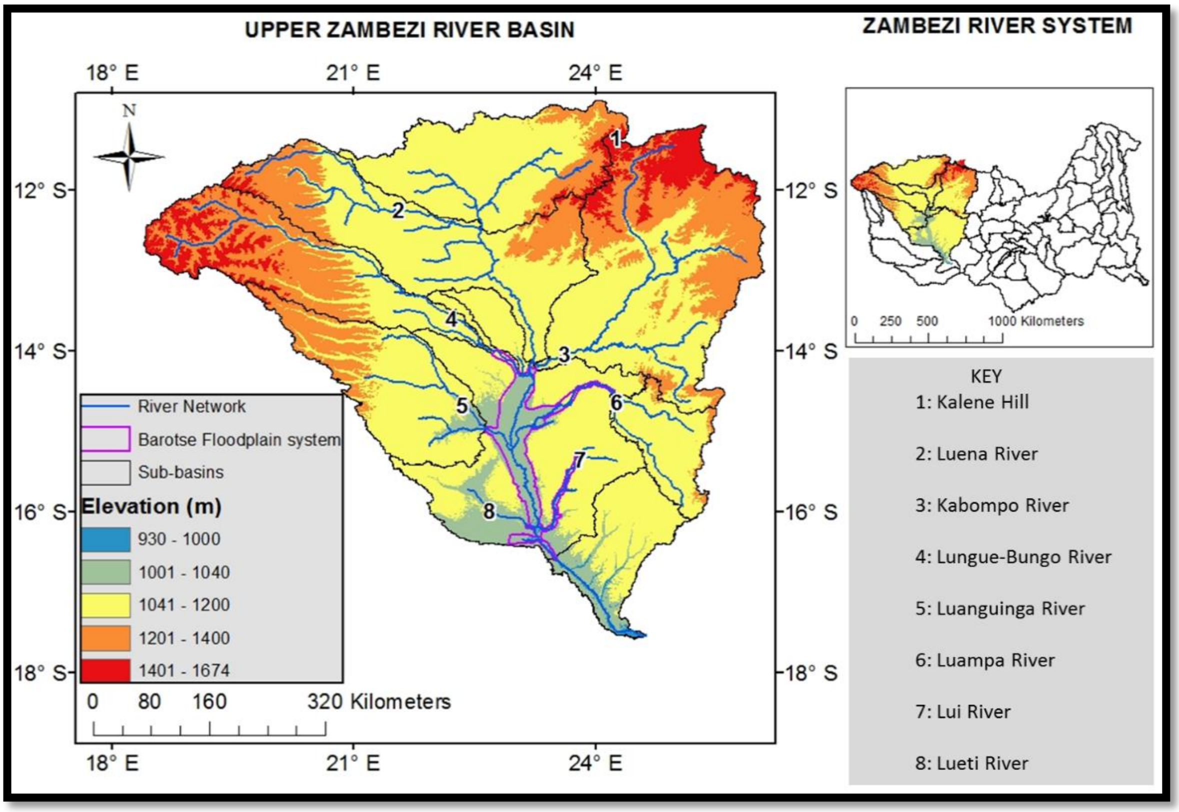

Figure 3.17: Location of the Upper Zambezi River basin in the Zambezi River system.

3.3.1 Topography and slope

The topography and slope characteristics of the Upper Zambezi River basin are illustrated in Figure 3.17 and 3.18, respectively. The upper sub-basins (north-east and north-west), including the Lungue-Bungo and Kabompo sub-basins, are characterised by high elevations between 1 041 m and 1 600 m and slope values between 5% and 15% (sloping to strong sloping areas according to FAO slope classification by Jahn *et al*., 2006; Table 3.1). The transitional areas between highlands and valleys have slopes between 16% and 62%, especially in the north-east. The high elevation and slope values suggest rapid runoff generation from these sub-basins. Flat to very gentle slopes (0% to 2%) dominate the Barotse floodplain, small plains and flatlands (centre of the basin) and these areas have elevation values between 1 000 m and 1 040 m.

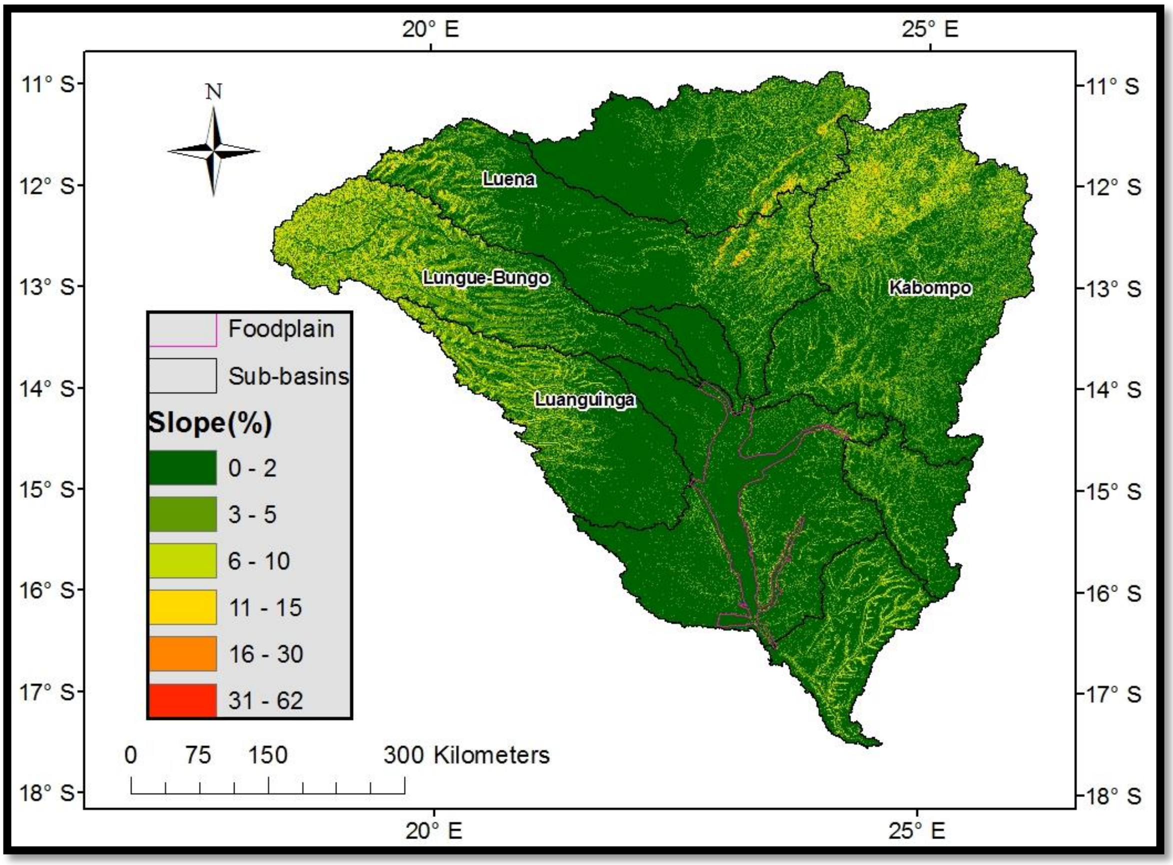

Figure 3.18: Slope characteristics of the Upper Zambezi River basin.

3.3.2 Geology and soil characteristics

The Luena, Luanguinga, and Lungue-Bungo River sub-basins are underlain predominantly by sandstones and conglomerates covered by the Kalahari sands, whereas the Kabompo sub-basin lies on the copper-rich sandstones, quartzite, arenites, and conglomerates (Ashton *et al*., 2001). The Barotse floodplain lies on the Karoo basalts (about 150 m thick) overlain by moist and permeable Kalahari sands (Turpie *et al*., 1999; Winsemius *et al*., 2006; Flint, 2008). Black and grey fertile soils enriched by silts and humus, which resulted from the decomposition of vegetation and aquatic species, remain on top of the Kalahari sands when floods recede in the floodplain (Moore and Fenton, 2007).

There is a considerable variation in the soil characteristics within the basin (Figure 3.19). The Barotse floodplain and small flatlands are dominated by Gleysols, which are commonly found in wetlands characterised by high groundwater levels. Aeronosols, which cover a large part of this basin (78%), are unconsolidated soils with low clay content and a high degree of porosity. Ferralsols dominate the north-eastern parts including the Kabompo sub-basin and

Kalene Hills and they are deeply weathered, acidic, leached and permeable soils with high iron content (Ashton *et al*., 2001).

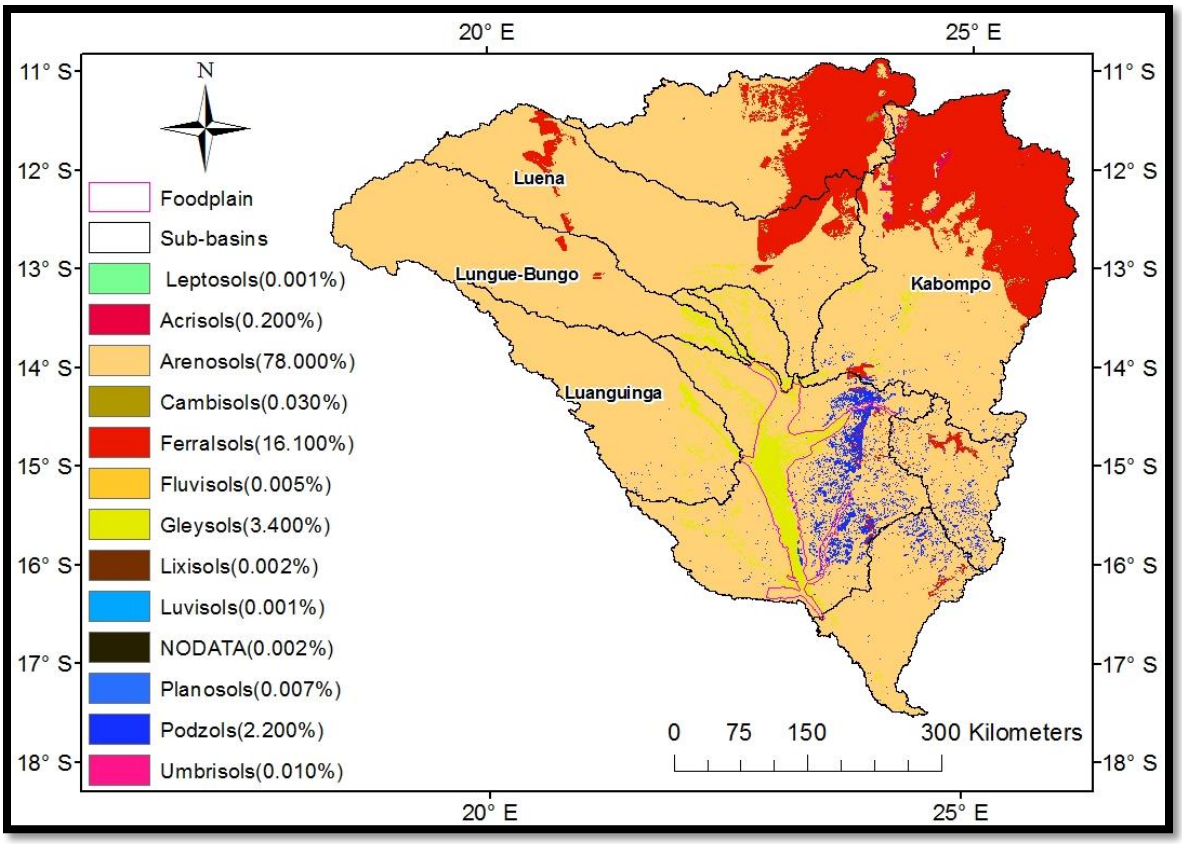

Figure 3.19: Distribution of different soils in the Upper Zambezi River basin (Source: Hengl *et al*., 2014).

3.3.3 Land cover and land use

Figure 3.20 illustrates that a large part of this basin is dominated by wood-savannas (59.3%) except for the upper course of the Zambezi River valley which is covered by grasslands. Forests are also found in the upper sub-basins especially in the Kabompo sub-basin in the north-east. The areas surrounding the Barotse floodplain (south-eastern part) are dominated by savannas. The permanent wetland areas, which cover about 1.5% of the whole basin, are expected to attenuate high flows as well as contribute to higher evapotranspiration losses. Major land use activities in this basin are livestock farming, wildlife, mining, fishing and tourism (Ashton *et al.*, 2001).

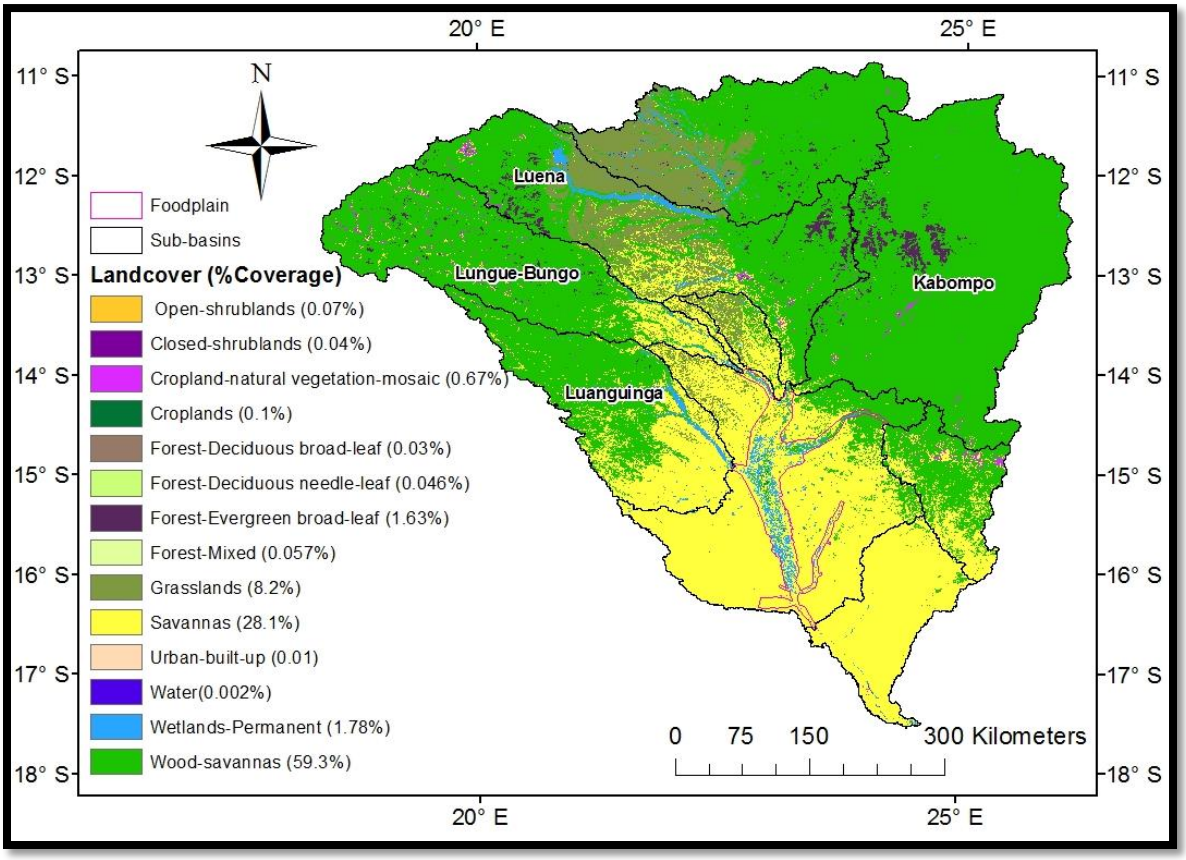

Figure 3.20: Land cover in Upper Zambezi River basin (Source: Broxton *et al*., 2014).

3.3.4 Climate

The basin is characterised by three climatic regimes: cool dry (April to August), hot dry (September to October), and a warm wet season (November to April) (Beilfuss and dos Santos, 2001). The rainfall in this basin is also controlled by the position of the ITCZ, and the mean annual rainfall is approximately 1 000 mm (Beilfuss and dos Santos, 2001; Beilfuss, 2012). The temperature varies with altitude; highly elevated areas experience lower temperatures compared to the floodplain and other low-lying areas. October is the hottest month and the coldest is July (World Bank, 2010). Generally, the area is moist and warm due to the effects of the Congo Air Masses (Timberlake, 2000).

3.3.4.1 Rainfall

The seasonal analysis in Figure 3.21, using area-averaged CRU monthly rainfall data for the selected sub-basins, indicates a unimodal pattern. The rainfalls in the upper sub-basins peak around December whereas the other remaining sub-basins peak around January. Generally, there is no substantial difference between the long-term monthly rainfall values across the basin except for the areas downstream of the Barotse floodplain (sub-basin or nodal point BP10). The peak values in the upper section of the basin are close to 250 mm month^{-1}, whereas values below 250 mm month^{-1} are experienced in the centre and lower parts of the basin. The spatial variation of mean annual rainfall presented in Figure 3.21 indicates a decrease in mean annual rainfall from the upper to the lower parts of the basin. The mean annual rainfall for the upper sub-basins is between 1 100 – 1 230 mm, whereas the values are 760 – 950 mm in the floodplain and the downstream areas. The inter-annual rainfall variation is very small as the annual CV values are less than 0.15 in all sub-basins. However, any seasonal and/or inter-annual variations of rainfall, especially in the upper sub-basins, will result in flow variation in the Zambezi River, thereby affecting the inundation characteristics in the Barotse floodplain (World Bank, 2010; Tirivarombo, 2013; Beyer *et al.*, 2016).

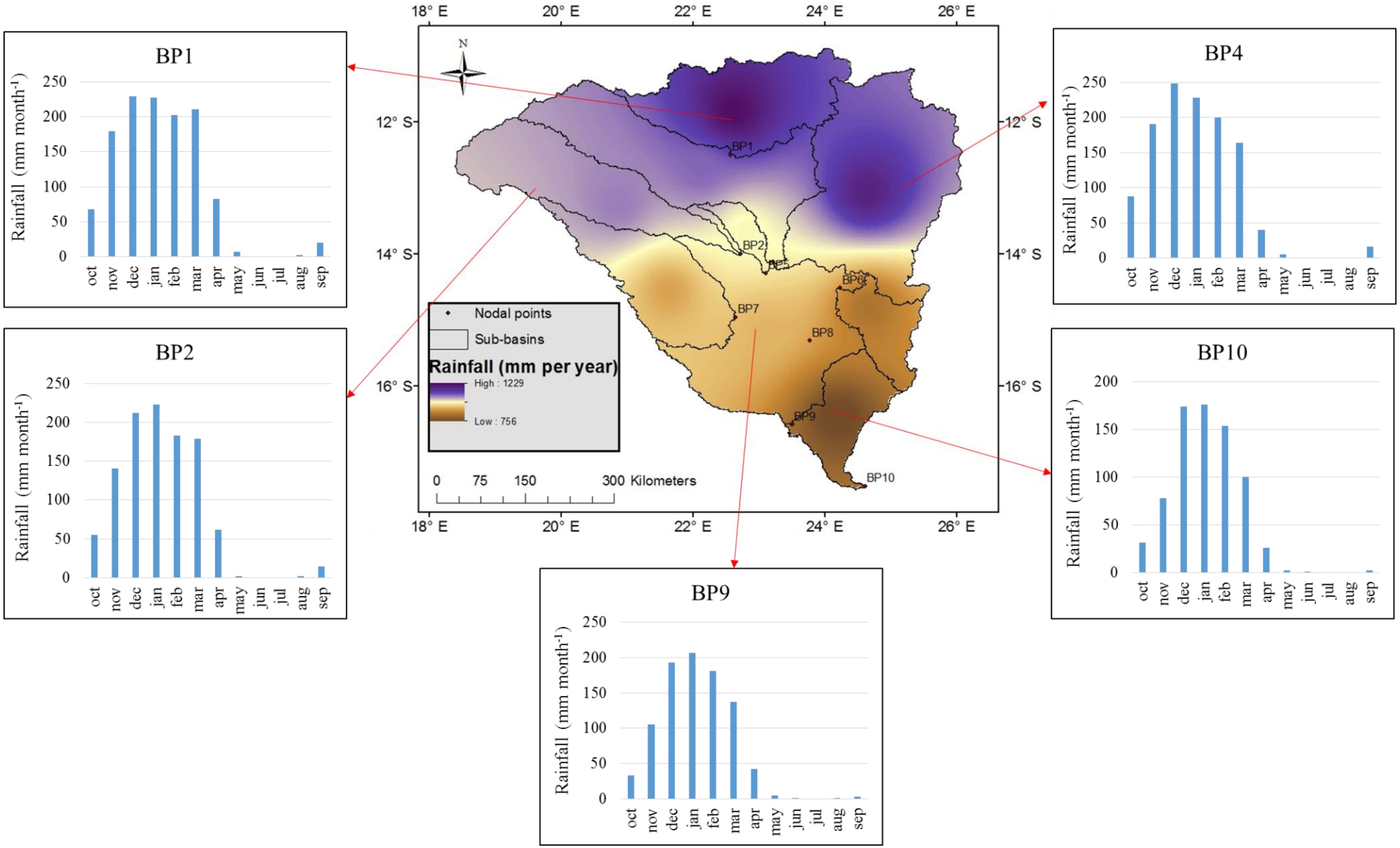

Figure 3.21: Rainfall seasonality in the Upper Zambezi River basin.

3.3.4.2 Temperature and potential evapotranspiration (PET)

Figure 3.22 illustrates the spatial variations of the mean annual temperatures derived from the mean monthly temperatures obtained from the IWMI Climatic Data Portal (New *et al*., 2002). The mean annual temperatures increase from the highlands toward the Barotse floodplain; however, the difference in terms of magnitude is minimal. The average maximum temperature is between 18°C and 27°C and the average minimum temperature ranges from 12°C to 15°C. The coldest month is July whereas October and November are the warmest months with average values of 16°C and 22°C, respectively (Euroconsult, 2007). The mean monthly potential evapotranspiration data were also obtained from the IWMI Climatic Data Portal, and these values were used to estimate the mean annual PET. The mean annual PET ranges between 1 466 mm y^{-1} and 1 611 mm y^{-1} (Table 3.4). The months of September and October contribute more to annual evapotranspiration (>10%) and this can be related to higher temperature and low rainfall experienced during these months. Similar to the mean annual temperature, the spatial variation of the mean PET shows an increase toward the Barotse floodplain (Figure 3.23).

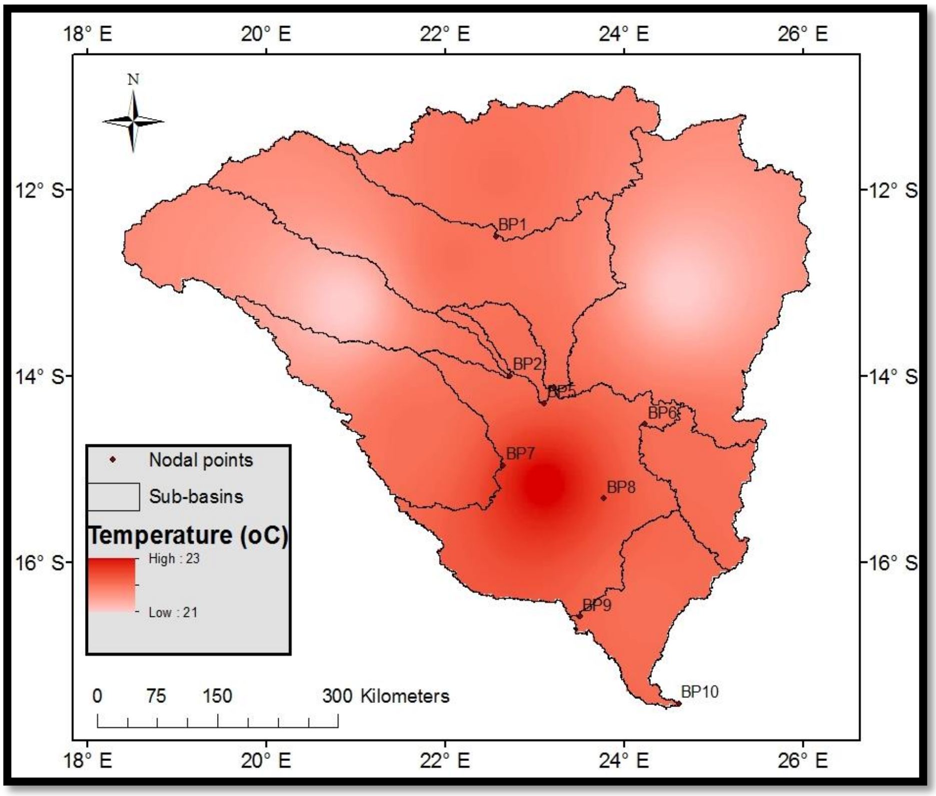

Figure 3.22: Variation of the mean annual temperature in the Upper Zambezi River basin.

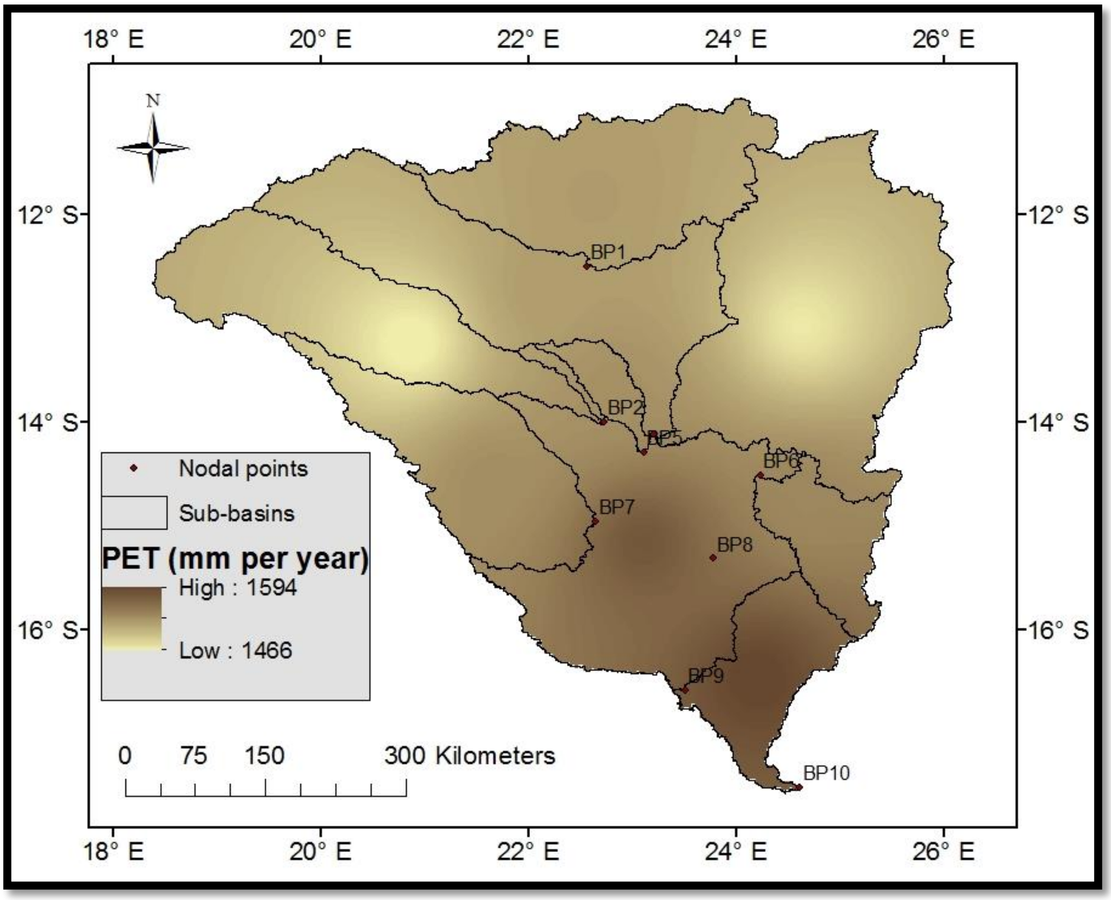

Figure 3.23: Variation of the mean annual potential evapotranspiration (PET) in the Upper Zambezi River basin.

Table 3.4: Sub-basin monthly and annual potential evapotranspiration in the Upper Zambezi River basin.

Sub-basin	Potential evapotranspiration (mm month^{-1})												Annual (mm)
	Jan	Feb	Mar	Apr	May	Jun	Jul	Aug	Sep	Oct	Nov	Dec	
BP1	120	113	118	118	117	110	122	146	160	154	129	118	1524
BP2	115	111	112	113	115	109	118	143	153	143	119	115	1466
BP3	120	114	118	118	117	109	121	145	160	154	128	119	1523
BP4	117	107	117	116	109	94	105	138	161	159	132	118	1473
BP5	123	114	121	118	114	101	113	142	165	163	135	123	1531
BP6	125	116	126	118	107	92	102	137	168	174	145	131	1539
BP7	125	117	122	119	113	102	112	138	162	161	137	128	1534
BP8	128	118	127	120	110	95	107	138	169	172	146	133	1563
BP9	129	118	127	120	112	98	112	141	169	174	145	132	1578
BP10	132	125	130	120	108	92	104	136	170	180	157	140	1594

3.3.4.3 Streamflow

The Zambezi River arises near the Kalene Hills in the north-western part of Zambia (Figure 3.17), and it flows southwards until it merges with the tributaries originating from the steep areas of the Angolan highlands e.g. the Luena River (Beilfuss and dos Santos, 2001; Kling *et al*., 2014). Further downstream, the river captures the runoff from its major tributaries, the Kabompo and Lungue-Bungo, which emerge from the north-western and the north-eastern parts, respectively. The two tributaries flow through an area of steep topography, which affects the shape and the timing of the response hydrographs. A few kilometres further down, the river increases its sinuosity by meandering along a flat and broad Barotse floodplain (Beilfuss and dos Santos, 2001). In the middle reaches of the floodplain, the river captures flow from other tributaries such as the Luanguinga River which drains the south-eastern parts of Angola (Ashton *et al*., 2001). In this study, the Upper Zambezi River basin is divided into nine sub-basin nodes, and their areas ranging from 4 100 to 71 900 km^2 (Table 3.5).

Figure 3.24 shows the location of the accessed streamflow gauging stations in this basin. Most of the Zambezi River tributaries are gauged but their data records are of short periods and contain a lot of missing values. Table 3.6 gives a summarised description and the percentage of missing values in the data record for each station in this basin. The longest records span from 41 to 44 years, and the missing data for most of the gauges are less than 10% except for station 1591002, which is located on the Zambezi River. Although station 1591200 has less than 10% missing values, its record is very short (4 years). Therefore, only two gauge stations (i.e. 1591820 and 1291100) were considered appropriate to be used for modelling this basin. The daily discharge data for the gauge station at Sioma/Ngonye Falls (BP9 in Table 3.6) were also used. Since there is only one reliable long-term gauging station in the upper sub-basins (ID: 1591820), it was difficult to understand the attenuation effects of the Barotse floodplain system, as the total inflow into the floodplain is not known.

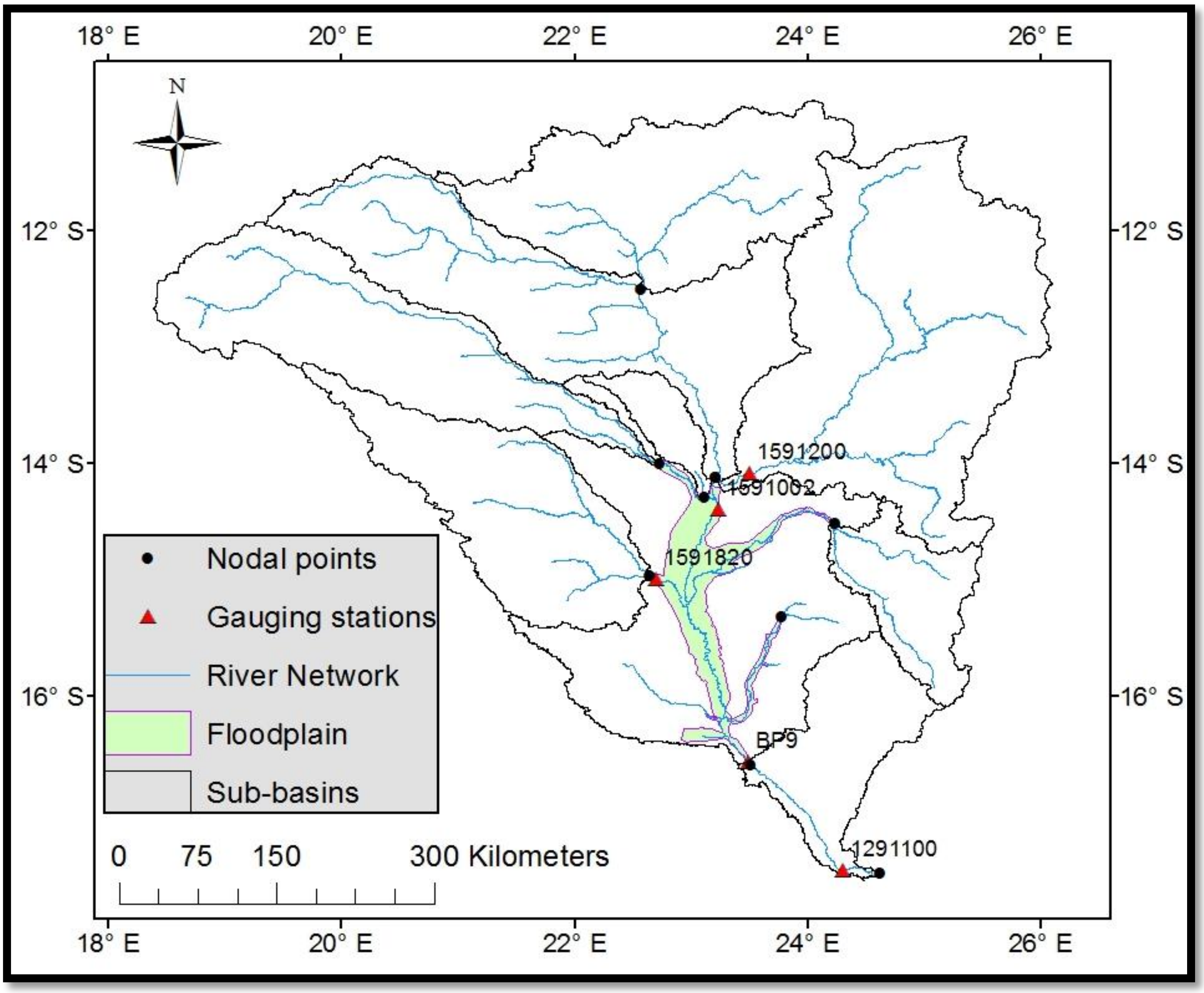

Figure 3.24: Location of the streamflow gauging stations in the Upper Zambezi River basin.

Table 3.5: Catchment areas for sub-basin nodes in the Upper Zambezi River basin.

Sub-basin node ID	Area (km^2)
BP1	40629
BP2	38964
BP3	51847
BP4	71908
BP5	5195
BP6	13903
BP7	32459
BP8	4128
BP9	54140
BP10	18763

Table 3.6: Streamflow gauging stations in the Upper Zambezi River basin.

Station ID	River	Longitude	Latitude	Start	End	Period (years)	% Missing values
1591200	Kabompo	23.5	-14.09	1975	1979	4	6
1591820	Luanguinga	22.7	-15	1958	2003	44	8
1591002	Zambezi	23.23	-14.4	1989	2003	14	39
1291100	Zambezi	24.3	-17.5	1964	2005	41	2
BP9	Zambezi	23.49	-16.57	1948	2014	66	9

Figure 3.25 shows the seasonal hydrographs for the three gauging stations (1591820, BP9 and 1291100) which display a single peak pattern. The Luanguinga (1591820) peaks in late March/early April, whereas the Zambezi River at Sioma Fall (BP9) peaks in late April/early May. The long-term (1965 – 2004) mean annual runoff for the Zambezi River (1291100) is approximately 37 × 10^9 m^3 with an annual CV of 0.38. The mean annual runoff for the Luanguinga River between 1958 and 1992 is around 2 × 10^9 m^3 with an annual CV of 0.34. The CV values (< 0.5) for the two gauging stations suggest that there is some variation between the annual runoffs, but it is of small magnitude.

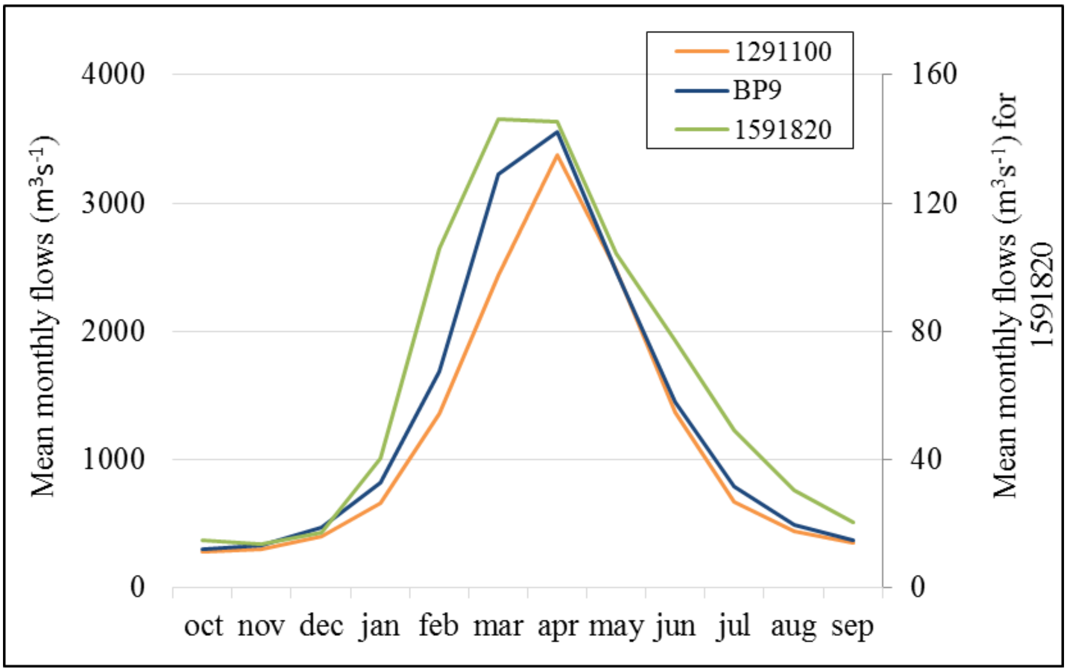

Figure 3.25: Mean monthly hydrograph for three gauges in the Upper Zambezi basin.

3.3.5 Water use

The total annual abstraction for irrigation, domestic and other activities is approximately 28.8 $\times 10^6$ m^3 (about 0.1% of annual basin runoff) (Beilfuss, 2012), which is relatively small when compared to the total runoff generated in this basin. There are no existing hydropower dams in this basin (Moore *et al*., 2008; World Bank, 2010) but some HEP and large-scale irrigation projects have been proposed to start in the near future (Beilfuss, 2012).

3.3.6 Barotse floodplain and associated flats

The Barotse floodplain, locally known as *Bulozi or Lyondo,* is located between 13°50'S to 16°40' S and 22°45'E to 23°45' E (Figure 3.17) and it extends from the confluence of the Zambezi River and the Lungue-Bungo tributary to a few kilometres upstream of the Ngonye Falls (Timberlake and Childes, 2004). The downstream end of the Barotse floodplain is controlled by natural basalt rock, acting as a natural dam that causes backwater effects into the floodplain (Flint, 2008). Being the second largest floodplain in the Zambezi River basin which drains a basin area of 320 $\times 10^3$ km^2, it is approximately 240 km long and 40 km wide (Beilfuss *et al*., 2001). The inundated areas for the Barotse floodplain occupy 5 500 km^2 of land but can extend up to 9 000 km^2 if other flatlands and small plains within the basin are included. The annual average storage for the floodplain is approximately 8.5 $\times 10^9$ m^3 (Turpie *et al*.,1999; Beilfuss, 2012) which could be about 23% of the average annual basin runoff. The maximum inundation depth ranges between 1.5 m and 3 m especially in the interior of the floodplain generally around April (Steenbergen *et al*., 2015).

The Barotse floodplain is characterised by depressions and abandoned channels (old channels) which experience flooding during the wet season and when the flow starts to recede, water remains only in the main channel and other depressions connected to the river (Steenbergen *et al*., 2015). Most of these floodplain features are connected to each other in a complex manner, with direct and indirect connections with the Zambezi River (e.g. Figure 3.26). The western and eastern parts of the floodplain are dominated by pans and dambos of different sizes covered by grasslands (Timberlake and Childes, 2004; Moore *et al*., 2008). A large part of the upper section of the Barotse floodplain is at a high elevation relative to the Zambezi River and some rural populations (Lozi people) have been residing in these areas since the 17th century, and they benefit from the ecological goods and services provided by the Barotse floodplain (Flint, 2008). At the beginning of the wet season, when the floodplain starts to inundate, the people leave the floodplain for the highlands and come back when the inundation starts to recede (Emerton, 2003; Moore e*t al*., 2008). Figure 3.27 and 3.28 show some rural houses located on the Barotse floodplain.

Different vegetation species are also found within the floodplain including *Acacia albida*, thicket, *Syzygium guineense*, *Echinochloa* and *Oryza* sp., in addition to birds as well as aquatic species (approximately 80 different types of fishes) (Turpie *et al*., 1999; Ramsar, 2007). Figure 3.29 is a LandsatLook image showing the Barotse floodplain and its related flatlands and small plains. The image on the right in Figure 3.29 shows the main part of the Barotse floodplain which is inundated for long periods of time.

Figure 3.26: A 3D Google Earth image showing detail of the geomorphology of the main channel and other floodplain features in the Barotse floodplain (Source: https://earth.google.com/web/@-14.8480635,22.98257525,1029.26325177a,6877.27730748d,35y,0.91172863h,67.15028773t,0r).

Figure 3.27: Natoga village in the Barotse floodplain (Source: https://farm6.staticflickr.com/5507/14158410929_22e59f4527_z.jpg).

Figure 3.28: Some temporary rural houses on the Barotse floodplain (Source: http://mw2.google.com/mw-panoramio/photos/medium/22959134.jpg).

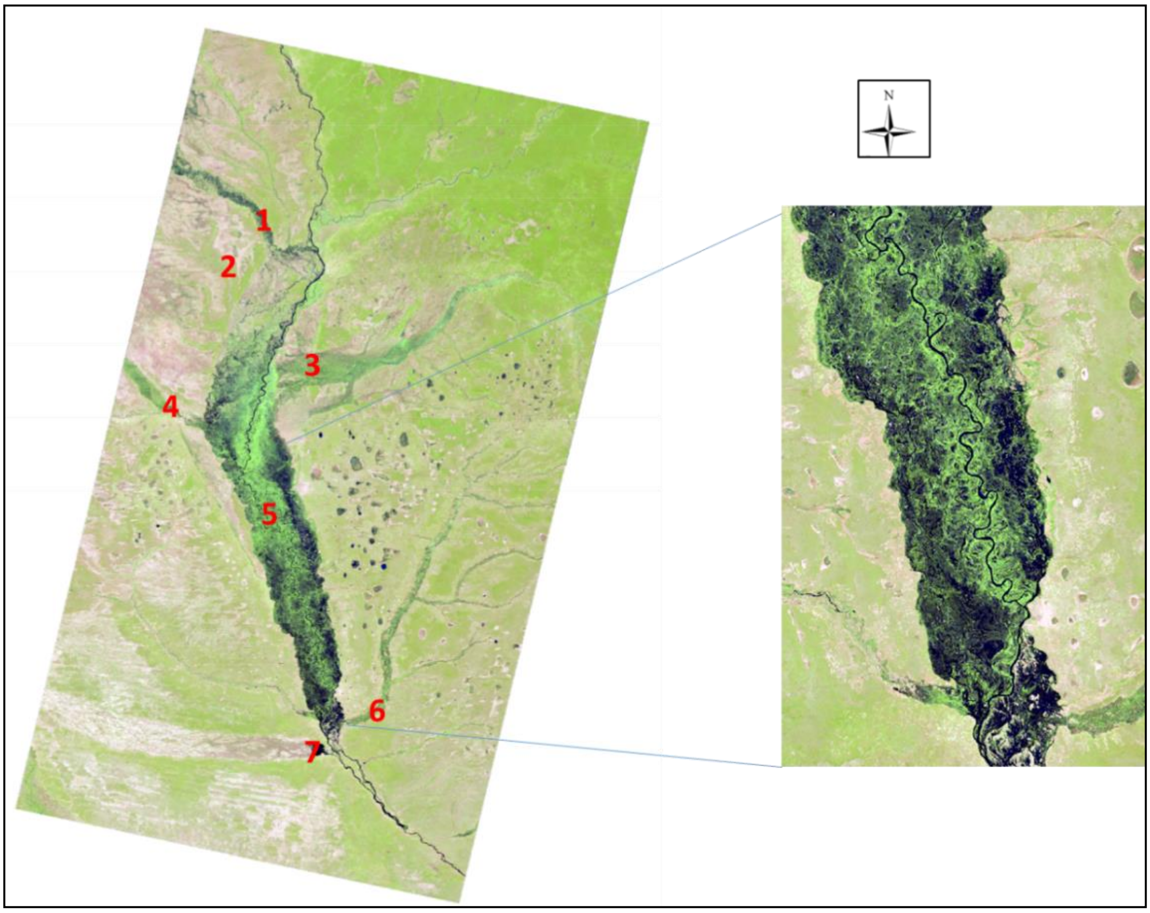

Figure 3.29: Barotse floodplain and its associated flats and plains (source: LandsatLook image; 30th April 2016): 1) swamps and floodplain of the Lungue-Bungo, 2) Liuwa plains National Park, 3) Luena flats, 4) Luanguinga floodplain, 5) Barotse floodplain, 6) Lui floodplain and 7) a broad floodplain which carries the overspill from the high floods of the Cuado River.

3.4 The Upper Great Ruaha River Basin

The Upper Great Ruaha River basin (approximately 2×10^4 km^2) is located in the south-west part of Tanzania. The basin is divided into the Usangu plains and highlands, which constitute 28% and 72% of the total basin area, respectively (Figure 3.30). The Usangu plains, at the interior of the basin, are characterised by alluvial fans and wetlands which are seasonally and permanently inundated (Kashaigili *et al*., 2006a; McCartney *et al*., 2008; Tumbo, 2015). While the wetlands owe their sustainability to the water balance in the basin, they play a significant role in regulating the flows of the Great Ruaha River, thereby serving as a major source of the inflow for the two HEP dams (Mtera and Kidatu Dams) that are located downstream of the Usangu plains (Figure 3.30). These dams collectively produce electricity serving more than 50% of the Tanzanian population (Mtahiko *et al.*, 2006). For the last two decades, significant flow reduction in the Great Ruaha River and its tributaries has been observed (SMUWC, 2001). Several studies such as SMUWC (2001), Kashaigili *et al*. (2006b) and Mwakalila (2011) have revealed that the irrigation abstractions contribute to this reduction.

Some studies have assessed the hydrological characteristics of this basin including an understanding of the dynamics of the Usangu wetlands using remote sensing images (Kashaigili *et al*., 2006a) and hydrological models (McCartney *et al*., 2008; Tumbo, 2015). Tumbo (2015) applied the Pitman monthly hydrological model with the inclusion of a wetland sub-model to understand the hydrological responses in the Great Ruaha River basin. Although this study is among a few of the detailed studies in the Upper Great Ruaha River basin, the uncertainties in the model simulations were related to inabilities to quantify some of the wetland parameters. It is likely that a detailed understanding of the spatial and temporal variations of water exchanges between channels and the Usangu wetlands would help to improve the quantification of some wetland parameters. Moreover, this information would be useful for the present and future sustainability of the Usangu wetlands and the activities downstream.

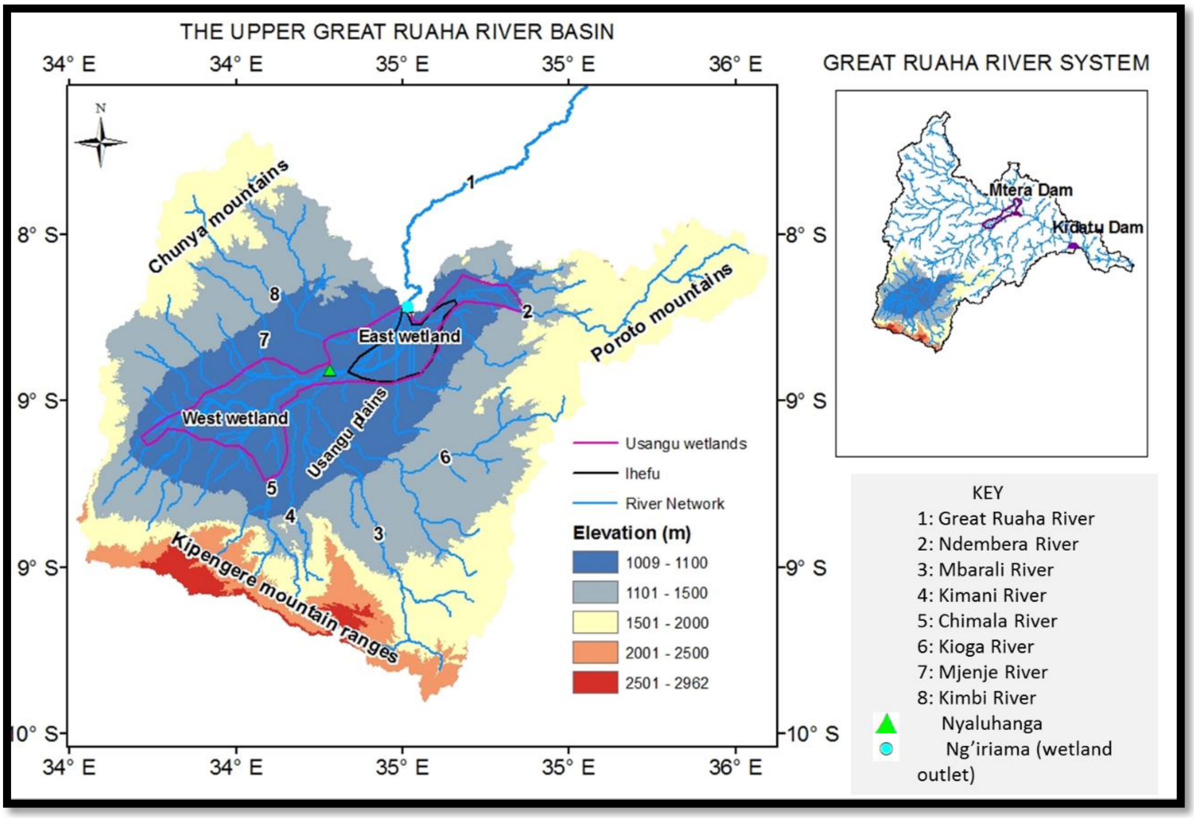

Figure 3.30: The Upper Great Ruaha River Basin and the Usangu wetlands.

3.4.1 Topography and slope characteristics

The topographical distribution of the Upper Great Ruaha River basin (Figure 3.30) indicates that the Usangu plains are characterised by elevations between 1009 m and 1 100 m. The high elevation values are observed in the southern parts of the basin, especially in the Kipengere Mountain ranges. The transitional areas between the mountains and the Usangu plains (Figure 3.31) are characterised with high slope values which can be classified as steep to very steep slopes according to the FAO soil classification by Jahn *et al*. (2006) (see Table 3.1). Many tributaries of the Great Ruaha River originate from these highly-elevated mountainous areas and the steep slopes have a positive impact on the generation of runoff. The Usangu plains (centre of the basin) are very gently sloping areas with slope values between 0% and 2% that support water accumulation.

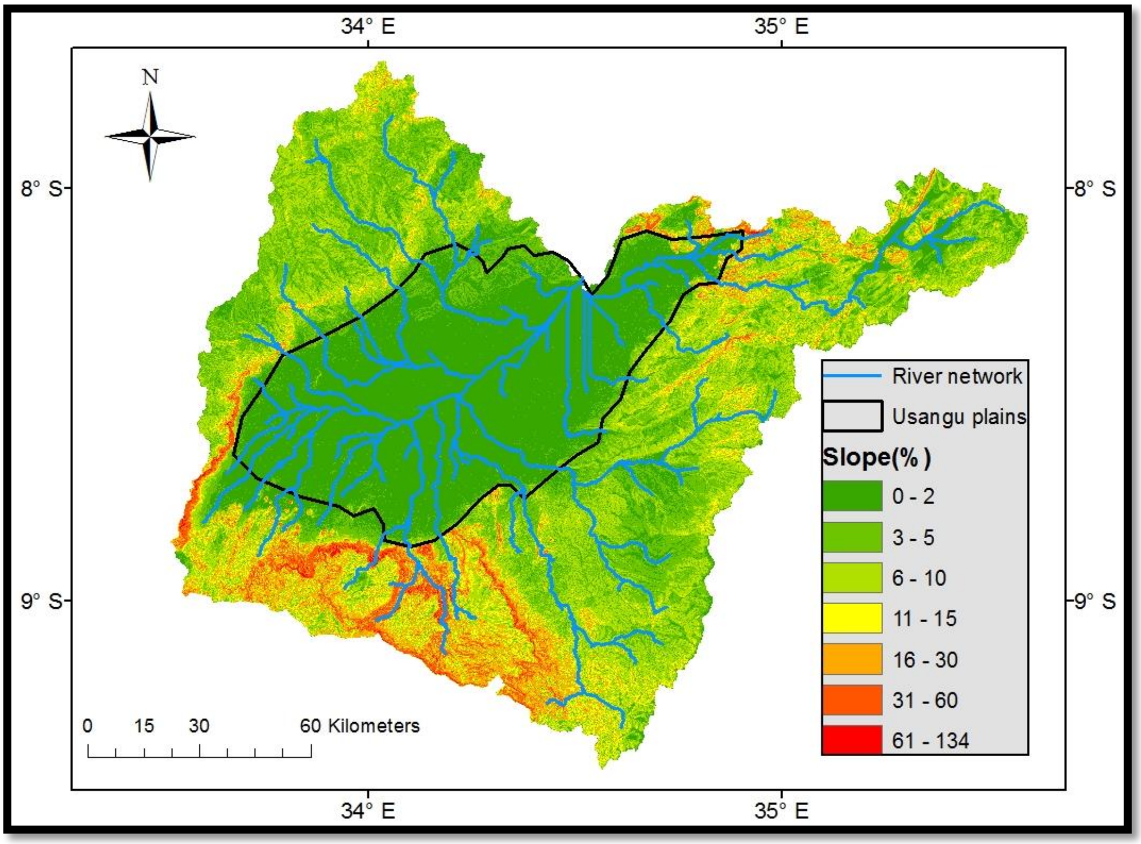

Figure 3.31: Slope characteristics of the Upper Great Ruaha River basin.

3.4.2 Geology and soil characteristics

Geologically, the Upper Great Ruaha River basin lies on the Pre-Cambrian basement rocks of gneiss and granite origin (McCartney *et al*., 2008). The Usangu plains form a depression bounded by fault lines and are dominated by lacustrine sediments deposited when the plains were still a lake (SMUWC, 2001). The south-west part of the Upper Great Ruaha River basin is surrounded by the Kipengere volcanic mountain ranges composed of basalts, pumice, and ash (SMUWC, 2001). The unconsolidated alluvial fan deposits found in the Usangu plains consist of materials which are highly permeable.

Figure 3.32 shows the distribution of the soil types in the Upper Great Ruaha River basin derived from the SoilGrids 1 km (Hengl *et al*., 2014). The northern and southern parts of the basin are dominated by Cambisols and Acrisols, respectively. The plains are covered by Fluvisols, whereas Leptosols form a boundary between the plains and the highlands. The Fluvisols are young soils mostly found in alluvial or lacustrine deposits and are characterised by clay, especially when the area has been frequently flooded. The Leptosols are normally found at the foot of the mountain where soils have been eroded or in rivers with gravel deposits (Nachtergaele, 2010).

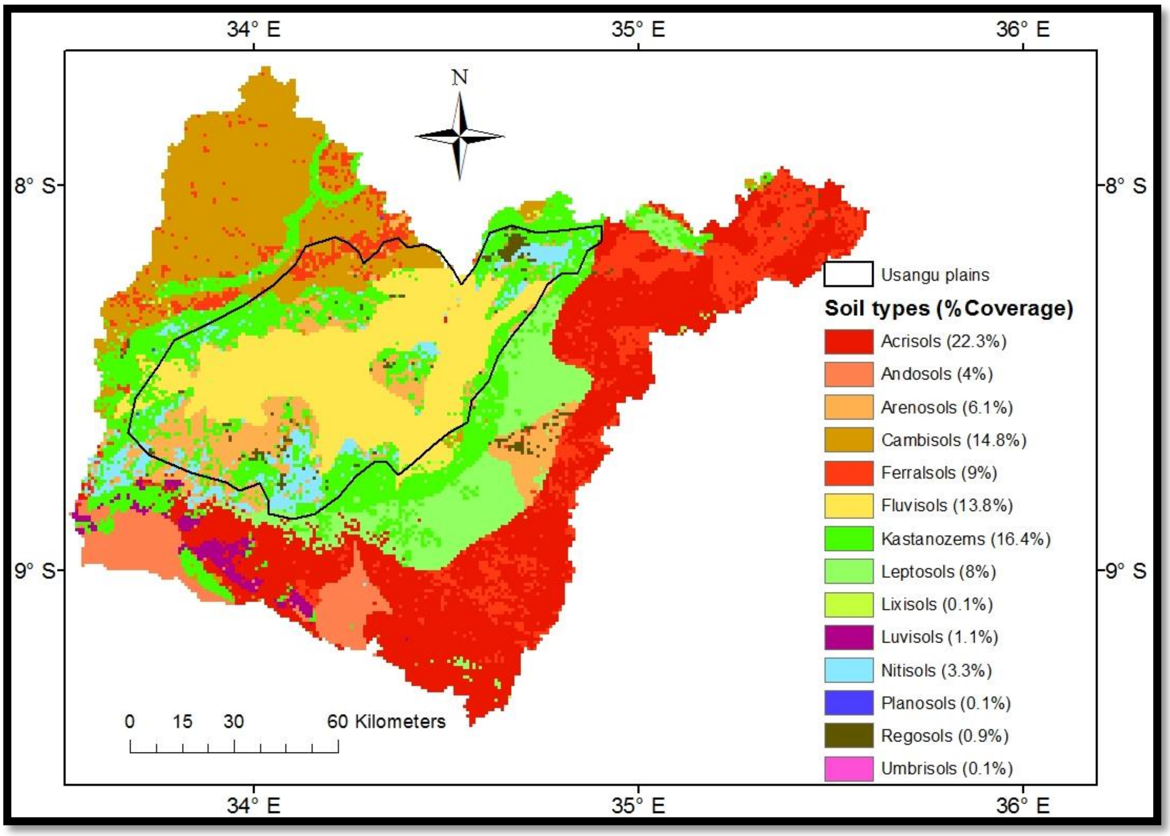

Figure 3.32: Distribution of the soils types in the Upper Great Ruaha River basin (Source: Hengl *et al.*, 2014).

3.4.3 Land cover and land use

The land cover of this basin has changed in time and space. Kashaigili *et al*. (2006b) grouped the land cover of the Upper Great Ruaha River basin into seven classes: 1) closed woodland, 2) open woodland, 3) vegetated swamp, 4) open bushland, 5) closed bushland, 6) bushed grassland, and 7) cultivated land and bare land. Vegetated swamp, closed and open woodland are found in the Usangu plains. Figure 3.33 shows that a large part of the Upper Great Ruaha River basin is covered by savanna and wood-savanna. Grasslands and other natural vegetation cover about 7.6%, whereas the permanent wetland areas are only 0.06% of the entire Upper Great Ruaha River basin. The main land use activities within this basin are irrigation (mainly paddy rice) and rain-fed agriculture especially in the western wetland, with livestock rearing and fishing being important in the eastern parts. However, irrigation and livestock rearing are the predominant activities that contribute to land cover change in the Upper Great Ruaha River basin (Mtahiko *et al.*, 2006; Kashaigili, 2008; Kihwele *et al.*, 2012).

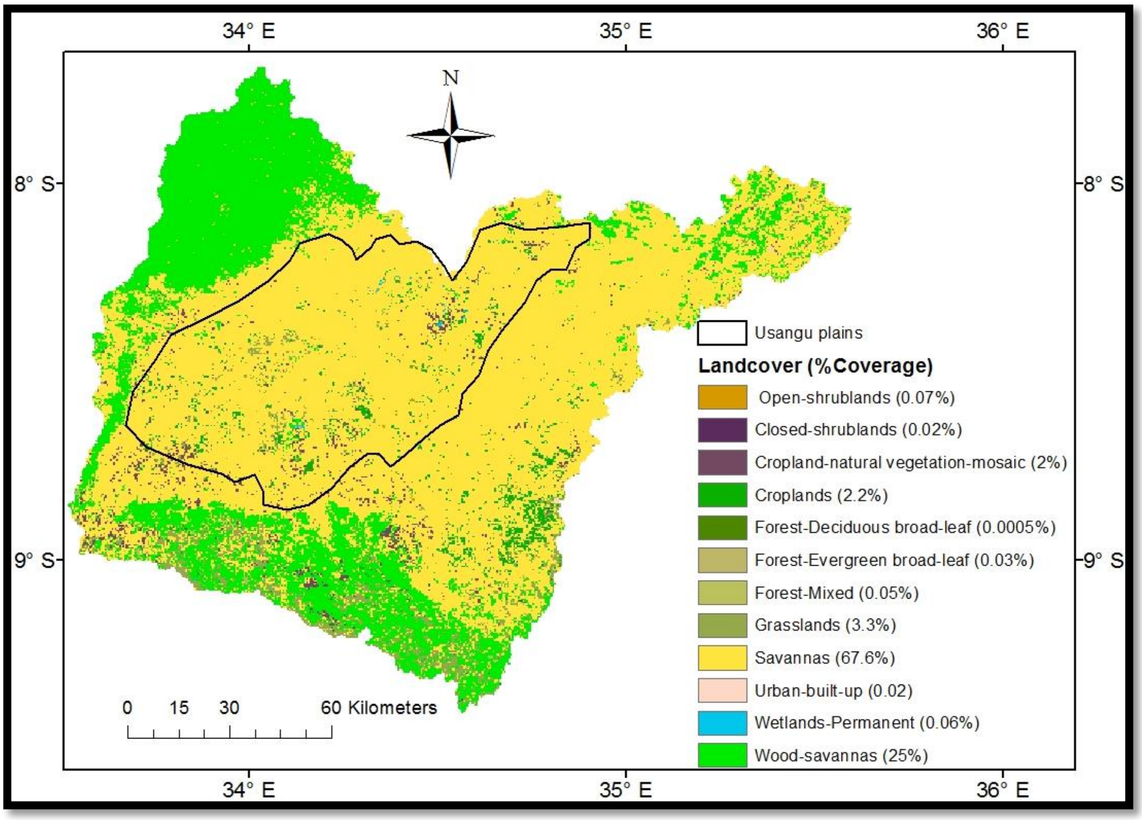

Figure 3.33: Land cover in the Upper Great Ruaha River basin (Source: Broxton *et al*., 2014).

3.4.4 Climate

Generally, the climatic conditions of the Upper Great Ruaha River basin are controlled by the movement of the ITCZ as well as the altitude (Kashaigili *et al*., 2006a; Tumbo and Hughes 2015). The ITCZ occurs when the north-east monsoon and the south-east air masses converge. The ITCZ reaches the southern part of Tanzania around January/February and changes its direction (northwards) around March/May. As a result, the wet season dominates from October to May and the dry season extends from June to September. The basin experiences large spatial variability in the mean annual precipitation (Tumbo, 2015). This could perhaps be an effect of an orographic influence of the highlands, with the mountainous areas receiving higher rainfall than the low-lying areas (Kashaigili *et al*., 2006a; McCarthy *et al*., 2008). Low-temperature values have been recorded in the highlands, whereas high temperatures values are experienced in the Usangu plains.

3.4.4.1 Rainfall

The monthly rainfall data for each sub-basin in the Upper Great Ruaha River basin were obtained from Tumbo (2015). These data are based on spatial interpolation of remotely sensed monthly rainfall estimates from the Climate Prediction Centre/Famine Early Warning System (CPC-FEWS v2) for the period 1960 – 2009. Tumbo (2015) explains how these rainfall values were derived.

The seasonal analysis using long-term mean monthly rainfall for some sub-basins indicated a unimodal type (Figure 3.34). However, a slight decrease in rainfall in February results in two rainfall seasons: short rains and long rains commonly known as *Vuli* and *Masika*, respectively. The *Vuli* occurs between late October/early November and February, whereas the *Masika* are experienced between March and May. Monthly peak values greater than 250 mm are observed in the highlands, whereas values less than 250 mm are common in the Usangu plains. The dry season is between June and late September/early October with August regarded as the driest month. Low amount of rainfall is experienced in the dry season, except for areas around the Kipengere Mountain ranges (southern parts) which receive comparatively higher rainfall (see 1ka8 in Figure 3.35) during this season. Generally, there is considerable spatial variation in the rainfall in the Upper Great Ruaha River basin. The rainfall in the Kipengere mountain ranges is associated with orographic lifting of air moving north from Lake Nyasa (Tumbo, 2015). The annual rainfall increases from the Usangu plains toward the highly elevated areas. For example, the sub-basins covering the Usangu plains receive about 1 200 mm y^{-1}, whereas the highlands may receive annual rainfall up to 2 000 mm or more, especially in the areas surrounding the Kipengere Mountain ranges (1ka8). Apart from the spatial variation in the mean annual rainfall, some variation in the annual rainfall has been experienced for the period 1960 – 2009. For instance, there was a decrease in the annual rainfall throughout the basin, especially for the period 1990 – 2009 (Figure 3.35). However, the annual coefficient of variation for the period 1960 – 2009 is less than 0.3 for all the sub-basins which suggests that the inter-annual rainfall variation is minimal.

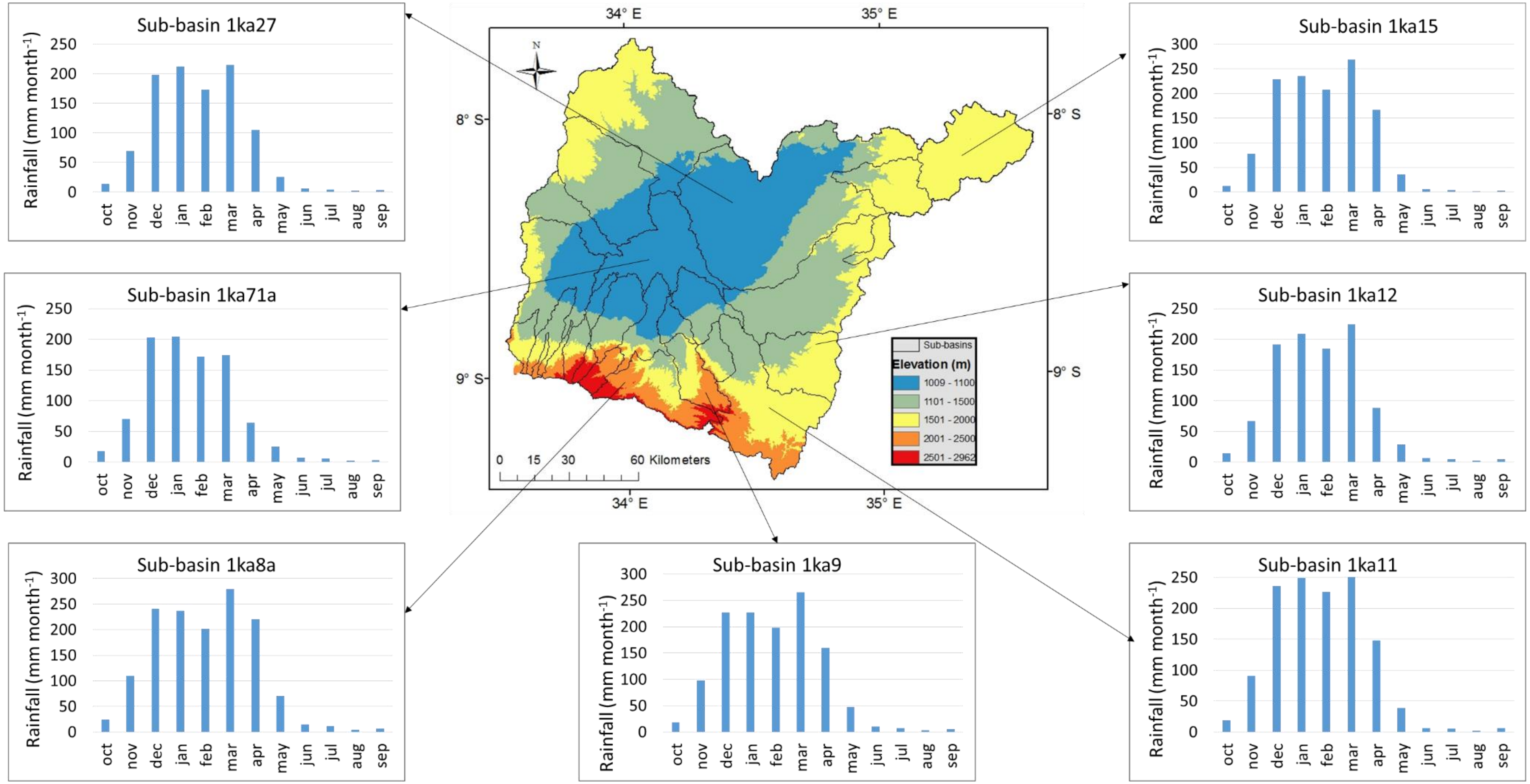

Figure 3.34: Rainfall seasonality for some of the sub-basins in the Upper Great Ruaha River Basin.

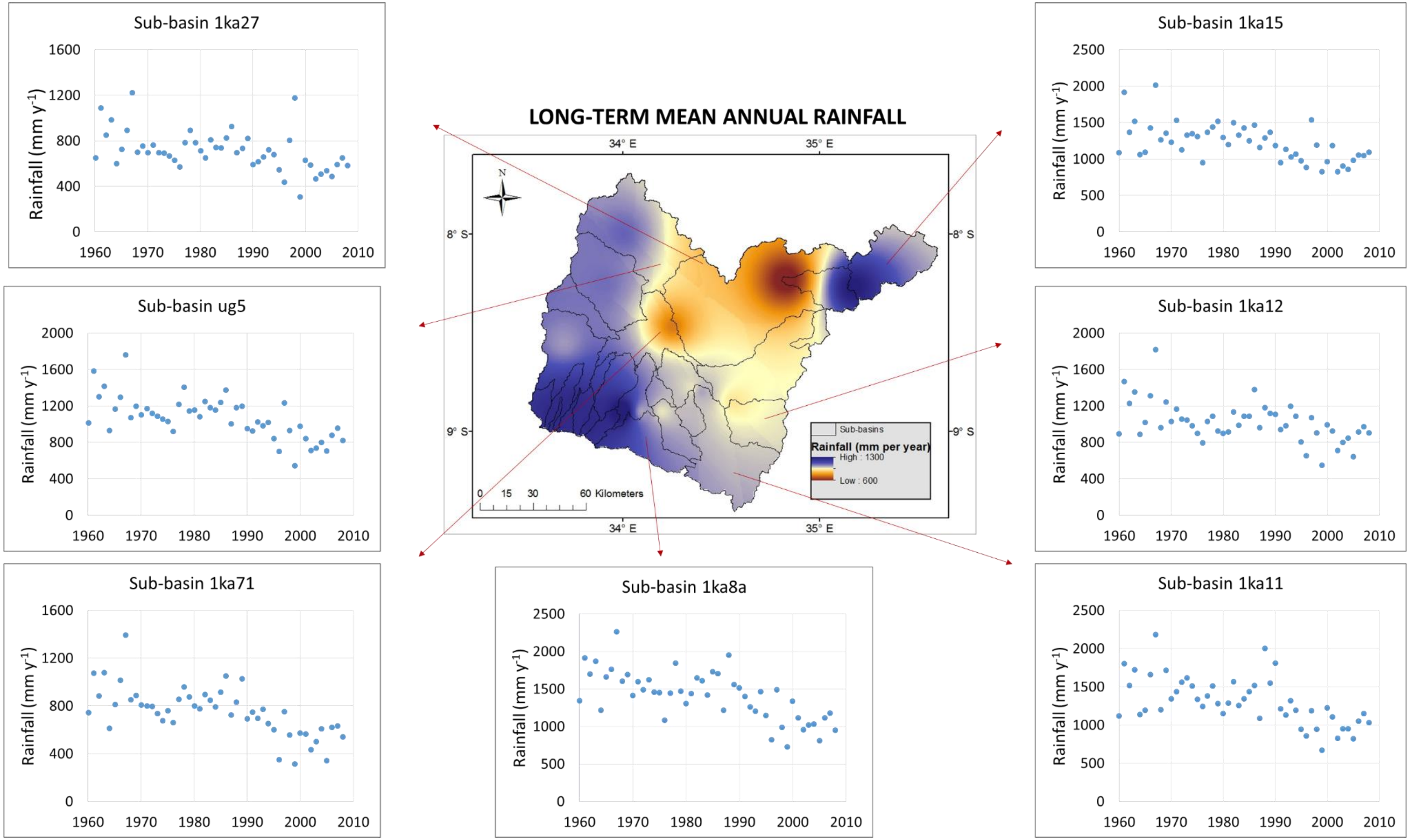

Figure 3.35: Spatial variations of the mean annual rainfall and the inter-annual rainfall variations for some of the sub-basins in the Upper Great Ruaha River basin for the period 1960 – 2009.

3.4.4.2 Temperature and potential evapotranspiration (PET)

The minimum and maximum mean monthly temperatures vary between 15^o – 24^oC and 28^o – 30^oC, respectively in the plains and from 5^o – 13^oC and 22^o – 27^oC in the highlands (Tumbo, 2015). Maximum temperatures are normally observed in October or November and low temperatures are observed between May and August (Wilson, 2003). Generally, the mean annual temperature in the Upper Great Ruaha River basin is approximately 18^oC in the highlands and 28^oC in the Usangu plains (Kashaigili *et al*., 2006b). The annual evapotranspiration ranges between 1 380 mm y^{-1} and 1 868 mm y^{-1} (Table 3.7). September, October and November have the higher proportion of the annual evapotranspiration demand (10% – 12.4%) in most sub-basins. The October contribution to annual PET is the highest in many sub-basins and can be related to higher temperatures and lower rainfall experienced during this month. The spatial variation in the mean annual PET can also be related to the fluctuation in temperatures and rainfall across the entire basin (Figure 3.36). As expected, higher values of annual PET are experienced in the Usangu plains and low values in the highlands.

Table 3.7: Sub-basin average monthly potential evapotranspiration in the upper Great Ruaha River basin.

Sub-basin	Potential evapotranspiration (mm month^{-1})												Annual (mm)
	Oct	Nov	Dec	Jan	Feb	Mar	Apr	May	Jun	Jul	Aug	Sep	
1ka71a	190	154	139	140	132	148	133	143	147	165	187	190	1868
1ka56	187	170	195	119	112	120	112	117	114	124	142	165	1677
1ka33	179	162	129	114	106	115	107	111	108	118	135	156	1540
1ka15	179	162	129	114	106	115	107	111	108	118	135	156	1540
1ka27	199	180	144	127	118	128	119	123	120	132	151	174	1714
1ka10	183	163	131	116	108	116	108	113	111	120	138	158	1566
1ka9	187	165	130	115	107	114	107	108	107	117	138	163	1557
1ka51	170	144	110	100	94	101	94	94	92	104	126	151	1380
1ka50a	172	145	111	101	94	102	95	96	94	104	129	154	1396
1ka16a	181	154	117	107	100	107	101	100	98	110	135	161	1471
1ka7a	193	165	126	113	107	114	107	107	105	117	143	171	1566
1ka8a	174	153	120	107	99	106	99	101	99	109	128	151	1447
1ka11	155	126	113	115	108	121	109	117	120	135	153	155	1527
1ka12	203	179	141	125	116	124	116	117	114	126	149	177	1685
ug5	198	178	140	125	116	125	118	122	119	131	150	174	1694
ug3	204	182	144	127	117	128	121	123	119	131	153	176	1726
ug18	198	175	135	121	113	123	116	119	117	128	149	175	1668
ug1	181	154	119	109	102	110	103	105	103	114	139	162	1501
ug17	170	143	110	100	93	101	94	95	92	103	127	152	1380
ug16	172	146	111	101	95	102	95	95	93	105	128	153	1396
ug15	201	171	130	119	111	119	112	111	109	123	150	179	1634
ug2	213	187	147	131	121	130	121	123	121	133	157	185	1768
ug20	224	197	155	137	127	137	128	129	127	140	165	194	1859
ug6	189	153	138	139	131	147	133	142	147	165	186	189	1859
ug21	186	150	136	137	129	145	131	140	144	162	183	186	1828
ug4	180	145	131	132	125	140	126	135	139	156	177	180	1765
ug22	183	148	133	135	127	142	128	137	142	159	180	183	1797

Note: ug represents ungauged sub-basin adopted from Tumbo (2015)

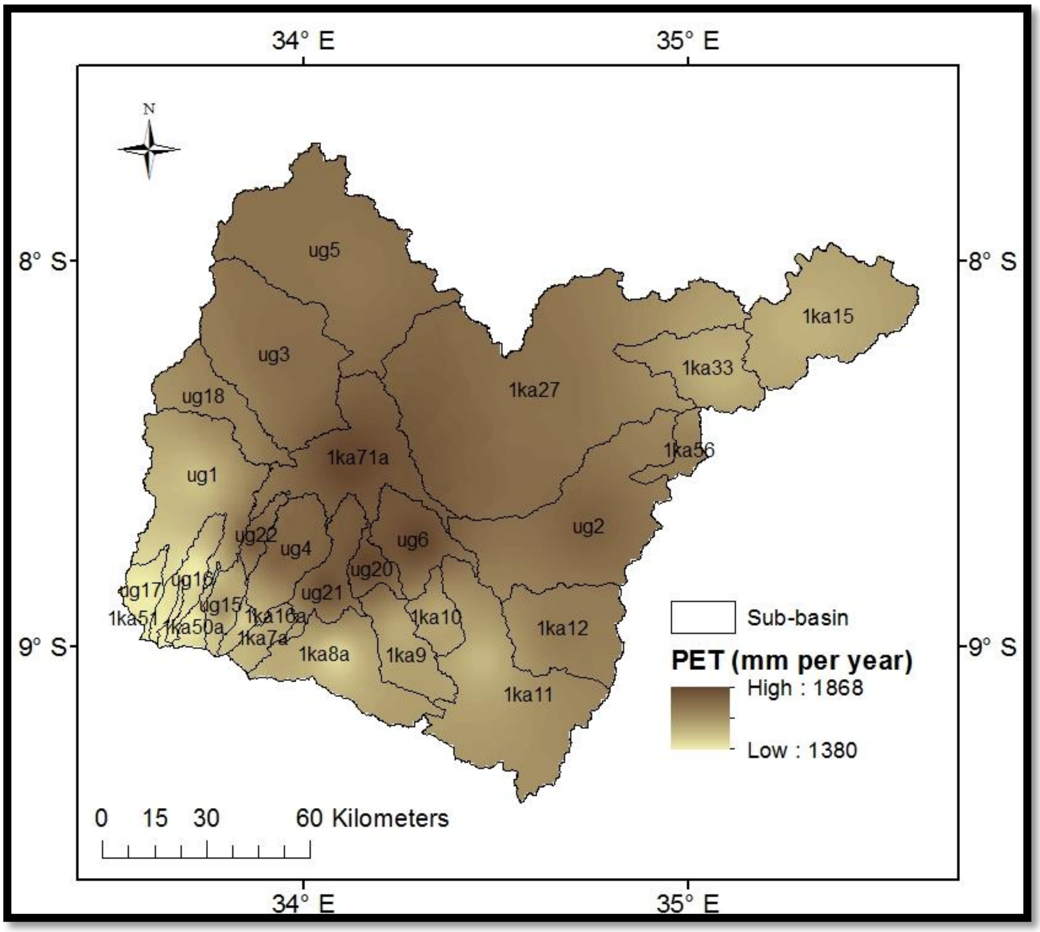

Figure 3.36: Variation of the mean annual potential evapotranspiration in the Upper Great Ruaha basin.

3.4.4.3 Streamflow

The Upper Great Ruaha River basin has both perennial and seasonal rivers which originate from the highlands of the basin. The perennial rivers draining into the Usangu Plains are the Great Ruaha, Mbarali, Kimani, Chimala, and Ndembera, whereas Kioga and Mjenje are seasonal rivers as indicated in Figure 3.30. The Great Ruaha River is the major source of water in the Usangu plains and it comprises of several tributaries that join to form a single river as they flow through a constriction at Nyaluhanga (Figure 3.30). The Great Ruaha River flows eastwards until it enters the permanent wetland known as Ihefu swamp (see Figure 3.41 below), and a few kilometres downstream the river exits the Usangu wetlands at Ng'iriama (Figure 3.30). In this study, the Upper Great Ruaha River basin includes 28 sub-basins and their areas are presented in Table 3.8.

Most of the perennial rivers were gauged (starting from the mid-1950s) but only a few gauging stations are currently operational (Table 3.9). Furthermore, the operational gauges have data for short periods and have missing values. The spatial distribution of the gauging stations in this basin is such that most gauges are upstream of the Usangu wetlands, and there are no gauges measuring the total inflows into or the outflows from the wetland (Figure 3.37). In addition, these gauges do not include all the key tributaries upstream to allow effective quantification of the total inflows into the Usangu wetlands. Gauging station 1ka71a is located where the Great Ruaha River enters the eastern wetland at Nyaluhanga (Figure 3.30 above). The gauging station 1ka59, which is located 80 km from the wetland outlet, is the only reliable gauging station normally used to estimate the outflows from the Usangu wetlands. There is not much substantial flow contribution into the Great Ruaha River between the wetland exit and where the gauge is located (Kashaigili *et al.*, 2006b). Table 3.9 summarises the extent of the data record for each gauging station (i.e. start and end year of the accessed data), and the percentage missing data.

Table 3.8: Catchment areas for the sub-basins in the Upper Great Ruaha River basin

Sub-basin ID	area (km^2)	Sub-basin ID	area (km^2)
1ka59	2539	ug4	500
1ka22	461	ug17	181
ug5	2149	ug21	420
1ka15	1221	ug16	277
1ka33	618	1ka51	38
ug3	1463	1ka50a	102
ug18	501	1ka16a	75
1ka56	182	1ka10	233
1ka27	4244	ug15	198
1ka71a	1055	1ka7a	169
ug1	1176	1ka12	807
ug20	175	1ka9	446
ug6	480	1ka8a	783
ug2	1709	1ka11	1600

Table 3.9: Streamflow gauging stations in the Upper Great Ruaha River basin

Station ID	River	Start	End	Latitude	Longitude	% Missing data	Status
1ka7a	Chimala	1962	1992	-8.9	34	52	Closed
1ka8a	Great Ruaha	1954	2009	-8.9	34.1	34	Operational
1ka9	Kimani	1954	2009	-8.9	34.2	17	Operational
1ka10	Mlomboji	1956	1983	-8.78	34.35	25	Closed
1ka11a	Mbarali	1955	2009	-8.8	34.4	17	Operational
1ka12	Halali	1956	1983	-8.85	34.57	20	Closed
1ka15	Ndembera	1956	2010	-8.3	35.2	12	Operation
1ka27	Great Ruaha	1965	1979	-8	34.58	36	Closed
1ka33	Ndembera	1957	2009	-8.2	34.8	52	Closed
1ka71	Great Ruaha	2001	2008	-8.4	34.23	52	Closed
1ka59	Great Ruaha	1963	2010	-7.8	34.15	15	Operation
1ka16	Lunwa	1964	1994	-8.957	33.83	58	Closed
1ka50a	Umrobo	1960	1994	-8.859	33.74	32	Closed
1ka51a	Mswiswi	1958	1976	-8.918	33.66	68	Closed

Source: Tumbo (2015)

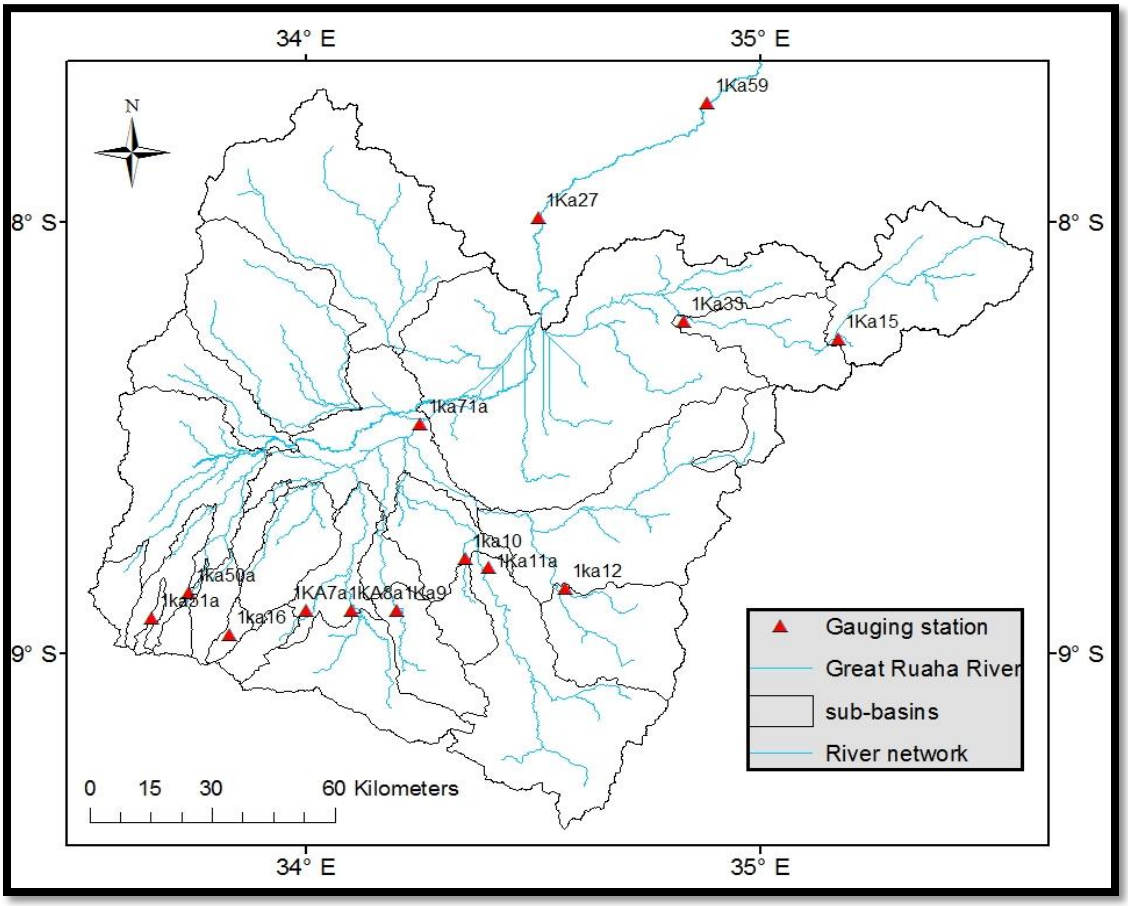

Figure 3.37: Location of the streamflow gauging stations in the Upper Great Ruaha River basin.

The mean monthly hydrographs for some of the gauged sub-basins show a unimodal pattern with a rising limb starting from late November/early December and most of the headwater sub-basins peaking in March except for the Ndembera River (gauge 1ka33) which peaks in April (Figure 3.38). The recession limb extends from May to September. A considerable decrease in the annual runoff since 1993 has been reported for the Great Ruaha River and its tributaries due to a rapid increase in water abstractions for irrigation purposes (Kashaigili *et al.*, 2006b; Mwakalila, 2011). In some years, zero flow was observed downstream of the Usangu wetland outlet (Kashaigili *et al.*, 2006a; McCarthy *et al.*, 2008), perhaps because of significant decrease of Usangu wetland inflows (about 70%) (Kashaigili *et al.*, 2006b). Table 3.10 presents the catchment area and the corresponding mean annual runoff for some of the gauged sub-basins. The mean annual runoff in the sub-basin 1ka59 is about 2 235 × 10^6 m^3, with the annual coefficient of variation greater than 1 (Table 3.10). This indicates a high variation of annual runoff which has been reported by other studies (Kashaigili, *et al.*, 2006b; McCartney *et al.*, 2008; Mwakalila, 2011; Tumbo, 2015).

Table 3.10: Mean annual runoff for some gauged sub-basins in the Upper Great Ruaha River basin.

Station ID	River	Catchment (km^2)	Mean Annual Runoff (× 10^6 m^3)	Annual coefficient of variation (CV)
1ka51	Umrobo	55	22	0.47
1ka16a	Lunwa	77	47	0.57
1ka7a	Chimala	167	99	0.55
1ka8a	Great Ruaha	795	489	0.32
1ka9	Kimani	448	211	0.45
1ka11	Mbarali	1 600	509	0.38
1ka12	Halali	807	201	0.6
1ka15	Ndembera	1221	203	0.56
1ka33	Ndembera	2 190	372	0.37
1ka27	Great Ruaha	19 941	1577	0.57
1ka59	Great Ruaha	24 620	2235	1.20

Modified from Tumbo (2015)

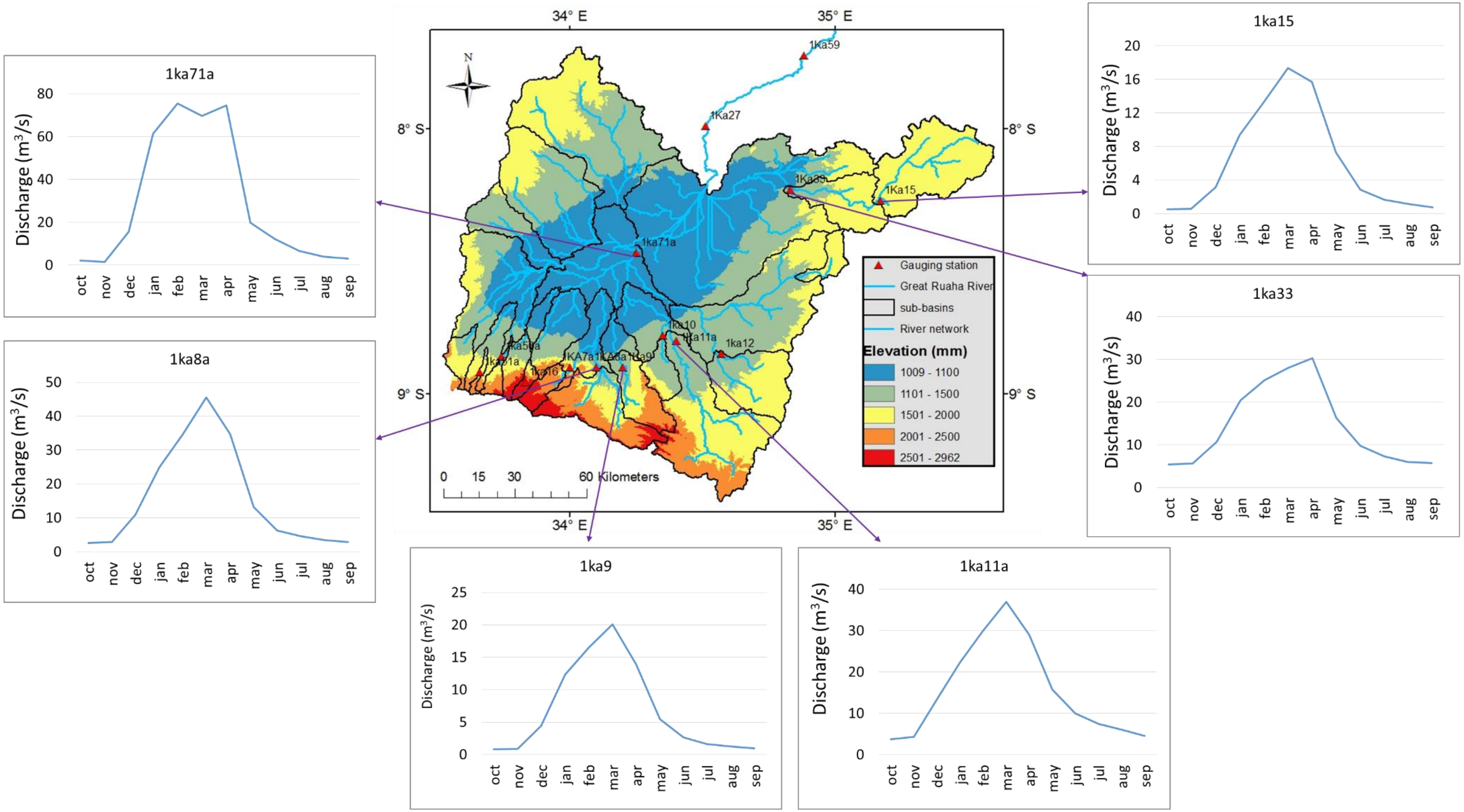

Figure 3.38: Streamflow seasonality for some gauged sub-basins in the Upper Great Ruaha River basin.

3.4.5 Water use

The main water uses in the Upper Great Ruaha River basin are: 1) abstractions for domestic use, 2) irrigation in the plains, and 3) pastoralists (Lankford *et al.*, 2004; WWF 2010), with abstraction for irrigation being the largest water use component. There are both large and small-scale irrigation farms, mainly for paddy rice which constitute about 15% of the rice production in Tanzania (Mtahiko *et al*., 2006; Lankford *et al*., 2009). The other small irrigation farms include maize, beans, tomatoes and vegetables. Water is abstracted from both perennial and seasonal tributaries flowing into the Usangu plains, thereby affecting the inundation patterns of the Usangu wetlands. The irrigated area in the Usangu plains is approximately 420 km^2 and 170 km^2 in wet and dry years, respectively (Tumbo, 2015). Figure 3.39 shows the location of the large-scale paddy rice farms in the Usangu plains with many of them located in the western wetland except for the Madibira Smallholder Agriculture Development Project which is in the eastern part. Some of these farms are shown in Figure 3.40; the top image is part of the Kapunga rice farm and the bottom one is a section of the Madibira farm.

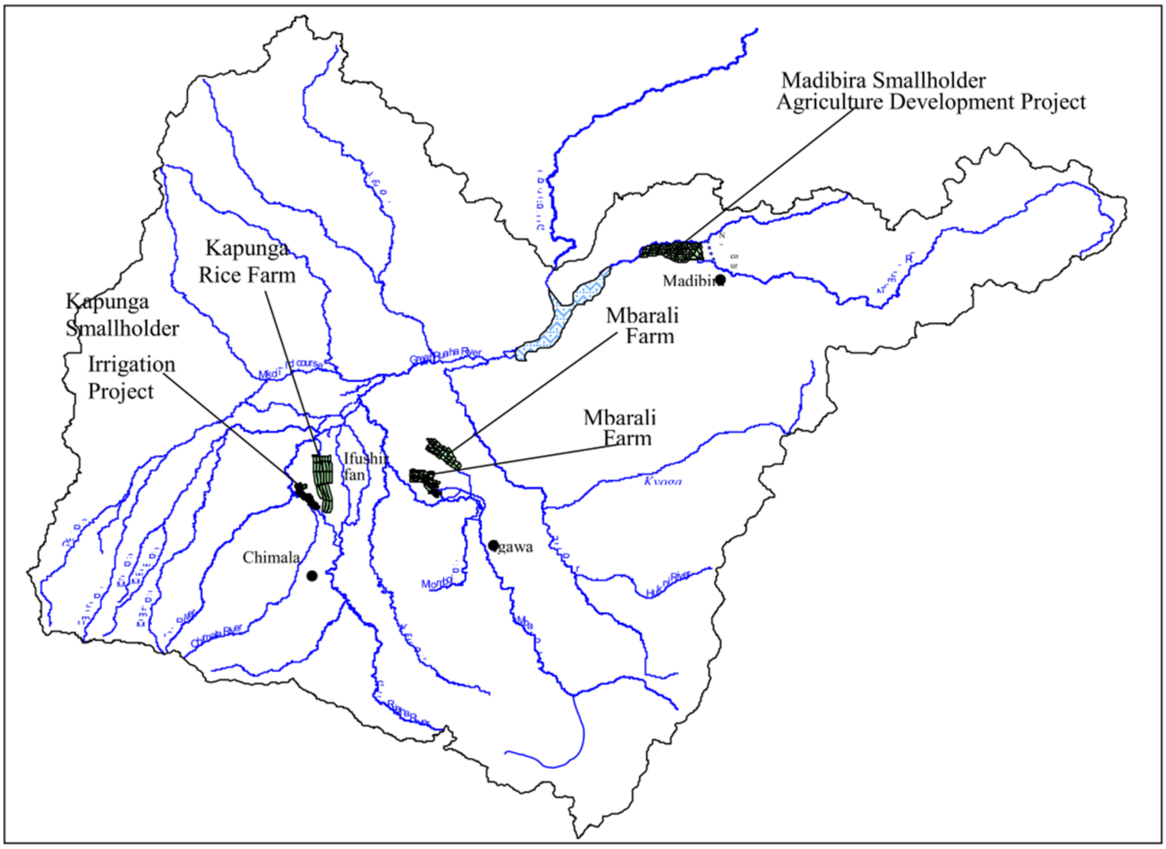

Figure 3.39: Location of the large-scale irrigation farms in the Upper Great Ruaha River basin (Source: SMUWC, 2001).

Figure 3.40: Google Earth images showing different paddy rice farms in the Usangu plains.

3.4.6 Usangu Wetlands

The Usangu wetlands are estimated to cover an area of about 2×10^3 km^2, and they are divided into two parts (west and east wetlands) by a slightly elevated ridge of underlying basement rock at Nyaluhanga (SMUWC, 2001; Kashaigili *et al*., 2006a; Mwakalila, 2011) (Figure 3.41). The western wetland is mostly seasonally flooded. The eastern wetland contains seasonal grassland and a permanently inundated swamp (Ihefu swamp) covering approximately 80 km^2 with an average inundation depth of 2 – 3 m (McCartney *et al*., 2008). The western wetland receives water from the rivers draining the highlands, whereas the eastern wetland receives inflows from the Great Ruaha River at Nyaluhanga and the Ndembera River. Moreover, the outflow from the eastern wetland is controlled by a rock bar at the wetland outlet (Ng'iriama) (Kashaigili *et al.*, 2006b; Mwakalila, 2011). When the flow in the *Ihefu* swamp starts to recede, the swamp divides into small five ponds (SMUWC, 2001). The topography of the Usangu wetlands is very flat, however, the eastern part of the eastern wetland is slightly higher (about 6 m higher than the Ihefu swamp), and it is assumed to be a perched section of the Usangu wetland (SMUWC, 2001). The Usangu wetland is characterised by numerous channels with varying connectivity to the main channel (Figure 3.42). Generally, these channels form a complex drainage network that contributes to water dispersion in different parts of the Usangu wetlands (Canisius *et al*., 2011; Mwakalila, 2011). Different vegetation and aquatic species are found in the wetlands; the eastern wetland is dominated by grasslands and aquatic vegetation whereas Miombo, Thorny trees and wood grasslands are found in the western wetland (SMUWC, 2001; Kashaigili *et al.*, 2006a; Mtahiko *et al*., 2006). Fishing is also dominant in the Ihefu swamp, whereas irrigation activities (i.e. paddy rice farms) are common in the western wetland.

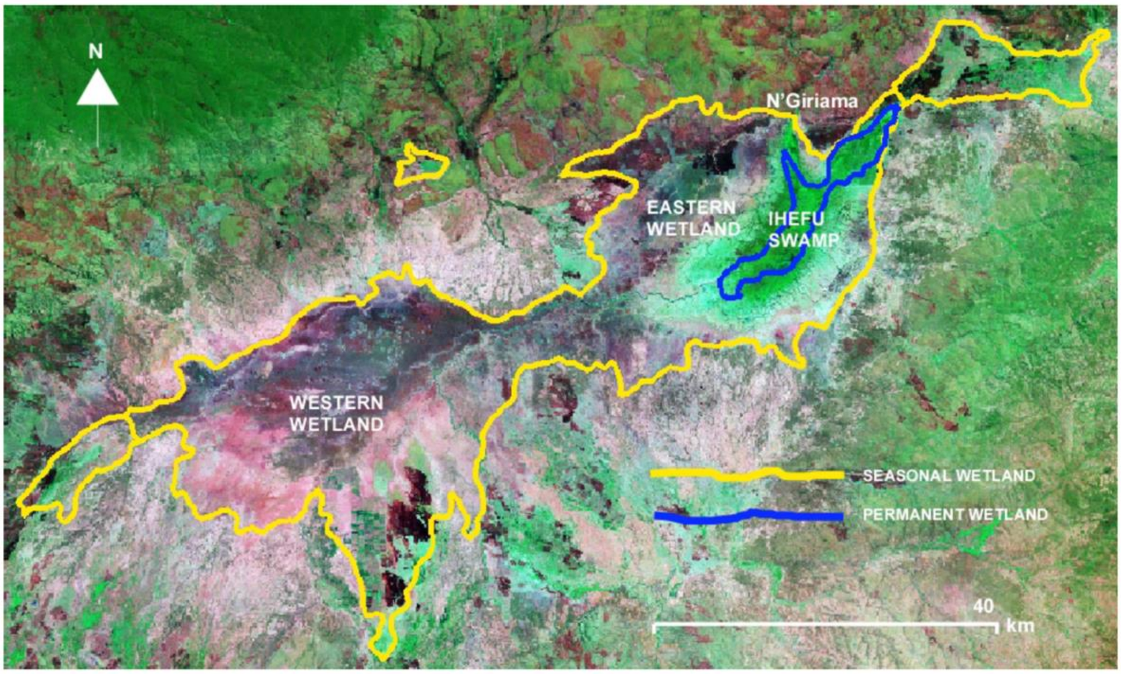

Figure 3.41: The Usangu wetlands (modified from Mwakalila, 2011).

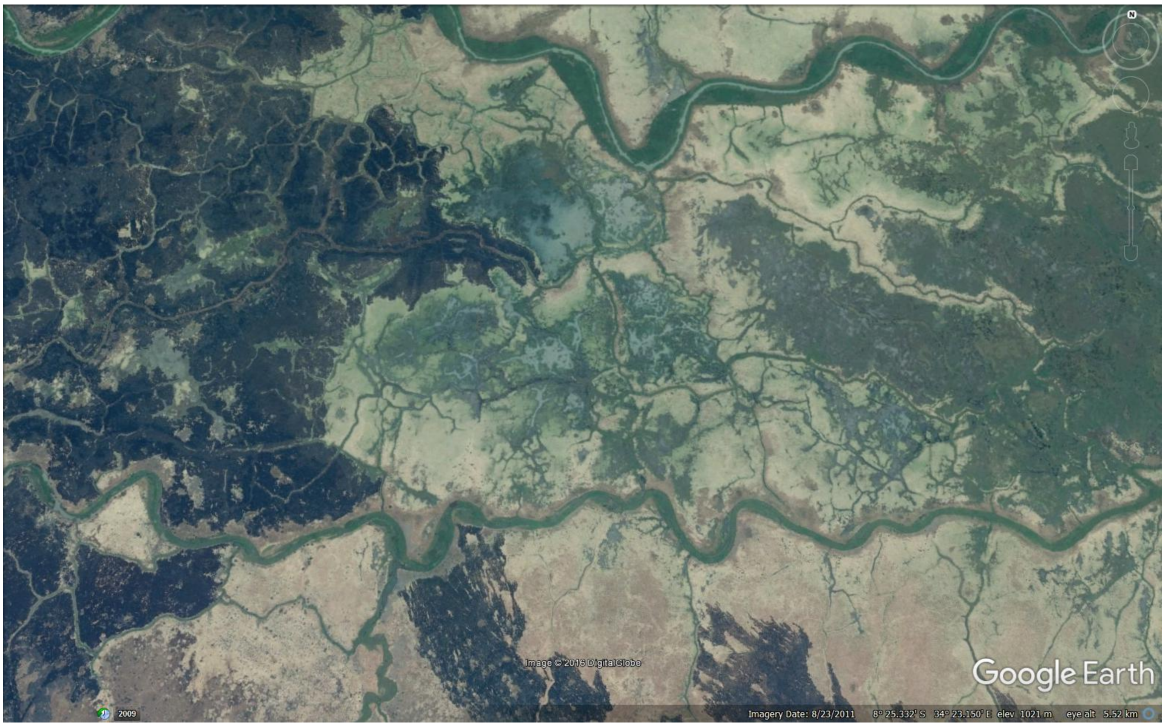

Figure 3.42: Google Earth image showing the distribution of different channels in the eastern wetland.

3.5 Conclusions

The physical and climatic characteristics of the three river basins including their wetlands have been presented in this chapter. The three river basins have a diverse physiography, and the wetlands in these basins have unique characteristics which influence the wetland inundation characteristics. For instance, the Usangu wetlands consist of numerous channels with variable connectivity to the main channel, and in the Barotse floodplain, a large part of the floodplain is above the main channel. In general, an understanding of the spatial and temporal variability of the physical and climatic characteristics is considered to be important in establishing the appropriate model parameters, thereby improving the results of the model simulation.

CHAPTER FOUR: METHODOLOGICAL FRAMEWORK

The rationale of the present study is to improve the understanding of hydrological response and efficient modelling of water resources availability for practical purposes at a basin-scale. The study focused on three basins containing large wetlands within southern Africa: 1) the Upper Zambezi River basin, 2) the Luangwa River basin, and 3) the Upper Great Ruaha River basin. A combined modelling approach is used, that involves combining the detailed high-resolution (time and space) LISFLOOD-FP hydraulic model (sub-grid version) with the basin-scale Pitman monthly hydrological model (Figure 4.1). The initial simulation results (with or without including wetland effects) from the basin-scale model are disaggregated to daily flows and are used to quantify the upstream boundary conditions for the LISFLOOD-FP model setup for the large wetlands under consideration. The LISFLOOD-FP model is validated as far as possible using observations of inundation extent or other information that can confirm the validity of the model setup. The outputs from the hydraulic model are then used to improve the understanding of the river–wetland water exchange dynamics and quantify the wetland parameters of the basin-scale model. The basin-scale model is then re-run with the wetland sub-model included and performance assessments conducted using any available observed data. While the version of the GW Pitman model used allows for parameter uncertainty, the LISFLOOD-FP model doesn't have specific uncertainty framework built into it ,but can be used within uncertainty framework (the component that was not specifically explored in this study). However, this is not considered to be a major restriction as the key uncertainties in water resources availability at the basin-scale will be captured by the final version of the Pitman model.

The two models used in this study were selected based on the review of three hydrological models and two hydraulic models presented in section 2.5 and 2.7. The GW Pitman hydrological model is less data intensive and includes the uncertainty analysis framework that suits data scarce basins of southern Africa. Its channel–wetland exchange function has been demonstrated to be appropriate for river basins containing large wetlands (Hughes *et al*., 2014). Further, it is linked to the disaggregation sub-model that is useful in disaggregating monthly to daily flows. Overall, the GW Pitman model remains one of the most widely used hydrological model in the southern Africa region (Hughes, 2013). The LISFLOOD-FP is a freely available hydraulic model that can be applied in wetlands of different sizes. The recent version that provides for the hydraulic characteristics of channels that are smaller in size compared to the grid size is useful for wetlands that interact with small channels. Unlike MIKE 21, the LISFLOOD-FP is not data intensive, thereby it suits data scarce basins and a significant number of studies have applied this model in different wetlands in Africa (see section 2.7.2). In addition, the Institute for Water Research (IWR; where this study was carried out) has established a strong collaboration with Bristol University (i.e. the model developers), hence more support was available during setting up the LISFLOOD-FP model.

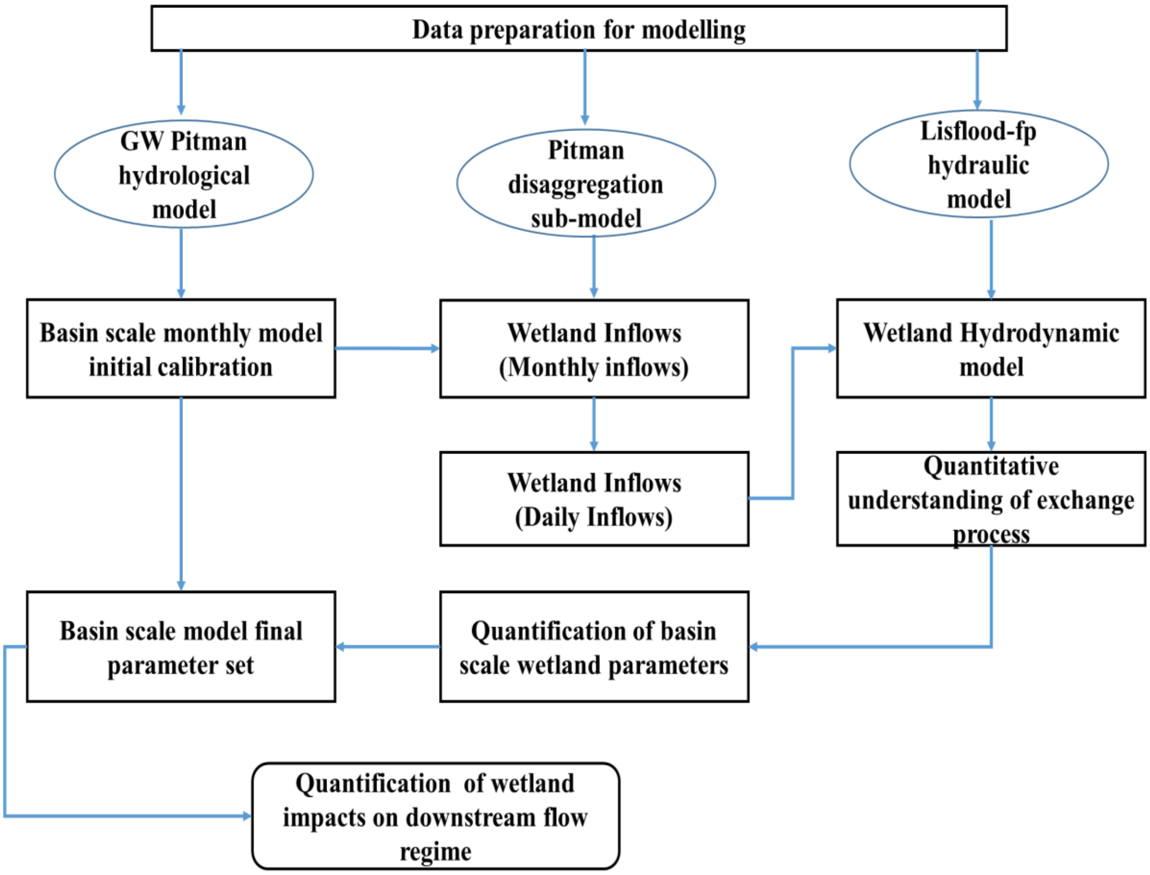

Figure 4.1: Flow chart diagram illustrating the combined modelling approach used in this study

4.1 Data preparation for modelling

4.1.1 Sub-basin delineation

ArcGIS is frequently being used for automatic delineation of basins (Tarboton, 2005; Pryde *et al.*, 2007). The hydrology tool and other ArcGIS extensions, such as Arc Hydro, TAUDEM and ArcSWAT are capable of delineating basins from topographical, land cover, slope or geological characteristics presented in a grid format (Jankowfsky *et al*., 2013; Li, 2014). In this study, the ArcSWAT (SWAT2012) extension was used to delineate each basin into sub-basins using the topography, slopes and main streams derived from the DEM. The streams were generated using a threshold value (assumed to be a catchment area), the selection of which is always critical and varies from basin to basin. To arrive at a reasonable threshold value, different values were tested through a trial and error method. For instance, the threshold values of 2 700 km^2 and 4 000 km^2 were used in the Luangwa and Upper Zambezi River basins, respectively.

To simplify the link between the LISFLOOD-FP and Pitman models, there was a need to identify the sub-basins that represent the major wetland inflows and those that represent the main wetland inundation effects. The downstream points of the inflow sub-basins should be correctly located to represent the wetland inflows to the LISFLOOD-FP model. The sub-basin delineation identified using ArcSWAT was therefore modified by creating nodal points at the downstream end of the key tributary inflow sub-basins, as well as the downstream ends of the main wetland areas. These nodal points were then used to setup the GW Pitman Model and the original sub-basin areas adjusted accordingly. To illustrate the approach, Figure 4.2 shows the delineated sub-basins and the sub-basin nodal points for the Luangwa basin and Table 4.1 presents areas of the original sub-basins and the new nodal point sub-basins.

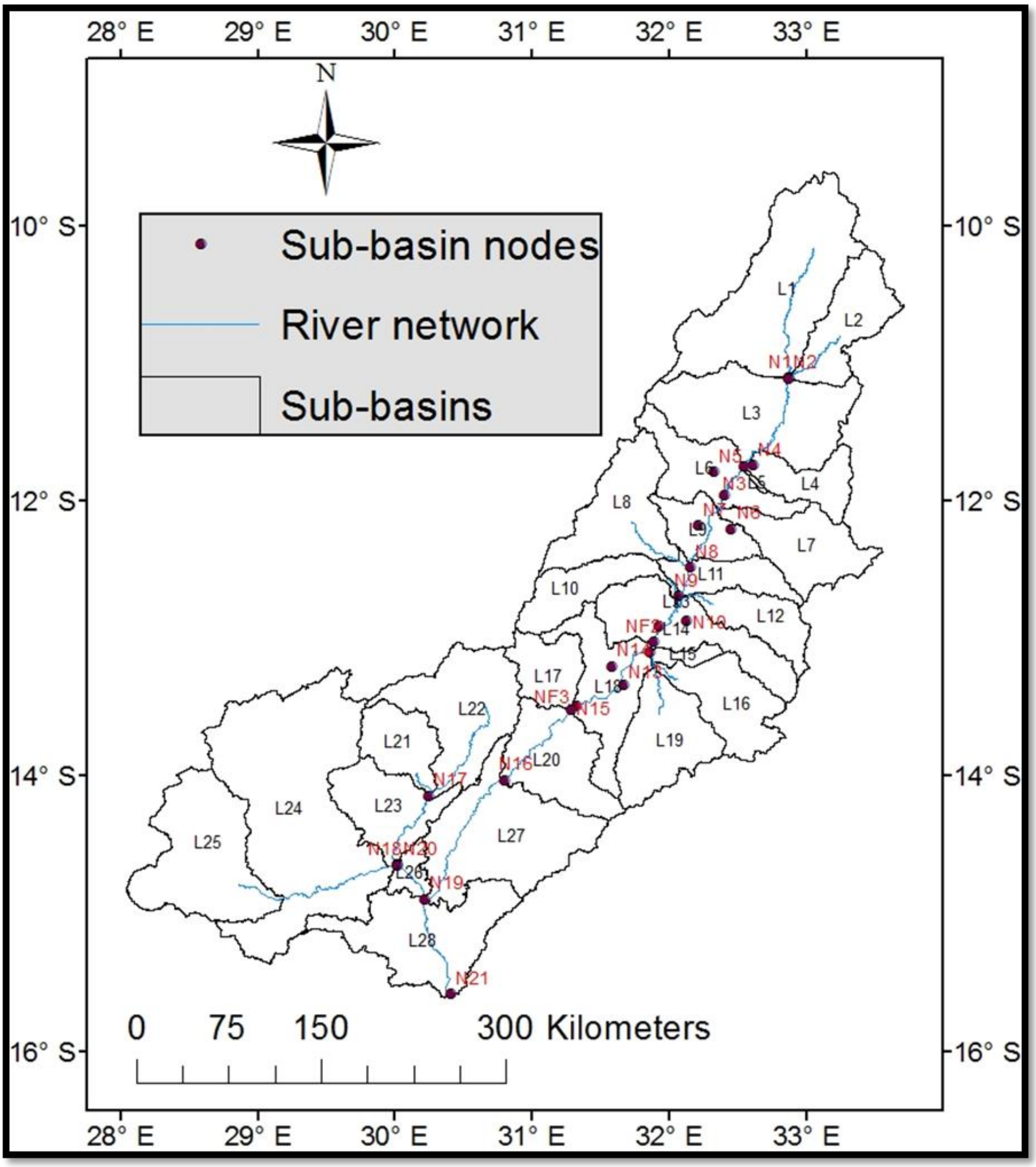

Figure 4.2: Original sub-basins and the created sub-basin nodal points in the Luangwa River basin. Note: Sub-basin name starts with ‘L’ and sub-basin node with ‘N’.

Table 4.1: Catchment areas of the original sub-basins and the new sub-basins nodes.

Sub-basin Name	Sub-basin Area (km^2)	Sub-basin Nodes	Sub-basin Node Area (km^2)	Remarks on Sub-basin Node areas
L1	12742	N1	12742	Same as L1
L2	4465	N2	4465	Same as L2
L3	9168	N3	8821	Part of L3 excluding wetland (inflows from East & West)
L4	2744	N4	3508	L4 and L5 & East part of L6
L5	86	N5	3511	West part of L6
L6	4647	NF1	805	Upper section of the floodplain
L7	4710	N6	5610	L7 and East part of L9 (about 40%)
L8	6150	N7	1467	West part of L9 (about 60%)
L9	2837	N8	6180	L8 & West part of L11
L10	3490	N9	5209	East part of L11 & L12 (minus FP part)
L11	2645	N10	2740	East part of L14 (about 50%) less FP
L12	3063	N11	6259	L10 & L13 & West part of L14 less FP
L13	29	NF2	1410	Middle section of the floodplain
L14	5950	N12	5146	L15 & L16
L15	668	N13	7178	L19 & East part of L18 (40%) less FP
L16	4478	N14	2763	West part of L18 (60%) less FP
L17	2841	NF3	880	Lower section of the floodplain
L18	5339	N15	2842	L17
L19	5482	N16	5427	L20
L20	5426	N17	10396	L21 and L22
L21	3164	N18	4572	L23
L22	7231	N19	9633	L27
L23	4571	N20	27997	L24 and L25
L24	19235	N21	8614	L26 andL28
L25	8762			
L26	997			
L27	9633			
L28	7617			

4.1.2 Extracting physical and hydrological characteristics for each sub-basin

The physical and hydrological characteristics of the sub-basins were established from both ground-based and satellite derived global datasets. Some of these characteristics are rainfall, evaporation, temperature, streamflow, soils, topography, and land cover. The data sources, including their limitations, are discussed in Chapter 3, and their choice was largely constrained by availability rather than reliability assessments. This is largely because there is no additional information to compare with at a local scale. Topography, soil and land cover were downloaded in grid format from the SRTM (Farr and Kobrick, 2000); the SoilGrids 1 km; (Hengl *et al*., 2014); and the USGS land cover (USGS LCI: Broxton *et al*., 2014) data sources, respectively. They were then processed into the required format using some ArcGIS tools such as Spatial Analyst (extraction then extraction by mask) and Data Management (projection and transformation). The initial step was to extract the data for the entire basin and then for individual sub-basin/sub-basin nodes.

Daily rainfall data gridded at 0.1° resolution (ARC2 satellite rainfall: Novella and Thiaw, 2013) and monthly rainfall at 0.5° resolution (CRU TS v. 3.22: Harris *et al*., 2014) were also downloaded in a grid format. The time series of monthly rainfall data were extracted using a program linked to the SPATSIM (Spatial and Time Series Information Modelling) platform (Hughes and Forsyth, 2006). The extraction process involved three main steps as shown in Figure 4.3. Initially, the raw data file was selected, followed by the selection of a point file which includes the centroid points for each sub-basin. The last step was to choose the required format between the single point and catchment/basin average. For sub-basin rainfall, the single point format was selected. Similar steps were used to extract the satellite gridded daily rainfall into time series (Figure 4.4). Potential evapotranspiration and temperature data from the IWMI Climate Data Portal (New *et al*., 2002) are also in a grid format and were downloaded as long-term mean monthly values (mm d^{-1}) for the centroid point of each sub-basin. The monthly values (mm $month^{-1}$) used in both models were computed from the long-term mean monthly values.

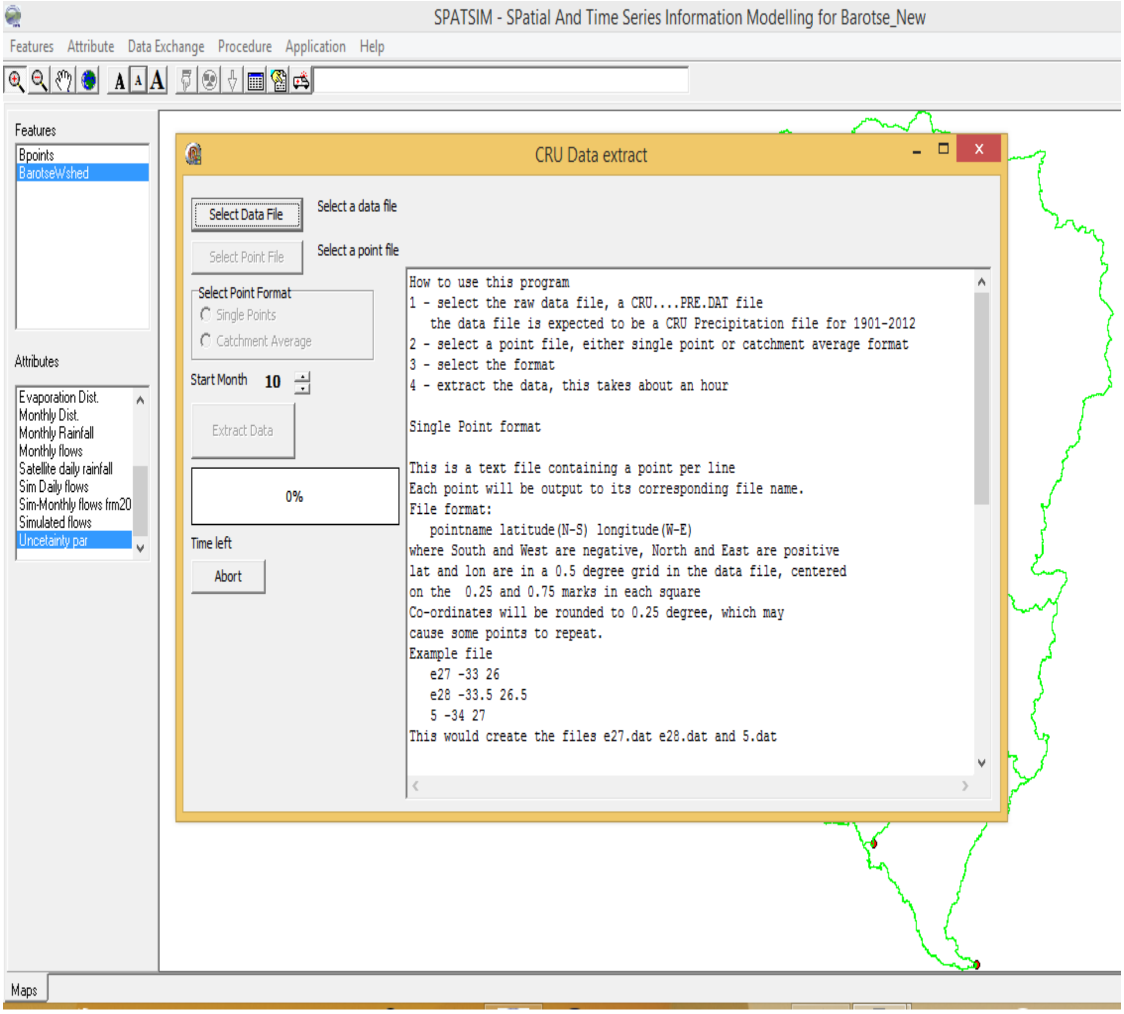

Figure 4.3: A screenshot of the CRU time series data extract program of SPATSIM.

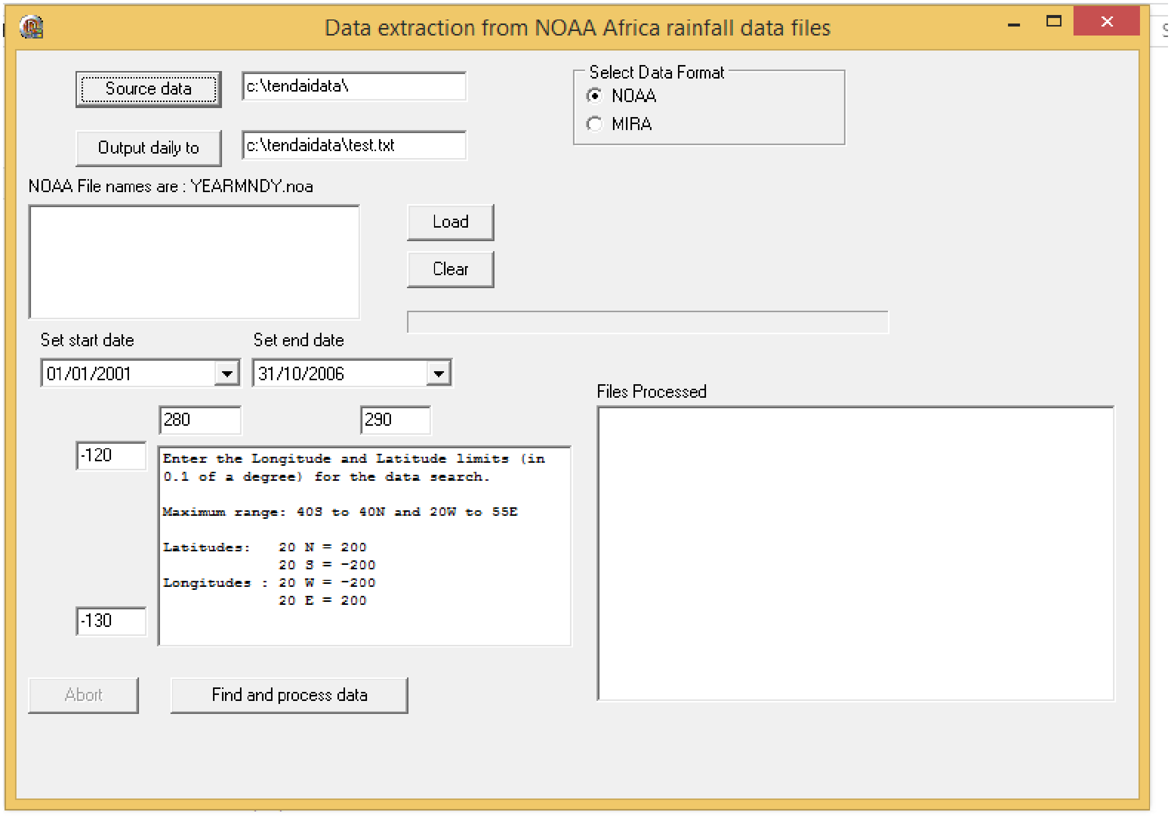

Figure 4.4: A screenshot of the ARC2 satellite time series data extract program.

4.1.3 Sub-basin similarity analysis

The sub-basin similarity analysis was used to identify sub-basins that are expected to have similar hydrological responses and consequently similar parameter values. This is required to assist with establishing the parameter sets for the Pitman model as most of the delineated sub-basins are not gauged, and therefore calibration is not possible. There are no universally accepted approaches for grouping sub-basins according to their similarity (Razavi and Coulibaly, 2013). However, spatial proximity, physiographic characteristics and various similarity indices are mostly applied (Parajka *et al*., 2005; Sawicz *et al*., 2011; Ali *et al*., 2012; Garambois *et al*., 2015). The use of multiple variables is required to attain an appropriate classification, but this is always subject to data availability. Slope, mean elevation, minimum elevation, maximum elevation, PET, mean annual precipitation (MAP), the Topographical Wetness Index (TWI: Beven and Kirkby, 1979); Aridity Index (AI: Budyko, 1974) and Hypsometric Integral (HI: Langbein, 1971) were used to group sub-basins according to their similarities in this study. Most of these variables were generated using ArcGIS techniques. The TWI, AI and HI were calculated using Equations 4.1 to 4.3, respectively by using the calculator tool in the ArcGIS. The influence of each variable on the classification process varies, and it was important to identify variables that explained the major differences between sub-basins. This was conducted using Principal Component Analysis (PCA) in SPSS version 21. All variables for each sub-basin were entered in the PCA, and the identified major variables were considered in the grouping of sub-basins. The resulting sub-basins found in the same group were assumed to have similar characteristics and were assigned similar model parameters values (or uncertainty ranges) during the model setup.

$$TWI = ln\left(\frac{a}{\tan\beta}\right) \qquad \text{(Equation 4.1)}$$

Where $'\beta'$ is a measure of water draining from a given point and

'a' is a measure of the water flowing towards a specified point.

$$AI = \frac{MAP}{PET} \qquad \text{(Equation 4.2)}$$

$$HI = \frac{Mean\ Elevation - Minimum\ Elevation}{Maximum\ Elevation - Mean\ Elavation} \qquad \text{(Equation 4.3)}$$

4.2 Spatial and Time Series Information Modelling (SPATSIM)

The Spatial and Time Series Information Modelling (SPATSIM) platform was developed at the Institute for Water Research (IWR), Rhodes University (Hughes and Forsyth, 2006). It is freely available software and can be downloaded from the IWR website (https://www.ru.ac.za/iwr/research/spatsim/). The full details of SPATSIM are not presented here but can be found in Hughes and Forsyth (2006) as well as within the 'Help' options that are part of the software package. The software forms a modelling framework, providing a common platform for the storage and analysis of data, as well as running various hydrological and water resource models. The main aim of SPATSIM is to improve the efficiency of the application of hydrological models for solving different types of water resources problems. There are currently multiple models that can be run through SPATSIM, including the GW Pitman model and its related versions, such as the Pitman Uncertainty model and the Pitman Disaggregation sub-model. Various past studies have used SPATSIM as a platform to run the Pitman model (e.g. Bharati and Gamage, 2011; Tshimanga *et al*., 2011; Kapangaziwiri *et al*., 2012; Hughes *et al*., 2014; Tumbo and Hughes, 2015; Slaughter *et al*., 2015; Hughes and Slaughter, 2016). SPATSIM manages data through data attributes, stored in database tables, and linked to spatial features. The features comprise ArcGIS created shapefiles (e.g. sub-basin polygons, points and river networks), while many different attribute types are allowed for so that all of the input and output information typically associated with running a hydrological model can be stored in a SPATSIM database (Table 4.2).

Table 4.2: The GW Pitman model attributes in the Spatial and Time Series Information Modelling (SPATSIM) platform.

Attribute Type	Attribute Requirement
Text	Catchment ID
	Downstream Area
Single real number	Catchment area (km^2)
	Catchment cumulative area (km^2)
Time series	Average rainfall (mm)
	Observed monthly flow (volume)
	Downstream outflow (volume)
	Uncertainty ensembles
One dimension array	GW-model parameters
	Mean monthly evaporation (monthly % of total annual)
	Reservoir model parameters
	Wetland model parameters
	Disaggregation parameters
Two dimensional array	Uncertainty parameters
	Monthly water distribution (fractions)

4.3 The GW Pitman model

4.3.1 The structure and parameters of the GW Pitman model

The main inputs for this model are rainfall and potential evaporation; these data are used to force the different basin processes (i.e. surface, sub-surface and groundwater processes) which are considered in the generation of stream flow (Figure 4.5). The processes are represented by the model algorithms and the model parameters (Table 4.3). The full details of the model algorithms are provided in many previous publications (see for example Kapangaziwiri, 2011) and are not repeated here. However, the following paragraphs provide brief descriptions of the model parameters and how they are used in the model process algorithms.

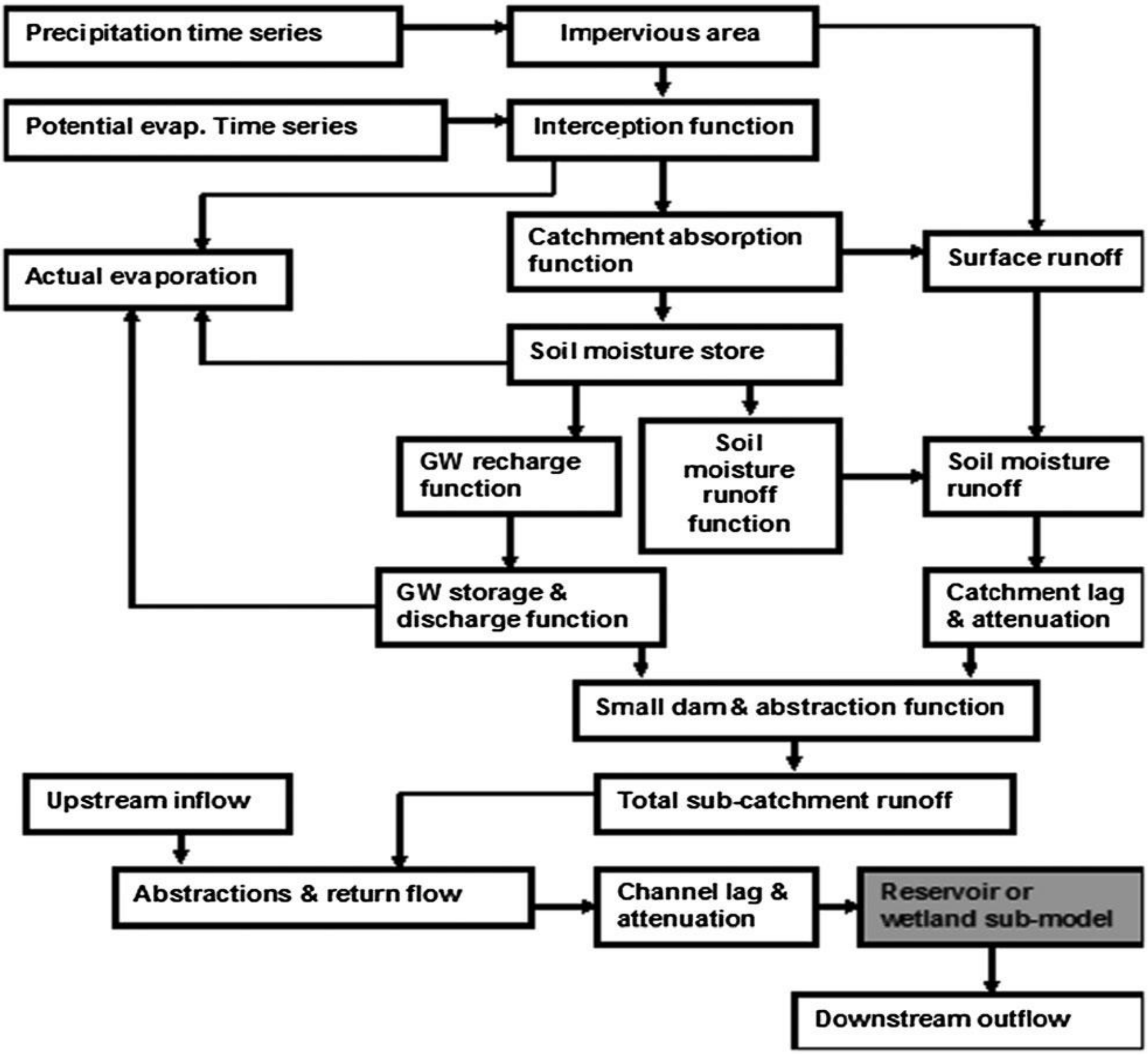

Figure 4.5: Structure of the GW Pitman model (Source: Hughes *et al*., 2014).

Table 4.3: The GW Pitman model parameters

Parameter	Units	Parameter description
RDF		Rainfall distribution factor
AI		Fraction of impervious area of the sub-basin
PI1 and PI2	mm	Interception storage for the two vegetation types
AFOR	%	Area of sub-basin under vegetation type 2
FF		Fraction ratio of potential evaporation rate for veg 2 relative to veg 1
PEVAP	mm y^{-1}	Annual potential evaporation (typically based on S-pan values)
ZMIN	mm $month^{-1}$	Minimum sub-basin absorption rate
ZAVE	mm $month^{-1}$	Mean sub-basin absorption rate
ZMAX	mm $month^{-1}$	Maximum sub-basin absorption rate
ST	mm	Maximum moisture storage capacity
SL	mm	Minimum moisture storage below which no GW recharge occurs
POW		Power of moisture storage-runoff equation
FT	mm $month^{-1}$	Runoff from the moisture storage at full capacity (ST)
GPOW		Power of moisture storage-GW recharge equation
GW	mm $month^{-1}$	Maximum groundwater recharge at full capacity (ST)
RSF	%	Controls the riparian evaporation losses from GW storage
R		Evaporation-moisture storage relationship parameter
TL	months	Lag of surface and soil moisture runoff
CL	months	Channels routing coefficient
DDENS	km km^{-2}	Drainage density
T	m^2 d^{-1}	Groundwater transmissivity
S		Storativity
GW Slope		Slope fraction initial groundwater gradient
Reservoir and water abstraction parameters		
A and B		Parameters in nonlinear area-volume relationship
MAXDAM	$m^3 \times 10^6$	Reservoir capacity
IWR	$m^3 \times 10^6$	Return flows from irrigation
IrrAreaDmd	km^2	Area irrigated from the small dams
NIrrDmd	$m^3 \times 10^6$	Annual volume of non-irrigation demand
EffRRF	mm	Amount of rainfall reduces the irrigation depth

Rainfall distribution function (RDF): This parameter controls the distribution of total monthly rainfall in the four iterations used in the model, and can be estimated from an understanding of the rainfall characteristics of the basin. Ideally, a month is divided into four iterations, and rainfall is distributed to each using a non-linear distribution. The original model used a fixed value of 1.28, however, some studies such as Mwelwa (2004), have used lower values in areas of southern Africa that frequently experience very high wet season monthly rainfalls.

Interception parameters (PI1 and PI2): Two main assumptions are considered in the model: 1) the total rainfall within a day is concentrated in a single storm event and; 2) the intercepted rainfall is lost through evaporation before the next day. PI1 and PI2 are parameters that control interception in the model. PI1 represents the primary vegetation type (natural vegetation), whereas PI2 represents secondary vegetation such as a planted forest. Past studies in South Africa have adopted values of 1.5 and 4 for PI and PI2, respectively (Kapangaziwiri, 2008). Parameter AFOR specifies the % of the sub-basin area that is covered by the secondary vegetation type.

Evapotranspiration from moisture store parameters (R and FF): R controls the ratio of actual to potential evaporation in a linear relationship with the relative soil moisture storage (Kapangaziwiri, 2008). The value of R ranges between 0 and 1 with higher values representing generally lower volumes of actual evapotranspiration and *vice versa.* FF scales the potential evaporation for the secondary vegetation type.

Infiltration and surface runoff parameters (ZMIN, ZAVE, ZMAX, and AI): The vertical movement of water in the basin is controlled by the infiltration capacity of the soils. ZMIN, ZAVE, ZMAX, and AI parameters guide the generation of surface runoff. The parameter AI accounts for surface runoff from impermeable areas. The ZMIN, ZAVE and ZMAX parameters define a triangular distribution of sub-basin absorption rates (Figure 4.6). No surface runoff is generated during periods of rainfall below ZMIN, whereas progressively higher rainfall amounts contribute to increasing volumes of surface runoff. Higher values of the parameters are assigned to sub-basins with coarser textured and well-drained soils, whereas smaller values are appropriate for finer textured soils.

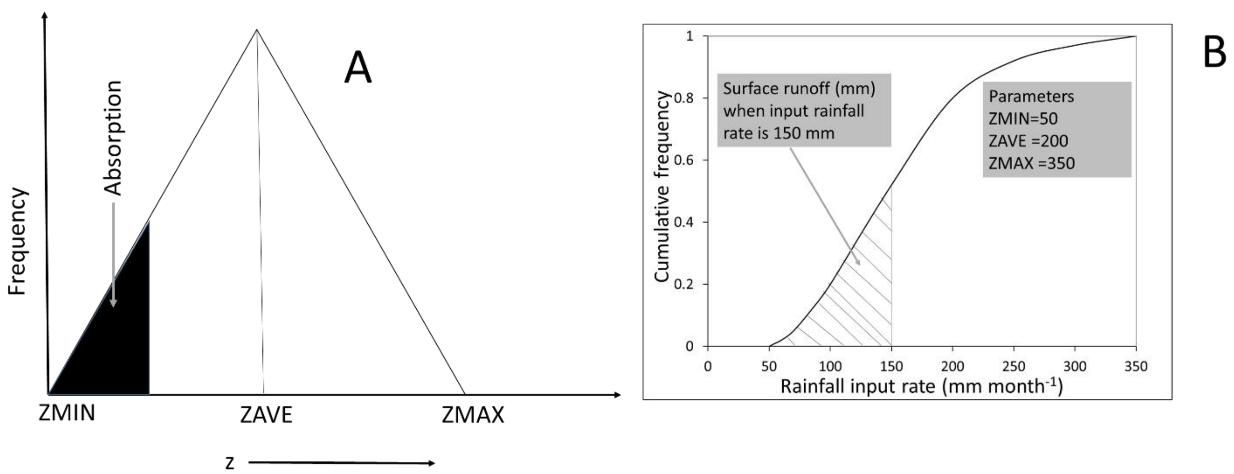

Figure 4.6: Frequency distribution of basin absorption rate, Z (A) and cumulative frequency curve of generated surface runoff, r is the rate of rainfall input (B).

Soil moisture storage and runoff parameters (ST, POW, and FT): ST is the maximum depth of subsurface unsaturated zone storage, with any rainfall inputs that exceed ST contributing to surface runoff. This parameter combines storage in soils (ST_{soil}) and the deeper unsaturated zone (ST_{unsat}). The value of ST_{soil} depends on soil porosity and soil depth, whereas ST_{unsat} depends on storativity and depth of fractured rocks (Kapangaziwiri, 2011). Deep, well-drained soils have higher ST values compared to shallower soils. FT and POW represent the scale and power parameters, respectively, of a non-linear relationship (Figure 4.7) between the soil moisture storage level (S) and the depth of interflow runoff.

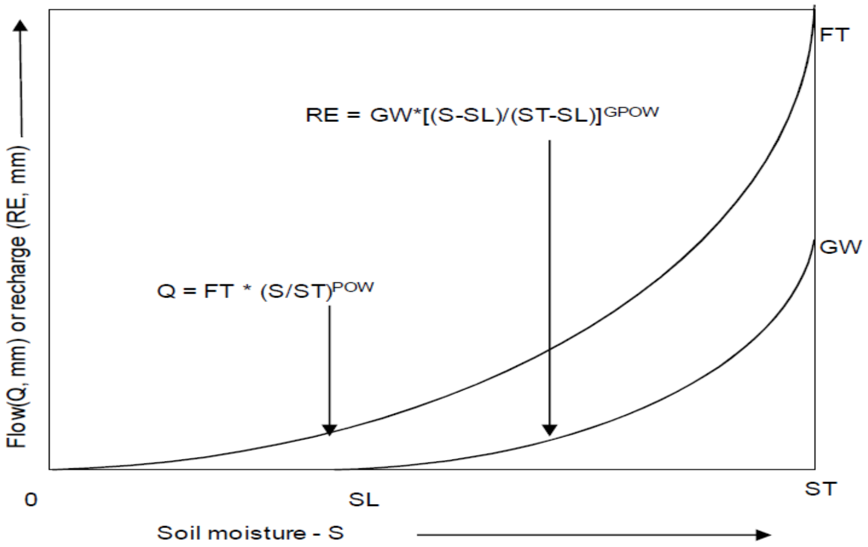

Figure 4.7: Soil moisture storage and subsurface runoff generation parameter relationship (Source: Kapangaziwiri, 2008).

Groundwater discharge and recharge parameters (DDENS, T, S, RSF, GPOW, GW, GW-slope and SL): The groundwater components are controlled by parameters that reflect recharge and discharge. These include drainage density (DDENS), transmissivity (T), storativity (S), ground water slope (GW-slope) and riparian strip factor (RSF). The calculation of recharge depth uses a similar non-linear relationship with unsaturated zone moisture storage as used for interflow runoff (Figure 4.7). GW represents the maximum recharge depth at ST, SL is the storage level at which the recharge ceases and GPOW is the power of the relationship. The riparian strip factor (RSF %) controls evaporation from groundwater through channel margins. The Pitman model uses a simple geometry presented in Figure 4.8 to simulate groundwater inflows and outflows (Hughes, 2013). A detailed explanation of this component of the GW Pitman model is not presented here but can be found in Hughes (2004). The basin area and drainage density parameter (DDENS) are used to divide the basin into representative slope elements. Subsequently, the drainage density (DDENS) and storativity (S) parameters are used to compute the geometry of the groundwater storage zone. The outflows from groundwater storage component can be determined from transmissivity (T) and internal model calculations of the groundwater gradients. Generally, the water balance components highlighted in this simple geometry include the recharge from the unsaturated zone, evapotranspiration losses from riparian zones, transmission losses to groundwater from upstream (when the gradients are negative) and discharge to the river channel (when the gradients are positive).

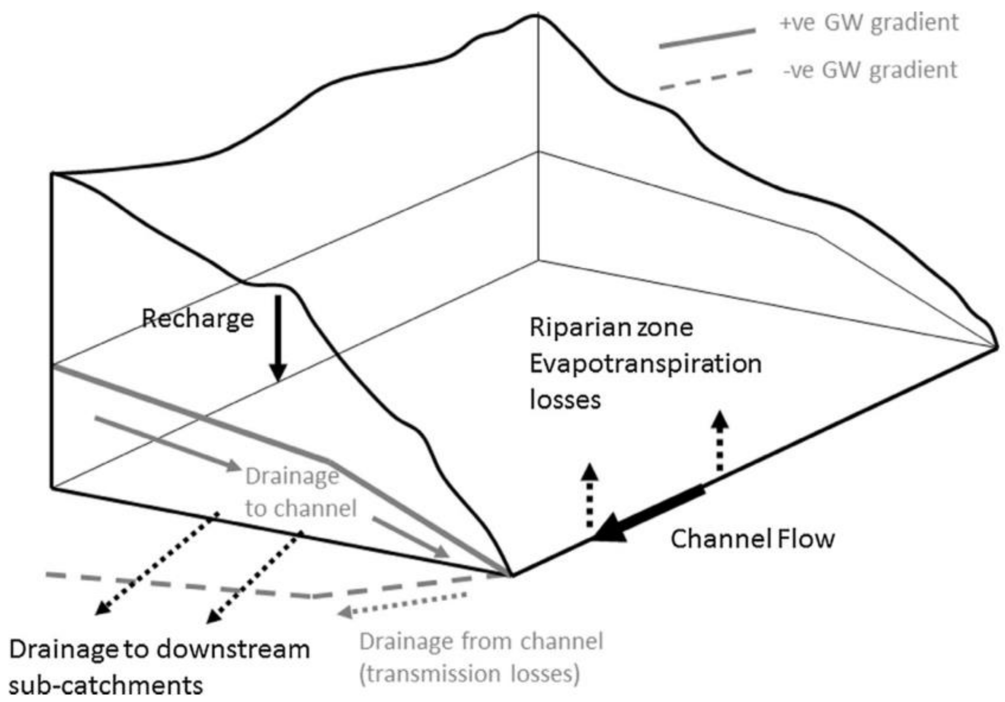

Figure 4.8: The geometry of the groundwater component in the GW Pitman model (Source: Hughes, 2013).

Routing parameters (TL and CL): TL and CL represent the runoff lag time and flow attenuation characteristics within the basin. CL (channel routing) is only used (i.e. CL > 0) in large basins where flow attenuation within a single sub-basin is significant at the monthly time scale. TL represents the sub-basin runoff attenuation and lag-time and is normally fixed to a value of 0.25 months.

Reservoir parameters and water abstraction parameters: The model can also be applied in basins where there are small dams, large reservoirs, and irrigation abstractions. The reservoir and water abstraction parameters are included in the model setup if a reservoir or other water abstractions exist in the basin. These parameters have not been used in the present study because the reservoir and irrigation abstractions were not included in the model setup because their influence o simulated flows were assumed to be negligible.

Pitman wetland sub-model parameters: The wetland component was included by Hughes *et al*. (2014) and Table 4.4 presents the parameters, model algorithms and brief descriptions. These parameters were established to reflect the key processes occurring during the channel–wetland exchanges in most wetlands. Wetland–groundwater interaction processes are not included because most of the groundwater–wetland processes are reported to have minor effects on the monthly water balance in large river–wetland systems in southern Africa (Wamulume *et al*., 2011; Hughes *et al*., 2014). The wetland sub-model can be applied in both natural lakes and seasonally inundated wetlands. Some of the parameters can be more-or-less directly estimated from relatively simple topographical analysis of the wetlands, whereas others are highly empirical and their estimation requires a good understanding of the channel–wetland exchange processes and/or hysteresis effects. The relationship between area and volume of inundation is assumed to be a power function defined by two parameters. The two parameters can directly be estimated from area–volume curves or indirectly from available satellite images. In the sub-model, the inundation area is limited to a given maximum inundation area (i.e. wetland local catchment area). Maximum inundation area, maximum and residual wetland volumes can also be estimated from area–volume curves, available satellite images or other hysteresis curves.

The wetland is assumed to be inundated from channel overbank spills when the volume of water in the channel is above a given channel-threshold (QThresh). For natural lakes or wetlands where the main river disappears within the lake/wetland, high values of QProp and a zero value of QThresh are used. This proportional value (QProp) varies with wetland type, but cannot easily be estimated without a clear understanding of channel–wetland characteristics. Wetland return flow (Rfract) is the proportion of the excess volume above a given wetland residual volume (the volume below which there are no returns to the river). Two options exist in the model regarding return flow; the wetland return flow may or may not be constrained by the volume of water in the channel. These options are designed to allow for situations where spillage from the channel and return flows back to the channel, can occur simultaneously as well as situations where return flows are severely restricted while the channel continues to spill. The selection of either of these options will clearly have a substantial impact on the shape of the inflow–inundation volume hysteretic curve.

Table 4.4: Parameters used within the Pitman wetland sub-model

Parameter(s)	Algorithm	Explanation
A and B	$IA = A \times IV^{B}$ (limited to maximum of MaxIA)	Scale and power parameters in the relationship between inundation area (IA $m^3 \times 10^6$) and volume (IV $m^3 \times 10^6$). Used to estimate rainfall additions and evapotranspiration losses.
MaxIA ($m^2 \times 10^6$)		Maximum inundation area.
QThresh ($m^3 \times 10^6$)	If QIN > QThresh Then QIV = QProp × QIN-QThresh Else QIV = 0	Monthly inflow volume below which there is no flow from the channel to the wetland.
QProp (fraction)		The proportion of monthly channel inflow (QIN $m^3 \times 10^6$) that contributes to inundation volume (QIV $m^3 \times 10^6$).

SRes ($m^3 \times 10^6$)	If IV > SRes then
	Rfract = AR × $(IV/SRes)^{BR}$
	(limited to maximum of 0.95)
	Else
	Rftact = 0
	
	Optional reduction of Rfract :
	Rfract = Rfract * QThresh / QIN
	
	Calculation of return flow:
	QRET = Rfract × (IV – SRes)
	QOUT = QIN – QIV + QRET
		Residual inundation volume below which there is no return flow to the channel.

AR and BR		Scale and power parameters in the function to calculate the proportion (Rfract) of inundated volume above SRes that returns to the channel (QRET $m^3 \times 10^6$) and contributes to downstream flow (QOUT $m^3 \times 10^6$). Rfract can be optionally reduced when the channel is spilling (on the assumption that spilling and return flow do not occur simultaneously in some wetland types).

4.3.2 Versions of the Pitman model

4.3.2.1 The structured uncertainty version of the GW Pitman model.

The structured uncertainty version of the GW Pitman model (Kapangaziwiri and Hughes 2008) including its modified versions (Hughes *et al*., 2010; Kapangaziwiri *et al.*, 2012) is based on the use of the basin physical and climatological characteristics (e.g. land cover, topography, geology, soils, rainfall and evapotranspiration) to establish *a priori* parameter sets using different empirical formulas and a regionalisation of the stream flow signatures used to constrain behavioural ensembles. The model uses parameter ranges (i.e. upper and lower bounds) with the defined distribution (normal, log-normal or uniform) to generate up to 10 000 ensembles using simple Monte Carlo sampling, with the generated parameter sets being independent of each other and across the sub-basin (Hughes *et al.*, 2010). For a distribution represented by normal or log-normal, the mean and standard deviation are defined before running the model, whereas simple parameter ranges are used for the uniform distribution (Kapangaziwiri, 2011).

The model results are saved in two files. The first file with the '.un1' extension contains the sampled parameter values, mean monthly flows, and mean monthly recharge, the slope of FDC, and the flows at 10%, 50%, and 90% for each ensemble. For gauged sub-basins, this file includes model performance results computed from the objective functions for each ensemble. The second file '.un2' includes the upper (5%), median (50%) and lower (95%) exceedance values for all the sub-basins and a series of observed flows for a gauged sub-basin. The generated ensembles are assessed using several statistical objective functions (see 4.3.3 below) and behavioural ensembles are identified using appropriate thresholds for the objective functions. This approach was applied in different studies within southern African basins (Hughes *et al*., 2010; Kapangaziwiri *et al.*, 2012; Tshimanga, 2012).

4.3.2.2 The single-run version

This version of the model applies the use of a single parameter set to simulate flows for each sub-basin (Hughes *et al*., 2010). The simulated flows are evaluated using the objective functions discussed in section 4.3.3 below as well as visual analysis of seasonal distributions, and the FDCs. In this version of the model, the parameters are manually calibrated, but when there are many sub-basins, the calibration processes is never a straightforward task. In such cases, the structured uncertainty version of the model can be run prior to the single-run version of the model to provide likely behavioural parameter sets to be used in calibrating a single run model. In a similar way, the single-run version can be used to 'manually' explore the effects of different parameter combinations prior to setting the parameter ranges in the structured uncertainty version. Therefore, the structured and single-run version of the model can be linked together to improve parameter estimations and in turn, the model simulation results.

4.3.2.3 The 2-stage model

This is one of the most recent approaches focused on using hydrological signatures as constraints to improve parameter estimations and uncertainty analysis in the Pitman model (Hughes, 2015a; Tumbo and Hughes, 2015). The approach involves two steps as indicated in Figure 2.11 in section 2.10. The initial step uses *a priori* parameter distributions under Monte Carlo sampling to generate up to 100 000 ensembles for the incremental natural flows of each sub-basin, and hydrological signatures are used to constrain all possible outputs to those considered behavioural. The hydrological constraints used in this approach include mean monthly streamflow (MMQ), mean monthly groundwater recharge, Q10, Q50 and Q90 on the flow duration curve as well as the percent time of zero flows. These constraints can be estimated from observed flow data, regional information on natural hydrological behaviour or previous model simulations (Hughes, 2015a; Tumbo and Hughes, 2015; Ndzabandzaba and Hughes, 2017). A behavioural ensemble its bounds fall within all established constraints, and these are automatically saved in the database for use in the second step. In the second step, all the saved behavioural parameter sets are re-sampled and the entire model is run for all sub-basins linked together to generate the cumulative streamflow volumes at all sub-basins outlets (Ndzabandzaba and Hughes, 2017). The final simulated flows can be further constrained using available observed data.

4.3.3 Model performance measures

The model performance statistical measures in the SPATSIM version of the GW Pitman model are the Nash-Sutcliffe coefficient of efficiency (CE), Percentage Bias of mean monthly flows (PBIAS) and coefficient of determination (R^2), determined using untransformed and natural log (ln) or transformed streamflow volumes. In addition, visual comparisons can be made between the observed and simulated time series, flow duration curves and seasonal distributions using the TSOFT facility that forms part of the SPATSIM framework.

Nash-Sutcliffe coefficient of efficiency (CE)

This measure is used to evaluate the residual variance of simulated data against the observed variance (Nash and Sutcliffe, 1970) and takes a value between $-\infty$ and 1. Negative values of CE indicate that the simulated flow represents the observed flows to a lesser degree than the mean observed flow, whereas a value of zero indicates that the simulated flow is no better estimator than the mean of observed flow (Kapangaziwiri, 2008). CE can be calculated as indicated in Equation 4.4. The same formula can be used to calculate the transformed values to obtain CE (ln) that reduces the effects of high flows.

$$CE = 1 - \frac{\sum_{i=1}^{n}\left(Q_{o_i} - Q_{S_i}\right)^2}{\sum_{i=1}^{n}\left(Q_{o_i} - \bar{Q}_o\right)^2} \qquad \text{(Equation 4.4)}$$

where Q_{o_i},$\bar{Q}_o$ and Q_{S_i}, are the observed monthly stream flow, mean of the observed stream flows and simulated monthly stream flow, respectively.

Coefficient of determination (R^2)

This statistical function provides an estimate of the general fit between the observed and simulated flows, and varies between 0 and 1. R^2 can be calculated as indicated in Equation 4.5. It is the most commonly used statistical objective function to define the linear relationship between two variables. However, R^2 is not sensitive to systematic differences between the observed and simulated flows (Tirivarombo, 2013).

$$R^2 = \frac{\sum_{i=1}^{n}\left(Q_{o_i} - \overline{Q_o}\right)\left(Q_{s_i} - \bar{Q}_s\right)}{\left[\left(\sum_{i=1}^{n}\left(Q_{o_i} - \overline{Q_o}\right)^2 \sum_{i=1}^{n}\left(Q_{s_i} - \bar{Q}_s\right)^2\right)\right]^{0.5}} \qquad \text{(Equation 4.5)}$$

Percentage bias of mean monthly flows (PBIAS)

PBIAS measures the percentage deviation of mean simulated flow volumes to observed flow volumes. A value of 0 represents the least bias, positive values indicate underestimation and negative values indicate overestimation. PBIAS can be calculated as;

$$PBIAS = \frac{\sum_{i=1}^{n}\left(Q_{o_i} - Q_{s_i}\right)}{\sum_{i=1}^{n} Q_{o_i}} \times 100 \qquad \text{(Equation 4.6)}$$

4.3.4 GW Pitman model setup for this study

The model was initially set up to simulate or quantify the wetland inflows required as upstream boundary conditions in the LISFLOOD-FP hydraulic model, and later re-run with the inclusion of the wetland sub-model parameters which were estimated from the hydraulic model. The setup was done on the SPATSIM platform for all three sub-basins (the Luangwa River basin, the Upper Zambezi River basin, and the Upper Great Ruaha River basin). However, for the Upper Great Ruaha River basin, the wetland monthly inflows were already generated from Tumbo (2015) and the initial simulations not repeated in this study.

Since the basins are largely ungauged and there is no adequate information to establish the model parameters, a combination of the structured uncertainty and single-run versions of the GW Pitman model was used. The main inputs (i.e. rainfall and potential evapotranspiration), were obtained from CRU TS 3.22 and IWMI Climate Data Portal datasets, respectively. The CRU TS monthly rainfall data extended from 1901 to 2013, whereas the potential evapotranspiration values were long-term monthly averages. In setting up the structured uncertainty model, some parameters were fixed, whereas those with high influence on runoff generation remained uncertain. These uncertain parameters were assumed to be uniformly distributed and parameter ranges were largely established using past experience (i.e. studies that have used the model) and some knowledge of basin physical characteristics. For example, low values of infiltration parameters (ZMIN, ZAVE, and ZMAX) were used for sub-basins in high elevated areas with coarse textured soils to account for more surface runoff, whereas sub-basins located in flat areas with finer soils were assigned higher values. In flat areas where soils are expected to be deep, higher values of ST were used. Moreover, low values of FT and GW parameters were used in flat sub-basins to account for low amounts of interflow and recharge. Higher values of POW and GPOW parameters used in low elevated areas to account for more variable amounts of recharge and interflow in these areas, whereas low values reflect less variable amounts in the two fluxes for high elevation areas. Generally, the initial parameter values adopted were consistent with those used in past studies (e.g. Mwelwa, 2004; Kapangaziwiri, 2011; Tshimanga, 2012; Tirivarombo, 2013; Tumbo, 2015).

For the case of the Luangwa River basin, a single gauging station downstream of the floodplain (data from 1930 to 1991) was used to assess the total model output. In the Upper Zambezi River basin, gauging stations (BP9, 1291100 and 1591820) were used, with the first two located a few kilometres downstream of the Barotse floodplain and the last one located upstream of the floodplain. Clearly, the wetland attenuation effects are included in the downstream observed data, but to avoid incorrectly estimating the wetland parameters, the wetland sub-model was not included in the initial setup of the model. This was not considered to be a major limitation as the uncertainties related to this would be captured by the final calibration of the GW Pitman model when the estimated wetland parameters are included in the model setup. The model was set to generate 10 000 ensembles, and these ensembles were filtered using thresholds established for each objective function. An ensemble was considered behavioural if the CE and PBIAS for both transformed and non-transformed values were > 0.5 and $\pm 15\%$, respectively. In addition, the best fit index that includes the effects of all objective functions (CE and PBIAS) was used to identify the most optimal behavioural ensemble. The index was calculated as $CE + CE(ln) + 1/[ABS(PBIAS) + ABS(PBIAS\,(ln))]$. The identified most optimal behavioural ensembles were then used to guide the establishment of the initial parameter set for the single-run model.

Using the single run version, several manual calibration runs were performed before arriving at the final calibration results. CE (> 0.5) and PBIAS ($\pm 15\%$), as well as visual comparisons of observed and simulated FDCs and seasonal distributions, were used to test the model performance. These objective function thresholds were applied in all basins, and the final calibrated model was considered appropriate enough to represent monthly wetland inflows. However, since daily wetland flows were required in the LISFLOOD-FP, the Pitman Disaggregation sub-model was used disaggregate the simulated monthly to daily flows.

4.4 Pitman Disaggregation sub-model

This sub-model was introduced by Slaughter *et al*. (2015) and was initially aimed at establishing a link between daily water quality modelling and monthly time-step water quantity models of natural hydrology and water use (system models). It can also be useful for various hydrological applications, including linking of monthly rainfall–runoff model results to the hydraulic modelling of wetland inundation at a finer (daily) time scale (Hughes and Slaughter, 2015). A detailed explanation of the model is found in the original document (Slaughter *et al*., 2015) and is summarised in Hughes and Slaughter (2015; 2016). The model uses daily rainfall data and five model parameters to disaggregate the monthly flows to daily flows. Three parameters (A, B, C) are used to establish the scaling relationship between monthly flow duration curve quantiles and the equivalent daily flow duration curve. The remaining parameters (R_{thresh} and K) are used to convert discrete daily rainfall values to a continuous antecedent rainfall time series. R_{thresh} is a threshold parameter that accounts for small values of daily rainfall that are not considered relevant to the generation of runoff, whereas K represents the storage response in the catchment (Slaughter *et al*., 2015). The daily FDC and the antecedent frequency distribution are used to generate the initial daily flow time series. Finally, a volume correction is included in the model computation to balance the total daily volumes with the monthly volume. To summarise, the six steps involved in the disaggregation processes are presented below as adopted from Hughes and Slaughter (2016):

i. Simulated monthly flow volumes are used to generate flow duration curves (M_FDC) of mean monthly flows.

ii. The mean monthly flow quantiles of the M_FDC are scaled (S_{PP}) to daily values (D_FDC) using three parameters (A, B, C) developed from the available observed daily flow data or regional estimates.

$$D\_FDC_{pp} = S_{PP} * M\_FDC_{PP} \qquad \text{(Equation 4.7)}$$

Where $S_{PP} = A.PP^{B} + C$ (If $S_{PP} < 0$ $then$ $S_{PP} = 0$) (Equation 4.8)

iii. Daily rainfall (P_i) is converted to a single continuous time series of antecedent rainfall (API) using K and R_{thresh} parameters.

$$API_i = API_{i-1}^{k} + R_{thresh} \qquad (\text{For } P_i > R_{thresh}) \qquad \text{(Equation 4.9)}$$

$$API_i = API_{i-1}^{k} \qquad (\text{For } P_i < R_{thresh}) \qquad \text{(Equation 4.10)}$$

iv. The generated antecedent rainfall time series is used to generate an antecedent rainfall frequency curve (API_DC).

v. The API time series and API_DC are used to establish the exceedance frequency for each day from which the initial daily flow estimates are obtained.

vi. The initial time series of daily flows (D_i) are volume corrected (DC_i) to balance with the monthly flow volumes (M_j).

$$DC_i = D_i + \left(M_j - \sum_{i=1}^{n} D_i\right) \times {D_i}^2 \Big/ \sum {D_i}^2$$

$$(\text{For } \sum_{i=1}^{n} D_i < M_j) \qquad \text{(Equation 4.11)}$$

The ARC2 global satellite daily rainfall data (Novella and Thiaw, 2013) for the period between October 2000 and September 2013 were used in this study. Applying this model in the absence of some local observed daily stream flow data is never a straightforward task and the simulated daily inflows are almost impossible to validate. However, the key issue was to obtain representative hydrographs that can be used as upstream boundary conditions in the LISFLOOD-FP model. The initial parameter values largely relied on the parameter values suggested by previous studies (e.g. Hughes and Slaughter, 2015; Slaughter *et al.*, 2015). According to Hughes and Slaughter (2015), the possible values for K and R_{thresh} are 0.95 – 0.99 and 1 – 10, respectively. Similar parameter values were assigned to all sub-basins as there was no information available to distinguish between different sub-basins.

4.5 LISFLOOD-FP hydraulic model

4.5.1 The structure and parameters of the LISFLOOD-FP hydraulic model

Some details about the LISFLOOD-FP model were presented in section 2.7.2, and the full details of the model algorithms for the most recent versions can be found in previous publications (see for example Bates *et al.*, 2010; Neal *et al.*, 2012). It is a freely available 2D hydraulic model that includes two equations that solve for continuity of mass (Equation 4.12) for each cell and continuity of momentum (Equation 4.13) between cells (Neal *et al.*, 2012). An explicit finite difference approach is used to solve the Saint Venant shallow water equation with the advection component ignored and the acceleration, water slope and friction slope components retained (Schumann *et al.*, 2013; Fernández *et al.*, 2016). The recent version of the model by Neal *et al.* (2012) known as a sub-grid model which was incorporated into the base model (Bates *et al.*, 2010) is applied in this study. The sub-grid model allows the inclusion of hydraulic characteristics of channels that are smaller in size compared to the grid size. Although a detailed description of the sub-grid model is not repeated here, a summary of the structure of the base model and the sub-grid model are shown in Figure 4.9.

$$h_{i,j}^{t+\Delta t} = h_{i,j}^{t} + \Delta t \frac{Q_{x\,i-1/2,j}^{t+\Delta t} - Q_{x\,i+\frac{1}{2},j}^{t+\Delta t} + Q_{y\,i-\frac{1}{2},j}^{t+\Delta t} + Q_{y\,i+1/2,j}^{t+\Delta t}}{A_{i,j}} \quad \text{(Equation 4.12)}$$

$$Q_{i+1/2}^{t+\Delta t} = \frac{q_{i+1/2}^{t} - g h_{flow}^{t} \Delta t S_{i+1/2}^{t}}{1 + g \Delta t n^2 \left| q_{i+1/2}^{t} \right| / \left(h_{flow}^{t} \right)^{7/3}} \Delta x \quad \text{(Equation 4.13)}$$

Where Δx is the cell width (m), Δt is a time step (sec), g is the acceleration due to gravity (m s^{-1}), q^t (m $^2s^{-1}$) is the flow from the previous time step (Q^t) divided by cell width (Δx), S is the water surface slope between cells, n is Manning's roughness coefficient, and h_{flow} (m) is the depth between cells through which water can flow.

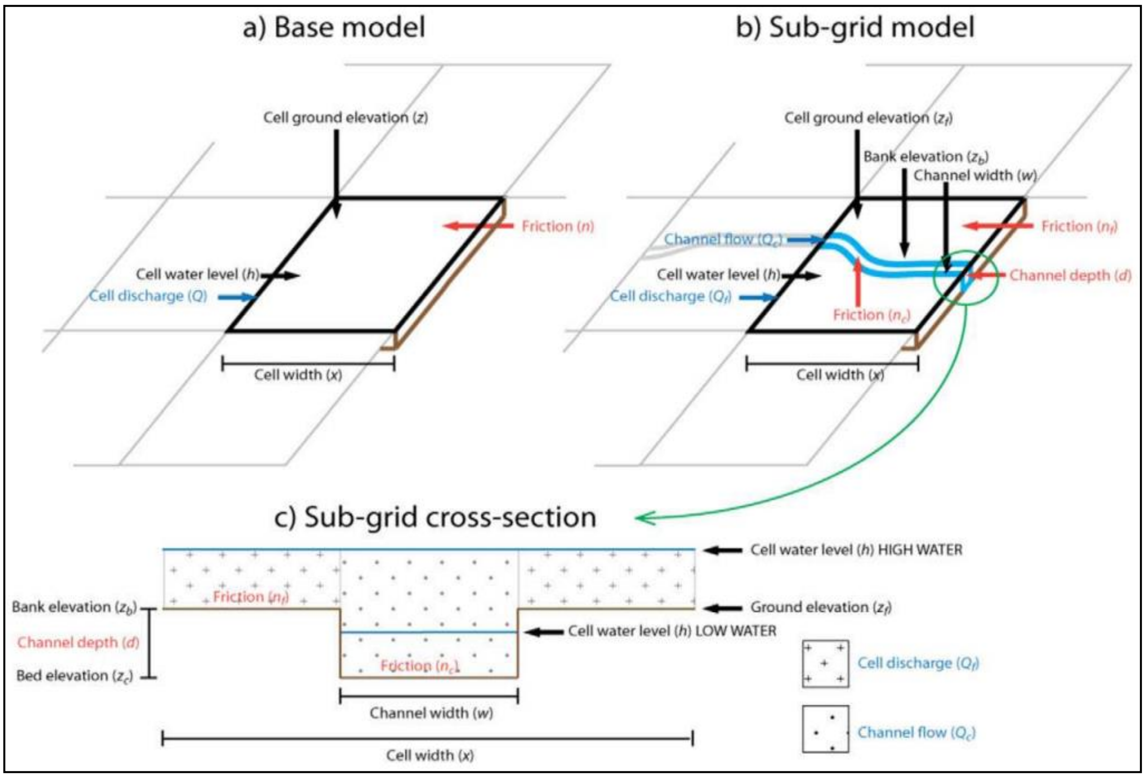

Figure 4.9: Conceptual diagram of the LISFLOOD-FP base model (a), sub-grid solver (b), and sub-grid section (c) (Source: Neal *et al*., 2012).

Topography, channel cross-sections, bankfull heights, model parameters (surface roughness (*n*), *p*, and *r*) and boundary conditions (discharge and water level) are required to set up the LISFLOOD-FP model. When channel width values are provided as the model inputs, bankfull depth can be estimated from the hydraulic geometry relationship proposed by Leopold and Maddock (1953) (Equation 4.14) which was summarised by Neal *et al*. (2012) as indicated in Equation 4.15. The parameters 'r' and 'p' are hydraulic radius parameters, and the inundation results are generally less sensitive to the variation of p than r. The topographical characteristics are mostly represented using a DEM. In some cases, particularly when the detailed river bathymetry data are not available, the bankfull elevations are represented using the grid elevations adjacent to the river boundary. Surface roughness is established using the land cover maps and other guidelines such as Chow (1959). The upstream and downstream boundary conditions specify inflows and outflow water levels in the model domain, respectively. When the observed boundary conditions are missing, upstream inflows are simulated using hydrological models, whereas a normal depth (i.e. depth of flow when the water surface slope is assumed to be similar to channel bed slope) is assumed to be a downstream boundary condition. With the assumption of normal depth, the water surface slope is estimated using the average channel bed slope.

$$\mathrm{d} = \left(\frac{\mathrm{c}}{\mathrm{a}^{\frac{\mathrm{f}}{\mathrm{b}}}}\right)\mathrm{w}^{\left(\frac{\mathrm{f}}{\mathrm{b}}\right)} \qquad \text{(Equation 4.14)}$$

$$\mathrm{d} = \mathrm{rw}^{\mathrm{p}} \qquad \left(For\ p = \left(\frac{f}{b}\right)\ and\ r = \left(\frac{c}{a^{\frac{f}{b}}}\right)\right) \qquad \text{(Equation 4.15)}$$

Where *d* represents bankfull depth,

w represents channel width values and

‘r’ and ‘p’ are scale and exponential hydraulic radius parameters.

a, b, c, f are coefficients and exponents that define the hydraulic geometry relationship

The model outputs include a series of water depths; maximum inundated depth and area in a grid format, as well as a single time series file of area and volume of inundation, outflow, and inflow at each specified time interval. The simulated results are compared with any available observed data (e.g. discharge at the downstream point, inundation extents and storage) to assess the model performance.

4.5.2 LISFLOOD-FP hydraulic model setup for this study

This section explains the methods used to set up the LISFLOOD-FP model for the three basins selected for the current study. Although the SRTM 30 m resolution DEM provides more detailed topographical characteristics, an initial analysis to compare the 90 m and 30 m

DEMs indicated that the 30 m DEM contained too much random noise, thereby affecting the model simulation results and increasing the model run time. Therefore, the SRTM 90 m resolution DEM was found to be more reliable, but filtering processes were necessary to reduce some of the local variations and noise effects but could not correct the vegetation bias. The DEM was pre-processed using the filter tool (low pass filter) of the ArcGIS 10.2 which calculates the mean value for each 3 × 3 neighbouring cells, and as a result, the high and low values within each neighbouring cells are averaged-out to reduce extreme values. The filtered SRTM 90 m resolution DEM was then used as topographical data in the model setup. It is important to note that, even though the filtering process is useful to reduce the noise effects, in some cases it may introduce some errors in the DEM (Trigg *et al.*, 2012; Baugh *et al.*, 2013). The presence of vegetation bias in the DEM could introduce some errors in the simulated inndation results. Recently (in the course of this study), a number of vegetation corrected DEMs have been released (e.g. O'Loughlin *et al.*, 2016) which can be used to reduce the effects of vegetation bias in the hydraulic modelling.

No channel cross-section details are available for the main river or the tributaries in all of the studied wetlands. The available global river cross-section datasets such as the global river bankfull width and depth dataset by Andreadis *et al*. (2013) have been used in many studies including some in southern Africa (Schumann *et al.*, 2013). When the river network from the Andreadis *et al*. (2013) dataset and the network derived from the SRTM 90 m DEM during the sub-basin delineation process, were overlaid on top of the Google Earth imagery, there was a somewhat better agreement between the latter river network and the Google Earth image compared to the former network (Figure 4.10). The reasons for this may be that the Andreadis *et al*. (2013) network was generated from a lower resolution DEM (15 arc sec) compared to the SRTM 90 m resolution DEM. Generally, the locations of the two river networks could not match properly with the observed river network on Google Earth. Moreover, the width values estimated from the Andreadis *et al*. (2013) dataset were found to be over-generalised and did not reflect widths measured using Google Earth in many places. Any attempt to use a river network with incorrectly-located coordinates and inaccurate width values will inevitably affect the simulated inundation results. Therefore, in this study, the river network was digitised using the Google Earth image and the width values were measured at different representative sections and interpolated for the whole network. The digitised river network together with the width values were then rasterised to the format required in the LISFLOOD-FP model setup.

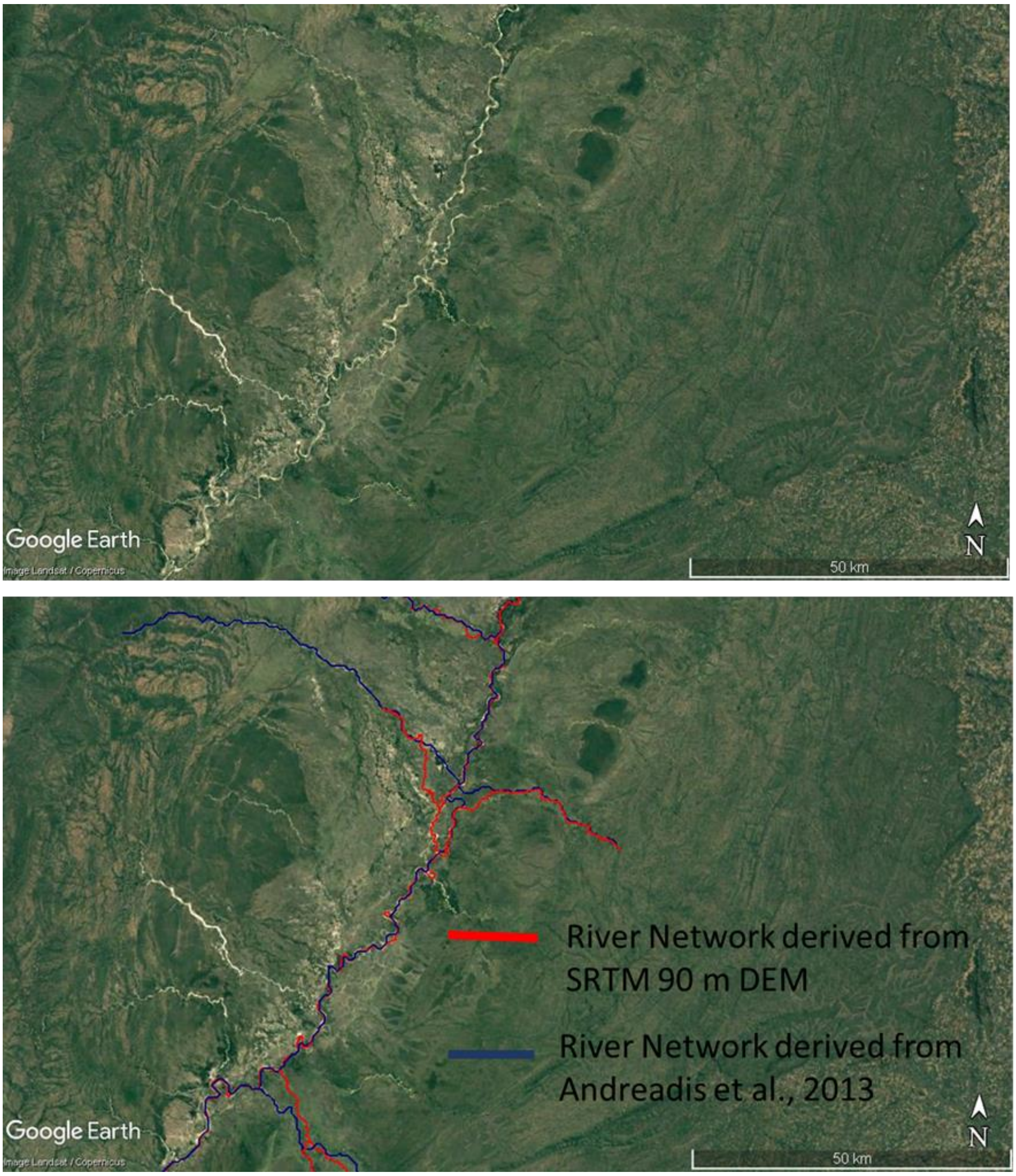

Figure 4.10: Comparison between two river networks generated from two different DEMs.

The bankfull depths were established using the width–depth relationship suggested by Neal *et al*. (2012) and the values of the scale (r) and power (p) parameters that define this relationship (see Equation 4.15) were set to reflect the actual width and depth values for each river network. A fixed value of p was used (i.e. the model default value of p=0.76), whereas a given range of parameter r was used. Bank elevations were represented using the grid elevations adjacent to the river boundary. The channel roughness (C_n) and the floodplain roughness (C_f) were established depending on the land cover and channel characteristics using the guidelines suggested by Chow (1959).

Disaggregated daily flows were used as the upstream boundary conditions. However, to limit the model run time, which is important in most detailed hydraulic models due to their computational demands, a short, but representative daily time series of wet and normal years were used in the setup of the LISFLOOD-FP (i.e. a complete hydrological year for each case) instead of the whole disaggregated time series (October 2000 – October 2013). The initial conditions in the wetland largely influence the simulated inundation results. The three studied wetlands consist of both seasonal and permanent inundated areas. In such wetlands, when the initial conditions are assumed to be dry (i.e. depth of water in the wetland is zero), the model tends to use a range of starting values as a 'warm-up period'. Thus, an addition of one year prior to the targeted ones (wet and normal years) was used as a warm-up period to create initial conditions in each wetland. An assumption of the normal depth (i.e. water surface is assumed to be parallel to the channel bed) was used as the downstream boundary condition at the end of the main channel. This depth was automatically estimated by the model using the average channel slope estimated from the Google Earth image. This was done by plotting a profile of a digitised channels in the Google Earth. For tributaries, the downstream boundary condition was assumed to be the water level in the downstream receiving channel. For wetlands with both dense vegetation and standing water, evapotranspiration was expected to have a great influence on the inundation characteristics and was considered in the model setup. The influence of direct rainfall on the inundation characteristics was also included in the model setup.

The Barotse floodplain covers one sub-basin, whereas the Luangwa and Usangu wetlands cover more than one sub-basin in the Pitman model setup. For the Luangwa and Usangu wetlands, the wetland sub-model parameters were required for each sub-basin. The LISFLOOD-FP was set up for each sub-basin starting from the one located upstream, and the outflows from this sub-basin were used as one of the inflow boundary conditions to the next sub-basin up to the last sub-basin. Although the setup was done for each sub-basin containing wetland effects, the setup for the entire wetland as a single unit was, however, used to establish likely parameter values, and the optimal values were used to inform parameter values in the individual sub-basin setups.

4.5.3 Validation of the LISFLOOD-FP model results

The simulated inundation extents were compared with the few available LandsatLook and Landsat level 1 images. Water pixels from the selected Landsat level 1 images were extracted using the Modified Normalised Difference Water Index (MNDWI) (Xu, 2006) which can be computed using Equation 4.16 and the results were used to represent the observed inundation extents. The extracted water pixels together with the simulated inundated extents were used to calculate the Flood Area Index (FAI) (Fernández *et al.*, 2016) using Equation 4.17 in order to assess the model performance. The simulated outflows from the wetlands were validated using the available observed daily flows for gauging stations located a few kilometres downstream of the wetland outlet, but this was only possible for the Barotse floodplain and the Usangu wetlands. Although the Landsat images were used to validate simulated inundation extents, it is clear that these images may not be that good to validate the model results because of some limitations discussed in section 2.4. Different researchers have proposed ways to deal with uncertainties of validation data (e.g. Pappenberger *et al.,* 2007; Schumann *et al.,* 2009). Pappenberger *et al.* (2007), proposed a fuzzy approach to deal with some of the uncertainties of validation data. The approach make use of the GLUE uncertainty framework. Generally speaking, the aim of applying the LISFLOOD-FP model was to get a likely representative simulation of wetland inundation dynamics and not to capture a specific observed event, and evidence from past studies has indicated that the model can provide likely inundation characteristics.

$$MNDWI = \frac{Green\ band - MIR}{Green\ band + MIR} \qquad \text{(Equation 4.16)}$$

$$FAI = \frac{M_i O_i}{(M_i O_i + M_i O_n + M_n O_i)} \qquad \text{(Equation 4.17)}$$

Where O is the observation and M corresponds to the model output,

M_iO_i is the number of inundated cells modelled and observed,

M_iO_n is number of non-inundated cells that the model simulated as inundated,

M_nO_i is the number of inundated cells that the model simulated as non-inundated, and

MIR is middle infrared.

4.6 Re-run and evaluation of the GW Pitman model for the entire basin

4.6.1 Establishment of Pitman wetland sub-model parameters from the LISFLOOD-FP model results

The Pitman wetland sub-model parameters are presented in Table 4.4. These parameters were estimated for each sub-basin with assumed wetland effects. Some of these parameters were directly estimated from the LISFOOD-FP results: maximum inundated area (MaxIA), the channel flow volume below which there is no flow into the wetland (QThresh) and the residual inundation volume below which there is no return flow from the wetland to the channel (SRes), others which are highly empirical were estimated manually. The scale (A) and power (B) parameters in the area–volume relationship were estimated by plotting the area–volume of inundation graph and varying A and B until a line of best fit was obtained. The remaining parameters were established using the time series for inundation volume, inflows, and outflows generated by LISFLOOD-FP. This was achieved by implementing the Pitman wetland sub-model algorithms in a spreadsheet version together with the LISFLOOD-FP results. The LISFLOOD-FP results (simulated daily flows and storage/volumes) are saved as mass file in the model results folder. This mass file can be opened in the excel sheets and the required LISFLOOD-FP results can be extracted and saved in different excel sheet. Then the simulated daily flows and storage/volumes can be converted to monthly values (as the wetland sub-model simulates monthly values) and added in the spreadsheet version of the wetland sub-model. The Pitman wetland sub-model parameters were manually calibrated by comparing the LISFLOOD-FP simulated monthly inundation volumes and outflows with those generated by the spreadsheet version of the Pitman wetland sub-model.

4.6.2 Re-run the Pitman model with the inclusion of wetland sub-model parameters.

The previously established parameter ranges used in the structured version of the model together with the wetland sub-model parameters were used to re-set this version of the model. The aim was to determine if there is any difference in model performance before and after inclusion of wetland sub-model parameters in the model setup. The performance of the original structured uncertainty model setup (before inclusion of wetland sub-model parameters) was compared to the performance after the wetland sub-model parameters were included in the model setup. The initial run suggested a need to revise the structure of the previous version of the wetland sub-model. This small revision involved the inclusion of an option to limit the return flows from the wetland back to the river when the river was still spilling onto the wetland. The revised version allows for the option to have return flows at any time. The estimated parameters were then used in the single-run version, and the final calibrated model was used to establish the likely impacts of the wetland on the downstream flow regime.

4.7 Regionalisation or direct estimation of wetland parameters of the basin-scale model

The final part of the results analysis was designed to provide guidelines on establishing the Pitman wetland sub-model parameters directly from their identified physical characteristics (i.e. without having to setup and run the LISFLOOD-FP model). While a sample of only three wetlands is certainly insufficient to develop clear guidelines, the three wetlands are considered sufficiently different (not only in their characteristics but also in their water exchange dynamics) to expect that these differences will be reflected in different wetland sub-model parameters. The approach adopted was to conceptually interpret the wetland sub-model parameters in terms of their physical characteristics, together with the better understanding of the different water exchange dynamics of the three wetlands that was obtained from the LISFLOOD-FP model.

4.8 Conclusions

This chapter discussed the methodological setup used in the present study. Three models (Pitman hydrological model, Pitman disaggregation sub-model and LISFLOOD-FP hydraulic model) were linked together to achieve the overall aim of the study. Generally, the quality of the model forcing data was expected to substantially influence the simulation results. There was no adequate information to be used in setting up and validating both hydraulic and hydrological models in the three basins. Some of the available data that were used in setting up these models have a number of limitations due to their spatial and temporal coverages as well as extraction methods. As a result, it was always expected that there would be quite large uncertainties in the simulated results related to the quality of model forcing data.

CHAPTER FIVE: A COMBINED MODELLING APPROACH: RESULTS AND DISCUSSION

Hydrological modelling in a river basin containing large wetlands requires a detailed conceptualisation of the interacting processes between channels and wetlands. Understanding these processes is vital for the estimation of model parameters (e.g. maximum inundation extents, wetland residual volume, and return flow). However, in data scarce basins these processes are not well understood therefore, parameter estimation can be very difficult. A combined modelling approach that was implemented in this study maximised the use of the LISFLOOD-FP hydraulic model to understand channel–wetland exchanges and wetland dynamics, and the results were used to quantify parameters and modify the structure of the basin-scale Pitman hydrological model.

This chapter presents the calibration results and a general discussion of the results of the combined modelling approach for the three selected basins as per the methodological sequence (explained in Chapter 4) which is summarised below:

- ❖ Data preparation for modelling.
  - a. Sub-basin delineation
  - b. Establishment of sub-basin characteristics
  - c. Sub-basin similarity analysis
- ❖ Initial setup of the GW Pitman model to simulate wetland inflows.
  - d. Parameter sampling using structured uncertainty version
  - e. Single-run version
- ❖ Disaggregation of simulated monthly flows to daily flows using the Pitman disaggregation sub-model.
- ❖ Simulation of wetland inundation characteristics using the LISFLOOD-FP model.
- ❖ Quantification of the Pitman wetland sub-model parameters.
- ❖ Re-run the Pitman model for the entire basin with the inclusion of the wetland sub-model and quantification of the wetland impacts on the downstream flow regimes.

It is important to note that, the first two components of the sequence were dealt with by a previous study by Tumbo (2015) for the Upper Great Ruaha River basin and are not repeated here.

5.1 The Luangwa River basin

5.1.1 Sub-basin delineated

A total of 28 sub-basins were delineated in the Luangwa River basin (Figure 5.1) and their characteristics are presented in Table 5.1. However, these sub-basins were modified to simplify the linkage between the LISFLOOD-FP and Pitman models by creating nodal points at the downstream end of the key tributary inflow sub-basins, as well as the downstream ends of the main wetland areas (NF1, NF2 and NF3). As a result 24 sub-basin nodes were formed and their upstream area characteristics are presented in Table 5.2. These sub-basins nodes were used in the setup of the GW Pitman model instead of the delineated sub-basins (Figure 5.1).

Table 5.1: Characteristics and indices for each sub-basin that were entered into the PCA

Sub-basin	Slope (%)	Mean Elev (m)	Min. Elev (m)	Max. Elev (m)	HI[1]	PET (mm y^{-1})	MAP (mm y^{-1})	AI[2]	TWI[3]
L1	7.0	1071.1	652.0	2311.0	0.3	1597.6	1012.7	1.6	9.0
L2	9.5	1168.3	657.0	2231.0	0.3	1599.9	937.7	1.7	8.8
L3	5.0	914.3	605.0	1683.0	0.3	1535.5	941.2	1.6	9.3
L4	3.3	968.3	604.0	1276.0	0.5	1608.3	904.8	1.8	9.6
L5	1.3	660.8	604.0	744.0	0.4	1497.2	1025.9	1.5	10.4
L6	4.6	849.7	579.0	1649.0	0.3	1535.5	1025.9	1.5	9.4
L7	3.9	1040.9	582.0	1529.0	0.5	1668.5	866.1	1.9	9.2
L8	7.6	1127.4	561.0	1842.0	0.4	1593.3	986.9	1.6	8.8
L9	2.2	645.9	555.0	1300.0	0.1	1668.5	1025.9	1.6	10.0
L10	6.0	1150.0	542.0	1727.0	0.5	1486.0	1025.9	1.4	9.1
L11	3.4	747.8	543.0	1242.0	0.3	1668.5	924.6	1.8	9.6
L12	4.2	944.7	555.0	1407.0	0.5	1668.5	854.4	2.0	9.1
L13	1.1	545.4	539.0	556.0	0.4	1668.5	924.6	1.8	10.7
L14	2.7	721.5	523.0	1218.0	0.3	1668.5	924.6	1.8	9.7
L15	3.0	653.4	525.0	1097.0	0.2	1756.4	928.6	1.9	9.8
L16	5.7	907.5	538.0	1645.0	0.3	1756.4	928.6	1.9	9.1
L17	7.7	1075.5	485.0	1758.0	0.5	1478.9	1001.8	1.5	8.9
L18	5.5	718.0	486.0	1701.0	0.2	1476.7	957.1	1.5	9.3
L19	4.7	842.7	539.0	1452.0	0.3	1478.9	958.0	1.5	9.2
L20	7.1	757.4	449.0	1328.0	0.4	1476.7	982.4	1.5	9.0
L21	6.2	1208.0	493.0	1615.0	0.6	1497.4	1026.3	1.5	8.9
L22	8.2	1086.3	488.0	1714.0	0.5	1497.4	1026.3	1.5	8.7
L23	10.5	919.2	408.0	1657.0	0.4	1549.6	961.5	1.6	8.5
L24	5.9	1092.1	406.0	1877.0	0.5	1550.8	944.4	1.6	9.1
L25	4.2	1091.5	463.0	1417.0	0.7	1562.6	852.3	1.8	9.5

[1] Hypsometric Integral

[2] Aridity Index

[3] Topographical Wetness Index

Sub-basin	Slope (%)	Mean Elev (m)	Min. Elev (m)	Max. Elev (m)	HI[1]	PET (mm y^{-1})	MAP (mm y^{-1})	AI[2]	TWI[3]
L26	16.9	664.9	365.0	1243.0	0.3	1662.5	866.4	1.9	8.0
L27	8.1	754.8	370.0	1414.0	0.4	1699.1	948.3	1.8	8.8
L28	10.6	658.6	323.0	1492.0	0.3	1679.1	720.0	2.3	8.6

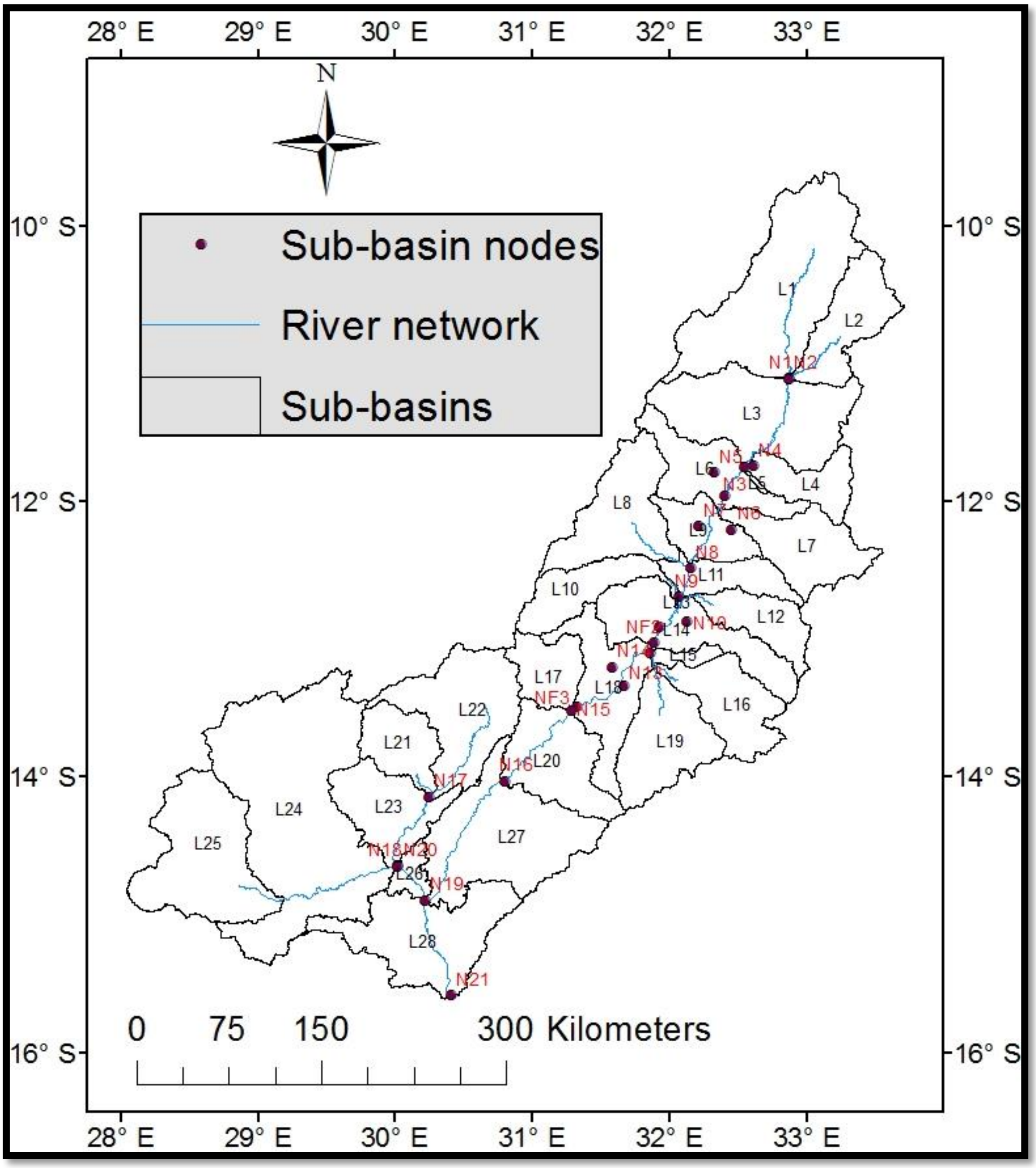

Figure 5.1: Sub-basins and sub-basin nodes formed in the Luangwa River basin.

Table 5.2: Areal characteristics upstream of each sub-basin node in the Luangwa River basin.

Sub-basin Name	Sub-basin Area (km^2)	Sub-basin Nodes	Sub-basin Node Area(km^2)	Remarks on Sub-basin Node areas
L1	12742	N1	12742	Same as L1
L2	4465	N2	4465	Same as L2
L3	9168	N3	8821	Part of L3 excluding wetland (inflows from East & West)
L4	2744	N4	3508	L4 and L5 & East part of L6
L5	86	N5	3511	West part of L6
L6	4647	NF1	805	Upper section of the floodplain
L7	4710	N6	5610	L7 and East part of L9 (about 40%)
L8	6150	N7	1467	West part of L9 (about 60%)
L9	2837	N8	6180	L8 & West part of L11
L10	3490	N9	5209	East part of L11 & L12 (minus FP part)
L11	2645	N10	2740	East part of L14 (about 50%) less FP
L12	3063	N11	6259	L10 & L13 & West part of L14 less FP
L13	29	NF2	1410	Middle section of the floodplain
L14	5950	N12	5146	L15 & L16
L15	668	N13	7178	L19 & East part of L18 (40%) less FP
L16	4478	N14	2763	West part of L18 (60%) less FP
L17	2841	NF3	880	Lower section of the floodplain
L18	5339	N15	2842	L17
L19	5482	N16	5427	L20
L20	5426	N17	10396	L21 and L22
L21	3164	N18	4572	L23
L22	7231	N19	9633	L27
L23	4571	N20	27997	L24 and L25
L24	19235	N21	8614	L26 andL28
L25	8762			
L26	997			
L27	9633			
L28	7617			

5.1.2 Sub-basin groups formed.

Sub-basin characteristics or variables presented in Table 5.1 were used to group sub-basins according to their similarities. From the PCA results, the first two principal components explained a total of 66.4% of the variation between the sub-basins (Table 5.3). Climatic variables (PET, MAP and AI), as well as the physical characteristics (i.e. slope, minimum elevation, and TWI), account for the first two principal components (Figure 5.2). These basin characteristics were predominantly used in the classification and resulted in three groups of sub-basins as shown in Figure 5.3. The first group consists of sub-basins primarily located in highly elevated areas with steep slopes (i.e. slopes values 7% – 16%), high MAP and low PET. The third group includes sub-basins with gentle slopes (1% – 3.9%), low MAP and high PET. Group two consists of sub-basins with characteristics between the above two extremes.

Sub-basins found in the same group were assumed to have more-or-less similar hydrological responses. Since the sub-basin nodes were used in the setup of the GW Pitman model, the group of each sub-basin node was established based on the dominant characteristics upstream of the nodal point (Figure 5.3). The final groups for sub-basin nodes are presented in Table 5.4.

Table 5.3: Total variance explained by 9 variables in the PCA

Component	Initial Eigenvalues		
	Total	% of Variance	Cumulative (%)
1	3.19	35.46	35.46
2	2.78	30.92	66.37
3	1.25	13.85	80.22
4	1.12	12.48	92.70
5	0.35	3.93	96.63
6	0.25	2.72	99.35
7	0.05	0.50	99.84
8	0.01	0.09	99.93
9	0.01	0.07	100.00

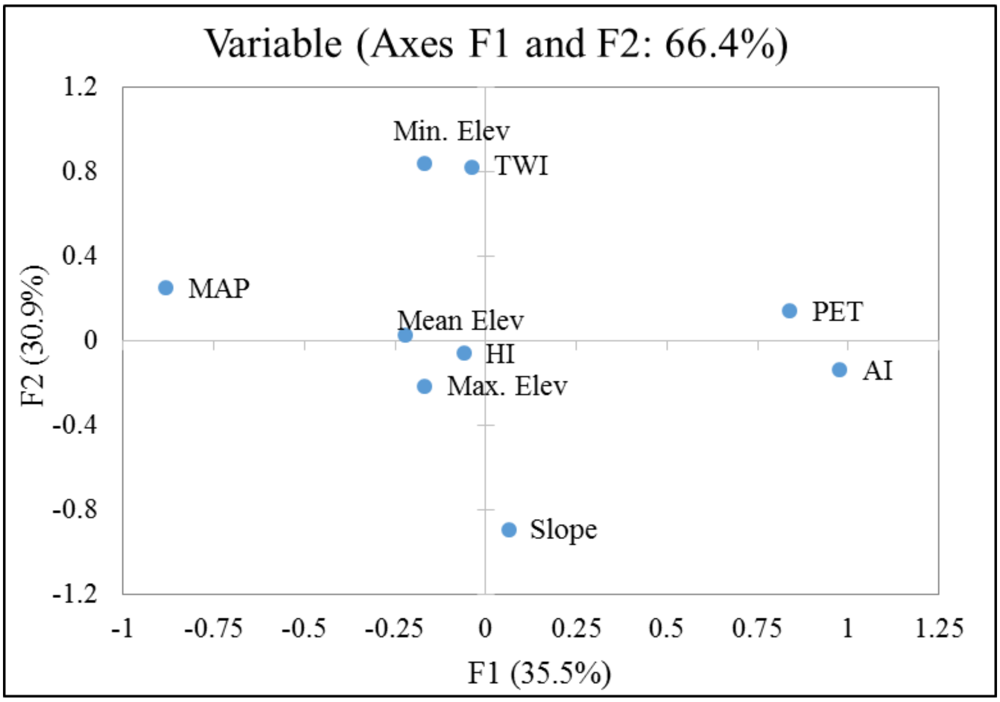

Figure 5.2: PCA biplot for the 9 variables of the Luangwa River basin.

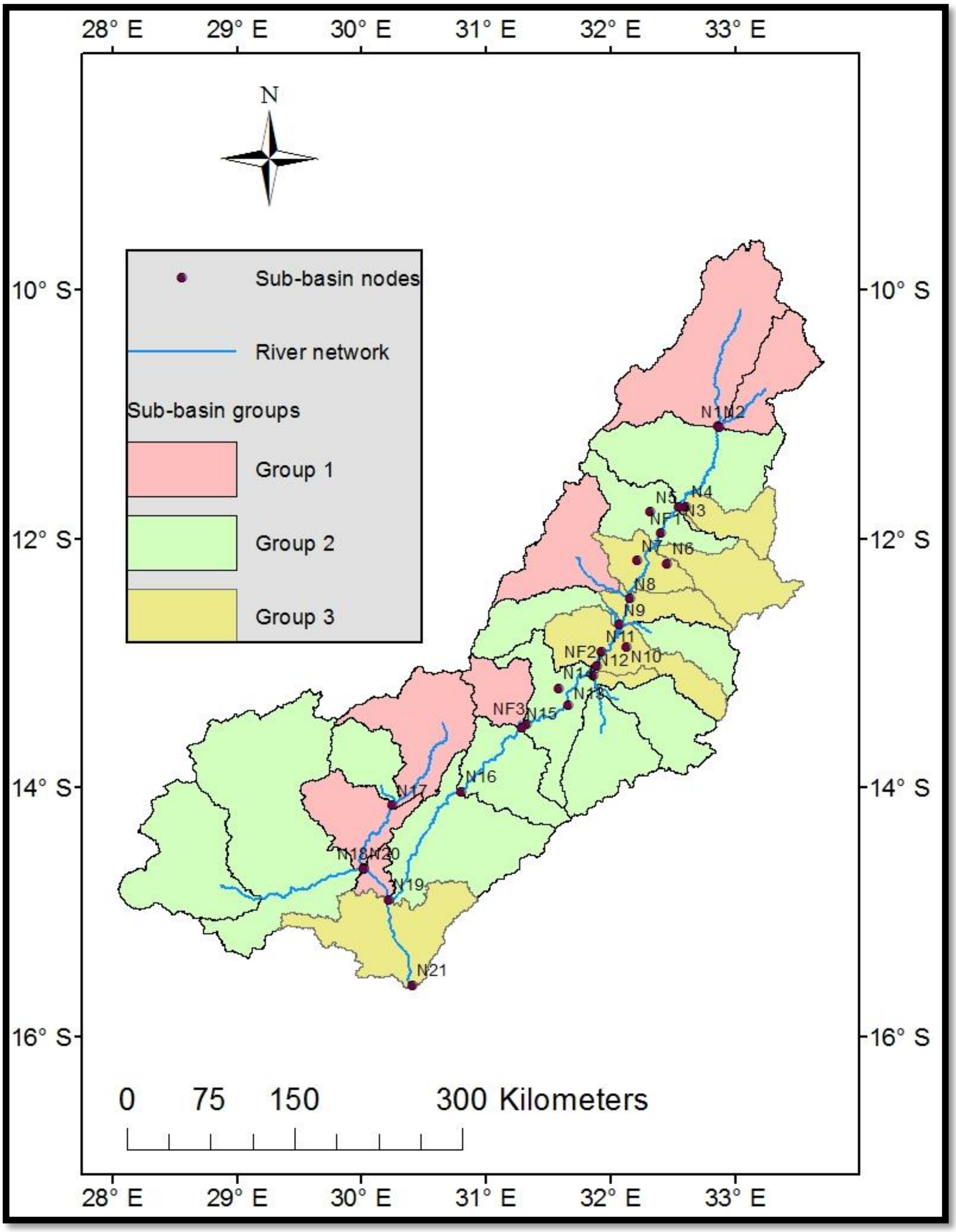

Figure 5.3: The sub-basin groups generated by the PCA and the location of sub-basin nodes used in the final model runs of the Luangwa River basin.

Table 5.4: Sub-basin node groups formed in the Luangwa River basin

Node	Remarks on sub-basin node areas	Group
N1	same as L1	1
N2	same as L2	1
N3	Part of L3 excluding wetland (inflows from East & West)	2
N4	L4 and L5 & East part of L6	2
N5	West part of L6	2
NF1	Upper section of the floodplain	3
N6	L7 and East part of L9 (about 40%)	2
N7	West part of L9 (about 60%)	3
N8	L8 & West part of L11	1
N9	East part of L11 & L12 (minus FP part)	3
N10	East part of L14 (about 50%) less FP	2
N11	L10 & L13 & West part of L14 less FP	2
NF2	Middle section of the floodplain	3
N12	L15 & L16	2
N13	L19 & East part of L18 (40%) less FP	2
N14	West part of L18 (60%) less FP	3
NF3	Lower section of the floodplain	3
N15	L17	1
N16	L20	3
N17	L21 and L22	1
N18	L23	3
N19	L27	3
N20	L24 and L25	2
N21	L26 andL28	3

5.1.3 Parameter sampling using the structured uncertainty version of the GW Pitman model

The model setup was done for the period October 1930 – September 1991. The initial uncertain parameter ranges were established using past experience of studies that have used the model in southern Africa (e.g. Mwelwa, 2004; Kapangaziwiri, 2011; Tshimanga, 2012; Tirivarombo, 2013; Tumbo, 2015) together with a reasonable understanding of basin physical characteristics. For instance, sub-basin nodes found in steep areas (Group 1) which are expected to have shallower soils were assigned lower values of the ST parameter and those located in relatively flat areas with finer and deep soils (Group 3), especially along the Luangwa Rift valley, were assigned higher values. Steep areas were also assigned low values of infiltration parameters (ZMIN and ZMAX) to allow more infiltration excess runoff volume in these areas compared to areas with gentle slopes. Low values of FT and GW parameters were assigned in flat areas including areas along the valley to reflect a minimal contribution of these fluxes to the total runoff and higher values were used in steep areas. The high value of RSF in flat areas and downstream reflects the assumption of higher losses through riparian margins than in steep and highly elevated sub-basins. Generally, a wide range of parameters was used to allow different parameter combinations. The parameters which were assumed to have minimal impacts on the generation of basin runoff remained fixed (Table 5.5). Sub-basin nodes in the same group were assigned similar parameter ranges with the assumption that they have a similar hydrological response.

Table 5.5: The parameter ranges used to set the uncertainty model

Parameter	Group1		Group2		Group3	
	min	max	Min	max	Min	Max
RDF	0.8		0.8		0.8	
PI1	1.5		1.5		1.5	
PI2	4		4		4	
AFOR	0		0		0	
FF	0		0		0	
PEVAP	varies with sub-basins					
ZMIN	40	80	40	100	60	100
ZAVE	0.5*(ZMIN+ZMAX)					
ZMAX	600	1000	800	1200	800	1250
ST	400	800	600	1000	700	1000
SL	0		0		0	
POW	2.5	3.5	2.5	3.5	2.5	3.5
FT	5	10	2	8	0	4
GW	5	15	5	10	2	8
R	0.4	0.7	0.4	0.7	0.2	0.5
TL	0.25		0.25		0.25	
CL	0		0		0	
GPOW	2.5	3.5	2.5	3.5	2.5	3.5
DDENS	0.4		0.4		0.4	
T	15		15		15	
S	0.001		0.001		0.001	
GW slope	0.01		0.01		0.01	
RWL	25		25		25	
RSF	0.2		0.2		1	

Only one sub-basin node is gauged (N21; located at the downstream outlet), and this gauging station was used to evaluate the model performance for the entire basin. Figure 5.4 illustrates that the high flows which occur less than 30% of the time are well simulated (the uncertainty bounds closely bracket the observed flow), whereas the uncertainty bounds for the moderate flows are somewhat over-estimated and low flows were under-estimated. The general pattern of the simulated ensembles could be related to the quality of the data used to establish the parameter ranges and/or the difficulty to clearly define some of the parameter ranges as well as the assumptions used in setting up the model. Using the established thresholds for each objective function, the majority of the simulated ensembles were satisfactory (about 95% of all generated ensembles were considered behavioural).

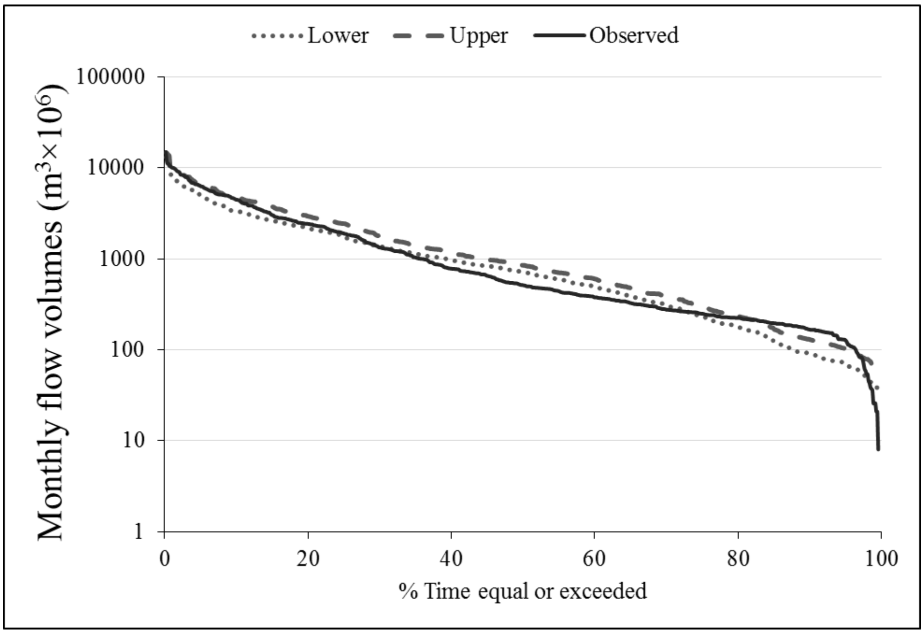

Figure 5.4: The FDCs of the observed and simulated bounds for the N21 sub-basin node of the Luangwa River basin.

Although the main purpose of running the model was to estimate the possible parameter values that could assist the manual calibration approach used in the GW Pitman model, most parameters were not individually identifiable (Figure 5.5). From this figure, different values of ST and ZMAX parameters have more-or-less the same values of CE and CE (ln). Simulated moderate and low flows are mainly related to the interaction of FT, POW, GW and GPOW parameters and different combination of these parameters may also result in the same model performance (equifinality). An index that combines the four parameters (FT/POW + GW/GPOW) can be used to minimise the equifinality issue and improve simulation of moderate to low flows. From Figure 5.6, given the other three parameters are fixed (GW, POW and GPOW), the index can be used to establish an appropriate/behavioural value of the FT parameter. However, the index is still constrained by the availability of data to establish the other three parameters. For example, most basins in southern Africa including the Luangwa, lack any accurate information on groundwater recharge that could be used to establish appropriate values of GW and GPOW. The same value of the index corresponds to different values of CE and CE (ln) (Figure 5.6). This suggests that the scatter plot cannot be used to establish one of these parameters. There is a need for appropriate data to establish these parameters in the Luangwa River basin.

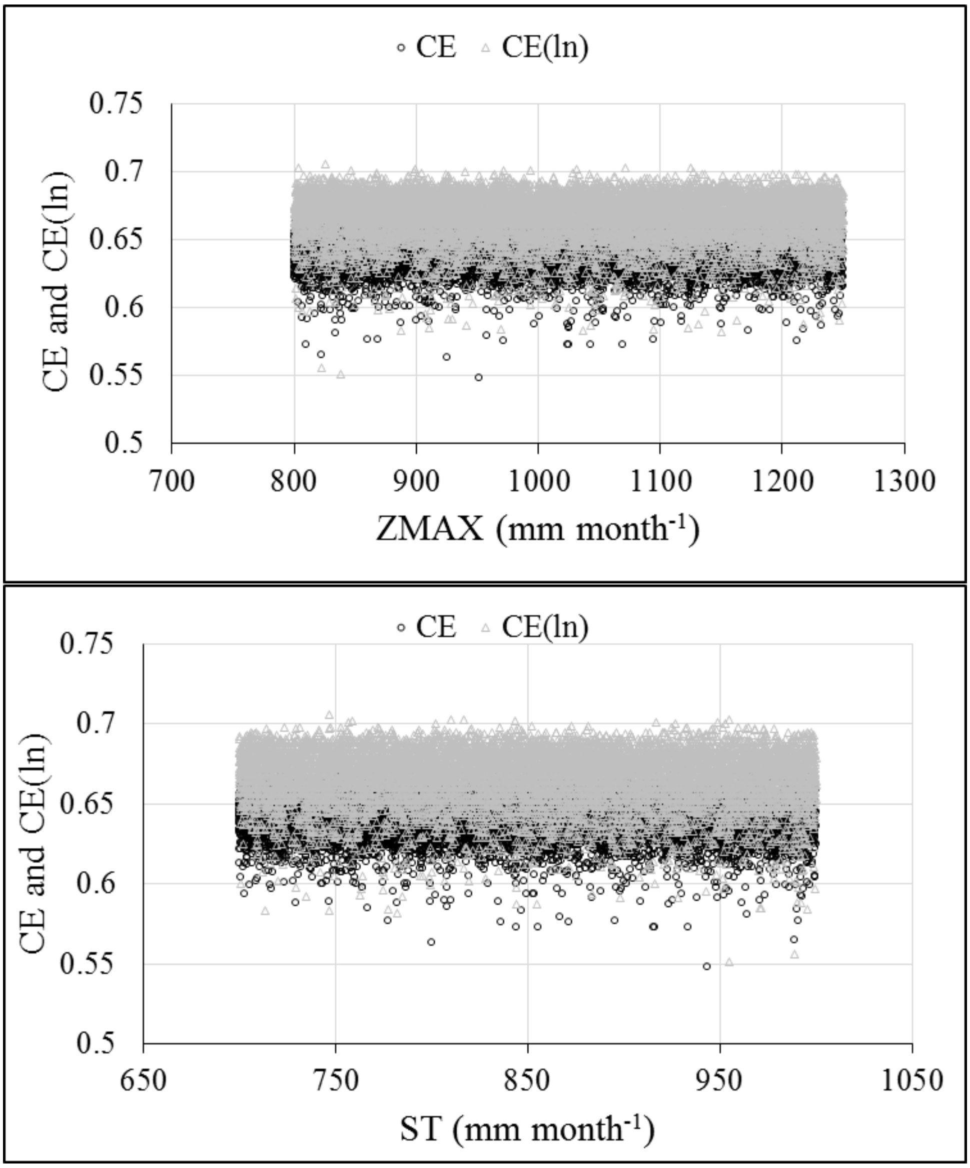

Figure 5.5: Scatterplots of the variation in CE and CE (ln) against ST and ZMAX parameter values for the N21 sub-basin node of the Luangwa River basin.

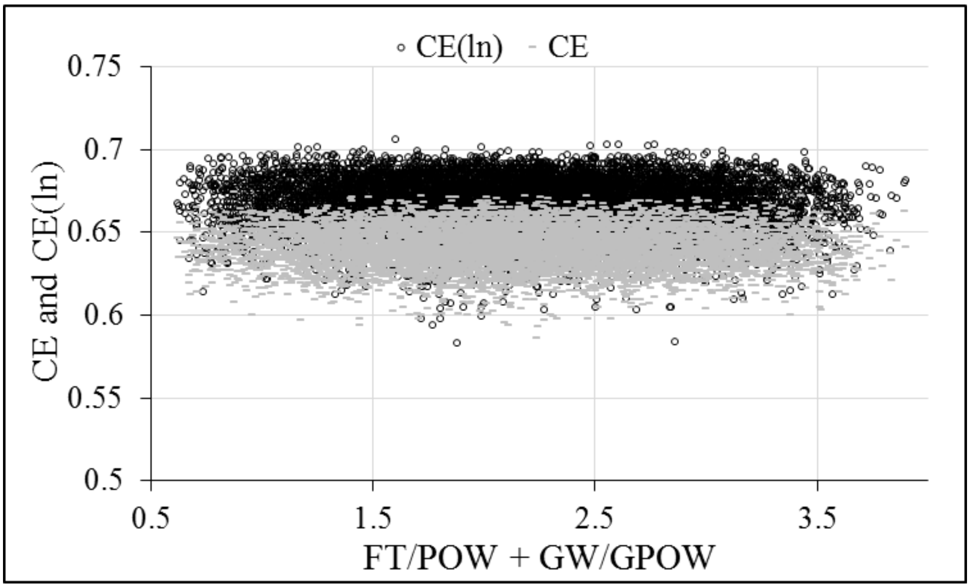

Figure 5.6: Scatterplots of the variation in CE and CE (ln) against FT/POW + GW/GPOW index for the N21 sub-basin node of the Luangwa River basin.

5.1.4 Simulation of wetland inflows using a single-run version of the GW Pitman model

The optimal behavioural ensemble, which was established using the Best Fit index (calculated as $CE + CE(ln) + 1/[ABS(PBIAS) + ABS(PBIAS\ (ln))]$) for sub-basin node N21 was used to guide the establishment of parameter values for the other sub-basin nodes in the initial setup of the model. The optimal ensemble number was used to identify parameter values for all the remaining sub-basin nodes. Although sub-basin nodes in the same group were given the same parameter ranges, the sampling process used is independent of the sub-basin nodes. Thus, different parameter values were obtained for each sub-basin node in a similar group. Mean parameter values were calculated for each group, and these values were used as an initial parameter set in the setup of the model (Table 5.6). Several simulation runs were performed before arriving at an acceptable model result. The parameter values used to setup the final model run are presented in Table 5.7.

Table 5.6: The initial set of calibration parameters for the GW Pitman model.

Parameter	Group1	Group2	Group3
RDF	0.8	0.8	0.8
PI1	1.5	1.5	1.5
PI2	4	4	4
AFOR	0	0	0
FF	0	0	0
PEVAP	varies with sub-basins		
ZMIN	62	75	79
ZAVE	0.5*(ZMIN+ZMAX)		
ZMAX	743	971	1077
ST	536	809	783
SL	0	0	0
POW	2.7	3.3	3.2
FT	7.4	5.2	2.6
GW	10.3	7.8	5.5
R	0.5	0.5	0.4
TL	0.25	0.25	0.25
CL	0	0	0
GPOW	2.7	3.3	3.3
DDENS	0.4	0.4	0.4
T	15	15	15
S	0.001	0.001	0.001
GW slope	0.01	0.01	0.01
RWL	25	25	25
RSF	0.2	0.2	1

Table 5.7: Final set of calibration parameters for the GW Pitman model

Parameter	Group1	Group2	Group3
RDF	0.8	0.8	0.8
PI1	1.5	1.5	1.5
PI2	4	4	4
AFOR	0	0	0
FF	0	0	0
PEVAP	varies with sub-basins		
ZMIN	61	76	76
ZAVE	0.5*(ZMIN+ZMAX)		
ZMAX	738	875	931
ST	541	732	793
SL	0	0	0
POW	3	3.1	3.1
FT	9	4	2
GW	10	7	6
R	0.5	0.5	0.4
TL	0.25	0.25	0.25
CL	0	0	0
GPOW	3	3.1	3.1
DDENS	0.4	0.4	0.4
T	15	15	15
S	0.001	0.001	0.001
GW slope	0.01	0.01	0.01
RWL	25	25	25
RSF	0.4	0.4	1

Reasonably good simulations of the high flows were achieved with CE and PBIAS values of 0.58 and 12.72%, respectively. The low flows simulations were achieved with CE (ln) and PBIAS (ln) values of 0.62 and 0.34%, respectively. The model somewhat under-estimated the low flow values, whereas the moderate flow values were over-estimated (Figure 5.7). From Figure 5.8 (top), high flows in most years are over-estimated, whereas for the period after 1960 most peak flows are under-estimated. Underestimated and over-estimated flows are expected to improve when the wetland parameters are included in the model setup. In general, the uncertainty in the simulated flows could have resulted from the relatively poor quality of the rainfall and the limitations of the observed flow data (only being available at the basin outlet), as well as the assumptions used during setting up the model, particularly with regard to the grouping of the sub-basins. However, the results were considered acceptable enough to establish representative inflows (after disaggregation) to the LISFLOOD-FP model.

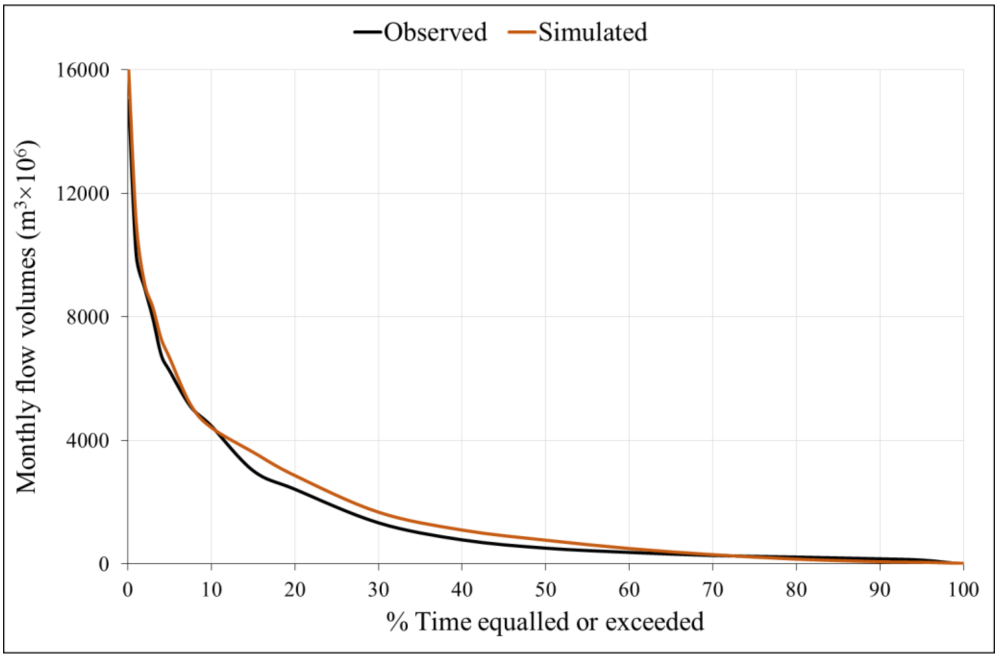

Figure 5.7 Observed and simulated monthly flow duration curves for N21 sub-basin node for the period 1930 – 1991.

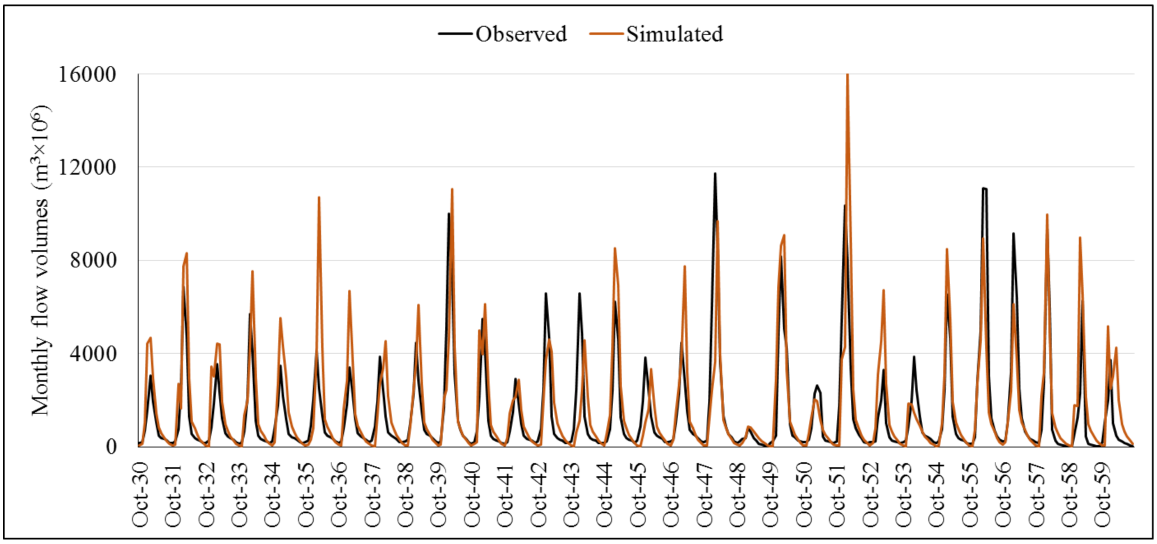

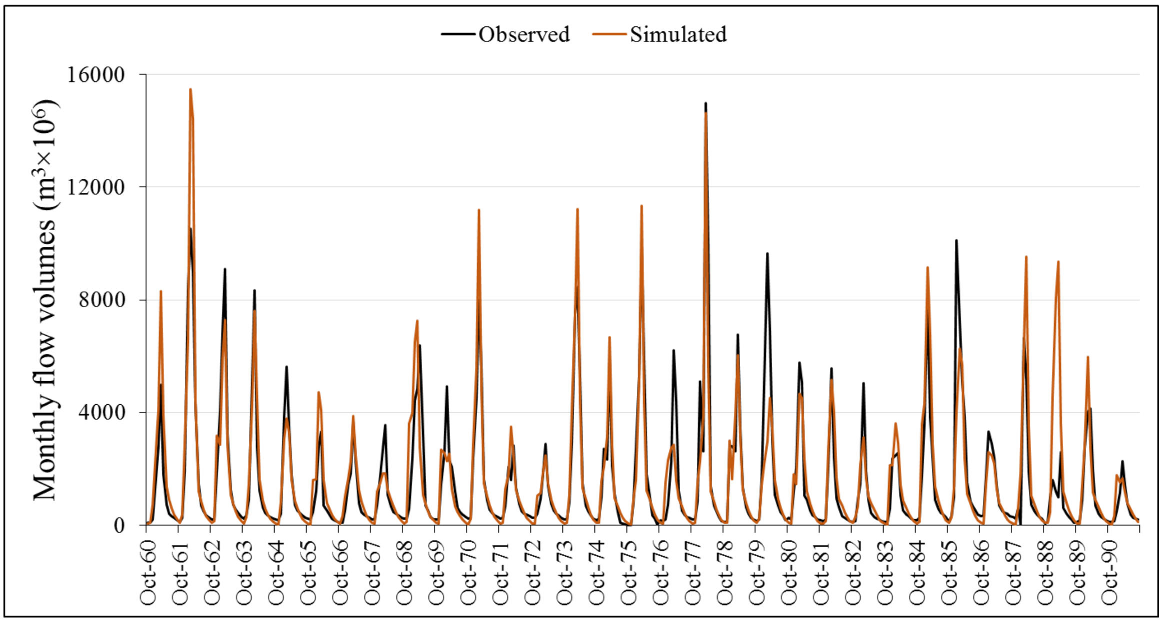

Figure 5.8: Time series of observed and simulated monthly flows for the N21 sub-basin node for the period October 1930 – September 1960 (top) and October 1960 – September 1991 (bottom).

5.1.5 Disaggregation of simulated monthly flows into daily flows using the Pitman disaggregation sub-model

Simulated monthly flows for each sub-basin node contributing to the floodplain inflows were disaggregated to daily flows for the period October 2000 – September 2013. Since none of these sub-basins has observed daily flows, which are important for establishing scaling parameters (A, B and C) and validating the model results, the whole disaggregation processes was never a straightforward task. Parameter values suggested by previous studies (e.g. Hughes and Slaughter, 2015; Slaughter *et al*., 2015) were used to establish likely parameter values (A = 0.4, B = -0.5, C = 0.9, K = 0.98 and R_{thresh} = 4). While the disaggregated daily flow magnitudes could not be validated, the onset and duration of simulated high peaks were compared with the information reported by the Dartmouth Flood Observatory (Adhikari *et al*., 2010) and the Robin Pope Safaris Blog (http://robinpopesafaris.net/blog/2000/01/its-monday-22nd-jan-2007-and-the-popes-go-flying/). According to the Robin Pope Safaris Blog, most of the areas in the Luangwa River basin experienced floods in late January and early February 2007 and 2010 (Figure 5.9). Similarly, most of the simulated high peaks in these years (2007 and 2010) are observed in late January and early February for the sub-basin nodes shown in Figure 5.10. Broadly speaking, there is a high degree of uncertainty in the simulated daily magnitudes which is mostly related to the appropriateness of the parameters used, as well as errors carried over from the simulated monthly flows. Overall, since the rationale was to obtain likely representative flow patterns that could be used in LISFLOOD-FP, the simulated daily flows are considered representative enough to be used as boundary conditions in the LISFLOOD-FP model.

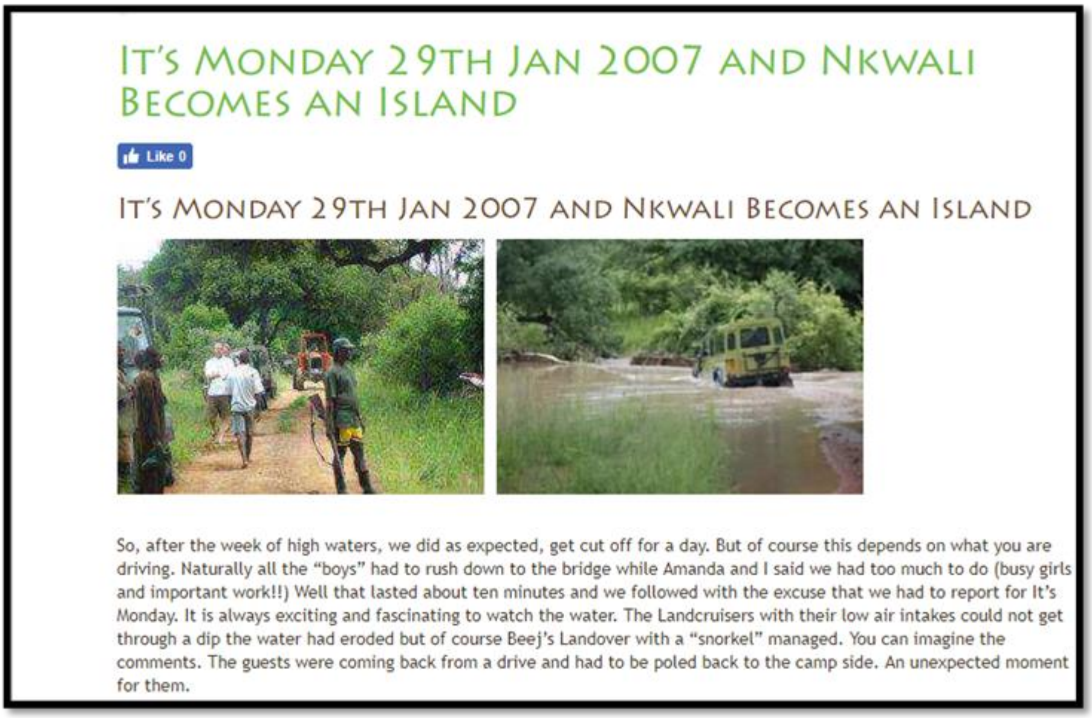

It's Monday 29th Jan 2007 and Nkwali Becomes an Island

Like 0

It's Monday 29th Jan 2007 and Nkwali Becomes an Island

So, after the week of high waters, we did as expected, get cut off for a day. But of course this depends on what you are driving. Naturally all the "boys" had to rush down to the bridge while Amanda and I said we had too much to do (busy girls and important work!!) Well that lasted about ten minutes and we followed with the excuse that we had to report for It's Monday. It is always exciting and fascinating to watch the water. The Landcruisers with their low air intakes could not get through a dip the water had eroded but of course Beej's Landover with a "snorkel" managed. You can imagine the comments. The guests were coming back from a drive and had to be poled back to the camp side. An unexpected moment for them.

http://robinpopesafaris.net/blog/2000/01/its-monday-29th-jan-2007-and-nkwali-becomes-an-island/

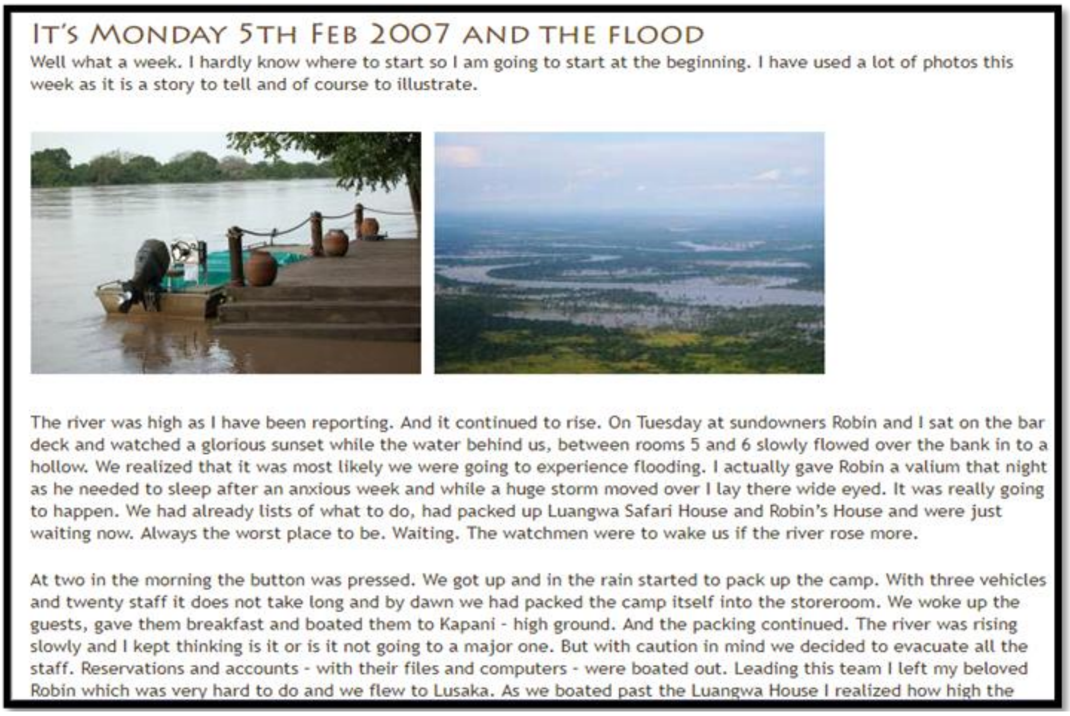

It's Monday 5th Feb 2007 and the Flood

Well what a week. I hardly know where to start so I am going to start at the beginning. I have used a lot of photos this week as it is a story to tell and of course to illustrate.

The river was high as I have been reporting. And it continued to rise. On Tuesday at sundowners Robin and I sat on the bar deck and watched a glorious sunset while the water behind us, between rooms 5 and 6 slowly flowed over the bank in to a hollow. We realized that it was most likely we were going to experience flooding. I actually gave Robin a valium that night as he needed to sleep after an anxious week and while a huge storm moved over I lay there wide eyed. It was really going to happen. We had already lists of what to do, had packed up Luangwa Safari House and Robin's House and were just waiting now. Always the worst place to be. Waiting. The watchmen were to wake us if the river rose more.

At two in the morning the button was pressed. We got up and in the rain started to pack up the camp. With three vehicles and twenty staff it does not take long and by dawn we had packed the camp itself into the storeroom. We woke up the guests, gave them breakfast and boated them to Kapani - high ground. And the packing continued. The river was rising slowly and I kept thinking is it or is it not going to a major one. But with caution in mind we decided to evacuate all the staff. Reservations and accounts - with their files and computers - were boated out. Leading this team I left my beloved Robin which was very hard to do and we flew to Lusaka. As we boated past the Luangwa House I realized how high the

Figure 5.9: Screenshot of the published information on early 2007 floods in the Luangwa (Source: http://robinpopesafaris.net/blog/2000/01/its-monday-5th-feb-2007-and-the-flood/)

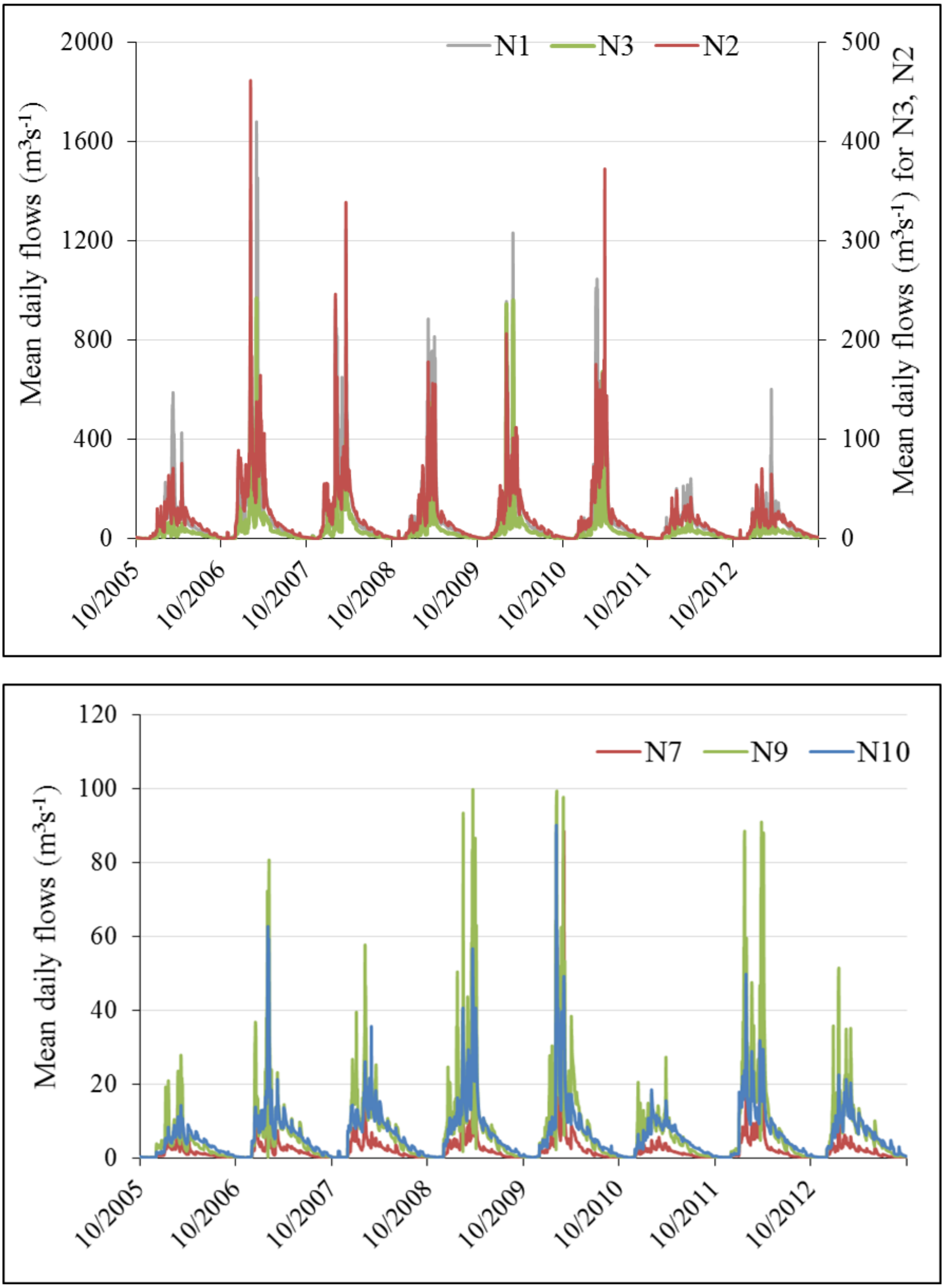

Figure 5.10: Disaggregated mean daily flows for some sub-basin nodes of the Luangwa River (October 2005 to September 2013).

5.1.6 Simulation of wetland inundation characteristics using LISFLOOD-FP model

The Luangwa floodplain (Figure 5.11) was divided into three sections; upper (Figure 5.12), middle (Figure 5.13) and lower (Figure 5.14). These figures also show the floodplain elevation and river width values used for setting up the model in each floodplain section. As explained in section 4.5.2, the widths were estimated/measured at different representative sections and interpolated for the whole river network. However, it is clear that in some sections especially where the main river or its tributaries was covered by vegetation, the values were difficult to estimate as the channel boundaries were covered by vegetation. The total length of the meandering river (i.e. main channel) in each of the three sections is 191 km, 194 km and 121 km for the upper, middle and lower, respectively. The channel bankfull depths were not provided as model input, the model generated these values at the beginning of the simulation using the width–depth relationship (see Equation 4.15). Figures 5.15 and 5.16 show the channel bankfull depths in each floodplain section. It can be seen that most of the low depth values (i.e. less than 1) are for tributaries. The channel depths in the middle section decreases and increase in the lower section because the floodplain at the lower section meets the Gorge where the channel become deep. The locations of tributary inflows used as upstream boundary conditions in each floodplain section are indicated using black circles (Figure 5.12 to 5.14). The downstream boundary condition for each floodplain section was defined using the normal depth (depth at which the water surface slope is assumed to be parallel to the channel bed slope). This depth was calculated using Manning's flow equation that defines the relationship between discharge and water surface. Since the water surface slope was not known, the average channel slope was used in the computation of normal depth. The average channel slope values used in the three floodplain sections were estimated from Google Earth imagery (i.e. 0.04 in the upper, 0.02 in the middle and 0.03 in the lower section).

The model runs were performed separately, starting with the upper section; the outflows from this section including the inflows from tributaries found in the middle section become upstream boundary conditions for the middle section. Subsequently, the output from the middle section together with inflows from tributaries in the lower section were used as upstream boundary conditions in the lower section. To limit the model run time, the model was run for a few representative years that include both wet and normal years. The period October 2006 – September 2007 represents the wet years, and October 2012 – September 2013 represents normal years. An addition of one year prior to the targeted ones was used as ‘warm up’ period. Thus, the model was run from October 2005 – September 2007, and October 2011 – September 2013. To gain some insight into parameter values, the model was initially run for the entire floodplain as a single unit, and the final estimated parameter values were used to guide parameter values for the individual floodplain sections. The parameter values were largely established based on basin physical characteristics. For instance, the Luangwa River mostly was a sandy bed, with the bankfull depth approximately 3 – 6 m. These characteristics led to the selection of parameter ranges for channel roughness (C_n) and hydraulic radius parameter (r) (Table 5.8). Floodplain vegetation is scattered and includes different species such as grasses, herbs, riparian woodland and Miombo woodland. The vegetation characteristics were used to decide on the parameter range for the floodplain roughness (C_f) (Table 5.8).

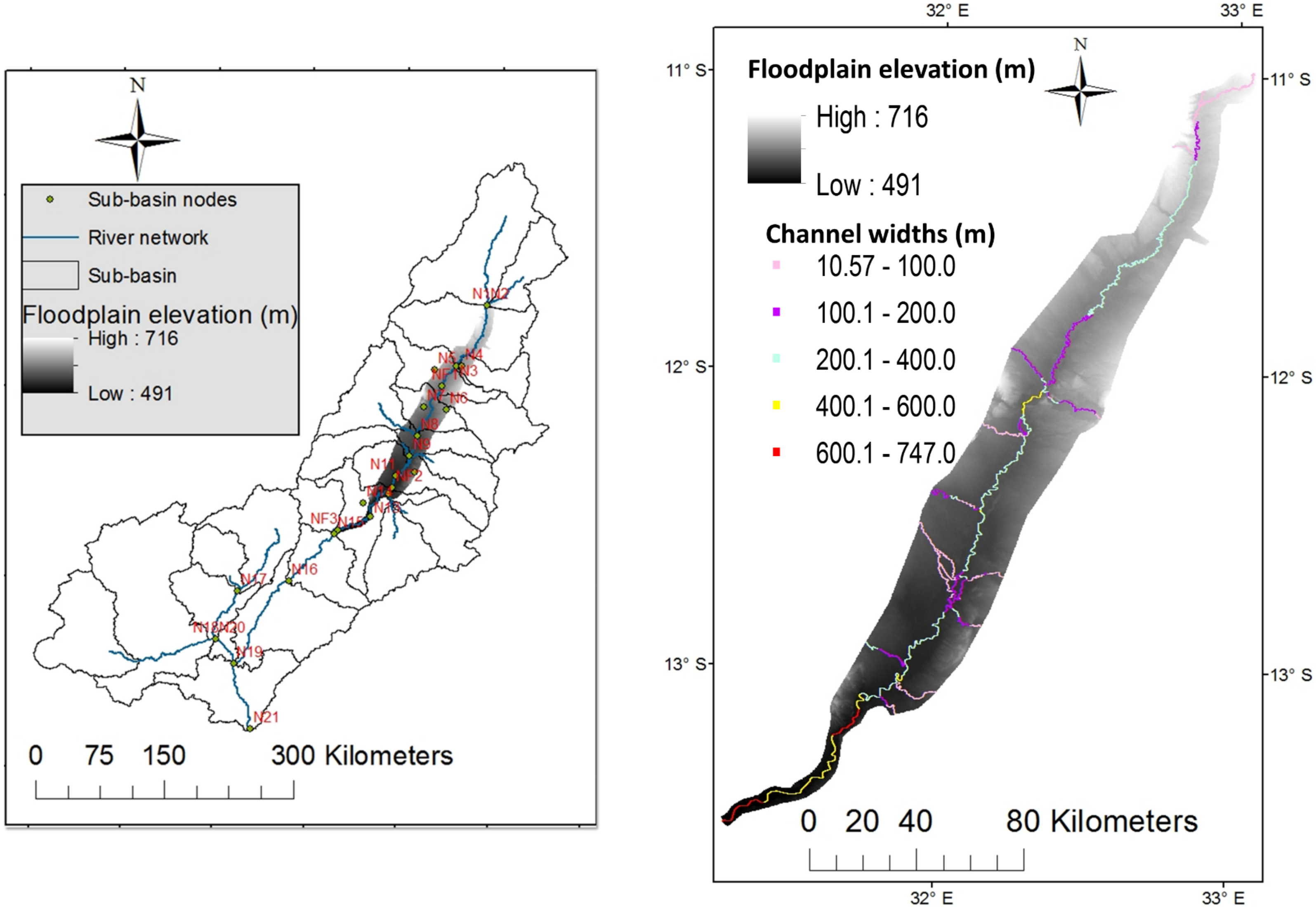

Figure 5.11: The location of the Luangwa floodplain in the Luangwa River basin

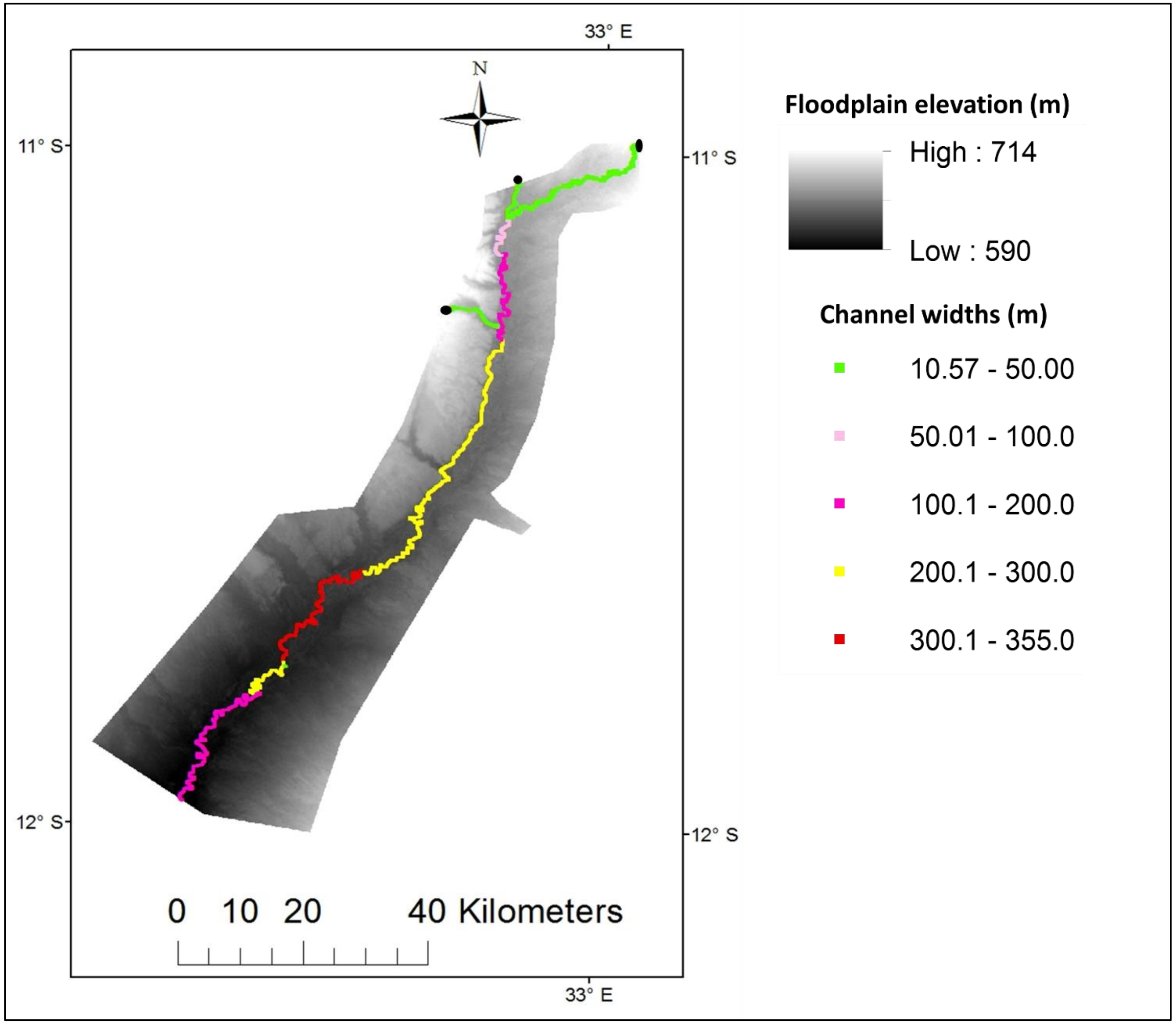

Figure 5.12: The elevation and channel width values for the upper section of the Luangwa floodplain.

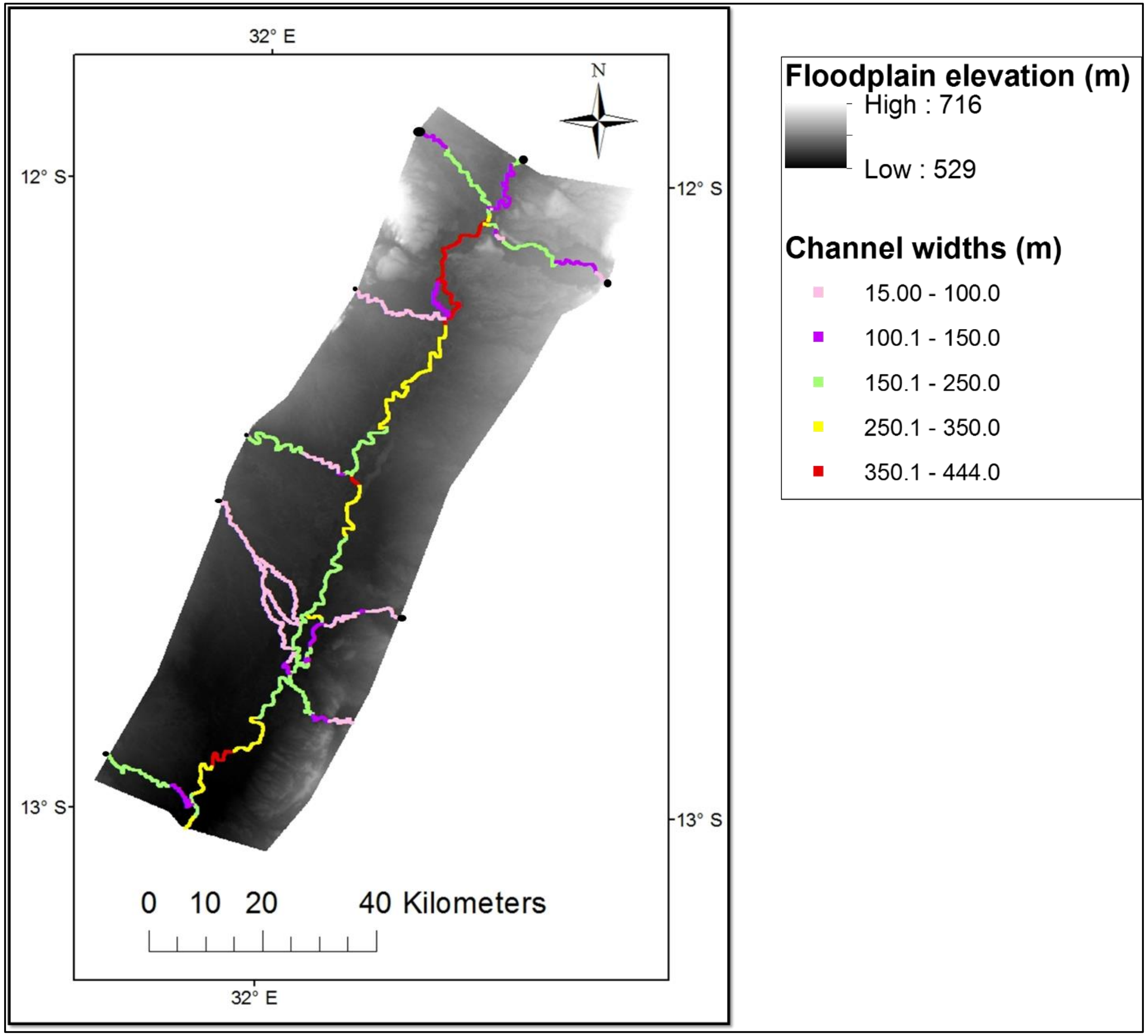

Figure 5.13: The elevation and channel width values for the middle section of the Luangwa floodplain.

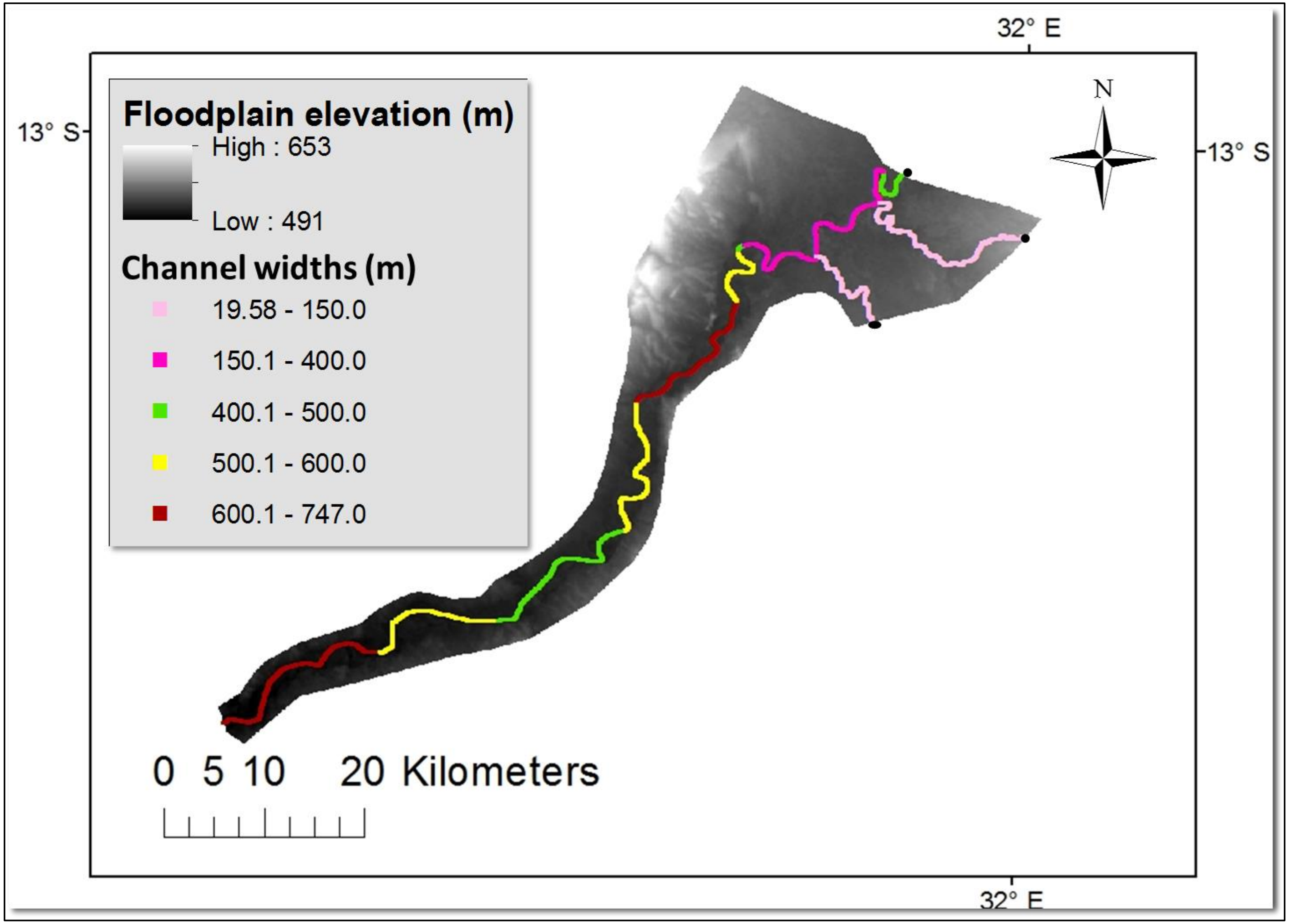

Figure 5.14: The elevation and channel width values for the lower section of the Luangwa floodplain.

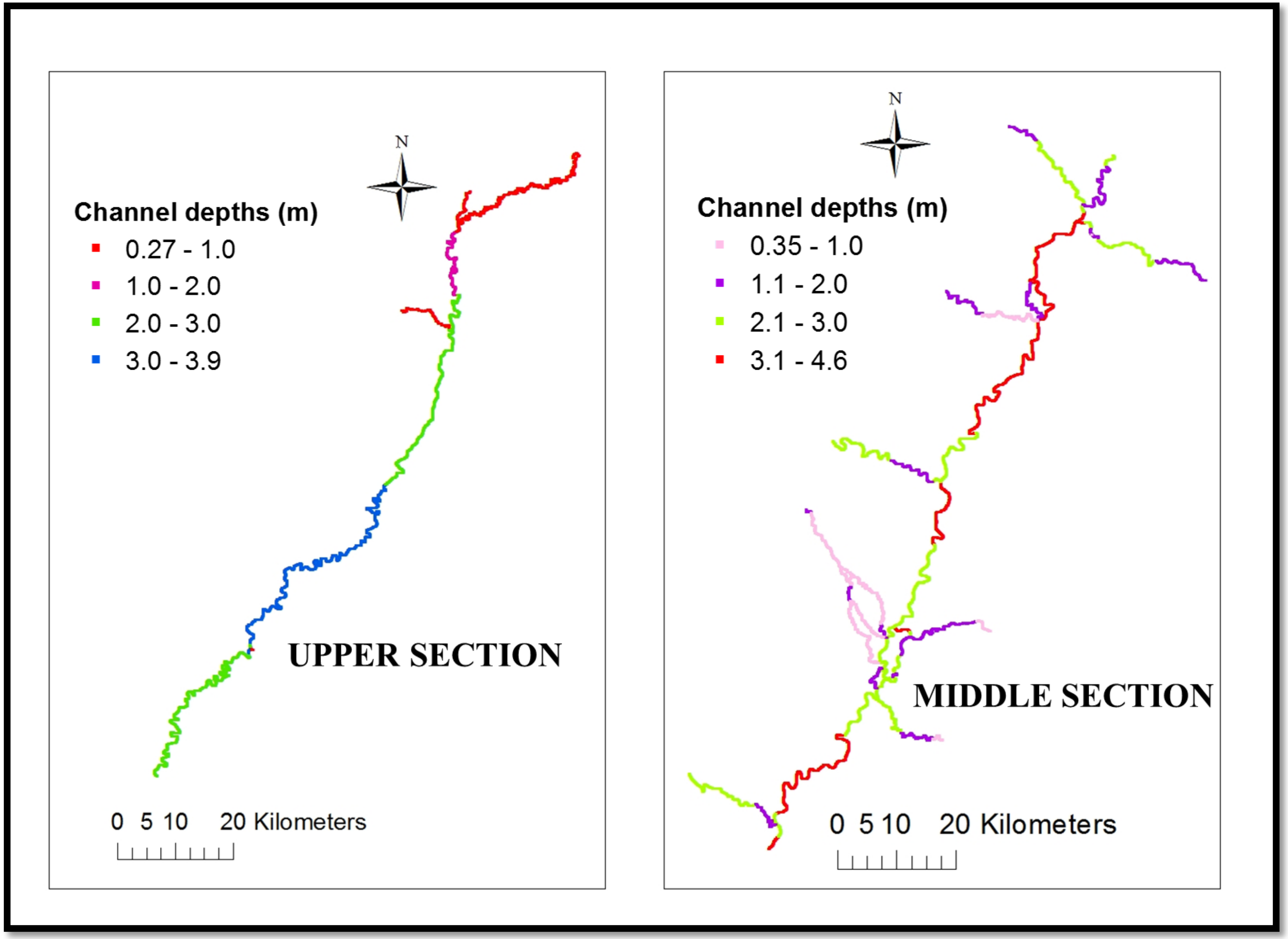

Figure 5.15: Channel depth values for upper and middle sections of the Luangwa floodplain.

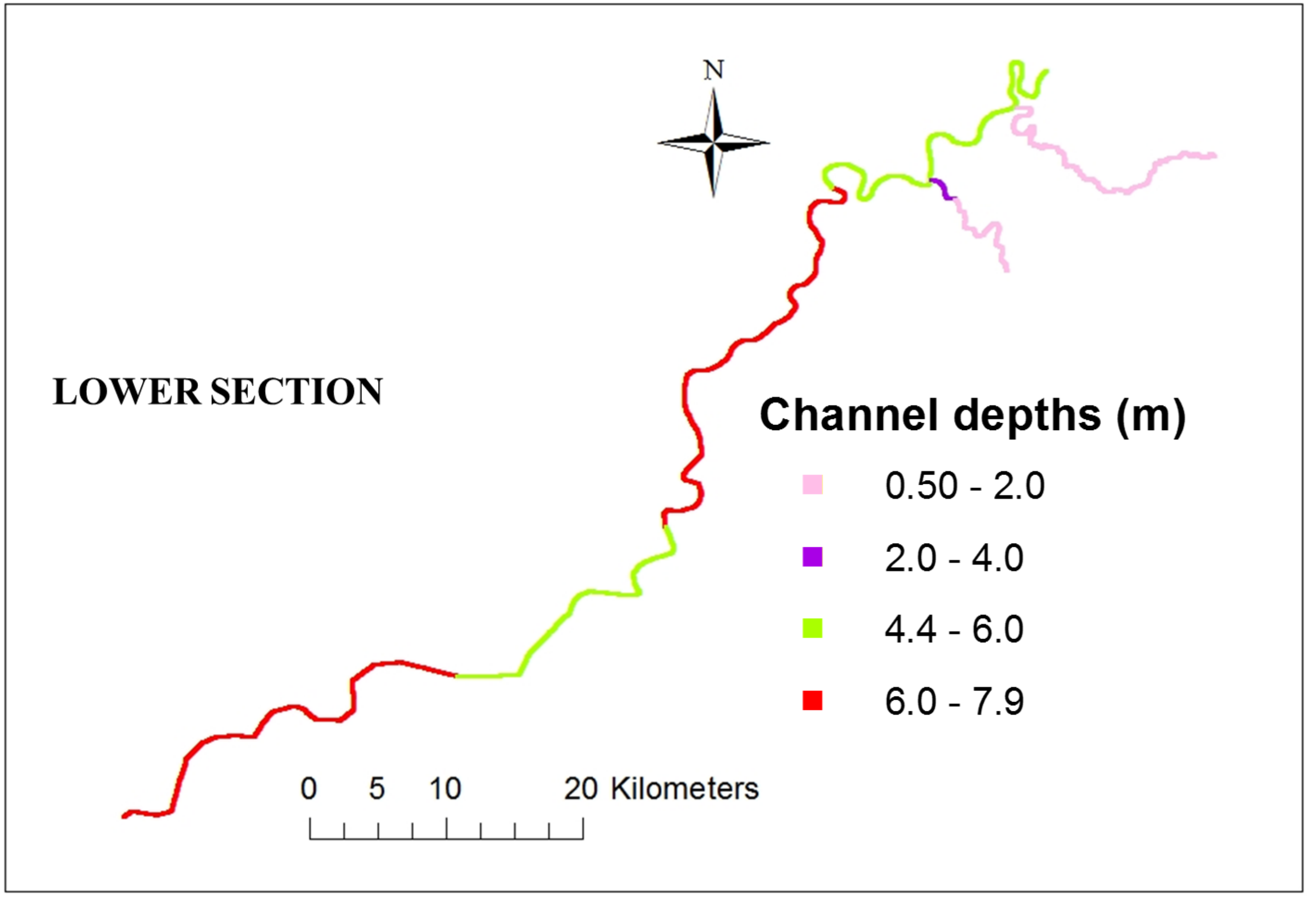

Figure 5.16: Channel depth values for the lower section of the Luangwa floodplain.

Table 5.8: Parameter ranges used to setup the LISFLOOD-FP model

Parameter	Parameter range	Final parameter value
Channel roughness (C_n)	0.015 – 0.035	0.015
Floodplain roughness (C_f)	0.06 – 0.08	0.08
p (fractional exponent in the Width–depth relationship)	0.76	0.76
r (scale coefficient in the Width–depth relationship)	0.04 – 0.055	0.052

In the absence of observed daily flows at the floodplain outlet, the simulated outflows could not be validated. Only the simulated inundation extents were partially validated using the limited observations of inundation extents from Landsat images. Regarding the quality of Landsat images, the images covering the period of maximum inundation (i.e. late February or early March) for the simulated years were largely obscured by cloud cover. The 26th March 2010 image was used to represent the wet season images. Other images used to validate the simulated inundation results include images acquired on 21st May 2007, 19th April 2013 and 5th May 2013. The results presented here are for simulations that involved the entire floodplain as a single unit as well as simulations for individual floodplain sections (middle and lower sections). The quality of the images on the upper section of the floodplain was very poor. Figure 5.17 shows different sections of the floodplain with the simulated inundation extent on 26th March 2010 and 21st May 2007 overlaid on the LandsatLook images. It is clear that most of the low-lying areas including the oxbows are well captured by the model (Figure 5.17 and 5.18). Additionally, simulated inundation extents on individual floodplain sections are reasonably good (Figure 5.19 and 5.20). For instance, inundation extents in the lower parts of the middle section of the floodplain are captured by the model (Figure 5.19). The results have indicated that the model over-estimated some of the inundation extents, especially during the dry season (see images during the dry seasons: Figure 5.21). Furthermore, the calculated Flood Area Index (FAI) values decreased during the dry season; an index value of about 35% was observed on 19th April 2013 and 39% on 26th March 2010. Even though the FAI values were generally low (less than 50%), the model captured more than 65% of the observed water pixels during the wet season. The average inundation depth was around 1.3 m, but inundation depths with values greater than 4 m were observed in oxbows and other depressions.

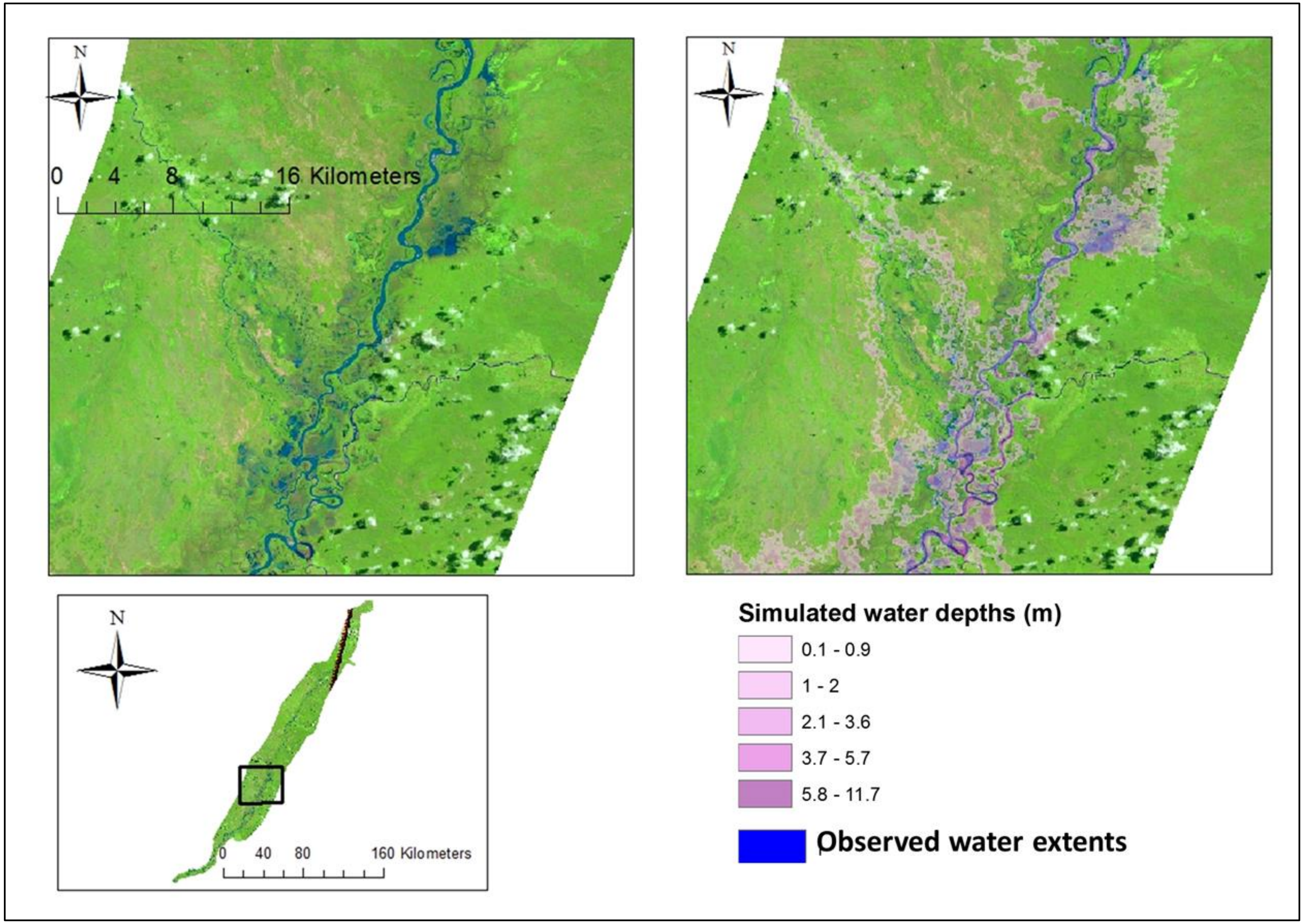

Figure 5.17: Comparison between observed and simulated flooding extents 26th March 2010 in the Luangwa floodplain (simulation for entire floodplain as a single unit).

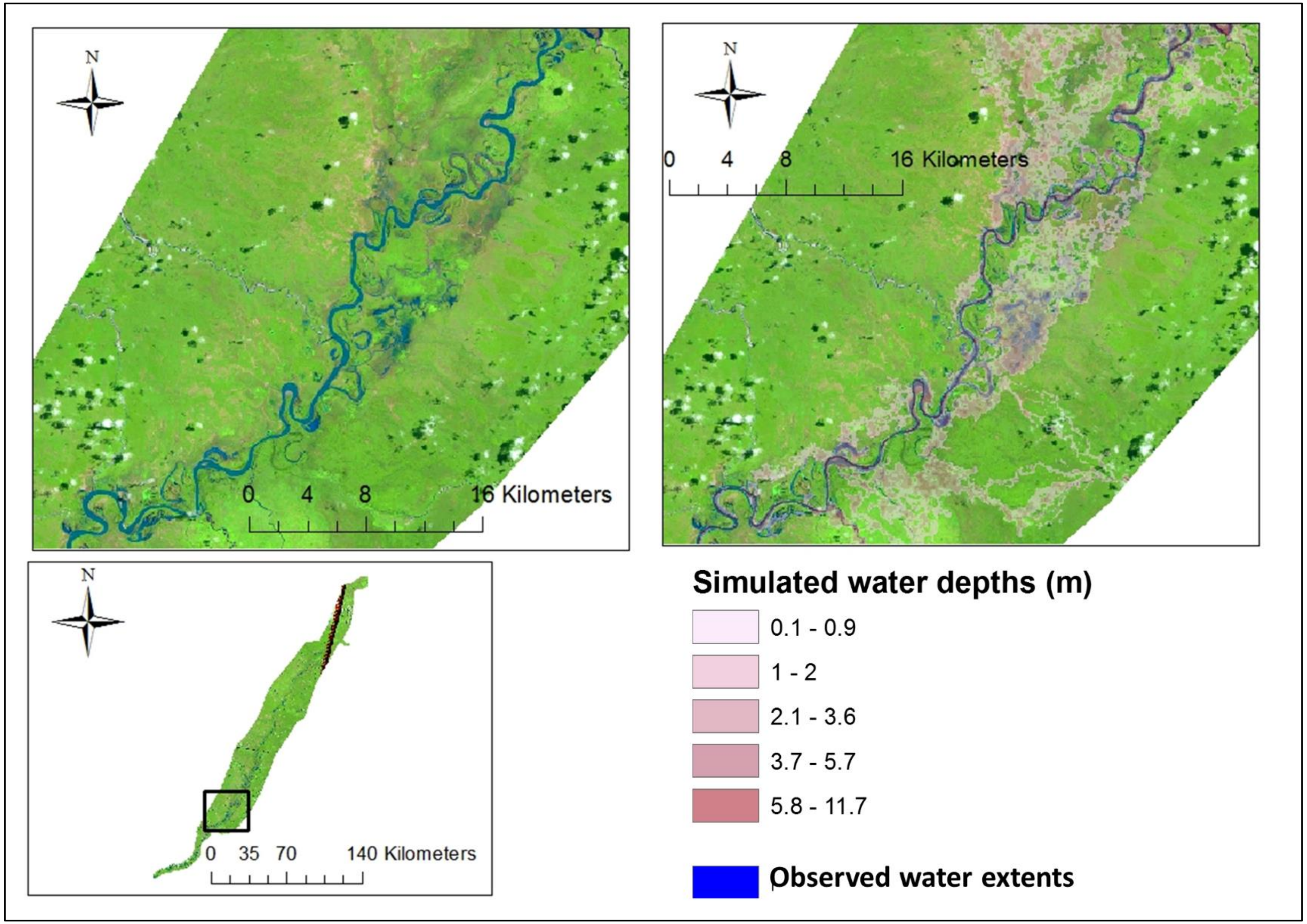

Figure 5.18: Comparison between observed and simulated flooding extents 26th March 2010 in the Luangwa River floodplain (simulation for entire floodplain as a single unit).

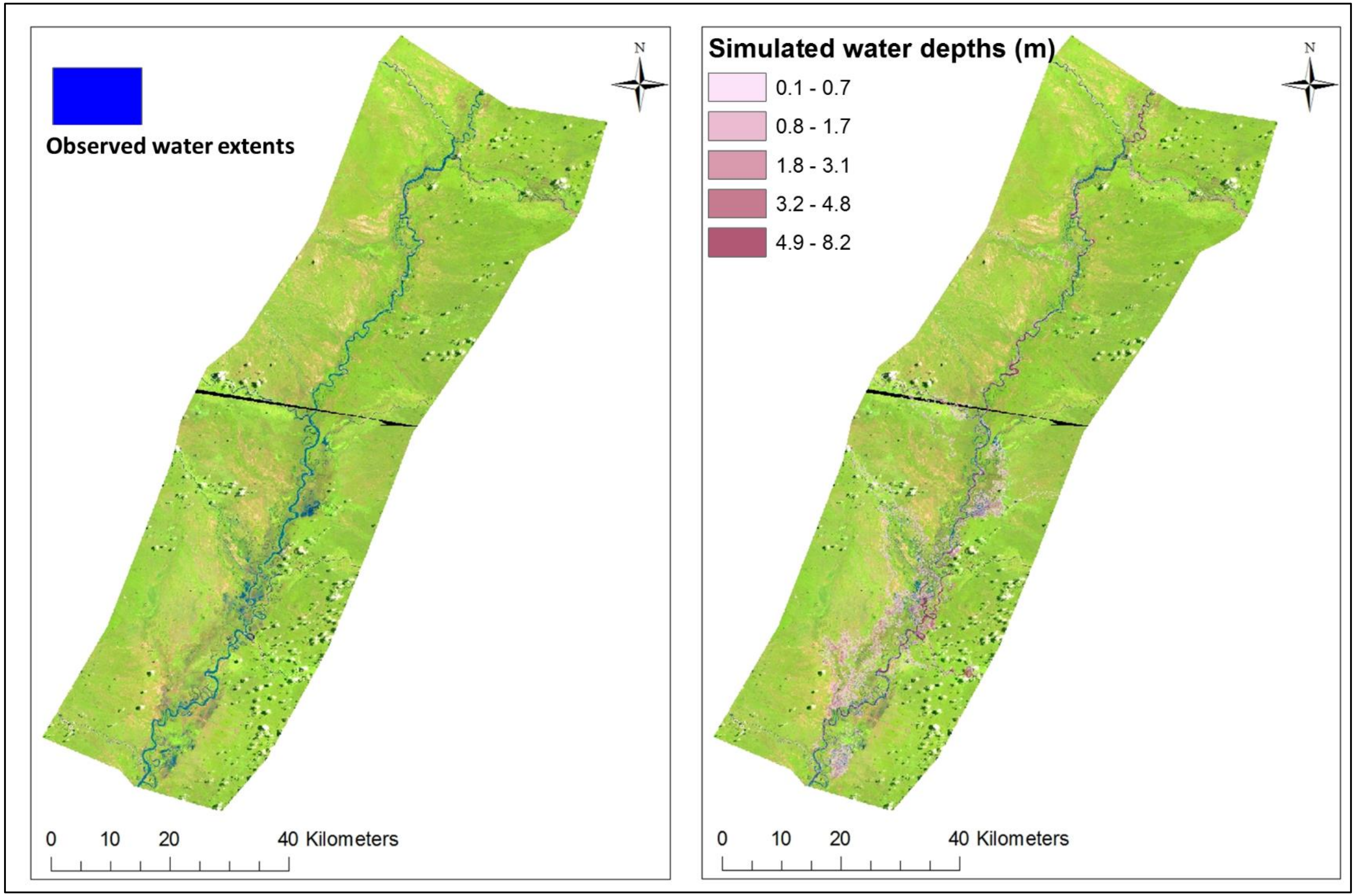

Figure 5.19: Comparison between observed and simulated flooding extents 26th March 2010 in the middle section of the Luangwa floodplain.

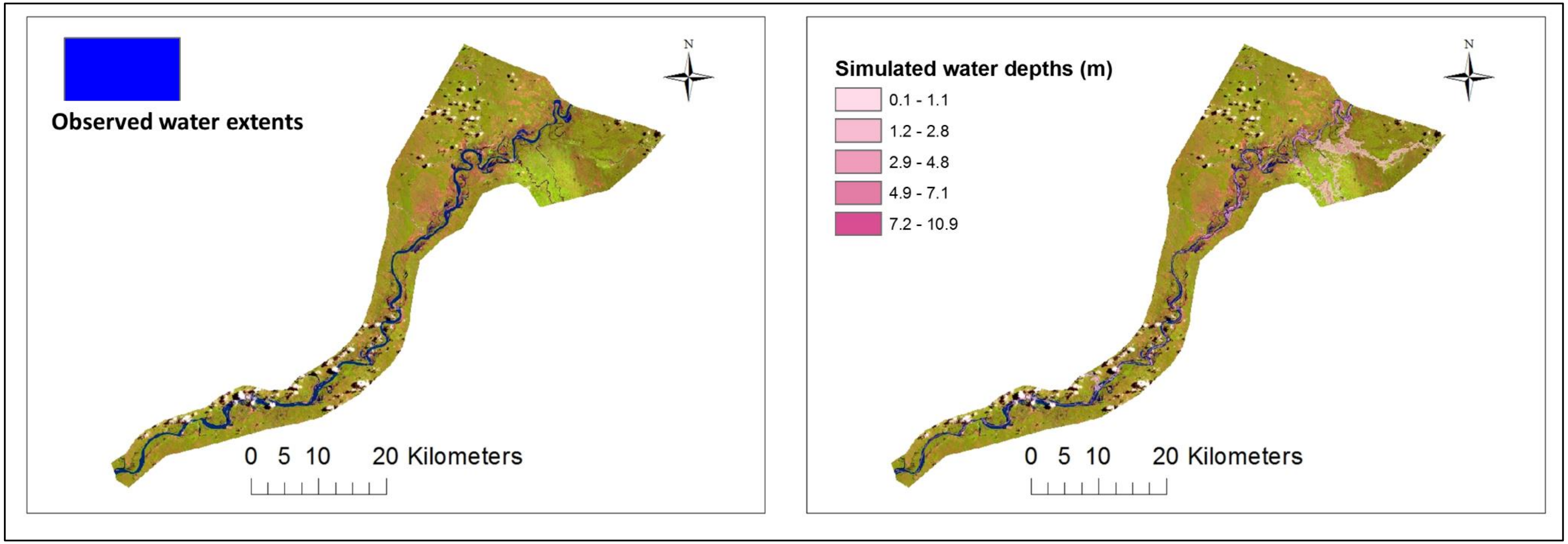

Figure 5.20: Comparison between observed and simulated flooding extents 26th March 2010 in the lower section of the Luangwa floodplain.

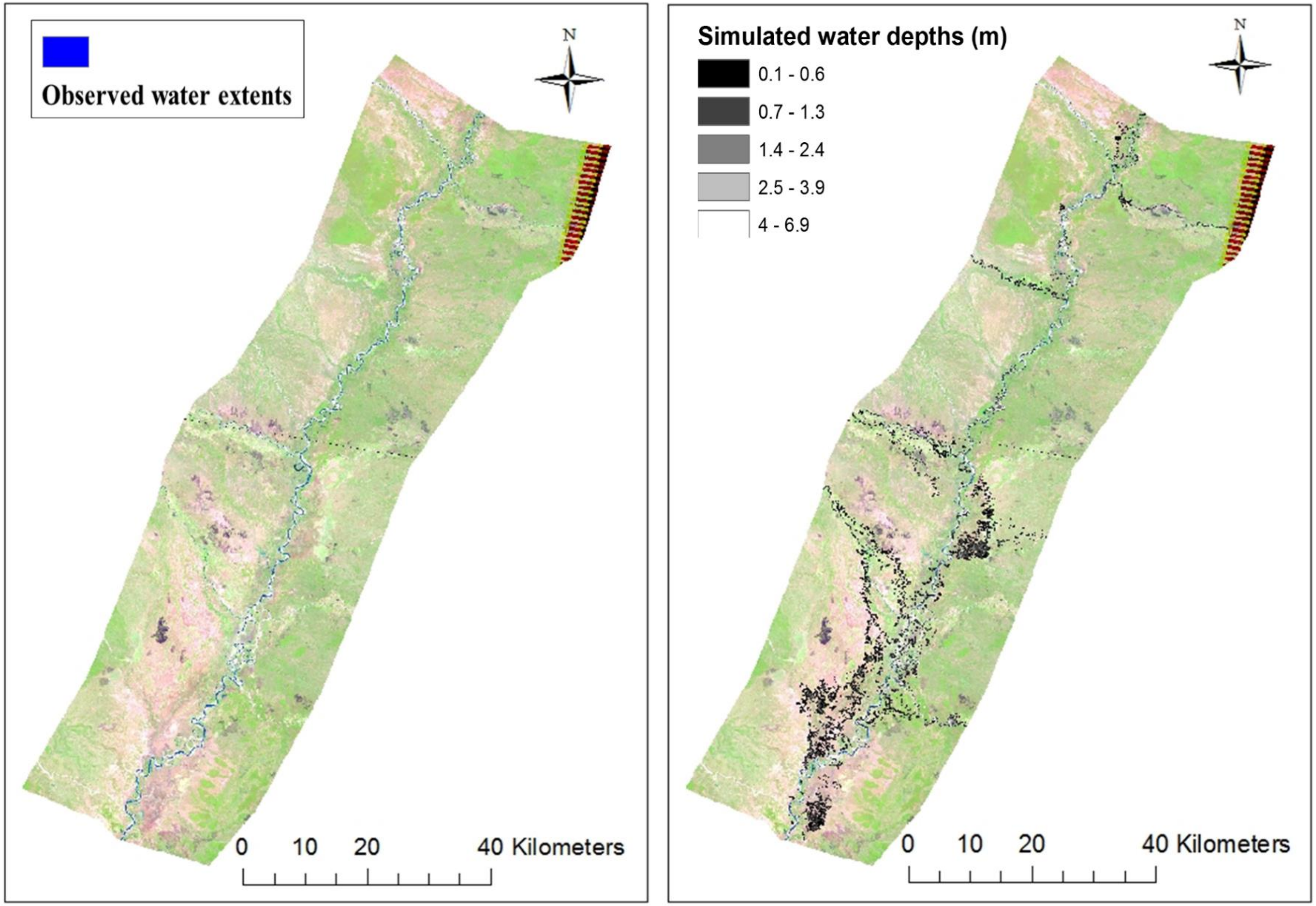

Figure 5.21: Comparison between the observed and simulated flooding extents on 21st May in the middle section of the Luangwa floodplain.

The storage–inflow and area–storage relationships for each 7-day simulation results form a nearly-closed anti-clockwise hysteresis behaviour. There is a low volume of water remaining on the floodplain at the end of the dry season (possibly in the few depressions and oxbows found within the floodplain). The maximum 7-day inundation extents and volumes for simulation of the entire floodplain were in the range of 400 – 700 km^2 and 900 – 1 500 $m^3 \times 10^6$, respectively (Figure 5.22). Maximum inundation area in the lower section of the floodplain was smaller compared to upper and middle sections (Figure 5.28). Part of this could be related to the topographic characteristics of this section (i.e. the floodplain becomes quite narrow) as indicated in Figure 5.14 above. The maximum inundation area and storage occur more-or-less simultaneously with the peak inflow suggesting a close relationship between the floodplain areas and the flow in the river channels. Although the storage–inflow relationship form a counter-clockwise hysteresis curve, the curves are somewhat complex especially during the rising limb. This could be related to multiple flow peaks and the complex nature of connectivity between the floodplain features and the main river, particularly during high flood magnitudes (see Figure 2.3 in section 2.2). In order to compare the hysteresis curves observed in both relationships, the variables of the hysteresis curves (i.e. area–storage or storage–inflow) were standardised/normalised by dividing each variable by the maximum value. The maximum separation distance between the rising and falling limbs is used (Table 5.9) to represent the magnitude of the hysteresis. The shape of the area–storage relationships during the wet and normal years are relatively similar, whereas their sizes are different (see Figure 5.23, 5.25, and 5.27. The higher the flood magnitude, the greater the hysteresis effect (Table 5.9). The difference in the hysteresis magnitude for the three wetland sections reflect the variations of their channel–wetland exchange processes. The greatest hysteresis effect is observed in the middle section (NF2). Generally, the difference in the size of the hysteresis loops between wet and normal hydrological years could be related to the differences in how the floodwater propagates and penetrates the floodplain as well as how long the return flow cycle lasts. During floods of greater magnitude the extent and volume of inundation is greater and this results in a greater hysteresis as it takes a longer relative time for the water to return to the river. The difference between inflows and outflows is minimal in the lower section because the effects of the floodplain in this section are very small and the hysteresis magnitudes are small regardless of the level of flooding.

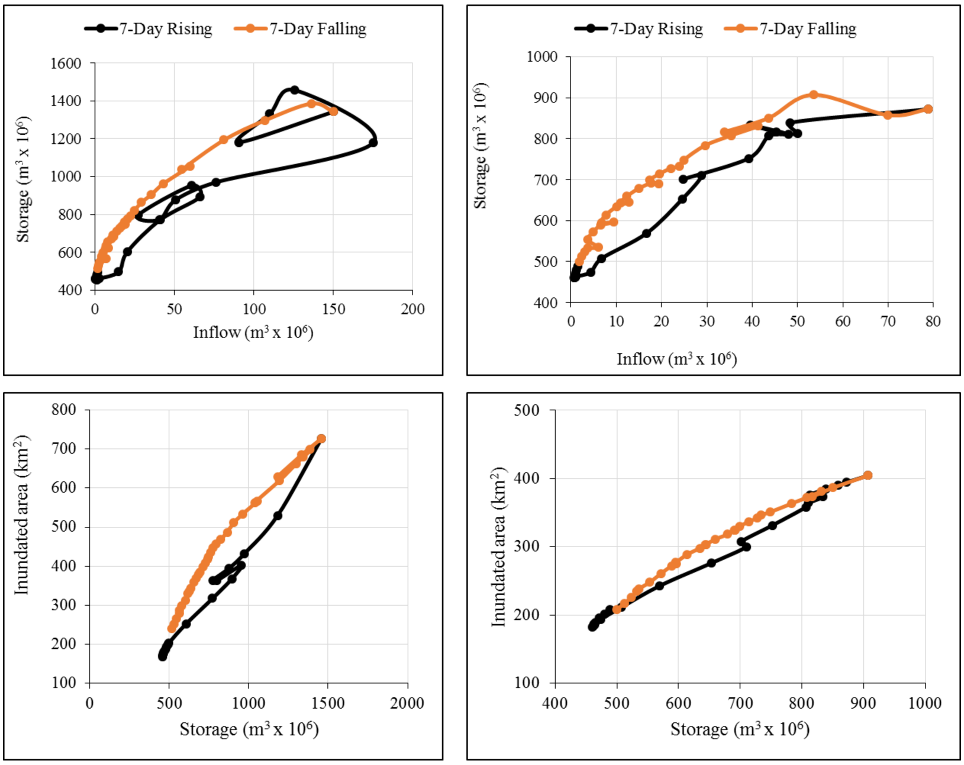

Figure 5.22: Storage–inflow and area–storage 7-day anticlockwise hysteresis for the wet (2006/07: Left) and normal (20012/13: Right) years in the entire Luangwa floodplain.

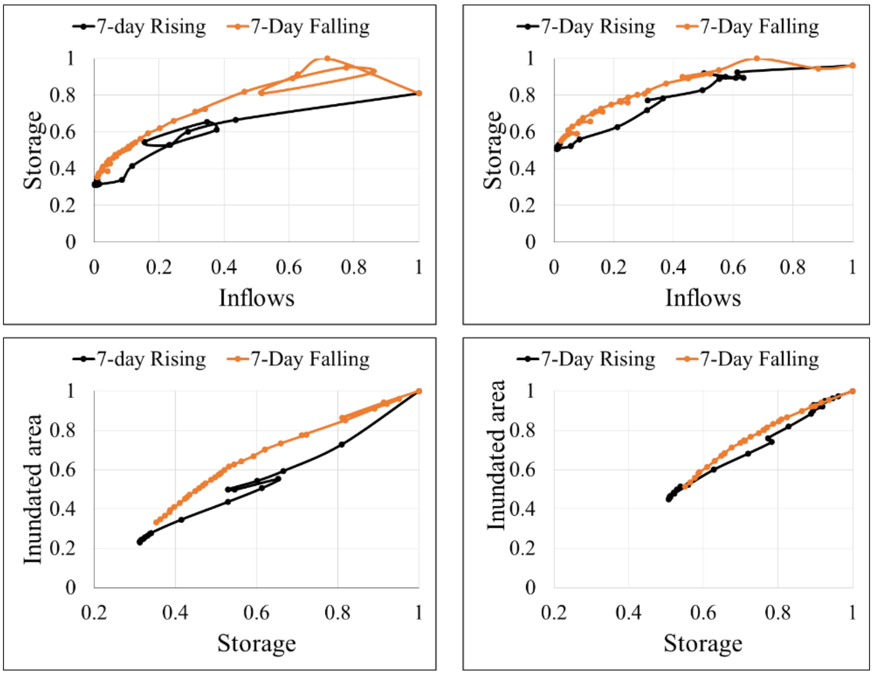

Figure 5.23: Standardised storage–inflow and area–storage 7-day anticlockwise hysteresis for the wet (2006/07: Left) and normal (20012/13: Right) years in the entire Luangwa floodplain.

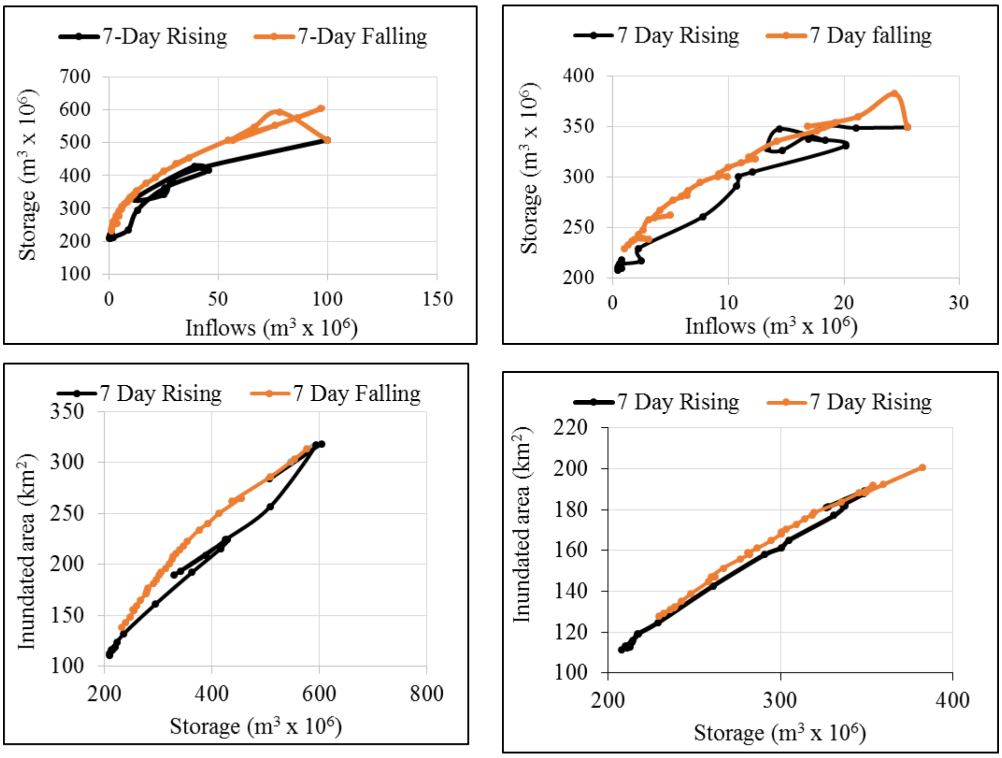

Figure 5.24: Storage–inflow and area–storage 7-Day hysteresis for wet (2006/07: Left) and normal (20012/13: Right) years in the upper section of the Luangwa floodplain.

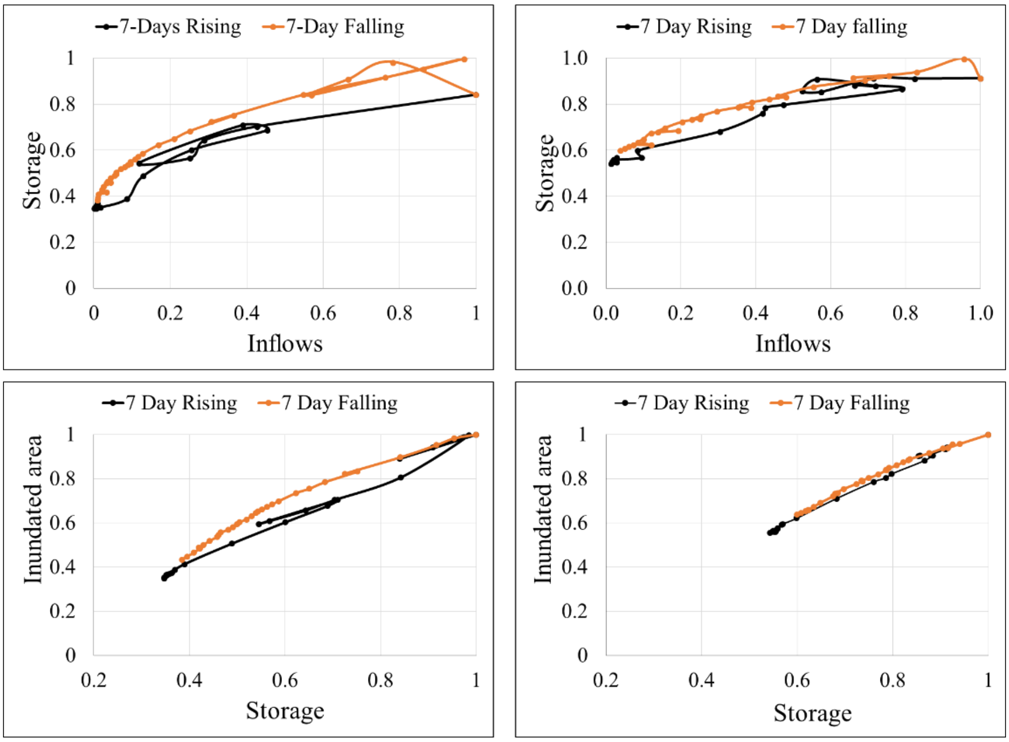

Figure 5.25: Standardized storage–inflow and area–storage 7-day hysteresis for wet (2006/07: Left) and normal (20012/13: Right) years in the upper section of the Luangwa floodplain.

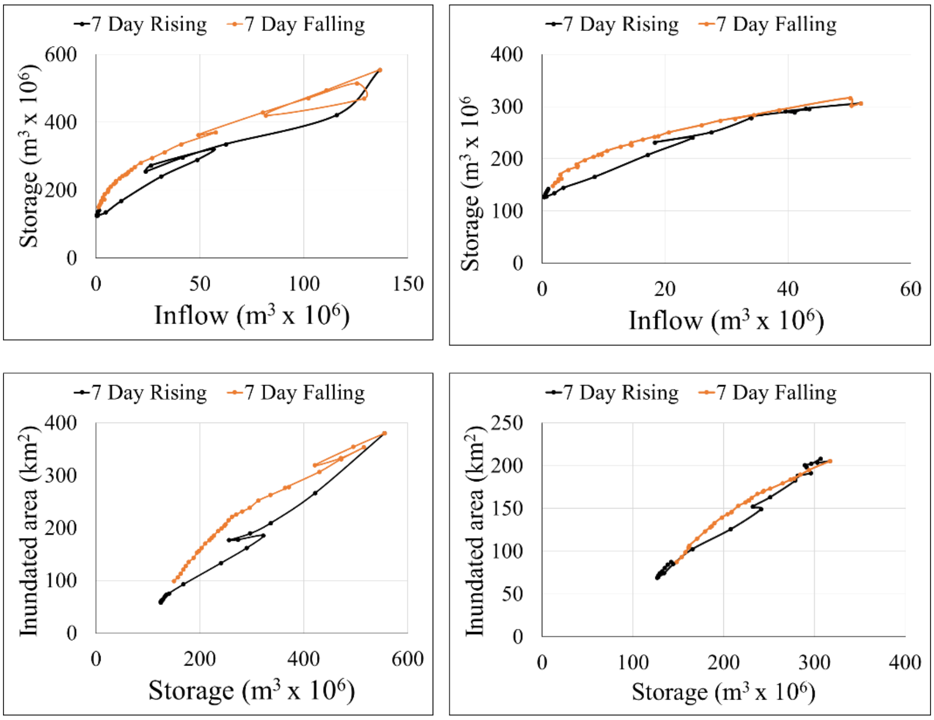

Figure 5.26: Storage–inflow and area–storage 7-day anticlockwise hysteresis for the wet (2006/07) and normal (20012/13) years in the middle section of the Luangwa floodplain.

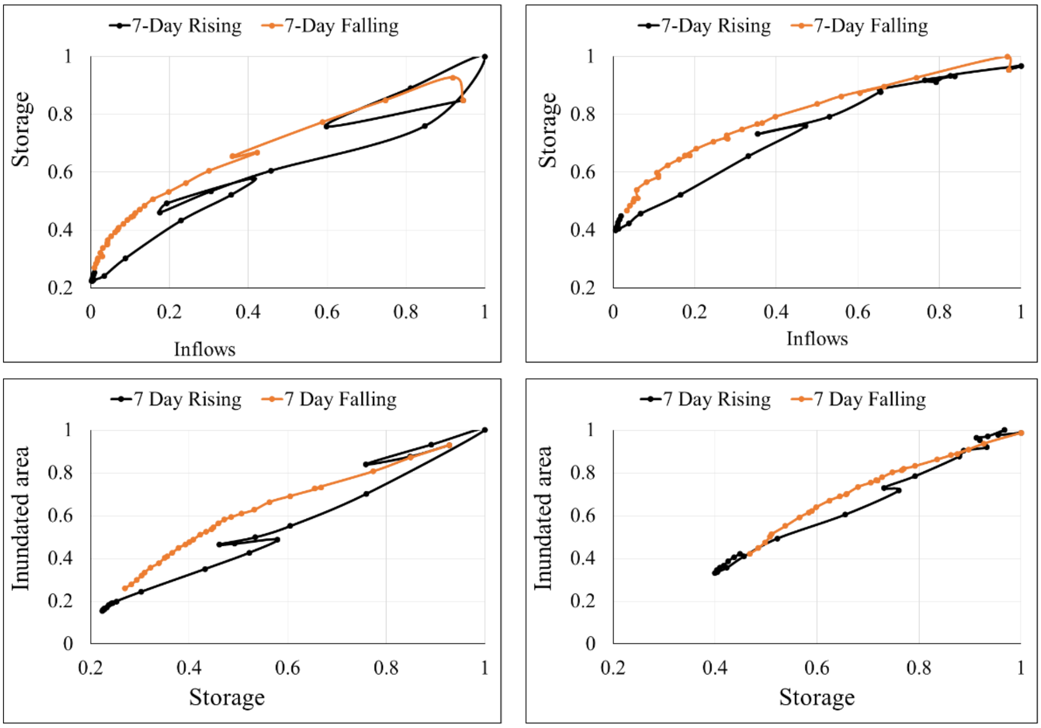

Figure 5.27: Standardised storage–inflow and area–storage 7-day anticlockwise hysteresis for the wet (2006/07) and normal (20012/13) years in the middle section of the Luangwa floodplain.

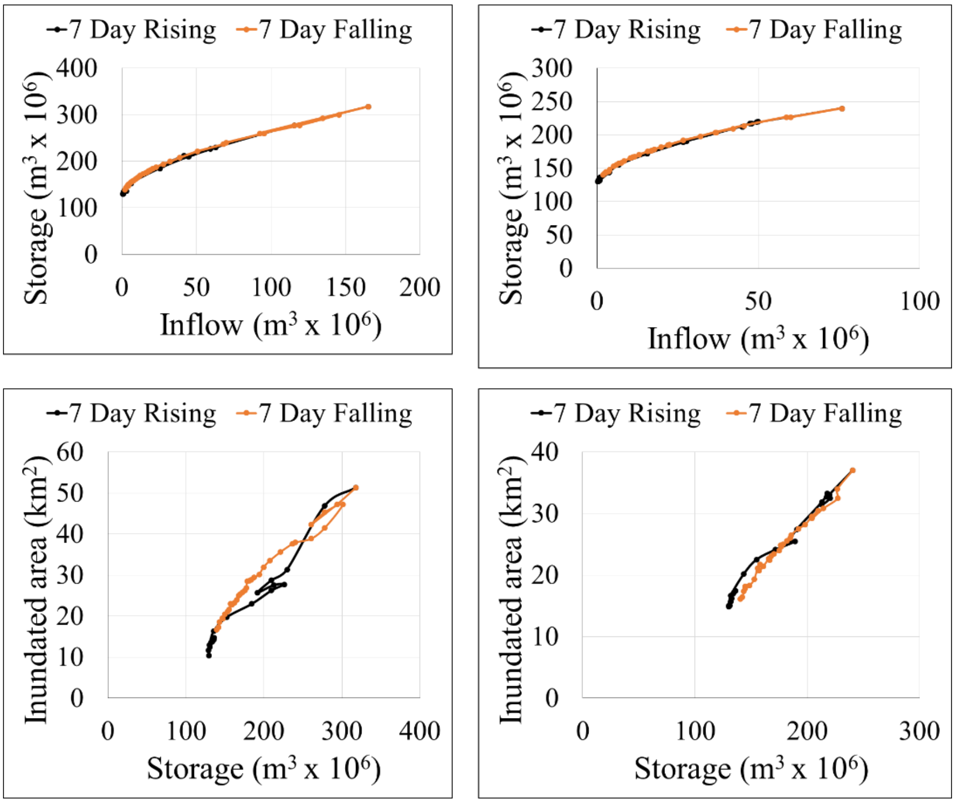

Figure 5.28: Storage–inflow and area–storage 7-day hysteresis for the wet (2006/07) and normal (20012/13) years in the lower section of the Luangwa floodplain.

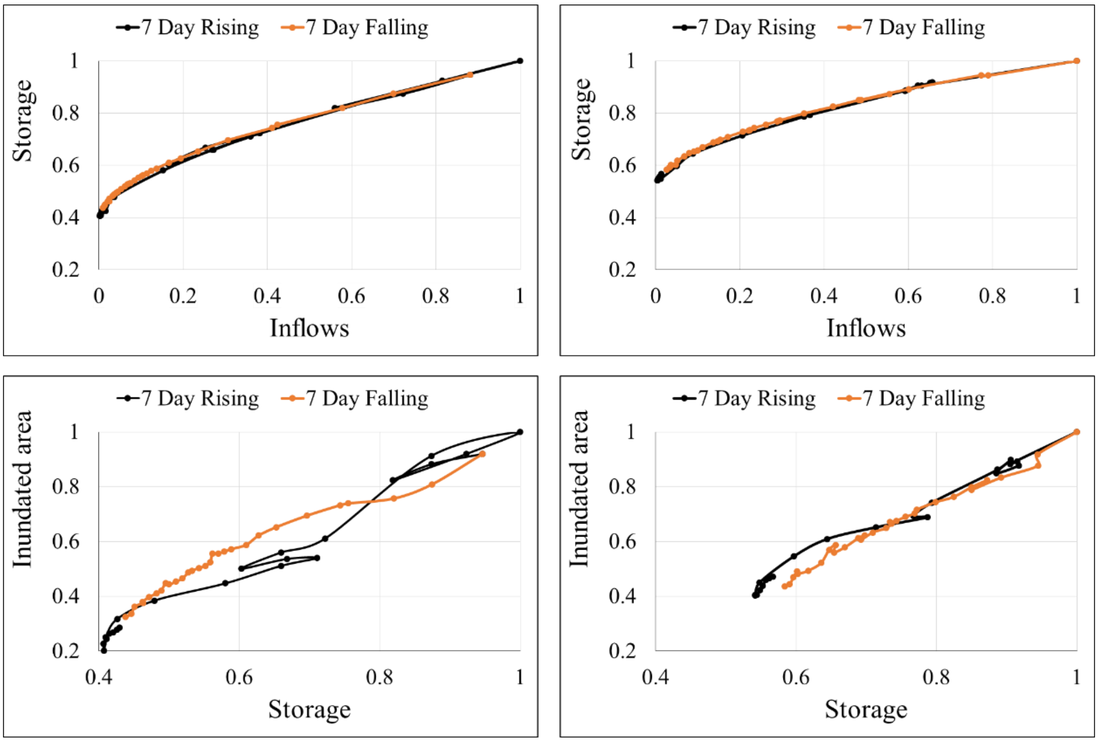

Figure 5.29: Standardised storage–inflow and area–storage 7-day hysteresis for the wet (2006/07) and normal (20012/13) years in the lower section of the Luangwa floodplain.

Table 5.9: Magnitude of the hysteresis curve in the Luangwa floodplain

Relationship	NF1		NF2		NF3	
	Wet year	Normal year	Wet year	Normal year	Wet year	Normal year
Area-storage	0.070	0.030	0.120	0.060	0.06	0.001
Storage-Inflow	0.120	0.030	0.130	0.050	0.000	0.000

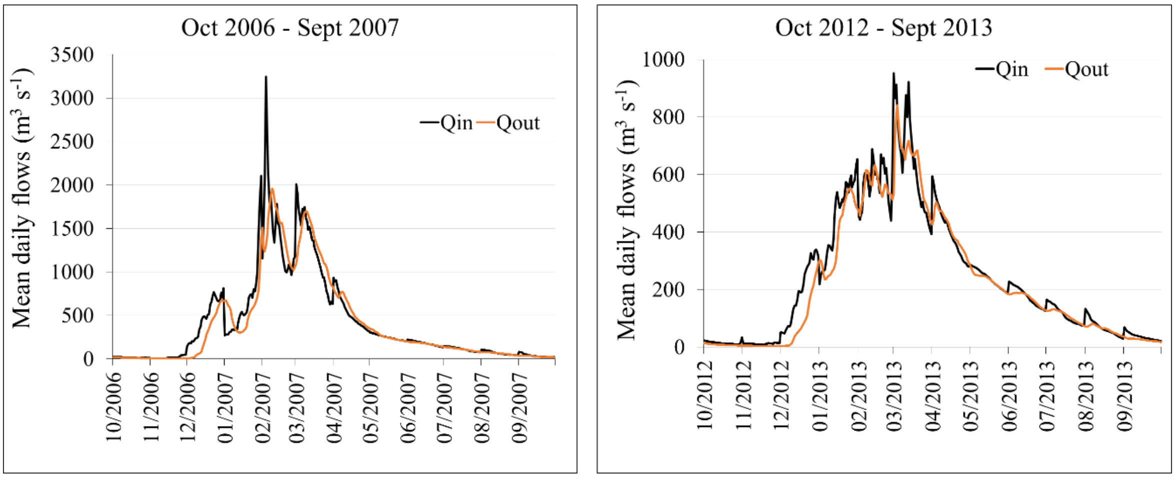

Figure 5.30: Mean daily inflows and outflows for the wet (2006/07) and normal (20012/13) years in the entire Luangwa floodplain.

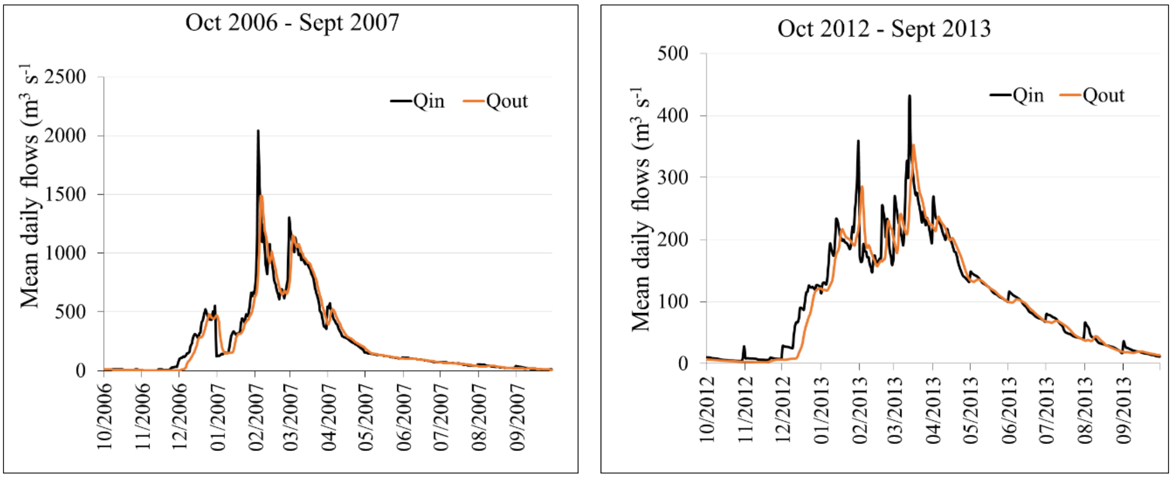

Figure 5.31: Mean daily inflows and outflows in the upper section of the Luangwa floodplain.

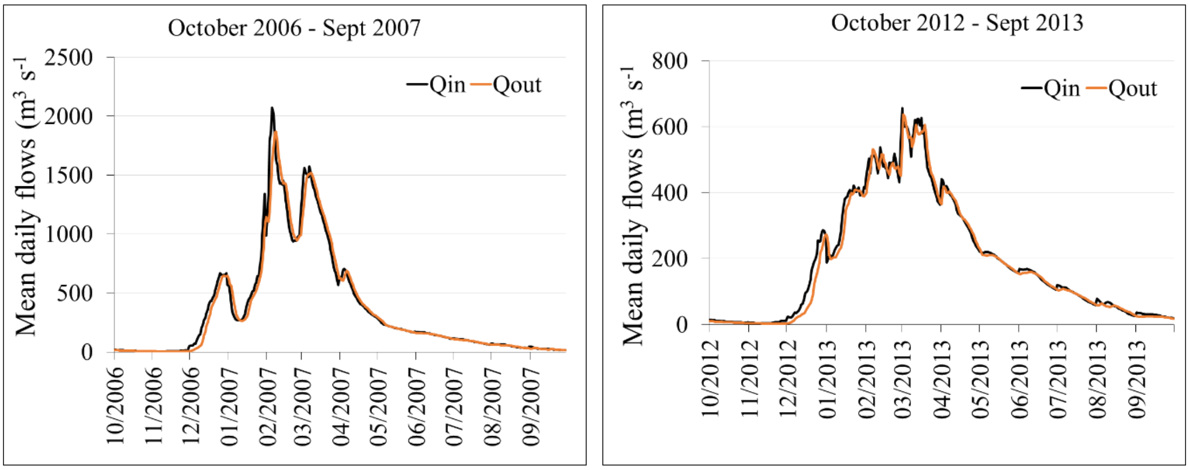

Figure 5.32 Mean daily inflows and outflows in the middle section of the Luangwa floodplain.

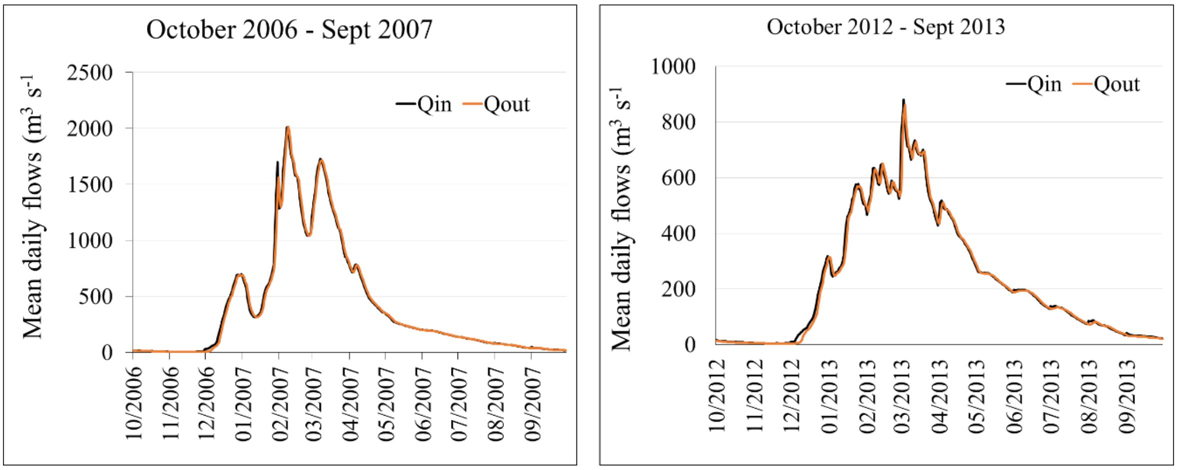

Figure 5.33: Mean daily inflows and outflows in the lower section of the Luangwa floodplain.

5.1.7 Quantification of Pitman wetland parameters

Table 5.10 presents the estimated parameter sets for the Pitman wetland sub-model established from the LISFLOOD-FP results for each sub-basin node with wetland effects. Some of these parameters were estimated directly from the LISFLOOD-FP results, whereas others were established through manual calibration by implementing the Pitman wetland sub-model in the excel sheet containing the LISFLOOD-FP results. The low value of the channel spill factor in the lower section corresponds to its channel characteristics (the channel is deep with low volumes of water spilling into the floodplain area). The maximum return flow fraction value illustrates that the return flows are not restricted by the amount of water in the channel relative to the capacity for spillage because spills and drainage back to the channel are expected to occur simultaneously in this floodplain. Figure 5.34, 5.35, 5.36 and 5.37 show the simulated monthly volume and outflow graphs for the LISFLOOD-FP and the Pitman wetland sub-model. The Pitman model is a monthly time-scale model, but the computations are done by dividing the monthly value into four iterations (i.e. 96 model iterations within two years). The results have indicated that there is a better agreement between the simulated outflows from the two models (the Pitman wetland sub-model and the LISFLOOD-FP) compared to the simulated volume (especially on the rising limb). Furthermore, the simulated results when the floodplain was divided into three sections are not as good as when the floodplain was simulated as a single unit. The reason could be that the floodplain is passing water down to the next section (or getting from the upstream section) and this was not being accounted for in the spreadsheet used to establish the wetland parameters. The fact that the LISFLOOD-FP model is accounting for downstream water transfers on the floodplain, while the Pitman model is not, could be a major issue to consider when setting up the model with more than one unit to represent the floodplain. The results suggest that some of the wetland parameters can be inferred from the results based on LISFLOOD-FP setup when the floodplain was a single unit. Generally speaking, the established parameters were considered appropriate enough to be used as the best-estimated parameter sets for the Pitman wetland sub-model.

Table 5.10: Estimated parameter set for the Pitman wetland sub-model based on the LISFLOOD-FP applications

Parameters and units	The estimated value for each sub-basin			
	Upper section (NF1)	Middle section (NF2)	Lower section (NF3)	Entire floodplain as a single unit
Local catchment area (Km^2)	500	450	200	2500
Residual wetland volume (RWV) in $m^3 10^6$	215	150	130	400
Initial wetland volume (WV) in $m^3 10^6$	212	140	130	550
A in $\mathrm{Area}(\mathrm{m}^2 10^6) = \mathrm{A}(\mathrm{WV}\ (m^3 10^6))^{\mathrm{B}}$	10.5	9	0.19	0.012
B in $\mathrm{Area}(\mathrm{m}^2 10^6) = \mathrm{A}(\mathrm{WV}\ (m^3 10^6))^{\mathrm{B}}$	0.82	0.87	1.004	1.18
Channel capacity for spillage (QCAP) $m^3 10^6$	100	80	160	80
Channel spill factor	0.25	0.15	0.06	0.2
AA in $\mathrm{RFF} = \mathrm{AA}\left(\frac{\mathrm{WV}}{\mathrm{RWV}}\right)^{\mathrm{BB}}$	0.32	0.3	0.33	0.09
BB in $\mathrm{RFF} = \mathrm{AA}\left(\frac{\mathrm{WV}}{\mathrm{RWV}}\right)^{\mathrm{BB}}$	1.9	1.8	1.7	2.6
Maximum return flow fraction	10.95	10.95	10.95	10.95

Annual evaporation (mm)	1535	1668.5	1668.5	1535

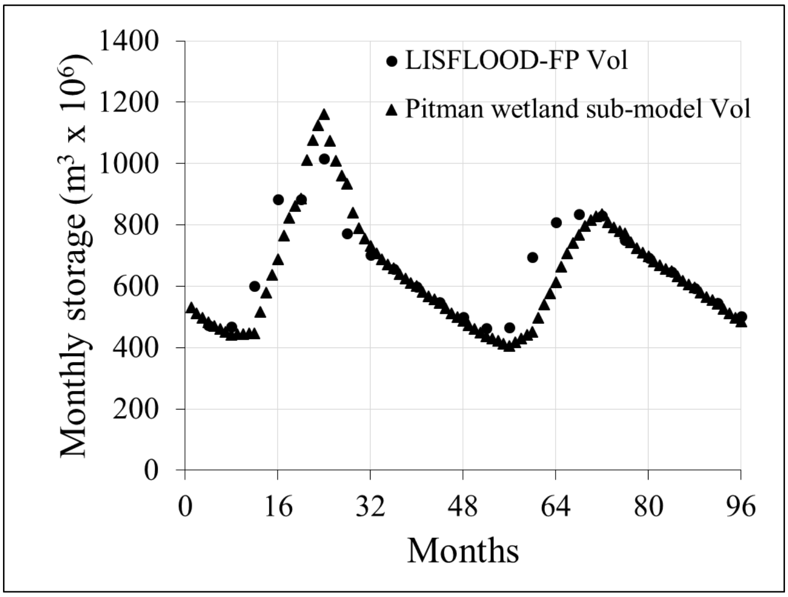

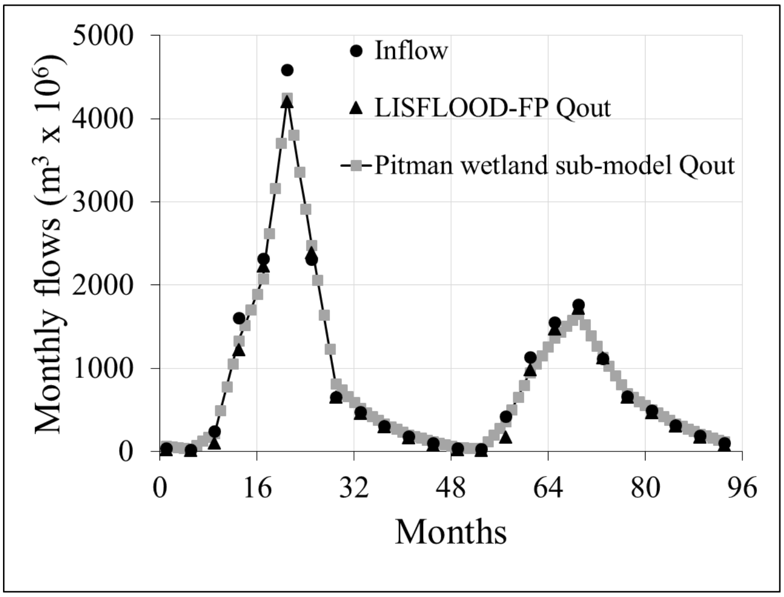

Figure 5.34: Comparison between the volume and flows simulated by the LISFLOOD-FP and Pitman wetland sub-model in the Luangwa floodplain (simulated as a single unit) for the period October 2011 to September 2013.

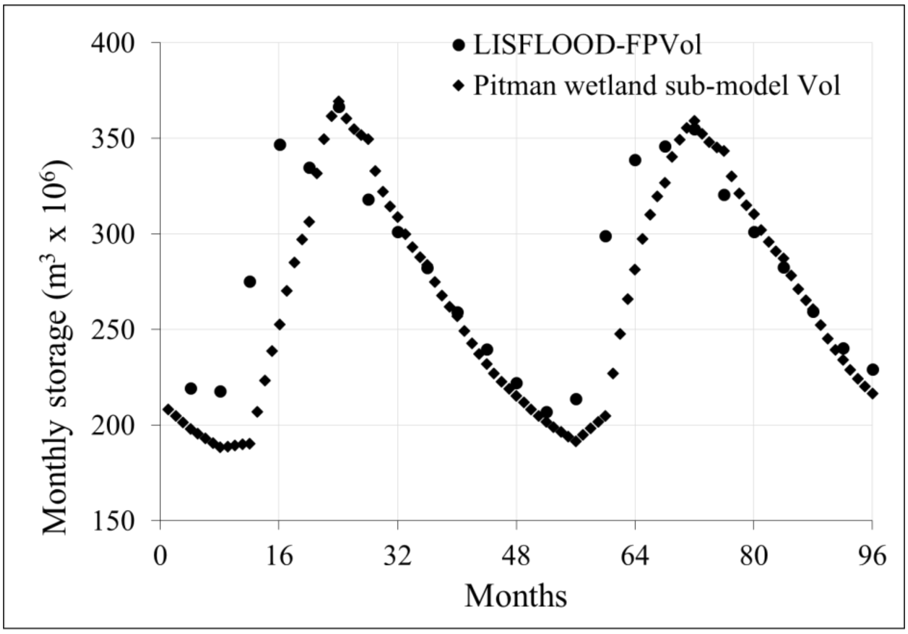

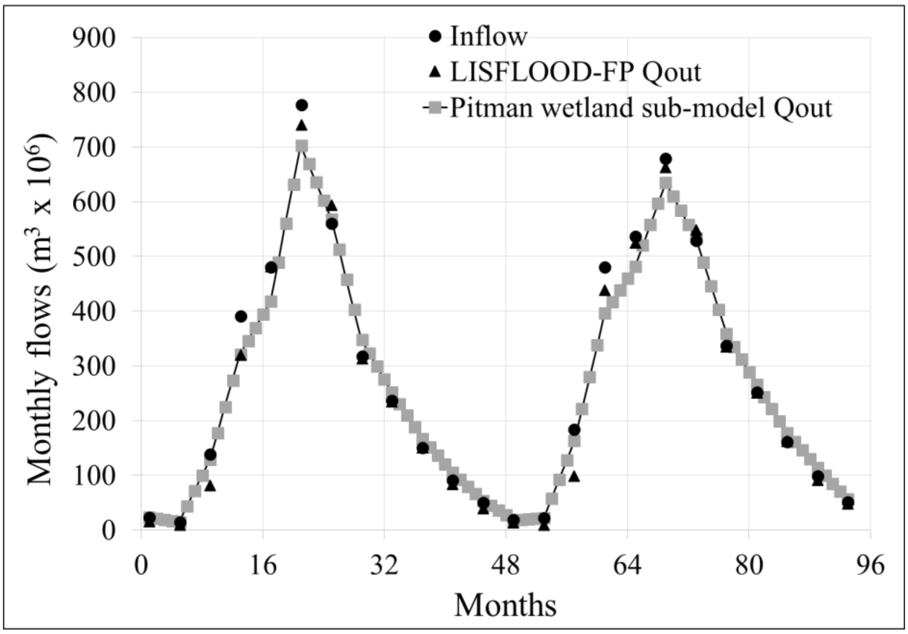

Figure 5.35: Comparison between the volume and flows simulated by the LISFLOOD-FP and Pitman wetland sub-model in the upper section (NF1) of the Luangwa floodplain for the period October 2011 to September 2013.

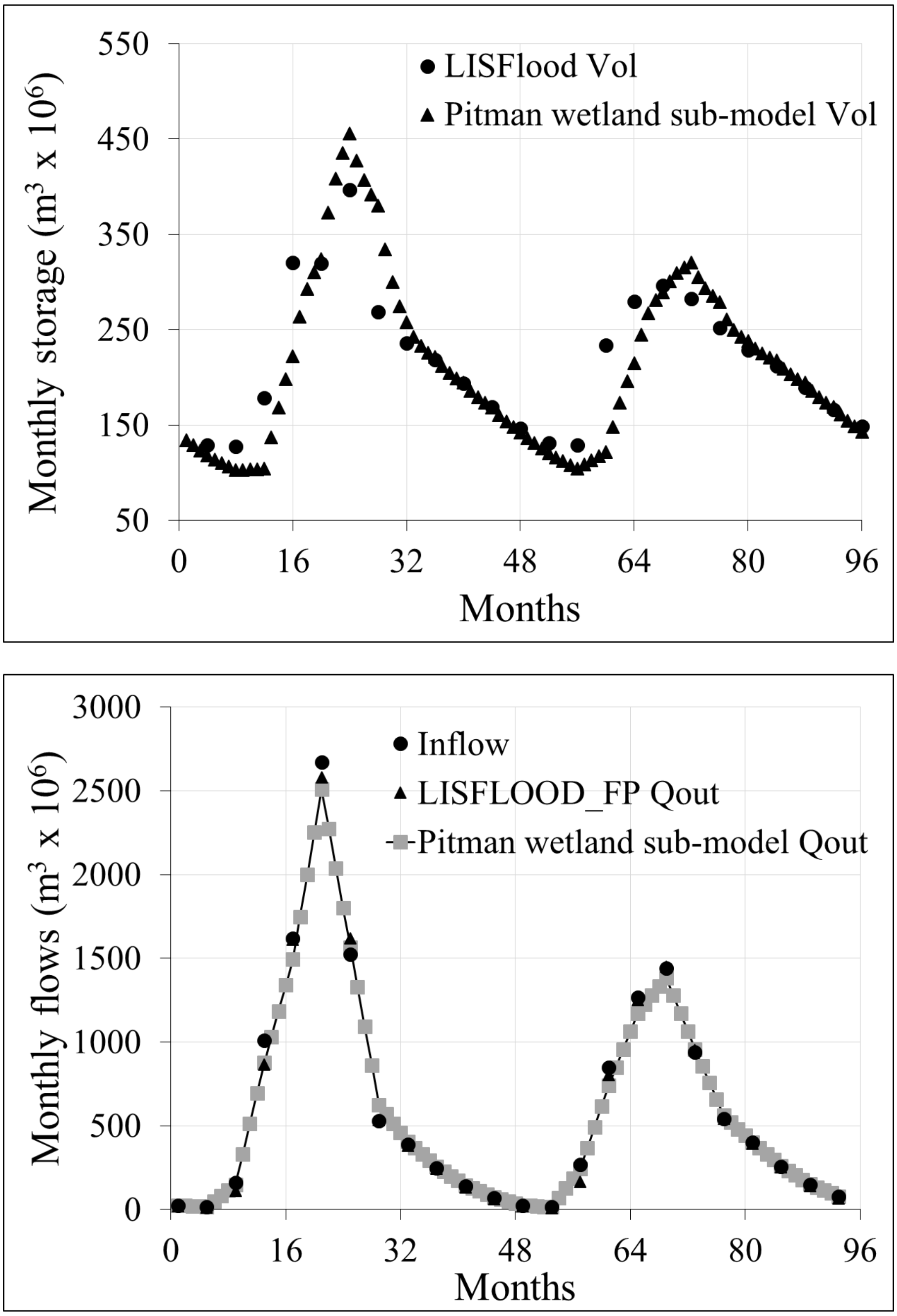

Figure 5.36: Comparison between the volume and flows simulated by the LISFLOOD-FP and Pitman wetland sub-model in the middle section (NF2) of the Luangwa floodplain for the period October 2005 to September 2007.

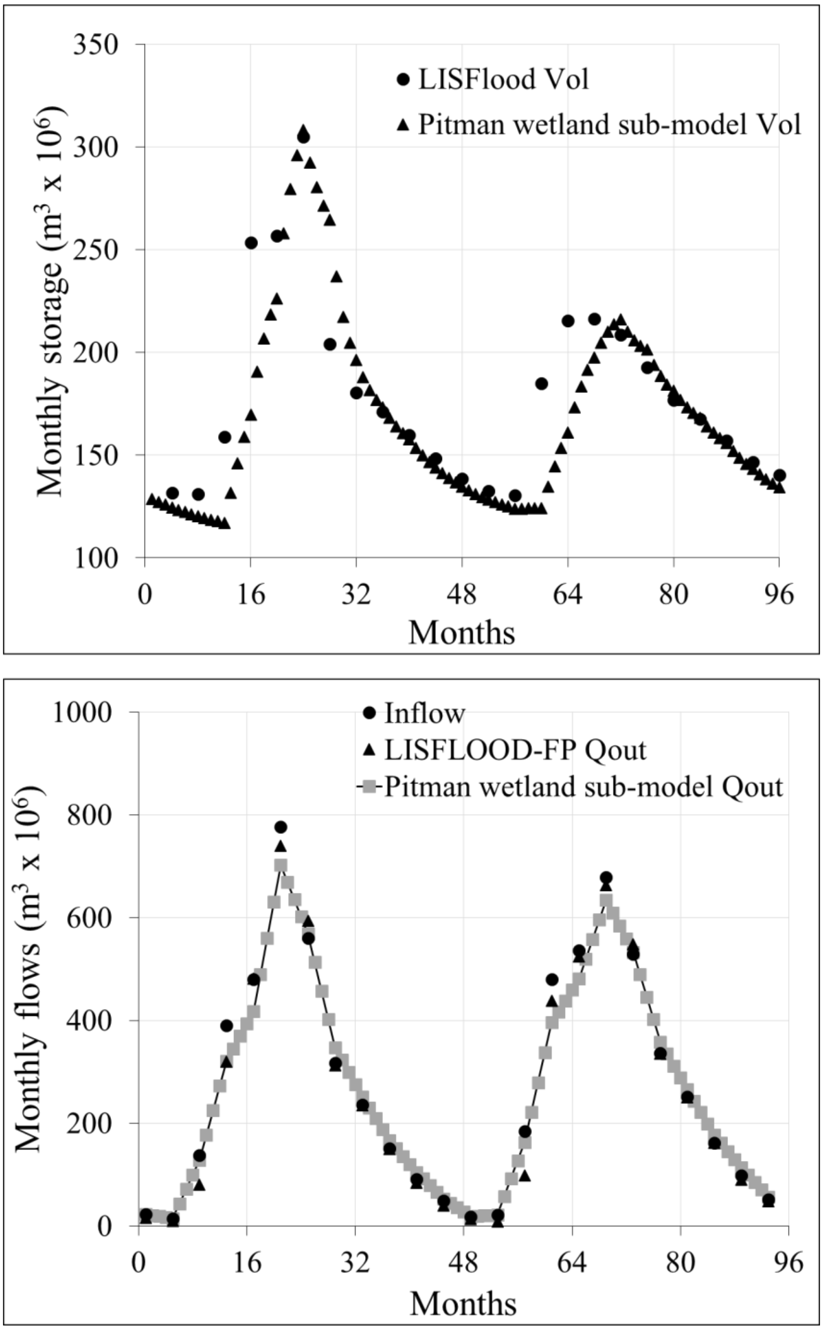

Figure 5.37: Comparison between the volume and flows simulated by the LISFLOOD-FP and Pitman wetland sub-model in the lower section (NF3) of the Luangwa floodplain for the period October 2005 to September 2007.

5.1.8 Re-run the Pitman model for the entire basin with the wetland sub-model included

The LISFLOOD-FP related estimated parameters for the Pitman wetland sub-model (Table 5.10) together with the final parameters (Table 5.5) used in the initial setup of the structured uncertainty version were used to re-set this version of the model. The aim was to see if there is a difference in parameter values estimated before and after inclusion of the wetland sub-model. The final parameter values established for the single run version after inclusion of wetland parameters in the model setup are presented in Table 5.11. The inclusion of the wetland parameters in the model setup gave somewhat improved simulation results, especially on the high and moderate flows (Table 5.12 and Figure 5.39). Most of the peak values which were over-simulated are reduced but generally the difference between the simulated results with and without wetland parameters is very small (Figure 5.38 and 5.39). The final results suggested that the influence of the Luangwa floodplain on the downstream flow regime of the Luangwa River is very small at the monthly time scale.

Table 5.11: Final parameter values established after inclusion of wetland sub-model in the model setup.

Parameter	Group1	Group2	Group3
RDF	0.8	0.8	0.8
PI1	1.5	1.5	1.5
PI2	4	4	4
AFOR	0	0	0
FF	0	0	0
PEVAP	varies with sub-basins		
ZMIN	50	58	66
ZAVE	0.5*(ZMIN+ZMAX)		
ZMAX	712	825	841
ST	539	643	768
SL	0	0	0
POW	2.8	3.0	3.0
FT	12.4	11	7
GW	9.5	8.7	4.6
R	0.5	0.5	0.4
TL	0.25	0.25	0.25
CL	0	0	0
GPOW	3.1	3.5	3.5
DDENS	0.4	0.4	0.4
T	15	15	15
S	0.001	0.001	0.001
GW slope	0.01	0.01	0.01
RWL	25	25	25
RSF	0.4	0.4	1

Table 5.12: Summarised model performance measures for sub-basin node N21

Statistical function	Before wetland sub-model	After wetland sub-model
CE(CE(ln)	0.58(0.62)	0.65(0.62)
Pbias (Pbias(ln))	12.72(0.34)	-5.57(-3.18)

Note: Values in the brackets are for transformed values

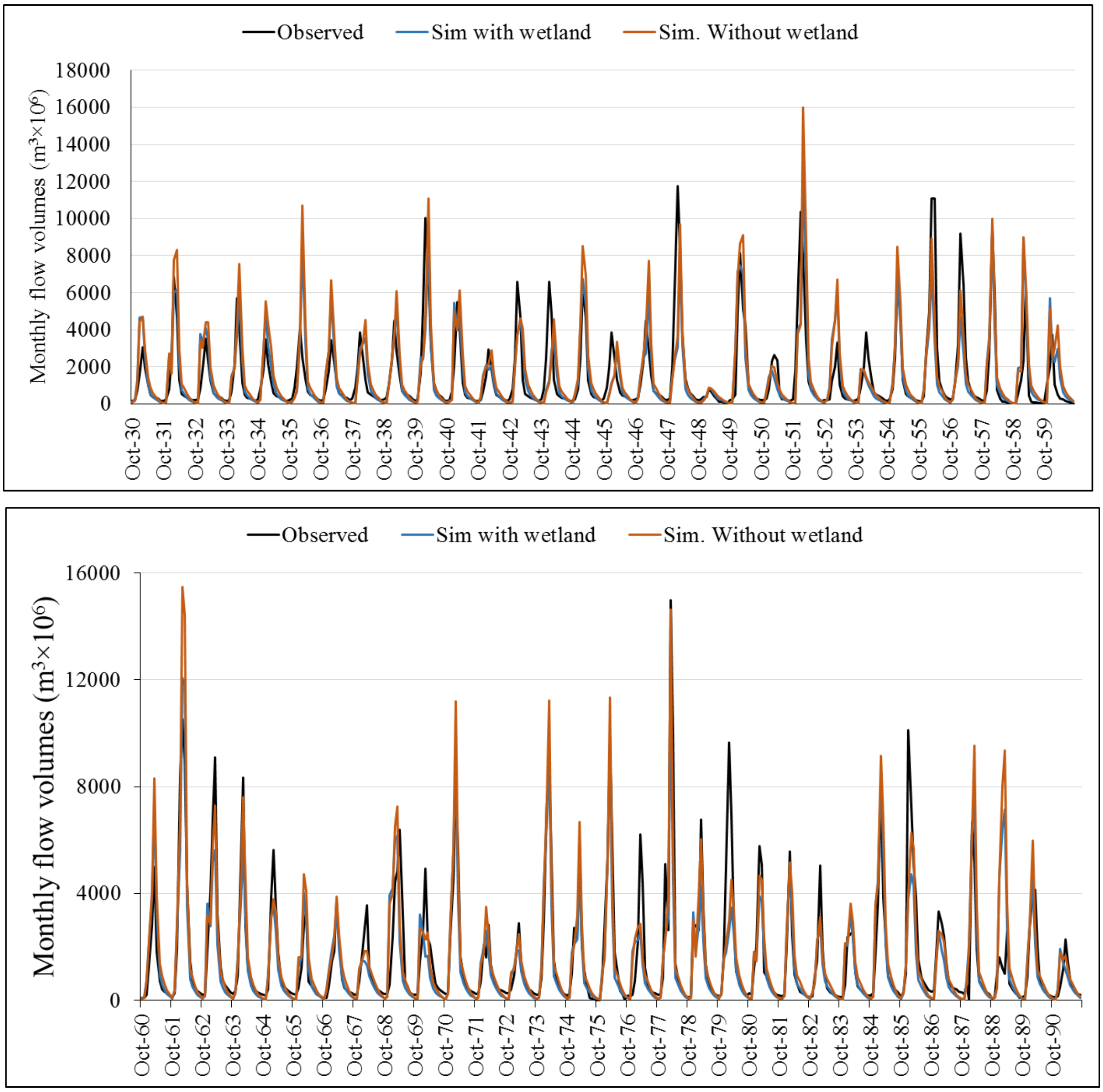

Figure 5.38: Observed and simulated flows (before and after wetland parameters) for sub-basin node N21 in the Luangwa River basin.

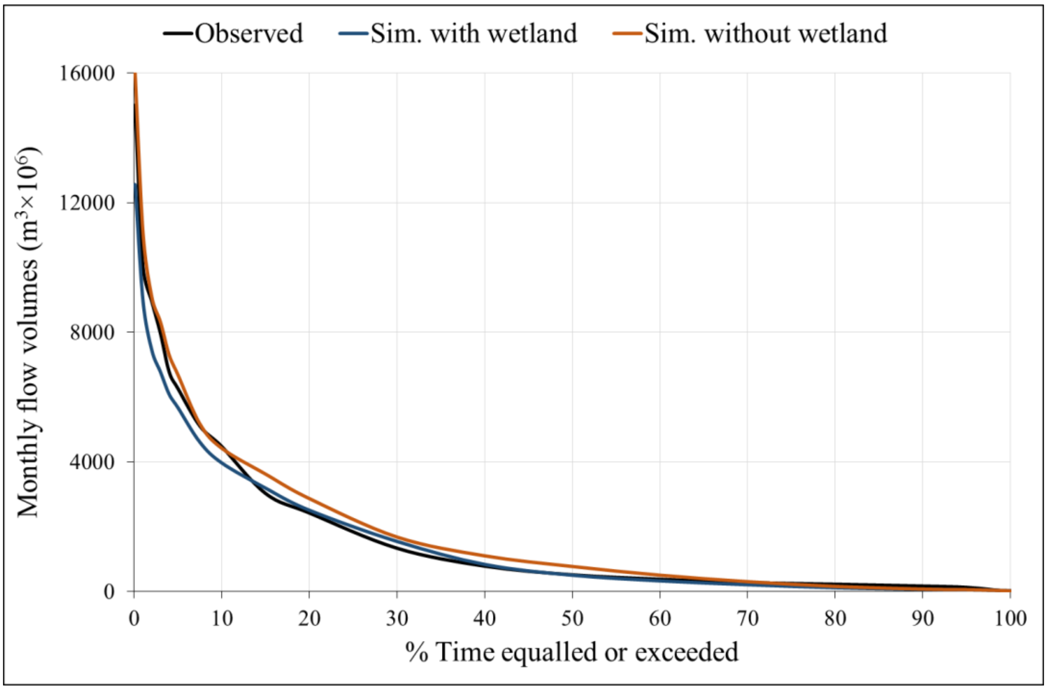

Figure 5.39 Observed and simulated FDCs (before and after wetland sub-model) for sub-basin node N21 in the Luangwa River basin.

5.2 The Upper Zambezi River basin

5.2.1 Sub-basin delineated

Nine sub-basins were delineated in the Upper Zambezi River basin (Figure 5.40). However, to include the effects of one tributary inflow in the setup of the LISFLOOD-FP model which was part of sub-basin B8, a nodal point was created (BP8) as indicated in Figure 5.40. Subsequently, to create consistency in setting up of the GW Pitman model, sub-basin nodes were created at the downstream end of the remaining sub-basins (Figure 5.40). The Barotse floodplain system is therefore found in the BP9 sub-basin node. The gauging stations used in the model setup are found in the three sub-basin nodes (BP7, BP9 and BP10) as shown in Figure 5.40.

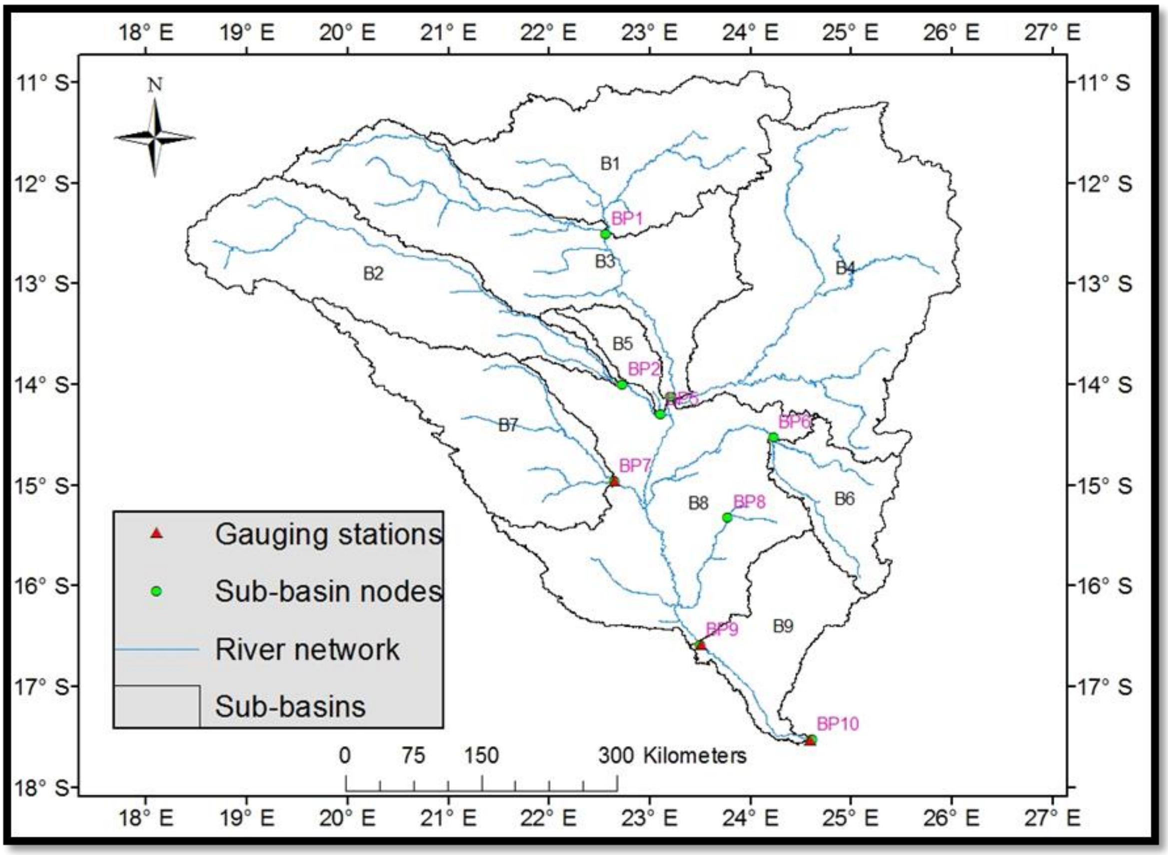

Figure 5.40: Sub-basins and sub-basin nodes in the Upper Zambezi River basin.

5.2.2 Sub-basin groups formed

The characteristics for each sub-basin node are presented in Table 5.13 and were used in the grouping process using the same approach as in the Luangwa River basin. Based on the PCA results (Table 5.14), the first two principal components explained a total of 79.3% of the variation between the sub-basin nodes. Figure 5.41 shows the physical variables (slope, elevation, TWI, and HI) and climatic variables (MAP and AI) that account for the first two principal components. Subsequently, these variables were primarily used in the classification of the sub-basin nodes, and four groups were formed (Table 5.15). The first group includes two sub-basin nodes (BP2 and BP4), whereas group two consists of BP7, BP1, and BP3. These first two groups have more or less similar characteristics, however, somewhat higher values of the slope are observed for sub-basin nodes in group one. Group three consists of sub-basin nodes BP6, BP8, and BP10, whereas the last group contains two sub-basin nodes (BP5 and BP9) characterised by very low slope values.

Table 5.13: Characteristics and indices for each sub-basin node that were entered in the PCA

Sub-basin node	Slope	Elev(mean)	Elev. Min	Elev. Max	TWI[4]	MAP	PET	AI[5]	HI[6]
BP1	1.9	1153.6	1055.0	1638.0	10.2	1228.5	1524.1	0.8	0.2
BP2	3.4	1284.8	1047.0	1674.0	9.7	1071.0	1466.1	0.7	0.4
BP3	1.9	1165.1	1025.0	1621.0	10.3	1085.2	1523.4	0.7	0.2
BP4	2.6	1236.8	1025.0	1564.0	9.8	1182.6	1472.5	0.8	0.4
BP5	0.7	1065.4	1029.0	1098.0	11.0	992.2	1531.0	0.6	0.5
BP6	1.5	1170.7	1066.0	1241.0	10.3	843.1	1539.2	0.5	0.6
BP7	2.1	1145.4	1018.0	1496.0	10.8	908.8	1533.7	0.6	0.3
BP8	1.3	1114.6	1047.0	1163.0	10.5	873.1	1562.6	0.6	0.6
BP9	1.1	1059.6	988.0	1227.0	10.6	927.1	1577.8	0.6	0.3
P10	1.9	1077.6	930.0	1211.0	10.2	756.3	1593.8	0.5	0.5

[4] Topographical Wetness Index

[5] Aridity Index

[6] Hypsometric Integral

Table 5.14: Total variance explained for the 9 variables in the PCA

Component	Initial Eigenvalues		
	Total	% of Variance	Cumulative %
1	5.63	62.53	62.53
2	1.51	16.80	79.33
3	1.18	13.14	92.47
4	0.41	4.58	97.05
5	0.22	2.48	99.52
6	0.02	0.24	99.77
7	0.02	0.21	99.97
8	0.00	0.03	100.00
9	0.00	0.00	100.00

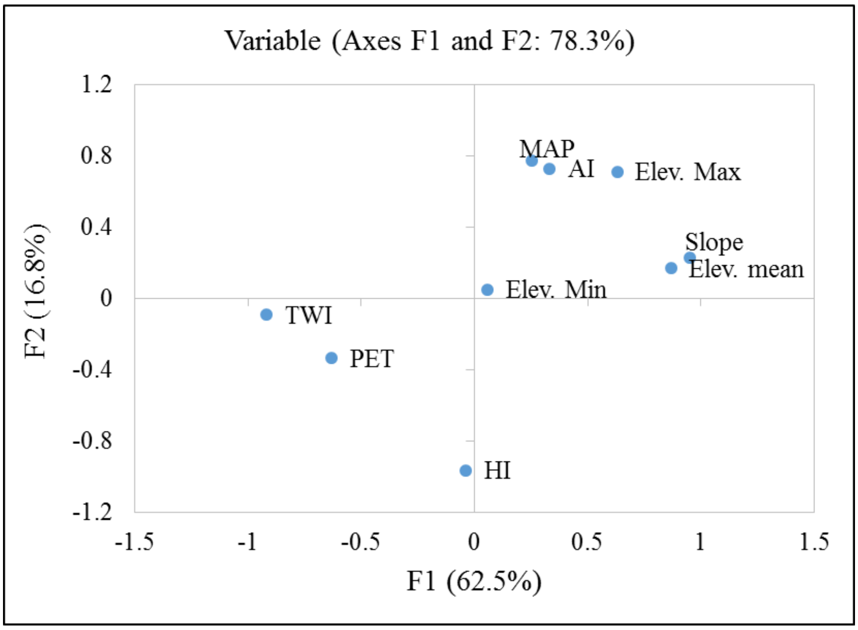

Figure 5.41: PCA biplot for the 9 variables of the Upper Zambezi River basin.

Table 5.15: Sub-basin groups generated by the PCA for the Upper Zambezi River basin

Group	Sub-basin nodes	Characteristics
1	BP2, BP4	High slope, high elevation and low TWI
2	BP1,BP3,BP7	Characteristics are somewhat similar to group 1
3	BP6, BP8, PB10	Characteristics somewhat similar to group 4
4	BP5, BP9	Gentle slope, low elevation and high TWI

5.2.3 Parameter sampling using structured uncertainty version of the GW Pitman model.

The same methods and criteria used to establish parameters in the Luangwa River basins were used in this basin (Table 5.16). Deep Kalahari sands that dominate the Barotse floodplain and surrounding areas (i.e. group 3 and 4 sub-basin nodes) suggested high values of the ST parameter. Additionally, very low slopes in group 3 and 4 suggested high values of the infiltration parameters (ZMIN and ZMAX) in these areas.

Table 5.16: Final parameter ranges used to set the uncertainty model

Parameter	Group 1		Group 2		Group 3		Group 4	
	min	max	min	max	min	max	Min	max
RDF	0.8		0.8		0.8		0.8	
PI1	1.5		1.5		1.5		1.5	
PI2	4		4		4		4	
AFOR	0		0		0		0	
FF	0		0		0		0	
PEVAP	varies with sub-basins							
ZMIN	100	300	100	300	200	300	200	300
ZAVE	0.5*(ZMIN+ZMAX)							
ZMAX	500	1000	800	1200	1000	1300	1000	1600
ST	500	900	1000	1400	1000	1500	1000	1600
SL	0		0		0		0	
POW	3	5	3	4	3	5	3	5
FT	10	40	10	30	10	30	10	20
GW	5	20	5	20	5	15	5	10
R	0.3	0.5	0.3	0.5	0.3	0.5	0.3	0.6
TL	0.25		0.25		0.25		0.25	
CL	0		0		0		0	
GPOW	3	5	3	4	3	5	3	5
DDENS	0.4		0.4		0.4		0.4	
T	30		30		30		30	
S	0.001		0.001		0.001		0.001	
GW slope	0.01		0.01		0.01		0.01	
RWL	25		25		25		25	
RSF	0.4		0.4		0.4		0.4	

Two gauging stations located in BP7 and BP9 sub-basins were used to evaluate model simulations. It should be noted that, even though BP7 sub-basin node is among the upstream sub-basin nodes, its gauging station was not sufficient enough to calibrate the upstream sub-basin nodes. Moreover, the gauging station in the BP9 sub-basin node includes wetland effects. Thus, the calibration process was not an easy task. Figure 5.42 illustrates the simulated FDCs of the upper and lower uncertainty bounds as well as the observed flows for BP7 and BP9 sub-basin nodes. Simulated flows for BP7 are reasonably good (i.e. narrow bounds of uncertainty), whereas there is some under-estimation of low flows in BP9. Generally, most of the simulated ensembles in the two sub-basin nodes were acceptable and about 2 000 ensembles were considered behavioural (based on the objective function statistics) in each sub-basin node. Despite a large number of simulated ensembles being considered behavioural, most of the parameters were not individually identifiable due to equifinality problems (Figure 5.43). The scatter plot of CE and CE (ln) against parameter ST for BP7 sub-basin node indicates that the range of parameter ST has been reduced to some extent (1 200 – 1 400 mm month^{-1}) compared to parameter ZMAX which is still similar to the initial range used (see Figure 5.43 and Table 5.16; group 2). Figure 5.44, a scatter plot of CE and CE (ln) against an index that combines the effects of FT, POW, GW and GPOW (FT/POW + GW/GPOW), indicates that the combined low flow index is identifiable for BP7 and not in BP9. This is likely to be related to the effects of the Barotse floodplain system on low flows. The fact that the incremental flows of BP9 are less important than the combined upstream inflows, although all of the other upstream sub-basins are not gauged, the result at BP9 in Figure 5.42 (even though the wetland effects have not yet been included) suggests that the simulations are reasonably good for generating inflows to the wetland.

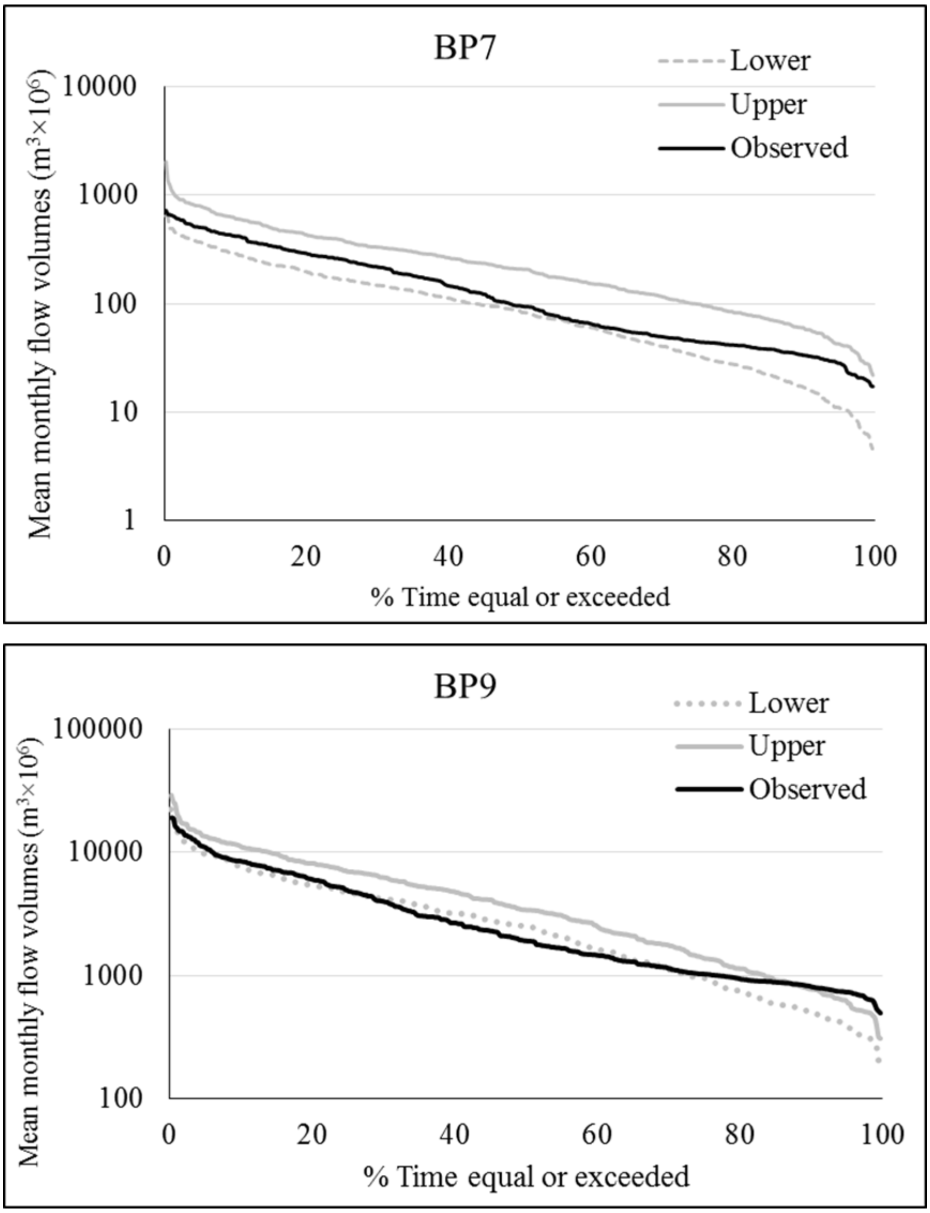

Figure 5.42: FDC of Observed and Simulated bounds for BP7 and BP9 sub-basin nodes.

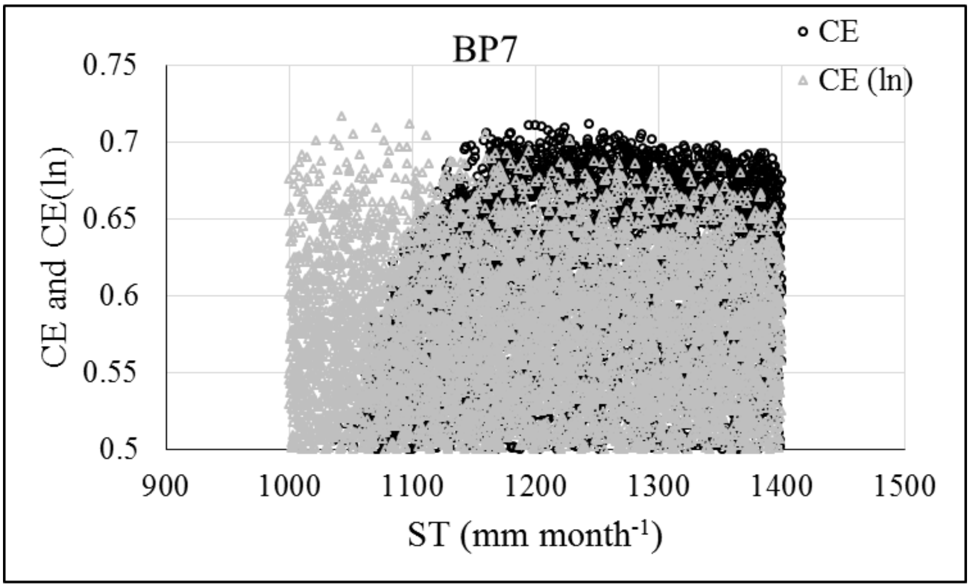

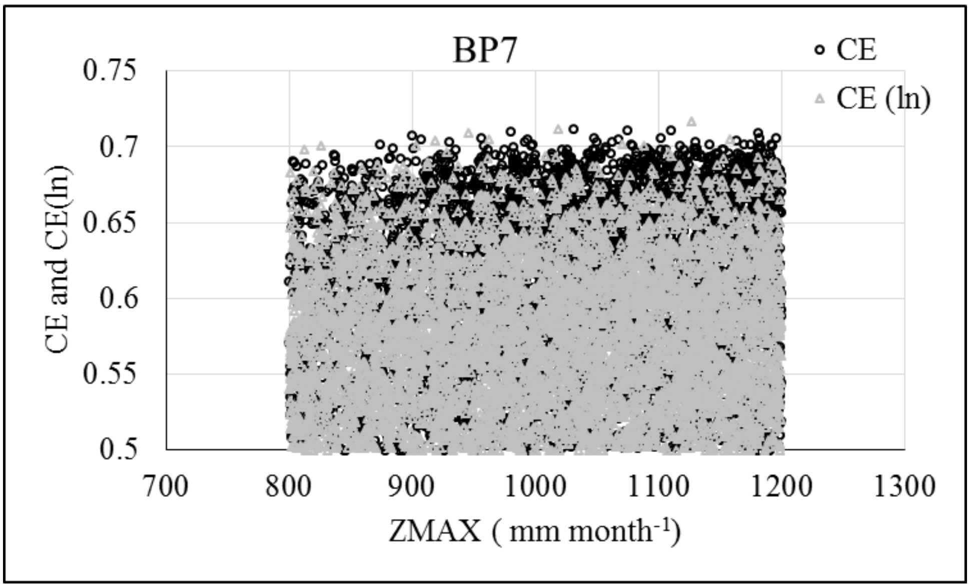

Figure 5.43: Scatterplots of the variation in CE and CE (ln) against ST and ZMAX parameter values for the BP7 sub-basin node of the Upper Zambezi River basin.

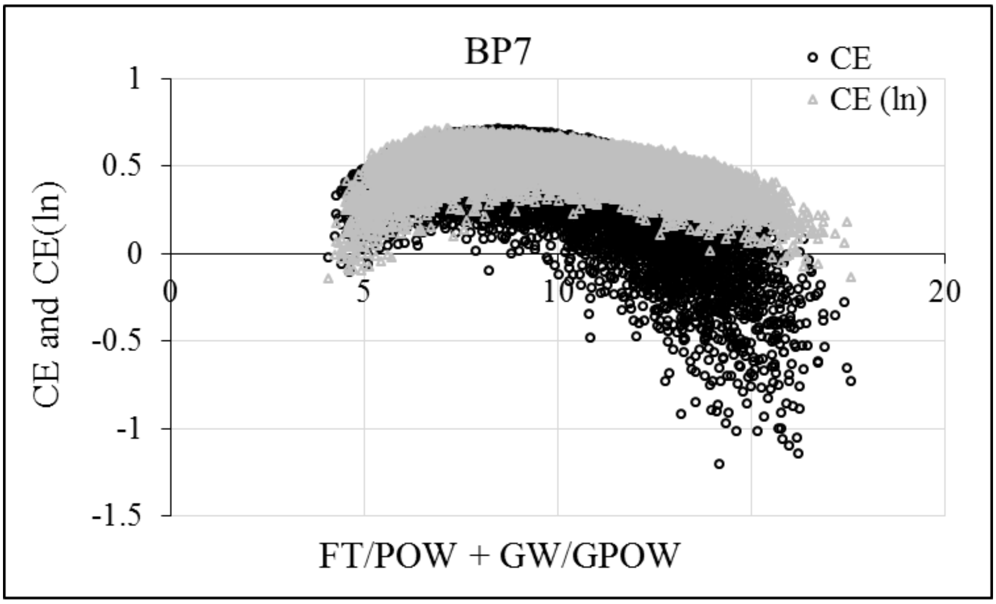

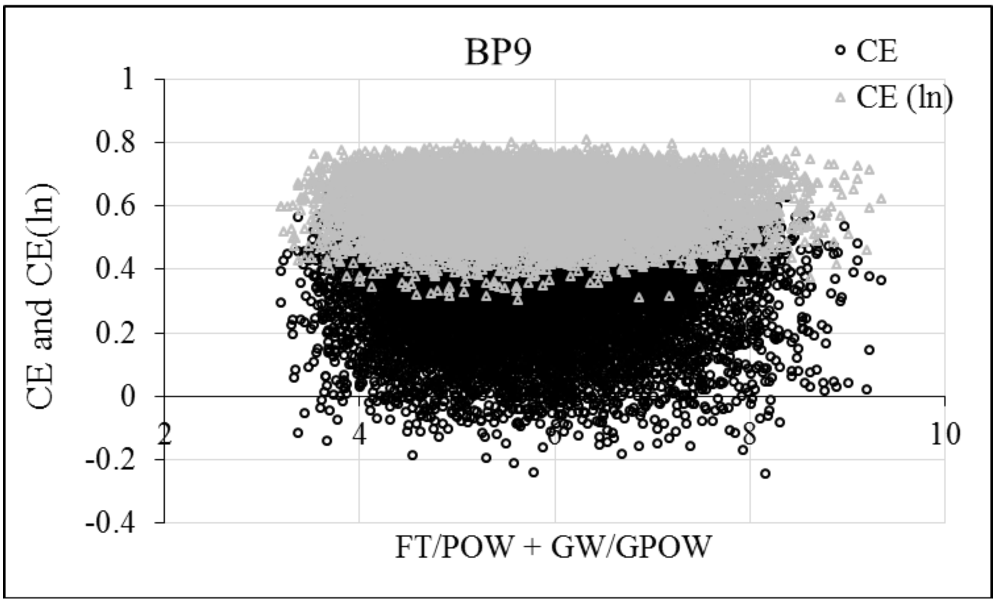

Figure 5.44: Scatterplots of the variation in CE and CE (ln) against FT/POW + GW/GPOW index for the BP7 sub-basin node of the Upper Zambezi River basin.

5.2.4 Simulation of wetland inflows using GW Pitman monthly model

The initial parameter set used to set a single run version was established from the identified optimal ensemble, and manually calibrated using the gauging stations located in BP7, and BP9 sub-basin nodes up until the final established parameter values in Table 5.17 were obtained.

Table 5.17: Final set of calibration parameters for the GW Pitman model

Parameter	group1	group2	group3	group4
RDF	0.8	0.8	0.8	0.8
PI1	1.5	1.5	1.5	1.5
PI2	4	4	4	4
AFOR	0	0	0	0
FF	0	0	0	0
PEVAP	varies with sub-basins			
ZMIN	100	270	300	300
ZAVE	0.5*(ZMIN+ZMAX)			
ZMAX	700	950	1000	1100
ST	800	1260	1300	1350
SL	0	0	0	0
POW	3.3	3.9	3.9	3.9
FT	40	28	25	18
GW	22	10	8	5 8
R	0.4	0.4	0.4	0.4
TL	0.25	0.25	0.25	0.25
CL	0	0	0	0
GPOW	3.3	3.6	3.8	3.9
DDENS	0.4	0.4	0.4	0.4
T	30	30	30	30
S	0.001	0.001	0.001	0.001
GW slope	0.01	0.01	0.01	0.01
RWL	25	25	25	25
RSF	0.4	0.4	0.4	0.8

For BP7 sub-basin node, the final simulations of moderate to high flows were achieved with CE and PBIAS of 0.65 and 7.7%, respectively. The low flow simulations were achieved with CE and PBIAS of 0.64 and 1.4%, respectively. Figure 5.45 indicates that there is a better simulations results for the period before 1970, whereas poor simulations are observed from 1982 to 1992 (both low and high flows are under-estimated). Additionally, the model has captured some extreme historical events such as those occurred in year 1977/1978. In general, high flows which occur less than 10% of the time are somewhat over-simulated and low flows are under-estimated (Figure 5.46).

For BP9 sub-basin node, the final simulation of high flows was achieved with CE and %PBIAS of 0.55 and 24.66%, respectively. Furthermore, low flow simulation was achieved with CE and %PBIAS of 0.58 and 3.60%, respectively. Simulated flows during the rising limb are over-estimated compared to the recessions (Figure 5.47). Over-simulated moderate flows (Figure 5.48) could be explained by uncertainties in the model setup for the upper sub-basin nodes as well as the floodplain attenuation effects which were not fully considered in the model setup. Additionally, the quality of data (i.e. rainfall and observed flow) could also contribute to the uncertainties in the simulated results.

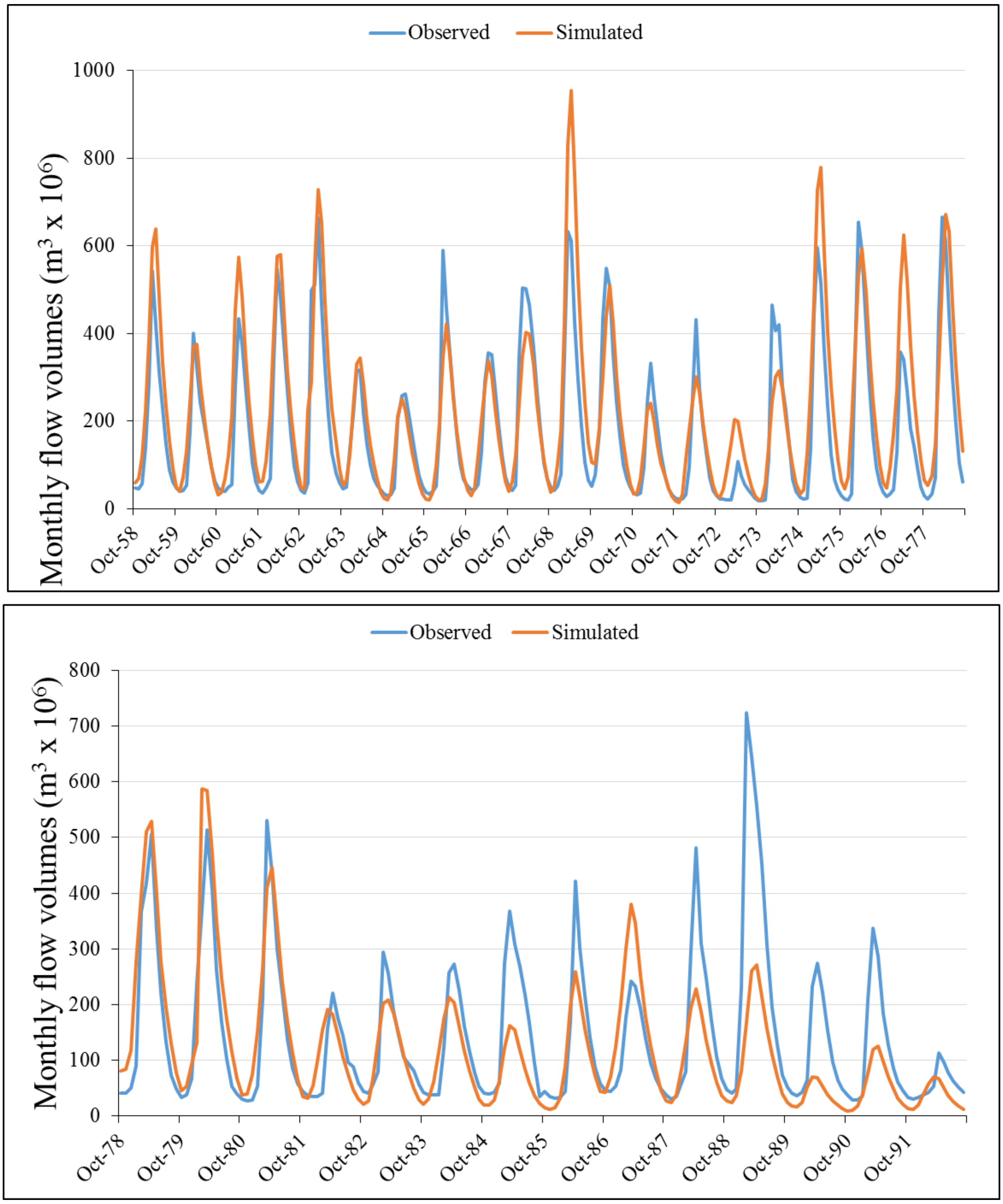

Figure 5.45: Observed and simulated monthly flows volumes for the period October 1958 – September 1978 (Top) and October 1978 – September 1992 for BP7sub-basin node.

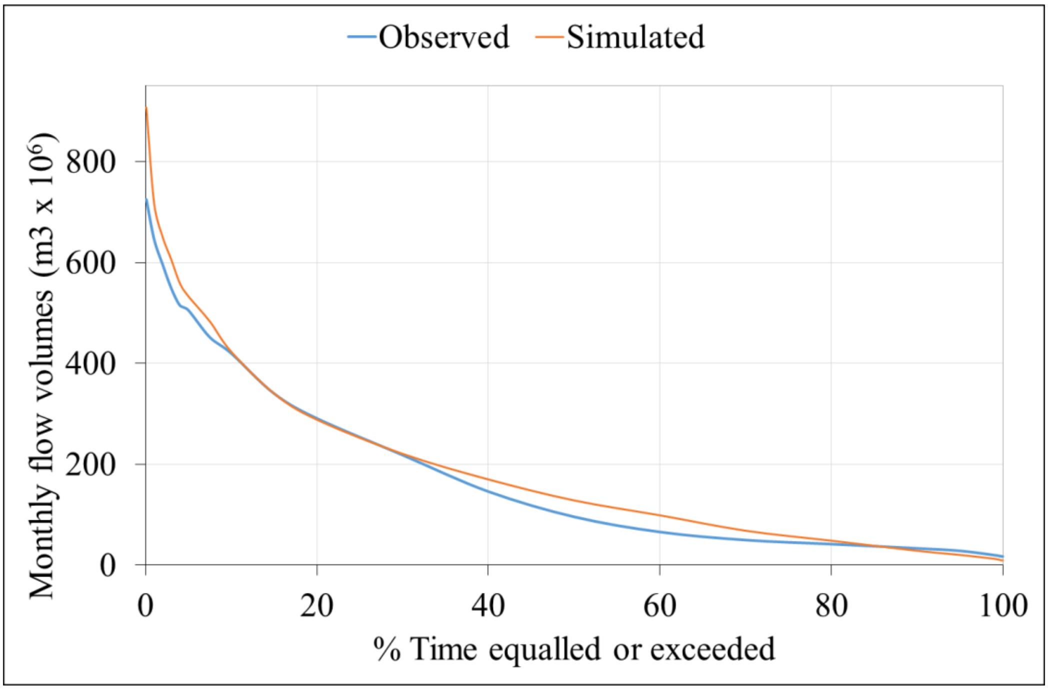

Figure 5.46: The FDCs of the observed and simulated monthly flows volumes for BP7sub-basin node for the period October 1958 – September 1992.

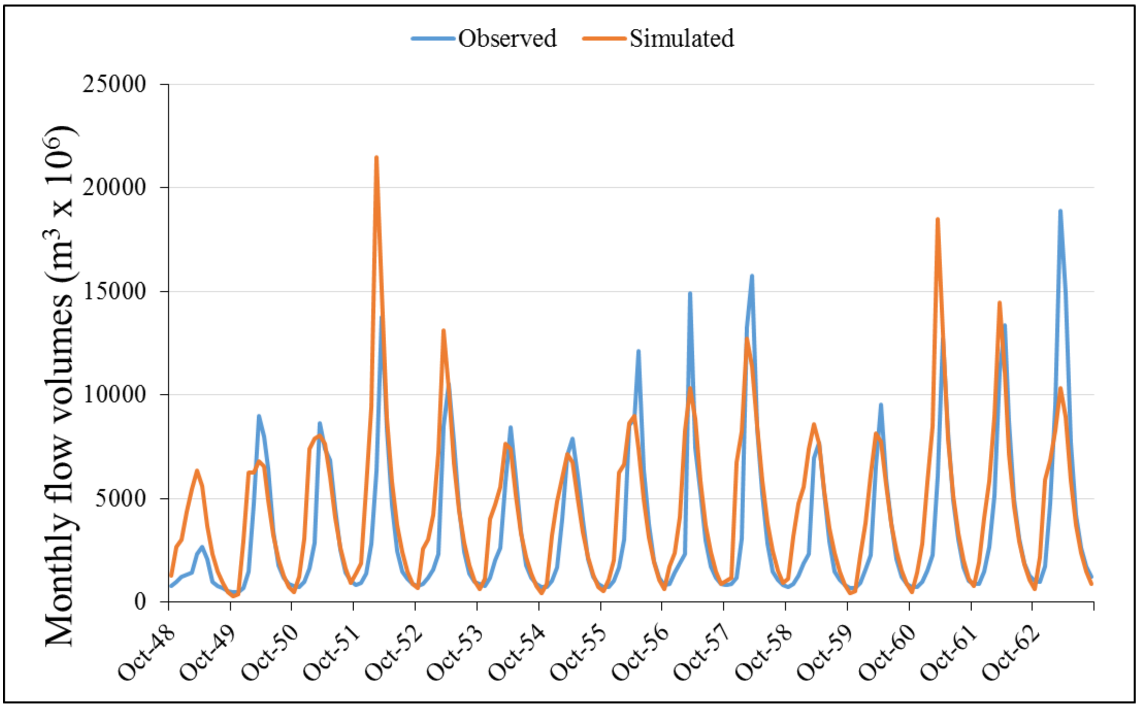

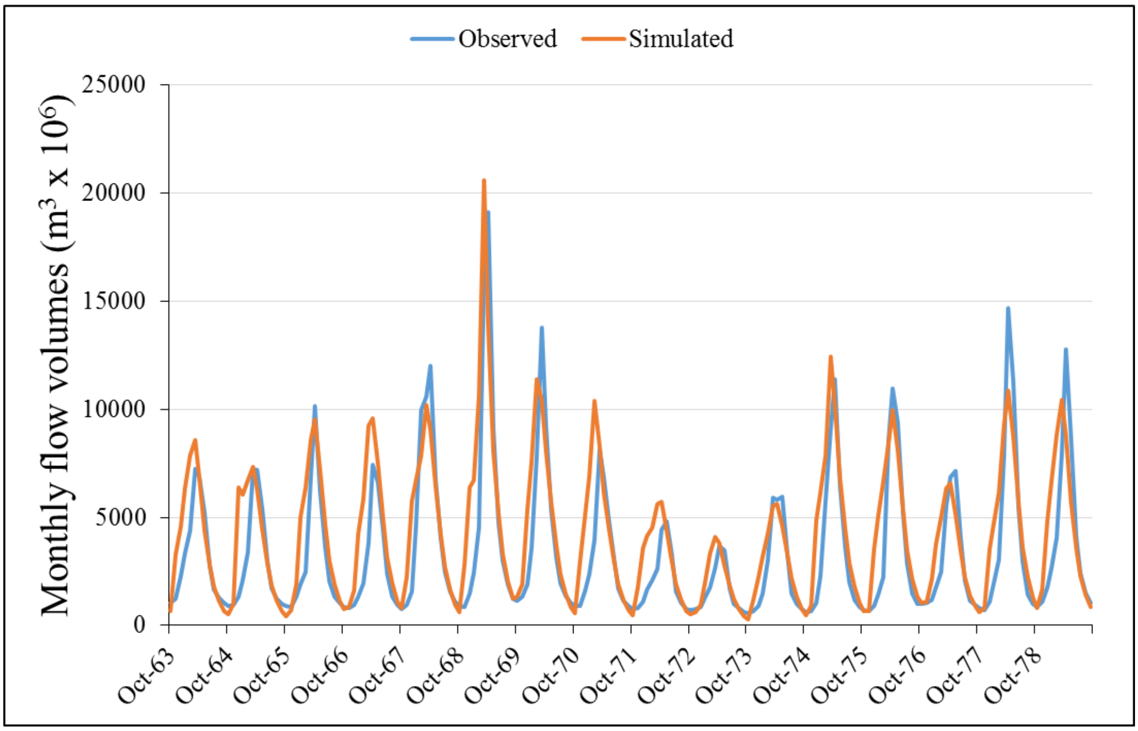

Figure 5.47 Observed and simulated monthly flows volumes for the period October 1948 – September 1963 (Top) and October 1963 – September 1979 for BP9 sub-basin node.

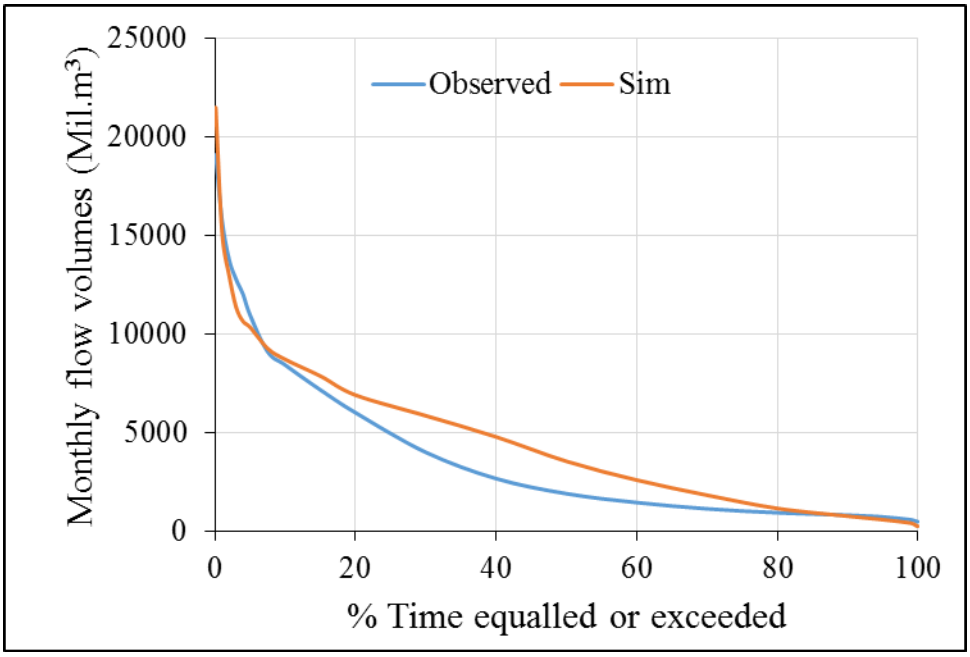

Figure 5.48: The FDCs of the observed and simulated monthly flows volumes for BP9sub-basin node for the period October 1948 – September 1979.

5.2.5 Disaggregation of simulated monthly flows into daily flows using the Pitman disaggregation sub-model

Disaggregation of monthly to daily flows from October 2000 to September 2013 was done for each sub-basin node contributing to the total floodplain inflows. The initial parameter values were established from past experience (studies that have applied the model) together with an understanding of the existing relationship between monthly and daily flows (e.g. higher peaks in daily flows than in monthly flows). The final possible parameter set used in the disaggregation processes includes: A = 0.4, B = -0.3, C = 0.9, K = 0.96 and R_{thresh} = 4 and these parameter values were used in all sub-basin nodes. In the absence of observed daily flows, the simulated daily flow magnitudes were not validated, and introduces uncertainties in the disaggregated daily flows. The published information on onset and duration of floods helped to somehow assess the disaggregated results. For instance, high peak flows indicated in Figure 5.49 can be related to historical high events in 2004, 2007, 2009 and 2010 as reported by Dartmouth Flood Observatory (2007) and Long *et al*., (2014). Since the key issue was to obtain reasonable representative hydrographs that can be used in the LISFLOOD-FP model, the simulated daily flows are considered adequate to be used as upstream boundary conditions in the LISFLOOD-FP model.

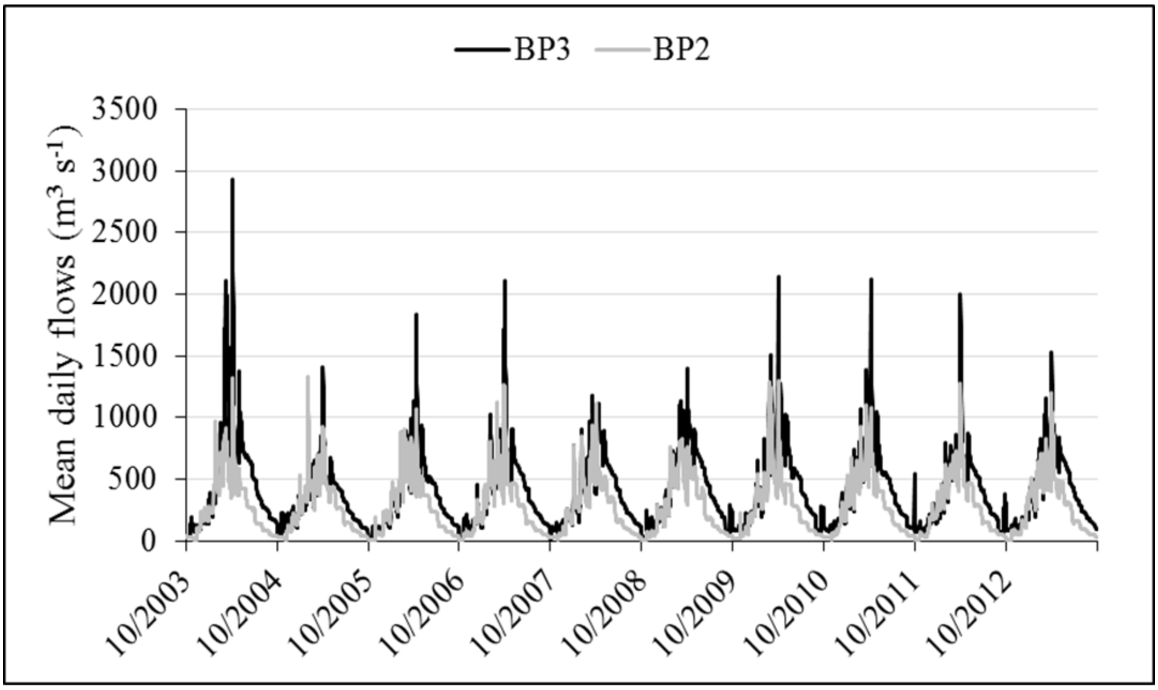

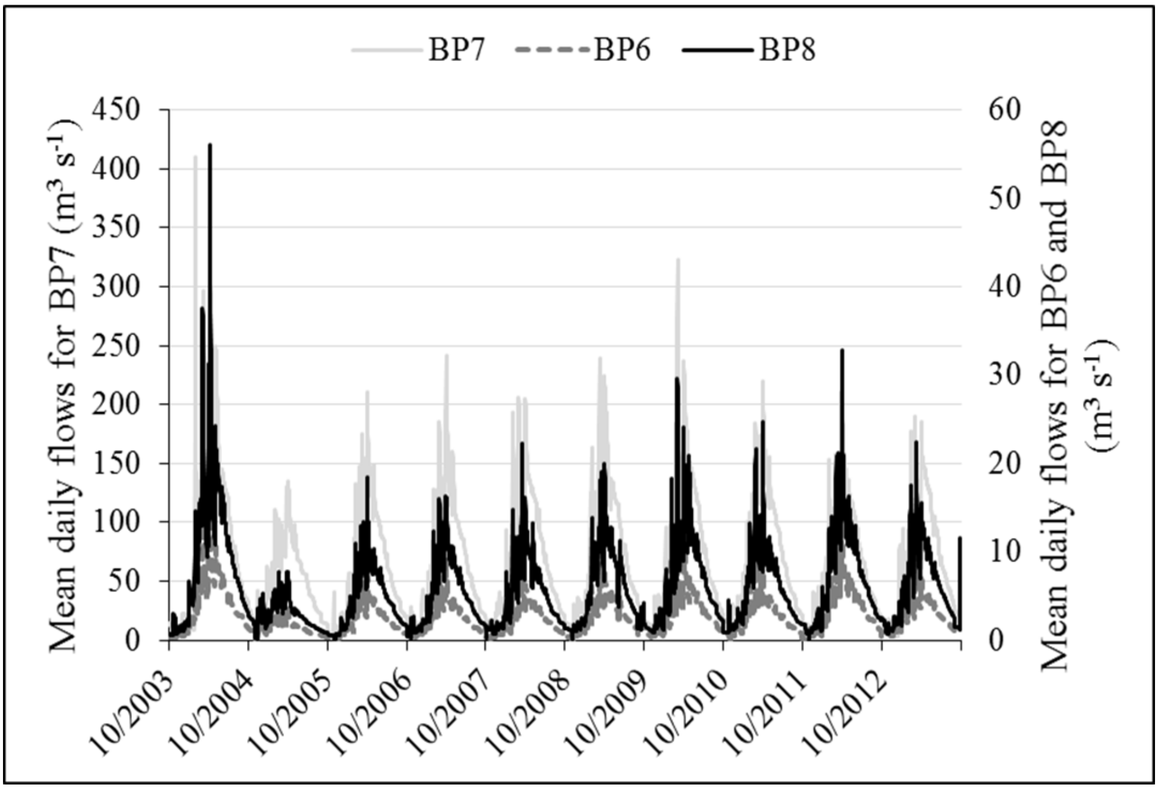

Figure 5.49: Mean daily flows for two sub-basins in Upper Zambezi River basin (Oct 2003 to Sept 2013).

5.2.6 Simulation of wetland inundation characteristics using LISFLOOD-FP model

Figure 5.50 illustrates the location of the Barotse floodplain system in the Upper Zambezi River basin. The floodplain is covered in a single sub-basin node (BP9) and receives inflows mainly from six upstream boundary conditions (Figure 5.50). The total length of the meandering river (the Zambezi) in the floodplain was estimated to be 394 km. Channel widths were estimated from Google Earth images (Figure 5.51), whereas channel depths (shown in Figure 5.52) were computed by the model at the beginning of simulation using the width–depth relationship (see Equation 4.15). The model setup was done for a representative hydrological period with a consideration of both wet and normal years (October 2002 – September 2007). However, an addition of one year (October 2001 – September 2002) was used as a warm-up period to establish an initial condition in the model domain. Furthermore, the selected period was also motivated by the availability of observed daily flows downstream of the Barotse floodplain which were used to validate simulated outflows from the floodplain.

The parameter values used to setup the LISFLOOD-FP model in this floodplain are presented in Table 5.18 and were established to reflect the characteristics of the river channels as well as the vegetation distribution in the Barotse floodplain system. For instance, the middle and lower parts of the floodplain are covered by denser vegetation which suggested higher values of floodplain roughness (0.07 – 0.1). The Zambezi River and its tributaries in this basin have sandy beds with the banks covered by dense vegetation. Thus, the channel roughness parameter ranges from 0.045 to 0.06. The downstream boundary conditions were presented using the normal depth assumption (depth at which the water surface slope is assumed to be parallel/equal to the channel bed slope). This depth was calculated through the Manning's flow equation that defines the relationship between discharge and water surface. Since the water surface slope was unknown, the average channel slope (0.001) estimated from the Google Earth image was used in the computation of normal depth. The simulated outflow from the wetland was calibrated using the Ngonye Falls gauging station (BP9) which is located a few kilometres from the wetland outlet.

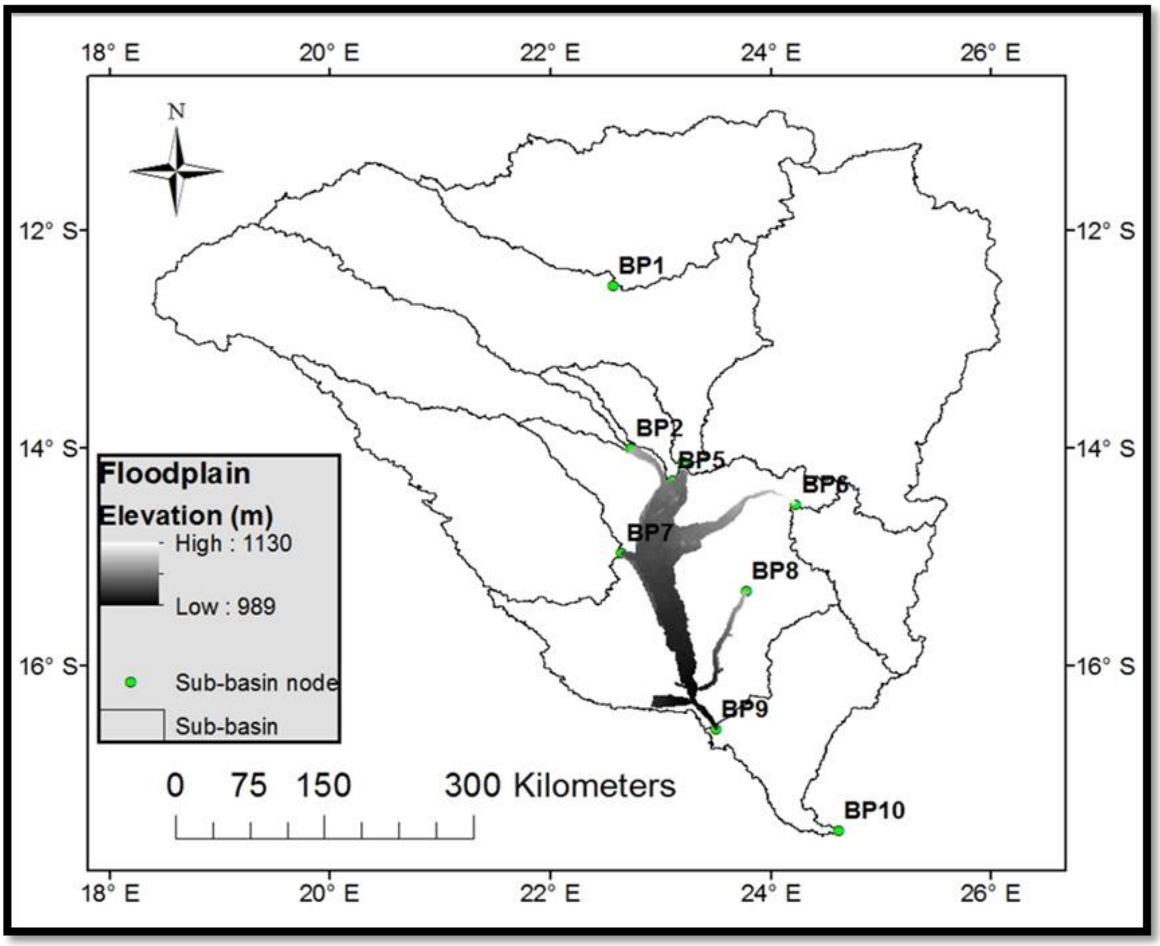

Figure 5.50: The location of the Barotse floodplain system in the Upper Zambezi River basin.

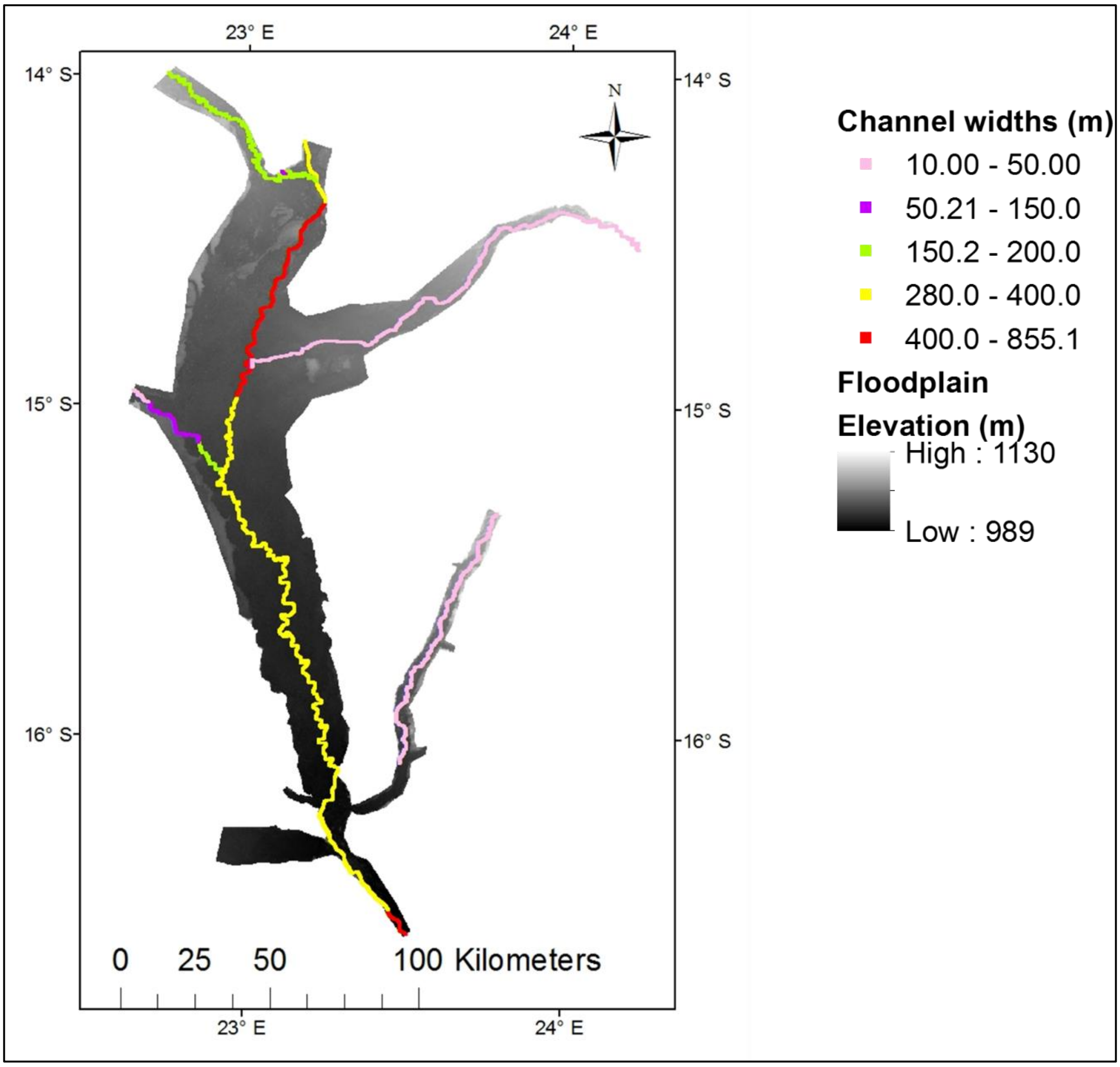

Figure 5.51: Elevation and channel width values in the Barotse floodplain system

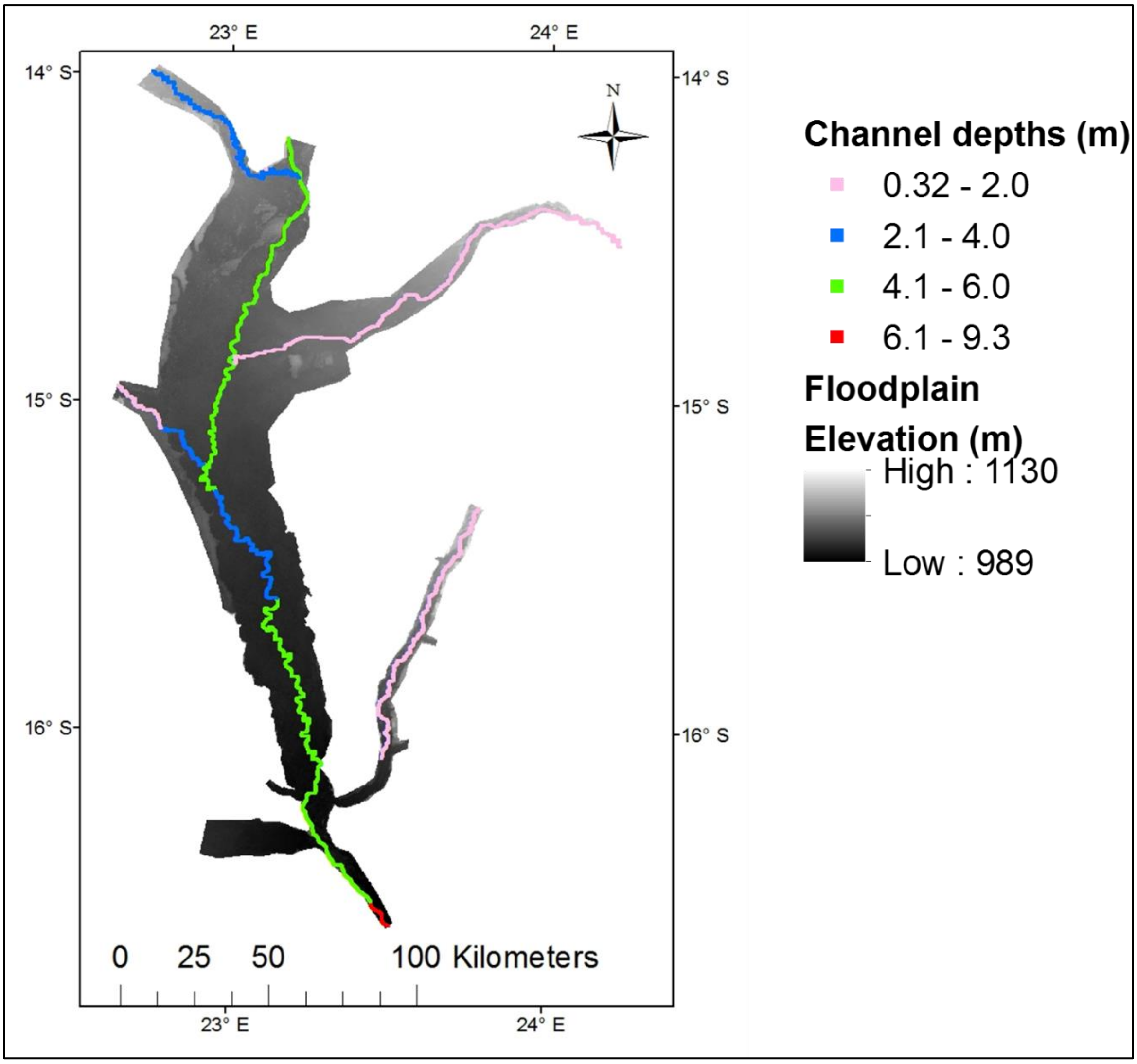

Figure 5.52: Elevation and channel depths in the Barotse floodplain system

Table 5.18: Parameter ranges used to set up the LISFLOOD-FP model

Parameter	Parameter range	Final established value
Channel roughness (C_n)	0.045 – 0.06	0.06
Floodplain roughness (C_f)	0.07 – 0.1	0.08
p (fractional exponent in the Width–depth relationship)	0.76	0.76
r(scale coefficient in the Width–depth relationship)	0.05 – 0.065	0.045
Average channel slope	0.001	0.001

Landsat images acquired on 12 March, 20 September 2004, 22 April 2007, were used to validate inundation extents through visual analysis. Figures 5.53 to 5.56 indicate different sections of the floodplain when the simulated inundation extents were overlaid on different LandsatLook images. Maximum inundation extents are observed between late February (upper section of the floodplain) and late April to early May (lower section). The simulated inundation extents were reasonably good especially for the middle and lower sections of the floodplain (most of the meander-cuts and isolated channels are filled with water as expected), whereas simulated inundated extents in the upper section of the floodplain were spatially inconsistent with observed inundation extents. Part of this could be related to the variation in topography in this section which might not be well represented in the DEM. Additionally, apart from the overflows from the Zambezi River, the right side of this section of the floodplain could be inundated from the tributary inflows. Under-simulation of the flooding extents in this area, therefore, could be linked to uncertainties in the simulated tributary inflows. Differences between simulated and observed flooding extents could also be related to the quality of the Landsat images used. Flood Area Index (FAI) values indicated that the model has captured some of the spatial variation of inundation extents during the wet season. FAI values close to 45% were observed in April 2007, whereas values less than 40% were observed during the dry season (September 2004). Despite the mismatches between the simulated and observed inundation extents, the results represent sensible simulations of the inundation extents in this floodplain. The average inundation depth was about 2 m. Inundation depth values less than 1 m were observed in the upper section of the floodplain, whereas high values (about 5 m) were observed in some depressions found in the middle and lower sections of the floodplain.

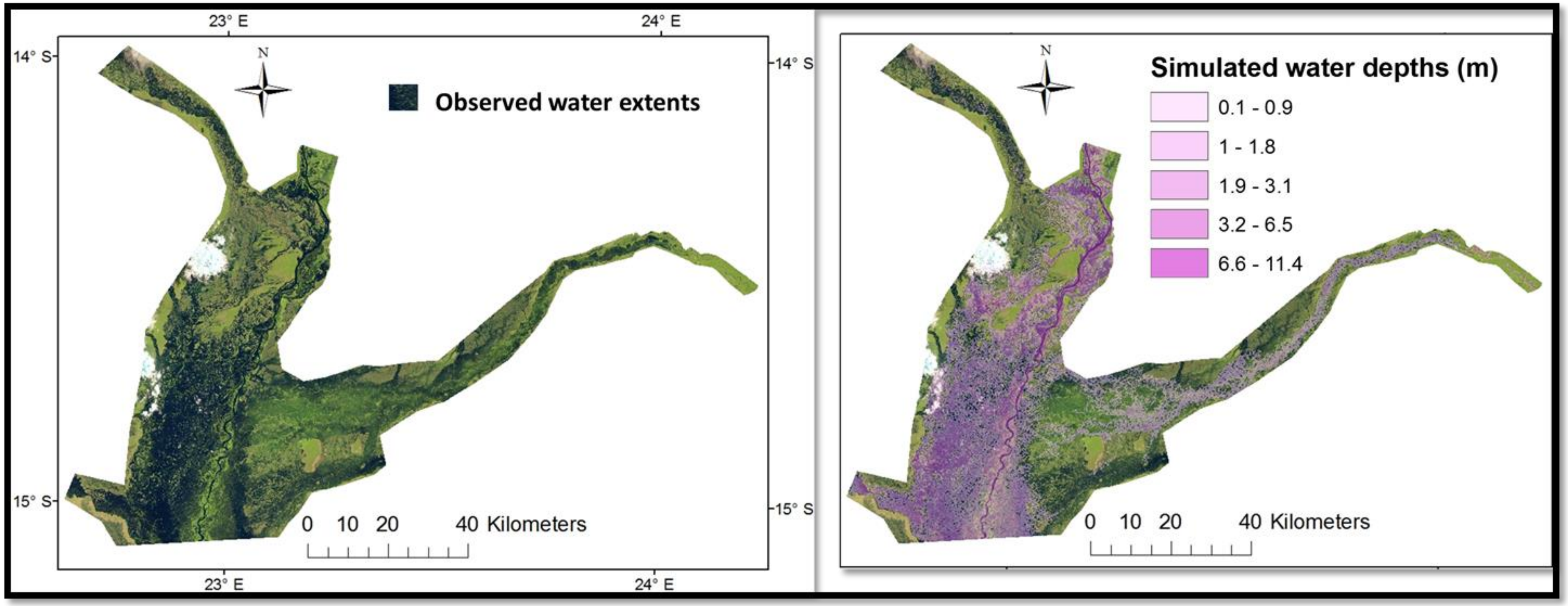

Figure 5.53: Comparison between observed and simulated flooding extents on 12 March 2004 in the upper section of the Barotse floodplain system.

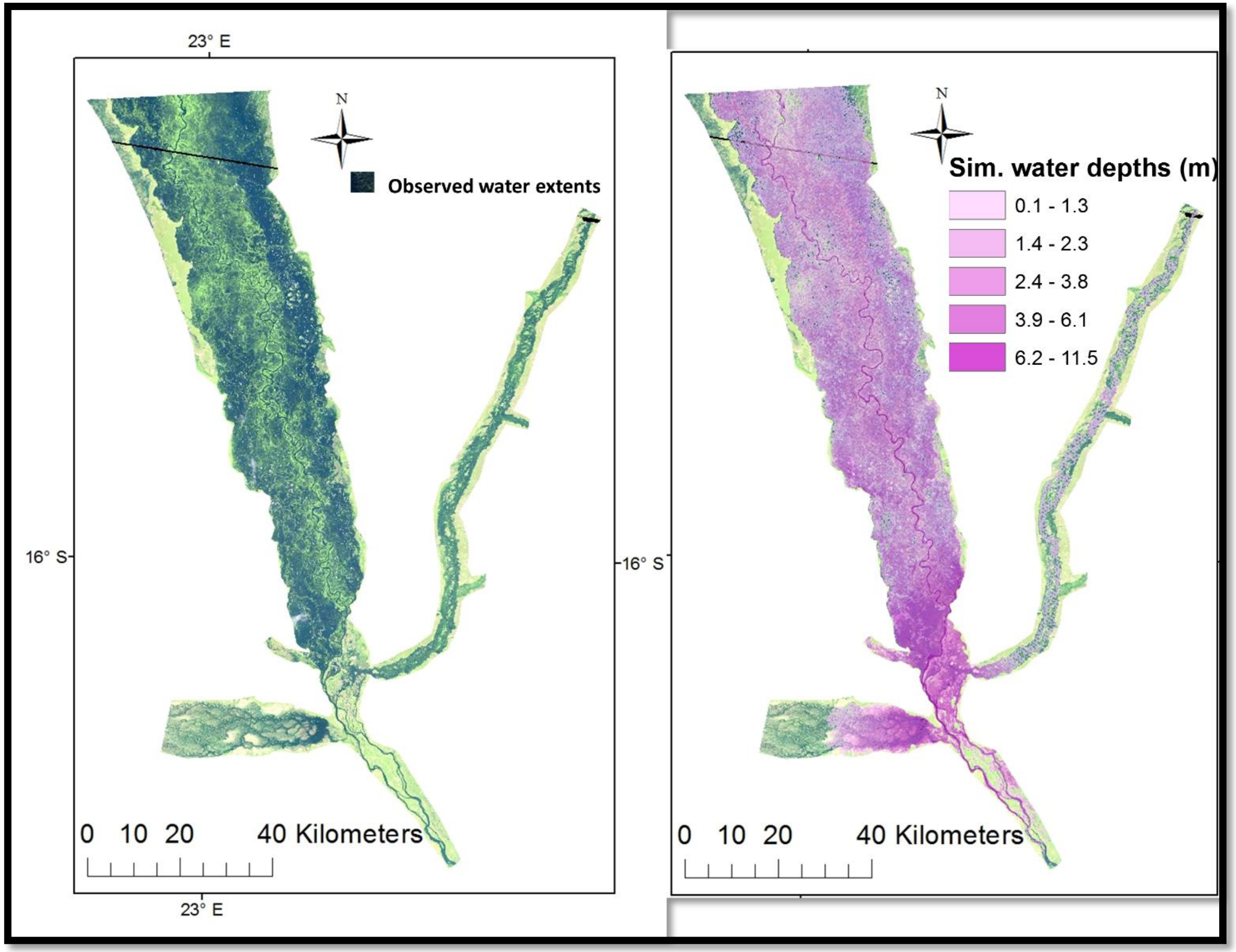

Figure 5.54: Comparison between observed and simulated flooding extents on 12 March 2004 in the middle and lower sections of the Barotse floodplain system.

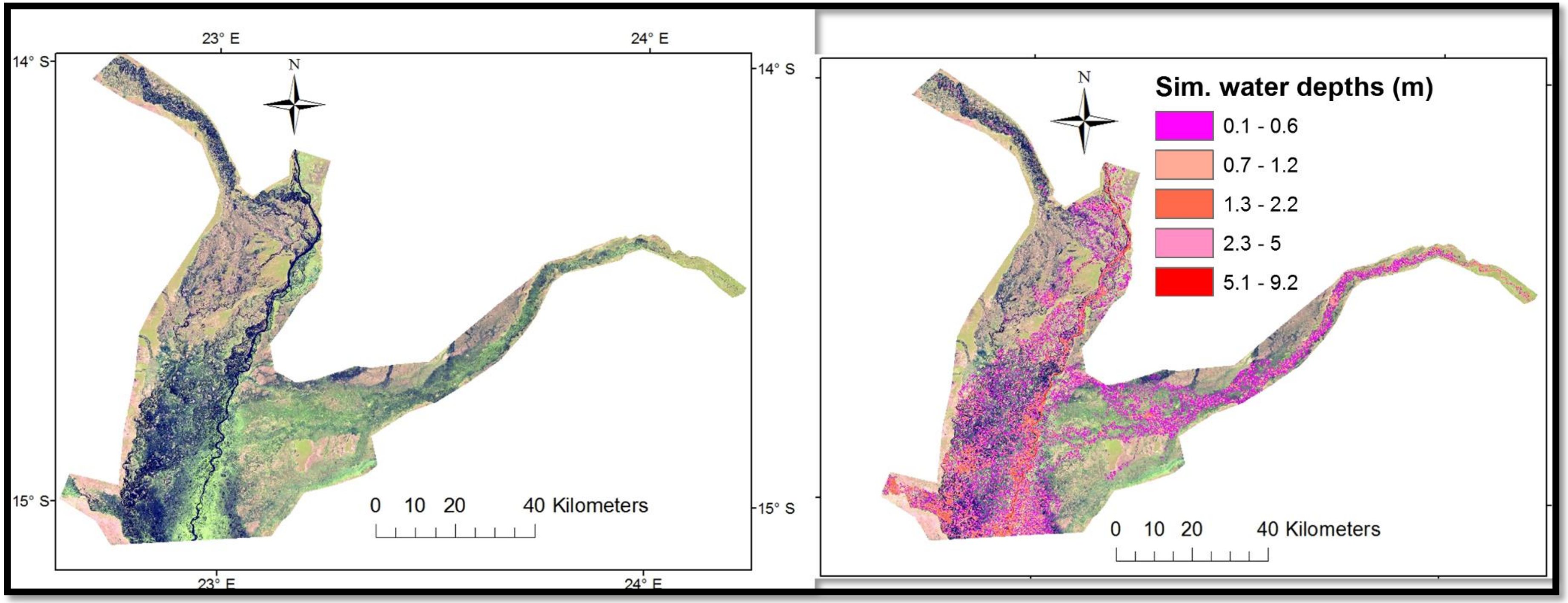

Figure 5.55: Comparison between observed and simulated flooding extents on 22 April 2007 in the upper section of the Barotse floodplain system.

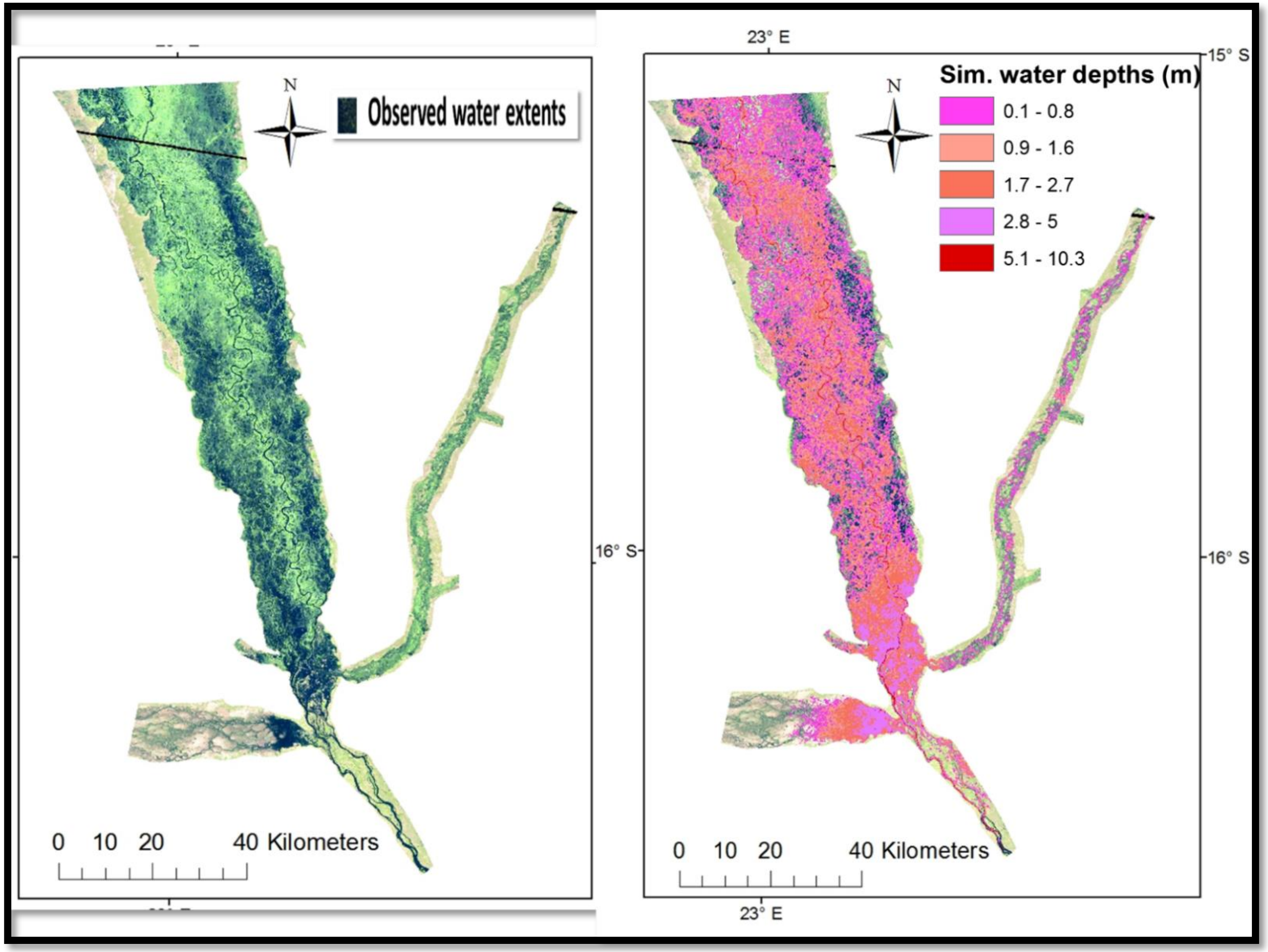

Figure 5.56: Comparison between observed and simulated flooding extents on 22 April 2007 in the middle and lower sections of the Barotse floodplain system.

The 7-day maximum inundation extents and volume were in the range of 5 000 – 6 000 km^2 and 6 000 – 12 000 $m^3 \times 10^6$, respectively (Figure 5.57). A counter-clockwise hysteresis loop was observed in both area–storage and storage–inflow relationships, and the earlier relationship suggests that there is substantial storage remaining on the floodplain at the end of the dry season. This could represent the storage in the isolated channels and backwater depressions found in the Barotse floodplain. It is clear that the storage–inflow relationship is complex due to multiple inflow peaks (Figure 5.57). As a result, the explanation of the interactions between the Barotse floodplain features and the channels become much complex. Standardised hysteresis curves for both relationships are presented in Figure 5.58 and the distance between the rising and falling curves indicated a high hysteresis effect when there is increased discharge during the wet year (Table 5.19). Daily inflow–outflow relationships showed that the Barotse floodplain system has a potential to attenuate flows, as the output hydrographs are smoothed and the high peaks are significantly reduced (Figure 5.59). Moreover, the floodplain delays time to peak to about 3 to 4 weeks and increases the low flows during the dry season. A comparison between the simulated outflows from the Barotse floodplain with the observed daily flows from a gauging station located a few kilometres downstream of the floodplain outlet (the Ngonye Fall gauging station or BP9) in Figure 5.60, indicates some agreement between the observed and simulated hydrographs (although it is a short record). Some of the high peaks and the flow patterns are well captured by the model. Over-estimated flows, especially in the rising and falling limbs, could be related to the uncertainties in the simulated wetland inflows used as upstream boundary conditions in the LISFLOOD-FP model. In general, the simulated inundation extents, storages and outflows were acceptable to be used to estimate the wetland sub-model parameters, as they largely reflect the characteristics of this floodplain.

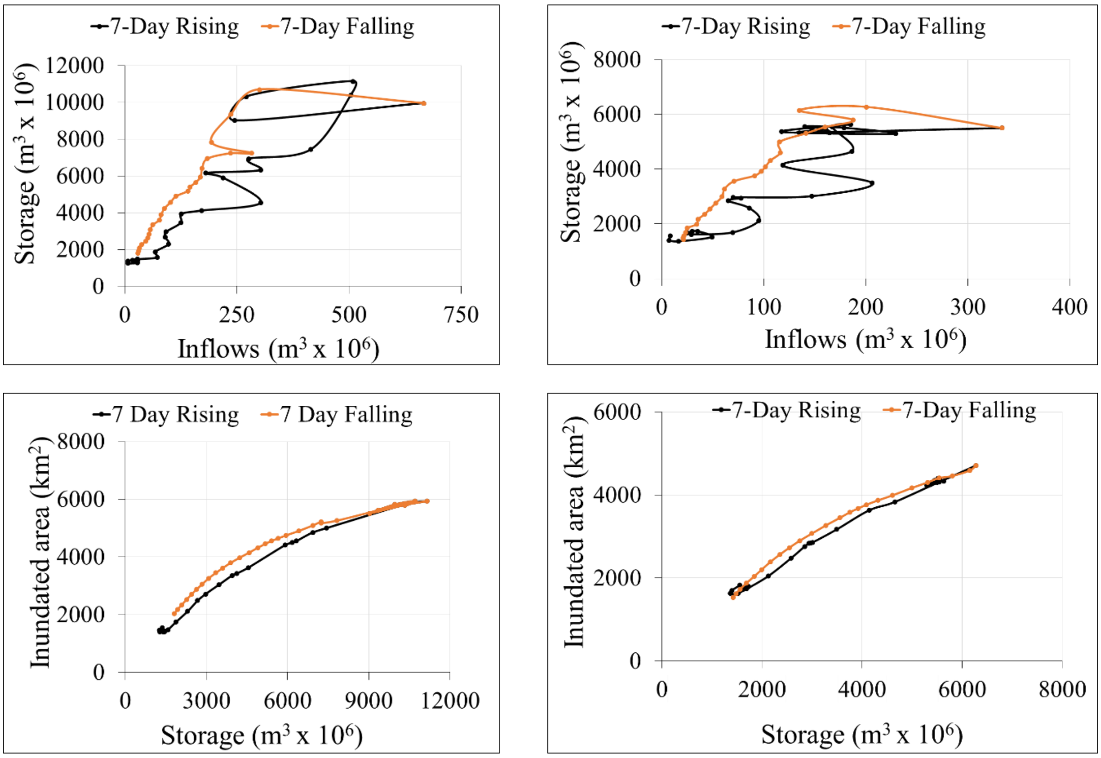

Figure 5.57: Storage–inflow and area–storage anti-clockwise hysteresis for the wet (left) and normal (right) years in the Barotse floodplain system.

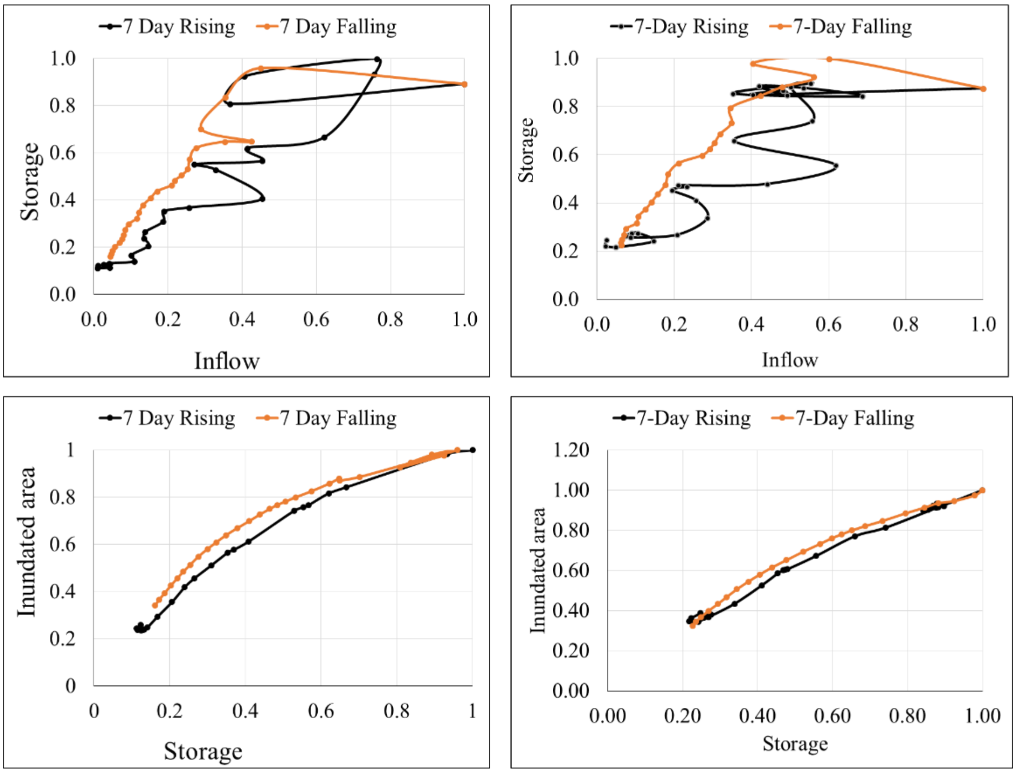

Figure 5.58: Standardised storage–inflow and area–storage anti-clockwise hysteresis for the wet (left) and normal (right) years in the Barotse floodplain system.

Table 5.19: Magnitude of the hysteresis curve in the Barotse floodplain

Relationship	Wet year	Normal year
Area–storage	0.070	0.040
Storage–inflow	0.380	0.200

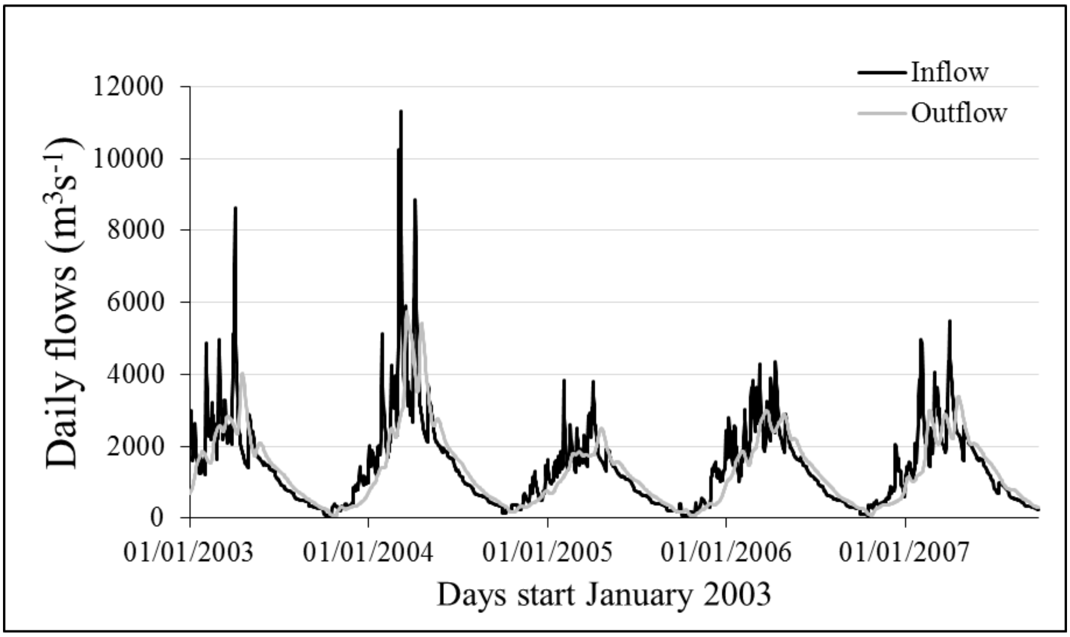

Figure 5.59: Daily inflows and outflows in the Barotse floodplain system for the period January 2003 to September 2007.

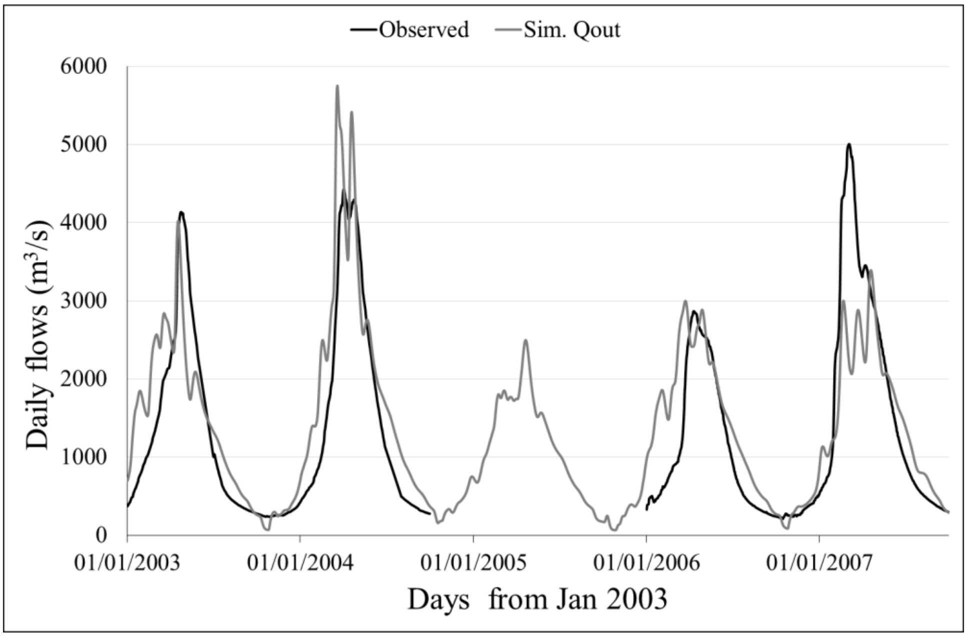

Figure 5.60: Comparison between observed and simulated daily flows (a gap on the observed flows indicates missing values) for the period January 2003 to September 2007.

5.2.7 Quantification of Pitman wetland parameters

The final estimated parameters for the Pitman wetland sub-model are given in Table 5.20. The scale and power parameters that define the relationship between the area and volume of inundation were directly estimated from the relationship between the simulated area and volume of inundation. The remaining parameters were established through manual calibration by implementing the Pitman wetland sub-model in the excel sheet containing the LISFLOOD-FP results. The large value of wetland residual volume (800 $m^3 \times 10^6$) reflects the volume of water remaining in the isolated channels and backwater depressions found in the middle and lower parts of the floodplain during the dry season. However, this is relatively small compared to the total amount of storage in the entire floodplain (1 100 $m^3 \times 10^6$). The return flows were not restricted by the volume of the channel inflows and thus, the value of the maximum return flow fraction was set to 10.95. Based on the comparison between simulated volume and outflows from the LISFLOOD-FP and Pitman wetland sub-model, it is clear that the simulated outflows and volumes from the two models are largely comparable (Figure 5.61). Thus, the estimated parameters can be used as wetland parameters in the new setup of the GW Pitman model.

Table 5.20: Estimated parameters for the Pitman wetland sub-model based on LISFLOOD-FP applications

Parameters and units	Estimated parameter value
Local catchment area (Km^2)	9500
Residual wetland volume (RWV) in $m^3 10^6$:	800
Initial wetland volume (WV) in $m^3 10^6$:	1600
A in $\mathrm{Area}(\mathrm{m}^2 10^6) = \mathrm{A}(\mathrm{WV}\ (m^3 10^6))^{\mathrm{B}}$	800
B in $\mathrm{Area}(\mathrm{m}^2 10^6) = \mathrm{A}(\mathrm{WV}\ (m^3 10^6))^{\mathrm{B}}$	0.69
Channel capacity for spillage (QCAP) $m^3 10^6$:	600
Channel spill factor	0.8
AA in $\mathrm{RFF} = \mathrm{AA}\left(\frac{\mathrm{WV}}{\mathrm{RWV}}\right)^{\mathrm{BB}}$	0.2
BB in $\mathrm{RFF} = \mathrm{AA}\left(\frac{\mathrm{WV}}{\mathrm{RWV}}\right)^{\mathrm{BB}}$	0.8
Maximum return flow fraction	10.95
Annual evaporation (mm)	1577.8

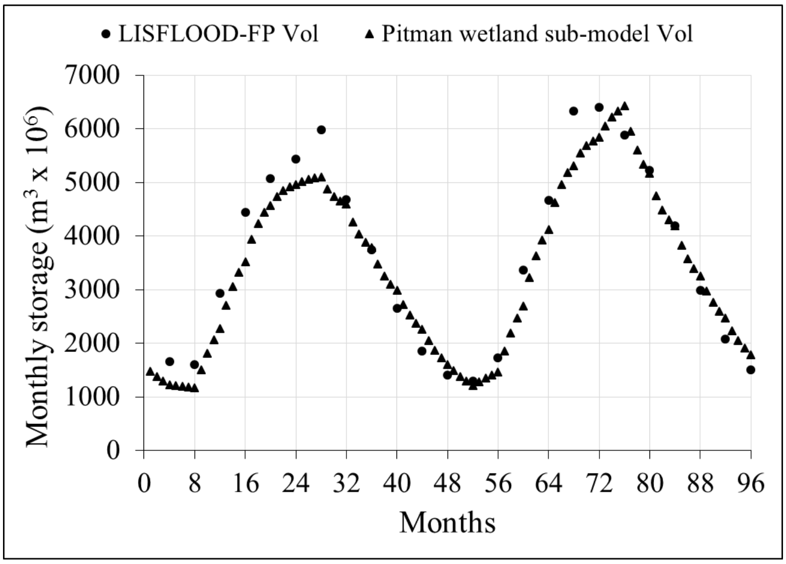

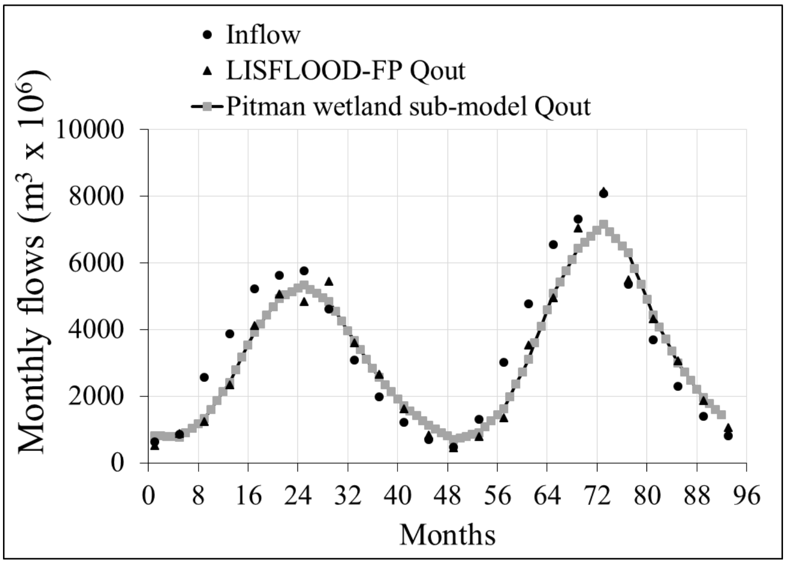

Figure 5.61: Monthly volume and flow simulated by LISFLOOD-FP and Pitman wetland sub-model in the Barotse Floodplain.

5.2.8 Re-run the Pitman model for the entire basin with the wetland sub-model included

The parameters (Table 5.16) used in the initial setup of the structured uncertainty version to generate wetland inflows together with LISFLOOD-FP related estimated wetland parameters (Table 5.20) were used to re-set this version of the model. Subsequently, the estimated parameters after the re-run of the structured uncertainty version were used in the setup of the single run version. The final estimated parameter values for the single run version after inclusion of wetland parameters in the model setup are presented in Table 5.21. Some of the parameters (initially established) have been modified when the wetland sub-model parameters were included in the model setup (see Table 5.17 and 5.21 for comparison). Notably improved simulation results were achieved after the inclusion of the wetland parameters in the model setup (Table 5.22). Simulated moderate and low flows are improved, and the peak flows which were previously (before the wetland sub-model) over-estimated are reduced (Figure 5.62 and 5.63). It can be concluded that the influence of the Barotse floodplain on both high and low flows in the Upper Zambezi River basin is substantial. Table 5.23 and Figure 5.64 suggest that the simulation results (downstream of the wetland at BP9) for the two models are broadly comparable.

Table 5.21: Final parameter values established after inclusion of wetland sub-model in the model setup.

Parameter	group1	group2	group3	group4
RDF	0.8	0.8	0.8	0.8
PI1	1.5	1.5	1.5	1.5
PI2	4	4	4	4
AFOR	0	0	0	0
FF	0	0	0	0
PEVAP	varies with sub-basins			
ZMIN	230	238	250	250
ZAVE	0.5*(ZMIN+ZMAX)			
ZMAX	636	1005	1219	1230
ST	816	1100	1200	1250
SL	0	0	0	0
POW	3.5	3.5	3.8	4
FT	20	16	15	15
GW	13	10	8	6
R	0.3	0.4	0.4	0.4
TL	0.25	0.25	0.25	0.25
CL	0	0	0	0
GPOW	3.5	3.7	3.8	4
DDENS	0.4	0.4	0.4	0.4
T	30	30	30	30
S	0.001	0.001	0.001	0.001
GW slope	0.01	0.01	0.01	0.01
RWL	25	25	25	25
RSF	0.4	0.4	0.4	0.8

Table 5.22: Summarised model performance measures for BP9 and BP7 sub-basin nodes.

Statistical function	BP9	
	Before wetland sub-model	After wetland sub-model
CE(CE(ln))	0.55(0.58)	0.77(0.86)
Pbias (Pbias(ln))	24.3(3.6)	8.97(1.92)

Note: Values in the brackets are for transformed values

Table 5.23: Summarised model performance measures for the LISFLOOD-FP and the Pitman model.

Statistical function	Simulation by LISFLOOD-FP	Simulation by Pitman wetland sub-model
CE(CE(ln))	0.73(0.76)	0.72(0.81)
Pbias (Pbias(ln))	13.92(3.15)	6.20(2.53)

Note: Values in the brackets are for transformed values

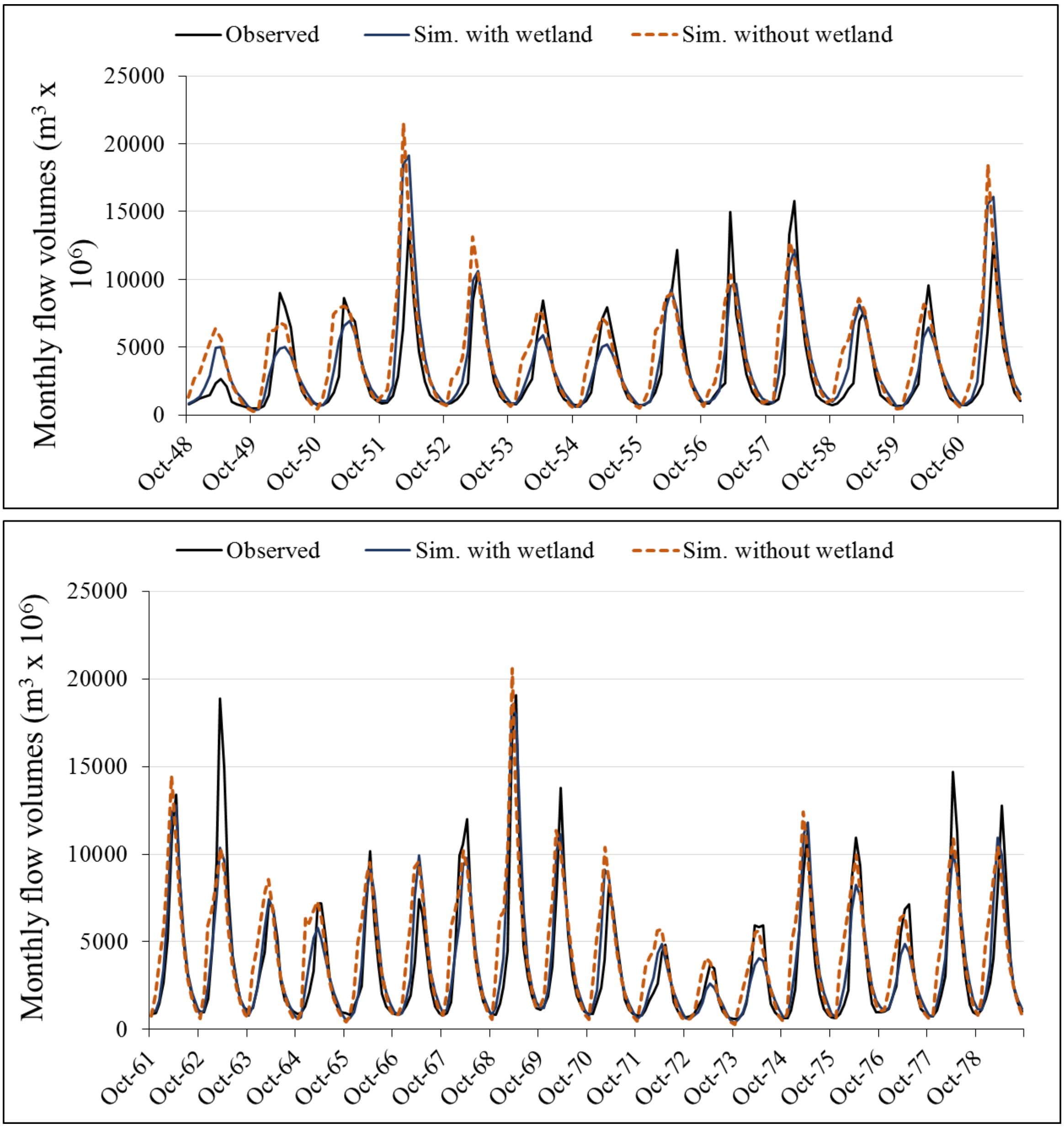

Figure 5.62: Observed and simulated flows (before and after inclusion of wetland sub-model) for sub-basin BP9 in the Upper Zambezi River basin.

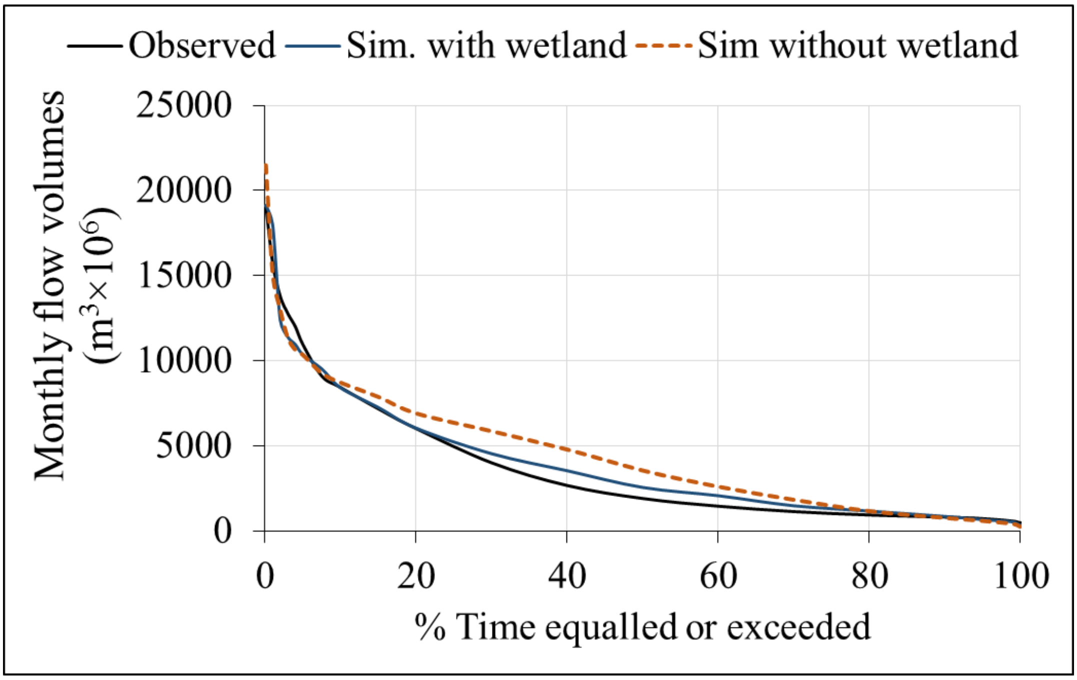

Figure 5.63: Observed and simulated FDCs before and after inclusion of wetland sub-model for BP9 sub-basin in the Upper Zambezi River basin.

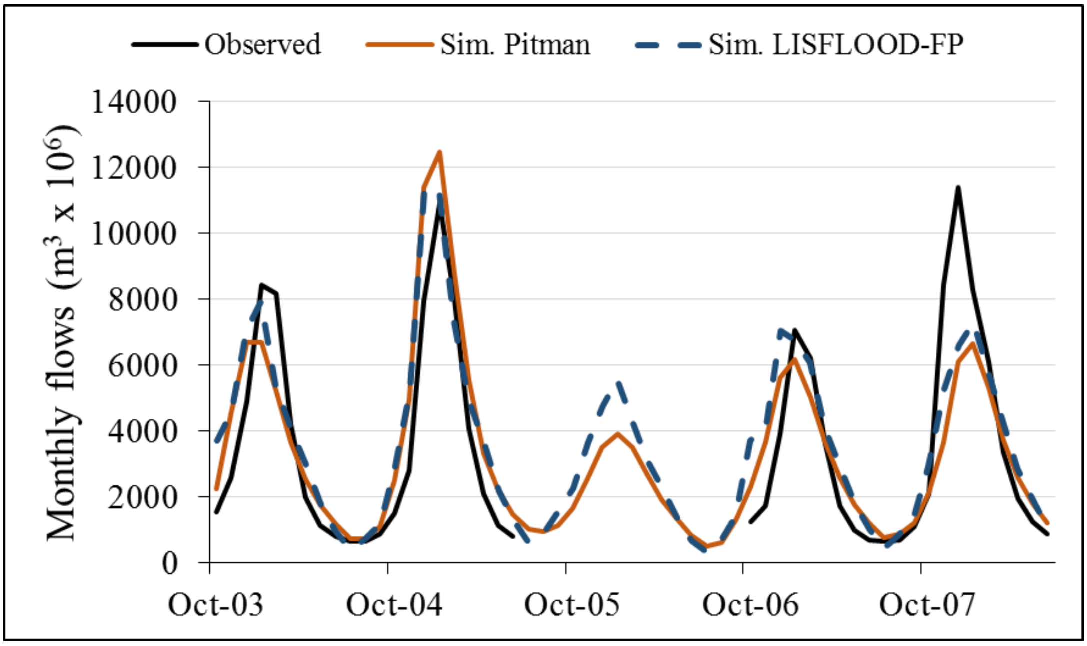

Figure 5.64: Comparison between observed and simulated monthly flows at BP9 (a gap on the observed flows indicates missing values) for the period January 2003 to September 2007.

5.3 The Upper Great Ruaha River basin (UGRRB)

5.3.1 Disaggregation of simulated monthly flows into daily flows

The simulated monthly wetland inflows (from Tumbo, 2015) were disaggregated into daily inflows for the period between October 2000 and September 2009. The scaling parameters were manually calibrated using the limited available historical daily and monthly flows in 1ka71 sub-basin until the best estimates were obtained. Figure 5.65 presents the FDCs of the observed (daily and monthly) and simulated daily flows established using the final estimated parameters (i.e. A = 0.3, B = -0.2, C = 0.8. K = 0.95 and R_{thresh} = 5). These parameter values were used in all sub-basins that contribute to wetland inflows. Observed daily flow records were available in some sub-basins, however, the records are very short, contain missing values and mostly precede the selected simulation period (October 2000–September 2009). Therefore, it was difficult to assess the simulated daily flows for all the sub-basins. The results in Figure 5.66 indicate that the simulated daily flows have low peaks (sub-basins are quite small) and nearly zero flows during the dry season. In general, there are many uncertainties in the simulated flows that were used as upstream boundary conditions in the LISFLOOD-FP model.

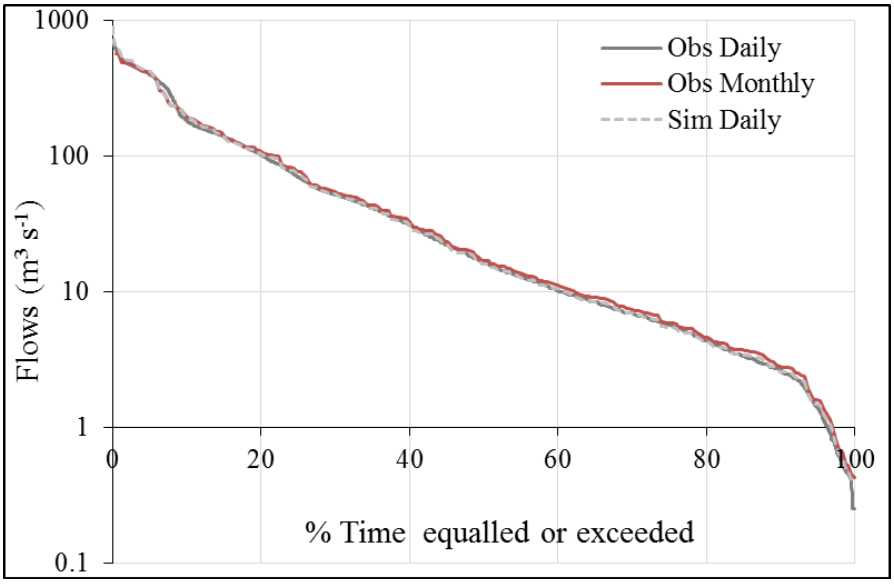

Figure 5.65: FDC of the observed (daily and monthly) and simulated daily flows after the establishment of the final scaling parameters.

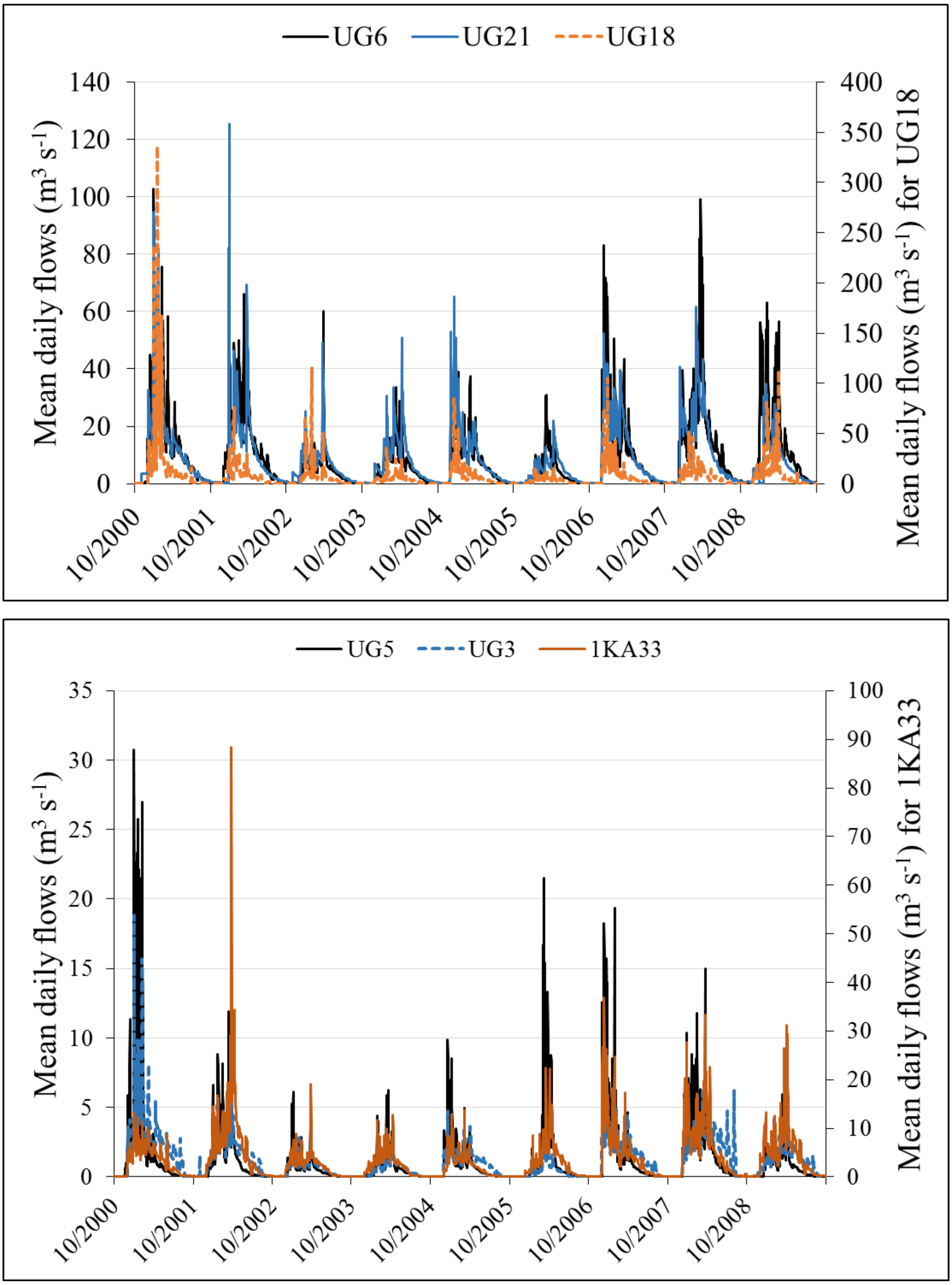

Figure 5.66: Disaggregated mean daily flows for 1KA33, UG3,UG5, UG21, UG6, UG21 and 1ka18 sub-basins of the Upper great Ruaha River basin (October 2000 to September 2009).

5.3.2 Simulation of wetland inundation characteristics using LISFLOOD-FP model

The location of the Usangu wetlands is shown in Figure 5.67. The model setup was done for the period October 2000–September 2009 with 2000/2001 used as a warm-up period and this matches the period for which observed downstream flows are available. The Usangu wetlands are covered by numerous channels of different sizes (Figure 5.68). Some have widths of less than 10 m and although they can be identified in Google Earth or Landsat Look images, they would be very difficult to include in a LISFLOOD-FP model setup. Most of these small channels were, therefore, initially ignored and only the main channels included in the model setup. The digitised channel widths for the whole network in the Usangu are shown in Figure 5.68. The total length of the main river meandering within the Usangu wetlands (the Great Ruaha River) is approximately 133 km. Channel depths generated at the beginning of the simulations are presented in Figure 5.68 with most of them having values between 0.3 m and 1 m which is quite low compared to river depths in other wetlands (see Figure 5.15, 5.16 and 5.52).

The initial assessment of the wetland inflows suggested a need to scale up the flow values before using them in the model setup. This was because a trial setup using these values as upstream boundary conditions generated zero outflows at the wetland outlet and a very small inundated area. The wetland inflows used in the model setup were the disaggregated daily flows from the simulated monthly flows of Tumbo (2015). It is likely that errors in the wetland inflows could be related to uncertainties in the simulated monthly flows by Tumbo (2015). For instance, most of the gauging stations used to validate the model simulations in the Tumbo (2015) study do not represent all the key upstream tributaries (especially those located in the western part of the basin), and mostly cover very short periods. Additionally, irrigation abstractions are common in most of these tributaries and data on irrigation use which were used for setting up the model were largely uncertain. According to Tumbo (2015), the computed irrigation demand was assumed to be fixed throughout the simulation period (1960 – 2010), but this is not practically feasible. For instance, management interventions for the period 2000 – 2007 improved the water use efficiency and reduced water use for irrigation. Thus, there is a possibility that adopting fixed values of irrigation water abstractions could under-estimate the flows during this period. Amongst others, these could be the reasons for too low values of the wetland inflows. Therefore, the wetland inflow values were scaled using Equation 5.1 to increase the high flows that contribute to wetland inundation and outflows. A value of n=3 was used in the final model setup.

$$X_i + n(F_i) \qquad \text{(Equation 5.1)}$$

$$F_i = \frac{X_i - X_{MIN}}{X_{MAX} - X_{MIN}} \qquad \text{(Equation 5.2)}$$

Where X_i is the original daily flow value

X_{MAX} is the maximum value in the daily time series

X_{MIN} is the minimum value in the daily time series

n is a multiplier ≥ 1

F_i is a daily scale factor

Another issue regarding the setting up the LISFLOOD-FP model related to the characteristics of channels within the wetlands. The Usangu wetlands (eastern and western) are dominated by numerous shallow and small (i.e. less than 10 m width) channels. Most of these channels are more easily identified in the western wetland than the eastern wetland which consists of a permanently inundated swamp (Ihefu). Additionally, the main river flowing into the swamp cannot clearly be seen from the LandsatLook or Google Earth images, possibly because of dense vegetation that surrounds a large part of the swamp. The initial setup of the model, which included clearly visible main channels in the wetland resulted in more storage in the wetland at the end of the simulation (dry season). This suggested that the channels that were ignored in the model setup, despite their small sizes, have an influence on the inundation dynamics of the Usangu wetlands including returning flows from the wetlands to the main channel. To improve the model simulation results, without explicitly including all of the small channels in the model, the simulated evaporative losses were increased. These additional volumes of water loss were assumed to represent drainage back to the main channel at the outlet and were therefore manually added to the outflows at the end of the model run. Clearly, this is simulating the inundation and outflow volumes for the wrong reason, but it represented a quick and pragmatic approach to improving the simulations. The basic assumption is that the greater the inundated area (and volume), the greater the real amount of return flow from the small channels and the greater the effect of the artificial evaporation scaling. Several model runs were performed to determine the appropriate additional value, and finally 4 mm of evaporation was added to each daily evaporation value. Figure 5.70 shows that the simulated wetland storage has been reduced.

The western wetland is found in the 1ka71 sub-basin while the eastern wetland is within the 1ka21 sub-basin. To simplify the establishment of wetland parameters in the two wetland sections (Figure 5.69), these wetland sections were simulated independently starting from the western wetland, and the outflows from this wetland together with tributary inflows found in the eastern wetland were used as upstream boundary conditions in the eastern wetland. However, the model was initially run for the two wetland sections (eastern and western) combined as a single unit to gain some insight into the parameter values to be used for each wetland section, and the estimated parameter values were used to guide parameter values for the specific wetland section (Table 5.24). The wetland physical characteristics largely guided the establishment of the initial parameter values. The Great Ruaha River and most of the channels flowing into the wetlands have sand-beds and in the eastern wetland, the main river is covered by vegetation, with the bankfull depths in most sections approximately 1 – 2 m. These characteristics led to the selection of parameter ranges for channel roughness (C_n) and hydraulic radius parameter (r). A value of 0.05 was used as channel roughness for channels in the western wetland and 0.07 for channels in the eastern wetland. Vegetation is scattered on the western wetland and denser in the eastern wetland, especially in the Ihefu swamp. The vegetation characteristics were used to select a parameter range for the floodplain/wetland roughness (C_f). A higher value of the wetland roughness was used in the eastern wetland (0.1) compared to the western wetland (0.07).

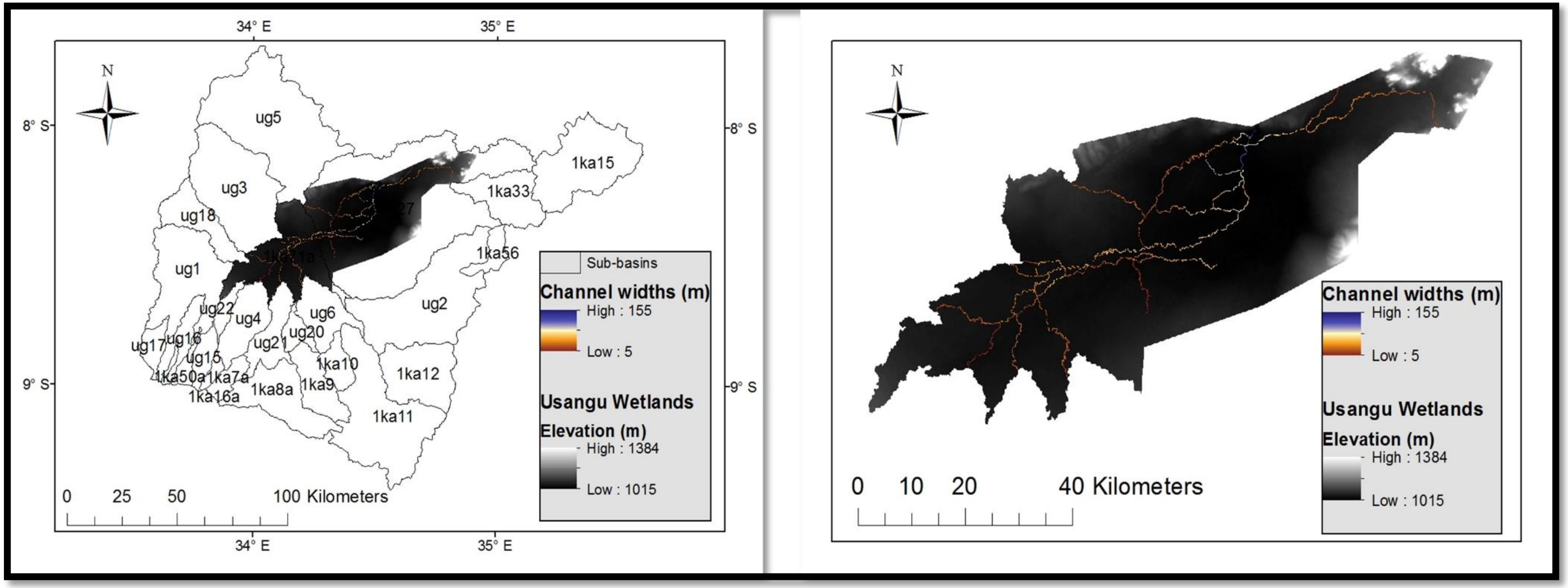

Figure 5.67: The location of the Usangu wetlands in the Upper Great Ruaha River basin.

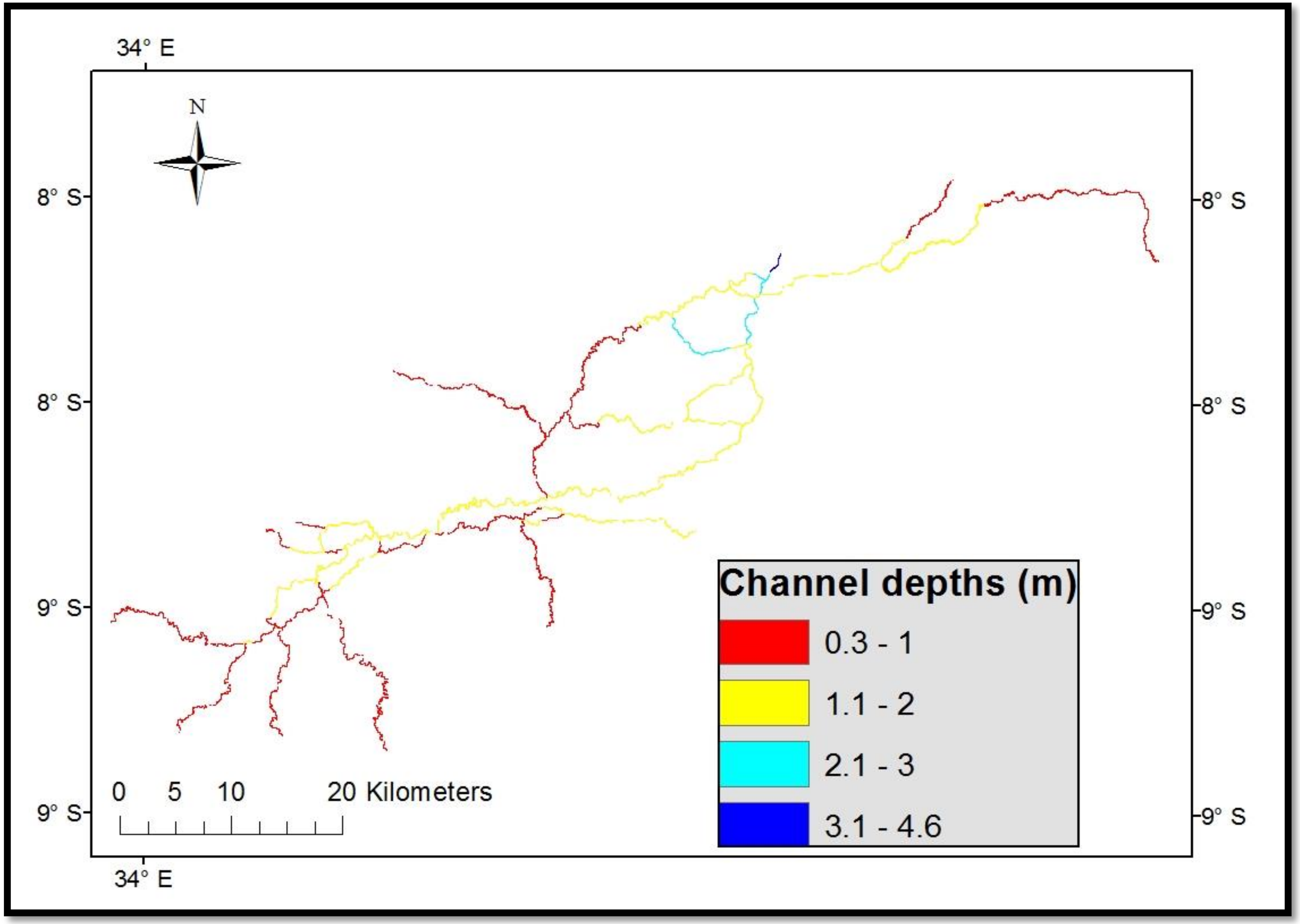

Figure 5.68: Channel depth values in the Usangu wetlands.

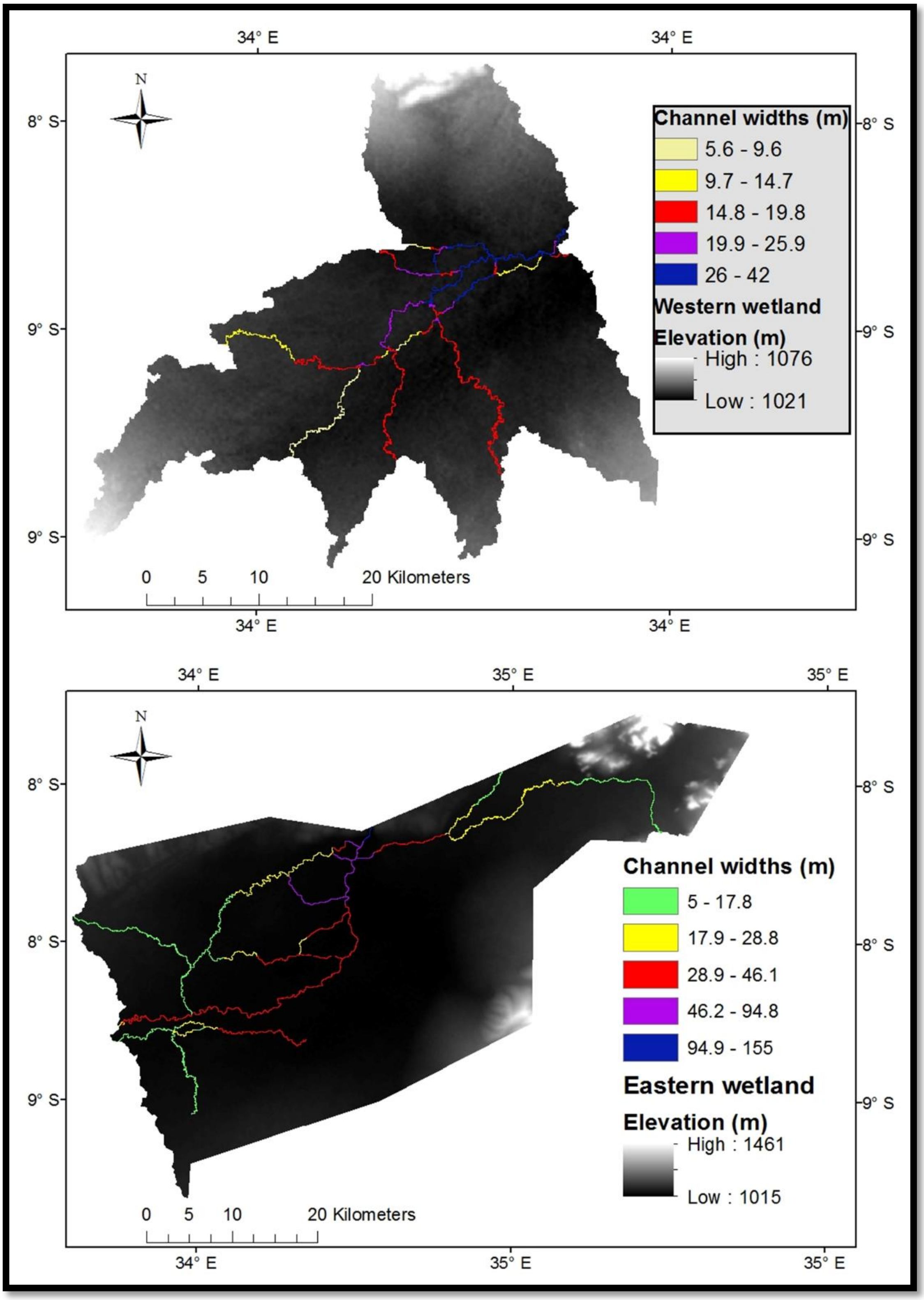

Figure 5.69: Elevation and channel widths in the western (Top) and eastern (Bottom) wetlands

Table 5.24: Parameter ranges used to setup the LISFLOOD-FP model

Parameter	Parameter range	Final value
Channel roughness (C_n)	0.02 – 0.07	0.05
Floodplain roughness (C_f)	0.05 – 0.1	0.08
p (fractional exponent in the Width–depth relationship)	0.76	0.76
r (scale coefficient in the Width–depth relationship)	0.055 – 0.15	0.1
Average channel slope	0.0001	0.0001

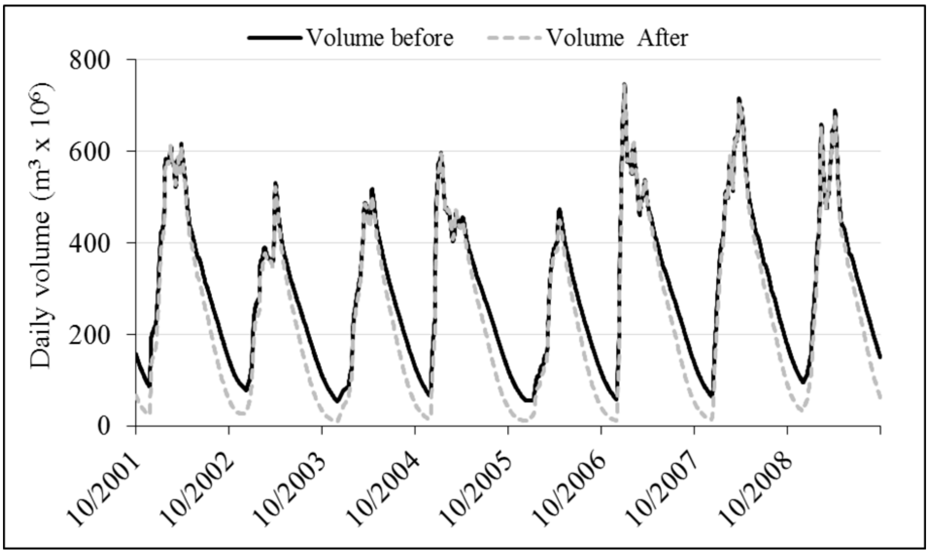

Figure 5.70: Simulated wetland storage before and after increasing evaporation values by 4 mm in the Upper Great Ruaha River basin.

The average inundation depth is about 0.7 m. From Figure 5.71, the 7-day maximum inundation area is between 600 km^2 and 700 km^2, whereas the maximum storage is in the range 500 $\times 10^6$ – 600 $\times 10^6$ m^3 when the two wetland sections were simulated as a single unit. Furthermore, the 7-day maximum storage and inundated area were in the range of 300 – 450$\times 10^6$ $m^3$and 250 – 300 km^2 in the western wetland (Figure 5.73). In the eastern wetland (1ka27), the maximum inundation area is 300 km^2 – 500 km^2 range and 200 $\times 10^6$ – 500 $\times 10^6$ m^3 for maximum storage (Figure 5.75). Simulated storage–inflow relationships show large magnitude counter-clockwise hysteretic relationships (Figure 5.71 5.73 and 5.75). Multiple inflow peaks in both the eastern and western wetland sections reflect the response of streamflows to short and long rains seasons in this basin. A nearly clockwise hysteresis loop in the area–storage relationship (normal year) illustrates that the inundation area is always higher than the storage at the beginning of the wet season, and low during the dry season. This means flooding water spreads quickly through the wetland (because large areas of the wetland are very flat), and the average inundation depth in most sections is less than 1 m. During the wet year, the area–storage relationship tends to form a figure of eight shaped hysteresis curve. In general, the standardised storage–inflow and area–storage relationships have indicated that whenever the peak flow increases, the hysteresis effect is great and the temporal fluctuation of the wetland inflows certainly influences the size of the hysteresis, particularly in the eastern wetland (Figure 5.76 and Table 5.25). In the western wetland, the hysteresis effect is much less than expected (Figure 5.74), and this could be related to uncertainties in the simulated results. The difference between inflows and outflows indicate that the Usangu wetland significantly attenuates high flows (Figure 5.77, 5.78 and 5.79).

The simulated outflows from the western wetland (1ka71) were not validated due to the lack of observed data, whereas simulated outflows from the eastern wetland (1ka27) were compared with the available daily flows for a gauging station (1ka59) located 80 km downstream of the wetland outlet. This gauging station was considered eligible to validate the wetland outflows as there are no substantial inflows between the wetland outlet and where the gauge is located. Simulated flows (i.e. recession and rise limbs) compare reasonably well with high peaks (Figure 5.80). Generally, the flow patterns are not well simulated (the model could not capture the observed peaks during short rains) (Figure 5.80). It is not easy to explain why the peaks were not captured, particularly in year 2006 when the wetland inflows were multiplied by a factor of 3. Increasing the multiplying factor might resolve the issue, but this would affect the simulated low flows (which are somewhat reasonable). Perhaps, the multiplying factor should vary across the tributary inflows, but clearly, this would be difficult especially in the absence of observed flow data. All in all, there is a wide range of uncertainty in the results and part of this could relate to the uncertainties in the model structure as well as wetland inflows. Additional field data are therefore required to resolve the issue.

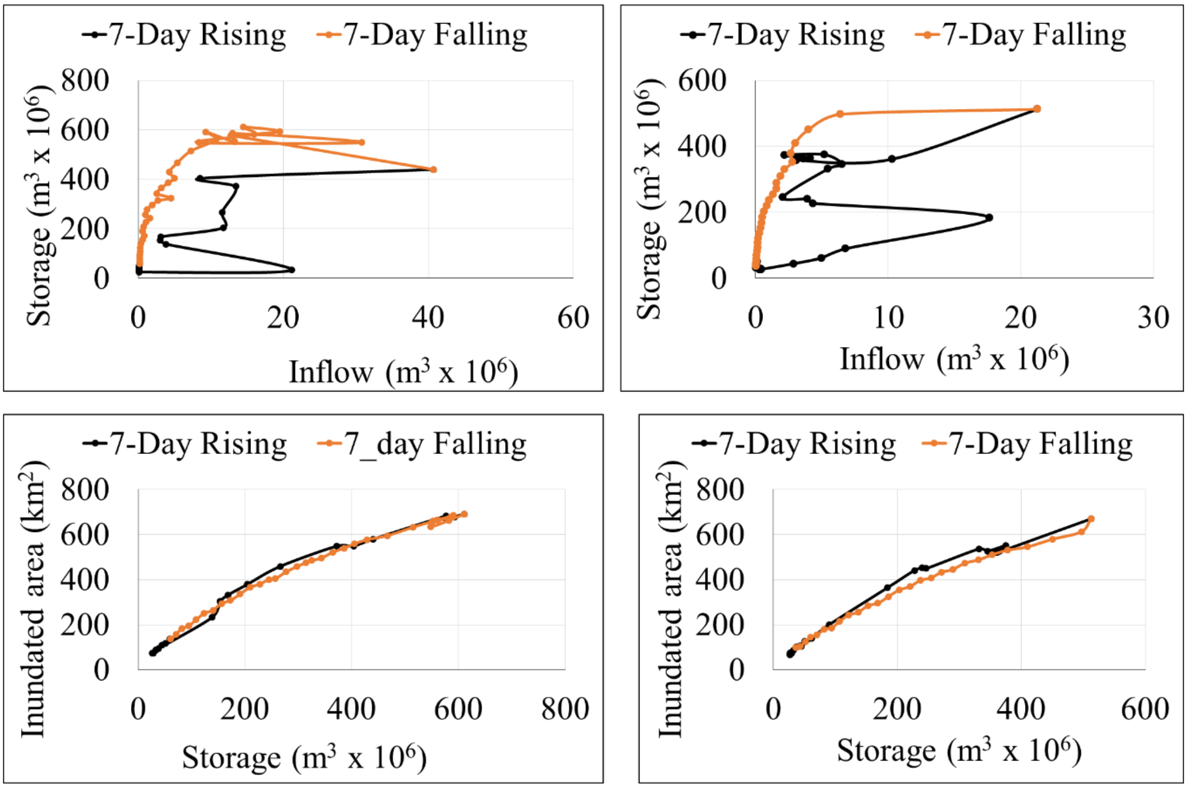

Figure 5.71 Storage–inflow and area–storage mean monthly hysteresis for 2001/02 (left) and 2002/03 (right) years in the Usangu wetlands (simulated as a single unit).

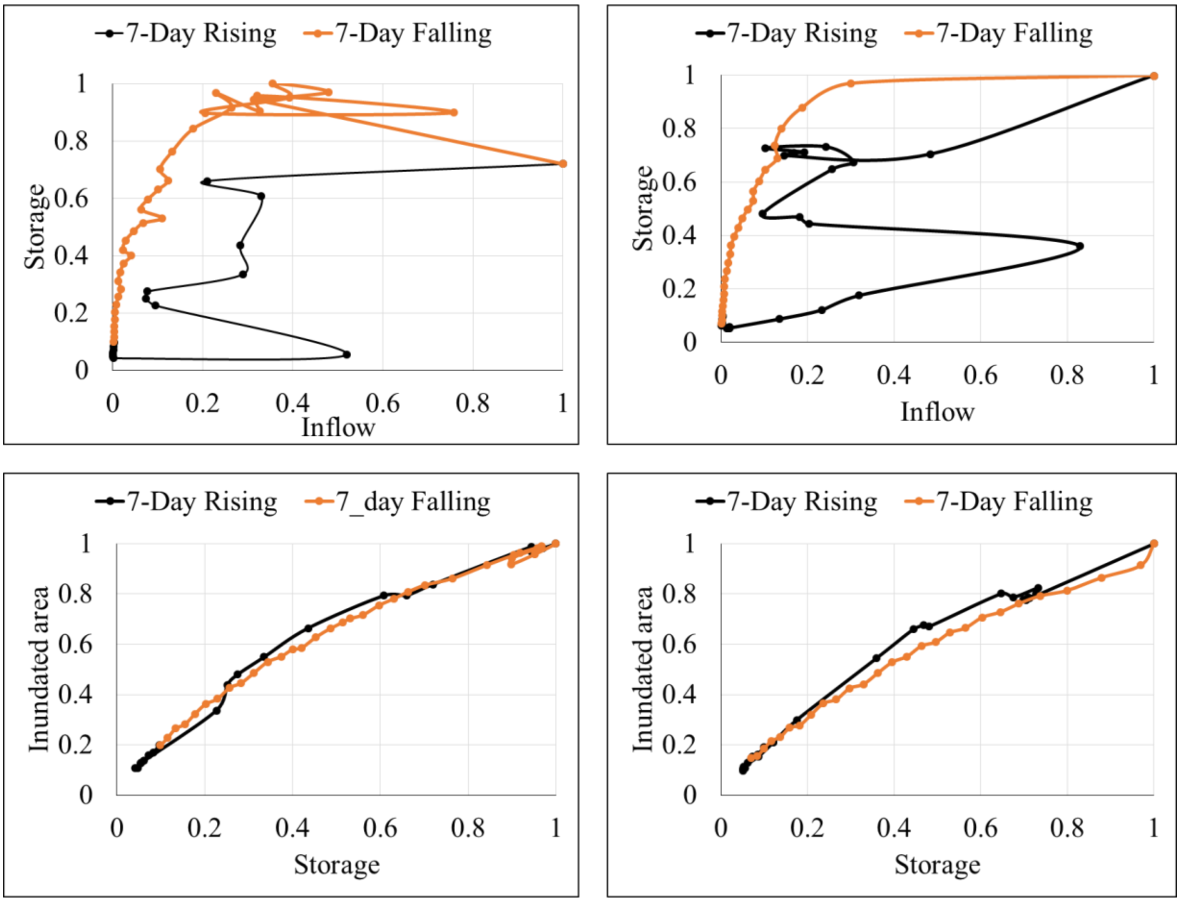

Figure 5.72: Standardised storage–inflow and area–storage mean monthly hysteresis for 2001/02 (left) and 2002/03 (right) years in the Usangu wetlands (simulated as a single unit).

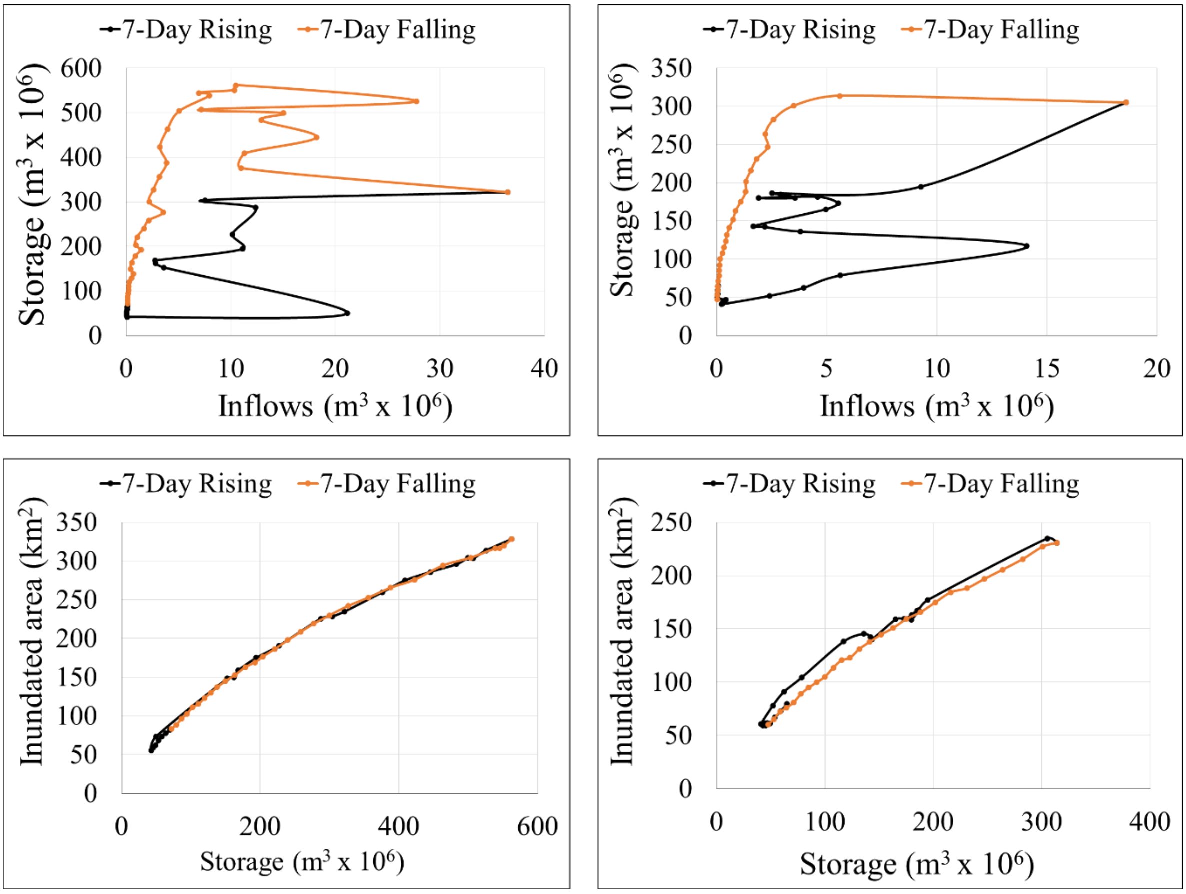

Figure 5.73: Storage–inflow and area–storage mean monthly hysteresis for 2001/02 and 2002/03 years in the western Usangu wetland (1ka71).

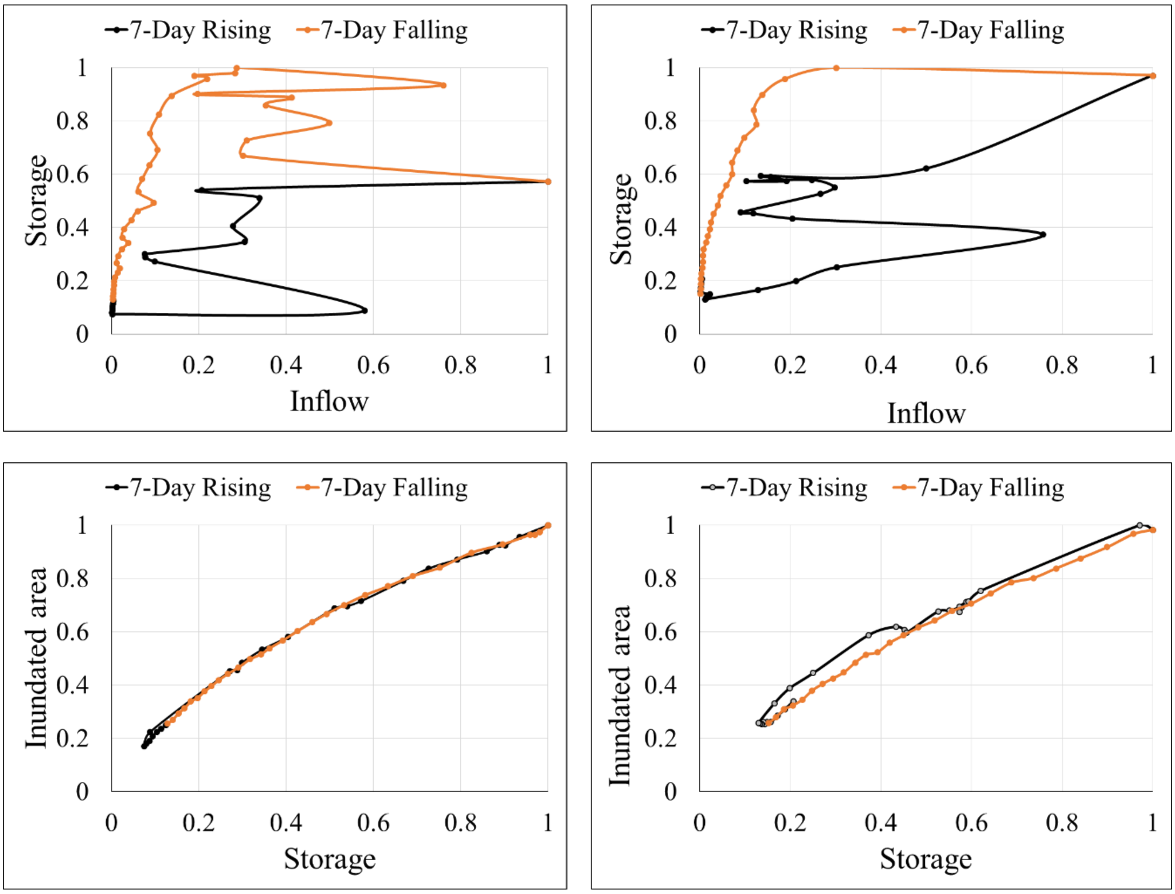

Figure 5.74: Standardised Storage–inflow and area–storage mean monthly hysteresis for wet (left) and normal (right) years in the western Usangu wetland (1ka71).

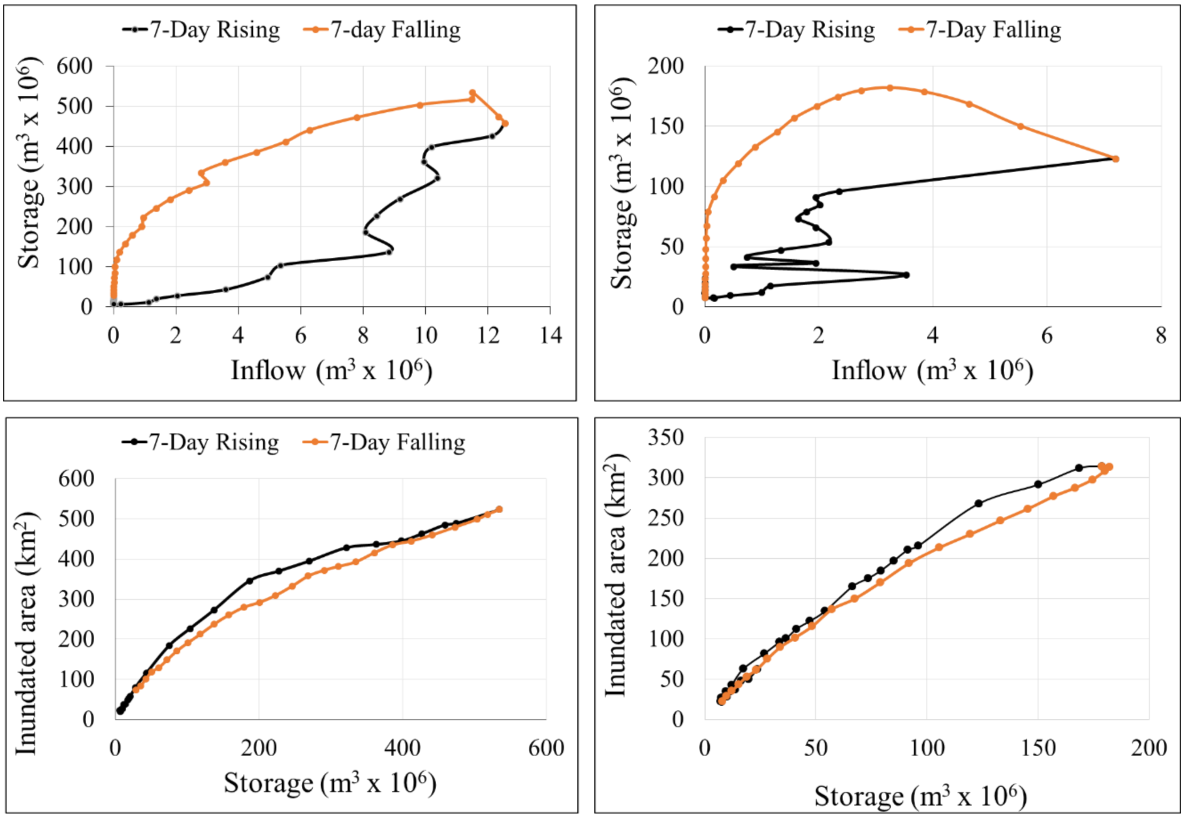

Figure 5.75: Storage–inflow and area–storage 7-day hysteresis for wet (left) and normal (right) years in the eastern Usangu wetland (1ka27).

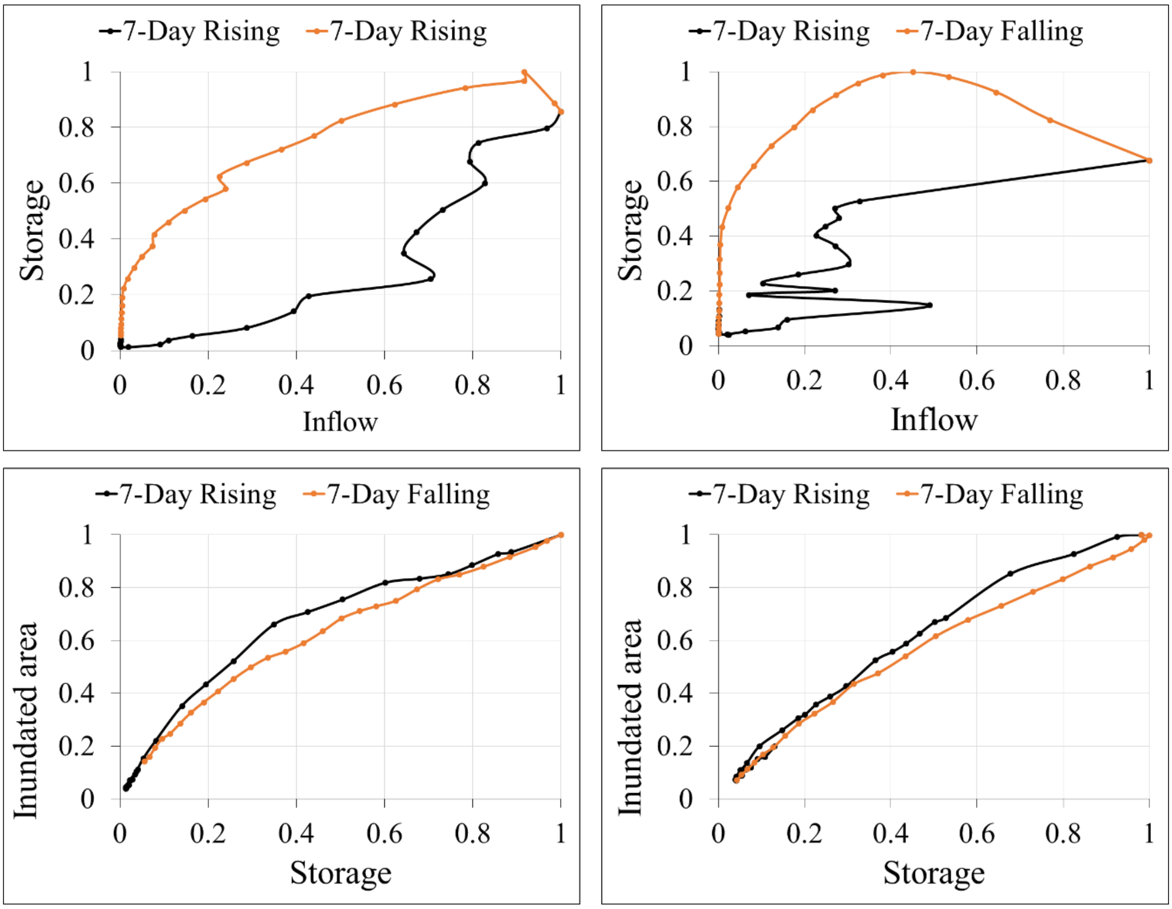

Figure 5.76: Standardised Storage–inflow and area–storage mean monthly hysteresis for wet (left) and normal (right) years in the eastern Usangu wetland (1ka27).

Table 5.25: Magnitude of the hysteresis in the Usangu wetlands

Relationship	Eastern wetland (1ka27)		Western wetland (1ka71)	
	Wet year	normal year	Wet year	normal year
Area-storage	0.09	0.06	0.01	0.02
Storage-Inflow	0.64	0.60	0.78	0.63

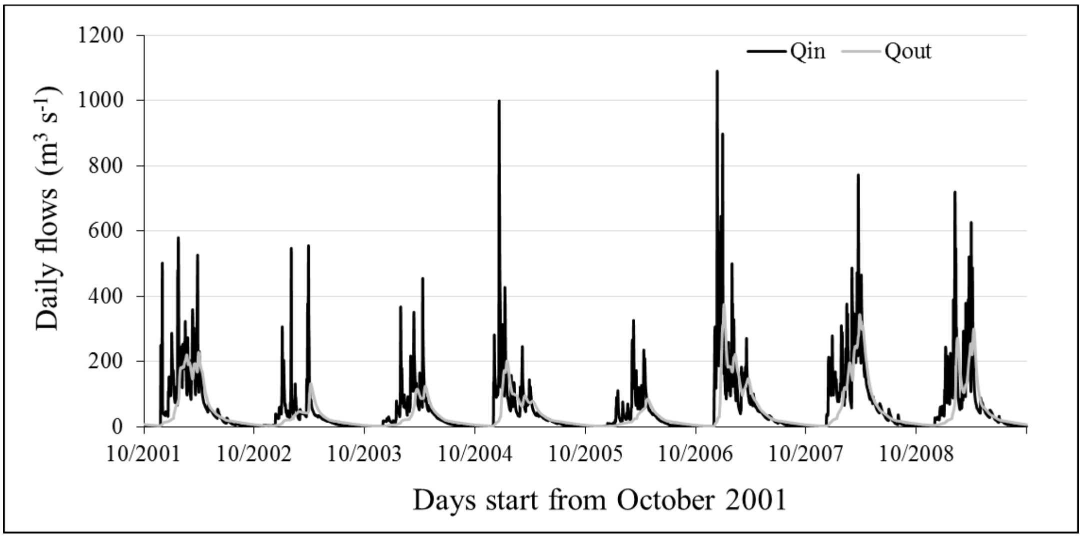

Figure 5.77: Daily inflows and outflows in the Usangu wetlands (simulated as a single unit).

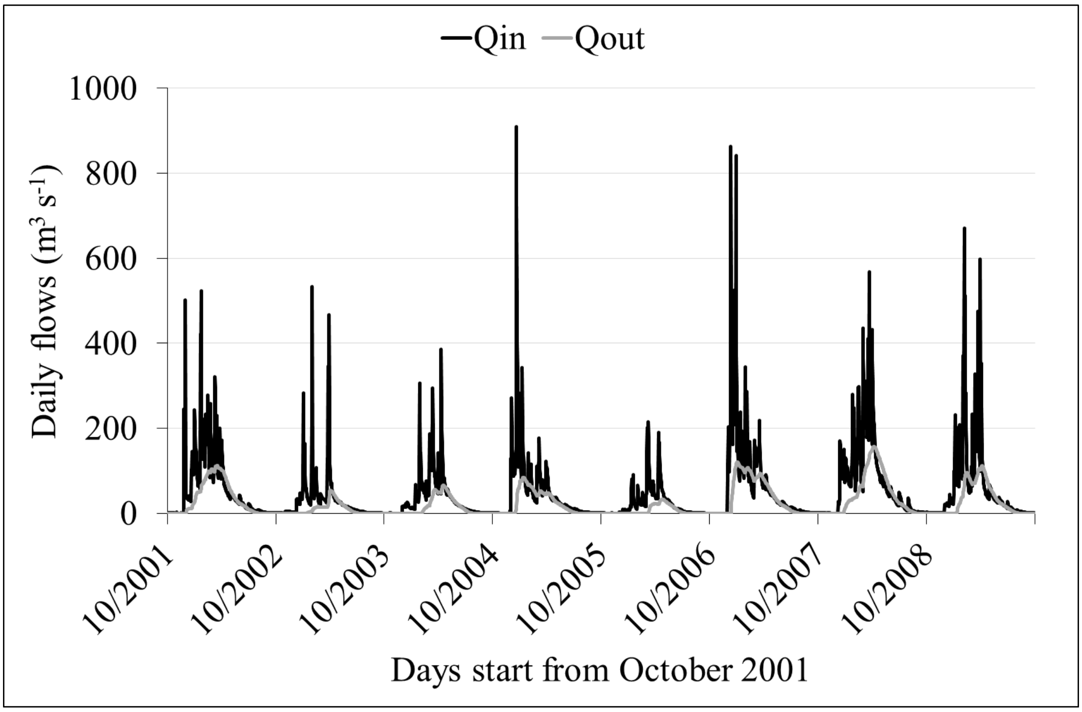

Figure 5.78: Daily inflows and outflows in the western Usangu wetland (1ka71).

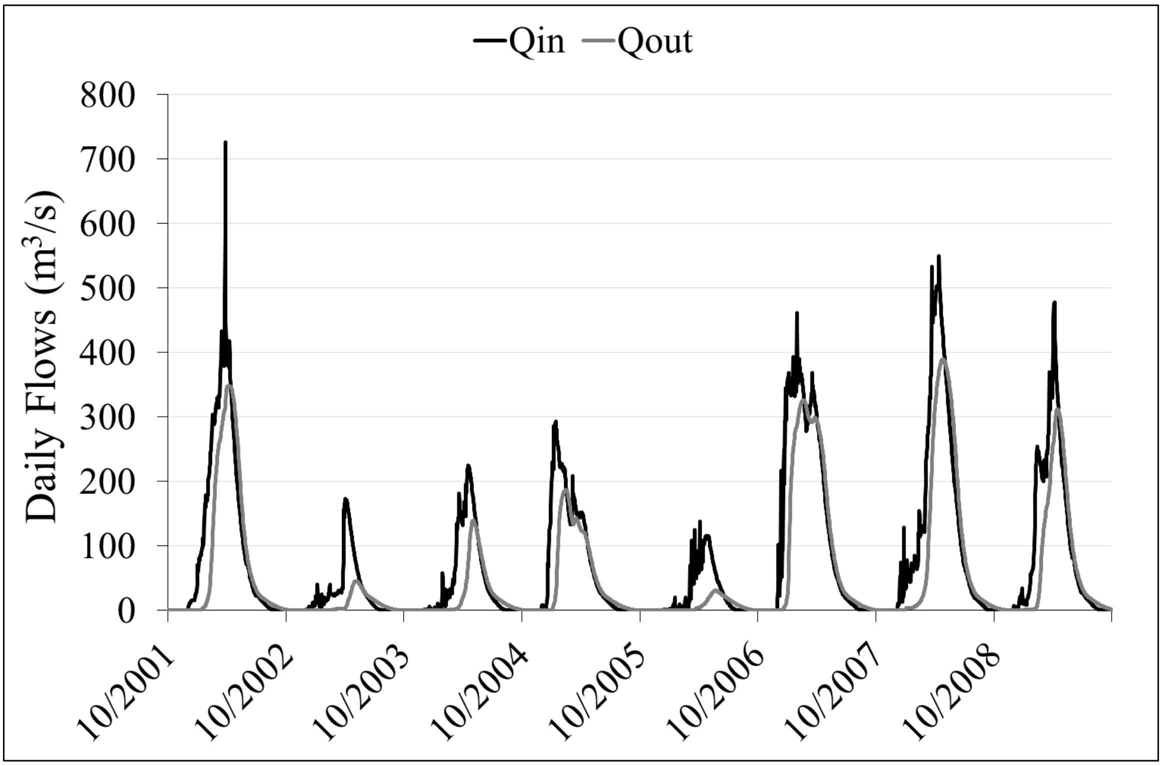

Figure 5.79: Daily inflows and outflows in the eastern Usangu wetland (1ka27).

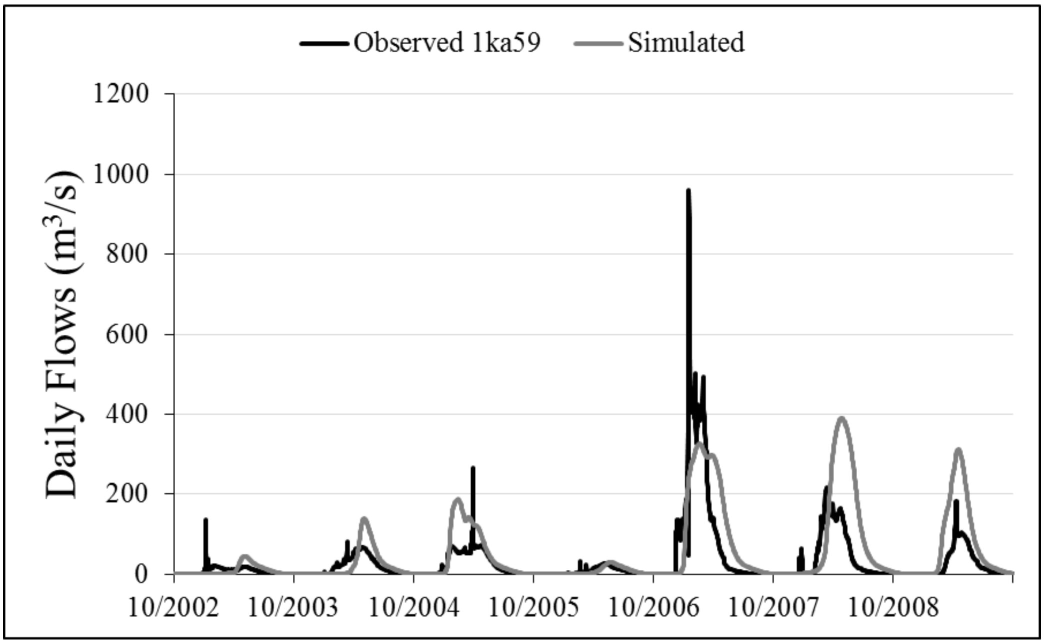

Figure 5.80: Observed (1ka59) and simulated daily outflows in the Usangu wetlands.

5.3.3 Quantification of Pitman wetland parameters

Wetland sub-model parameters were estimated from the LISFLOOD-FP results for the two sub-basins. A similar approach applied in the other basins was used in this basin; most of the parameters were established through manual calibration by implementing the Pitman wetland sub-model in an excel sheet containing the LISFLOOD-FP results. The quantified wetland parameters for each sub-basin are presented in Table 5.26. A zero value of channel capacity for spillage and high value of spill factor in the eastern wetland (1ka27) were used because the Great Ruaha River tends to disappear in the Ihefu swamp which is part of the eastern wetland. Furthermore, the wetland residual storage value is higher in the eastern wetland than the western due to the presence of a permanently inundated swamp. Return flows are limited by the volume of water in the channel (i.e. no return flows during spilling onto the wetland). Better agreement between the two models was achieved for simulated storage volumes, compared to simulated outflows (Figure 5.81, 5.82 and 5.83). This illustrates the difficulties of simulating the exchange processes for this wetland, regardless of the model being used. Part of the problem lies with the uncertainties relating to the inflows, but the effects of the complex network of small channels in the eastern wetland (which were not explicitly simulated) are also expected to contribute to the difficulties.

Table 5.26 Estimated parameter set for the Pitman wetland sub-model in the Usangu wetlands

Parameters and units	The estimated wetland parameter values for each sub-basin		
	Western (1ka71)	Eastern (1ka27)	Whole wetland as unit
Local catchment area (Km^2)	800	600	1600
Residual wetland volume (RWV) in $m^3 10^6$	20	60	80
Initial wetland volume (WV) in $m^3 10^6$	40	20	20
A in $\mathrm{Area}(\mathrm{m}^2 10^6) = \mathrm{A}(\mathrm{WV}\ (m^3 10^6))^{\mathrm{B}}$	680	680	760
B in $\mathrm{Area}(\mathrm{m}^2 10^6) = \mathrm{A}(\mathrm{WV}\ (m^3 10^6))^{\mathrm{B}}$	0.65	0.67	0.65
Channel capacity for spillage (QCAP) $m^3 10^6$	20	0	0
Channel spill factor	0.7	0.9	0.9
AA in $\mathrm{RFF} = \mathrm{AA}\left(\frac{\mathrm{WV}}{\mathrm{RWV}}\right)^{\mathrm{BB}} \frac{\mathrm{QCAP}}{\mathrm{Q}}$	0.11	0.4	0.15
BB in $\mathrm{RFF} = \mathrm{AA}\left(\frac{\mathrm{WV}}{\mathrm{RWV}}\right)^{\mathrm{BB}} \frac{\mathrm{QCAP}}{\mathrm{Q}}$	0.5	0.35	0.8
Annual evaporation (mm)	1867	1714	1714

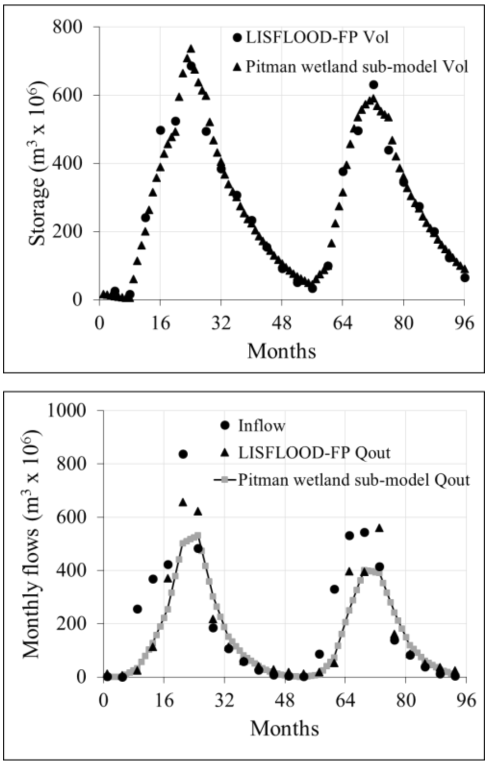

Figure 5.81: Monthly volume and flow simulated by LISFLOOD-FP and Pitman wetland sub-model in the Usangu wetlands (simulated as a single unit).

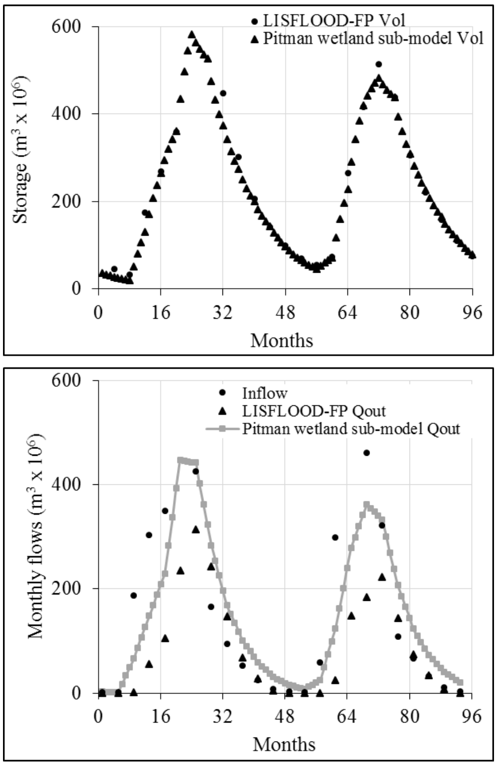

Figure 5.82: Monthly volume and flow simulated by LISFLOOD-FP and Pitman wetland sub-model in the western Usangu wetland (1ka71 sub-basin).

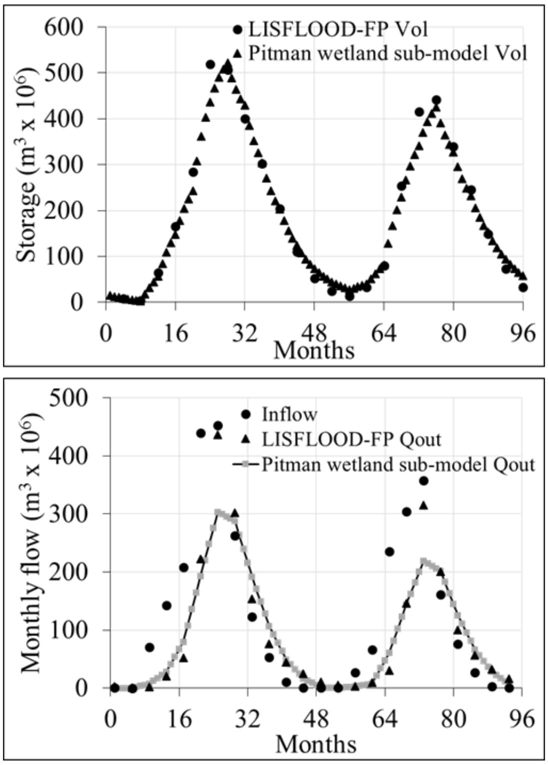

Figure 5.83: Monthly volume and flow simulated by LISFLOOD-FP and Pitman wetland sub-model in the eastern Usangu wetland (1ka27 sub-basin).

5.3.4 Re-run the Pitman model for the entire basin with the wetland sub-model included

The final estimated parameter values established by Tumbo (2015) together with the quantified wetland parameters were used to reset the uncertainty version of the model and the results are presented in Figure 5.84 (top). High flows are underestimated, whereas the low flows are somewhat high. This suggested that the estimated wetland parameters overestimated the impacts of the Usangu wetlands, possibly because the whole setup of the LISFLOOD-FP in the Usangu was difficult, and the dynamics of the Usangu wetlands were not well understood. Clearly, the simulated results are not good compared to that of Tumbo (2015) as indicated in Figure 5.84. Performance measures for the optimal ensemble indicates poor results especially in high flows (values are beyond the minimum requirements). Therefore, additional field data related to exchange dynamics could improve the setup of the LISFLOOD-FP to achieve acceptable estimated wetland parameters from the LISFLOOD-FP results.

Table 5.27: Summarised model performance measures for 1ka59 sub-basin

Statistical function	Simulation by Tumbo (2015)	Current simulation after wetland sub-model
CE(CE(ln))	0.53(0.59)	0.30(0.63)
Pbias (Pbias(ln))	-7.13(1.13)	-48.50(13.10)

Note: Values in the brackets are for transformed values

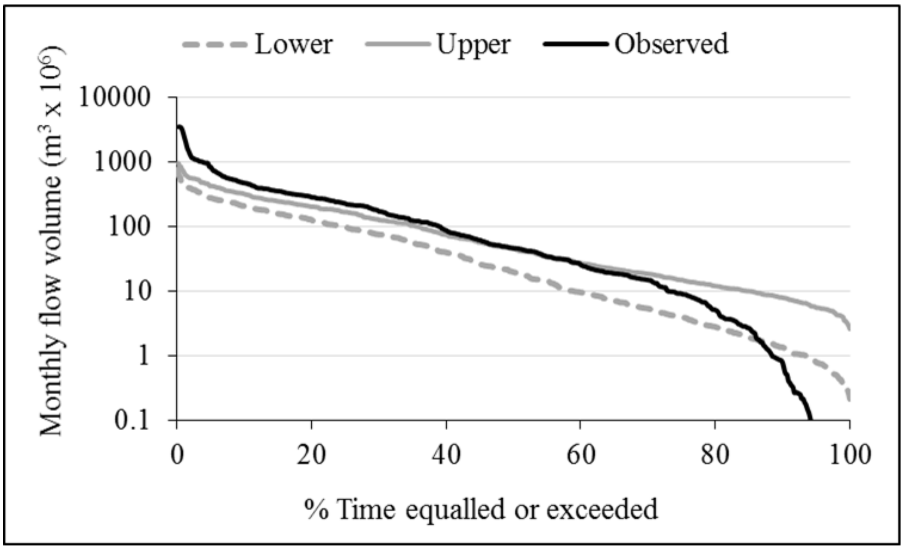

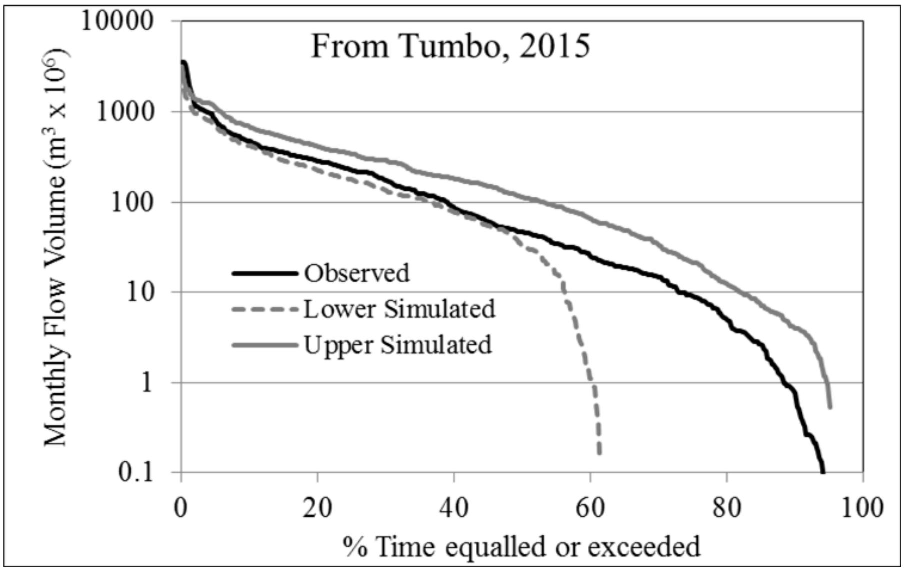

Figure 5.84: Observed and simulated uncertainty bounds after inclusion of wetland parameters in the Pitman model.

5.4 Regionalisation or direct estimation of wetland parameters of the basin-scale model.

The wetland sub-model parameters (Table 5.28) were interpreted in terms of their physical characteristics, together with the better understanding of the different water exchange dynamics of the three wetlands that were obtained from the LISFLOOD-FP model. The detailed explanations of the physical characteristics of the basins and the wetlands are presented in Chapter 3, of which some of the key physical characteristics of the three wetlands were used to help understand and interpret the wetland sub-model parameters. Standardised storage–inflow and area–storage hysteresis curves are different across the three studied wetlands and between wet and normal years. Higher flood discharges (wet years) tend to have a greater hysteresis effect compared to lower flood discharges (normal year) and the temporal fluctuation of the wetland inflows increases the size of the hysteresis.

The relative residual storage computed as a ratio between residual wetland storage and the total size of the individual wetlands are: Luangwa NF1 (0.36), NF2 (0.27), NF3 (0.41), Barotse (0.073), western Usangu (0.03) and Eastern Usangu (0.06). Clearly, the Luangwa has the highest relative residual storage and this is related to the number of cut-off channels evident on the floodplain. However, this result is rather inconsistent with the relatively low hysteresis of the Luangwa and could be a modelling artefact. The low value in the Barotse floodplain could reflect the small volume of water (compared to the total inundated volume) that remains in abandoned channels and other depressions connected to the river, possibly because the Barotse is very wide and shallow.

The relative spill capacity (channel spillage capacity relative to maximum simulated discharge) is about 0.03 to 0.04 for the Upper and Middle Luangwa, 0.075 for the Barotse and very low for the Usangu. This is consistent with the nature of the floodplains, and the Luangwa has many more low lying floodplain features that are directly connected to the channel (promoting quite early spill) compared to the Barotse (Figure 5.85), while the Usangu is a depression type wetland (rather than a floodplain) with a very limited size main channel passing through (notably in the eastern wetland). The channel spill factor (proportion of upstream inflow that contributes to floodplain storage) for the Usangu also reflects the wetland type and most of the inflows will spill onto the wetland. It is hard to explain why the Luangwa floodplain sections have such low spill factors compared to the Barotse when both have many low lying features connected to the floodplain. This is possibly because of the greater extent of these features across the Barotse, while many of the active ones in the Luangwa are quite close to the channel (see Figure 5.85 for comparison).

Figure 5.86 illustrates the relationship between the return flow fraction and the stored volumes relative to the residual volume. It is difficult to make any generalisations about the return flows. However, it is clear that the Luangwa returns more water at relatively low storages and this suggests a better channel–floodplain connectivity than the Barotse or western Usangu wetland. Figure 5.85 shows that the nature of channel–floodplain connectivity determines the possibility of return flows to occur even during high inflows in the Luangwa compared to the Barotse. The Usangu wetlands (eastern and western) are slow to return water and this could be because the small channels found in this wetland were not adequately catered for in the model, and the final calibrated Pitman model could not properly account for the extra evaporation losses which were designed to account for this effect. Further consideration is that the Usangu and Barotse relative storages (compared to the residual storage) are much higher than that of the Luangwa. That illustrates that the AA and BB parameters are both scale dependent, making it difficult to make direct comparisons between these parameter values across different wetlands. Regionalising the AA and BB parameters will therefore not be realistic objective and it may be necessary to perform the type of analysis represented by Figure 5.86 to check that appropriate AA and BB parameters are quantified for different types of wetland.

Table 5.28: Summary of the estimated wetland sub-model parameters

Parameters and units	LUANGWA			BAROTSE	USANGU	
	Upper section (NF1)	Middle section (NF2)	Lower section (NF3)		Western (1ka71)	Eastern (1ka27)
Local catchment area (Km^2)	500	450	200	9500	800	600
Residual wetland volume (RWV) in $m^3 10^6$:	215	150	130	800	20	60
Initial wetland volume (WV) in $m^3 10^6$:	212	140	130	1600	40	20
A in $\text{Area}(\text{m}^2 10^6) = \text{A}(\text{WV}\ (m^3 10^6))^{\text{B}}$	10.5	9	0.19	800	680	680
B in $\text{Area}(\text{m}^2 10^6) = \text{A}(\text{WV}\ (m^3 10^6))^{\text{B}}$	0.82	0.87	1.004	0.69	0.65	0.68
Channel capacity for spillage (QCAP) $m^3 10^6$:	100	80	160	600	20	0
Channel spill factor	0.25	0.15	0.06	0.8	0.7	0.9
AA in $\text{RFF} = \text{AA}\left(\frac{\text{WV}}{\text{RWV}}\right)^{\text{BB}}$	0.32	0.3	0.33	0.2	0.11	0.4
BB in $\text{RFF} = \text{AA}\left(\frac{\text{WV}}{\text{RWV}}\right)^{\text{BB}}$	1.9	1.8	1.7	0.8	0.5	0.35
Maximum return flow fraction	10.95	10.95	10.95	10.95	0.95	0.95
Annual evaporation (mm)	1535	1668.5	1668.5	1577.8	1867	1714

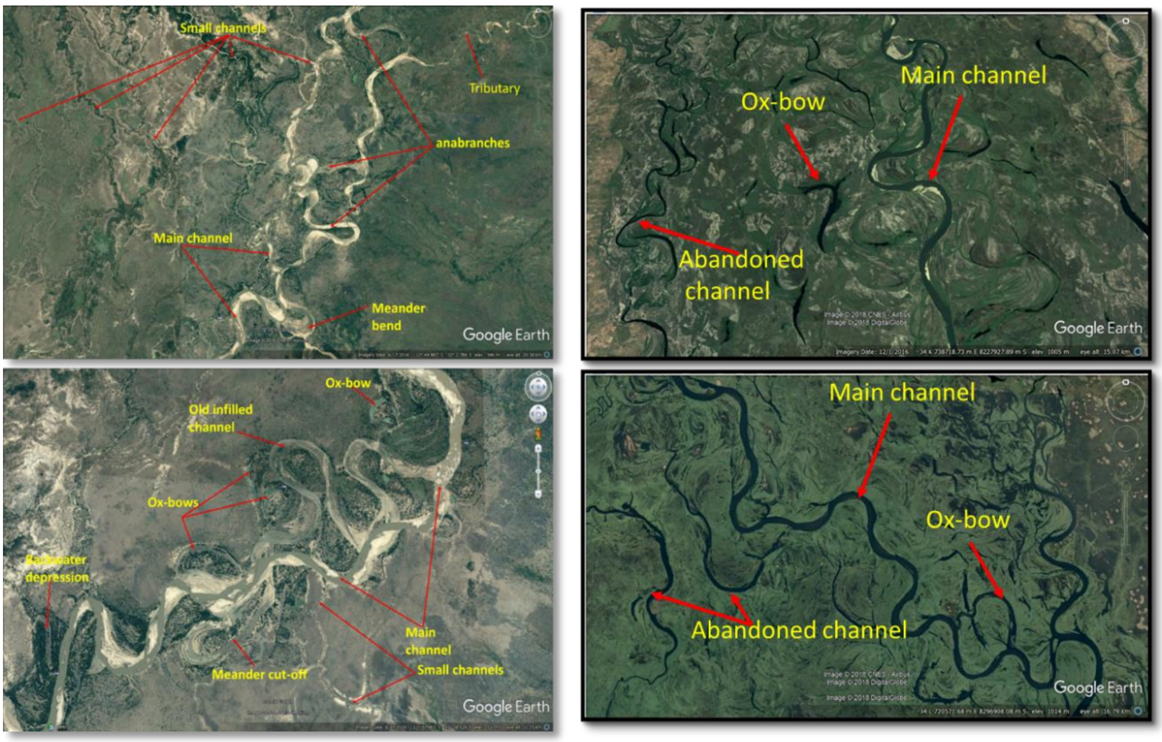

Figure 5.85: Interactions between the Luangwa River and the floodplain features (left), the Zambezi River and Barotse floodplain features (right).

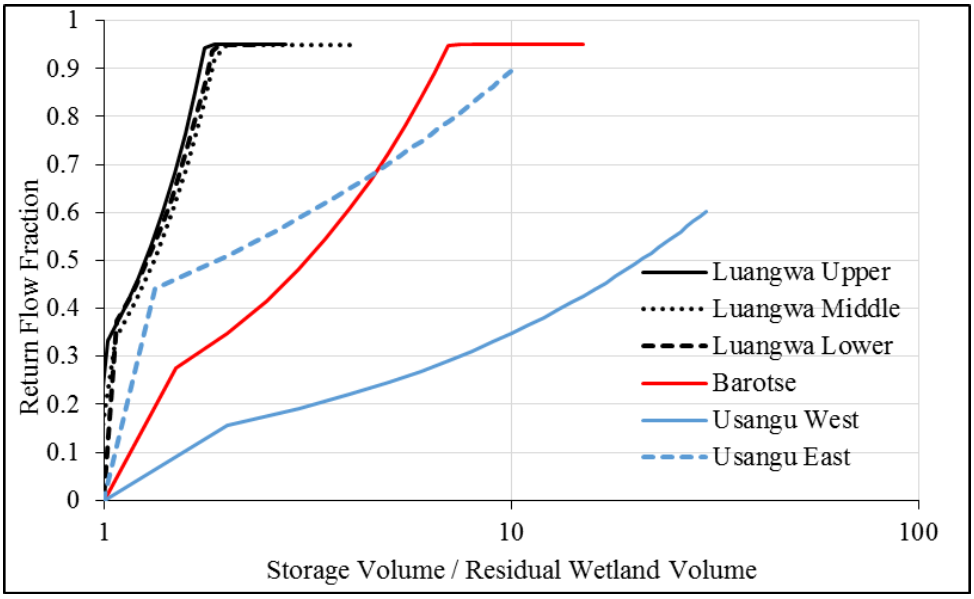

Figure 5.86: Return flows against standardised plot of the stored volume relative to the residual volume.

5.5 General discussions and conclusions

Each basin was divided into smaller units (sub-basins/sub-basin nodes) depending on their physical characteristics, mainly topography and slope. Sub-basins with more-or-less similar characteristics were grouped together using Principal Component Analysis (PCA). Sub-basins found in the same group were assumed to have similar hydrological responses, thus assigned similar parameter values. Basin physical characteristics were also used to derive parameters required in the model setup (both hydraulic and hydrological models). These data were obtained from global data sets, and are subject to a number of uncertainties due to their coarse resolution and/or temporal coverage and some of the derived physical characteristics could not reflect the real physical characteristics of the basin. However, this was the best information available for understanding the sub-basin physical characteristics and establishing parameter values for ungauged areas

Most of the upstream sub-basins were ungauged, and the wetland inflows required as upstream boundary conditions in the LISFLOOD-FP model were generated using the Pitman model. In general, the whole process of generating wetland inflows introduced uncertainties, as most of the available gauging stations are located downstream of the Luangwa and Barotse floodplains (i.e. include the wetland effects). For the Luangwa, a single gauging station was used to calibrate 24 upstream sub-basins nodes. In the Upper Zambezi River basin, apart from the downstream gauging station, one upstream sub-basin is gauged, yet it was not sufficient to calibrate all upstream sub-basins. Thus, the downstream gauging stations were mainly used to calibrate the model simulations in the two river basins for both structured and single run versions of the Pitman model. The structured version was run to provide likely behavioural parameter sets to be used in calibrating a single run model, but most of the parameters were not individually identifiable due to equifinality problems. Part of the problem is related to the difficulty of clearly defining some of the parameter ranges. The scatter plots of the CE and CE (ln) against an index (FT/POW + GW/GPOW) should assist in the establishment of some parameters which interact together to generate moderate and low flows. However, they were not very useful due to the limited information about basin physical characteristics that could be used to reject certain parameter combinations (See Figure 5.6 and 5.44 above). Despite these challenges, the number of simulated behavioural ensembles suggested that the simulations were reasonably good for generating inflows to the wetland.

Optimal ensemble sets (established using index: $CE + CE(ln) + 1/[ABS(PBIAS) + ABS(PBIAS\ (ln))]$) were used as the initial parameter sets for the setup of the single model run, and manually calibrated using any gauging station data. Simulated monthly flows were either over- or under-estimated in some years which could be related to either the quality of data used and/or assumptions made during setting up the model. For instance, the quality of the observed flows in the Luangwa River gauging station could be impacted by inadequate rating curves that are not often updated (Beilfuss and dos Santos, 2001). Initially, part of the uncertainties in the simulated wetland inflows was expected to be reduced when the estimated wetland parameters (using LISFLOOD-FP) were included in the revised setup of the Pitman model.

Disaggregation was used to obtain representative hydrographs of daily flows that can be used as upstream boundary conditions in the LISFLOOD-FP model. Parameter values suggested by previous studies (e.g. Hughes and Slaughter, 2015; Slaughter *et al*., 2015) were used to establish likely parameter values. The duration of high peaks correlated with what has been reported by some researchers, but generally the disaggregated daily flow magnitudes were not validated and some under/overestimation resulted. This is possibly because of the appropriateness of the parameters used, as well as errors carried over from the simulated monthly flows through the volume correction processes in the model. Generally, the flow patterns were appropriate enough to be used, especially in the Luangwa and Barotse as the key objective was to obtain possible representative flow patterns that could be used in the LISFLOOD-FP model.

The approach used to set up the LISFLOOD-FP model varied between the three wetlands. The Luangwa floodplain was divided into three sections and flows from the upper sections become upstream inflows to the next downstream section. The same was true for the Usangu wetlands which are naturally divided into two sections (western and eastern) by a narrow constriction at the centre (hydraulic control). Channel characteristics (locations and widths) were digitised from Google Earth images. However, this was easier for channels with large widths (especially in Luangwa and Barotse floodplains) than for small channels (widths < 10 m) such as those found in the Usangu wetlands and therefore, most of these small channels in Usangu were not included in the model setup. In areas where the channels were covered by dense vegetation, it was difficult to estimate the widths as well as establishing the channel location. For the Usangu, the setup process was not straightforward; the initial runs generated almost zero outflows and very small inundation extents and this prompted an increase in the simulated wetland inflows by a variable factor. Further, after several model runs, the results indicated that the model simulates more storage in the wetland at the end of the simulation (i.e. dry season) and insufficient outflow. This effect was assumed to be related to the influence of small channels (previously ignored in the model setup) on the inundation dynamics. To avoid the need to include all of the minor channels in the model setup, the simulated evaporative losses were increased and these additional volumes of water loss were assumed to represent drainage back to the main channel at the outlet and were manually added to the outflows at the end of the model run. This whole process is highly uncertain, but the approach improved the simulated inundation results in the Usangu wetlands.

The rapid rise of the hydrograph in the Luangwa floodplain could suggest that a large part of the floodplain gets inundated during the early months of the wet season. Most of the tributaries of the Luangwa River originate from steep escarpment areas that are expected to have quick responses to rainfall and promote early spills even before the Luangwa River overtops its banks. The Luangwa example illustrates that some large wetlands can have a minimal influence on the downstream flow (the difference between inflows and outflows in daily time scale was minimal). However, the Barotse floodplain significantly modifies the Zambezi River hydrographs in the Upper Zambezi River basin by reducing peak flows, delaying time to peak and stabilising or increasing downstream flows during the dry season. This is comparable to what was reported by other studies (World Bank, 2010; McCartney *et al*., 2013; Cai *et al*., 2016). The average monthly inundated area (about 5 500 km^2) is closely equivalent to the reported value by Turpie *et al*. (1999). The Usangu wetlands clearly have a major influence on the flow regime of the Great Ruaha River, although the results of the combined modelling approach used in this study were largely unsatisfactory. Area–storage and storage–inflow relationships form hysteresis curves but the shape of these curves varies across the three wetlands. Anticlockwise hysteresis curves are common in the floodplains (Luangwa and Barotse) and the inundation area during the rising limb is larger than during the recession for a given storage value, while different types of hysteresis were observed in the Usangu wetlands. The anticlockwise hysteresis observed in the Luangwa and Barotse floodplains is common in river–floodplain systems and have been observed in similar systems by other researchers (e.g. Rudorff *et al*., 2014a; Chen *et al*., 2015; Zhang and Werner, 2015). Standardised hysteresis curves indicated that the hysteresis effect increases with the increase in flood magnitude except in the western Usangu, and this could be associated with uncertainties in the model results. Moreover, the temporal fluctuation of the wetland inflows was found to have an influence on the shape of the hysteresis. The channel–wetland exchanges are complex in all three wetlands due to topographic and structure settings of the wetlands as well as fluctuations of the wetland inflows. In combination these influence the shape of the hysteresis curves.

The LISFLOOD-FP results present a major step in understanding channel-wetland exchanges and dynamics in the three wetlands. However, the observed inconsistencies of spatial distribution between inundated and non-inundated areas could be related to the accuracy of the SRTM DEM, boundary conditions, and land cover characteristics used in the model setup. The SRTM DEM data suffer from random noise effects (Rodriguez *et al*., 2006; Bates *et al*., 2014; Yan *et al*., 2015). Although the SRTM 90 m DEM used to represent the topographic characteristics was filtered to reduce noise effects, it is likely that there were still a number of pixels that could falsely affect the inundation extents. Moreover, Radar-based technology applied in the SRTM does not penetrate the water surface. Since this DEM was produced around February 2000, when water levels in some channels are almost at bankfull height, it is possible that the channel characteristics such as bed elevation could have been overestimated in some areas. Even though this effect was somewhat lowered by adjusting the values of channel roughness and hydraulic parameter (r), it is likely that there is an unresolved degree of uncertainty in the model results associated with this effect. In some sections especially where the main river or its tributaries was covered by vegetation, the width values were difficult to estimate, particularly in the eastern Usangu wetland. The vegetation bias in the SRTM 90 m DEM could have also contributed to the quality of simulated LISFLOOD-FP results and new datasets such as MERIT DEM (Yamazaki *et al*., 2017) could improve the simulation results. Generally, the results have indicated low values of Flood Area Index (FAI) during the dry season which could be related to wetting and drying ability of the LISFLOOD-FP model as pointed out by (Neal *et al*., 2012). In the Usangu and Luangwa wetland were the wetland were divided into more than one section there is possibility that back water effect (elevated downstream water levels tend to move upstream) have occurred. In addition, this effect could be more evident in the Usangu wetland where the two sides of the wetland are separated by elevated land at the centre and the outlet of the eastern wetland is controlled by hydraulic constriction. One of the solutions for this effect could be to transfer the downstream water levels to the upstream model as an outflow boundary condition to allow for this hydraulic effect rather than assuming the normal depth/slope at the downstream point.

Most of the final estimated Pitman wetland parameter values from the LISFLOOD-FP results reflect the characteristics of these wetlands. For example, a zero value of channel capacity for spillage and high value of spill factor in the Usangu wetland (eastern wetland, 1ka27) reflects the fact that the Great Ruaha River tends to disappear in the Ihefu swamp. The wetland residual volume in the Barotse floodplain system reflects the presence of isolated channels and backwater depressions found in its middle and lower parts. In the Luangwa floodplain, better results were obtained when the floodplain was set as a single unit compared to simulations of more than one wetland sections. This could possibly relate to the fact that the spreadsheet used to estimate Pitman wetland sub-model parameters did not account for the water transfer from the upstream to the next section downstream while the LISFLOOD-FP model does. This highlighted the important need to consider the effects of all water transfers in the wetland sub-model to accommodate the simulation of wetlands that involve more than one section.

In general terms, the results from the LISFLOOD-FP model assisted the establishment of wetland parameters and an assessment of the structure of the wetland sub-model. The Luangwa example (mostly because of its high level of channel-floodplain connectivity), suggested a modification of the structure of the Pitman wetland sub-model to allow for return flows to occur at any time and not be limited by high water levels in the main channel. Overall, the revised setups of the Pitman model, with the wetland sub-model parameters included, improved the model results, particularly in Luangwa and Barotse river basins and the following can be concluded:

- ❖ The influence of the Luangwa floodplain on downstream flow regime is almost negligible on a monthly time scale, whereas the Barotse floodplain significantly influences the downstream flow regime.
- ❖ There is still a high degree of unresolved uncertainty in the simulated results for the Upper Great Ruaha River basin which could be related to the limited information/data used to set up the LISFLOOD-FP model. Additional field data collection could improve the model results.
- ❖ Despite the improvement in the model results for the three river basins after inclusion of the estimated wetland parameters in the Pitman model setup, data availability to force both LISFLOOD-FP and the Pitman model could lead to better results in modelling river basins containing large wetlands in Africa.

- The degree of equifinality when using the structured uncertainty version of the model is high, and the recent uncertainty approach applied with the Pitman hydrological model that uses hydrological signatures as model constraints to quantify possible parameter sets is recommended for future studies (Hughes, 2015a; Mohobane, 2015; Tumbo and Hughes, 2015; Ndzabandzaba and Hughes, 2017).

CHAPTER SIX: CONCLUSIONS AND RECOMMENDATIONS

6.1 Conclusions

The current study aimed to improve water resources assessment modelling of data-scarce African river basins that include large wetlands. This was achieved through a combined modelling approach that includes the use of the high-resolution LISFLOOD-FP hydraulic model to establish an in-depth understanding of channel–wetland exchanges and wetland dynamics to estimate the wetland parameters required for the basin-scale Pitman hydrological model. The final model results, with the wetland parameters included in the model, were used to quantify the impacts of wetlands on flow river regimes. Due to the fact that different types of wetlands are expected to function (and impact) differently, three river basins that include large wetland areas within southern Africa were considered as case studies. The interpretation of the different parameter values in relation to the physical characteristics of the three wetlands are expected to be of value for the estimation of wetland parameters for other wetlands, although this was not directly assessed during the study. The following can be concluded from this study:

6.1.1 Establishment of wetland inflows

The basin physical characteristics derived from global datasets can be used for similarity analysis (grouping sub-basins with similar characteristics), and establishing some model parameters. However, due to their low spatial resolutions and accuracy, it is likely that some of the basin characteristics were not well represented. Complex basin processes such as those related to groundwater movement (recharge and discharge) are mostly not known, and the groundwater parameter ranges used in the setup of the model were largely uncertain. Generally, with a limited amount of information related to basin characteristic, initial parameter ranges used in the uncertainty model were difficult to estimate. A higher degree of equifinality was observed in the uncertainty model results, despite the fact that the number of behavioural ensembles were reasonably good. The scatter plots (see Figure 5.5 and 5.43) indicated a wide range of likely parameter values and this is a reflection that the basin physical information was not sufficient to establish the possible parameter ranges and it can be concluded that the parameter ranges used in the model setup determine the possible estimated parameter values. Regardless of such difficulties, the results were quite satisfactory for generating wetland inflows.

The initial setup of the GW Pitman model for Luangwa and Upper Zambezi River basins to generate wetland inflows were evaluated using downstream gauging stations that include wetland effects. The results highlighted that in such situations, it is important to understand the likely impacts of each wetland on the downstream flow regime as these impacts largely influence the model results. However, this is not always possible because of the limited information related to wetland dynamics. There is a need to establish reliable gauging stations in rivers that contribute to wetland inflows.

The disaggregation sub-model proved to be useful to link a monthly time-scale hydrological model with the detailed hydraulic model that operates on a daily time-scale, despite the lack of observed information that can be used to validate the disaggregated daily flows. The simulated daily flows were considered appropriate to be used as upstream boundary conditions in the LISFLOOD-FP model. Generally, uncertainty in the disaggregated daily flows is related to the quality of the simulated monthly flows as well as the rainfall data used in the disaggregation processes.

6.1.2 Understanding the wetland–channel exchange processes and quantification of the wetland parameters of the basin-scale model

The study demonstrated that amongst other factors, wetland characteristics (i.e. complex topographical and structural settings) as well as flood magnitude, determine the inundation dynamics in wetlands. Moreover, small channels such as those found in the Usangu wetlands despite their size, could have influence on the inundation dynamics of the Usangu wetlands. Conversely, the nature of connectivity between the floodplain features and channels in the Luangwa allows channel spills and drainage back to the channel to occur simultaneously. Most of Luangwa River's tributaries originate from high escarpment areas that allow different areas of the floodplain to become inundated even at the early stage of the wet season. Simulated inundation results indicated meaningful hysteresis curves in the area–storage and storage–inflow relationships, but the size and shape of these curves varied across the wetland types and with flood magnitude. An anticlockwise hysteresis type was observed in the area–storage and storage–inflow relationships for the Luangwa and Barotse floodplains, while there appeared to be no dominant type of hysteresis curve for the Usangu depression wetland. For the anticlockwise hysteresis, when the river starts to spill, the inundation area increases quickly as the water spreads across the floodplain, and during the recession flooding extent decreases until only ponding remains in depressions/oxbows and other abandoned channels. The counter-clockwise hysteresis type found in the Luangwa and Barotse floodplains has also been observed in other river–floodplain systems by some researchers (e.g. Rudorff *et al*., 2014a; Chen *et al*., 2015; Zhang and Werner, 2015).

In the Usangu wetlands, the largest inundation area and storage occurred after the peak discharge. The same was true for the Barotse floodplain. Amongst other factors, this could be related to complex exchange processes attributed by spatial heterogeneity of the lateral movement of floodwater in these areas. Standardised hysteresis curves confirmed the increase of hysteresis effects with an increase in flood magnitude. Moreover, temporal fluctuation of the wetland inflows strongly influences the hysteresis size and mostly increases the hysteresis effect. Generally, the distinct hysteresis curves in floodplains and depression wetlands, respectively, are a reflection of complex channel–wetland exchanges and vary considerably with wetland type, as well as within a given wetland (somewhat different curves were observed in the upper, middle and lower sections of the Luangwa floodplain). Hysteresis curves are evident in large wetlands and thus, it is recommended that they should be incorporated into models that are used in water resource assessments, including assessment of floods and river ecosystems.

Daily inflow–outflow relationships indicated a significant peak reduction, as well as a delayed time to peak of several weeks in the Barotse floodplain and Usangu wetlands, while the impacts of the Luangwa floodplain on the Luangwa River are minimal even on a daily time scale. This implies that the Barotse and Usangu wetlands could play a more important role in reducing the impacts of flood events than the Luangwa. Furthermore, the Luangwa is an example of a large linear floodplain that has minimal flow attenuation effects, even at the daily time-scale.

Although there are unresolved uncertainties in the LISFLOOD-FP results, the model results provide useful information to establish wetland parameters as well as to assess and improve the structure of Pitman wetland sub-model. The simple spreadsheet used to estimate wetland parameters did not account for the wetland (rather than channel) water transfers from the upstream to the next section downstream (the condition that is included in the LISFLOOD-FP model) when the floodplains were divided into more than one section. This restricted the value of the spreadsheet for estimating the parameter values and in future studies a method allowing for the upstream wetland inflows as well as the channel inflows should be included. The same situation applies to the Pitman model structure and the only way in which a downstream transfer of water can be modelled is through return flows to the channel. It is therefore necessary to be very careful how the Pitman model is set up if a single wetland is distributed across more than one sub-basin.

6.1.3 Re-calibration of the basin-scale model with a channel–wetland exchange function included

Statistical objective functions indicated an improvement in the model simulation results when the estimated wetland parameters (by the LISFLOOD-FP model) were included in the Pitman model setup, particularly in the Luangwa and Barotse river basins. The Luangwa River basin illustrated the importance of allowing the return flows to occur at any time in the model. The physical characteristics (and simulated inundation dynamics) in Luangwa highlighted that channel spillage and drainage back to the channel can occur simultaneously. The earlier version of the model restricted return flows when the amount of water in the channel exceeded the channel spill capacity parameter, and after the modification, the simulated results in the Luangwa River basin were improved. Generally, the impacts of the Luangwa floodplain on the downstream flow regime are very small, especially at the monthly time scale, whereas the Barotse floodplain system and the Usangu wetlands significantly regulate the flows of the Zambezi River and the Great Ruaha River, respectively. These findings are important for both practical and research purposes in these river basins. The minimal influence of the Luangwa floodplain is consistent with reports that flooding from the Luangwa River reaches the Zambezi River (western end of the Cahora Bassa Dam) within a few days and almost at the same magnitude as reported by several researchers (e.g. Beilfuss, 2012; Kling *et al*., 2014). Beilfuss (2012) argued that the natural flooding patterns within the Cahora Bassa Dam resemble that of the Luangwa River.

The understanding of the role played by the Barotse floodplain could be important for the operation of Kariba Dam as well as a recently proposed hydro-electric power plant at Ngonye Falls (located approximately 50 km downstream of the Barotse wetland). Additionally, this information could be useful for the Lozi people living and benefiting from ecological goods and services in the floodplain as they will be able to understand the possible duration over which the floodplain is inundated during wet or dry years. In the Upper Great Ruaha River basin, although the results are somewhat encouraging (the wetlands have significant impacts on the Great Ruaha River), there is still a need for further improvement of model performance and this will only be possible with additional field data collection.

This study demonstrated the potential of the combined modelling approach towards the improvements of model parameterisation (and structure). In fact, it presents a first attempt to estimate wetland parameters of the basin scale model (the Pitman) from a detailed hydraulic model (LISFLOOD-FP) in the large ungauged river basins in southern Africa. Given the fact that the two models were forced under limited data conditions, the results are informative enough to be used for both research and practical purposes.

6.1.4 Regionalisation of the estimated wetland parameters

Most of the wetland parameters were either estimated directly or reflect the type of wetland that is being modelled. Relative residual storage in Luangwa reflected the volume of water that remains in oxbows and other cut-off channels that are close to the main river. Likewise, in the Barotse the residual wetland storage is very small compared to the huge volume of water that inundates this floodplain. The channel spill factor and channel capacity for spillage in Usangu agree with its characteristics in that the large value of the spill factor and a zero value for channel capacity for spillage in the eastern wetlands reflects the fact that there are no major channels passing through the wetland. The study highlighted the possibility of interpreting some of the wetland parameters physically, while others such as those related to non-linear return flow and the area–volume relationships are still difficult to interpret. Perhaps, more than one wetland in each wetland type would have improved the regionalisation processes as the estimated parameters could have been compared for wetlands in the same category before concluding on the likely possible parameter ranges for each wetland type. However, the limited time resources available during this study precluded the inclusion of more wetlands.

6.2 Recommendations

6.2.1 Simulation of wetland inflows

- To account for the equifinality problem, future studies should use the recent uncertainty approach applied with the Pitman hydrological model. It uses hydrological signatures to quantify possible parameter sets. These hydrological signatures which are used as model constraints do not rely only on the observed flow data, and hence can be applied even in ungauged river basins. So far this version of the model has been successfully applied in some studies (Hughes, 2015a; Mohobane, 2015; Tumbo and Hughes, 2015; Ndzabandzaba and Hughes, 2017).

- ❖ The quality of simulated flows depends on the climatic data inputs (i.e. rainfall, evapotranspiration), the parameters and observed flows used for calibration or validation. In these data scarce basins, the model was forced using data derived from global datasets which are subject to uncertainty related to spatial resolution and temporal coverages. To improve the model simulations, data from different datasets should be assessed before being used in the model setup.
- ❖ For basins containing substantial wetland areas, the inflows and outflows should be gauged (i.e. upstream and downstream) to improve quantification of the wetland storage. Conversely, if the wetland receives water from several main tributary rivers these should also be gauged. Above all, it is advisable that there should be an improvement in data collection and monitoring including the establishment of gauging networks in ungauged rivers. Rating curves should also be periodically updated, especially for rivers affected by sedimentation and fluctuating bed levels. It is likely that without adequate observational data, research findings will remain uncertain and so will their applications.

6.2.2 Simulation of wetland inundation characteristics

- ❖ Since the LISFLOOD-FP is a raster-based model and a DEM is used to represent the topographical characteristics in the wetland, DEM accuracy should be considered to minimise errors in the model results. Moreover, for wetlands covered with dense vegetation, vegetation bias should be reduced in the DEM as this tends to affect the model simulation results (e.g. inundation extents, water depths), and a number of no-fee vegetation corrected DEMs have been released recently (e.g. O'Loughlin *et al*., 2016; Yamazaki *et al*., 2017; Allen and Pavelsky, 2018; Zhao *et al*., 2018).
- ❖ For a wetland that receives inflows from rivers of different sizes, the major channels should be identified, and well-represented in the model setup. Poor representation of the channel location and size in the DEM could affect the spatial distribution of the inundation results. Furthermore, the study demonstrated the importance of representing small channels in some wetlands such as the Usangu. Thus, an assessment of these channels should, if possible, be done prior to setting up of a model to identify whether they influence wetland inundation dynamics.
- ❖ The study identified the importance of assessing the freely available global river widths datasets before applying them. The initial assessment of the Global River

Bankfull Width and Depth dataset by Andreadis *et al*. (2013) revealed that most of the channel locations, width and depth values estimated in this dataset did not match with the locations observed from the 90 m SRTM DEM as well as the higher resolution Google Earth images. One of this could be how most of these values were estimated in African rivers; the downstream river widths are applied to their upstream tributaries, resulting in rivers being too wide. Whenever possible, future studies should emphasise the use of high-resolution images to estimate river location and widths, as suggested by Schumann *et al*. (2013).

6.2.3 Pitman wetland parameter estimations and revision of the GW Pitman model

The approach applied in the current study depends on the validity of the simulation results from the hydraulic model as these results were used to establish the wetland parameters for the simulations using the Pitman model. The approach is not limited to the combination of the LISFLOOD-FP and Pitman models, and different model combinations can be used to achieve a similar study purpose.

6.2.4 Recommendations for further studies

- ❖ Future studies should apply the estimated wetland parameters in related/similar wetlands to see whether they can give appropriate results.
- ❖ Future studies may investigate different model combinations or how the Pitman model can be combined with other types of hydraulic models to achieve similar purposes.
- ❖ In the present study, the LISFLOOD-FP model was validated using low-resolution satellite images. For future studies, the use of high-resolution images to calibrate and validate the model results is recommended.
- ❖ The wetland function does not include exchanges with groundwater in the current version of the Pitman wetland sub-model. However, groundwater-wetland interactions might be significant in other wetlands. Therefore, future modifications of the Pitman wetland sub-model structure should consider including a groundwater-wetland function to increase its applicability to such wetlands. The same is true for the LISFLOOD-FP model, which does not include a groundwater component in its structure.

- Use of additional field data related to exchange dynamics to refine the model setup of the Upper Great Ruaha River basin is recommended in future studies.

REFERENCES

Abbaspour, K., 2015. *SWAT-Calibration and uncertainty programs (CUP)*, Available at: http://www.neprashtechnology.ca/wp-content/uploads/2015/06/Usermanual_SwatCup.pdf.

Abbaspour, K.C., Johnson, C.A. and van Genuchten, M.T., 2004. Estimating Uncertain Flow and Transport Parameters Using a Sequential Uncertainty Fitting Procedure. *Vadose Zone Journal*, 3(4), p.1340.

Abbaspour, K.C., Yang, J., Maximov, I., Siber, R., Bogner, K., Mieleitner, J., Zobrist, J., Srinivasan, R., 2007. Modelling hydrology and water quality in the pre-alpine/alpine Thur watershed using SWAT. *Journal of Hydrology*, 333(2–4), pp.413–430.

Acreman, M. and Holden, J., 2013. How wetlands affect floods. *Wetlands*, 33(5), pp.773–786.

Acreman, M.C. and Miller, F., 2007. Hydrological impact assessment of wetlands. In: Ragone S, Hernández-Mora N, de la Hera A, Bergkamp G, McKay J (eds) The global importance of groundwater in the 21st century. *Proceedings of the International Symposium on Groundwater Sustainability (ISGWAS),* National Groundwater Association Press, Ohio pp.225–255.

Aghakouchak, A., Habib, E. and Bárdossy, A., 2010. Modeling Radar Rainfall Estimation Uncertainties : *Journal of Hydrologic Engineering*, 15(4), pp.265–274.

Ajami, N.K., Duan, Q. and Sorooshian, S., 2007. An integrated hydrologic Bayesian multimodel combination framework: Confronting input, parameter, and model structural uncertainty in hydrologic prediction. *Water Resources*, 43 (W01403), pp.1–19.

Alexander, L.C., Autrey, B., DeMeester, J., Fritz, K.M., Goodrich, D.C., Kepner, W.G., Lane, C.R., LeDuc, S.D., Leibowitz, S.G., McManus, M., Pollard, A.I., Raanan-Kiperwas, H., Ridley, C.E., Schofield, K. and Wigington, P.J., 2015. Connectivity of Streams and Wetlands to Downstream Waters: A Review and Synthesis of the Scientific Evidence, U.S. Environmental Protection Agency, Washington, DC p331.

Ali, G., Tetzlaff, D., Soulsby, C., McDonnell, J.J. and Capell, R., 2012. A comparison of similarity indices for catchment classification using a cross-regional dataset. *Advances in Water Resources*, 40, pp.11–22.

Allen, G.H and Pavelsky, T.M., 2018. Global Extent of Rivers and Streams. *Science*, 361(6402), 585-588.

Allen, R.G., Pereira, L.S., Raes, D. and Smith,M., 1998. Crop evapotransipration: Guidelines for computing crop water requirements, FAO Irrigation and Drainage Paper 56, Food and Agriculture Organization of the United Nations, Rome, Italy.

Allen, R.G., Pereira, L.S., Howell, T.A. and Jensen, M.E., 2011. Evapotranspiration information reporting: I. Factors governing measurement accuracy. *Agricultural Water Management*, 98(6), pp.899–920.

Allen, Y., 2015. Landscape Scale Assessment of Floodplain Inundation Frequency using

Landsat Imagery. *River res. Applic*, 32(7), pp.1609–1620.

Alsdorf, D., Bates, P., Melack, J., Wilson, M. and Dunne, T., 2007. Spatial and temporal complexity of the Amazon flood measured from space. *Geophysical Research Letters*, 34(8), pp.1–5.

Amarnath, G., Umer, Y M., Alahacoon, N. and Inada, Y., 2015. Modelling the flood-risk extent using LISFLOOD-FP in a complex watershed: Case study of Mundeni Aru River Basin, Sri Lanka. *International Association of Hydrological Sciences*, 370(131), pp.131–138.

Amoros, C. and Bornette, G., 2002. Connectivity and biocomplexity in waterbodies of riverine floodplains. *Freshwater Biology*, 47(4), pp.761–776.

Andersen, J., Refsgaard, J.C. and Jensen, K.H., 2001. Distributed hydrological modelling of the Senegal River Basin - Model construction and validation. *Journal of Hydrology*, 247(3–4), pp.200–214.

Anderson, R.M., Koren, V.I. and Reed, S.M., 2006. Using SSURGO data to improve Sacramento Model a priori parameter estimates. *Journal of Hydrology*, 320(1–2), pp.103–116.

Andersson, J.C.M., Pechlivanidis, I.G., Gustafsson, D., Donnelly, C. and Arheimer, B., 2015. Key factors for improving large-scale hydrological model performance. *European Water*, 49, pp.77–88.

Andersson, L., Wilk, J., Todd, M. C., Hughes, D. A., Earle, A. and Kniveton, D., 2006. Impact of climate change and development scenarios on flow patterns in the Okavango River. *Journal of Hydrology*, 331(1), pp.43-57.

Andreadis, K.M., Schumann, G.J.P. and Pavelsky, T., 2013. A simple global river bankfull width and depth database. *Water Resources Research*, 49(10), pp.7164–7168.

Ao, T., Ishidaira, H., Takeuchi, K., Kiem, A.S., Yoshitari, J., Fukami, K. and Magome, J., 2006. Relating BTOPMC model parameters to physical features of MOPEX basins. *Journal of Hydrology*, 320(1), pp.84–102.

Arnold, J.G., Allen, P.M. and Bernhardt, G., 1993. A comprehensive surface-groundwater flow model. *Journal of Hydrology*, 142(1–4), pp.47–69.

Arnold, J.G., Srinivasan, R., Muttiah, R.S. and Williams, J R., 1998. Large area hydrologic modeling and assesment Part I: Model development. *JAWRA Journal of the American Water Resources Association*, 34(1), pp.73–89.

Arnold, J.G., Arnold, J.G., Moriasi, D.N., Gassman, P.W., Abbaspour, K.C., White, M.J., Srinivasan, R., Santhi, C., Harmel, R.D., Van Griensven, A., VanLiew, M.W., Kannan, N. and Jha, M., 2012. Swat: Model Use, Calibration, and Validation. *Asabe*, 55(4), pp.1491–1508.

Arora, V.K., 2002. The use of the aridity index to assess climate change effect on annual runoff. *Journal of Hydrology*, 265(1–4), pp.164–177.

Ashton, P.J., Love, D., Mahachi, H. and Dirks, P.H.G.M., 2001. An Overview of the Impact of Mining and Mineral Processing Operations on Water Resources and Water Quality in the Zambezi, Limpopo and Olifants Catchments in Southern Africa. Contract Report to the Mining, Minerals and Sustainable Development (South Africa) Project, CSIR Environmentek, Pretoria, South Africa and Geology Department, University of Zimbabwe, Harare, Zimbabwe. Report No. ENV-P-C 2001-042, p336.

Astle,W.L., Webster, R. and C. J. Lawrance., C.J., 1969. Land Classification for Management Planning in the Luangwa Valley of Zambia. *Journal of Applied Ecology,* 6(2), pp.143-169.

Awange, J.L., Ferreira, V.G., Khandu., Andam-Akorful, S.A., Agutu, N.O. and He, X.F., 2016. Uncertainties in remotely sensed precipitation data over Africa. *International Journal of Climatology*, 36(1), pp.303–323.

Bárdossy, A. and Singh, S.K., 2008. Robust estimation of hydrological model parameters. *Hydrology and Earth System Sciences*, 12(6), pp.1273–1283.

Beck, J.S. and Basson, G.R., 2008. Klein River Estuary (South Africa): 2D numerical modelling of estuary breaching. *WaterSA*, 34(1), pp.33–38.

Bates, P. and De Roo, A.P., 2000. A simple raster-based model for flood inundation simulation. *Journal of Hydrology*, 236(1–2), pp.54–77.

Bates, P.D., Horritt, M.S. and Fewtrell, T.J., 2010. A simple inertial formulation of the shallow water equations for efficient two-dimensional flood inundation modelling. *Journal of Hydrology*, 387(1–2), pp.33–45.

Bates, P.D., Neal, J.C. and Alsdorf, D., 2014. Observing Global Surface Water Flood Dynamics. *Surv Geophys*, 35(3), pp.839–852.

Bauer, P., Kinzelbach, W., Babusi, T., Talukdar , K. and Baltsavias., E., 2002. Modeling concepts and remote sensing methods for sustainable water management of the okavango delta , Botswana. *ISPRS Commission VI Workshop "Developments and Technology Transfer in Geomatics for Environmental and Resource Management" held in Dar es Salaam, Tanzania, March 25-28, 2002. The International Archives of the Photogrammetry, Remote Sensing and Spatial Information Sciences,* 34(6/W6), pp.136–143.

Baugh, C.A., Bates, P.D., Schumann, G. and Trigg, M.A., 2013. SRTM vegetation removal and hydrodynamic modeling accuracy. *Water Resources Research,* 49(9), pp.5276–5289.

Beilfuss, R., 2012. A Risky Climate for Southern African Hydro. Assessing Hydrological Risks and Consequences for Zambezi River Basin Dams. International Rivers, Berkeley, CA, USA, p60.

Beilfuss, R.D., Dutton, P. and Moore, D., 2000. Land cover and land use change in the Zambezi Delta. I*n Biodiversity of Zambezi Basin Wetlands Volume III. Land Use Change and Human Impacts. Consultancy Report for IUCN ROSA, Chapter 2,* Bulawayo Foundation for Africa and Harare: The Zambezi Society, pp.31–105.

Beilfuss, R and Dos Santos, D., 2001. Patterns of hydrological change in the Zambezi Delta, Mozambique, Working Paper 2, Program for the Sustainable Management of Cahora

Bassa Dam and The Lower Zambezi Valley Report, International Crane Foundation, Sofala, Mozambique, p89.

Berkowitz, J.F. and White, J.R., 2013. Linking Wetland Functional Rapid Assessment Models with Quantitative Hydrological and Biogeochemical Measurements across a Restoration Chronosequence. *Soil Sci. Soc. Am. J.*, 77(4), pp.1442–1451.

Beven, K., 1989. Changing ideas in hydrology—the case of physically-based models. *Journal of Hydrology,* 105(1), pp.157-172.

Beven, K., 2006. Searching for the Holy Grail of scientific hydrology: Qt=(S, R, Δt)A as closure. *Hydrology and Earth System Sciences*, 10(5), pp.609–618.

Beven, K., 2016. Facets of uncertainty: epistemic uncertainty, non-stationarity, likelihood, hypothesis testing, and communication. *Hydrological Sciences Journal*, 61(9), pp.1652–1665.

Beven, K.J., 2005. On the concept of model structural error. *Technology*, 52(6), pp.167–175.

Beven, K.J. and Binley A.M., 1992. The future of distributed models: Model calibration and uncertainty prediction. *Hydrological Processes*, 6(3), pp.279–298.

Beven, K.J. and Freer, J., 2001. A dynamic TOPMODEL. *Hydrological Processes*, 15(10), pp.993–2011.

Beven, K.J., Smith, P.J. and Freer, J.E., 2008. So just why would a modeller choose to be incoherent? *Journal of Hydrology*, 354(1–4), pp.15–32.

Beyer, M., Wallner, M., Bahlmann, L., Thiemig, V., Dietrich, J. and Billib, M., 2016. Rainfall characteristics and their implications for rain-fed agriculture: a case study in the Upper Zambezi River Basin. *Hydrological Sciences Journal*, 61(2), pp.321–343.

Bharati, L. and Gamage, N., 2011. Application of the Pitman Model to Generate Discharges for the Lhasa Basin , China Model setup in the Koshi basin. *Hydro Nepal: Journal of Water, Energy and Environment*, 7, pp.30–34.

Biancamaria, S., Bates, P.D., Boone, A. and Mognard, N.M., 2009. Large-scale coupled hydrologic and hydraulic modelling of the Ob river in Siberia. *Journal of Hydrology*, 379(1–2), pp.136–150.

Bishop, M.P., Shroder, J.F., Bonk, R. and Olsenholler, J., 2002. Geomorphic change in high mountains: A western Himalayan perspective. *Glob Planet Change*, 32(4), pp.311–329.

Blasone, R.-S., Vrugt, J.A., Madsen, H., Rosbjerg, D., Robinson, B.A. and Zyvoloski, G.A., 2008a. Generalized likelihood uncertainty estimation (GLUE) using adaptive Markov Chain Monte Carlo sampling. *Advances in Water Resources*, 31(4), pp.630–648.

Blasone, R.-S., Madsen, H. and Rosbjerg, D., 2008b. Uncertainty assessment of integrated distributed hydrological models using GLUE with Markov chain Monte Carlo sampling. *Journal of Hydrology*, 353(1–2), pp.18–32.

Bloschl, G., 2005. Rainfall-runoff modeling of ungauged catchments. *Encyclopedia of Hydrological Sciences*, pp.1–19.

Bontemps, S., Defourny, P., van Bogaert, E., Arino, O., Kalogirou, V. and Ramos, J., 2011, GlobCover 2009-Products description and validation report, 2.2, ESA GlobCover project, p53.

Boyle, D.P., Gupta, H. V. and Sorooshian, S., 2000. Toward improved calibration of hydrologic models: Combining the strengths of manual and automatic methods. *Water Resources Research*, 36(12), pp.3663–3674.

Bravo, J.M., Allasia, D., Paz, A.R., Collischonn, W. and Tucci, C.E. M., 2012. Coupled Hydrologic-Hydraulic Modeling of the Upper Paraguay River Basin. *Journal of Hydrologic Engineering*, 17(5), pp.635–646.

Broxton, P.D., Zeng, X., Sulla-Menashe, D. and Troch, P.A., 2014. A global land cover climatology using MODIS data. *Journal of Applied Meteorology and Climatology*, 53(6), pp.1593–1605.

Budyko, M.I., 1974. Climate and life, Academic Press, Orlando, New York, p508.

Bullock, A. and Acreman, M., 2003. The role of wetlands in the hydrological cycle. *Hydrology and Earth System Sciences*, 7(3), pp.358–389.

Butts, M.B., Payne, J.T., Kristensen, M. and Madsen, H., 2004. An evaluation of the impact of model structure on hydrological modelling uncertainty for streamflow simulation. Journal of Hydrology, 298(1–4), pp.242–266.

Bytheway, J.L. and Kummerow, C.D., 2013. Inferring the uncertainty of satellite precipitation estimates in data-sparse regions over land. *Journal of Geophysical Research Atmospheres*, 118(17), pp.9524–9533.

Channan, S., Collins. and Emanuel, W.R., 2014. Global mosaics of the standard MODIS land cover type data. University of Maryland and the pacific Northwest National Laboratory, College Park, Maryland, USA.

Canisius, F., Turral, H. and Mbilinyi, B.P., 2011. Analysis of seasonal land use in Usangu wetlands, Tanzania: an object-oriented technique for multi-temporal analysis with high-resolution data. *International Journal of Remote Sensing*, 32(7), pp.1885-1900.

Chang, H., Yun, C., Wu, J. and Yu, J., 2012. Detecting floodplain inundation frequency using MODIS time-series imagery. *1st International Conference on Agro-Geoinformatics, Agro-Geoinformatics held on 2-4 2012, Shangai China*, pp.349–354.

Chen, L., Jin, Z., Michishita, R., Cai, J., Yue, T., Chen, B. and Xu, B., 2014. Dynamic monitoring of wetland cover changes using time-series remote sensing imagery. *Ecological Informatics*, 24, pp.17–26.

Chen, X., Chen, L., Zhao, J. and Yu, Z., 2015. Modeling the hydrodynamic interactions between the main channel and the floodplain at McCarran Ranch in the lower Truckee River , Nevada. *Nat. Hazards Earth Syst. Sci*, 15(9), pp.2161–2172.

Chen, Y., Huang, C., Ticehurst, C., Merrin, L. and Thew, Peter., 2013. An evaluation of MODIS daily and 8-day composite products for floodplain and wetland inundation mapping. *Wetlands*, 33(5), pp.823–835.

Chesworth, W., Arbestain, M.C., Macias, F. and Spaargeren, O., 2016. Cambisols, Encyclopidia of Soil Science, Springer Dordrecht, Berlin, Heidelberg, New York.

Chow, V.T., 1959. Open Channel Hydraulics, MacGraw-Hill, New York.

Christensen, S., 2004. A synthetic groundwater modelling study of the accuracy of GLUE uncertainty intervals. *Hydrology Research*, 35(1), pp.45–59.

Clilverd, H.M., Thompson, J.R., Heppell, C.M., Axmacher, J.C., Sayer, C.D. and Axmacher, J.C., 2013. River – floodplain hydrology of an embanked lowland Chalk river and initial response to embankment removal. *Hydrological Sciences Journal*, 58(3), pp.627–650.

Coe, M.T., Costa, M.H. and Howard, E.A., 2008. Simulating the surface waters of the Amazon River basin: impacts of new river geomorphic and flow parameterizations Michael. *Hydrol. Process.*, 22(14), pp.2542–2553.

Cohen, S., Willgoose, G. and Hancock, G., 2008. A methodology for calculating the spatial distribution of the area-slope equation and the hypsometric integral within a catchment. *Journal of Geophysical Research: Earth Surface*, 113(3), pp.1–13.

Confesor, R.B. and Whittaker, G.W., 2007. Automatic Calibration of Hydrologic Models With Multi-Objective Evolutionary Algorithm and Pareto Optimization1. *JAWRA Journal of the American Water Resources Association*, 43(4), pp.981–989.

Conway, 2009., Persechino, A., Ardoin-bardin, S., Hamandawana, H., Dieulin, C. and Mahe, G. Rainfall and Water Resources Variability in Sub-Saharan Africa during the Twentieth Century. *American Meteorological Society*, 10, pp.41–59.

Coulthard, T.J., Ramirez, J.A., Barton, N., Rogerson, M. and Brücher, T., 2013. Were rivers flowing across the Sahara during the last interglacial? Implications for human migration through Africa. *PloS one*, 8(9), p.1-12.

Coxon, G., Freer, I.K.W., Wagener, T., Woods, R. and Smith, PJ., 2015. A novel framework for discharge uncertainty quantification applied to 500 UK gauging stations. *Water Resources Research*, 51(7), pp.5531–5546.

Curie, F., Gaillard, S., Ducharne, A. and Bendjoudi, H., 2007. Geomorphological methods to characterise wetlands at the scale of the Seine watershed. *The Science of the total environment*, 375(1–3), pp.59–68.

Czgani, S., Pirkhoffer, E., Halmai, Á. Lóczy, D., 2016. Application of MIKE 21 in a multi-purpose floodway zoning along the lower Hungarian Drava section. *REVISTA DE GEOMORFOLOGIE*, 18, pp.1–14.

Dahri, Z.H., Ludwig, F., Moors, E., Ahmad, B., Khan, A. and Kabat, P., 2016. An appraisal of precipitation distribution in the high-altitude catchments of the Indus basin. *Science of the Total Environment*, 548–549, pp.289–306.

Dams, J., Batelaan, O., Nossent, J. and Chormanski, J., 2009. Improving hydrological model parameterisation in urbanised catchments: Remote sensing derived impervious surface cover maps. *Water and Urban Development Paradigms*, pp.405–410.

Dawson, C. and Mirabito, C.M., 2008. The Shallow Water Equations (SWE). Institute for Computational Engineering and Sciences University of Texas at Austin, USA.

Day, G., Dietrich, W.E., Rowland, J.C. and Marshall, A., 2008. The depositional web on the floodplain of the Fly River, Papua New Guinea. *Journal of Geophysical Research: Earth Surface*, 113(1), pp.1–19.

De Almeida, G.M. and Bates, P., 2013. Applicability of the local inertial approximation of the shallow water equations to flood modeling. *Water Resources Research*, 49(8), pp.4833–4844.

Dennis, I. and Dennis, R., 2012. Climate change vulnerability index for South African aquifers. *Water SA*, 38(3), pp.417–426.

DHI, 2004. The MIKE SHE User Reference. DHI Water and Environment, Horsholm, Denmark, p.462.

DHI, 2007. MIKE 21 FLOW MODEL Hydrodynamic Module Step-by-step training guide, p.120.

Di Baldassarre, G. and Montanari, A., 2009. Uncertainty in river discharge observations: A quantitative analysis. *Hydrol. Earth Syst. Sci*, 13(6), pp.913–921.

Dingman, S.L. and Sharma, K.P., 1997. Statistical development and validation of discharge equations for natural channels. *Journal of Hydrology*, 199(1–2), pp.13–35.

Dixon, J.W., 2014. Geomorphic characteristics of small seeps and fens in a glaciated landscape. *Landform Analysis*, 27, pp.15–25.

Domeneghetti, A. (2016). On the use of SRTM and altimetry data for flood modeling in data-sparse regions. *Water Resources Research*, 52, pp.2901–2918.

Droogers, P. and Allen, R.G., 2002. Estimating reference evapotranspiration under naccurate data conditions. *Irrigation and drainage systems*, 16(1), pp.33–45.

Du, B., Arnold, J.G., Saleh, A. and Jaynes, D.B., 2005. Development and Application of Swat To Landscapes With Tiles and Potholes. *Transactions of the ASAE*, 48(3), pp.1121–1133.

Duan, Q., Sorooshian, S. and Gupta, V., 1992. Effective and efficient global optimization for conceptual rainfall-runoff models. *Water Resour. Res*. 28 (4), pp.1015–1031.

Duan Q., Schaake J., Andreassian V., Franks S. and Goteti G., Guptaf, H.V., Gusevg, Y.M., Habetsh, F., Halli, A., Hayj, L., Hoguek, T., Huangl, M., Leavesleyj, G., Liangl, X., Nasonovag, O.N., Noilhanh, J., Oudinc, L., Sorooshianm, S., Wagenern, T. and Woodo., E.F., 2006. Model Parameter Estimation Experiment (MOPEX): An overview of science strategy and major results from the second and third workshops. *Journal of Hydrology*, 320(1–2), pp.3–17.

Eberhart, R. and Kennedy, J., 1995. A new optimizer using particle swarm theory. In MHS'95. *Proceedings of the Sixth International Symposium on Micro Machine and Human Science, 4-6 October, 1995*, Nagoya, Japan, pp.39–43.

Edwards, B.L., Keima, R.F., Johnson, E.L., Hupp, C.R., Marre, S. and King, S.L., 2016. Geomorphic adjustment to hydrologic modifications along a meandering river: Implications for surface flooding on a floodplain. *Geomorphology*, 269, pp.149–159.

Efstratiadis, A. and Koutsoyiannis, D., 2010. One decade of multi-objective calibration approaches in hydrological modelling: a review. *Hydrological Sciences Journal*, 55(1), pp.58–78.

Ellery, W.N., Grenfell, M., Grenfell, S., Kotze, D.C., McCarthy, T.S., Tooth, S., Grundling, P.L., Beckedahl, H., Le Maitre, D and Ramsay, L., 2009. WET-Origins: controls on the distribution and dynamics of wetlands in South Africa. Wetland Management Series. WRC Report No. TT 334. Water Research Commission, Pretoria.

Esmaeilabadi, A.E., 2014. *Evapotranspiration: application, scaling and uncertainty*.Published PhD. thesis. School of Civil and Environmental Engineering, Faculty of Engineering University of New South Wales, Sydney, Australia. http://users.monash.edu.au/~jpwalker/theses/AliErshadi.pdf.

Euroconsult, 2008. Integrated Water Resources Management Strategy and Implementation Plan for the Zambezi River Basin. SADC-WD/ Zambezi River Authority SIDA/ DANIDA, Norwegian Embassy Lusaka.

Euroconsult, and Mott MacDonald. 2007. "Integrated Water Resources Management Strategy and Implementation Plan for the Zambezi River Basin. Final Report, Rapid Assessment". Gaborone, Botswana and Lusaka, Zambia: South African Development Community Water Division and Zambezi River Authority.

Falorni, G., Teles, V., Vivoni, E.R., Bras, R.L., and Amaratunga, K.S., 2005. Analysis and characterization of the vertical accuracy of digital elevation models from the Shuttle Radar Topography Mission. *Journal of Geophysical Research: Earth Surface,* 110(2), pp.1–20.

Farr, T.G. and Kobrick, M., 2000. Shuttle radar topography mission produces a wealth of data. *Eos, Transactions American Geophysical Union*, 81(48), p.583.

Feng, L., Hu, C., Chen, X., Cai, X., Tian, L. and Gan, W., 2012. Assessment of inundation changes of Poyang Lake using MODIS observations between 2000 and 2010. *Remote Sensing of Environment*, 121, pp.80–92.

Fekete, B.M., Looser, U., Pietroniro, A. and Robarts, R.D., 2012. Rational for monitoring discharge on the ground. *Journal of Hydrometeorology*, 13, pp.1977–1986.

Fernández, A., Reza, M., Durand, M., Mark, B., Moritz, M., Chul, H., Neal, J., Shastry, A., Laborde, S., Chian, S., Hamilton, I. and Xiao, N., 2016. Testing the skill of numerical hydraulic modeling to simulate spatiotemporal flooding patterns in the Logone floodplain, Cameroon, 539, pp.265–280.

Flint, L.S., 2008. Socio-Ecological Vulnerability and Resilience in an Arena of Rapid Environmental Change: Community Adaptation to Climate Variability in the Upper Zambezi Floodplain. Working Paper on Social-Ecological Resilience SeriesNo:2008-004, Research Institute for Humanity and Nature (RIHN), Dakar, Senegal, p54.

Fossey, M., Rousseau, A.N. and Savary, S., 2015. Assessment of the impact of spatio-temporal attributes of wetlands on stream flows using a hydrological modelling framework: A theoretical case study of a watershed under temperate climatic conditions. *Hydrological Processes*, 30(11), pp.1768-1781.

Frazier, P. and Page, K., 2006. The effect of river regulation on floodplain wetland inundation, Murrumbidgee River, Australia. *Marine and Freshwater Research*, 57(2), p.133.

Frazier, P. and Page, K.E.N., 2009. A Reach-Scale Remote Sensing Technique to relate wetland inundation to river flow. *River. Res. Applic*, 25(7), pp.836–849.

Gall, M., Boruff, B.J. and Cutter, S.L., 2007. Assessing Flood Hazard Zones in the Absence of Digital Floodplain Maps: Comparison of Alternative Approaches. *Natural Hazards Review*, 8(1), pp.1–12.

Gallardo, B., González-Sanchís, M., Cabezas, A., Gascón, S. and Comín, F., 2009. Modelling the response of floodplain aquatic communities across the lateral hydrological gradient. *Marine and Freshwater Research,* 60(9), p.924–935

Gallart, F., 2007. Using internal catchment information to reduce the uncertainty of discharge and baseflow predictions. *Advances in Water Resources*, 30(4), pp.808–823.

Garambois, P.A., Roux, H., Larnier, K., Labat, D. and Dartus, D., 2015. Parameter regionalization for a process-oriented distributed model dedicated to flash floods. *Journal of Hydrology*, 525, pp.383–399.

Gassman, P.W., Reyes, M R., Green, C.H. and Arnold, J.G., 2007. The Soil and Water Assessment Tool: Historical Development, Applications, and Future Research Directions. *American Society of Agricultural and Biological Engineers,* 50(4), pp.1211–1250.

Gassman, P.W., Sadeghi, A.M. and Srinivasan, R., 2014. Applications of the SWAT Model Special Section: Overview and Insights. *Journal of Environmental Quality*, 43(1), pp.1–8.

Gebregiorgis, A.S. and Hossain, F., 2013. Understanding the dependence of satellite rainfall uncertainty on topography and climate for hydrologic model simulation. *IEEE Transactions on Geoscience and Remote Sensing*, 51(1), pp.704–718.

Gibbs, M.S., Clarke, K. and Taylor, B., 2015. Linking spatial inundation indicators and hydrological modelling to improve assessment of inundation extent. To be published in *Ecological Indicators*, 60, pp.1298–1308.

Gill, M.K., Kaheil, Y.H., Khalil, A., McKee, M. and Bastidas, L., 2006. Multiobjective particle swarm optimization for parameter estimation in hydrology. *Water Resources Research,* 42(7), pp.1–14.

Gilvear, D., Winterbottom, S. and Sichingabula, H., 2000. Character of channel planform change and meander development: Luangwa River, Zambia. *Earth Surface Processes and Landforms*, 25(4), pp.421–436.

Goteti, G., Famiglietti, J.S. and Asante, K., 2008. A Catchment-Based Hydrologic and Routing Modeling System with explicit river channels. *Journal of Geophysical Research Atmospheres*, 113(14), pp.1–15.

Gray, R., Schulze, R. and Horan, M., 2012. Techniques For Assessing Impacts Of Wetlands On Hydrological Responses Under Varying Climatic Conditions : A Case Study From

The Thukela Catchment. *16th SANCIAHS National Hydrology Symposium*. University of Pretoria, 1-3 October 2012, Pretoria, South Africa, pp.1–14.

Grenfell, M.C., Ellery, W. and Grenfell, S.E., 2008. Tributary valley impoundment by trunk river floodplain development: A case study from the kwaZulu-Natal Drankensberg foothills, eastern South Africa. *Earth Surface Processes and Landforms*, 33(13), pp.2029–2044.

Grenfell, S., Ellery W.N., Grenfell, W.C., Ramsay, F.Y and Fluge, T.J., 2010. Sedimentary facies and geomorphic evolution of a blocked-valley lake: Lake Futululu, northern Kwazulu-Natal, South Africa. *Sedimentology*, 57(5), pp.1159–1174.

Grismer, M.E., Orang, M., Snyder, R. and Matyac, R., 2002. Pan Evaporation to Reference Evapotranspiration Conversion Methods by. *Journal of Irrigation and Drainage Engineering*, 128(3), pp.180–184.

Grundling, A.A.T., Berg, E.C. and Price, J, S.J.S., 2013. Assessing the distribution of wetlands over wet and dry periods and land-use change on the Maputaland Coastal Plain, north-eastern KwaZulu-Natal, South Africa. *South African Journal of Geomatics*, 2(2), pp.120–139.

Guerrero, J.L., Westerberg, I.K., Halldin, S., Xu, C.Y. and Lundin, L.C., 2012. Temporal variability in stage-discharge relationships. *Journal of Hydrology*, 446–447, pp.90–102.

Guillermo, A.M., Karl, D., Malonzo, M., Fesalbon, R.M. and Inocencio, L.C., 2015. Parameterization and Sensitivity Analysis using SUFI-2 In SWAT-CUP for calibration of watershed model in Tanjay River Negros Oriental. *In: The 36th Asian Conference on Remote Sensing 2015 (ACRS 2015): Fostering Resilient Growth in Asia. Proceedings of a meeting held 24-28 October 2015*, Quezon City, Metro Manila Philippines.

Gupta, H. V., Clark, M.P., Vrugt, J.A., Abramowitz, G. and Ye, M., 2012. Towards a comprehensive assessment of model structural adequacy. *Water Resources Research*, 48(8), pp.1–16.

Hails, A.J., 1996. Wetlands, Biodiversity and the Ramsar Convection. The Role of the Convection on Wetlands in the Conversation and wise use of Biodiversity, Grand Switzerland: Ramsar Convection Bureau. New Delhi, India: Ministry of Environment and Forests.

Hamerlynck, O., Zeine, S.A.M., Mutua, J.Y., Mukhwana, L.V. and Yena, M., 2016. Reflooding the Faguibine floodplain system, northern Mali: potential benefits and challenges. *African Journal of Aquatic Science*, 41(1), pp.109–117.

Harris, I., Jones, P.D., Osborn, T.J., Lister, D.H., 2014. Updated high-resolution grids of monthly climatic observations the CRU TS3.1 dataset. I*nt. J. Climatol.* 34 (3), pp.623–642.

Harrison, M.E., 2013. Using conceptual models to understand ecosystem function and impacts of human activities in tropical peat-swamp forests. *Wetlands*, 33(2), pp.257–267.

Hargreaves, G. H., and Allen, R. G., 2003. History and evaluation of Hargreaves evapotranspiration equation. *Journal of Irrigation and Drainage Engineering*, 129(1), pp.53-63.

Hattermann, F.F., Krysanova, V. and Hesse, C., 2008. Modelling wetland processes in regional applications. *Hydrological Sciences Journal*, 53(5), pp.1001–1012.

Heimhuber, V., Tulbure, M.G. and Broich, M., 2016. Modeling 25 years of spatio-temporal surface water and inundation dynamics on large river basin scale using time series of Earth observation data. H*ydrol. Earth Syst*, 20(6), pp.2227–2250.

Hengl T, de Jesus, J.M., MacMillan, R.A., Batjes, N.H., Heuvelink GBM., Ribeiro, E., Samuel-Rosa, A., Kempen, B., Leenaars, J.G.B., Walsh, M.G., and Ruiperez Gonzalez, M., 2014. SoilGrids1km — Global Soil Information Based on Automated Mapping. PLoS ONE 9(8), pp.1-17.

Hooijer, A., 2003. Quantifying wetland hydrological functions: Some examples of innovative methods using water table information some examples of innovative methods using water table information. *Proceedings of the 1st WETHYDRO workshop held on 12-14, October 2003,* Gonadz, Poland, pp. 75–87.

Hrachowitz,M., Savenije, H.H.G., Blöschl, G., McDonnell, J.J., Sivapalan, M.,. Pomeroy, J.W., Arheimer, B., Blume, T Clark, M.P., Ehret, U., Fenicia, F., Freer, Gelfan, A., Gupta,H.V., Hughes, D.A., Hut, R.W., Montanari, A., Pande, S., Tetzlaff, D., Troch, P.A., Uhlenbrook, S., Wagener, T., Winsemiuns, H.C., Woods, R.A., Zehe, E and Cudennec, C., 2013. A decade of Predictions in Ungauged Basins (PUB)—a review, *Hydrological Sciences Journal,* 58(6), pp.1198-1255.

Huang, A., Peng, W., Liu, X., Du, Y., Zhang, S., Wang, S., and Du, F., 2017. Characteristics and Factors Influencing the Hysteresis of Water Area–Stage Curves for Poyang Lake. *Water*, *9*(938), pp.1-20.

Hudson, P.F., Sounny-Slittine, M.A. and Lafevor, M., 2013. A new longitudinal approach to assess hydrologic connectivity: Embanked floodplain inundation along the lower Mississippi River. *Hydrological Processes*, 27(15), pp.2187–2196.

Hughes, D.A., 1980. Floodplain inundation: Processes and relationships with channel discharge. *Earth Surface Processes*, 5, pp.297–304.

Hughes, D.A., 2004a. Three decades of hydrological modelling research in South Africa. *South African Journal of Science*, 100, pp.638–642.

Hughes, D.A., 2004b. Incorporating groundwater recharge and discharge functions into an existing monthly rainfall – runoff model. *Hydrological Sciences–Journal* , 49(2), pp297-311.

Hughes, D. A., 2006. An evaluation of the potential use of satellite rainfall data for input to water resource estimation models in southern Africa. In Climate Variability and Change—Hydrological Impacts. *Proceedings of the Fifth FRIEND World Conference held on November 2006 at* Havana, Cuba, pp.75–80.

Hughes, D.A., 2007. Modelling Semi-Arid and Arid Hydrology and Water Resources – The Southern African Experience. In: Wheater, H., Sorooshian, S. and Sharma, K.D., (ed). Hydrological Modelling in Arid areas. Cambridge University Press, pp.29–40.

Hughes, D. A., 2013. A review of 40 years of hydrological science and practice in southern Africa using the Pitman rainfall-runoff model. *Journal of Hydrology*, 501, pp.111–124.

Hughes, D.A., 2015a. Hydrological modelling, process understanding and uncertainty in a southern African context: lessons from the northern hemisphere. *Hydrological Processes*, 30(14), pp.2419–2431.

Hughes, D.A., 2015b. Scientific and practical tools for dealing with water resource estimations for the future. *IAHS-AISH Proceedings and Reports*, 371, pp.23–28.

Hughes, D.A. and Forsyth, D.A., 2006. A generic database and spatial interface for the application of hydrological and water resource models. *Computers and Geosciences*, 32(9), pp.1389–1402.

Hughes, D.A. and Mantel, S.K., 2010. Estimating the uncertainty in simulating the impacts of small farm dams on streamflow regimes in South Africa. *Hydrological Sciences Journal*, 55(4), pp.578–592.

Hughes, D.A, Andersson, L., Wilk, J. and Savenije, H.H.G., 2006. Regional calibration of the Pitman model for the Okavango River. *Journal of Hydrology*, 331, pp.30–42.

Hughes, D.A., Kapangaziwiri, E. and Sawunyama, T., 2010. Hydrological model uncertainty assessment in southern Africa. *Journal of Hydrology*, 387(3–4), pp.221–232.

Hughes, D.A., Kingston, D.G. and Todd, M.C., 2011. Uncertainty in water resources availability in the Okavango River basin as a result of climate change. *Hydrology and Earth System Sciences*, 15(3), pp.931–941.

Hughes, D.A., Gush, M., Tanner, J.L. and Dye, P., 2013. Using targeted short-term field investigations to calibrate and evaluate the structure of a hydrological model. *Hydrological Processes*, DOI: 10.1002/hyp.9807.

Hughes, D.A.; Tshimanga, R.M.; Trivarombo, S., Tanner, J., 2014. Simulating wetland impacts on streamflow in southern Africa using a monthly hydrological model. *Hydrological Processes*, 28(4), pp1775–1786.

Hughes, D.A. and Slaughter, A., 2015. Daily disaggregation of simulated monthly flows using different rainfall datasets in southern Africa. *Journal of Hydrology: Regional Studies*, 4, pp.153–171.

Hughes, D.A. and Slaughter, A.R., 2016. Disaggregating the components of a monthly water resources system model to daily values for use with a water quality model. *Environmental Modelling and Software*, 80, pp.122–131.

Hughes, R.H. and Hughes, J.S., 1992. A Directory of African Wetlands. IUCN Publication Services Unit, Cambridge, p.805.

Hunter, N.M., Bates, P.D., Horritt, M.S., De Roo, A.P.J., and Werner, M.G.F.,2005. Utility of different data types for calibrating flood inundation models within a GLUE framework, *Hydrol. Earth Syst. Sci*., 9(4), 412-430.

Hunter, N.M., Bates, P.D., Horritt, M.S., Wilson, M.D., 2007. Simple spatially-distributed models for predicting flood inundation: A review. *Geomorphology*, 90(3–4), pp.208–225.

Hunter, N.M., Horritt, M.S., Bates, P.D., Wilson, M.D. and Werner, M.G.F., 2005. An adaptive time step solution for raster-based storage cell modelling of floodplain inundation. *Advances in Water Resources*, 28(9), pp.975–991.

Jahn, R., Blume, H.P., Asio, V.B., Spaargaren, O. and Schad, P., 2006. *Guidelines for soil description*, Food and Agriculture Organization of The United Nations, Rome, p97.

Jankowfsky, S., Branger, F., Braud, I., Gironás, J. and Rodriguez, F., 2013. Comparison of catchment and network delineation approaches in complex suburban environments: Application to the Chaudanne catchment, France. *Hydrological Processes*, 27(25), pp.3747–3761.

Jarvis, A., Rubiano, J., Nelson, A., Farrow, A., Mulligan, M., 2004. Practical use of SRTM data in the tropics: Comparisons with digital elevation models generated from cartographic data. Centro Internacional de Agricultura Tropical (CIAT), p32.

Jensen, O. and Wu, X., 2016. Embracing Uncertainty in Policy-Making: The Case of the Water Sector. *Policy and Society*, 35(2), pp.115–123.

Jones, K., Lanthier, Y., Van der Voet, P., Van Valkengoed, E., Taylor, D. and Fernández-Prieto, D., 2009. Monitoring and assessment of wetlands using Earth Observation: the GlobWetland project. *Journal of environmental management*, 90(7), pp.2154–69.

Jovanovic, N., Mu, Q., Bugan, R.D.H. and Zhao, M., 2015. Dynamics of MODIS evapotranspiration in South Africa. *Water SA*, 41(1), pp.79–91.

Joubert, R. and Ellery, W., 2013. Controls on the formation of Wakkerstroom Vlei, Mpumalanga province, South Africa. *African Journal of Aquatic Science*, 38(2), pp.135–151.

Jiang, Y., Liu, C., Huang, C. and Wu, X., 2010. Improved particle swarm algorithm for hydrological parameter optimization. *Applied Mathematics and Computation*, 217(7), pp.3207–3215.

Jiang, Y., Li, X. and Huang, C., 2013. Automatic calibration a hydrological model using a master-slave swarms shuffling evolution algorithm based on self-adaptive particle swarm optimization. *Expert Systems with Applications*, 40(2), pp.752–757.

Jung, D., Choi, Y. and Kim, J., 2017. Multiobjective Automatic Parameter Calibration of a Hydrological Model. *Water*, 9(3), pp.187.

Jung, H.C., Alsdorf, D., Lee, H., Wilson, M., Beighley, E., Durand, M., Shum, C K., Kim, J W. and Andreadis, K., 2010. Hydrodynamic Modeling of the Congo Wetlands Using LISFLOOD and Satellite Based Measurements. In: *European Geosciences Union (EGU) General Assembly 2010, held 2-7 May, 2010 in* Vienna, Austria,. p.6202.

Junk, W.J., Bayley, P.B. and Sparks, R.E., 1989. The flood pulse concept in river-floodplain systems. *Can. Spec. Publi. Fish. Acquat. Sci*, 106, pp.110–127.

Kakuru, W., Turyahabwe, N. and Mugisha, J., 2013. Total Economic Value of Wetlands Products and Services in Uganda. *The Scientific World Journal*, 2013, pp.1–13.

Kapangaziwiri, E., 2008. *Revised parameter estimation methods for the Pitman monthly rainfall-runoff model*. published MSc. Thesis. Rhodes University Grahamstown South Africa. http://hdl.handle.net/10962/d1006172.

Kapangaziwiri, E., 2011. *Regional application of the Pitman monthly rainfall-runoff model in southern Africa incorporating uncertainty*. Published PhD thesis. Rhodes University Grahamstown South Africa. http://hdl.handle.net/10962/d1006178.

Kapangaziwiri, E., Hughes, D.A. and Wagener, T., 2012. Incorporating uncertainty in hydrological predictions for gauged and ungauged basins in southern Africa. *Hydrological Sciences Journal*, 57(5), pp.1000–1019.

Kapangaziwiri, E. and Hughes, D., 2008. Towards revised physically based parameter estimation methods for the Pitman monthly rainfall-runoff model. *Water Sa*, 34(2), pp.183–192.

Karim, F., Kinsey-Henderson, A., Wallace, J., Arthington, A. and Pearson, R., 2012. Modelling wetland connectivity during overbank flooding in a tropical floodplain in north Queensland, Australia. *Hydrological Processes*, 26(18), pp.2710–2723.

Karim, F., Dutta, D., Marvanek, S., Ticehurst, C. and Petheram, C., 2013. Hydrodynamic modelling of potential impacts of climate change on hydrological connectivity of floodplain wetland. In *20th International Congress on Modelling and Simulation Adelaide, Australia, 1–6 December 2013,* pp.2332–2338.

Karim, F., Kinsey-Henderson, A., Wallace, J., Godfrey, P., Arthington, A.H. and Pearson, R.G., 2014. Modelling hydrological connectivity of tropical floodplain wetlands via a combined natural and artificial stream network. *Hydrological Processes*, 28(23), pp.5696–5710.

Karim, F., Petheram, C., Marvanek, S., Ticehurst, C., Wallace, J. and Hasan, M., 2016. Impact of climate change on floodplain inundation and hydrological connectivity between wetlands and rivers in a tropical river catchment. *Hydrological Processes,* 30(10), pp.1574–1593.

Karim, F., Dushmanta, D., Marvanek, S., Petheram,C., Ticehurst,C., Lerat, J., Kim, S and Yang, A., 2015. Assessing the impacts of climate change and dams on floodplain inundation and wetland connectivity in the wet–dry tropics of northern Australia. *Journal of Hydrology*, 522, pp80–94.

Karim, F., Petheram, C., Marvanek, S., Ticehurst, C., Wallace, J., Gouweleeuw, B., Chan, F., Marinova, D., Anderssen, R S., 2011. The use of hydrodynamic modelling and remote sensing to estimate floodplain inundation and flood discharge in a large tropical catchment. In *19th International Congress on Modelling and Simulation , Perth, Australia, 12–16 December 2011*. pp.3796–3802.

Kashaigili, J.J., 2008. Impacts of land-use and land-cover changes on flow regimes of the Usangu wetland and the Great Ruaha River, Tanzania. *Physics and Chemistry of the Earth*, 33(8–13), pp.640–647.

Kashaigili, J.J., Mbilinyi, B.P., Mccartney, M. and Mwanuzi, F., 2006a. Dynamics of Usangu plains wetlands : Use of remote sensing and GIS as management decision tools. *Physics* *and Chemistry of the Eart*h, 31, pp.967–975.

Kashaigili, J.J., Mccartney, M.P., Mahoo, H.F., Lankford, B.A., Mbilinyi, B.P. and Yawson, D., 2006b. *Use of a Hydrological Model for Environmental Management of the Usangu Wetlands, Tanzania*, Research Report. International Water Management Institute, Colombo, Sri Lanka, p.37.

Kavetski, D., Franks, S.W. and Kuczera, G., 2002. Confronting input uncertainty in environmental modelling. In:Q. Duan, et al., eds. Calibration of watershed models water science and applications. Washington, DC. American Geophysical Union Books, Washington DC, pp.49-68.

Kavetski D., Kuczera G. and Franks S.W., 2006. Calibration of conceptual hydrological models revisited: 1. Overcoming numerical artefacts. *Journal of Hydrology*, 320, (1-2), pp.173–186.

Kiamehr, R. and Sjöberg, L.E., 2005. Effect of the SRTM global DEM on the determination of a high-resolution geoid model: A case study in Iran. *Journal of Geodesy*, 79(9), pp.540–551.

Kihwele, E., Mnaya, B., Birkett, C. and Wolanski, E., 2012. The role of vegetation in the water budget of the Usangu wetlands, Tanzania. *Wetlands Ecol Manage*, 20, pp.389–398, pp.

Kling, H., Stanzel, P. and Preishuber, M., 2014. Impact modelling of water resources development and climate scenarios on Zambezi River discharge. *Journal of Hydrology: Regional Studies*, 1, pp.17–43.

Kolka R.K., Thompson J.A., 2012. Wetland geomorphology, soils, and formative processes. In: D. Batzer (ed), Ecology of freshwater and estuarine wetlands. University of California Press, Berkeley, pp.7–42.

Kossi, K., 2017. Modelling of flood hazard extent in data sparse areas: a case study of the Oti River basin, West Africa. *Journal of Hydrology, Reginal studies*, 10, pp.122-132.

Kotze, D.; 2000. The contribution of wetlands to the attenuation of floods. The Mondi Wetlands Programme. School of Applied Environmental Sciences, University of Natal, SA, p7.

Kotze, D.; Marneweck, G.; Batchelor, A.; Lindley, D.; Collins, N., 2009. WET-EcosServices: A technique for rapidly assessing ecosystem services supplied by wetlands. WRC Report TT 339/09. Pretoria, South Africa: Water Research Commission.

Kouwen, N., 1988. WATFLOOD: a Micro-Computer Based Flood Forecasting System Based on Real-Time Weather Radar. *Canadian Water Resources Journal*, 13(1), pp.62–77.

Kreiselmeier, J., 2015. *Development of a Flood Model Based on Globally-Available Satellite Data for the Papaloapan River , Mexico*. Published thesis. Department of Earth Sciences, Uppsala University, Uppsala. urn:nbn:se:uu:diva-256399.

Kupfer, J.A. and Meitzen, K.M., 2012. Modeling flood inundation and hydrological connectivity across the congaree river floodplain. *Proceedings of the 2012 South*

Carolina Water Resources Conference, held October 10-11, 2012 at the Columbia Metropolitan Convention Center, pp.1–4.

Kuzmin, V., Seo, D.J. and Koren, V., 2008. Fast and efficient optimization of hydrologic model parameters using a priori estimates and stepwise line search. *Journal of Hydrology*, 353, pp.109–128.

Lankford, B.A., Tumbo, S., and Rajabu, K., 2009. Water competition, variability and river basin governance: a critical analysis of the Great Ruaha River, Tanzania. In: F. Molle and P. Wester, eds. River basin development in perspective. Oxfordshire: Centre for Agriculture and Biosciences International (CABI), pp.171–195

Lankford, B., Van Koppen, B., Franks, T. and Mahoo, H., 2004. Entrenched views or insufficient science? Contested causes and solutions of water allocation; insights from the Great Ruaha River Basin, Tanzania. *Agricultural Water Management*, 69(2), pp.135–153.

Larocque, M., Biron, P.M., Buffin-Bélanger, T., Needelman, M., Cloutier, C. and McKenzie, J., 2016. Role of the geomorphic setting in controlling groundwater–surface water exchanges in riverine wetlands: A case study from two southern Québec rivers (Canada). *Canadian Water Resources Journal / Revue canadienne des ressources hydriques*, 41(4), pp.1–15.

Leauthaud, C., Belaud, G., Duvail, S., Moussa, R., Grunburger, O. and Albergel, J., 2013. Characterizing floods in the poorly gauged wetlands of the Tana River Delta , Kenya , using a water balance model and satellite data. *Hydrol. Earth Syst. Sci*, 17(8), pp.3059–3075.

Lee, H., Yuan, T., Jung, H.C., Beighley, E., 2015. Mapping wetland water depths over the central Congo Basin using PALSAR ScanSAR, Envisat altimetry, and MODIS VCF data. *Remote Sensing of Environment*, 159, pp.70–79.

Lefsky, M.A., 2010. A global forest canopy height map from the moderate resolution imaging spectroradiometer and the geoscience laser altimeter system. *Geophysical Research Letters*, 37(15), pp.1–5.

Lehner, B., and Döll, P. (2004). Development and validation of a global database of lakes, reservoirs and wetlands. *Journal of Hydrology*, *296*(1-4), 1–22.

iLehner, B., Verdin, K. and Jarvis, A., 2006. HydroSHEDS Technical Documentation v1.0 1. World Wildlife Fund, Washington, DC, USA. p.1-27.

Lehner, B., Verdin, K. and Jarvis, A., 2008. New global hydrography derived from spaceborne elevation data. *Eos,* 89(10), pp.93–94.

Leopold, L.B. and Maddock, T., 1953. *The Hydraulic Geometrv of Stream Channels and Some Physiographic Implications. Geological survey professional paper 252 Quantitative*. U. S. Government Printing Office, Washington, p.57.

Lewin, J., 1978. Floodplain geomorphology. *Progress in Physical Geography*, 2(3), pp.408–437.

Lewin, J. and Hughes, D., 1980. Welsh floodplain studies. *Journal of hydrology,* 46(1980), pp.35–49.

Lewin, J. and Ashworth, P.J., 2014. The negative relief of large river floodplains. *Earth-Science Reviews*, 129, pp.1–23.

Li, Z., 2014. Watershed modeling using arc hydro based on DEMs: a case study in Jackpine watershed. *Environmental Systems Research*, 3(1), pp.1–12.

Liang, D., Falconer, R.A. and Lin, B., 2006. Comparison between TVD-MacCormack and ADI-type solvers of the shallow water equations. *Adv. Water Resour*. 29 (12), 1833–1845.

Liechti, T.C., Matos, J.P., Ferràs S.D., Boillat, J. and Schleiss, A., 2014. Hydrological modelling of the Zambezi River Basin taking into account floodplain behaviour by a modified reservoir approach. *International Journal of River Basin Management*, 12(1), pp.29–41.

Liersch, S. and Hattermann, F., 2011. How to integrate wetland processes in river basin modeling? A West African case study. In *SWAT conference June 2011*. p.29.

Liu, Y. and Gupta, H. V., 2007. Uncertainty in hydrologic modeling: Toward an integrated data assimilation framework. *Water Resources Research*, 43(W07401), pp.1–18.

Liu, Y., Yang, W. and Wang, X., 2010. Development of a SWAT extension module to simulate riparian wetland hydrologic processes at watershed. *Hydrol. Process*, 22(16), pp.2901–2915.

Long, D., Longuevergne, L. and Scanlon, B., 2014. Uncertainty in evapotranspiration fromland surfacemodeling, remote sensing, and GRACE satellites. *Water Resources Research*, 50(2), pp.1131–1151.

Loveland, T.R., Reed, B.C., Brown, J.F., Ohlen, D.O., Zhu, Z., Yang, L. and Merchant, J.W., 2000. Development of a global land cover characteristics database and IGBP DISCover from 1 km AVHRR data. *International Journal of Remote Sensing*, 21(6–7), pp.1303–1330.

Lu, J., Sun, G., McNulty, S.G., Amatya, D.M., 2005. A Comparison of Six Potential Evapotranspiration Methods for Regional Use in the Southeastern United States. *Journal of the American Water Resources Association*, 41(3), pp.621–633.

MacKay, H., Finlayson, C M., Fernández-Prieto, D., Davidson, N., Pritchard, D. and Rebelo, L.M., 2009. The role of Earth Observation (EO) technologies in supporting implementation of the Ramsar Convention on Wetlands. *Journal of environmental management*, 90(7), pp.2234–42.

Madsen, H., 2001. Automatic calibration of the MIKE SHE integrated hydrological modelling system. *4th DHI Software Conference, 6-8 June, 2001, Scanticon Conference Centre, Helsingør, Denmark.* pp.6–8.

Mahay, F.H., 2008. *Ecohydrology Study of Kirumi Wetland using Hydroinformatics Tools*. Published thesis. UNESCO-IHE Institute for Water Education, Delft, the Netherlands. http://www.hydroinformatics.org/knowledgebank.php?id=3.

Malone, R.W., Green, T.R., Timothy, R., Yagow, G., Baffaut, C., Gitau, M.W., Qi, Z., Amatya, D.M., Parajuli, P.B., Bonta, J.V. and Green, T.R., 2016. Parameterization

Guidelines and Considerations for Hydrologic Models. Transactions of the ASABE, 58(6), pp.1681–1703.

Martinez-Martinez, E.A., Nejadhashemi, A.P., Woznicki, S.A and Love, B.J., 2014. Modeling the hydrological significance of wetland restoration scenarios. *Journal of environmental management*, 133, pp121–34.

Masafu, CK, Trigg, MA, Carter, R & Howden, NJK 2016, 'Water availability and agricultural demand: An assessment framework using global datasets in a data scarce catchment, Rokel-Seli River, Sierra Leone' *Journal of Hydrology: Regional Studies*, 8, pp. 222-234.

Matthew, B.S. and Day, J.A, 2014. Wetlands in changed landscapes: the influence of habitat transformation on the physico-chemistry of temporary depression wetlands. *PloS one*, 9(2), pp.1–15.

Mazvimavi, D. and Wolski, P., 2006. Long-term variations of annual flows of the Okavango and Zambezi Rivers. *Physics and Chemistry of the Earth*, 31(15–16), pp.944–951.

Mazvimavi, D., Burgers, S.L.G.E. and Stein, A., 2006. Identification of basin characteristics influencing spatial variation of river flows. *International Journal of Applied Earth Observation and Geoinformation*, 8, pp.165–172.

Mccartney, M., 2007. Technical Note : Hydrology of the Lukanga Swamp, Zambia. IWMI Research Report NO: H040529, International Water Management Institute, pp.1–6.

McCartney, M.P., Kashaigili, J.J., Lankford, B.A. and Mahoo, H.F., 2008. Hydrological modelling to assist water management in the Usangu wetlands , Tanzania. *Intl. J. River Basin Management*, 6(1), pp.51–61.

McCartney, M., Rebelo, L. M., Senaratna Sellamuttu, S and De Silva, S., 2010. Wetlands, agriculture and poverty reduction. Colombo, Sri Lanka: International Water Management Institute. (IWMI Research Report 137).

Mccartney, M., Rebelo, L., Mapedza, E., de Silva, S. and Finlayson, C.M., 2011. The Lukanga Swamps: Use, Conflicts, and Management, *Journal of International Wildlife Law and Policy*, 14(3–4), pp.293–310.

McCarthy, T.S., Tooth, S., Kotze, D.C., Collins, N.B., Wandrag, G. and Pike, T., 2010. The role of geomorphology in evaluating remediation options for floodplain wetlands: The case of Ramsar-listed Seekoeivlei, eastern South Africa. *Wetlands Ecology and Management*, 18(2), pp.119–134.

Mcclain, M.E., 2013. Balancing Water Resources Development and Environmental Sustainability in Africa : A Review of Recent Research Findings and Applications. *AMBIO*, 42, pp.549–565.

Mccorquodale, A., Georgiou, I., Davis, M. and Pereira, J., 2010. *Hydrology and hydrodynamic modeling of the Mississippi River in the Southeast Louisiana – Part I: A report Submitted to the Lake Pontchartrain Basin Foundation.* Pontchartrain Institute for Environmental Studies University of New Orleans New Orleans, LA 70148, p321.

McCowan, A., 2001. Improving the performance of a two-dimensional hydraulic model for floodplain applications. *Conference on Hydraulics in Civil Engineering, The Institution of Engineers, Australia. 28-30 November 2001, Hobart, Australia.*

Mcginness, H.M., Thoms, M.C. and Southwell, M.R., 2002. Connectivity and fragmentation of flood plain- river exchanges in a semiarid , anabranching river system. In: *The Structure, Function and Management Implications Fluvial Sedimentary Systems. Proceedings of an international symposium held at* Alice Springs, Australia, September 2002. IAHS Pubi. NO:. 276, pp.19–26.

Mcmillan, H., Krueger, T. and Freer, J., 2012. Benchmarking observational uncertainties for hydrology: Rainfall, river discharge and water quality. *Hydrological Processes*, 26(26), pp.4078–4111.

Meek, B.D., Chesworth, W. and Spaargaren, O., 2016. Regosols, Encyclopidia of Soil Science. DOI: 10.1007/978-1-4020-3995-_479.

Meier, P., Frömelt,A and Kinzelbach, W., 2011. Hydrological real-time modelling in the Zambezi river basin using satellite-based soil moisture and rainfall data. *Hydrology and Earth System Sciences*, 15(3), pp.999–1008.

Mekonnen, B.A., Mazurek, K.A. and Putz, G., 2016. Incorporating landscape depression heterogeneity into the Soil and Water Assessment Tool (SWAT) using a probability distribution. *Hydrological Processes*, 30(13), pp.2373–2389.

Memon, A.A., Muhammad, S., Rahman, S. and Haq, M., 2015. Flood monitoring and damage assessment using water indices: A case study of Pakistan flood-2012. *Egyptian Journal of Remote Sensing and Space Science*, 18(1), pp.99–106.

Mengistu, S.G. and Spence, C., 2016. Testing the ability of a semidistributed hydrological model to simulate contributing area. *Water Resources Management*, 52, pp.4399–4415.

Mertes, L.A.K., 1997. Documentation and significance of the perirheic zone on inundated floodplains. *Water Resources Research*, 33(7), pp.1749–1762.

Merz, R., Blöschl, G. and Parajka, J., 2006. Regionalisation methods in rainfall-runoff modelling using large samples. *LResults of the Model Parameter Experiment–MOPEX. IAHS Publ*, 307(307), pp.117–125.

Meyer, P.D., Ming, Y., Neuman, S.P. and Cantrell, K.J., 2004. *Combined Estimation of Hydrogeologic Conceptual Model and Parameter Uncertainty*, Pacific Northwest National Laboratory, Richland, WA 99352.

Milzow, C., Kgotlhang, L., Kinzelbach, W., Meier, P. and Bauer-Gottwein, P., 2009. The role of remote sensing in hydrological modelling of the Okavango Delta, Botswana. *Journal of environmental management*, 90(7), pp.2252–60.

Mitchell, S.A., 2012. The status of wetlands, threats and the predicted effect of global climate change: the situation in Sub-Saharan Africa. *Aquatic Sciences*, 75(1), pp.95–112.

Mitsch, W. and Gosselink, J.G., 2015. *Wetlands of the World*, Hoboken, New Jersey, JohnWiley and Sons, p75.

Mohobane, T., 2015. *Water resources availability in the Caledon River Basin past , present* *and future*. Published thesis. Rhodes University Grahamstown, South Africa. http://hdl.handle.net/10962/d1019802.

Moore, A.E., Cotterill, F.P.D., Main, M.P.L. and Williams, H.B., 2008. The Zambezi River. *large Rivers: geomorphology and Management*, (2007), pp.311–332.

Montanari, A., 2005. Large sample behaviors of the generalized likelihood uncertainty estimation (GLUE) in assessing the uncertainty of rainfall-runoff simulations. *Water Resources Research*, 41(8), pp.1–13.

Montovan, P., and E. Todini (2006), Hydrological forecasting uncertainty assessment: Incoherence of the GLUE methodology, *J. Hydrol.* 330(1–2), pp.368–381.

Moradkhani, H., Sorooshian, S., Gupta, H.V. and Houser, P.A., 2005. Dual state-parameter estimation of hydrological models using ensemble Kalman filter, Adv. *Water Resour*, 28(2),135–147.

Morris, K., Ferwerda, F. and Papas, P., 2013. *Wetland connectivity models*, Technical Report Series No. 241. Department of Sustainability and Environment, Arthur Rylah Institute for Environmental Research, Heidelberg, Victoria.

Mtahiko, M.G.G., Gereta, E., Kajuni, A. R., Chiombola, E.A.T, Ng'umbi, G.Z., Coppolillo, P. and Wolanski, E., 2006. Towards an ecohydrology-based restoration of the Usangu wetlands and the Great Ruaha River, Tanzania. *Wetlands Ecology and Management*, 14, pp.489–503.

Mukolwe, M.M., Yan, K., Di Baldassarre, G. and Solomatine, D., 2015. Testing new sources of topographic data for flood propagation modelling under structural, parameter and observation uncertainty. *Hydrological Sciences Journal*, 61(9), pp.1707–1715.

Mu, Q., Zhao, M. and Running, S.W., 2011. Improvements to a MODIS global terrestrial evapotranspiration algorithm. *Remote Sensing of Environment*, 115(8), pp.1781–1800.

Mwakalila, S., 2011. Assessing the Hydrological Conditions of the Usangu Wetlands in Tanzania. *Journal of Water Resource and Protection*, 3(12), pp.876–882.

Mwanza, D.D., 2003. Water for sustainable development in africa. *Environment, Development and Sustainability,* 5, pp.95–115.

Mwelwa, E.M., 2004. *The Application of the monthly time step Pitman Rainfall-Runoff Model to the Kafue River Basin of Zambia.* Published Masters Thesis. Rhodes University, Grahamstown South Africa. http://hdl.handle.net/10962/d1006171.

Musambachime, C.M., 2016. *One Zambia, One nation, One Country*, Xlibris, p672.

Mwita, E., Menz, G., Misana, S., Becker, M., Kisanga, D. and Boehme, B., 2013. Mapping small wetlands of Kenya and Tanzania using remote sensing techniques. *International Journal of Applied Earth Observation and Geoinformation*, 21, pp.173–183.

Nachtergaele, F., 2010. The classification of Leptosols in the World Reference Base for Soil Resources. In *19th World Congress of Soil Science, Soil Solutions for a Changing World, 1 – 6 August 2010, Brisbane, Australia*. pp. 25–27.

Nash, J.E., Sutcliffe, J.V., 1970. River flow forecasting through conceptual models. Part I – A discussion of principles. *J. Hydrol*. 10, 282–290.

Ndiritu, J.G., 2009. *AUTOMATIC CALIBRATION OF THE PITMAN MODEL USING THE SHUFFLED COMPLEX EVOLUTION METHOD*. WRC Report Number: KV 229/09, South Africa.

Ndomba, P., Magoma, D., Mtalo, F.W. and Norbert, J., 2010. Application of SWAT in Natural Wetland Catchments. A case of Rugezi Catchment in Rwanda. *Nile Basin Water Science and Engineering*, 3(3), pp.1–13.

New, M., Lister, D., Hulme, M., Makin, I., 2002. A high-resolution data set of surface climate over global land areas. *Climate Research*, 21(1), pp.1–25.

Ndzabandzaba, C. and Hughes, D.A., 2017. Regional water resources assessments using an uncertain modelling approach : The example of Swaziland. *Journal of Hydrology : Regional Studies*, 10, pp.47–60.

Neal, J., Schumann, G. and Bates, P., 2012. A subgrid channel model for simulating river hydraulics and floodplain inundation over large and data sparse areas. *Water Resources Research*, 48(W11506), pp.1–16.

Négrel P.H., Petelet-Giraud E., Sgouridis F., 2005. Integration of European Wetland research in sustainable management of the water cycle. Significance of wetlands in the water cycle, EUROWET, p22.

Neitsch, S.L., Arnold, J.G., Kiniry, J.R. and Williams, J.R., 2005. Soil and water assessment tool: Theoretical documentation. Ver. 2005. Grassland, Soil and Water Res. Lab., Agric. Res. Service–Blackland Res. Center, Texas Agric. Exp. Stn. http://swatmodel.tamu.edu/media/1292/swat2005theory.pdf.

Newman, A.E. and Keim, R.F., 2013. Mesoscale connectivity through a natural levee. *Hydrology and Earth System Sciences*, 17(2), pp.691–704.

Nguyen, N.Y., Ichikawa, Y. and Ishidaira, H., 2016. Estimation of inundation depth using flood extent information and hydrodynamic simulations. *Hydrological Research Letters*, 10(1), pp.39–44.

Nicholas, A.P. and Mitchell, C.A., 2003. Numerical simulation of overbank processes in topographically complex floodplain environments. *Hydrological Processes*, 17(4), pp.727–746.

Nicholson, S.E., 2013. The West African Sahel: A Review of Recent Studies on the Rainfall Regime and Its Interannual Variability. *Hindawi Publishing Corporation*, 2013, pp.1-32. dx.doi.org/10.1155/2013/45352.

Niu, Z., Zhang, H., Wang, X., Yao, W., Zhou, D., Zhao, K., Zhao, H., Li, N., Huang, H., Li, C., Yang, J., Liu, C., Liu, S., Wang, L., Li, Z., Yang, Z., Qiao, F., Zheng, Y., Chen, Y., Sheng,Y., Gao, X., Zhu, W., Wang, W., Wang, H., Weng, Y., Zhuang, D., Liu, J., Luo, Z., Cheng, X., Guo, Z. and Gong, P., 2012. Mapping wetland changes in China between 1978 and 2008. *Chinese Science Bulletin*, 57(22), pp.2813–2823.

Norbiato, D. and Borga, M., 2008. Analysis of hysteretic behaviour of a hillslope-storage kinematic wave model for subsurface flow. *Advances in Water Resources*, 31(1), pp.118–131.

Novella, N.S. and Thiaw, W.M., 2013. African rainfall climatology version 2 for famine early warning systems. *Journal of Applied Meteorology and Climatology*, 52(3), pp.588–606.

Nyirenda, V.R., Nahonyo, C.L. and Mushimbalume, M., 2013. Efficacy of chilli Capsicum oleoresin guns usage by local hunters as African elephant repellent from crop raiding in the Luangwa Valley , Zambia. *International Journal of Biodiversity and Conservation,* 5(7), pp.418–425.

O'Kane, J.P., 2005. Hysteresis in hydrology. *Acta Geophys. Pol.*, 53(4), pp.373–383.

Ollis, D.J., Ewart-Smith, J.L., Day, J.A., Job, N.M., Macfarlane, D.M., Snaddon, C.D., Sieben, E.J.J., Dini, J.A. and Mbona, N., 2015. The development of a classification system for inland aquatic ecosystems in South Africa. *Water SA*, 41(5), pp.727–745.

O'Loughlin, F., Trigg, M.A., Schumann, G.J.P. and Bates, P.D., 2013. Hydraulic characterization of the middle reach of the Congo River. *Water Resources Research,* 49(8), pp.5059–5070.

O'Loughlin, F.E., Paiva, R.C.D., Durand, M., Alsdorf, D.E. and Bates, P.D., 2016. A multi-sensor approach towards a global vegetation corrected SRTM DEM product. *Remote Sensing of Environment*, 182, pp.49–59.

Pryde, J.K., Osorio, J., Wolfe, M.L., Heatwole, C., Benham, B.C.A., 2007. Comparison of watershed boundaries derived from SRTM and ASTER digital elevation datasets and from a digitized topographic map. An ASABE Meeting Presentation Paper Number: 072093. Minneapolis Convention Center Minneapolis, Minnesota, p10.

Oguntunde, P.G., Friesen, J., van de Giesen, N. and Savenije, H., 2006. Hydroclimatology of the Volta River Basin in West Africa: Trends and variability from 1901 to 2002. *Physics and Chemistry of the Earth*, 31(18), pp.1180–1188.

Opperman, J.J., Luster, R., McKenney, B.A., Roberts, M. and Meadows, A., 2010. Ecologically Functional Floodplains:Connectivity, Flow Regime, and Scale. *Journal of the American Water Resources Association*, 46(2), pp.211–226.

Ollis, D.J., Snaddon, C.D., Job, N.M. and Mbona, N., 2013. Classification System for Wetlands and other Aquatic Ecosystems in South Africa. User Manual: Inland Systems. SANBI Biodiversity Series 22. South African National Biodiversity Institute, Pretoria.

Overton, I.C., 2005. Modelling floodplain inundation on a regulated river: integrating GIS, remote sensing and hydrological models. *River Research and Applications*, 21, pp.991–1001.

Pagliero, L., Bouraoui, F., Willems, P. and Diels, J., 2014. Large-Scale Hydrological Simulations Using the Soil Water Assessment Tool, Protocol Development, and Application in the Danube Basin. *Journal of Environment Quality*, 43(1), p.145.

Paiva, R.C.D., Collischonn, W. and Tucci, C.E.M., 2011. Large scale hydrologic and hydrodynamic modeling using limited data and a GIS based approach. *Journal of*

Hydrology, 406(3–4), pp.170–181.

Pamba, S., Shaghude, Y.W. and Muzuka, A.N.N., 2016. Hydrodynamic Modelling on Transport, Dispersion and Deposition of Suspended Particulate Matter in Pangani Estuary, Tanzania. *Estuaries:*In: Diop, S., Scheren, P. and Machiwa, F.J., (eds): A Lifeline of Ecosystem Services in the Western Indian Ocean. Estuaries of the World. Springer, Cham, pp.141–160.

Pappenberger, F. and Beven, K.J., 2006. Ignorance is bliss : Or seven reasons not to use uncertainty analysis. *Water resources research*, 42(W05302), pp.1–8.

Pappenberger, F., Frodsham, K., Beven, K.J., Romanovicz, R., Matgen, P., 2007. Fuzzy set approach to calibrating distributed flood inundation models using remote sensing observations. *Hydrol. Earth Syst. Sci.*, 11(2), pp.739–752, 2007

Parajka, J., Merz, R. and Blöschl, G., 2005. A comparison of regionalisation methods for catchment model parameters. *Hydrology and Earth System Sciences Discussions*, 2(2), pp.509–542.

Patro, S., Chatterjee, C., Singh, R. and Raghuwanshi, N., 2009. Hydrodynamic modelling of large flood-prone river system in India with limited data. *Hydrol. Process*, 23(19), pp.2774–2791.

Paz, A.R., Collischonn, W. and Lopes Da Silveira, A.L., 2006. Improvements in large-scale drainage networks derived from digital elevation models. *Water Resources Research*, 42(8), pp.1–7.

Pender, G. and Néelz, S., 2007. Use of computer models of flood inundation to facilitate communication in flood risk management. *Environmental Hazards*, 7(2), pp.106–114.

Penman H. L., 1948. Natural evaporation from open water, bar soil and grass. *Proceedings of the Royal Society of London* 193, pp.120-145.

Persits, F., Ahlbrandt, T. S., Tuttle, M., Charpentier, R. R., Brownfield, M. E., and Takahashi, K. (1997). Maps showing geology, oil and gas fields and geological provinces of Africa. Verson 2.0, USGS Open File Report 97-470A.

Petersen, G. and Fohrer, N., 2010. Two-dimensional numerical assessment of the hydrodynamics of the Nile swamps in southern Sudan. *Hydrological Sciences Journal*, 55(1), pp.17–26.

Phillips, J.D., 2013. Hydrological connectivity of abandoned channel water bodies on a coastal plain river. *River Research and Applications*, 29(2), pp.149–160.

Pitman, W.V., 1973. A mathematical model for generating river flows from meteorological data in South Africa. Report no. 2/73, Hydrological Research Unit, University of the Witwatersrand, Johannesburg, South Africa.

Popov, L.V. and Gavrin, Y.S., 1970. Use of aerial photography in evaluating the flooding and emptying of river floodplains and the development of floodplain currents. *Soviet Hydrology*, 5, pp. 413–426.

Pryde, J.K., Osorio, J., Wolfe, M. L., Heatwole, C., Benham, B. and Cardenas, A., 2007.

Comparison of watershed boundaries derived from SRTM and ASTER digital elevation datasets and from a digitized topographic map . *ASABE Annual International Meeting*, 300(72093), pp.1–10.

Qin, C-Z., Zhu, A-X., Pei, T., Li, B-L. and Zhou, C-H., 2011. An approach to computing topographic wetness index based on maximum downslope gradient. *Precision Agriculture*, 12(1), pp.32–43.

Radwan, M., Willems, P. and Berlamont, J., 2004. Sensivity and uncertainty analysis for river quality modelling. *Journal of Hydroinformatics*, 6, pp.83-99.

Rafiei, E.A., Kappas, M., Hoang Khanh Nguyen, L. and Renchin, T., 2017. Hydrological Modeling in an Ungauged Basin of Central Vietnam Using SWAT Model. *Hydrology and Earth System Sciences*, 4(16), pp.2–17.

Refsgaard, J.C., 1997. Parameterisation, calibration and validation of distributed hydrological models. *Journal of Hydrology*, 198(1–4), pp.69–97.

Refsgaard, J.C., 2007. *Hydrological Modelling and River Basin Management.* Published PhD Thesis. University of Copenhagen. http://www.geus.dk/program-areas/water/denmark/rapporter/geus_special_rap_1_2007.pdf

Refsgaard, J.C., van der Sluijs, J.P., Brown, J. and van der Keur, P., 2006. A framework for dealing with uncertainty due to model structure error. *Advances in Water Resources*, 29(11), pp.1586–1597.

Refsgaard, J.C., Nilsson, B., Brown, J., Klauer, B., Moore, R., Bech, T., Vurro, M., Blind, M., Castilla, G., Tsanis, I., Biza, P., 2005. Harmonised techniques and representative river basin data for assessment and use of uncertainty information in integrated water management (HarmoniRiB). *Environmental Science and Policy* 8(3), pp.267–277.

Rahman, M.M., Thompson, J.R. and Flower, R.J., 2016. Environmental Modelling and Software An enhanced SWAT wetland module to quantify hydraulic interactions between riparian depressional wetlands , rivers and aquifers. *Environmental Modelling and Software*, 84, pp.263–289.

Rak, G., Kozelj, D. and Steinman, F., 2016. The impact of floodplain land use on flood wave propagation. *Natural Hazards*, 83(1), pp.425–443.

Ramsar, 2007. The Ramsar Convention on wetlands. Information Sheet on Ramsar wetlands (RIS): Luangwa floodplain, 2006-2008 version. Compiled by the Zambian Wildlife Authority ZAWA, Chilanga, Zambia. http://www.ramsar.org/ ris/key_ris_index.htm.

Rayburg, S. and Thoms, M., 2009. A coupled hydraulic–hydrologic modelling approach to deriving a water balance model for a complex floodplain wetland system. *Hydrology Research*, 40(4), pp.364–377.

Razavi, T. and Coulibaly, P., 2013. Classification of Ontario watersheds based on physical attributes and streamflow series. *Journal of Hydrology*, 493, pp.81–94.

Rebelo, A.J., Le Maitre, D.C., Esler, K.J. and Cowling, R.M., 2015. Hydrological responses of a valley-bottom wetland to land-use/land-cover change in a South African catchment: Making a case for wetland restoration. *Restoration Ecology*, 23(6), pp.829–841.

Rebelo, L.M., Finlayson, C.M. and Nagabhatla, N., 2009. Remote sensing and GIS for wetland inventory, mapping and change analysis. *Journal of environmental management*, 90(7), pp.2144–53.

Renard, B., Kavetski, D., Thyer, Kuczera, G. and Franks, S., 2010. Understanding predictive uncertainty in hydrologic modeling: The challenge of identifying input and structural errors. *Water Resources Research*, 46(5), pp.3-79.

Rodriguez, E., Morris, C.C., and Belz, J.J., 2006. A global assessment of the SRTM performance. *Photogrammetric Engineering and Remote Sensing*, 72(3), pp249–260.

Rokni, K., Ahmad, A., Selamat, A. and Hazini, S., 2014. Water feature extraction and change detection using multitemporal landsat imagery. *Remote Sensing*, 6(5), pp.4173–4189.

Rowberry, M.D., McCarthy, T.S., Thompson, M., Nomnganga, A. and Moyo, L., 2011. The spatial and temporal characterisation of flooding within the floodplain wetland of the Nyl River, Limpopo Province, South Africa. *Water SA*, 37(4), pp.445–452.

Rubarenzya, M.H., Willems, P. and Berlamont, J., 2007. Identification of uncertainty sources in distributed hydrological modelling: Case study of the Grote Nete catchment in Belgium. *Water SA*, 33(5), pp.633–642.

Rudorff, C.M., Melack, J.M. and Bates, P.D., 2014. Flooding dynamics on the lower Amazon floodplain: 1. Hydraulic controls on water elevation, inundation extent, and river-floodplain discharge. *Water Resources Research*, 50(1), pp.619–634.

Sahoo, G.B., Ray, C. and De Carlo, E.H., 2006. Calibration and validation of a physically distributed hydrological model, MIKE SHE, to predict streamflow at high frequency in a flashy mountainous Hawaii stream. *Journal of Hydrology*, 327(1–2), pp.94–109.

Sakamoto, T., Van Nguyen, N., Kotera, A., Ohno, H., Ishitsuka, N. and Yokozawa, M., 2007. Detecting temporal changes in the extent of annual flooding within the Cambodia and the Vietnamese Mekong Delta from MODIS time-series imagery. *Remote Sensing of Environment*, 109(3), pp.295–313.

SANBI., 2009. Further Development of a Proposed National Wetland Classification System for South Africa. Primary Project Report. Prepared by the Freshwater Consulting Group (FCG) for the South African National Biodiversity Institute (SANBI), SA.

Sanders, B.F., 2007. Evaluation of on-line DEMs for flood inundation modeling. *Advances in Water Resources*, 30(8), pp.1831–1843.

Sarp, G., Toprak, V. and Duzgun, S., 2011. Hypsometric properties of the hydrolic basins located on western part of nafz. *34th International Symposium on Remote Sensing of Environment - The GEOSS Era: Towards Operational Environmental Monitoring held on April 2011 in Sydney, Australia, pp.1*–4.

Sawicz, K., Wagener, T., Sivapalan, M., Troch, P.A and Carrillo, G., 2011. Catchment classification : empirical analysis of hydrologic similarity based on catchment function in the eastern USA. *Hydrol. Earth Syst. Sci.*, 15(9), pp.2895–2911.

Schoen, J.H., Stretch, D.D. and Tirok, K., 2014. Wind-driven circulation patterns in a shallow estuarine lake: St Lucia, South Africa. *Estuarine, Coastal and Shelf Science*, 146, pp.49–

59.

Schuijt, K., 2002. Land and Water Use of Wetlands in Africa: Economic Values of African Wetlands. IIASA Interim Report . IIASA, Laxenburg, Austria.

Schulze, R.E., 1984. Hydrological Models for Application to Small Rural Catchments in Southern Africa: Refinements and Development. WRC Report 63/2/84, Pretoria, RSA.

Schulze, R.E., Chapman, R.A., Angus, G.R. and Schmidt, E.J., 1987. Distributed model simulation of impacts of upstream reservoirs on wetlands. In: Walmsley, R.D. and Botten, M.L. *Proceedings, Symposium on Ecology and Conservation of Wetlands in South Africa. Ecosystems Programme, FRD-CSIR, Pretoria, RSA. Occasional Report, 24, pp.115-123.*

Schulze, R.E., 1989. ACRU: Background Concepts and Theory. ACRU Report No. 36, Dept. Agric. Eng., Univ. of Natal, Pieter- maritzburg, RSA.

Schulze, R.E., 1995. Hydrology and Agrohydrology: A Text to Accom pany the ACRU 3.00 Agrohydrological Modelling System. WRC Report TT 69/95, Water Research Commission, Pretoria.

Schulze, R.E., 2001. National Landcover Classification: Development of a Decision Support System for the ACRU Model. Internal Report, School of Bioresources Engineering and Environmental Hyrology, University of Natal, Pietermaritzburg, p25.

Schulze, R.E. and Smithers, J.C., 2002. The ACRU Modelling System as of 2001: Background, Concepts, Structure, Output, Typical Applications and Operations. In: Schulze, R.E. (Ed) Modelling as a Tool in Integrated Water Resources Management: Conceptual Issues and Case Study Applications. WRC Report 749/1/02. Water Research Commission, Pretoria, RSA.

Schulze, R.E. and Pike, A., 2003. *Development and Evaluation of an Installed Hydrological*, School of Bioresources Engineering and Environmental Hydrology University of Kwa-Zulu-Natal, Pietermaritzburg, RSA.

Schulze, R.E. and Pike, A., 2004. Development and Evaluation of an Installed Hydrological Modelling System. WRC Report No. 1155/1/04. Water Research Commission, Pretoria. p179.

Schumann, G.J., DI Baldassarre, G and Bates, P.D., 2009. the utility of space-borne radar to render maps of observed possibility of inundation. *IEEE Transactions on Geoscience and Remote sensing*, 4(8), pp.739-752.

Schumann, G.J., Neal, J.C., Voisin, N., Andreadis, K.M., Pappernberger, F., Phanthuwongpakdee, N., Hall, C and bates, P.D., 2013. A first large-scale flood inundation forecasting model. *Water Resources Research*, 49(10), pp.6248–6257.

Schuol, J. and Abbaspour, K.C., 2006. Calibration and uncertainty issues of a hydrological model (SWAT) applied to West Africa. *Advances in Geosciences*, 9, pp.137–143.

Schuyt, K.D., 2005. Economic consequences of wetland degradation for local populations in Africa. *Ecological Economics*, 53(2), pp.177–190.

Scown, M.W., Thoms, M.C. and De Jager, N.R., 2015. Floodplain complexity and surfacemetrics: Influences of scale and geomorphology. *Geomorphology*, 245, pp.102–116.

Scown, M.W., Thoms, M.C. and De Jager, N.R., 2016. An index of floodplain surface complexity. *Hydrology and Earth System Sciences,* 20(1), pp.431–441.

Seong, C., Herand, Y. and Benham, B.L., 2015. Automatic calibration tool for hydrologic simulation program-FORTRAN using a shuffled complex evolution algorithm. *Water (Switzerland),* 7(2), pp.503–527.

Sichingabula, H.M., 1998. Rainfall Variability, Drought and Implications of its Impacts on Zambia, 1886-1996 in Water Resources Variability in Africa during the 20th Century. *International Association of Hydrological Sciences,* 252, pp.125-134.

Shen, D., Wang, J., Cheng, X., Rui, Y. and Ye, S., 2015. Integration of 2-D hydraulic model and high-resolution LiDAR-derived DEM for floodplain flow modeling. *Hydrology and Earth System Sciences Discussions*, 12(2), pp.2011–2046.

Shook, K., Pomeroy, J.W., Spence, C. and Boychuk, L., 2013. Storage dynamics simulations in prairie wetland hydrology models: Evaluation and parameterization. *Hydrological Processes*, 27(13), pp.1875–1889.

Shook, K.R. and Pomeroy, J.W., 2011. Memory effects of depressional storage in Northern Prairie hydrology. *Hydrological Processes*, 25(25), pp.3890–3898.

Sikorska, A.E., Scheidegger, A., Banasik, K. and Rieckermann, J., 2013. Considering rating curve uncertainty in water level predictions. *Hydrology and Earth System Sciences*, 17(11), pp.4415–4427.

Singh, O., Sarangi, A. and Sharma, M.C., 2008. Hypsometric integral estimation methods and its relevance on erosion status of North-Western Lesser Himalayan watersheds. *Water Resources Management*, 22(11), pp.1545–1560.

Singh, V.P., 1995. *Computer models of watershed hydrology, V. P. Singh, ed.,* Water Resources Publications, Highlands Ranch, Colorado, pp.1–22.

Sivan, D., Greenbaum, N.,Cohen-Seffer, R., Sisma-Ventura, G. and Almogi-Labin, A., 2011. The origin and disappearance of the late Pleistocene-early Holocene short-lived coastal wetlands along the Carmel coast, Israel. *Quaternary Research*, 76(1), pp.83–92.

Sivapalan, M., Takeuchi, K., Franks, S.W., Gupta, V.K., Karambiri, H., Lakshmi, V., Liang, X., McDONNELL, J.J., Mendiondo, E.M., O'Connell, P.E., Oki, T., Pomeroy, J.W., Schertzer, D., Uhlenbrook, S. and Zehe, E., 2003. IAHS Decade on Predictions in Ungauged Basins (PUB), 2003–2012: Shaping an exciting future for the hydrological sciences. *Hydrological Sciences Journal*, 48(6), pp.857–880.

Silberstein, R.P., 2006. Hydrological models are so good, do we still need data? *Environmental Modelling and Software* 21 (9), pp.1340–1352.

Singh, V.P. and Woolhiser, D.A., 2002. Mathematical modelling of watershed hydrology. *J. Hydrol. Eng,* 7(4), pp.270–292.

Slaughter, A.R., Retief, D.C.H. and Hughes, D.A., 2015. A method to disaggregate monthly flows to daily using daily rainfall observations: model design and testing. *Hydrological Sciences Journal*, 60(11), pp.1896–1910.

Simard, M., Pinto, N., Fisher, J.B. and Baccini, A., 2011. Mapping forest canopy height globally with spaceborne lidar. *Journal of Geophysical Research: Biogeosciences*, 116(4), pp.1–12.

SMUWC (Sustainable Management of Usangu Wetlands and its Catchment)., 2001. Final Report, Water Resources. Supporting Report 7, vol. 3, Directorate of Water Resources Dar es Salaam, Tanzania, p203.

Sørensen, R., Zinko, U. and Seibert, J., 2006. On the calculation of the topographic wetness index: evaluation of different methods based on field observations. *Hydrology and Earth System Sciences*, 10(1), pp.101–112.

Spalding-Fecher, R., Yamba, F., Walimwipi, H., Kling, H., Tembo, B., Nyambe, I., Chapman, A. and Cuamba, B., 2014. *Water Supply and Demand Scenarios for the Zambezi River Basin. Climate Change and Upstream Development Impacts on New Hydropower Projects in the Zambezi Project.* Report for Climate and Development Knowledge Network. University of Cape Town, Cape Town, p92.

Stedinger, J.R., Vogel, R.M., Lee, S.U. and Batchelder, R., 2008. Appraisal of the generalized likelihood uncertainty estimation (GLUE) method. *Water Resources Research*, 44(W00B06), pp.1–17.

Steenbergen, F., Kool, M., Vuik, R. and Pol, B., 2015. *Floodplains in Zambia: The Scope for Shallow Well Development. Overview paper NO: 16*. Spate Irrigation Foundation, p16.

Stelling, G.S., Kernkamp, H.W.J., Laguzzi, M.M., 1998. Delft Flooding System: a powerful tool for inundation assessment based upon a positive flow simulation. Hydroinformatics'98, Babovic, Larsen (eds). Balkema: Rotterdam, pp.449–456.

Strahler, A.N., 1952. Hypsometric (area–altitude) analysis of erosional topography. *Geol Soc Amer Bull*, 63, pp.1117–1141.

Sulebak, J., 2000. *Applications of Digital Elevation Models*. DYNAMAP Project, Oslo, pp11.

Syme, W., 1991. Dynamically linked two dimensional / one dimensional hydrodynamic modelling program for rivers, estuaries, and coastal waters. M.Eng.Sc. Thesis, Dept. of Civil Engineering, The University of Queensland. http://trove.nla.gov.au/version/38572527.

Syvitski, J.P.M., Overeem, I., Brakenridge, G.R. and Hannon, M., 2012. Floods, floodplains, delta plains - A satellite imaging approach. *Sedimentary Geology*, 267–268, pp.1–14.

Teng, J., Vaze, J., Dutta, D. and Marvanek, S., 2015. Rapid Inundation Modelling in Large Floodplains Using LiDAR DEM. *Water Resources Management*, 29(8), pp. 2619–263.

Teng, J., Jakeman, A.J., Vaze, J.,Croke, B.F.W., Dutta, D. and Kim, S., 2017. Flood inundation modelling: A review of methods, recent advances and uncertainty analysis. *Environmental Modelling & Software*, 90, pp.201–216.

Ticehurst, C., Guerschman, J.P. and Chen, Y., 2014. The strengths and limitations in using the daily MODIS open water likelihood algorithm for identifying flood events. *Remote*

Sensing, 6(12), pp.11791–11809.

Thiemann, M., Trosset, M., Gupta, H., Sorooshian, S., 2001. Bayesian recursive parameter estimation for hydrologic models. *Water Resources Research*, 37(10), pp.2521–2535.

Thompson, J.R., 2004. Simulation of wetland water-level manipulation using coupled hydrological/hydraulic modeling. *Physical Geography*, 25(1), pp.39–67.

Thoms, M.C., Southwell, M. and McGinness, H.M., 2005. Floodplain–river ecosystems: Fragmentation and water resources development. *Geomorphology*, 71(1-2), pp.126–138.

Thyer, M., Renard, B., Kavetski, D., Kuczera, G., Franks, S.W. and Srikanthan, S., 2009. Critical evaluation of parameter consistency and predictive uncertainty in hydrological modeling: A case study using Bayesian total error analysis. *Water Resources Research*, 45(W00B14), pp.1–22.

Timberlake, J., 2000. *Biodiversity of the Zambezi Basin*, Occasional Publications in Biodiversity No: 9. Biodiversity Foundation for Africa, Famona, Bulawayo, Zimbabwe.

Timberlake, J.R. and Childes, S.L., 2004. Biodiversity of the Four Corners Area: Technical Reviews. Volume One (Chapters 1-4). Biodiversity Foundation for Africa, Famona, Bulawayo, Zimbabwe.

Tirivarombo, S., 2013. *Climate variability and climate change in water resources*. Published PhD. Thesis. Rhodes University Grahamstown South Africa. http://hdl.handle.net/10962/d1002955.

Tockner, K., Pennetzdorfer, D., Reiner, N., Schiemer, F. and Ward, J. V. 1999. Hydrological connectivity, and the exchange of organic matter and nutrients in a dynamic river-floodplain system (Danube, Austria). *Freshwater Biology*, 41, pp.521–535.

Tockner, K., Malard, F. and Ward, J. V, 2000. An extension of the Food pulse concept. *Hydrol. Process.*, 14, pp.2861–2883.

Tockner, K., Bunn, S.E., Quinn, G., Naiman, R., Stanford, J.A., Gordon, C., 2008. Floodplains: critically threatened ecosystems. In: Polunin, N.C. (Ed.), Aquatic Ecosystems. Cambridge University Press, Cambridge, pp. 45–61.

Tockner, K., Lorang, S. and Stanford, J.A., 2010. River flood plains are model ecosystems to test general hydrogeomorphic and ecological concepts. *River. Res. Applic.*, 26, pp.76–86.

Todd, J.M., Muneepeerakul, R., Pumo, D., Azaele, S., Miralles-Wilhelm, F., Rinaldo, A. and Rodriguez-Iturbe, I., 2010. Hydrological drivers of wetland vegetation community distribution within Everglades National Park, Florida. *Advances in Water Resources*, 33(10), pp.1279–1289.

Tomscha, S.A., Gergel, S.E. and Tomlinson, M.J., 2017. The spatial organization of ecosystem services in river-floodplains. *Ecosphere*, 8(3), pp. 1–27.

Tooth, S., McCarthy, T.S., Brandt, D., Hancox, P.J. and Morris, R., 2002. Geological controls on the formation of alluvial meanders and floodplain wetlands: The example of the Klip River, eastern Free State, South Africa. *Earth Surface Processes and Landforms*, 27(8), pp.797–815.

Tooth, S. and McCarthy, T.S., 2007. Wetlands in drylands: Geomorphological and sedimentological characteristics with emphasis on examples from southern Africa. *Progress in Physical Geography*, 31(1), pp.3–41.

Tooth, S., McCarthy, T., Rodnight, H., Keen-Zebert, A., Rowberry, M. and Brandt, D., 2012. Late Holocene development of a major fluvial discontinuity in floodplain wetlands of the Blood River, Eastern South Africa. *Geomorphology*, 205, pp.128–141.

Trambauer, P., Dutra, E., Maskey, S., Werner, M., Pappenberger, F., Van Beek, L.P.H. and Uhlenbrook, S., 2014. Comparison of different evaporation estimates over the African continent. *Hydrology and Earth System Sciences*, 18(1), pp.193–212.

Trigg, M.A., Wilson, M.D., Bates, P.D., Horritt, M.S., Alsdorf, D.E., Forsberg, B.R. and Vega, M.C., 2009. Amazon flood wave hydraulics, *Journal Hydrol.*, 374(1–2), 92–105.

Trigg, M.A., Bates, P.D., Wilson, M.D., Schumann, G. and Baugh, C., 2012. Floodplain channel morphology and networks of the middle Amazon River. *Water Resources Research*, 48(W10504), pp.1–17.

Trigg, M. A., Michaelides, K., Neal, J. C., and Bates, P. D., 2013. Surface water connectivity dynamics of a large scale extreme flood. *Journal of Hydrology*, 505, pp.138–149.

Tristram, D., Hughes, D. and Bradshaw, K., 2014. Accelerating a hydrological uncertainty ensemble model using graphics processing units (GPUs). *Computers and Geosciences*, 62, pp.178–186.

Tshimanga, R.M., 2012. *Hydrological Uncertainty Analysis and Scenario-Based Streamflow Modelling For The Congo River Basin*. Published PhD thesis. Rhodes University Grahamstown South Africa. http://hdl.handle.net/10962/d1006158.

Tshimanga, R.M., Hughes, D.A. and Kapangaziwiri, E., 2011. Initial calibration of a semi-distributed rainfall runoff model for the Congo River basin. *Physics and Chemistry of the Earth, Parts*, 36, pp.761–774.

Tshimanga, R.M. and Hughes, D.A., 2012. Climate change and impacts on the hydrology of the Congo Basin: The case of the northern sub-basins of the Oubangui and Sangha Rivers. *Physics and Chemistry of the Earth*, 50–52, pp.72–83.

Tulbure, M.G., Broich, M., Stehman, S.V. and Kommareddy, A., 2016. Remote Sensing of Environment Surface water extent dynamics from three decades of seasonally continuous Landsat time series at subcontinental scale in a semi-arid region. *Remote Sensing of Environment*, 178, pp.142–157.

Tumbo, M.H., 2015. *Uncertainties in modelling hydrological responses in gauged and ungauged sub-basins*. Published PhD thesis. Rhodes University Grahamstown South Africa. http://hdl.handle.net/10962/d1018568.

Tumbo, M. and Hughes, D. A., 2015. Uncertain hydrological modelling: application of the Pitman model in the Great Ruaha River basin, Tanzania. *Hydrological Sciences Journal*, 60(11), pp.1–16.

Turpie, J., Brad, S., Lucy, E. and Jon, B., 1999. Economic Value of The Zambezi Basin Wetlands. Zambezi Basin wetlands conservation and resource utilisation project: IUCN Regional Office for Southern Africa.

UNEP., 1992. World Atlas of Desertification. Edward Arnold, London.

USDA, 2008. Hydrogeomorphic Wetland Classification System : An Overview and Modification to Better Meet the Needs of the Natural Resources Conservation Service. Technical Note No. 190–8–76. United States Department of Agriculture, USA.

Valentová, J., Valenta, P. and Weyskrabová, L., 2010. Assessing the retention capacity of a floodplain using a 2D numerical model. *Journal of Hydrology and Hydromechanics*, 58(4), pp.221–232.

Valimba, P., 2004. *Rainfall variability in southern africa , its influences on streamflow variations and its relationships with climatic variations*. Published PhD thesis. Rhodes University grahamstown South Africa. http://hdl.handle.net/10962/d1006159.

Vanderhoof, M.K., Alexander, L.C. and Todd, M.J., 2015. Temporal and spatial patterns of wetland extent influence variability of surface water connectivity in the Prairie Pothole Region, United States. *Landscape Ecology*, 31(4), pp.805–824.

Van Griensven, A. and Meixner, T., 2004. Dealing with unidentifiable sources of uncertainty within environmental models. In: Pahl C, Schmidt S, Jakeman T. (Eds.), *Proceedings of the iEMSs International Congress, June 2004 International Congress*: *"Complexity and Integrated Resources Management". International Environmental Modelling and Software Society,* Osnabrück, Germany, pp.14–17.

Van Griensven, A., Xuan, Y., Haguma, D and Niyonzima, W., 2008. Understanding riverine wetland-catchment processes using remote sensing data and modelling. In: iEMSs 2008. *International Congress on Environmental Modelling and Software Integrating Sciences and Information Technology for Environmental Assessment and Decision Making 4th Biennial Meeting of iEMSs*, pp. 462–468.

Van Straaten, P 2002. Rocks for Crops: Agrominerals of sub-Saharan Africa. ICRAF, Nairobi, Kenya, p338.

Viessman, W. and Lewis, G.L., 2003. Introduction to Hydrology 5th (Ed). Upper Saddle River, N. J. Prentice Hall, Englewood Cliffs, New Jersey, p612.

Visser, H., Folkert, R.J.M., Hoekstra, J. and Wolff, J.J.D.E., 2000. Identifying Key Sources of Uncertainty in Climate. *Climatic Change*, 45(3–4), pp.421–457.

Vrugt, J.A., Gupta, H.V., Bastidas, L.A., Bouten, W. and Sorooshian, S., 2003. Effective and efficient algorithm for multiobjective optimization of hydrologic models. *Water Resources Research*, 39(8), pp.1–19.

Villarini, G., Mandapaka, P.V., Krajewski, W.F. and Moore, R.J., 2008. Rainfall and sampling uncertainties: A rain gauge perspective. *Journal of Geophysical Research Atmospheres*, 113(11), pp.1–12.

Vining, K.C., 2002. Simulation of Streamflow and Wetland Storage, Starkweather Coulee Subbasin, North Dakota, Water Years 1981-98. Water-Resources Investigations Report

NO: 02–4113. Bismarck, North Dakota, p28.

Wagener, T. and Gupta, H.V., 2005. Model identification for hydrological forecasting under uncertainty. S*tochastic Environmental Research and Risk Assessment*, 19(6), pp.378–387.

Wagener, T. and Kollat, J., 2007. Numerical and visual evaluation of hydrological and environmental models using the Monte Carlo analysis toolbox. *Environ. Model. Software* 22(7), pp.1021-1033.

Wagener, T. and Montanari, A., 2011. Convergence of approaches toward reducing uncertainty in predictions in ungauged basins. *Water Resour Res*, 47 (W06301), doi:10.1029/2010WR009469.

Wagener, T. and Wheater, H.S., 2006. Parameter estimation and regionalization for continuous rainfall-runoff models including uncertainty. *Journal of Hydrology*, 320(1), pp.132–154.

Wagener, T., Mcintyre, N., Lees, M.J., Wheater, H.S. and Gupta, H.V., 2003. Towards reduced uncertainty in conceptual rainfall-runoff modelling : Dynamic identifiability analysis. *Hydrol. Process.*, 17(2), pp.455–476.

Wagener, T., Boyle, D.P., Lees, M.J., Wheater, H.S., Gupta, H.V. and Sorooshian, S., 2001. A framework for development and application of hydrological models. *Hydrology and Earth System Sciences*, 5(1), pp.13–26.

Wamulume, J., Landert, J., Zurbrügg, R., Nyambe, I., Wehrli, B. and Senn, D. B., 2011. Exploring the hydrology and biogeochemistry of the dam-impacted Kafue River and Kafue Flats (Zambia). *Physics and Chemistry of the Earth*, 36(14–15), pp.775–788.

Wang, Y. and Brubaker, K., 2015. Multi-objective model auto-calibration and reduced parameterization: Exploiting gradient-based optimization tool for ahydrologic model. *Environmental Modelling and Software*, 70, pp.1–15.

Wen, L., Ralph, T., Hosking, T., Barma, D. and Saintilan, N., 2013a Assessing stream restoration works in the southern Macquarie Marshes using hydrodynamic modeling. *In 20th International Congress on Modelling and Simulation.* Adelaide, Australia, pp.1–6.

Wen, L., Macdonald, R., Morrison, T., Hameed, T., Saintilan, N. and Ling, J., 2013b. From hydrodynamic to hydrological modelling: Investigating long-term hydrological regimes of key wetlands in the Macquarie Marshes, a semi-arid lowland floodplain in Australia. *Journal of Hydrology*, 500, pp.45–61.

Wang, M., Hjelmfelt, A.. and Garbrecht, J., 2000. DEM aggregation for watershed modeling. *Journal of the American Water Resources Association*, 36(3), pp.579–584.

Wang, X., Yang, W. and Melesse, A.M., 2008. Using hydrological equivalent wetland concept within SWAT to estimate streamflow in watersheds with numerous wetlands. *American Society of Agricultural and Biological Engineers*, 51(1), pp.55–72.

Wang, X., Shang, S., Qu, Z., Liu, T., Melesse, A.M and Yang, W., 2010. Simulated wetland conservation-restoration effects on water quantity and quality at watershed scale. *Journal of environmental management*, 91(7), pp.1511–25.

Ward, D.P., Hamilton, S.K., Jardine, T.D., Pettit, N.E., Tews, E. K., Olley, J.M. and Bunn, S.E., 2013. Assessing the seasonal dynamics of inundation, turbidity, and aquatic vegetation in the Australian wet-dry tropics using optical remote sensing. *Ecohydrology*, 6(2), pp.312–323.

Warmink, J., Janssen, J., Booij, M.J., and Krol, M.S., 2010. Identification and classification of uncertainties in the application of environmental models. *Environmental Modelling and Software*, 25(12), pp.1518–1527.

Westerberg, I., Guerrero, J.L., Seibert, J., Beven, K.J. and Halldin, S., 2011. Stage-discharge uncertainty derived with a non-stationary rating curve in the Choluteca River, Honduras. *Hydrological Processes*, 25(4), pp.603–613.

Westerhoff, R.S., 2015. Using uncertainty of Penman and Penman-Monteith methods in combined satellite and ground-based evapotranspiration estimates. *Remote Sensing of Environment*, 169, pp.102–112.

Wilson, M.D., Bates, P., Alsdorf, D., Forsberg, B., Horritt, M., Melack, J., Frappart, F. and Famiglietti, J., 2007. Modeling large-scale inundation of Amazonian seasonally flooded wetlands. *Geophysical Research Letters*, 34(15), pp.4–9.

Wood, M., Hostache, R., Neal, J., Wagener, T., Giustarini, L., Chini, M., Corato, G., Matgen, P. and Bates, P., 2016. Calibration of channel depth and friction parameters in the LISFLOOD-FP hydraulic model using medium resolution SAR data. *Hydrology and Earth System Sciences*, 20, pp.4983–4997.

WMO, 1983. Guide to Climatological Practices, Second edition. WMO-No. 100. Third Edition working draft 3 May 2007 available from: http://www.wmo.int/pages/prog/wcp/ccl/ guide/guide_climat_practices.html.

Wiens, J.A., 2002. Riverine landscapes : taking landscape ecology into the water. *Freshwater Biology*, 47(4), pp.501–515.

Wilk, J. and Hughes, D.A., 2002. Simulating the impacts of land-use and climate change on water resource availability for a large south Indian catchment. *Hydrological Sciences Journal*, 47(1), pp.19–30.

Wilson, R.T., 2003. Livestock production and farm animal genetic resources in the Usangu Wetland of the Southern Highlands of Tanzania. *Livestock Research for Rural Development*, 15(1), pp.11–24.

Wilson, M.D., Bates, P., Alsdorf, D., Forsberg, B., Horritt, M., Melack, J., Frappart, F. and Famiglietti, J., 2007. Modeling large-scale inundation of Amazonian seasonally flooded wetlands. *Geophysical Research Letters*, 34(15), pp.4–9.

Winsemius, H.C., 2009. *Satellite data as complementary information for hydrological modelling*. Published PhD. Thesis,Water Resources Section, Faculty of Civil Engineering and Geosciences, Delft University of Technology. Delft. uuid:2db8e9e7-03cf-43ab-976b-8ea8941a7a05.

Winsemius, H.C., Savenije, H.H.G., Gerrits, A.M.J., Zapreeva, E.A., Klees, R., 2006. Comparison of two model approaches in the Zambezi river basin with regard to model reliability and identifiability. *Hydrology and Earth System Sciences Discussions*, 2(6), pp.2625–2661.

Winsemius, H.C., Savenije, H.H.G. and Bastiaanssen, W.G.M., 2008. Constraining model parameters on remotely sensed evaporation: justification for distribution in ungauged basins? *Hydrology and Earth System Sciences*, 12(6), pp.1403–1413.

Winsemius, H.C., Schaefli, B., Montanari, A., Savenije, H. H G., 2009. On the calibration of hydrological models in ungauged basins: A framework for integrating hard and soft hydrological information. *Water Resources Research*, 459(W12422), pp.1–15.

Wolski, P., Savenije, H.H.G., Murray-Hudson, M. and Gumbricht, T., 2006. Modelling of the flooding in the Okavango Delta, Botswana, using a hybrid reservoir-GIS model. *Journal of Hydrology*, 331(1–2), pp.58–72.

World Bank., 2010. The Zambezi River Basin–A multi-sector investment opportunity analysis. Report, Volume 4, The World Bank, Washington DC, p139.

Xu, C., 2002. *Text book of Hydrologic models (Lärobok i Avrinningsmodeller),* Department of Earth Sciences Hydrology, Uppsala University, Sweden, p168.

Xu, H., 2006. Modification of normalised difference water index (NDWI) to enhance open water features in remotely sensed imagery. *International Journal of Remote Sensing*, 27(14), pp.3025–3033.

Yadav, M., Wagener, T. and Gupta, H., 2007. Regionalization of constraints on expected watershed response behavior for improved predictions in ungauged basins. *Advances in Water Resources,* 30(8), pp.1756–1774.

Yamazaki, D., Kanae, S., Kim, H., Oki, T., 2011. A physically based description of floodplain inundation dynamics in a global river routing model. *Water Resources Research*, 47(4), pp.1–21.

Yamazaki, D., O'Loughlin, F., Trigg, M.A., Miller, Z.F., Pavelsky, T.M and Bates, P.D. 2014. Development of the Global Width Database for Large Rivers. *Water Resources Research* 50(4), pp.3467–3480.

Yamazaki, D., Loughlin, F.O., Trigg, M. and Bates, P., 2015. GWD-LR : A satellite-based global database of river channel width. *EGU General Assembly 2015, held on 12-17 April, 2015 in Vienna, Austria. id.4250*.

Yamazaki, D., Ikeshima, D., Tawatari, R., Yamaguchi, T., O’Loughlin, F., Neal, J.C., Sampson, C.C., Kanae, S and Bates, P. D.., 2017. A high-accuracy map of global terrain elevations, Geophys. Res. Lett., 44, pp.5844–5853.

Yan, K., Di Baldassarre, G., Solomatine, D.P. and Schumann, G.J., 2015. A review of low-cost space-borne data for flood modelling: topography, flood extent and water level. *Hydrological Processes*, 29(15), pp.3368–3387.

Yan, K.; Pappenberger, F., Umer, Y.M., Solomatine, D.P. and Di Baldassarre, G., 2014. Regional versus physically-based methods for flood inundation modelling in data scarce areas: An application to the Blue Nile. In: M. Piasecki (Ed.), *Proceedings of the HIC 2014, 11th international conference on hydroinformatics,* New York, pp.849–855.

Yang, J., Reichert, P., Abbaspour, K.C., Xia, J. and Yang, H., 2008. Comparing uncertainty analysis techniques for a SWAT application to the Chaohe Basin in China. *Journal of Hydrology*, 358(1–2), pp.1–23.

Yao, C., Li, Z., Yu, Z. and Zhang, K., 2012. A priori parameter estimates for a distributed, grid-based Xinanjiang model using geographically based information. *Journal of Hydrology*, 468–469, pp.47–62.

Zahera, 2011. Modelling Seasonally Flooded Wetlands in the Semi-arid Sahelian Zone. Nile Basin. *Water Science and Engineering Journal*, 4(2), pp.83–93.

Zarch, M.A., Sivakumar, B. and Sharma, A., 2015. Assessment of global aridity change. *Journal of Hydrology*, 520, pp.300–313.

Zhang, G.X., Feng, X.Q. and Jun Xu, Y., 2013. Simulation of hydrological processes in the Zhalong wetland within a river basin, Northeast China. *Hydrology and Earth System Sciences*, 17(7), pp.2797–2807.

Zhang, Q. and Werner, A.D., 2015. Hysteretic relationships in inundation dynamics for a large lake-floodplain system. *Journal of Hydrology*, 527, pp.160–171.

Zhang, X., Hörmann, G., Gao, J. and Fohrer, N., 2011. Structural uncertainty assessment in a discharge simulation model. *Hydrological Sciences Journal*, 56(5), pp.854–869.

Zhang, Y., Li, C., Trettin, C.C., Li, H and Sun, G., 2002. An integrated model of soil, hydrology, and vegetation for carbon dynamics in wetland ecosystems. *Global Biogeochemical Cycles*, 16 (4), pp.9:1–17.

Zhang, Z., Wagener, T., Reed, P. and Bhushan, R., 2008. Reducing uncertainty in predictions in ungauged basins by combining hydrologic indices regionalization and multiobjective optimization. *Water Resources Research*, 44(W00B04), pp.1–13.

Zhao, X., Su, Y., Hu, T., Chen, L., Gao, S., Wang, R., Jin, S. and Guo, Q., 2018. A global corrected SRTM DEM product for vegetated areas A global corrected SRTM DEM product for vegetated areas. *Remote Sensing Letters*, 9(4), pp.393–402.

Zhiqiang, T., Qi, Z., Mengfan, L., Yunliang, L., Xiuli, X. and Jiahu, J., 2016. A study of the relationship between wetland vegetation communities and water regimes using a combined remote sensing and hydraulic modeling approach. *Hydrology Research*, pp.1–15.